

City Research Online

City St George's, University of London

Citation: Halai, H. (2018). Compensation grouting to control deep excavation ground movements. (Unpublished Doctoral thesis, City, University of London)

This is the accepted version of the paper.

This version of the publication may differ from the final published version. To cite this item please consult the publisher's version.

Permanent repository link: https://openaccess.city.ac.uk/id/eprint/20078/

Copyright and Reuse: Copyright and Moral Rights remain with the author(s) and/or copyright holders. Copies of full items can be used for personal research or study, educational, or not-for-profit purposes without prior permission or charge, unless otherwise indicated, provided that the authors, title and full bibliographic details are credited, a hyperlink and/or URL is given for the original metadata page and the content is not changed in any way. For full details of reuse please refer to City Research Online policy.

City Research Online: http://openaccess.city.ac.uk/ publications@citystgeorges.ac.uk

Compensation grouting to control deep excavation ground movements

By

Hitesh Halai

A dissertation submitted for the Degree of Doctor of Philosophy

City, University of London

School of Mathematics, Computer Sciences and Engineering

Department of Civil Engineering

Research Centre for Multi-Scale Geotechnical Engineering

“Nothing in the world is worth having or worth doing unless it means effort, pain, difficulty…”

—Theodore Roosevelt

CONTENTS

LIST OF TABLES i
LIST OF FIGURES iv
AKNOWLEDGEMENTS xviii
DECLARATION xix
ABSTRACT xx
LIST OF SYMBOLS xxi
SUBSCRIPTS xxiii
ABBREVIATIONS xxiv
1. INTRODUCTION
1.1 Background 1
1.2 Aims 3
1.3 Outline of report 4
2. EXCAVATION GROUND MOVEMENTS-LITERATURE REVIEW
2.1 Introduction 6
2.2 Ground movement mechanisms 7
2.2.1 Vertical stress relief 9
2.2.2 Horizontal stress relief 10
2.3 Empirical observations 11
2.4 Semi-empirical prediction methods 17
2.5 Summary 20
3. COMPENSATION GROUTING - LITERATURE REVIEW
3.1 Introduction 22
3.2 Compaction grouting process 25
3.3 Theory 27
3.3.1 Mechanisms 27
3.3.1.1 Shear failure 29
3.3.1.2 Cavity expansion 30
3.4 Case studies of compaction grouting 31
3.4.1 Bolton Hills Tunnels, Baltimore, U.S.A. 31
3.4.2 Deep excavation, Shanghai, China 33

3.5 Summary 35

4. CENTRIFUGE MODELLING

4.1 Introduction 36

4.2 Principles of centrifuge modelling 37

4.3 Scaling Laws 38

4.4 Scaling effects and errors 40

4.4.1 Vertical acceleration field 40

4.4.2 Rotational acceleration field 41

4.4.3 Particle size 42

4.4.4 Boundary effects 43

4.5 The Geotechnical Centrifuge Testing Facility 44

4.6 The Acutronic 661 geotechnical centrifuge 44

4.7 Data acquisition and motion control 46

4.8 Instrumentation and calibration 47

4.9 Digital imaging and analysis 49

5. MODEL AND APPARATUS DEVELOPMENT

5.1 Model design requirements 51

5.1.1 Excavation modelling 51

5.1.2 Compensation grouting modelling 53

5.2 Apparatus design and development 55

5.2.1 Strongbox and model boundary conditions 55

5.2.2 Soil properties and stress history 57

5.2.3 Ground water supply 59

5.2.4 Model excavation apparatus 59

5.2.4.1 Model retaining wall and prop 59

5.2.4.2 Excavation simulation 61

5.2.5 Compensation grouting apparatus 64

5.2.5.1 Grouting injection tubes 64

5.2.5.2 Grout injection system 66

5.2.6 Location of instrumentation 68

5.3 Experimental procedure 69

5.3.1 Sample preparation 69

5.3.2 Model preparation 70
5.4 Testing 73
6. EXPERIMENTAL WORK
6.1 Details of tests 76
6.2 Comparison of LVDT and image processing vertical measurements at the retained surface 82
6.2.1 Excavation tests 83
6.2.2 Grouting and excavation tests (without a brass collar) 85
6.2.3 Grouting and excavation tests (with a brass collar) 86
6.3 Image processing of wall and formation level displacements 89
6.4 Observations and Results 91
6.4.1 Soil and wall movements 91
6.4.1.1 Tests 2HH, 3HH and 10HH 92
6.4.1.2 Tests 6-9HH 96
6.4.1.3 Tests 10-11HH 103
6.4.1.4 Tests 12-13HH 106
6.4.2 Injection and local pore pressure response 109
6.4.3 Far field pore pressures 113
6.5 Soil strengths 113
6.6 Summary 114
6.6.1 Test details 114
6.6.2 Measurement of vertical soil and horizontal wall displacements 114
6.6.2.1 Excavation tests 115
6.6.2.2 Grouting tests 115
6.6.3 Observations 117
6.6.4 Soil strengths 118
7. DISCUSSION
7.1 Introduction 119
7.2 Consideration of the test results within existing frameworks 120
7.3 Influence of the grouted volume 122
7.3.1 Vertical displacements at the retained surface 123
7.3.2 Horizontal wall displacements 125
7.4 Influence of the timing of grout injection 126

7.4.1 Vertical displacements at the retained surface 126
7.4.2 Horizontal wall displacements 129
7.5 Influence of the position of grouting 131
7.5.1 Vertical displacements at the retained surface 131
7.5.2 Horizontal wall displacements 136
7.6 Summary 138
7.6.1 Volume of injected grout 138
7.6.2 Timing of injection grouting 139
7.6.3 Position of grouting 140
8. CONCLUSION
8.1 Introduction 143
8.2 Experimental procedure 143
8.3 Conclusions 144
8.3.1 Grouted volume 145
8.3.2 Grout injection timing 145
8.3.3 Position of grouting 146
8.4 Implications and limitations of the research 149
8.5 Recommendations for further research 151
REFERENCES 153
TABLES
FIGURES

LIST OF TABLES

Table 2. 1 Support stiffness categories for excavations (after Carder, 1995).

Table 3. 1 Physical and geotechnical properties of Shanghai Clay (after Liu, 2003).

Table 3. 2 Ground settlement changes due to compaction grouting in Shanghai, China (after Liu, 2003).

Table 4. 1 Scaling factors relating parameters at prototype scale to centrifuge model scale.

Table 5. 1 Previous methods for modelling excavations in a geotechnical centrifuge.

Table 5. 2 Speswhite kaolin clay properties (after Grant, 1998).

Table 6. 1 Details of tests conducted showing development of experimental technique with comments on performance of apparatus.

Table 6. 2 Summary of simulated excavation durations and SPT support pressures for all tests.

Table 6. 3 Difference in settlements between LVDTs and image processing targets (15 mm below the surface) above the wall and at distances x= 0.25H, 0.5H, 1.0H and 1.5H behind the wall during excavation and up to 133 s post excavation completion in tests 2HH, 3HH and 10HH.

Table 6. 4 Difference in settlements between LVDTs and image processing targets (15 mm below the surface) above the wall and at distances x= 0.25H, 0.5H, 1.0H and 1.5H behind the wall in tests 6-7HH, where no brass collar was provided at the front of the injection tube.

Table 6. 5 Difference in settlements between LVDTs and image processing targets (15 mm below the surface) above the wall and at distances x= 0.25H, 0.5H, 1.0H and 1.5H behind the wall in test 8HH, where a brass collar was provided at the front of the injection tube.

Table 6. 6 Difference in settlements between LVDTs and image processing targets (15 mm below the surface) above the wall and at distances x= 0.25H, 0.5H, 0.75H, 1.0H and 1.5H behind the wall in tests 10HH and 12HH, where a brass collar was provided at the front of the injection tube.

Table 6. 7 Difference in settlements between LVDTs and image processing targets (15 mm below the surface) above the wall and at distances x= 0.25H, 0.5H, 0.75H, 1.0H and 1.5H behind the wall in tests 9HH, 11HH and 13HH, where a brass collar was provided at the front of the injection tube.

Table 6. 8 Pre-test hydrostatic pore pressures established in model, measured by the top and bottom far field PPTs.

Table 6. 9 Summary of event times relative to the start of excavation and injected volumes in test 6HH.

Table 6. 10 Summary of event times relative to the start of excavation and injected volumes in test 7HH.

Table 6. 11 Summary of event times relative to excavation initiation and injected volumes in test 8HH.

Table 6. 12 Summary of event times relative to the start of excavation and injected volumes in test 9HH.

Table 6. 13 Summary of event times relative to the start of excavation and injected volumes in test 10HH.

Table 6. 14 Summary of event times relative to the start of excavation and injected volumes in test 11HH.

Table 6. 15 Summary of event times relative to the start of excavation and injected volumes in test 12HH.

Table 6. 16 Summary of event times relative to the start of excavation and injected volumes in test 13HH.

Table 6. 17 Average pressure losses measured between the Injection system PT and Manifold PT (close to the point of injection tube into the back wall of the strongbox).

Table 6. 18 Initial cavity volumes of the injection tubes in tests 6-13HH.

Table 6. 19 Radial distance between the injection grouting tube and locally installed injection zone pore pressure transducer.

Table 6. 20 Peak injection pressures, associated injected volumes, overburden stresses above each tube and normalised injection pressures against overburden stresses for all grouting tests.

Table 7. 1 Normalised magnitude of maximum horizontal wall displacement at the end of simulated excavation in tests 3HH and 10HH shown in the context of expected limits in firm clays from monitoring data by Moorman (2004).

Table 7. 2 Normalised impact of the injection passes in tests 7HH, 9HH, 10HH and 11HH on the vertical surface settlements above the injection tube relative to test 3HH.

Table 7. 3 Total injected volumes in test 6-13HH at the end of simulated excavation.

Table 7. 4 Effect of timing between injection passes on the compensation effect in single point injection tests 7HH and 10HH.

Table 7. 5 Normalised impact of the injection passes in all grouting tests on the horizontal wall displacements at a depth d= 0.75H below the retained surface relative to test 3HH.

Table 7. 6 Normalised impact of injection between single point injections in tests 7HH, 9HH, 10HH and 11HH and dual point simultaneous injections in test 12HH and 13HH on the vertical displacements at the retained surface above the injection location.

LIST OF FIGURES

Figure 2. 1 Typical pattern of displacements behind retaining walls (after Burland *et al.,* 1979).

Figure 2. 2 Typical profiles of movement for braced and tieback walls (after Clough and O'Rourke, 1990).

Figure 2. 3 Types of settlement profiles (after Hsieh and Ou, 1998).

Figure 2. 4 Vertical soil response to vertical unloading caused by excavation (after Burland *et al.,* 1979).

Figure 2. 5 Horizontal soil response to vertical unloading caused by excavation (after Burland *et al.,* 1979).

Figure 2. 6 Effect of factor of safety against basal heave (FS_{Heave}) and support system stiffness (K_1) on normalised maximum horizontal wall movements in soft to medium clays (after (a) Terzaghi, 1943; Bjerrum and Eide, 1956, (b) Mana and Clough, 1981 and (c) Clough *et al.,* 1989).

Figure 2. 7 Summary of settlements adjacent to open cuts in various soils, as a function of distance from edge of excavation (after Peck, 1969).

Figure 2. 8 Observed maximum: (a) wall deflections and (b) vertical settlements for stiff clays, residual soils and sands (after Clough and O'Rourke, 1990; reproduced from Moorman, 2004).

Figure 2. 9 Summary of vertical soil and horizontal wall displacements adjacent to excavations in stiff to very hard clays (after Clough and O'Rourke, 1990).

Figure 2. 10 Dimensionless settlement envelopes for estimating settlements adjacent to excavations in different soil types (after Clough and O'Rourke, 1990).

Figure 2. 11 Subdivision of case history data by Long (2001).

Figure 2. 12 Normalised maximum horizontal wall displacements against excavation depths observed in soft and stiff clays (after Moormann, 2004).

Figure 2. 13 Normalised maximum vertical settlements against excavation depths observed in soft and stiff clays (after Moormann, 2004).

Figure 2. 14 (a) Normalised ground surface displacements due to excavation and (b) settlements normalised against maximum settlement behind the wall in soft to firm clays (after Gaba *et al.,* 2017).

Figure 2. 15 (a) Normalised ground surface displacements due to excavation and (b) settlements normalised against maximum settlement behind the wall in stiff clays (after Gaba *et al.,* 2017).

Figure 2. 16 Relationship between normalised maximum ground settlements and lateral wall movements (after Mana and Clough, 1981).

Figure 2. 17 Normalised ground settlement profile envelopes (after Mana and Clough, 1981).

Figure 2. 18 Proposed method for predicting a spandrel type settlement profile (after Ou *et al.,* 1993).

Figure 2. 19 Modified method for predicting a spandrel type settlement profile following Ou *et al.* (1993) (after Hseih and Ou, 1998).

Figure 2. 20 Proposed method for predicting a concave settlement profile (after Hseih and Ou, 1998).

Figure 3. 1 Development of ground movement ahead of a tunnel heading in clay (after Mair *et al.,* 1995).

Figure 3. 2 Basic principle of compensation grouting (after Mair and Hight, 1994).

Figure 3. 3 Compensation grouting process (modified after Mair *et al.,* 1995).

Figure 3. 4 Soil displacements induced by compensation grouting (after Soga *et al.,* 2004).

Figure 3. 5 Compaction grouting concept (after Graf, 1969).

Figure 3. 6 Typical compaction grouting processes with: (a) top down and (b) bottom up methods (after ASCE, 2010).

Figure 3. 7 Modes of soil mass deformation by compaction grouting (after Wong *et al.,* 1996).

Figure 3. 8 Conical shearing failure above spherical grout bulb (after Wong, 1974).

Figure 3. 9 Distributions of normalised radial displacements with normalised radial distance to grout bulbs from compaction grouting (after Wong *et al.,* 1996).

Figure 3. 10 Cylindrical shear failure mechanism above a spherical expanding cavity in clay (after Cirone, 2016).

Figure 3. 11 Injection pressure-cavity radius relationship representing the two mechanisms that occur during the compaction grouting process as proposed by Cirone (2016).

Figure 3. 12 Layout of the compaction grout bulbs over the first tunnel shield in Baltimore, U.S.A. (after Baker *et al.,* 1983).

Figure 3. 13 Influence of the compaction grouting on soil settlements above the tunnel at various times in Baltimore, U.S.A. (after Baker *et al.,* 1983).

Figure 3. 14 Displacement-depth profiles for grouted and ungrouted sections of the tunnels in Baltimore, U.S.A. (after Baker *et al.,* 1983).

Figure 3. 15 Layout of the excavation and buildings in Shanghai, China (after Liu, 2003).

Figure 3. 16 Procedure of compaction grouting during the deep excavation in Shanghai, China (after Liu, 2003).

Figure 4. 1 Inertial stresses in a centrifuge model induced by rotation about a fixed axis compared to a corresponding prototype (after Taylor, 1995).

Figure 4. 2 Stress variation with depth in a centrifuge model compared to a corresponding prototype (after Taylor, 1995).

Figure 4. 3 Geometry of a typical model on the Acutronic 661 geotechnical centrifuge at City, University of London showing a) elevation of the model inflight; b) plan view of model inflight with components of induced acceleration (after Grant 1998).

Figure 4. 4 Schematic diagram of the previous Acutronic 661 geotechnical centrifuge testing facility at City, University of London, prior to upgrading and refurbishment of the facility (after Grant, 1998).

Figure 4. 5 Schematic diagram of the current Acutronic 661 geotechnical centrifuge testing facility at City, University of London (used from tests 6HH onwards).

Figure 4. 6 General arrangement of the dual TELI and PULNIX CCD camera setup for tests 2HH and 3HH showing: a) schematic plan view of positions and b) typical fields of view captured by each camera (before January 2014).

Figure 4. 7 General arrangement of the single TELI CCD camera setup for test 6HH onwards showing: a) schematic plan view of position and b) typical field of view captured by the TELI camera (after January 2014).

Figure 5. 1 Simulation of excavation methods using two fluids adopted by: (a) McNamara (2001) and (b) Elshafie (2008).

Figure 5. 2 Schematic diagram of model and tests apparatus developed by Chin (1996) for modelling fracture grouting in a geotechnical centrifuge.

Figure 5. 3 Schematic diagram showing the granular grout injection apparatus developed by Lu (1996) for centrifuge modelling compaction grouting.

Figure 5. 4 Compensation grouting apparatus developed by Au (2001).

Figure 5. 5 Expandable latex balloon system developed by Au (2001) for the modelling of idealised compaction grouting.

Figure 5. 6 Conceptual image of the aluminium strongbox used in the centrifuge model tests.

Figure 5. 7 Schematic diagram showing the layout of the excavation in the centrifuge model tests conducted.

Figure 5. 8 Comparison of failure modes behind and in front of a retaining wall (after Padfield and Mair, 1984).

Figure 5. 9 Variation of overconsolidation ratio with soil depth in the centrifuge model.

Figure 5. 10 Variation in K_o with soil depth in the centrifuge model.

Figure 5. 11 Theoretical total vertical and horizontal stresses and hydrostatic pore pressures with the water table used in the model.

Figure 5. 12 Diagram showing the standpipe configuration for setting up the correct water table level within the model.

Figure 5. 13 Detailed drawing of the model retaining wall.

Figure 5. 14 Details of the cast silicone RTV rubber seals used on the front and back faces of the model retaining wall.

Figure 5. 15 Photograph showing the 3 mm external diameter black tracking targets inserted into the front rubber seal of the model retaining wall for tracking of horizontal wall displacements.

Figure 5. 16 Detailed drawing of the aluminium prop plate.

Figure 5. 17 Prop plate support frame and spacers.

Figure 5. 18 Conceptual diagram of the apparatus arrangement for modelling of the excavation.

Figure 5. 19 (a) Photograph of the collar clamp used to secure the SPT filled excavation support latex bag to the prop plate during flight and (b) schematic diagram showing configuration of latex support bag and collar clamp.

Figure 5. 20 Non-linear distribution of the total vertical and horizontal stresses with the model excavation depth and comparison with the stresses imposed by the Sodium polytungstate solution.

Figure 5. 21 Details of the latex bag used for containing the excavation heavy Sodium polytungstate (SPT) support fluid.

Figure 5. 22 Photograph of the natural latex bag used to contain the SPT fluid and support the pre-cut excavation during flight.

Figure 5. 23 Detail of the SPT drainage fitting connection to the excavation support latex bag, manifold and external SPT pressure transducer.

Figure 5. 24 Conceptual diagram (exploded) of the heavy fluid pump (HFP) used to drain the SPT fluid in excavation only tests 2HH and 3HH.

Figure 5. 25 Photograph showing the position and arrangement of the heavy fluid pump on the swing.

Figure 5. 26 Photograph showing the configuration used for the draining and pressure measurement of the SPT excavation support fluid and injection pressures from tests 7HH onwards.

Figure 5. 27 Photograph showing the rotary solenoid assembly used to drain the SPT fluid in test 6HH.

Figure 5. 28 Typical detail of the grout injection tube within the model (see Figure 5.29 for details A to C).

Figure 5. 29 Details A to C from Figure 5.28 of the grout injection tube construction within the model.

Figure 5. 30 Photographs of: (a) the grout injection tube without the front brass retaining collar used in tests 6-7HH, (b) the front brass retaining collar used in tests 8-13HH, (c) the wire wrap seating grooves in the inner Nylon mandrel injection pipe and (d) application of the outer wire wrap around the latex membrane.

Figure 5. 31 Photograph showing details of the grout injection system.

Figure 5. 32 Photograph showing details of the de-airing standpipe used to prime and fill the injection system.

Figure 5. 33 Plan and section view of the LVDT gantry set up in the model tests.

Figure 5. 34 Positions of the far field PPTs used to assess hydrostatic pore pressure equilibrium within the model prior to testing.

Figure 5. 35 Positions of the installed PPTs locally around the grout injection tube locations in the grouting tests 6-13HH.

Figure 5. 36 Photographs showing: (a) insertion of the de-stoned Druck PDCR-81 PPT and (b) the slotted ballast sleeve attached behind the de-stoned PPT to ensure its positioning at the bottom of the SPT filled excavation support latex bag.

Figure 5. 37 Clay sample stress history during one dimensional consolidation in the hydraulic press prior to model making.

Figure 5. 38 Photograph showing the final trimming of the top model surface using an aluminium box cutter.

Figure 5. 39 Photograph showing the excavation trimming guide being used to rough cut the excavation cavity using the brass tube cutter.

Figure 5. 40 Guide and cutter for forming the 40 mm deep slot for the model wall toe embedment.

Figure 5. 41 Schematic drawing of the model wall embedment slot cutter and guide (after McNamara, 2001).

Figure 5. 42 Photograph showing the pin location system on the wall embedment slot cutter for quick adjustment of the cutting depth.

Figure 5. 43 Diagram showing the clay coring apparatus for insertion of the grout injection tube.

Figure 5. 44 Photograph showing the prepared model, apparatus and instrumentation setup following the model making procedure, ready for flight.

Figure 6. 1 Schematic illustration of the grouting positions for each test relative to the retained surface and back face of the model wall.

Figure 6. 2 Typical SPT excavation support pressure response recorded by the externally located PT during excavation simulation in test 7HH.

Figure 6. 3 Pressure transducer readings (from the external PT for tests 2-3HH and internal PT for tests 6-13HH) of the SPT support fluid pressure during the simulated excavation period.

Figure 6. 4 Staged SPT excavation support pressure response in tests 2-3HH (using the HFP to remove the SPT fluid) during excavation simulation.

Figure 6. 5 Effect of spinning down the model in test 8HH on the far field pore pressures (following an unresponsive solenoid-plug valve assembly on the first actuation attempt).

Figure 6. 6 Differences in vertical displacements between LVDTs and image processing targets above the wall and at distances x= 0.25H, 0.5H, 1.0H and 1.5H behind the wall in tests: (a) 2HH (b) 3HH and (c) 10HH, up to 133 s after excavation completion (prior to injection in test 10HH).

Figure 6. 7 Retained surface vertical displacements measured by LVDTs and image processing targets (15 mm below the surface) in test 6HH above the wall and at distances x= 0.25H, 0.5H, 1.0H and 1.5H behind the wall.

Figure 6. 8 Retained surface vertical displacements measured by LVDTs and image processing targets (15 mm below the surface) in test 7HH above the wall and at distances x= 0.25H, 0.5H, 1.0H and 1.5H behind the wall.

Figure 6. 9 Differences in vertical displacements between LVDTs and image processing targets during test 6HH above the wall and at distances x= 0.25H, 0.5H, 1.0H and 1.5H behind the wall.

Figure 6. 10 Differences in vertical displacements between LVDTs and image processing targets during test 7HH above the wall and at distances x= 0.25H, 0.5H, 1.0H and 1.5H behind the wall.

Figure 6. 11 Differences in vertical displacements between LVDTs and image processing targets during test 8HH above the wall and at distances x= 0.25H, 0.5H, 1.0H and 1.5H behind the wall.

Figure 6. 12 Retained surface vertical displacements measured by LVDTs and image processing targets (15 mm below the surface) in test 10HH above the wall and at distances x= 0.25H, 0.5H, 0.75H, 1.0H and 1.5H behind the wall.

Figure 6. 13 Retained surface vertical displacements measured by LVDTs and image processing targets (15 mm below the surface) in test 12HH above the wall and at distances x= 0.25H, 0.5H, 0.75H, 1.0H and 1.5H behind the wall.

Figure 6. 14 Differences in vertical displacements between LVDTs and image processing targets during test 10HH above the wall and at distances x= 0.25H, 0.5H, 0.75H, 1.0H and 1.5H behind the wall.

Figure 6. 15 Differences in vertical displacements between LVDTs and image processing targets during test 12HH above the wall and at distances x= 0.25H, 0.5H, 0.75H, 1.0H and 1.5H behind the wall.

Figure 6. 16 Retained surface vertical displacements measured by LVDTs and image processing targets (15 mm below the surface) in test 9HH above the wall and at distances x= 0.25H, 0.5H, 1.0H and 1.5H behind the wall.

Figure 6. 17 Retained surface vertical displacements measured by LVDTs and image processing targets (15 mm below the surface) in test 11HH above the wall and at distances x= 0.25H, 0.5H, 0.75H, 1.0H and 1.5H behind the wall.

Figure 6. 18 Retained surface vertical displacements measured by LVDTs and image processing targets (15 mm below the surface) in test 13HH above the wall and at distances x= 0.25H, 0.5H, 0.75H, 1.0H and 1.5H behind the wall.

Figure 6. 19 Differences in vertical displacements between LVDTs and image processing targets during test 9HH above the wall and at distances x= 0.25H, 0.5H, 1.0H and 1.5H behind the wall.

Figure 6. 20 Differences in vertical displacements between LVDTs and image processing targets during test 11HH above the wall and at distances x= 0.25H, 0.5H, 0.75H, 1.0H and 1.5H behind the wall.

Figure 6. 21 Differences in vertical displacements between LVDTs and image processing targets during test 13HH above the wall and at distances x= 0.25H, 0.5H, 0.75H, 1.0H and 1.5H behind the wall.

Figure 6. 22 Horizontal wall target displacements measured using the embedded image processing targets from the TELI and PULNIX cameras in tests 2-3HH.

Figure 6. 23 Vertical formation level target displacements measured using the embedded image processing targets from the TELI and PULNIX cameras in tests 2-3HH.

Figure 6. 24 Gantt chart showing the injection events (with grout volumes injected) in tests 6-13HH with reference to the fraction of excavation progression (relative support fluid level) and time elapsed after excavation in baseline test 3HH to enable comparison of movements.

Figure 6. 25 Vertical LVDT retained surface displacements at the end of excavation and 133 s after for tests 2HH, 3HH and 10HH (prior to the start of injection in 10HH).

Figure 6. 26 Horizontal displacements of the retaining wall and soil beneath using image processing for tests 2HH, 3HH and 10HH at the end of excavation and 133 s after (prior to the start of injection in test 10HH).

Figure 6. 27 Vertical displacements at the formation level using image processing for tests 2HH, 3HH and 10HH at the end of excavation and 133 s after (prior to the start of injection in test 10HH).

Figure 6. 28 Development of the excavation induced maximum vertical surface settlements measured by the LVDTs at distance x= 0.5H (position of S_{vmax}) behind the wall in tests 2HH, 3HH and 10HH, up to 133 s after excavation.

Figure 6. 29 Development of the excavation induced maximum horizontal wall displacements (S_{hmax}) at depth d= 0.75H (90 mm) below the retained surface in tests 2HH, 3HH and 10HH, up to 133 s after excavation.

Figure 6. 30 Development of vertical surface settlements (S_v) measured by LVDTs at distances x= 0.25H and 0.5H (above the injection tube) behind the wall in tests 6-9HH.

Figure 6. 31 Development of horizontal wall displacements (S_h) at depth d= 0.75H (90 mm) below the retained surface in tests 6-9HH.

Figure 6. 32 Vertical LVDT retained surface displacements at the start of the 1st injection events in tests 6-9HH against the end of excavation surface settlement envelope in baseline test 3HH.

Figure 6. 33 Horizontal wall movements at the start of the 1st injection events in tests 6-9HH against the end of excavation wall displacements profile in baseline test 3HH.

Figure 6. 34 Vertical formation level movements at the start of the 1st injection events in tests 6-9HH against the end of excavation formation level movement envelope in baseline test 3HH.

Figure 6. 35 Vertical LVDT retained surface displacements at the end of the injection events in tests 6-9HH (and start of the 2nd injection event in test 7HH) compared to equivalent stages in baseline test 3HH.

Figure 6. 36 Horizontal wall movements at the end of the injection events in tests 6-9HH (and start of the 2nd injection event in test 7HH) compared to equivalent stages in baseline test 3HH.

Figure 6. 37 Vertical formation level movements at the end of the injection events in tests 6-9HH (and start of the 2nd injection event in test 7HH) compared to equivalent stages in baseline test 3HH.

Figure 6. 38 Rupture lines behind and in front of the wall and shear bands above the injection location at the end of test 8HH (traced following removal of the model from the centrifuge swing and removal of the latex injection tube).

Figure 6. 39 Rupture lines behind and beneath the wall and shear bands above the injection location at the end of test 9HH (traced following removal of the model from the centrifuge swing and removal of the latex injection tube).

Figure 6. 40 Photographs of the post-test resin castings of the cavities created by the injection tubes for tests: (a) 6HH and (b) 7HH, showing the tapered shape created without the provision of the front brass retaining collar on the injection tubes.

Figure 6. 41 Photographs of the typical uniform cylindrical post-test resin castings of the cavities created by the injections tubes provided with the front brass retaining collar for tests: (a) 9HH and (b) 11HH.

Figure 6. 42 Development of vertical surface settlements (S_v) measured by LVDTs at distances x= 0.25H, 0.5H and 0.75H (above the injection tube) behind the wall in tests 10-11HH.

Figure 6. 43 Development of horizontal wall displacements (S_h) at depth d= 0.75H (90 mm) below the retained surface in tests 10-11HH.

Figure 6. 44 Vertical LVDT retained surface displacements at the start of the 1st injection events in tests 10-11HH.

Figure 6. 45 Horizontal wall movements at the start of the 1st injection events in tests 10-11HH.

Figure 6. 46 Vertical formation level movements at the start of the 1st injection events in tests 10-11HH.

Figure 6. 47 Vertical LVDT retained surface displacements at the end of the injection events in tests 10-11HH (and start of the 2nd injection event in test 10HH) compared to equivalent stages in baseline test 3HH.

Figure 6. 48 Horizontal wall movements at the end of the injection events in tests 10-11HH (and start of the 2nd injection in 10HH) compared to equivalent stages in baseline test 3HH.

Figure 6. 49 Vertical formation level movements at the end of the injection events in tests 10-11HH (and start of the 2nd injection in 10HH) compared to equivalent stages in baseline test 3HH.

Figure 6. 50 Development of vertical surface settlements (S_v) measured by LVDTs at distances x= 0.25H, 0.5H and 0.75H behind the wall in tests 12-13HH.

Figure 6. 51 Development of horizontal wall displacements (S_h) at depth d= 0.75H (90 mm) below the retained surface in tests 12-13HH.

Figure 6. 52 Vertical LVDT retained surface displacements at the start of the 1st injection event in tests 12-13HH.

Figure 6. 53 Horizontal wall movements at the start of the 1st injection event in tests 12-13HH.

Figure 6. 54 Vertical formation level movements at the start of the 1st injection event in tests 12-13HH.

Figure 6. 55 Vertical LVDT retained surface displacements at the end of the injection events in tests 12-13HH (and start of the 2nd injection events) compared to equivalent stages in baseline test 3HH.

Figure 6. 56 Horizontal wall movements at the end of the injection events in tests 12-13HH (and start of the 2nd injection events) compared to equivalent stages in baseline test 3HH.

Figure 6. 57 Vertical formation level movements at the end of the injection events in tests 12-13HH (and start of the 2nd injection events) compared to equivalent stages in baseline test 3HH.

Figure 6. 58 Rupture lines behind and beneath the wall toe and open soil fractures surrounding the injection tube location at the end of test 13HH (traced following removal of the model from the centrifuge swing and removal of the latex injection tube).

Figure 6. 59 Injection pressure and locally installed injection zone PPT response during test 6HH.

Figure 6. 60 Injection pressure and locally installed injection zone PPT response during test 7HH.

Figure 6. 61 Injection pressure and locally installed injection zone PPT response during test 8HH.

Figure 6. 62 Injection pressure and locally installed injection zone PPT response during test 9HH.

Figure 6. 63 Injection pressure and locally installed injection zone PPT response during test 10HH.

Figure 6. 64 Injection pressure and locally installed injection zone PPT response during test 11HH.

Figure 6. 65 Total injection pressure response from both injection tubes and locally installed injection zone PPT response during test 12HH.

Figure 6. 66 Total injection pressure response from both injection tubes and locally installed injection zone PPT response during test 13HH.

Figure 6. 67 Schematic illustrating the development of the plastic soil zone around the injection tube during injection and its coincidence with the local pore pressure transducer based on cavity expansion theory in an infinite elastic-perfectly plastic soil.

Figure 6. 68 Typical response of the far field PPTs and standpipe PT during consolidation prior to testing.

Figure 6. 69 Readings and locations of undrained shear strengths (S_u), using a 19 mm hand shear vane, taken of the soil model immediately after the tests (3-13HH).

Figure 7. 1 Normalised settlements behind the retaining wall at the end of simulated excavation in tests 3HH and 10HH shown in the context of expected settlements for excavation in various soils from field monitoring data after Peck (1969) and Gaba *et al.* (2017).

Figure 7. 2 Normalised settlement profile behind the retaining wall at the end of simulated excavation in tests 3HH and 10HH shown in the context of typical bounding profiles in soft-firm soils from field monitoring after Hseih and Ou (1998) and Gaba *et al.* (2017).

Figure 7. 3 Normalised changes in vertical displacements and injection pressures with injected volume above the injection location relative to the reference test from the start of injection in tests 8HH, 9HH, 10HH and 11HH.

Figure 7. 4 Normalised changes in horizontal wall displacements at depth d= 0.75H, below the retained surface and injection pressures with injected volume, relative to the reference test from the start of injection in tests 8HH, 9HH, 10HH and 11HH.

Figure 7. 5 Development of vertical displacements above the injection location at the retained surface in grouting tests 7HH, 9HH, 10HH and 11HH relative to test 3HH during the simulated excavation.

Figure 7. 6 Development of vertical displacements above the injection location at the retained surface in grouting tests 7HH, 9HH, 10HH and 11HH relative to test 3HH after the simulated excavation.

Figure 7. 7 Development of horizontal wall displacements at depth d= 0.75H, below the retained surface, in grouting tests 7HH, 9HH, 10HH and 11HH relative to test 3HH during the simulated excavation.

Figure 7. 8 Development of horizontal wall displacements at depth d= 0.75H, below the retained surface, in grouting tests 7HH, 9HH, 10HH and 11HH relative to test 3HH after the simulated excavation.

Figure 7. 9 Development of vertical displacements above the injection location at the retained surface in grouting tests 6-9HH relative to test 3HH during the simulated excavation.

Figure 7. 10 Development of vertical displacements above the injection location at the retained surface in grouting tests 6-9HH relative to test 3HH after the simulated excavation.

Figure 7. 11 Development of vertical displacements above the injection location at the retained surface in grouting tests 7HH,10HH and 12HH relative to test 3HH during the simulated excavation.

Figure 7. 12 Development of vertical displacements above the injection location at the retained surface in grouting tests 7HH, 10HH and 12HH relative to test 3HH after the simulated excavation.

Figure 7. 13 Development of vertical displacements above the injection location at the retained surface in grouting tests 9HH, 11HH and 13HH relative to test 3HH during the simulated excavation.

Figure 7. 14 Development of vertical displacements above the injection location at the retained surface in grouting tests 9HH, 11HH and 13HH relative to test 3HH after the simulated excavation.

Figure 7. 15 Development of horizontal wall displacements at depth d= 0.75H, below the retained surface, in grouting tests 6-9HH relative to test 3HH during the simulated excavation.

Figure 7. 16 Development of horizontal wall displacements at depth d= 0.75H, below the retained surface, in grouting tests 6-9HH relative to test 3HH after the simulated excavation.

Figure 7. 17 Development of horizontal wall displacements at depth d= 0.75H, below the retained surface, in grouting tests 7HH, 10HH and 12HH relative to test 3HH during the simulated excavation.

Figure 7. 18 Development of horizontal wall displacements at depth d= 0.75H, below the retained surface, in grouting tests 7HH, 10HH and 12HH relative to test 3HH after the simulated excavation.

Figure 7. 19 Development of horizontal wall displacements at depth d= 0.75H, below the retained surface, in grouting tests 9HH, 11HH and 13HH relative to test 3HH during the simulated excavation.

Figure 7. 20 Development of horizontal wall displacements at depth d= 0.75H, below the retained surface, in grouting tests 9HH, 11HH and 13HH relative to test 3HH after the simulated excavation.

Figure 8. 1 Summary of the compensation effect on vertical displacements above the injection tube location at the retained surface between grouting tests (after the first injection pass) and reference test 3HH.

Figure 8. 2 Summary of the effects on wall displacements at depth d= 0.75H, below the retained surface, between grouting tests (after the first injection pass) and reference test 3HH.

Figure 8. 3 Schematic illustration of regions identified from model tests where injection grouting can provide positive compensation of the retained surface and the effects on wall displacements.

AKNOWLEDGEMENTS

My time with the Research Centre for Multi-Scale Geotechnical Engineering at City, University of London working toward my Ph.D. has been a wonderful experience. This is because of the kindness, support and nurturing gifted to me throughout the duration by the Academic staff and other members of the group.

Firstly, I wish to acknowledge with many thanks my first supervisor, Dr Andrew McNamara for his help, guidance and continued faith in my ability to complete my Ph.D. Without his continued support, good humour and encouragement, even at the darkest of times when faced with setbacks and problems, I could not have completed this research. He has been an unending source of practical ideas and solutions and has always patiently guided me in the right direction at all times.

I would also like to equally thank my second supervisor Professor Sarah Stallebrass for her nurturing nature, technical knowledge and for always being available to advise during the writing up of this thesis. Her valuable guidance, availability to discuss ideas and encouragement throughout the duration of the PhD has been invaluable and very much appreciated. Thanks are also due to Dr Richard Goodey, Professor Neil Taylor and Dr Sam Divall for their practical and technical knowledge, valuable insight, assistance and advice during the development of the apparatus, testing and write up.

The experimental work required considerable input and dedication of highly skilled technical staff. I would therefore like to thank Mr Melvyn Hayes, Mr Keith Osborne and Mr Jim Hooker for manufacturing and assembling the apparatus and the much needed assistance, often at short notice, during model preparation and testing.

My time at City, University of London has been made a very enjoyable experience by many members who have created an atmosphere of friendship and good humour at all times. Thanks are therefore due to Dr Brett McKinley, Dr Binh Thanh Le, Dr Sadegh Nadimi, Miss Greta Tanghetti, Miss Jignasha Panchal, Dr Joanna Fonseca and also Dr Neil Phillips and Dr Rohit Gorasia during their time here.

A special thanks to my family for their continuous love, financial support and belief in me and finally to my wonderful and boisterous niece Jasmin for always putting a smile on my face even after the most difficult of days.

DECLARATION

I grant powers of discretion to the University Librarian to allow this dissertation to be copied in whole or in part without further reference to me. This permission covers only single copies made for study purposes, subject to normal conditions of acknowledgement.

ABSTRACT

The research conducted concerns the application of compensation grouting, particularly compaction grouting, as a method to reduce and control the ground movements generated in the soil by a deep retained excavation in firm to stiff clays. Compaction grouting involves the injection of grout into the soil to create a spherical or cylindrical grout bulb. This research investigates the effectiveness and limitations of the method to provide a preliminary understanding of the influence of the grouting volume, timing and position on the vertical settlements at the retained surface and horizontal displacements of the wall relative to the behaviour observed from the corresponding scenario in which only excavation occurs.

Experimental data were obtained from a series of 10 successful centrifuge model tests undertaken at 100 *g*. The plane strain models consisted of a pre-formed 12 m deep (at prototype scale) retained excavation temporarily supported by the pressure of a dense fluid acting against the wall and formation surface and a relatively flexible retaining wall propped at the top. The dense fluid was removed and the subsequent soil movements at the retained surface, wall and the formation level were measured, using a combination of transducers and analysis of digital images taken of targets embedded in the front face of the model and wall. Three reference tests were conducted to establish the magnitude and pattern of soil and wall displacements generated by excavation alone. Idealised compaction grouting was modelled simultaneously with excavation in the remaining tests with the injection of 'grout' (water) into sealed latex tubes (supported by a perforated Nylon tube), inserted in the soil behind the excavation. The start of injection relative to the timing of the excavation varied amongst the tests. Grouting was continued until positive compensation of the local surface settlement was noted or significant horizontal displacements of the wall were observed.

The tests showed that there appears to be no distinct relationship between the grout volume and the displacements at the retained surface above the injection and at a wall depth of 0.75 times the excavation depth, H due to injection. However, it was seen that for injections below a depth of 0.25H different critical volumes existed beyond which a positive compensation of the retained surface deteriorated or negative compensation increased at a greater rate. This was also reflected in the wall behaviour.

The different injection initiation times showed that greater positive compensation effects could be achieved with injections up to a depth of 0.5H when conducted during the excavation, rather than in the period after. Timing had no influence on injections below this depth. The influence of injection timing was found to be secondary to the injection position.

A linear relationship between the depth of injection and either positively or negatively compensated settlements was noted from the tests. Positive compensation of the ground surface is possible for injections conducted above a depth of 0.5H. However, below this depth a significant negative compensation effect on surface settlements and horizontal wall movements was noted regardless of timing or volume. Greater positive compensation effects and reduced negative effects on the wall were noted with increasing distance from the wall. Regions behind the wall have been identified where grouting provides positive compensation of the surface with minimal influence on the wall and where only negative effects are observed at both the surface and wall.

LIST OF SYMBOLS

a	Acceleration (m/s^2).
aE_n	Factor (or decimal fraction), *a*, of simulated excavation complete in test *n*.
B	Excavation half width.
c_v	Coefficient of consolidation.
d	Depth below retained soil surface.
D	Wall embedment length.
E	Young's Modulus.
$E_{concrete}$	Young's Modulus of concrete.
FS_{Heave}	Factor of safety against basal heave.
g	Earth's gravitational acceleration constant (9.81 m/s^2).
G	Shear modulus of soil.
H	Excavation depth.
h	Height of soil.
H_d	Embedded depth of wall.
k	Coefficient of permeability.
K_o	Coefficient of Earth pressure at rest.
K_1	Support system stiffness (after Clough *et al.,* 1989).
K_a	Passive Earth pressure coefficient.
K_p	Active Earth pressure coefficient.
L	Drainage path length.
N	Acceleration scaling factor.
N_c	Bearing capacity factor (from Skempton, 1951).
ϕ'_{cs}	Critical state angle of friction.
P_o	Original *in situ* soil stress.
P_c	Limiting pressure to create upward heave (after Wong, 1974).
$P_{c, lim}$	Limiting cavity pressure defined by cavity expansion theory at the onset of plastic equilibrium in soil surrounding cavity.
P_i	Injection pressure.
P_{up}	Limiting pressure to create upward heave (after Cirone, 2016).
q	Surcharge on soil surface.
R_e	Effective radius of model.

r_i	Initial cavity radius.
r_p	Radius to plastic-elastic boundary around cavity.
r_{PPT}	Radius between injection tube centre to local injection zone pore pressure transducer centre.
R_t	Radius from the centre of rotation to the top of the soil model.
S_h	Horizontal wall displacement.
S_u	Undrained shear strength.
S_v	Vertical displacement.
t	Time.
T_n+b	Time b after completion of simulated excavation in test n.
T_v	Dimensionless time factor (for consolidation).
u	Pore pressure.
u_o	Initial hydrostatic pore pressure.
u_{inj}	Pore pressure local to injection tube during injection.
V_E	Volume expansion in soil achieved by grouting.
V_i	Total injected grout volume.
V_o	Initial volume of cavity created by injection tube.
V_{SH}	Volume of heave at ground surface owing to grout injection.
w/c	Water-cement ratio.
x	Distance behind retaining wall.
α	Compensation factor.
ΔP_{loss}	Pressure losses in injection pipe work between injection system and injection manifold pressure transducers.
$\delta S_{h(d=0.75H)}$	Difference in horizontal wall displacements at soil depth d= 0.75H between the excavation only test data and injection test data.
ΔS_v	Difference in vertical displacements between LVDT and image processing target measurements.
δS_v	Difference in vertical soil displacements at the retained surface between the excavation only test and injection test data.
Δu	Excess pore pressure.
ΔV	Change in injected volume.
δV_i	Injected grout volume during injection pass.

$\delta V_{i,PEAK}$	Injected grout volume during injection pass at peak injection pressure.
$\Delta\delta S_{h,\ inj\ only}$	Changes in δS_h (at d= 0.75H) from the start of injection.
$\Delta\delta S_{v,\ inj\ only}$	Change in δS_v (above the injection location) from the start of injection.
η	Grouting efficiency.
ξ	Compensation grouting efficiency.
ρ	Density (kg/m^3).
σ	Total stress.
σ'	Effective stress.
σ_r	Radial total stress.
σ_θ	Tangential total stress.
ω	Angular velocity.

SUBSCRIPTS

h	Horizontal component.
inj	Parameter in grout injection test.
inj only	Parameter relating to the effects of injection with the effects of excavation removed from grout injection test data.
LVDT	Measurement made using LVDT data.
m	Parameter in model.
max	Maximum value.
p	Parameter in prototype.
PEAK	Peak value.
ref	Parameter in excavation only reference test.
Target	Measurement made using imaging targets.
v	Vertical component.

ABBREVIATIONS

FEM	Finite Element Method.
AIR	Apparent Influence Range (after Ou *et al.,* 1993).
DAQ	Data Acquisition.
NI	National Instruments.
SRIP	Slip Ring Interface Panel.
LAN	Local Area Network.
PXI	PCI eXtensions of Instrumentation (PC-based platform for measurement and automation systems)
CCD	Charged Coupled Device.
LVDT	Linear Variable Differential Transformer.
PPT	Pore Pressure Transducer.
PT	Pressure Transducer.
DPI	Digital Pressure Indicator.
SPT	Sodium polytungstate.
HF	Heavy Fluid.
HFP	Heavy Fluid Pump
BSPP	British Standard Parallel Pipe Thread.
LED	Light Emitting Diode.
OCR	Overconsolidation Ratio.
LH	Left Hand.
RH	Right Hand.
OD	Outside Diameter.

1. INTRODUCTION

The research undertaken concerns the influence of compensation grouting to control and minimise surface settlements behind the retaining wall of deep a single propped excavation. The study focuses on the use of idealised compaction grouting at varying positions behind the retaining wall and beneath the retained surface to investigate the effectiveness of the technique and provide an understanding of its limitations.

1.1 Background

In urban centres such as London, the increasing demand on space, both commercial and residential, and on infrastructure from the rapidly growing economy and population are driving the development of larger and taller structures to accommodate these needs. However, the planning restrictions on building heights and limited land availability have often curtailed the construction of very tall large buildings in these environments. With such restrictions civil engineers, in recent years, have seen greater demand on the utilisation of underground spaces with construction of deeper basements and underground stations. The excavation and construction of deep basements and stations causes large stress changes in the ground, inevitably resulting in movements in the surrounding ground. The magnitude and extent of these ground movements are dependent on several factors including the soil nature, duration of excavation works, construction method employed and the propping and support systems implemented to maintain excavation stability before completion of the permanent sub-structure.

If allowed, the realisation of the deep excavation induced ground movements in the surrounding ground surface can have damaging consequences on nearby existing structures and buried services. In a congested urban environment these movements can also have serious financial repercussions if not controlled. Prediction and control of these movements involve complex analyses and design processes and a detailed understanding of the construction process. However even with the plethora of sophisticated numerical analyses tools currently available, the intrinsically complicated stress changes and site-specific complications, inherent in deep basement and station constructions, prevent these tools from providing very accurate predictions of ground movement. Consequently, current practices often adopt overly conservative designs of the excavation supporting wall and propping system to compensate for the lack of confidence in the expected ground movement magnitudes. This is often reflected in complex arrangements and thick retaining wall solutions which add significantly to the excavation duration and costs.

The last six decades have seen the research and exploration of new methods to control ground surface movements around excavations such as anti-heave piles (McNamara, 2001), permeation grouting, jet grouting and underpinning, each with varying degrees of success and each often limited to specific soil types and conditions. In contrast, the excavation of underground tunnels in a variety of soils has seen repeated successful implementation of grout injections into the ground either behind or ahead of the advancing tunnel face. This technique, commonly referred to as compensation grouting has shown to be capable of reversing and controlling any excavation induced ground movements within specified tolerances when used in conjunction with the observational method proposed by Peck (1969). The most recent example of this was demonstrated in the Crossrail project in London, U.K. which showed effective implementation of compensation grouting in combination with a live active ground surface movement monitoring system in response to tunnelling induced movements across a number of sites.

It is therefore clear that a potential exists in the implementation of compensation grouting technology in the form of a new technique applicable to deep retained excavations to enable closer control of surrounding ground movements. Having greater confidence in the control of ground movements would enable reduction of the complex propping arrangements and retaining wall solution thus hastening excavation and construction. The development of this new potential technique therefore provides an attractive proposition.

The limitations and soil conditions under which compensation grouting technology can be deployed in tunnelling applications is well understood, principally through empirical data from previous studies and experience. In contrast, very little is known about its application to deep retained excavations. It would therefore be useful to understand the potential of using compensation grouting to limit and control ground movements behind a retaining structure, its limitations, the effects on the retaining structure and how and in what circumstances its performance can be maximised.

Owing to the inherently complex nature of retained excavations movements in three dimensions and soil response to compensation grouting, finite element analysis cannot yet quantify, with sufficient confidence and accuracy, the soil and retaining structure response to grout injection behind the retaining wall. This is further limited by the frequent requirement to simplify the analyses undertaken into two dimensions. However, another useful method to investigate the potential performance of the new technique is via small scale physical model tests undertaken in a geotechnical centrifuge. With this

method realistic *in situ* soil stresses and boundary conditions can be replicated and repeated and the injection of grouting can be scaled down and idealised.

1.2 Aims

The primary aim of the research undertaken was to develop a preliminary understanding of the effectiveness of the novel application of compensation grouting to limit and control the retained ground surface movements around deep excavations. To achieve this the following points formed the key parameters of investigation in this research study:

- Volume of injected grout
- Timing of grout injection
- Position of grouting; both below the retained surface and distance behind the retaining wall

The exploration of the soil at the retained and formation levels and retaining wall response to grout injections to these parameters, both during and after excavation, have been carried out through centrifuge modelling techniques. To this end several tasks were carried out and form the basis for the discussion and conclusions:

- Apparatus development to enable the simulation of a single propped 12 m deep excavation in the geotechnical centrifuge at City, University of London.
- Development of centrifuge modelling apparatus to allow modelling of an idealised grout mass injection behind the model excavation.
- Execution of a parametric study on the ground and retaining wall response subject to the varied locations, volumes and times of grouting behind the model excavation.
- Comparison of the data from grouting tests with that from excavation only reference tests to assess the performance of the grouting apparatus and grouting locations.

1.3 Outline of report

This thesis details the approach to the research, describes the development of the model testing apparatus and explains and interprets the response of the model in the series of tests conducted. Chapter 2 presents a literature review of the various case studies available to date which have focused on ground movements around deep excavations in medium to stiff clays. An overview is provided of the expected magnitudes and profiles of soil and wall movements from empirical observations to enable comparisons to be made later against the data recorded in the excavation only reference test conducted. Some of the available semi-empirical frameworks for predicting ground settlement magnitudes and profiles are also detailed.

An outline of the compensation grouting technique and the different processes encompassed by its definition are provided in chapter 3. The chapter focusses on one of the processes, compaction grouting, owing to its idealised form having been adopted in the model tests in this study. Details of the process and the general limitation of its use in different soils are described. A brief review is undertaken of the relevant theory concerning the mechanisms used to model and understand compaction grouting in loose coarse-grained soils, with considerations made for the translation of these mechanisms to clay soils. The behaviours and findings are presented from two case studies where compaction grouting was successfully deployed in the field to control settlements around a tunnelling excavation and a diaphragm walled deep excavation.

Chapter 4 discusses the range of modelling techniques and outlines the relevancy and merits of using the geotechnical centrifuge modelling method for simulation of construction events at prototype scale. A background to centrifuge modelling principles and associated scaling laws are explained in detail. Inherent errors will always be present within any form of model testing and those relevant to this research are discussed along with the typical solutions applied in this study. Details of the geotechnical centrifuge facility used at City, University of London and the changes made following a significant refurbishment of the facility are presented as these affected the development of apparatus.

Various studies have focused individually on the modelling of excavations and compensation grouting in the centrifuge. Chapter 5 provides a summary of the approaches adopted in these studies within the context of the model requirements for this study. The design and development of the centrifuge testing apparatus was carried out over a significantly extended period owing to its complexity. The chapter presents a description

of the excavation and grout simulation apparatus and their continual development during the study in addition to the model preparation and testing procedures adopted.

Chapter 6 presents the results from the successful tests in a manner which enables a stage by stage understanding of the progression of the test series, the development of apparatus faults in certain tests and their impact on the soil, wall and injection behaviours. The results of appropriately grouped tests, based on their location within the model, are presented in an unprocessed form. The general quality of data from the instrumentation and image processing is assessed and discussed, with explanations provided for the problems which influenced the test results.

In chapter 7 the direct effects of injection in the grouting tests, both locally above the grouting position and at the depth along the wall coinciding with the maximum displacement observed during the reference test, are analysed against the effects generated solely due to excavation. This enables the effectiveness of the compensation of settlements and horizontal displacements achieved at these locations to be quantified with respect to the injected volume, timing and position.

Chapter 8 summarises the key findings of the research and final conclusions are drawn with reference to the applicability and accuracy of the results. Suggestions are provided for the regions behind the excavation, in the adopted model geometry, where injection has the potential to be either beneficial or detrimental to the vertical retained surface and horizontal retaining wall displacements, in comparison to those expected solely due to excavation. These suggestions are based on the identified trends from chapter 7. Recommendations are made for further research that will enable a better understanding of the effectiveness of the application of the compensation grouting behind deep excavations.

2. EXCAVATION GROUND MOVEMENTS-LITERATURE REVIEW

This chapter provides a review of the current understanding of ground movements induced by deep excavations and the two approaches available in estimating the ground and wall movements. The various findings from field data up to the most recent databases of field case studies published by previous authors have been examined to provide an outline of expected magnitudes and profiles of vertical retained surface soil and horizontal wall displacements for excavations in firm to stiff soils. This will enable comparisons to be made later during the analyses of the results against the movements recorded for a similar soil type expected during the excavation only model tests conducted in this study to assess the performance of the apparatus and model.

2.1 Introduction

Any form of excavation or unloading of the ground will cause both vertical and horizontal movements. The extent and magnitude of these movements, as highlighted by Padfield and Mair (1984), are dependent on several factors including, but not limited to, soil properties, excavation technique, phasing of excavation stages and treatment of ground water. Often it is the case that the sequencing, phasing and support details differ from those envisaged by the designer which provides difficulty in accurately predicting the ground movements (Padfield and Mair, 1984).

Even with the continued improvements made in construction technologies there is always a necessity to control movements, particularly vertical ground movements behind a retaining structure to within tighter tolerances. In an urban environment these movements, if not mitigated, can have damaging consequences on surrounding structures and services leading to severe financial implications for the client or contractor. One possible means of controlling and remediating the ground movements expected from deep excavation is compensation grouting, discussed further in chapter 3. However, it is necessary to gain a firm understanding of the extent and magnitude of settlement expected solely from excavation, as well as the mechanisms that enable them, to correctly plan the compensation grouting programme.

In the last three decades there has been an improved understanding of the mechanisms and magnitudes of movements through empirical examinations of field case studies presented by various authors (e.g. Clough and O'Rourke, 1990; Carder, 1995; Fernie and Suckling, 1996; Hseih and Ou, 1998; Long, 2001; Moormann, 2004 and Gaba *et al.,*

2017) and availability of prediction and modelling methods such Finite Element Modelling (FEM). This has made it possible to make better general predictions of the upper and lower bounds of movements that might be expected during construction events.

2.2 Ground movement mechanisms

Padfield and Mair (1984) originally categorised the forms of movements around excavations as being either local or global. Global movements are typically 'elastic,' as described by Gaba *et al.* (2017), and arise from the unloading effect of the vertical stress relief in the ground with the weight of the soil removed within the excavation. Global movements are largely independent of the nature of the retaining wall and are of particular importance for large deep excavations in clay where movements continue for long periods, have a large lateral spread and are deep seated. In contrast, local movements are typically plastic and are associated with shear deformations as the soil mobilises shear strength and changes in active and passive pressures occur in response to removal of lateral support provided by the soil. These local movements typically occur over a short period of time. In the active zone behind the wall, settlements spread to a lesser extent than global movements but lead to more severe horizontal and vertical differential movements (Padfield and Mair, 1984). It is the differential movements and rotations at the interfaces with overlying buildings and services that have the greatest influence on the structural damage caused to overlying and surrounding structures and services (Boscardin and Walker, 1998). In agreement with Mana and Clough (1981), Padfield and Mair (1984) proposed the strong dependency of the magnitudes and patterns of these movements on the stiffness of the wall and support system. However, Clough and O'Rourke (1990) and later confirmed by Long (2001), Moorman (2004) and Gaba *et al.* (2017) showed from their extensive databases of over 300 field case studies in various soil types and conditions that this dependency and relationship to support stiffness was only apparent for soft soils where basal heave within the excavation was a concern. For medium to stiff soils where a sufficiently high factor of safety against basal heave (FS_{Heave}) was present (e.g. $FS_{Heave} \geq 2.5$) the authors showed that wall and support stiffness had no clear correlation to the soil and wall movements recorded, suggesting instead better efficiency and lower costs with the adoption of flexible walls (e.g. sheet pile walls) in stiff soils without significant increase in ground movements. This increased efficacy was noted to be possible if overall system stiffness was not significantly reduced. Use of a more flexible wall also aided to reduce bending moments induced in the wall by the soil.

Burland *et al.* (1979) noted that the mode and magnitude of deformation of the retaining wall and ground, both within the excavation and behind the wall, were dependent on the relief of vertical and horizontal stress. They explained that horizontal soil movement resulting from horizontal stress relief was a function of the mode of deformation of the wall. Padfield and Mair (1984) and Burland *et al.* (1979) described movements expected from cantilevered walls to be different from those associated with propped walls. Both publications state that horizontal soil and wall movements for cantilevered walls will be greater than their vertical components and typically take the form shown in Figure 2.1(a). For a wall propped near the surface, deflections would occur at depth and in general vertical movements would exceed horizontal movements, Padfield and Mair (1984), as illustrated in Figure 2.1(b).

Excavations generally proceed in three main stages: 1) installation of retaining wall, 2) excavation of soil and installation of lateral support system and 3) construction of permanent substructure and removal of supports. Clough and O'Rourke (1990) described the deflection behaviour in response to excavation, illustrated in Figure 2.2. During the initial stage of excavation, before the first level of lateral support has been installed, the wall will behave and deform in a cantilever form, shown in Figure 2.2(a). As excavation proceeds and supports are installed at upper horizons, significant movements into the excavation at greater depths begin to develop as illustrated in Figure 2.2(b). The movements over these two stages accumulate to present the wall deflections and surface displacements shown in Figure 2.2(c). Clough and O'Rourke (1990) described the soil surface settlements occurring during stage one being predominantly triangular in shape and those during the second and third final stage cumulating to a trapezoidal shape, having made similar findings using case study data from retained excavations in clay. Hseih and Ou (1998) described the triangular and trapezoidal profiles as spandrel and concave settlement profiles, respectively, as shown in Figure 2.3. These general movements and patterns only account for the response to excavation and neglect the effect of other important factors known to affect deflection and settlement behaviour, such as soil conditions, wall and support stiffness, installation methods, dewatering of the ground and installation of foundations within the excavation, Clough and O'Rourke (1990).

2.2.1 Vertical stress relief

Burland *et al.* (1979) highlighted the importance of vertical stress relief on excavation movements in clay. The movements can often be deep seated as described by McNamara (2001). Burland *et al.* (1979) described the movement associated with vertical unloading being inversely analogous to the profile caused by vertical loading of the ground with settlement beneath the loaded zone and heave at the further extents, as illustrated in Figure 2.4. In the short term heave occurs within the excavation and some settlement is observed behind the wall. However, with the onset of drainage in the long term the established heave continues and spreads from within the excavation to the ground outside, particularly if there is a net long term relief of stress at the excavation base, as shown in Figure 2.4(c).

Burland *et al.* (1979) also highlighted the influence of vertical stress relief on the horizontal movements of the walls. The unloading of the soil is again described as being inversely analogous to the loading of the soil above the excavation zone as shown in Figures 2.5(a) and 2.5(b). The heave within the excavation induces deep seated inward movements of the wall and retained soil, resulting in settlements behind the walls, shown in Figure 2.5(c). Burland *et al.* (1979) described these inward movements as being uncontrollable by internally placed propping.

In soft to medium clays the aspect of basal heave failure and movements becomes a dominant source of ground movements. If the exaction geometry and soil properties are not able to resist the upward movement of the soil plug within the excavation base then it is likely that the implementation of any ground improvement techniques, such as compensation grouting, to reduce excavation related surface ground movements will be ineffective. Mana and Clough (1981) and later Clough *et al.* (1989) presented Figures 2.6(b) and 2.6(c), respectively, using measurement data from case studies and parametric plane strain finite element analyses. Figure 2.6(b) shows the magnitude of maximum horizontal wall displacements normalised by the excavation depth were highly sensitive to the factor of safety against basal heave (FS_{Heave}) up to values of around 2.5, calculated using the methods proposed by Bjerrum and Eide (1956) and Terzaghi (1943), shown in Figure 2.6(a). Clough *et al.* (1989) also proposed a relationship between the magnitude of normalised maximum horizontal wall displacements and the overall stiffness of the support system, K_1 (see Figure 2.6(c)) which related the bending stiffness of the retaining wall (EI) to the average vertical spacing of struts, h, and unit weight of water, γ_w.

2.2.2 Horizontal stress relief

Ground movements associated with horizontal stress relief consist of two source components: 1) movement associated solely with the soil mass excavation process and 2) movement solely due to wall installation (for *in situ* cast walls), McNamara (2001).

Clough and O'Rourke (1990) highlighted that for soils with high, locked in pre-excavation horizontal stresses, the soil deformations surrounding the excavation extend further from the wall compared to other soils, even at relatively shallow depths. For soils with lower values of coefficient of earth pressure at rest, K_o, the extent of deformations will tend to be less, Potts and Fourie (1984). Similar behaviour and relationships between pre-excavation lateral pressures, soil stiffness and displacements were also observed by Powrie and Li (1991) from a series of finite element analyses. They found that by modelling high pre-excavation lateral pressures the soil stiffness increased, leading to smaller displacements and reduced bending moments on the *in situ* retaining wall.

Installation of embedded walls induce complex stress changes, McNamara (2001). The concept that installation of retaining walls, particularly diaphragm walls, cause changes in *in situ* stresses thus influencing soil behaviour during excavation is well recognised, Rampello *et al.* (1998). The reduction in horizontal stress caused by the installation of the walls, particularly in overconsolidated soil has been addressed in detail and described by several researchers (e.g. Pantelidou, 1994; Kantartzi, 1993 and Carder, 1995). Anderson *et al.* (1985) undertaking tests on bored cast *in situ* piles in normally and overconsolidated clays, showed that 90% of the initial effective horizontal stress, σ_h', associated with K_o was recovered 30 days after the dramatic reduction during excavation. They established that K_o values would eventually re-establish over time. Several authors (e.g. Stewart, 1989; Powrie, 1986 and Lings *et al.,* 1991) have reported significant reduction in initial K_o values following wall installation in overconsolidated clay, with Stewart and Powrie reporting values of between 1 and 1.2 and Lings *et al.* (1991) reporting values of K_o which were less than 1 for heavily overconsolidated Gault Clay.

Powrie and Kantartzi (1993) showed from centrifuge model tests, investigating installation effects of diaphragm walls, that much of the overall settlement associated with diaphragm wall installation occurred immediately after trench excavation; the post installation movements (after 17 days at prototype scale) were relatively smaller in magnitude. Similar behaviour was also found by Pantelidou (1994) who reported that most of overall movement occurred by the end of the excavation of a model wall. Tedd

et al. (1984) reported that 30% of the overall movements occurred during the secant pile wall construction at Bell Common Tunnel in stiff overconsolidated clay. In the idealised case of a plane strain excavation, Powrie and Kantartzi (1996) concluded that the installation of a diaphragm wall in an overconsolidated clay would lead to the most significant movements being developed within a distance x= 1H either side of the excavation.

Powrie *et al.* (1998) simulated stress paths similar to those associated with the process of installing a diaphragm wall in clay and subsequent excavation in front in triaxial tests using reconstituted kaolin clay samples. They concluded that uncertainties in the *in situ* stresses and previous stress history of the soil had only a minor effect on the soil behaviour subsequent to wall installation. This was due to the stress changes imposed during installation moving the stress state of the soil outside the influence of its geological and pre-installation stress history. Rampello *et al.* (1998) stated that the changes in lateral effective stresses due to wall installation defined the recent history of the soil at the start of the excavation. Following simulation of wall construction, movements in the ground behind the wall were shown to be dominated by decreases in σ'_h and movements in the ground in front of the wall were dominated by decreases in σ'_v, Rampello *et al.* (1998).

2.3 Empirical observations

The state of the art report published by Peck (1969) was the first attempt to produce a method to predict excavation induced ground movements using observed relationships and behaviours from case histories of excavations supported by strutted and tieback soldier and sheet piles in Chicago, U.S.A., and Oslo, Norway. Compiled settlement data from case histories in different soils were normalised against the excavation depths and plotted against the normalised distances behind the supporting wall, as illustrated in Figure 2.7. Peck summarised the movements observed from these soil conditions into three categories. Peck (1969) attempts to also distinguish between the quality of workmanship and account for basal stability for soft clays, however fails to differentiate movements associated with individual construction activities. Figure 2.7 presents soil behaviour for sands, stiff clays and soft clays. The figure shows spandrel settlement curves for all three soil types, with the smallest values in zone 1 for sand and soft to hard clay extending back a distance x= 2H behind the wall based on average workmanship. The magnitude of maximum settlements found for this zone were limited to 1% of the excavation depth. For very soft to soft clays maximum settlements occur immediately

behind the wall reaching a magnitude of about 1-2% of the excavation depth and extend back a distance four times the excavation depth. A limitation of Peck's study is that it applies to excavations where supports have been installed early at shallow depths, as late installation of supports is generally regarded as an important cause of subsequent displacement, as highlighted later by Burland *et al.* (1979) and O'Rourke (1981). O'Rourke (1981), having analysed time dependent movements in sands and soft clays, recommended excavation be limited to less than 5 m below the lowest strut. Both Burland *et al.* (1979) and O'Rourke (1981) called for the installation of struts as quickly and as early as possible following excavation to avoid excessive wall and surface ground movements to develop.

The findings presented by Goldberg *et al.* (1976), who extended the work of Peck (1969) by including more wall types (e.g. secant pile and diaphragm walls), showed reductions in the observed soil settlements for cast *in situ* walls. In relating maximum vertical settlements (S_{vmax}) behind the wall to maximum horizontal wall deflection (S_{hmax}), Goldberg *et al.* (1976) found most of the data plotted as S_{vmax}/S_{hmax} lay within a ratio of 0.5-2. They showed that, for soft clays, settlements generally exceeded horizontal wall displacements, which was attributed to consolidation induced settlements owing to lowering of the water table around the excavation. Fundamentally the authors showed that settlement in sands and stiff clays were typically less than half the values presented by Peck (1969) for similar soils. For softer clays settlement magnitudes were greater than 1% of the excavation depth and settlements were generally found to occur within distances x= 1.0-1.5H behind the excavation. Their analysis of the case studies showed for sands, gravels and stiff clays maximum normalised wall displacements, $S_{hmax}/H<$ 0.35%. As with Peck (1969), the findings presented by Goldberg *et al.* (1976) are limited by the fact that movements associated with individual activities (i.e. strut installation, wall installation) are not isolated from the observations. However, it is clear from the improvement in settlement values obtained by Goldberg *et al.* (1976) that significant advances in wall, support and construction technology were made in the period 1969-1976.

Clough and O'Rourke (1990) presented data from various case studies on horizontal and vertical displacements as an update to the database collated by Goldberg *et al.* (1976). They divided the case histories into two categories of soils: 1) stiff clays, residual soils and sand and 2) soft to medium clays and distinguished between effects solely due to the normal excavation cycles and support installation. They also isolated unusual

construction effects or late strut installation. The database primarily focused on sheet pile and soldier pile walls. Clough and O'Rourke (1990) reported that in category 1 soils the magnitude of S_{hmax} tends to average about 0.2%H, with S_{vmax} being about 0.15- 0.5%H, as shown in Figure 2.8. In Figure 2.9, Clough and O'Rourke (1990) suggested for excavations in stiff to very hard clays, horizontal wall movements tended to equal or exceed the vertical settlement counterparts and proposed an upper bound ratio of 2.5:1 for S_h/S_v and suggested a bounding triangular settlement profile to predict movements for different soil types, as summarised in Figure 2.10. It can be seen that the zone of influence reaches a distance of three times the excavation depth for stiff to very hard clays.

Since the early work of Peck (1969) there has been a steady growth in the number of databases and site specific soil conditions. In the U.K. these include Burland (1979), Carder (1995) and Fernie and Suckling (1996), each progressively adding to the data and knowledge base of those before and other case histories in relevant soil conditions and types pertaining to the U.K. Burland *et al.* (1979) found that significant movements from excavations in London Clay can extend up to 3H behind the wall, consistent with the envelopes presented by Clough and O'Rourke (1990) for stiff to hard clays, see Figure 2.10. Carder (1995) reported case histories of bored pile and diaphragm walls in stiff soils and presented upper bound values for S_{hmax} of 0.125%H, 0.2%H and 0.4%H for high, moderate and low stiffness support systems used during excavation, respectively. In contrast, Carder (1995) found that movements extended as far as 4H behind the wall. Fernie and Suckling (1996) reported similar finding to Burland *et al.* (1979) with S_{vmax} on average being 0.15%H for stiff U.K. soils. In considering the horizontal wall deflections of bored piles diaphragm walls and sheet pile walls, in terms of the dimensionless system stiffness, K_1 (defined by Clough and O'Rourke, 1990), it was found that for $FS_{Heave} > 3.0$, lateral deflections of walls embedded wholly in stiff soils was less than 0.3%H, Gaba *et al.* (2017). Gaba *et al.* (2017) reported that these deflections were about 0.15%H for walls embedded in stiff London Clay, when adopting a top-down construction method.

A later study by Long (2001) presented an extensive database from the analysis of 296 case histories. The study focused largely on the validation of the observations presented by Clough and O'Rourke (1990) for a large range of different soils from sites all around the world. Long (2001) collated the data into four categories: 1) stiff to medium dense

soils, 2) stiff to medium dense soils with embedment into stiff stratum, 3) stiff to medium dense soils with a low factor of safety against heave, FS_{Heave} and 4) cantilever walls. Further subdivisions were made for internally propped and anchored walls, top down construction and soil strengths. Figure 2.11 illustrates the category divisions by Long (2001). For excavations with walls wholly embedded in stiff clay, for top down (high support stiffness) constructions and retaining predominantly stiff clay with a large FS_{Heave}, Long (2001) reported normalised S_{hmax} values between 0.05-0.25%H and S_{vmax} values being generally less than 0.2%H. Gaba *et al.* (2017) noted that these values were larger than values presented by Clough and O'Rourke (1990), Carder (1995) and Carder *et al.* (1997) which was possible if the total settlement data presented by Long included those due to wall installation. Long (2001) concluded that when large wall deflections (greater than 0.25%H) were observed for walls wholly embedded in stiff soils, these movements were always attributed to one or more of the following reasons:

- movements associated with an initial cantilever stage at the beginning of the construction sequence,
- an overly flexible retaining system,
- creep of anchorages,
- structural yielding of the wall.

Moormann (2004) summarised the findings from an extensive database of over 500 case histories in the study published by Moormann and Moormann (2002) which built on the previous work presented by several authors, including Clough and O'Rourke (1990) and Long (2001). The authors focused their analysis on excavations in soft to firm soils (i.e. $S_u < 75$ kPa - type 1) and stiff clays (i.e. $S_u \geq 75$ kPa – type 2), sands and layered soils and rocks. In general, the data scatter indicated no simple relationship between S_{hmax} and H. However, ignoring cases histories with extraordinary movements, both soil types 1 and 2 showed a clear tendency for S_{hmax} to increase with H. The studies presented the following conclusions for the two soil types for horizontal wall movements and vertical soil settlements:

Horizontal wall displacements, S_h

- The S_{hmax} (H) data for type 1 soils had the widest scatter, with 40% of the cases lying in the range $0.5\% < S_{hmax}/H < 1\%$, 33% of the cases in the soil type having $S_{hmax}/H < 0.5\%$ and 27% of the cases with $S_{hmax}/H > 1.0\%$ (on average $S_{hmax}/H = 0.87\%$, as illustrated in Figure 2.12).
- Significantly smaller S_{hmax}/H values were observed for type 2 soils with only 8% of cases having a measured $S_{hmax}/H > 1.0\%$ and the average measurements being S_{hmax}/H equal to 0.25%.
- For the majority in both soil types (67% of cases histories), the position of S_{hmax} was found to occur at depths d= 0.5-1.0H below the retained surface. In 21% of cases histories S_{hmax} occurred at the top of the excavation, probably owing to late installation of the initial high-level support, thus enabling movements expected with cantilever walls.

Vertical soil settlements, S_v

- For stiffer clays ($S_u \geq 75$ kPa) S_{vmax} behind the wall was found to be on average 0.18%H compared to 1.07%H for soft to medium clays ($S_u < 75$ kPa), see Figure 2.13.
- 70% of all case studies showed S_{vmax} occurred within a distance $x \leq 0.5H$ behind the wall (in stiff clays), in line with the findings presented by Goldberg *et al.* (1976) but was shown to increase to within $x \leq 2.0H$ behind the wall in soft clays.
- Contrary to the postulate of Peck (1969) of a constant volume displacement ($S_{vmax}/S_{hmax} = 1.0$) but similar to Goldberg *et al.* (1976) the authors found that in general for excavations in soft clays as well as for all soil conditions $0.5 \leq S_{vmax}/S_{hmax} \leq 1$, with an upper limit of 2.0 (particularly for stiff clay).

The most recent publication presented by Gaba *et al.* (2017) provided a renewed summary of all available databases of the expected soil and wall movements in different soil types observed from field case histories presented by previous authors. Gaba *et al.* (2017) presented alternative envelopes and upper bounds to vertical ground surface movements observed from the case histories for both soft to firm soils and stiff clays in which a variety of wall types and support stiffnesses (according to the categorisations proposed by Carder, 1995, as shown in Table 2.1) were utilised during excavation. Figures 2.14(a) and 2.14(b) illustrate the normalised vertical settlements against the excavation depth and

settlements normalised against the maximum vertical settlements, respectively, plotted against normalised distance behind the wall for all the reviewed case histories by Gaba *et al.* (2017) for excavations in soft to firm clays. In providing an upper bound limit to the reported movements, Gaba *et al.* (2017) found vertical settlements in these soil conditions to extend as far back as distance x= 3H behind the wall. Maximum settlements, in the order of magnitude of 2.0-2.2%H, were noted to occur up to distance x= 1H behind the wall but more typically at distance x= 0.5H. This was contrary to the envelope presented by Cough and O'Rourke (1990) for similar soils, shown in Figure 2.10(c). The envelope by Cough and O'Rourke for normalised settlements, S_v/S_{vmax} shows movements being limited to distance x= 2H behind the wall, with maximum settlements expected to occur up to distance x= 0.75H

In considering vertical surface settlements from previously presented case histories for excavations and walls embedded in competent stiff clays, Gaba *et al.* (2017) proposed the envelope profiles shown in Figure 2.15, accounting for the data in which both high and low support stiffnesses were represented. In revising the spandrel envelopes presented by Clough and O'Rourke (1990) in Figure 2.9 for excavations in stiff to very hard London Clay, Gaba *et al.* (2017) proposed a concave settlement envelope for high stiffness support excavations with maximum vertical settlements limited to magnitudes less than 0.1%H, occurring up to distances of x= 0.75H behind the wall. For low support stiffness excavations (according to Table 2.1) maximum vertical settlements between 0.3-0.4%H were noted to occur at the wall, as would be expected. This range was similar to that reported by Clough and O'Rourke (1990). Again, in contrast to the general upper bound envelope presented by Clough and O'Rourke in Figure 2.10(b) for stiff to very hard clays, a greater extent of movements was proposed by Gaba *et al.* (2017), reaching as far back as distance x= 3.5H behind the wall, as shown in Figure 2.15(b). Maximum settlements were still expected to occur at distances up to x= 0.75H behind the wall for low support stiffness excavation, shown in Figure 2.15(b).

2.4 Semi-empirical prediction methods

The literature presented in this chapter so far has focused primarily on observed normalised values of maximum horizontal wall and vertical soil displacements and the extent of settlement behind the wall for deep excavations. However, determining the profile of a ground surface settlement trough behind the retaining wall is also of particular importance during design as it enables deformations, distortions and strains that will be imposed on the overlying structure or service, to be estimated. This facilitates an understanding of the severity of damage that is likely to occur. Several researchers have proposed methods that allow prediction of the surface settlement, using analytical solutions and finite element models in conjunction with characterisation from field observations.

The approaches described herein for estimating soil and wall displacements are defined as semi-empirical methods. These methods rely on the numerical computation of the maximum horizontal wall displacements, S_{hmax} using finite element or sub-grade reaction methods. These provide good approximations of the wall displacement owing to the close proximity of the soil to the wall and the known structural properties and behaviour of the wall material (e.g. steel or concrete). This is in contrast to the vertical soil displacements behind the wall, which are further afield from the excavation (source of ground movements) and are highly dependent on the constitutive model used and estimation of the soil properties and parameters in finite element analysis. The calculated S_{hmax} value is then linked to maximum vertical displacements, S_{vmax} at the retained surface using empirical observations from case studies in similar soil conditions before finally linking S_{vmax} to settlements, S_v as a function of the normalised distance behind the wall, x/H using settlement profiles with assumed shapes observed from empirical studies such as those presented in section 2.3.

Mana and Clough (1981) used previously unavailable field data to update the case histories presented by Peck (1969) and Goldberg *et al.* (1976) for soft to medium clays to identify the limiting bounds shown in Figure 2.6. The authors isolated data from case histories with unusual construction effects and incorporated cases where movements were generated solely by excavation induced stress relief and where prudent construction procedures had been employed. The specifics of these unusual construction effects were not provided by the authors. However, the effects from de-watering induced consolidation, wall installation and late placement of the primary struts (i.e. placed at a

depth greater than $2S_u/\gamma$) were noted to have been isolated. The data showed the normalised maximum lateral wall displacement, S_{hmax}/H was related to the normalised maximum vertical settlement, S_{vmax}/H by a ratio 0.5-1.0, as shown in Figure 2.16. In comparing their finite element study with the collected field data, shown in Figure 2.6(b), which indicated good agreement, they proposed a method to estimate the ground settlement profile. This method required estimation of S_{hmax} using the lowest calculated FS_{Heave} during the various excavation stages from Figure 2.6 and S_{vmax}, assuming S_{vmax}= 0.6-1.0S_{hmax}. The estimated S_{hmax} value could then adjusted to provide S^*_{hmax}. This adjusted value of S^*_{hmax} allowed the influence of wall and strut stiffness, depths to firm layers of soil, excavation widths, strut preloads and correlation between the undrained shear strength, S_u and Young's Modulus, E of the clay soil to be accounted for using influence coefficients. These coefficients were quantified and presented in chart form by the authors from parametric finite element analysis studies. The coefficients when multiplied by the original S_{hmax} provide S^*_{hmax}. An adjusted S^*_{vmax} could then be calculated using the same relationship where S^*_{vmax} = 0.6-1.0S^*_{hmax}, before determining the ground settlement profile using the S^*_{vmax} value in the normalised settlement profile shown in Figure 2.17. Comparisons using this method were made using data from a well-documented case study and were shown to be in good agreement with the field measurements.

As discussed briefly in section 2.2, Ou *et al.* (1993) and Hseih and Ou (1998) derived two soil settlement profiles from their in depth study of case histories in Taiwan: 1) the spandrel type in which S_{vmax} occurs close to or immediately behind the wall and 2) the concave type, where S_{vmax} occurs some distance away from the supporting wall, illustrated in Figure 2.3. The focus of both publications was on movements generated solely due to excavations under plane strain conditions. Ou *et al.* (1993) noted that the magnitude and shape of the wall deflection controlled the settlement profile. Spandrel type settlements occurred if a large amount of wall deflection occurred during the early stage of excavation and initial support installation where cantilever conditions exist and subsequent excavation produces relatively smaller deflections, Hseih and Ou (1998). For concave settlement profiles, Hseih and Ou noted that relatively small movements would occur at the top of the wall owing to the high level support restraint, resulting in lateral deflections shifting down as the excavation progressed.

Ou *et al.* (1993) proposed a tri-linear settlement profile for predicting the spandrel type settlement profile, based on the Taiwan case histories, illustrated in Figure 2.18. The profile is presented as normalised vertical soil movements and horizontal distance behind the wall against the sum of the excavation depth, H and wall penetration depth, D. However, Hseih and Ou (1998) later noted that the penetration depth is likely to be an arbitrary parameter and modified the profile to the bi-linear line in Figure 2.19.

Hseih and Ou (1998) described the primary zone of influence depicted in Figure 2.19, which reached back a distance x= √2H behind the wall. In the secondary zone movements are more uniform and the slope of the normalised settlements is less steep; movements in this zone were considered less damaging, than the primary zone, to overlying structures by the authors. For the spandrel type profile, the position of S_{vmax} occurred immediately behind the wall, Ou *et al.* (1993).

An apparent influence range (AIR), was also defined by Ou *et al.* (1993), within which significant differential movements and distortions would occur that could cause damage to overlying buildings and services. It was concluded that the AIR could be estimated based on the active zone of soil behind the retaining wall with an upper limit equal to the total length of the wall or the total length minus the embedded depth if penetrated into a hard stratum. In constructing their proposal for predicting concave settlement profiles (see Figure 2.20), Hseih and Ou (1998) considered case histories where the vertical settlements at the wall approximately equalled $0.5S_{vmax}$ which is consistent with the range of $0.5\text{-}0.75S_{vmax}$ presented by Clough and O'Rourke (1990) in soft to firm clays. Using the findings presented by Ou *et al.* (1993), where S_{vmax} occurs at distance x= 0.5H behind the wall and the extent of the active zone, according to Rankine theory, being approximately equal to the extent of the primary influence zone for a spandrel profile up to distance x= 2H, as with Clough and O'Rourke (1990), the authors were able to define the primary influence zone for this type of settlement curve. Hseih and Ou (1998) considered the secondary influence zone for the spandrel profile, presented in Figure 2.19, which showed a significantly shallower slope than the primary zone and suggested that this region would be less affected by different excavation and strut installation. With this consideration, Hseih and Ou (1998) used the same extent and magnitude profile to describe the secondary influence zone for the concave settlement curve in Figure 2.20.

The proposed settlement profiles in Figures 2.19-2.20 were evaluated by Hseih and Ou (1998) against several case histories from around the world that had been presented by

previous authors (i.e. Clough and O'Rourke, 1990 and Tedd *et al.,* 1984) and against the prediction methods presented by Peck (1969), Bowles (1988) and Clough and O'Rourke (1990). Good agreement was found between the field observations from the case studies and the proposed methods for soft and stiff clays and generally gave better predictions of the angular distortion at the surface than Peck (1969), Bowles (1988) and Clough and O'Rourke (1990). However, Hseih and Ou (1998) noted that the reliability of both methods was dependent on making good predictions for S_{hmax} using finite element analysis or a sub-grade reaction method. S_{hmax} could then be used to predict S_{vmax} using relationships presented by different authors for a range of soil conditions.

2.5 Summary

The local and global ground movements and their mechanism owing to excavations have been described. The expected profiles of the vertical settlements at the retained soil surface owing to the vertical stress relief from excavation have been presented. The sources of movements from the horizontal stress relief by excavation have also been briefly addressed. The influence of the support system stiffness has been shown by more recent case study databases to have no clear dependency on the horizontal wall and retained soil surface displacements for excavation in medium to stiff soils where a factor of safety against basal heave greater than 2.5 exists. However, in soft to medium clays the aspect of basal heave failure has been shown to be a more significant source of ground movements where a clear relationship has been observed from case study data between maximum wall displacements, overall support system stiffness and factor of safety against basal heave.

Empirical studies from field measurements of wall and ground movements up to the most recently published by Gaba *et al.* (2017) have been discussed. The findings from these studies, with predominant focus on excavations in medium to stiff clays considering the expected soil type in the model tests conducted in this study, have shown the lateral spread of vertical movements at retained soil surface to extend back behind the wall up to a distance x= 3.5H. Maximum settlements, S_{vmax} have been noted to generally occur somewhere between distances of x= 0.5-0.75H behind the wall and typically less than 0.1-0.2%H in magnitude. Moorman (2004) highlighted from a database of over 500 case studies that maximum horizontal wall displacement for excavations in both soft to medium and stiff clays generally occurred between depths of d= 0.5-1.0H below the retained surface.

Various semi-empirical prediction methods from different authors have been described which enable calculation of the vertical retained soil surface displacements. The findings from these semi-empirical predictions methods for excavations in clay have been discussed and have been demonstrated by the publishing authors to have good correlation with field measurements, showing the validity of the methods to reasonably approximate soil settlements. This has commonly, amongst the reviewed literature, noted to be true only if the correct assumptions and soil properties are adopted early on during either the finite element or sub-grade reaction methods to predict the maximum horizontal wall displacement.

The soil and wall movements generated by excavations and their manifestations as angular distortions, horizontal strains and deflections ratios are a significant concern in their ability to cause damage to sensitive overlying and adjacent structures and buried services. Several authors (i.e. Boscardin and Cording, 1989; Boone, 1996; Finno *et al.,* 2005 and Son and Cording, 2005) have provided detailed guidance on the assessment of the levels of damage induced on different overlying structures from excavation induced ground movements. These authors have provided design limits and criteria on the distortions and strains that can be allowed before realisation of these levels of damage. However, examining these parameters and limits both in available literature and later against measurements made in the model tests conducted was considered to be outside the scope of this study.

3. COMPENSATION GROUTING - LITERATURE REVIEW

This chapter provides an introduction to the compensation grouting technique. The details of the process and limitations of the employment of the technique in the field are identified. This chapter focusses only on the information pertinent to the compaction grouting method owing to the modelling methods adopted in this study. Mechanisms which describe the process of compaction grouting to realise heave at the ground surface are described. Two case studies are examined and the key findings and performance of the compaction grouting employed in the field within the individual projects are detailed.

3.1 Introduction

Tunnelling, particularly in soft ground, always results in ground loss towards the tunnel and its face owing to stress changes in the ground which manifest itself as ground movements at higher levels, Mair and Hight (1994) (see Figure 3.1). The resulting ground movements will affect overlying buildings thereby inducing distortions and tensile strains, which depending on their magnitude can lead to damage in the form of cracking, particularly in masonry buildings, Mair and Hight (1994). In order to reduce and control excessive movements in the ground and building settlement, several construction techniques can be applied from within the tunnel excavation to reduce volume loss (i.e. face support, creating a pilot tunnel, ground treatment, etc.). External measures such as underpinning the concerned structure, strengthening the ground around the tunnel or beneath the building again by means of ground treatment can also be applied. There have been several ground treatment technologies developed and employed within construction projects around the world to provide ground stabilisation and strengthening. These include jet grouting, ground freezing, permeation grouting and compensation grouting, Bruce (1994).

Compensation grouting, a term first introduced by Mair and Hight (1994), is a relatively new and novel technique to compensate, control and correct ground settlements experienced during bored tunnelling in soft ground. Figure 3.2 illustrates the basic principle behind compensation grouting. The technique involves the injection of grout between the tunnel excavation and building foundations and soil surface to compensate for the ground loss and stress relief owing to the tunnel excavation. Littlejohn (2003) further describes the two approaches to compensation grouting:

- Concurrent grouting is the proactive injection of grout as settlement develops. It is typically specified when it is anticipated that the magnitude of settlements will cause damage. The location and volume of grout are determined from predicted settlement profiles.
- Corrective grouting is a reactive process where the injection of grout is only initiated when a pre-determined settlement or distortion limit of the structure ground is observed. The positioning and timing of injection are determined using the observational method, proposed by Peck (1969) to maintain distortions and settlements within pre-determined tolerances.

With both approaches to compensation grouting it is usually necessary to install grouting tubes well in advance of the tunnelling excavation to undertake a phase of pre-treatment to 'condition' and 'tighten' the ground, Mair and Hight (1994). The pre-treatment phase is intended to allow the main compensation grouting phase to be more effective in controlling ground settlements and distortions and is typically carried out until a response is observed in the monitoring instrumentation on the structure.

Good quality real-time monitoring and instrumentation of the ground and concerned structures is required to enable decisions regarding the positioning, timing and volume of the selected process of compensation grouting to be made, Mair and Hight (1994). The real time monitoring and feedback has often been reported in case studies to enforce changes by the contractor to the original grouting plan for the project. Figure 3.3 shows the general compensation grouting procedure that would be adopted on a project with emphasis on the key elements of successful compensation grouting monitoring, instrumentation and performance limits.

The first critical step in the grouting operation is to establish performance limits (stage 1 in Figure 3.3) (e.g. relative settlements, angular distortions and horizontal strains) that can be allowed to manifest in the ground from the underground excavation before a certain level of damaged is incurred by overlying structures and buried services. These limits are typically based on the guidance provided in widely recognised literature from several authors (i.e. Boscardin and Cording, 1989; Boone, 1996; Finno *et al.,* 2005 and Son and Cording, 2005) concerning the selection of values from damage assessment criteria. Once these limits are identified, a 'traffic light' system is implemented with the active monitoring and instrumentation which signals the grouting contractor and designer when the magnitudes of these limits, are being approached (amber) and have been

exceeded (red) during and after the excavation event has passed. This trigger value system enables the grouting contractor and designer to determine when the grouting operation should be initiated to mitigate the occurrence of costly damages to surrounding and overlying structures.

Compensation grouting can be achieved using a variety of different grouting processes but there are broadly two processes which have been most commonly used on successful grouting projects in the field:

- Compaction grouting
- Fracture grouting

A third process which is a variation of compaction grouting is 'pressure filtration' grouting, sometimes referred to as 'intrusion grouting', Mair and Hight (1994).

Only the process of compaction grouting is relevant to this study as a result of idealising of the process in the model tests conducted in this study, with injection of grout into sealed latex membranes. The details of the modelling equipment and test results are discussed further in chapters 5 and 6.

In order to better understand the effectiveness of compensation grouting Soga *et al.* (1999) and Au (2001) proposed terms of grouting efficiency (η) and a compensation factor (α). These terms relate the increase in soil volume owing to injection (V_E), the injected grout volume (V_i) and the subsequent volume of heave realised at the surface (V_{SH}), as shown in Figure 3.4. However in practice, determining V_E locally around the subsurface injection is extremely difficult. Therefore, using the product of the two terms, η and α, provides a more practical and direct assessment of the compensation grouting efficiency (ξ), shown in Equation 3.1. This term relates V_i to V_{SH}, both of which are relatively easy to measure from the grouting activities in the field.

$$\xi = \eta.\alpha = \frac{V_{SH}}{V_{INJ}} \tag{3.1}$$

3.2 Compaction grouting process

Mair (1994) describes compaction grouting as a process in which a low slump, high viscosity and stiff grout is injected into the ground to form an approximately spherical or cylindrical 'bulb,' depending on the grouting procedure adopted, Rawling *et al.* (2000). Figure 3.5 shows the concept behind the compaction grouting process.

The grout, typically cementitious, has sufficient silt size particles to provide plasticity, with sufficient sand size particles to develop internal friction. Owing to the low slump (ideally 30 mm ± 20 mm, Rawling *et al.,* 2000), low water cement ratio (w/c) and high viscosity and stiffness of the grout, it typically has a limited mobility within the ground. The grout is generally unable to enter the soil pores but instead remains as a homogenous mass. This causes the surrounding ground around the expanding grout 'bulb' to densify, Mair and Hight (1994). As the growing mass continues and overcomes the natural compressibility of the soil, the grout displaces the surrounding ground to compensate for settlements occurring above the injection point, Rawling *et al.* (2000). A complex system of radial and tangential stresses develop in the ground as the grout bulb continues to expand; this creates a major zone of shearing and plastic deformation to occur locally around it, causing the soil density to reduce and displaces the granular soils plastically or induces elastic movements further afield in clays, Rawling *et al.* (2000).

The rheological properties of the typical grout used generates large shear stresses and in turn large magnitudes of pipe friction when injected. Consequently, high powered pumps are required to generate the necessarily large back pressures to overcome these frictional effects and mobilise the grout along the pipework with sufficient pressure capacity to overcome, at minimum, the soil overburden at the injection depth thus allowing initiation of the grout bulb expansion in the soil.

The delivery of grout typically occurs over a short period of time. With the inherent low permeability of clay soils the injection process results in an undrained soil response during the expansion of the grout cavity. Vesic (1972) described using cavity expansion theory, that an undrained cavity expansion in an infinite medium elastic-perfectly plastic clay soil results in positive excess pore pressures, Δu, within a plastic soil zone, immediately surrounding the cavity. In the elastic soil zone, further afield and outside the plastic zone, zero changes in Δu are observed. In a finite elastic-perfectly plastic soil, Vesic (1972) showed that undrained cavity expansions resulted in small negative Δu in the elastic zone with large positive Δu in the plastic zone.

Au (2001) simulated single and multiple point compaction grout bulb expansions in normally consolidated and a range of overconsolidated (OCR≥ 2) Speswhite kaolin clay samples using a modified oedometer apparatus. These tests simulated idealised compaction grout injections using water and epoxy resin injected into latex 'balloons' (see Figure 5.5). Au observed larger magnitudes and a larger zone of positive Δu, during injection in the normally consolidated soil in comparison to the reducing extent of the zones and magnitudes of positive Δu recorded for single point injections in increasingly overconsolidated clays. In heavily overconsolidated clays (OCR≥ 5) Au (2001) noted that due to the dilative nature of the soil, negative Δu was generated at some distance away from the injection point. These negative Δu generated during injection were stated to at least partially compensate for the positive Δu around the cavity. These excess pore pressure behaviours resulted in reduced negative final long term compensation grouting efficiencies ($\xi < 0$) in the normally consolidated samples. A dramatic increase was observed in the long term ξ when the OCR was increased from 1 to 2, with near perfect efficiencies ($\xi = 1$) being reached at larger increasing values of OCR.

It is due to these consolidation induced settlements and the potential for net negative grouting efficiencies, that compaction grouting is typically reserved for granular soils where the process is likely to be drained and will avoid complications associated with consolidation, Mair and Hight (1994). This is provided that the injection rates are kept sufficiently low to allow excess pore pressures to dissipate. However, Essler *et al.* (2000) details some of the cases where compaction grouting was successfully deployed near tunnelling excavations in silty clayey soils. The process of hydro fracture grouting, the details of which are not addressed in this study, is more commonly used and successful in overconsolidated clay soils. The fracturing process result in a larger spread of lower magnitudes of Δu in the soil during injection due to the lower injection pressures required, further reaching grout fractures and the propagation mechanism of the fractures highlighted by Au (2001). This results in reduced magnitudes of consolidation induced settlements in a less localised area (in comparison to compaction grouting) in the long term period after injection leading to values ξ being closer to 1. However larger regions of consolidation induced settlements can be observed with the further reaching fracture grouting when compared to the more localised regions associated with compaction grouting.

Compaction grouting is typically delivered through vertically installed open ended grout tubes or casings. ASCE (2010) states that the casing should ideally be installed tightly

into the borehole, with little or no annulus, such that the grout will be forced to expand radially and is restrained from travelling upward along the tube.

Compaction grouting can be employed either to form discrete inclusions or injected in overlapping stages, Rawling *et al.* (2000). In either form ascending or descending stages of grouting can be adopted. Descending staged grouting involves inserting grout in the first pass near the surface via a grouting tube, with subsequent injections made at greater depths, which require re-drilling and extension of the tube to the next deeper injection point between each pass. This method is more suited to applications requiring improvement of soil density as the upper layers are treated first thus reducing unwanted heave from subsequent injections. Ascending staged grouting requires the first phase of grouting to be carried out at the deepest depth, with subsequent stages made at higher elevations. This method is more economical than descending staged grouting and can be used in a controlled manner, through multiple injection points at lower pressures near the surface to induce heave. Figure 3.6 shows the details of the top down (descending) and bottom up (ascending) processes of compaction grouting.

One of the key limitations of compaction grouting is the inability to react quickly to further settlements from the same grout position following the initial grouting phase due to the use of non-reusable injection pipes and hard setting grouts. These grouts are virtually impossible to break through, Au (2001), unless a relatively weak cement binder is employed or the re-drilling of the grouting tube is adopted by the contractor.

3.3 Theory

This section provides an outline of the two mechanisms which are understood in current literature to model the behaviour of compaction grouting at the onset of heave at the ground surface.

3.3.1 Mechanisms

Owing to the application of compaction grouting typically in granular soils in the field, much of the available literature focusses on the response and behaviour of granular soils to compaction grouting. Several authors (e.g. Graf, 1969; Wong *et al.,* 1996; El-Kelesh *et al.,* 2001) proposed, in common, that heave at the ground surface due to compaction grouting can be explained by considering two main mechanisms or modes: 1) shear failure of a conical wedge of soil above the point of injection and 2) cavity expansion, shown in Figure 3.7.

Although the conical shear failure mechanism due to a spherical cavity was proposed by these authors with particular focus on granular soils ($\phi' > 0$) it is possible to translate it to be applicable to undrained expansions in clay soils ($\phi' = 0$).

According to El-Kelesh *et al.* (2001), in the case of shallow injections, the compaction grouting process follows a cavity expansion model until a failure mechanism develops under the influence of the free surface. The occurrence of each mode is dependent on the cavity pressure magnitude acting at the grout-soil interface. El-Kelesh *et al.* (2001) and El-Kelesh and Matsui (2002) found that the occurrence of each mechanism in loose granular soils could be categorised by a critical depth of injection of about 5 m. This was also observed by Nishimura *et al.* (2011) who saw visible heave for compaction grouting injections above the critical depth. A significant difference in performance of the compaction grouted piles in the tests conducted by El-Kelesh and Matsui (2002) was noted above and below this critical depth. Above this critical depth, it was suggested that the injection process is controlled mainly by the overburden pressure and soil shear strength. Beneath this depth injections were noted as having no appreciable effect on the surface and injections at such depths were highly affected by compressibility of the soil.

The initial theory of elasticity presented by Timoshenko and Goodier (1970) has been used as a basis for the development of a well-defined mathematical framework of cavity expansion theory. To date there are a large range of closed form solutions presented by different authors (e.g. Gibson and Anderson, 1961; Palmer, 1971; Vesic, 1972; Menard, 1975; Carter *et al.,* 1986 and Bolton and Whittle, 1999) using cavity expansion theory that have been developed, which are applicable to different problems encountered in geotechnical engineering. The full derivation, mathematical workings and description of the kinematics of the solutions relevant to grout injection are detailed in the papers. As such only the relevant expressions to explain the process, in particular the relationship between the injection pressure and cavity size are considered herein.

3.3.1.1 Shear failure

Graf (1969) first proposed the concept of a conical shearing envelope, based on observations in the field (shown as Mode 2 in Figure 3.7), developing when the available injection pressure, after maximum compaction of the soil surrounding a grout bulb was achieved, caused uplifting of the soil above the grout bulb.

Based on the observations of Graf (1969), Wong (1974) described the onset of ground surface heave occurring when the upward force exerted by the grouted bulb was equal to the total downward force exerted by the weight of the cone of soil plus the downward shearing resistance along the cone surface, as shown in Figure 3.8. In granular soils it was assumed that the conical surface was inclined by an angle θ to the horizontal that is equivalent to the application of the Mohr-Coulomb failure criterion to any point along the conical surface, as defined in Figure 3.8. An example was provided by Wong (1974) where the typical internal angle of friction for grout bulb injection in a loose soil is $\phi' = 30^0$ and the maximum and minimum principal stresses are vertical and horizontal, respectively, provide an angle of $\theta = 45^0 + \phi'/2 = 60^0$. This angle is inline with the observations provided by Graf (1969) and later by El-Kelesh *et al.* (2001). Based on these assumptions Wong (1971, 1974) proposed a model which related the grout bulb radius, R and the limiting grout injection pressure, P_c that satisfied heave at the ground surface given by the following Equation 3.2:

$$P_c = \gamma d \frac{\left(\frac{d}{R}\right)^2 + 3\left(\frac{d}{R}\right)\tan\theta + 3\tan^2\theta}{3\tan^2\theta} \cdot \left[1 + \frac{2(1-\sin\phi')\cos(180^0 - |\theta - \phi'|)}{\cos\phi'\cos\theta}\right] \quad (3.2)$$

Where d= injection depth; R= radius of spherical grouted mass; P_c= limit injection pressure at onset of heave; γ= unit weight of soil; ϕ= internal angle of friction of soil.

Graf (1969) noted that the heave resulting from this form of mechanism manifested as a "bubble" in the horizontal plane at the surface above the injected grout mass. Wong *et al.* (1996) noted from field measurements that the horizontal and vertical zones of influence of the compaction grouting extended a distance up to approximately eight times the radius of the grout bulb, indicated in Figure 3.9. The zone of influence was defined by the author as the extent to which displacements of the soil, resulting in its compaction, were observed around the grout 'bulb'.

Using the same approach as Wong (1974), Cirone (2016) obtained a relationship for the cylindrical shear failure mechanism developed in clay soils above an ideal spherical cavity created by compaction grouting. Considering the depth of injection (d) below the soil surface, weight of soil of the cylindrical shaped envelope created above the spherical cavity (W), the downward shearing resistance of the clay soil along the cylindrical surface provided by the undrained shear strength (S_u) and any overburden stress at the surface (q) (i.e. from an overlying structure), a relationship was established to enable the limiting pressure to create upward heave, P_{up} at shallow depths to be found, shown in Equation 3.3 and Figure 3.10

$$P_{up} = \gamma(d - \frac{2}{3}R) + S_u \frac{2d}{R} + q \tag{3.3}$$

Both models, owing to their simplicity, ignore the effects from previous or neighbouring injections, as would likely be the case when employed in the field. If multiple injections are made at close spacing and at great depths, the conical mechanism would overlap or would be different in clay, thus significantly affecting the limiting injection pressure at uplift of the surface. A key limitation in these models proposed by Wong (1974) and Cirone (2016) is the lack of any consideration for deformations that occur during the expansion of the grout bulb.

3.3.1.2 Cavity expansion

In modelling the compaction grouting technique it is assumed that the injection process continues until reaching a limiting condition, which in the case of compaction grouting is the heave of the ground surface.

Cirone (2016), for clay soils, suggested the use of the well-established limiting cavity pressure expression ($P_{c,\,lim}$), shown in Equation 3.4, defined by many previous authors (i.e. Gibson and Anderson, 1961; Yu, 2000 and Hill, 1950) for an ideal spherical grout mass by undrained cavity expansion theory in an elastic-perfectly plastic infinite medium. Equation 3.4 represents the mechanics and soil response during injection in contrast to Equations 3.2 and 3.3 which represent the soil at the failure condition. Equation 3.4 describes the pressure at which the zone of soil surrounding a spherical cavity reaches a fully plastic state of equilibrium, after the start of expansion (prior to which the soil is

assumed to be in an elastic state), where no further changes in the internal cavity pressure occur but the cavity continues to expand,

$$P_{c,lim} = P_o + \frac{4}{3} S_u \left(1 + ln\left(\frac{G}{S_u} \right) + ln\left(1 - \frac{r_i}{r} \right)^3 \right) \quad (3.4)$$

Where P_o is the original *in situ* stress in the soil, G is the soil shear modulus and r_i/r is the cavity ratio between the initial cavity radius (initial radius of the grouting pipe- r_i) and the cavity radius (r) see for example Yu (2000).

In combining Equations 3.3 and 3.4, Cirone (2016) proposed a model which described the compaction grouting process, shown diagrammatically in Figure 3.11. At the start of the compaction grouting process the injection pressure or internal spherical cavity pressure rises rapidly to a constant value described by Equation 3.4, typically achieved when the radius of the expanding cavity is twice the initial radius. As the radius of the cavity increases, the second mechanism described by Equation 3.3 is activated. The intersection point of these two equations, shown in Figure 3.11, is the limiting pressure determining the maximum bulb radius which can be expanded without causing excessive plastic deformations at the ground surface. El-Kelesh *et al.* (2001) described a similar model for cavity expansions in loose granular soils based on the cavity expansion solution for spherical cavities in an infinite soil mass presented by Vesic (1972).

3.4 Case studies of compaction grouting

The following case studies presented focus on the use of compaction grouting during the construction of two tunnels and adjacent to a diaphragm walled excavation to control ground surface displacements developed by the construction activity.

3.4.1 Bolton Hills Tunnels, Baltimore, U.S.A.

Compaction grouting was used for the first time to control settlement during the construction of the Bolton Hills Tunnels in Baltimore, U.S.A., Baker *et al.* (1983). Steel lined twin tunnels 5.88 m in diameter were constructed in soil consisting of interbedded stiff clays, dense sand and gravels. The tunnels were constructed between depths of 12-23 m below the surface with a ground water table 13 m below surface. Some 39 buildings, predominantly masonry in structure with foundations 3 m below the surface were prevented from settling by compaction grouting, Mair *et al.* (1994). The grouting contractor had initially specified the compaction grouting be placed directly beneath the

foundations via pre-installed grout pipes within the vicinity of the footings of each building through the building basements. The grouting was to be initiated when a settlement in excess of around 6 mm was recorded from the extensive monitoring and instrumentation put in place. The concern with this approach was that of controlling the differential heave that would have occurred as a result of the grout being placed directly beneath at relatively shallow depths. This would have required the coordination of multiple injection points beneath multiple footings which would have inevitably created logistical issues. The alternative method put forward by the engineers was to install the tubes from the edge of the street surface and place grout 'bulbs' near the tunnel crown. This procedure would allow the movements to be dealt with near the source before being able to affect the structures. By placing the grout at depth, the influence of a single grout bulb was spread out over a large portion of the structure to be protected, Baker *et al.* (1983). In this way, delays in placing the grout bulb did not produce serious structural distortions and each bulb could be placed sequentially rather than having to grout simultaneously, as with the initial scheme.

The grouting program was carried out by injecting through 75 mm diameter grout pipes installed vertically or at an incline from the street surface, as shown in Figure 3.12. Grouting at each pipe begun after the tail of the shield had advanced by 5 ft beyond the pipe and was maintained until pressures of 400-500 psi were reached or extraction of the grout pipe by a few feet did not result in lower injection pressure nor an increased rate of grout ‘take’ was recorded. As no precise details of the site soil properties were provided by the authors it is difficult to assess the relative ratio between these limiting injection pressures and the overburden pressures that would have been present prior to commencing injection.

Grouting at each pipe was carried out sequentially. A double acting piston pump capable of pumping 3.5 ft^3/min at pressures up to 1000 psi was used. Baker *et al.* (1983) noted that these high pressures were quickly dissipated over a short distance of grout flow owing to internal shearing resistance within the pipework. The grout consisted of a well graded sandy soil with 15-25% fines passing through a 74 μm sieve mixed with ordinary Portland cement in a 1:2 ratio. Water was added to provide a cone slump between 25-50 mm. The volume of grout injected at each point ranged between 30-60 ft^3.

It was observed that the grouting produced maximum settlements of 125 mm immediately above the first tunnel crown, however these attenuated to movements of 10-13 mm at the

ground surface for both tunnels, shown in Figures 3.13 and 3.14. Baker *et al.* (1983) showed that grout volume stayed close to the injection point resulting in densification of the soil within a 5 ft radius around the bulb. It was also highlighted that the soil ahead of each grout bulb was displaced forward, having been prevented from rearward displacement by the last injection bulb. The high pressures used were sufficient to cause shearing deformations in the soil above each bulb, resulting in heave movements extending 20-30 ft above the crown, Baker *et al.* (1983). The zone of influence of the grout bulbs was recorded through detailed measurements of the ground surface over time to be conical in shape above the bulbs extending upwards at angle of about 30^0.

3.4.2 Deep excavation, Shanghai, China

Liu (2003) reported on the use of compaction grouting to protect seven six storey masonry buildings during an adjacent deep excavation in soft Shanghai Clay. The excavation, as illustrated in Figure 3.15, was 277 m long by 19.6 m wide along the main central section, which was 15 m deep, with the two wider ends at a slightly greater depth of 17 m. The retaining structure was a 0.6 m thick concrete diaphragm wall with a depth of 26 m, supported by steel braces at four levels (1.2, 5.2, 9.0 and 12.5 m) below the retained soil surface with prop preloads varying between 500 to 2180 kN. The Shanghai Clay consisted of various layers of clay of different properties, as shown in Table 3.1, with shear strengths varying between 9.6 to 26.2 kPa. It is likely that such low values do not represent undrained shear strengths, although no information was provided by the author as to how these presented values were obtained. The formation of the excavation was in a particularly soft stratum of grey clay with the lowest shear strength value. The masonry structures being protected were 3.9 m to 14.7 m away from the excavation.

The maximum settlement at the surface, S_{vmax} was expected to occur about 10 m or 0.67H behind the wall with a magnitude in excess of about 0.4%H or 60 mm owing to the surcharge applied by the adjacent structures. The influence zone of the excavation on surface settlements was expected to extend to a distance x= 2-3H behind the wall. The authors state that these expected movements and profiles of ground movement were based on well documented field monitoring data from excavations in similar ground conditions. Compensation grouting was designed to be carried out from the surface 3 m behind the diaphragm wall, parallel to the wall. The horizontal spacing of the grouting points was 3 m. Liu (2003) highlights that the grouting process was expected to not only compensate for the ground surface settlement but also increase deformations in the wall. Consequently, the most effective method of achieving compensation would be to carry

out grouting concurrently with the excavation process. For practical reasons the grouting was carried out after the placement of each of the braces at each excavation stage, of which there were four in total, with three main grouting stages. It was necessary to limit grout gel times, tightly control grout volumes and limit pressures to prevent high excess pore pressure generation behind the wall and also to not structurally damage the wall.

The compaction grout points shown in Figure 3.15 consisted of three open ended vertically placed plastic pipes, 40 mm diameter, for the three grouting stages. The horizontal spacing between the pipes was 250 mm. Figure 3.16 shows the three stages of grouting following each excavation stage and placement of braces. The ascending compaction grouting technique was adopted over the three stages. The three pre-drilled pipes located at each injection point were used sequentially to inject grout at depths from 4 to 1 m, 8 to 4 m and 11 to 8 m during the three grouting stages, respectively, as shown in Figure 3.16. Grout volumes were calculated using a simple linear relationship between the predicted ground loss owing to deformation of the wall and a multiplication factor which was initially set at two to account for additional volume loss as a result of consolidation, compaction of the soil and bleed. This factor was increased to three in the later grouting stages. Grouting limiting pressures were also raised from 0.25 MPa to 0.5 MPa in the final grouting stage, however no explanation was provided by the author why these changes were made,

Grouting was carried out by inserting a 25 mm diameter grout pipe into the pre-drilled set pipes. A chemical grout consisting of cement and sodium silicate was used in 1:1 ratio to provide a gel time of one minute and the grouting was initiated within 0.5 hour of the placing of the brace. Grouting was carried out using a double acting piston pump with a flow rate of 20 l/min.

Instrumentation was put in place to monitor ground surface settlement, brace reaction forces and earth pressure response between the wall and grouting locations. The response from the brace reaction forces presented pressure increments ranging from 250 to 400 kPa. No detailed information was provided by Liu (2003) in order allow these to be computed as actual reaction forces, which would help better understand their magnitude and influence on the concrete wall. Liu (2003) reported that the grout zone of influence was again conical in shape extending at about 32^0 to the vertical, which is similar to the observation made by Baker *et al.* (1983). The calculated volume of surface heave from measurements taken was approximately half of the grouted volume, representing $\xi \approx 0.5$.

The limited data presented by Liu (2003) on the measured earth pressure changes showed increases of approximately 25 kPa through the grouted depths down to the formation level. The ground settlement data, presented in Table 3.2, shows that the grouting had a significant positive response in reducing settlement rates both during and after the grouting process to a distance 15 m from the grouting point. However, what is not clear from this data is the duration of monitoring following grouting and whether the values presented for the 'after grouting' settlement changes subsequently increased with soil consolidation in the long term.

3.5 Summary

The application, principles and general process of compensation grouting as first introduced by Mair and Hight (1994) have been described. The successful implementation of compensation grouting has been shown from literature to be highly dependent on the use of active monitoring and instrumentation with the establishment of appropriate performance limits. The compensation grouting efficiency parameter ξ has been described which enables practical assessment of the performance of the grouting.

A detailed outline of the compaction grouting method under the description for compensation grouting has been provided, considering the focus and methods adopted in the model tests within this study. Compaction grouting uses generally high solids content grouts injected into the ground to create a near spherical or cylindrical grout bulb. This grout causes densification of the surrounding soil and localised lifting of the soil surface above. The practices of implementing compaction grouting have been described with the expected effects on surrounding pore pressures and consequential effects on long term grouting efficiencies in normally consolidated and overconsolidated clays. Two of the mechanisms available in literature have been detailed which describe the behaviour of single point compaction grouting injections. These mechanisms are described by the development of a conical or cylindrical shear failure plane above the grout bulb and by cavity expansion theory to provide calculation of the limiting pressure to cause uplift of the soil surface above.

The details of two case studies where compaction grouting was successfully applied above tunnels in silty clay and granular soil and behind an excavation in soft clay have been detailed. The practical aspects of implementing the compaction grouting for both case studies have been described and the influences on the excavation induced ground movements from the grouting activity have been outlined.

4. CENTRIFUGE MODELLING

An introduction to the geotechnical centrifuge modelling fundamental principles is presented in this chapter. The essential considerations necessarily made in the design of any centrifuge test are explained in detail. An outline is provided of the inherent errors associated with this modelling technique and solutions adopted for this study. A detailed description of the geotechnical centrifuge facility at City, University of London used in this study is also presented.

4.1 Introduction

To provide solutions to complex construction problems it is necessary for geotechnical engineers to understand the behaviour of the soil with which they are working and its interaction with the surrounding environment. Soil behaviour is governed by stress level and stress history. This consequently requires the correct *in situ* stress levels with soil depth to be modelled to reflect the stiffness and strength aspects of soil behaviour, McNamara (2001).

Today there exists modelling methodologies with varying degrees of rigour to understand the non-linear behaviour of soil. Three methods often adopted to improve understanding of soil behaviour and interactions are; 1) numerical modelling, 2) soil testing and 3) physical modelling. It is well recognised in both industry and academia that the first two methods are capable of providing good approximations to soil-structure behaviour of relatively simple constructions. However, for more complex construction events, such as that being investigated in this study, the capability of these methods is highly dependent on the soil constitutive model (for numerical modelling), stress histories and paths and selection of appropriate and representative soil properties encountered in the field.

Physical modelling, particularly full prototype scale and small-scale centrifuge modelling has the capability to control and simulate the boundary conditions, real soil properties, stress paths and soil behaviours experienced in the real world event. As such it is generally accepted that physical modelling used as a tool enables a far more accurate representation of the soil-structure interactions and behaviours from such complex constructions in comparison to numerical modelling. It is for these reasons that physical modelling was selected as the methodology for investigating the technique of applying compensation grouting behind a retained deep excavation to control ground movements in this study.

The main methods of physical modelling available include: 1) full scale testing, 2) reduced scale modelling under normal gravity conditions and 3) reduced scale modelling under an increased gravity field (centrifuge modelling). The huge scale and cost of most geotechnical problems often precludes the use of full scale testing. A significant limitation of the second method is the lack of ability to correctly model soil stresses and consequently the stress dependent behaviour of any soil-structure interactions. However, the third method provides a solution which overcomes the limitation of the previous two by permitting the correct scaled modelling of the *in situ* stresses with depth, history and magnitude in a reduced size model. This reason makes centrifuge modelling a far more attractive method than small scale testing under normal gravity conditions.

4.2 Principles of centrifuge modelling

Newton's laws of motion form the backbone of centrifuge modelling. They state that the action of pulling a mass out of its straight flight path around one of constant radius, r will impose a radial acceleration towards the axis of rotation described by:

$$a = \omega^2 r \tag{4.1}$$

Where a - acceleration (m/s^2)

ω - angular velocity (radians/s)

r - radius from centre of rotation (m).

As a result the mass, in this case a soil model, will experience an equal and opposite radial acceleration outwards towards the model base. In an engineering context it is common practice to relate this inertial radial acceleration, a to Earth's gravitational acceleration, g via a scaling factor, N with:

$$a = Ng \tag{4.2}$$

Using a centrifuge allows a soil model contained within a strongbox at the end of a centrifuge arm to be accelerated. This permits an inertial radial acceleration field N times Earth's gravity to be induced in the soil. The result of the radial acceleration field increases the self-weight of the model in the direction of its base, McNamara (2001). Soil stresses are dependent on soil density and the gravitational field. The scaling of the latter allows stresses in the soil model to approximately increase linearly with depth from zero values at the surface.

4.3 Scaling Laws

In order to correctly model a stress profile and stress history resembling those in a corresponding prototype soil it is necessary to maintain stress similarity through the depth of the model. Consequently, the vertical stress at a depth d_m in the model should be equal to the corresponding depth d_p in the prototype;

$$d_p = Nd_m \tag{4.3}$$

For a soil of density, ρ in the prototype the total vertical stress, σ_v at depth d_p is given by:

$$\sigma_{v,p} = \rho g d_p \tag{4.4}$$

Central to centrifuge modelling is the ability to apply an acceleration of N times Earth's gravity to a soil model. Thus, for a soil in the model of density, ρ the vertical stress at depth d_m can be written as:

$$\sigma_{v,m} = \rho N g d_m \tag{4.5}$$

To obtain stress similarity between model and prototype:

$$\sigma_{v,m} = \sigma_{v,p} \tag{4.6}$$

And so;

$$\rho N g d_m = \rho g d_p \tag{4.7}$$

If the density of material in both prototype and model are the same, it can be shown that Equation 4.7 can be reduced to Equation 4.3. Consequently, it follows that if the same soil is used between model and prototype and the model is carefully prepared to achieve similar soil packing and stress history, Taylor (1995), then it is possible to achieve closely resembling stress profiles as indicated in Figure 4.1.

The validation of Equation 4.3 provides a scaling law of $1/N$ which can be applied to length and consequently the model dimensions and geometric properties of other components used in the model (i.e. bending stiffness of a retaining wall). Table 4.1, modified after Powrie (1986), Culligan-Hensley and Savvidou (1995) and Wood (2004) provides a detailed list a few of the scaling factors relevant to centrifuge modelling.

Another significant benefit of centrifuge and small-scale modelling is that for consolidation and seepage. Consolidation (a diffusion event) relates to the dissipation of excess pore pressures and is important when attempting to replicate construction events relating to a prototype problem such as grouting and excavation which are time-dependent.

Taylor (1995) described the easiest method of examining the scaling laws for consolidation time using dimensional analysis. The degree of consolidation is defined by the dimensionless time factor T_v as:

$$T_v = \frac{c_v t}{L^2} \tag{4.8}$$

Where c_v - coefficient of consolidation

t - time

L - drainage path length

Relating the same time factor or degree of consolidation in model and prototype gives:

$$\frac{c_{v,m} t_m}{L_m^2} = \frac{c_{v,p} t_p}{L_p^2} \tag{4.9}$$

and

$$\frac{L_m^2}{L_p^2} = \frac{1}{N^2} \tag{4.10}$$

which gives,

$$t_m = \frac{1}{N^2} \frac{c_{v,p} t_p}{c_{v,m}} \tag{4.11}$$

By using the same soil from the prototype, the scale factor for consolidation and time in the model is $1/N^2$. This increase in the speed of modelling time dependent events owing to the reduced scale of geometry in the centrifuge allows events to be observed in minutes or hours that would otherwise take months or years at prototype scale. For example, in a $1/100^{th}$ scale test at a 100 *g*, a period of one minute equates to approximately one week at the prototype scale. Time related events such as grouting and excavation are controlled by seepage. It is the seepage law in centrifuge modelling that implies the time scaling advantage in the simulation of events.

Using the seepage scaling law, Equation 4.12 describes the relationship between time in the model and prototype in the context of seepage by considering the different soil permeabilities;

$$t_m = \frac{1}{N^2}\frac{k_p}{k_m}t_p \tag{4.12}$$

Where k - coefficient of permeability (m/s).

Notwithstanding the rewards in modelling seepage related events in the centrifuge, the extremely low permeability of clay soils such as London Clay deem it unfavourable for use. This is owing to the extended time required for sample consolidation and achieving effective stress equilibrium conditions. It is therefore advisable to use a more permeable clay such as Speswhite kaolin. Kaolin is a comparatively coarser grained clay with a relatively high permeability. Consequently, a kaolin clay sample can be rapidly consolidated, minimising the model preparation and centrifuge test duration down to a window of two weeks as opposed to several months for London Clay, McNamara (2001).

4.4 Scaling effects and errors

It is not possible to replicate precisely all the details of the prototype through physical modelling. This necessitates approximations to be made and to recognise the errors and effects of these and their influence on the model. The errors and effects relevant to this study are discussed in the following sections.

4.4.1 Vertical acceleration field

For the purpose of problems encountered in civil engineering Earth's gravity is uniform for the practical range of soil depths, Taylor (1995). In contrast the centrifuge generates a non-linear acceleration field through the model depth owing to the variation in radius from the centre of rotation over the height of the model as can be seen from Equation 4.1 and Figure 4.1. It thus becomes necessary to carefully select an effective radius for which the average gravity scaling factor N is determined, Taylor (1995), through Equation 4.13. This restricts the errors in vertical stresses between model and prototype.

$$Ng = \omega^2 R_e \tag{4.13}$$

Where R_e - effective radius of model (m).

Taylor (1995) showed through detailed calculations that the coincidence of model and prototype vertical stresses occur at two thirds of the model depth from its surface. The

maximum difference between model and prototype stresses occur at the base of soil model, described as the maximum over-stress and the maximum under-stress occurs one third from the model surface. By considering the relative magnitudes of under and over-stress, depicted by the hatched areas in Figure 4.2, it is possible to show that the effective radius to minimise the error in stress distribution can be found from Equation 4.14.

$$R_e = R_t + \frac{h_m}{3} \tag{4.14}$$

Where R_t - radius to the top of the soil

h_m - height of soil in model

Generally, for most geotechnical centrifuges, where h_m/R_e is less than 0.2, the maximum error in the stress profile is less than 3% of the prototype stress.

4.4.2 Rotational acceleration field

Stewart (1989) described the radial acceleration field acting in a direction that passes through the axis of rotation of the centrifuge. The lateral component of this acceleration field imposes an error in principal stress magnitude and direction within the reference frame of the soil. Consider a model setup such that the centre line of the soil, perpendicular to the plane at the model base, passes through the axis of rotation, as depicted in Figure 4.3. In moving along a direction normal to this line, horizontally within the reference frame of the model, the direction and magnitude of acceleration and hence the principal stresses change with the radius to the axis of rotation, Grant (1998). The greatest lateral acceleration will occur at the shortest model radius, the soil surface and largest offset from the centre line (i.e. the model boundaries). Logically it follows that any critical measurements be taken along the centre line of the model, Stewart (1989), and where feasible events occur near the centre of the model. McNamara (2001) suggested orientating the smallest dimension, or minor axis of the strongbox such that it is tangential to the circle describing the rotational path of the model to minimise these effects. With a maximum radius of 1.8 m and model soil dimensions ± 0.1 m from the centre line, McNamara (2001) stated that maximum horizontal accelerations were approximately 5% of the vertical for a typical plane strain strongbox used on the geotechnical centrifuge at City, University of London.

4.4.3 Particle size

One of the key purposes of physical modelling is to replicate the stress-strain behaviour expected in the prototype. In centrifuge modelling the scaling laws apply to both model dimension and soil grain size. It would therefore appear logical to apply this scaling to the soil thus increasing the particle size, where a fine sand in a 1:100 scale model might be thought of as representing a gravel. However, Taylor (1995) states that using this same argument, a clay soil model could be thought of representing a fine sand at prototype scale. This clearly presents a flaw in the argument as the stress-strain characteristics of a fine sand are very different to that of a clay. At a high acceleration the soil grain size would be significant relative to the model dimensions and so it would be unlikely that the model would mobilise the same stress-strain curve as in the prototype, Taylor (1995). It is therefore implied that in conducting tests, the modeller use the same soil type as that of the prototype soil.

Speswhite kaolin clay was used for the tests in this study owing to its relatively high permeability, minimising sample preparation and test times as well as having well published characteristics (e.g. Al Tabbaa, 1987 and Grant, 1998). The main merit in choosing a laboratory clay like kaolin over a realistic prototype soil, such as London Clay, has been addressed in section 4.3. Taylor (1995) highlights the need to compare grain size with some important critical dimension in the model to assess potential problems of grain size effects. For coarse grained soil it is generally accepted that only when the grain size exceeds $1/30^{th}$ of the critical model dimension does a significant grain size effect become present.

For centrifuge tests using kaolin and modelling retained excavations previous researchers have compared the ratios between model wall dimensions and the kaolin grain size (2 μm) at model scale and at prototype scale under increased acceleration. Powrie (1986), Stewart (1989), Richards and Powrie (1998) and McNamara (2001) found ratios ranging between of $5x10^4$ and $6x10^6$. The model retaining wall height of 120 mm used for the 100 *g* tests carried out in this study imply ratios of $6x10^4$ and $6x10^6$ at model and prototype scale, respectively. With values lying with the range of previous work, the use of Speswhite kaolin in the model tests of this study can be justified.

4.4.4 Boundary effects

Scaling and boundary effects, imposed by the containment of the soil model and the implicit restrictions from the available centrifuge swing bed plan area and clearance height, provide definition of the scaling ranges available in replicating the prototype. This limitation dictated the use of a plane strain model for this study. Phillips (1995) gives guidance on soil containers and states that the geotechnical centrifuge model is normally used in simulating the behaviour of an infinite half space with a local disturbance. Therefore, the boundaries of the container should replicate the behaviour of the far field half space. In replicating static events, particularly in plane strain, it is necessary to create one dimensional consolidation boundaries which are ideally frictionless and rigid walls to prevent out of plane soil displacement. However, it is not possible in practice to have container walls that are completely frictionless. In clay tests, Phillips (1995) highlighted that this wall friction can be reduced by lubricating the smooth walls with water resistant grease. The effects of side wall friction on the event being modelled can be further reduced, especially for plane strain models, by ensuring that the strongbox is sufficiently wide. This ensures that side wall friction is not a significant proportion of the resisting forces. Phillips (1995) suggested, for two and three-dimensional models the length should be twice as long as the soil depth. Another means suggested by which the effect of side wall friction can be reduced is to take measurements along the centre line of the model, away from the boundaries.

The rectangular strongbox used for this study was constructed from 6082-T651 aluminium plates with an internal plan area of 550 x 200 mm. The depth of clay was limited to 300 mm to allow a clear view of the cross section of the model through an 85 mm thick Perspex window on the front face of the plane strain model. For the tests in this study, Castrol Spheerol EPL-2 (a general bearing and gearbox lithium-based grease) was used. It was selected based on its very good resistance to water and wash-out, mechanical stability and availability. The right internal face of the strongbox wall represented the line of symmetry of the excavation cross section as viewed from the Perspex window. Grant (1998) highlighted the need to use high viscosity lubricants to minimise the friction component of sliding between the clay and Perspex. It was suggested that lower viscosity lubricant did not ensure sufficient cover between the soil and Perspex. For this study a thin layer of silicone fluid with a viscosity of 12500 cS was applied to the inside face of the Perspex window prior to securing to the model. The high

viscosity of this lubricant aimed to ensure that the clay was not in contact with the Perspex surface through the test.

4.5 The geotechnical centrifuge testing facility

The Research Centre for Multi Scale Geotechnical Engineering at City, University of London has a purpose built Acutronic 661 geotechnical centrifuge. The centre became only the third centre in the U.K. to have a geotechnical centrifuge testing facility when commissioned in 1989, Grant (1998). Since this time the facility has undergone several redevelopments, upgrades and modifications. The most recent and significant change was carried out in 2013-2014. During this time the centrifuge underwent a full offsite refurbishment carried out by Thomas Broadbent and Sons Ltd before being relocated to a newly constructed facility. In this process significant enhancements to the data acquisition and motion control systems were made whilst the testing programme described within this thesis was being conducted. This meant two initial tests in this study were conducted with the older facility and systems, described in detail by Grant (1998), McNamara *et al.* (2012) and Schofield and Taylor (1988). Figure 4.4 shows the schematic general arrangement of the facility prior to its upgrade. However, the main bulk of tests for this study were carried out in the new updated facility described herein and depicted in Figure 4.5.

4.6 The Acutronic 661 geotechnical centrifuge

The Acutronic 661 beam centrifuge is a 40 *g*/tonne machine with a swinging platform on the end of two parallel beam arms. It has a maximum operating speed of 345 rpm which gives 200 *g* acting approximately at an effective radius (R_e), of 1.5 m. This allows a maximum testing capacity of a 400 kg package at 100 *g* or a 200 kg package at 200 *g*. Figure 4.3 shows the important geometrical details for a typical 300 mm high plane strain model in an aluminium strongbox. The swinging platform has a working area of 500 x 720 mm in plan by 500 mm height, however a usable plan area of 330 x 720 mm is available at a height of 970 mm above the swing bed, in the central region between the beam arms. This space allows a variety of strong model containers of either rectangular or cylindrical form to be accommodated. The radius to the swinging platform bed inflight is 1.8 m allowing effective radii typically between 1.4 to 1.6 m to be achieved. The package weight and centrifuge are balanced by a 1.45 tonne counterweight. Its position is adjustable pre-flight via a geared screw mechanism. The centrifuge is directly driven through a gearbox by a 30 kW motor located beneath the central cast iron pedestal.

Continuous running of the centrifuge for at least two days is often required for clay soil models to establish effective stress equilibrium within the model. In order to allow safe unmanned running of the machine during this period, four strain gauged sensors are installed onto the stiffening flanges of the cast iron central pillar pedestal; the pedestal is fixed to the reinforced concrete floor using grouted anchors. The sensors provide real time feedback to the control flight computer which monitors any out of balance load which may be present during flight. A pre-set cut off out of balance load of 15 kN is set to provide a safety mechanism to prevent any damage to the machine, surrounding structure and model by shutting power to the drive motor and decelerating the beam and swing platform to a stationary state. In the tests reported any out of balance forces exceeding 3 kN monitored immediately after spinning up the package were reduced by stopping the centrifuge and adjusting the counterweight position by the amount calculated by the flight computer, before spinning back up to speed. This provided additional confidence in leaving the model continuously spinning unmanned overnight.

To minimise energy input required from the drive system, a fibreglass fairing is positioned on the leading edge of the swing. For safety and energy efficiency the entire rotating assembly is enclosed within a thick circular reinforced concrete structure accessed via a lockable steel frame reinforced curved fibreglass door which opens out into a foyer space. The entire space is closed off by a Kevlar safety door. Various interlocks are in place which immediately decelerate the centrifuge to a stop before allowing access for safety reasons. The internal walls are lined with an energy absorbent material to decelerate and retain objects in the rare event of any pieces of equipment or large fragments of debris coming loose from the swing during flight.

During flight the temperature within the enclosed circular space is maintained at room temperature by a 30 kW air conditioning system to offset the heat generated by the drive system and bearings. This prevents major fluctuations in signal outputs from temperature sensitive instrumentation and aids in maintaining a constant humidity in the room.

The centrifuge is operated and tests conducted from the safety of a separate control room. An isolated system is used solely for the operation and control of the centrifuge. Various slip ring and stator assemblies located above the central pillar of the centrifuge allow communication and control of the systems on board from the control room.

A slip ring interface panel (SRIP) located in the control room provides the key interface for communications of signals and control of power for many of the on board systems. It

is linked to an on board programmable logic controller and Ethernet switch via a single fibre optic cable connection which passes through a single channel fibre optic slip ring. The slip ring interface panel allows actuation of power for the 64 channel instrument junction boxes, a 64 channel signal filter and amplifier rack, the on board data logging, motion control and imaging PC (PXI), on board dimmable LED lighting driver, on board solenoids and rotary valves DC power supply and CCD camera power supply. Ethernet connections on the SRIP permit remote access and control of the PXI via a dedicated local area network connection to a PC in the control room.

A 16 channel electrical slip stack and stator assembly located on the central pillar provides additional interface for the video analogue output from the CCD camera, power for the motion control driver, switching signals for solenoid and rotary valves and dimming of the on board LED lights. The three latter functions are controlled via various switches on a secondary interface panel within the control room.

A 4 channel fluid slip stack and stator assembly with a 10 bar maximum working capacity allows two compressed air and two mains water pressure feeds to be supplied to the swing and model. The flow rate and pressure of these feeds is controlled via needle valves and pressure regulators located on a fluid control panel within the control room.

4.7 Data acquisition and motion control

Two 32 channel junction boxes mounted beside the swing bed provide an interface for various instruments types to be used with the model. The junction boxes are capable of providing a ±5 V, ±10 V and a variable voltage DC supply to the instruments. The output signals from instruments are passed through an on board signal conditioning rack. Here the signals pass through a low pass filter and can be amplified by 1, 2, 10, 100, 500 or 1000 times to account for sensitive low output voltage instruments such as pressure transducers and strain gauges. Different gains can be chosen to maximise the output voltage within the required working range of the instrument. Gains are selected to keep the amplified output voltage within a ±5 V range. The signals are then sent to a National Instruments data acquisition card (DAQ) for analogue to digital conversion and logging. The DAQ cards are located on board a National Instruments (NI) PXI chassis run and managed with a solid state PC controller. This permits the storage of instrument outputs onto a solid state memory. Custom designed LabVIEW software interfaces are used to initiate logging and monitor instrumentation response during flight via the SRIP and LAN connection to the remote PC in the control room.

Two on board rack mounted Maxon DC motor control driver boards are powered via the SRIP and a logic controller. These permit either axial or rotary motion through two independently controlled DC brush type Maxon motor assemblies with planetary reduction gearboxes and optical rotary encoders. The encoders allow either absolute or relative positions of the motor output shaft to be communicated back to the drivers which in turn feedback to the National Instruments motion controller card located within the PXI chassis. Actuation and control of these motors is achieved through NI Motion Assistant software installed on the PXI solid state PC.

The benefit of having both data acquisition and motion control interfaced through the PXI is that they can be controlled via the single remote control room PC and actuation of the motors can be easily tied in with instrument response.

4.8 Instrumentation and calibration

To investigate the response of grouting behind the model retaining wall during and after excavation it was necessary to monitor ground movements, pore water pressures and total fluid pressures in the model.

Linear variable differential transformers (LVDTs) with a stroke of ±15 mm and ±5 V outputs at each extreme were used to monitor vertical displacement of the retained soil surface. For all tests a minimum of seven LVDTs were located at longitudinal distances 0.25, 0.5, 1.0, 1.5, 2.0, 2.5 and 3.0 times the excavation depth, H behind the model wall with an additional LVDT on top of the wall centre line. For the final four tests in the study, where grouting was carried at distance x= 0.75H behind the wall, an additional LVDT was placed at the corresponding position on the soil surface. The LVDTs were calibrated prior to each test against a modified micrometre at 1 mm intervals over a ±8 mm range from their mid stroke position. The LVDTs used had the capacity to measure accurately displacements to a resolution of ±10 μm.

Two GE Druck PDCR-81 miniature pore water pressure transducers (PPTs) were used to measure changes in pore water pressure during inflight consolidation and establishment of effective stress equilibrium. A third miniature pore pressure transducer was used in close proximity to the injection points for each grouting test to measure the injection induced pore water response. Porous ceramic stones fixed within the stainless steel housing on the face of the pore pressure transducers in front of the diaphragm permitted only the pore water pressure within the soil to be measured. The pore pressure transducers

were calibrated prior to installation before each test. Each pore pressure transducer was inserted into a port of a distilled water filled de-airing chamber. A vacuum pressure of -100 kPa was applied to the chamber to ensure the stone and void behind it were fully de-aired and saturated with water for correct measurement of pore pressures. The de-airing chamber was then pressurised and the times 10 gain transducer output voltage recorded via the PXI PC against a calibrated Druck DPI101 Digital Pressure Indicator (DPI). This provided an output voltage of 0.8 V over the 300 kPa working range of the PPTs.

A de-stoned PDCR-81 pore pressure transducer was used as a total pressure transducer (PT) for measuring the heavy Sodium polytungstate support fluid pressure at formation level internally within the latex bag which supported the excavation (discussed further in section 5.2.6). This pressure transducer was calibrated along with the PPTs previously discussed. An XP5 miniature flush diaphragm pressure transducer, manufactured by Measurement Specialties Ltd, with a 5 bar working range was also used externally to the excavation to confirm the heavy fluid support pressure. A Druck PDCR810 pressure transducer with a 15 bar working range was used in the base of the standpipe assembly (discussed in section 5.2.6) to confirm the water head pressure in the standpipe and verify the level of the water table being imposed on the model. The XP5 and PDCR810 pressure transducers were calibrated directly against the DPI within a 2.5 bar and 3.5 bar range, respectively, given the pressures expected for each transducer in the model tests.

Two additional PDCR810 pressure transducers were also used to measure fluid pressures within the injection system. One was located at the injection system ‘pump’ source and the second in the injection manifold, as detailed in sections 5.2.3 and 5.2.6. For the initial two injection grouting tests 60 bar range pressure transducers were selected owing to availability and some uncertainty in maximum grouting pressure that would be achieved. Following these tests another two available PCDR 810 pressure transducers with a 3.5 bar working range were selected instead for all subsequent tests. These were calibrated against a Budenberg dead weight tester using hydraulic oil whilst connected to the logging PXI. This method allowed the pressure transducers to be calibrated against more stable pressures up to 20 bar when compared to the DPI.

4.9 Digital imaging and analysis

Two machine vision 5 megapixel CMOS USB cameras manufactured by The Imaging Source GmbH were available to provide live video feeds and allow image capturing via the on-board NI PXI PC and LabVIEW software. For the series of tests undertaken in this study one of these cameras was used to monitor and confirm actuation of the Maxon DC motor used during the tests.

Small charged coupled device (CCD) cameras were mounted to a frame behind the fibre glass fairing to enable a view of the front plane of the model through the 80 mm Perspex window. The analogue live feed signals from the cameras were fed to an isolated monitor and dedicated image capturing PC in the control room. An in-house designed image capturing software allowed the digital conversion of images from the live feeds. The software allowed correlation of the images to instrumentation data during tests via manual logging of the image epoch number against the sample counter within the LabVIEW logging program. The first two baseline tests conducted in this study, using the previous centrifuge facility setup (see Figure 4.4), used two CCD cameras to capture the full extent of the front model plane. Figure 4.6 shows the arrangement and extent of the model captured using this arrangement. Following the upgrade of the facility (see Figure 4.5), only one of these CCD cameras was available. It was positioned to focus on the predominant area of soil movement and grouting response for subsequent tests. Figure 4.7 shows the single CCD camera arrangement and typical field of view obtained. Positioning the camera central axis perpendicular to the front model plane reduced distortions of the images towards the edges as highlighted by McNamara (2001).

The camera and image capturing setup formed the basis of the image processing system used in conjunction with these tests. It was developed as a joint research study at City, University of London and described in detail by Taylor *et al.* (1998) and Grant (1998). The system enabled subsurface movements of the soil and model retaining wall to be monitored during the plane strain tests through the Perspex window. During model preparation a 10 mm spaced grid of black marker beads (3 mm diameter by 6 mm long cylinders) were pressed into the front clay surface to give discrete observable targets. The method of tracking the position of these embedded targets relative to fixed targets, of known position, etched into the Perspex window face in contact with the soil revolves around the use of close range photogrammetry. Much of the background to close range photogrammetry is given by Cooper and Robson (1996) and details of the image analysis system by Taylor *et al.* (1998).

For the dual CCD camera setup (see Figure 4.6) different capturing frequencies were used during the various stages of the model being on the swing. During initial spin up image capturing was set at 2 second intervals and then adjusted to 20 minute intervals during the pre-test consolidation period. For the test, the frequency was returned to 2 second intervals. McNamara (2001) reported this to be the smallest frequency possible to maintain correlation and synchronicity between the two sets of images from the two cameras. In all subsequent tests using the single CCD camera setup (see Figure 4.7) it was possible to use a capturing frequency of 1 second during spin up and the test phase. A 20 minute interval was still used during the pre-test consolidation period.

5. MODEL AND APPARATUS DEVELOPMENT

Previous approaches in the physical modelling of excavations and compensation grouting are discussed in the context of model design requirements for this study. The design and development of apparatus used in modelling the excavation is presented. A discussion is provided on the continual development of the method and apparatus carried out to model compensation grouting inflight. Model preparations and test procedures are also described.

5.1 Model design requirements

5.1.1 Excavation modelling

In modelling excavation processes on the centrifuge it is necessary to simulate the stress path associated with construction and excavation as closely as possible. This often requires consideration of various aspects and their effects such as, wall type and installation, reduction of vertical and horizontal stresses in excavation of soil and installation of bracing systems. The four main available techniques in modelling excavations on the centrifuge are summarised in Table 5.1. Lam *et al.* (2012) concluded that their inflight excavation technique provided appropriate initial ground conditions before excavation and enabled realistic progressive development of passive resistance on the excavation side with removal of actual soil and installation of props at multiple levels. The inherent complexity, difficulty and time required in developing such apparatus for this study was considered unfeasible in light of the expected complexity in developing compensation grouting equipment. In view of this it was decided to simplify the excavation process by preforming the excavation profile before flight and use a heavy fluid to support the excavation before the test. Use of specially fabricated templates and jigs provided a consistent and accurate excavation profile between tests. Although the technique of draining a heavy fluid suffers from the introduction of pre-excavation lateral wall movements and bending moments, Lam *et al.* (2012), it was considered to offer a simplistic, quick and consistent method of modelling the excavation in this study.

Previous centrifuge modellers (i.e. Elshafie, 2008 and McNamara, 2001) have made use of two independent, contained mediums to provide horizontal (wall) and vertical (formation level) support pressures to their pre-cut excavation inflight, as pictured in Figure 5.1. Independent control of the drainage of a heavy fluid and either compressed air or another heavy fluid allowed a stress reduction profile to be maintained to mimic the expected stress reduction path in the field. A stiff separating plate was provided between

the two fluids to prevent interaction of the applied pressures. Although this is a simpler system to allow better modelling of the excavation process, McNamara (2001) reported that carrying out the excavation process during the tests was complicated and often required several people to assist in the procedure. Iterations were also required in the design of a stiff separating plate to prevent its interaction with the expected soil heave. In view of this it was decided to adopt a single contained supporting heavy fluid system to provide both vertical and horizontal support pressures during flight in the model tests within this study. The need to maintain the research focus on soil and wall response to compensation grouting further justified this approach.

With the heavy fluid drainage approach, both McNamara (2001) and Elshafie (2008) highlighted the need to control supporting fluid drainage rates. McNamara (2001) permitted free drainage of the contained heavy fluid into a vented reservoir located beside the model through small bore pipe work. The compressed air, supporting the excavation base, within a specially formed latex bag was simultaneously reduced to provide the required stress reduction profile. A solenoid connected to the drainage pipework permitted a three staged excavation process to be modelled to allow actuation of hydraulic props between each stage. The total time for heavy fluid drainage and compressed air reduction was reported to be about 4 minutes in the 100 *g* tests. McNamara (2001) noted a slight and gradual decrease in the drainage flow rate leading to a non-linear stress reduction path owing to the falling heavy fluid head. This resulted in the later stages of the simulation process taking considerably longer than the initial stages. However, the response from locally installed pore pressure transducers provided confidence in the entire event being modelled as an undrained event. Alternatively, Elshafie (2008) used different sized orifice plates and pipe lengths to control the drainage flow rate of his two separate supporting fluids to model the excavation in sand. The orifice plates were sized to provide a more linear reduction of the fluid levels and maintain the difference required in horizontal and vertical support pressures during drainage. The total simulation time of the excavation process was reported to be approximately 12.5 minutes for the 75 *g* tests in sand.

In light of the lessons learnt from these two methods it was decided to develop a piston pump to provide better control of the supporting heavy fluid to be used in this study. Use of a sealed pump system to withdraw the heavy fluid was considered to allow a controlled linear reduction of the fluid level and pressures and also permit pauses to enable grouting to be initiated in later grout injection tests. The details of the system developed to permit

simulation of the excavation process are discussed in section 5.2.4. However, owing to limitations in space and problems with consistent performance it was later decided to adopt the free drainage approach, described by McNamara (2001), for simplicity.

5.1.2 Compensation grouting modelling

Various approaches have been adopted in the physical modelling of compensation grouting techniques. Bolton *et al.* (1994) and Chin and Bolton (1999) reported their work investigating factors influencing fracture grouting in heavily overconsolidated clay in a mini drum centrifuge. A series of tests using a single part adhesive with no solid suspensions and dyed water were carried out to study fracture behaviour. Delivery was made through an embedded 3 mm internal diameter brass injection pipe with a Dural nozzle tip to encourage fracturing of the soil. Figure 5.2 shows a schematic of the model and apparatus setup. Use of a single part adhesive prevented the issue of rapid solids separation from the liquid medium and consequent potential blockage of the injection system under the increased acceleration field. To allow post-test inspection of the adhesive injection it was necessary to set the resin within the model in an oven as it did not gel within the duration of the test. In the unset state it would have been possible for the injected adhesive mass to deform under the soil self-weight and consequently affect the observed compensation effect. It would have therefore been necessary, if using a resin or adhesive, in the grouting tests for this study to use a material that set within a relatively short time frame after injection. Consideration would have also had to be made in dealing with the increased rate of the solid-fluid separation effect when using any form of suspension 'grout' in the centrifuge tests in this study.

Lu (1996) developed a series of apparatus with varying success to model compaction grouting in front of an advancing tunnel head in a soft kaolin clay model. A positive displacement pump was initially developed using compressed air to drive the piston to inject a fine cement paste into the clay model. However, constriction of the injection syringe at the outlet significantly increased the grout injection pressure causing consolidation of the grout medium. The water was found to separate from the formed paste and the solids created a dense filter cake plug thus completely blocking the pump. A peristaltic pump system was also initially developed however it was found a suitable grout to work with this system would require a very high water content and would only allow fracture grouting with a high level of bleeding. This bleeding effect would have been detrimental to the compaction grouting effect. The final solution developed and implemented, illustrated in Figure 5.3, allowed the injection of dry sand to create a dense

grout bulb using an Archimedes screw to feed the sand into the model from a hopper. Owing to the large size and single point injection ability of this system it was considered unfeasible for this study. The injection of a sand grout bulb would also create a permeable drain within the clay model, affecting the pore pressure response of the soil around the bulb and the excavation and consequently the compensation effect observed from compaction grouting.

Au (2001) carried out a series of 1 *g* test with a modified oedometer, injecting different materials to model fracture and compaction grouting in normal and overconsolidated kaolin clay, seen in Figure 5.4. Injections were delivered through a 3 mm internal diameter copper tube. Computer controlled piston pumps were used to inject grout into the models. Idealised compaction grouting was modelled with the expansion of a 1.2 mm thick latex balloon dipped and sealed onto the end of the injection tube, with the injection of water and single part epoxy resin, shown in Figure 5.5. A sealed system was used to ensure the injected volume remained the same. The short gel time epoxy resin used allowed the injected mass to set and retain its shape shortly after injection. Fracture grouting was modelled with the injection of dyed water, Laponite-water mixture, epoxy resin and a cement-bentonite grout through the open end of the injection tube. The injection of dyed water and Laponite were shown to bleed significantly and allowed the fracture to collapse shortly after making it difficult to trace the path and shape of the fracture. It was for these reasons that mainly epoxy resin and the cement bentonite grouts were used which provided greater compensation grouting efficiencies. It was necessary to mix the cement bentonite grout with a high water cement ratio of up to 0.6 to prevent the separation effect previously observed by Lu (1996) and permit injection within the capacity of the piston pump system.

In developing apparatus for this study it was clear from previous work it would be necessary to use a quick setting grout to truly assess the impact of grouting on the soil surface and model excavation. Initially a prototype inflight rotating mixer for the grout was fabricated to allow containment, mixing and injection of two part resin grouts into the soil model. The mixer was intended to permit the use of suspension grouts in the centrifuge without the problems of fluid solid separation. It was intended to use grouts of different viscosity with and without filler to allow simulation of compaction and fracture grouting. A disposable piston pump was also developed to receive the mixed grout from the mixer and allow injection into the model directly through a model scale tube à manchette embedded into the model behind the retaining wall.

Approximately two years of the study were spent on the development of the inflight mixer and cradle system, disposable piston pump and exploring different grouts. Following a critical review of the apparatus development progress, it was decided to abandon this approach of simulating grouting in the centrifuge model. Several hurdles, such as determining the mixer rotational speed to maintain suspension and developing the system for reliability, were evaluated to require significantly more time and work owing to its complexity. Consequently, a much simpler idealised approach and apparatus was developed to deliver and simulate compensation grouting, as discussed in section 5.2.5.

Consideration of the problems experienced when using high viscosity, non-Newtonian suspensions as a grout (e.g. resin, slurries) on the centrifuge led to the decision to use a single-phase Newtonian fluid. This provided a more confident understanding of its behaviour inflight when pumped and would also be less demanding on the pumping system. Water was selected owing to its very low viscosity. With known properties and behaviour, water would require much lower injection pressures to mobilise and deliver it into the model via the injection tubes, discussed in section 5.2.5. However, owing to the detrimental bleeding effect shown previously with injection of water it was clear the injected volume would need to be contained within an expandable impermeable membrane. This limited the injections to be carried out within the test to be more akin to compaction grouting than fracture grouting, thus determining the focus of this research. It was also acknowledged that the injected water 'grout' would also not set or gel like a typical grout and had no shear strength. Both of these characteristics of the grout injection material were expected to produce different behaviours when injected into the soil behind the excavation in comparison to a typical suspended particulate setting and higher viscosity grout adopted in the field.

5.2 Apparatus design and development

5.2.1 Strongbox and model boundary conditions

All centrifuge tests conducted within this study were carried out using a rectangular aluminium strongbox (shown in Figure 5.6). The internal dimensions were 550 x 200 mm in plan by 375 mm in height. The left and right side walls and base of the box were constructed from 38.1 mm thick aluminium plate. The back and front walls were constructed from 25.4 mm thick plate. These were stiffened using 76.2 x 50.8 x 6.35 mm thick aluminium channels bolted along the length of the plates. The channels and thick side walls minimised lateral deflection of the soil. This maintained one dimensional

consolidation boundaries in the press and plane strain conditions in the centrifuge tests. All aluminium surfaces of the strongbox, particularly the smooth internal faces in contact with the clay, were anodised. This was necessary to prevent pitting of the surface owing to the de-ionised water used in the model and consequent increase in friction between boundaries and soil. The surface of the base plate had 3 mm radius drainage grooves machined in a herringbone pattern which were connected to drainage valves located externally on the left and right side wall plates. For all tests a 3 mm thick porous plastic layer and filter paper were placed above the drainage grooves. This setup provided a drainage path for pore water to freely drain during consolidation in the press and for pore pressure equalisation in the centrifuge. It also prevented any clay escaping and blocking the drainage channels that would influence the intended water table set. The front plate of the strongbox was detached, following removal of the sample from the consolidation press, to provide access to the clay for model preparation. Following the model preparation process, the front plate was replaced with the clear 85 mm thick Perspex window, mentioned in section 4.4.4. This thickness was found to prevent out of plane movement of the soil owing to the self-weight of the model soil inflight. The rear aluminium plate of the strongbox was used for the insertion of pore pressure transducers (see section 4.8 and 5.2.6) and the grouting injection tubes (discussed in section 5.2.5) via machined G1/4 BSPP (British Standard Pipe Parallel) threaded holes and brass compression fittings.

Figure 5.7 illustrates schematically the model geometry adopted for the simulation of the model excavation. A wall, 120 mm deep (H) with a 40 mm embedment (D) was used to model a prototype 12 m deep retained excavation with a 4 m deep embedded toe. The depth of clay below the retained surface was 297 mm and 180 mm below the formation level. A stiff fixed prop was provided at the crest of the excavation. This geometry left the retained soil extending a distance x= 3.25H behind the wall towards the left strongbox wall boundary, 1.5H below the formation surface and d= 2.5H below the retained soil surface. McNamara (2001), with the exception of the propping system, adopted a similar excavation geometry, stress history and centrifuge acceleration scale factor, N, equal to 100. It was shown with these tests that significant vertical surface settlement extended only as far back as 3H; this was within the far left boundary of the strongbox and was consistent with influence zones expressed in the literature, discussed in chapter 2.

Modelling of the half space is common practice with plane strain centrifuge models; a half excavation width, B, of about 160 mm at model scale equating to 16 m at 100 *g* was

adopted. The right strongbox wall provided a line of symmetry to the finite excavation width throughout the centrifuge testing series. This geometry was selected as it was considered representative of a practical excavation geometry that might be expected in an urban environment. Initial calculations showed this formation half width to be approximately 2.2 times larger than the expected width of the theoretical passive Coulomb failure wedge, approximately 70 mm (for ϕ_{cs}'=23.5^0, K_p≈3, assuming a wall friction angle δ=ϕ_{cs}'/2). Padfield and Mair (1984) highlighted the influence of wall friction on the stress field near the wall resulting in a curved failure zone, seen in Figure 5.8. This curvature worked to reduce the extent of the failure zone in front of the wall. Although the model wall used could not be considered to have a wall friction expected for a concrete or steel wall this calculation provided confidence in the limiting influence of the boundary wall on the formation. It was also appreciated that the expected passive side failure mechanism made no consideration of wall flexibility, propping system or soil movements.

5.2.2 Soil properties and stress history

The benefits of using kaolin clay for centrifuge tests in this study has been previously discussed in chapter 4. Table 5.2 details the engineering properties of the Speswhite kaolin clay used. The kaolin clay was sourced from IMERYS Minerals Ltd in powder form and is commercially available as Speswhite Quality China clay.

Previous modelling of excavation in clay soils in the centrifuge (i.e. Powrie, 1986 and Richards and Powrie, 1998) have been carried out on stiff overconsolidated samples, consolidated to 1250 kPa and then swelled to 80 kPa. For this study, it was considered preferable to use a less stiff overconsolidated soil, for the initial baseline test, principally to verify if measurable movements were achieved and make adjustments to the soil pre-consolidation pressures for remaining tests, if necessary. It was desirable to have a soil stiffness and strength that provided a measurable response with the compensation grouting injection in the later tests.

Kopsalidou (2000) and McNamara (2001) conducted a series of numerical analyses prior to centrifuge tests conducted by McNamara (2001). The focus of these analyses was to identify a suitable stress history and magnitudes of displacement expected in the centrifuge tests. McNamara (2001) used a one dimensional consolidation pressure of 500 kPa followed by swelling to 250 kPa prior to further consolidation and pore pressure equalisation in the centrifuge. With a similar model geometry but stiffer excavation

support system, relative to that adopted for this study, McNamara (2001) reported vertical surface settlements and horizontal wall displacement in the order of 1 mm. The adoption of a more flexible wall and less stiff support system, discussed in section 5.2.4, with this stress history was expected to provide soil movements of larger magnitude than those observed by McNamara (2001).

A water table set 25 mm below the retained clay surface along the model centre line was adopted. A lower than expected standpipe pressure was observed in an early excavation only baseline test after spinning up, owing to an unknown leak in the standpipe assemble, described in section 5.2.3. An attempt was made shortly after spinning up to correct the leak with no success. This lead to the establishment of lower unknown level of water table below surface. The impact of the lower unknown water table in this early test, 2HH is discussed further in chapter 6. Following test 2HH the O-ring seals in the standpipe assembly were changed. The assembly was filled with water and outlets sealed before being pressure tested on the bench to the working pressures expected inflight to avoid a reoccurrence in subsequent tests.

Adopting a water table 25 mm below the clay surface provided an increased effective overburden stress near the top surface of the retained clay behind the wall to prevent potential blow out of soil in later grout injection test events. The overconsolidation ratio (OCR) variation with depth of the models at 100 *g,* following one-dimensional compression of the clay samples to 500 kPa is presented in Figure 5.9. Using Equation 5.1, after Mayne and Kulhawy (1982), and the Speswhite kaolin clay properties in Table 5.2 the resulting theoretical variation of K_o with depth was found, as shown in Figure 5.10. Consequently, the theoretical vertical and horizontal total and effective stresses were determined using the saturated bulk unit weight of the clay γ_{sat}= 17.44 kN/m^3, shown in Figure 5.11, using the known pore pressure distributions associated with the water tables.

$$K_o = (1 - \sin\phi'_{cs}).OCR^{\sin\phi'_{cs}} \tag{5.1}$$

Previous researchers (Grant, 1998; McNamara, 2001; Rose, 2012; Divall, 2013 and Gorasia, 2013) found that adopting the same stress history described above generated a medium to stiff clay soil model with S_u ranging between about 40 and 80 kPa, increasing with depth.

5.2.3 Ground water supply

A standpipe assembly located adjacent to the strongbox on the swing, illustrated in Figure 5.12, was used to provide the ground water supply to the clay model. Water was continuously supplied to the assembly via a channel on the fluid slip ring. The water table level, discussed in section 5.2.2, in the clay model was set by the adjustable overflow pipe height within the assembly. The top of the overflow pipe was set to coincide with the radius from the centre of rotation to the top of the water table along the longitudinal model centre line (see Figure 5.12). This setup allowed a constant head of water to be maintained within the standpipe and was monitored using a pressure transducer mounted in the base. Nylon pipe (8 mm external diameter and 6 mm bore) was used to connect the standpipe water column to the soil model through the base of the strongbox.

5.2.4 Model excavation apparatus

5.2.4.1 Model retaining wall and prop

A decision was made relatively early in the study to use a single prop arrangement at the crest of the excavation that would represent a stiff support. The use of a single prop with the model wall versus a multi propped excavation was understood to provide a sufficiently low support system stiffness to allow measurable movements to be generated that could be potentially be compensation for in the later grouting tests.

The model wall used throughout this study is illustrated in Figure 5.13. The rectangular wall measuring 225 mm in height by 190 mm width was made from Acetal Copolymer (POM-C) (E_{Acetal} = 2.8 GPa) supplied by Bay Plastics Ltd, and was machined to a thickness of 8.65 +0.1 mm. This thickness provided a model wall with a prototype scale bending stiffness of 1.52 x 10^5 kNm^2/m length, corresponding to a prototype concrete wall approximately 0.4 m thick (assuming $E_{concrete}$ = 30 GPa). This prototype bending stiffness was also equal to that of the stiffest sheet pile wall section commercially available, PU32, manufactured by ArcelorMittal (assuming E_{steel} = 205 GPa) that can be installed in a stiff clay.

The wall was made 10 mm narrower than the width of the strongbox to make provisions for seals which would prevent seepage of water from the retained soil into the excavation following its simulation. The white silicone rubber seals, shown in Figure 5.14, were cast from Zhermack HT45 RTV silicone mould making compound, supplied by W.P. Notcutt Ltd. The 6 mm projection from the model wall sides provided 1 mm compression of the

seal profiles against the back wall of strongbox and Perspex window. To prevent excessive friction from this compression that may have provided restraint to the wall, the seal profile was formed with a concave recess for the provision of silicone grease. The addition of grease also enhanced the water retaining effects of the seals. The seals were cast around Acetal pins inserted into the ends of the wall at 20 mm vertical centres to secure the seals to the wall, see Figures 5.13 and 5.14.

In order to monitor the profile and lateral deflections of the wall during excavation and subsequent compensation grouting it was decided to use black tracking targets similar to those used to monitor subsurface soil movements, discussed in section 4.9. The black targets were embedded into the front silicone rubber seal during the casting process at 10 mm vertical centres, shown in Figure 5.15.

Figure 5.16 shows the details of the prop. The prop plate was fabricated from 12 mm thick aluminium plate. A width of 199.8 mm allowed a 0.1 mm clearance between the prop, Perspex window and strongbox back plate. The length of the prop plate was machined to 151.25 mm to allow for the model wall thickness within the pre-cut excavation box and ensure the wall was pushed back, such that the back face of the wall was in contact with the retained soil vertical face. Although a stiff prop was required it was necessary to minimise rotational restraint of the wall at the prop level. Consequently, the front edge in contact with the wall was reduced to a thickness of 3 mm extending back 10 mm from the wall (see Figure 5.16).

The prop plate was held in position using the support frame and bolt spacers, illustrated in Figure 5.17, with the support frame bolted down above the strongbox to prevent any movement of the prop. Figure 5.18 illustrates the prop, support frame and space configuration within the strongbox and model. The prop plate had a 12 mm diameter hole machined to allow the collar of the excavation support latex bag, discussed in section 5.2.4.2, to be secured using an aluminium collar clamp, shown in Figure 5.19. The hole and clamp arrangement allowed filling of the latex bag with the heavy support fluid and its venting to atmosphere during the test.

5.2.4.2 Excavation simulation

Previous centrifuge studies modelling excavations have made use of toxic and corrosive solutions such as zinc chloride (i.e. Powrie, 1986; Stewart, 1989 and Richards, 1995) and safer but mildly corrosive zinc iodide (i.e. McNamara, 2001) to support pre-cut excavations inflight. The high solubility of the crystals of these compounds in water provide high density solutions. However as both solutions presented health hazards an alternative liquid was sought. Elshafie (2008) successfully used Sodium polytungstate solution as a replacement heavy fluid. The non-toxic, non-corrosive Sodium polytungstate solution (SPT) was supplied by Sometu Ltd in Germany at a specific gravity of 2.82. Its density, like the other heavy fluids used by previous researchers, could be reduced by adding distilled water or increased through evaporation of water from the solution.

Figure 5.11 shows the expected total horizontal and vertical stresses required from the Sodium polytungstate solution to support the excavation inflight. As the solution could only provide a lateral earth pressure coefficient, K equal to unity it was difficult to match the expected non-linear variation of horizontal total stress with depth. Figure 5.20 shows the difference between theoretical and imposed total vertical and horizontal stresses over the excavation depth. The solution was diluted to a specific gravity of 1.78 to match the saturated bulk unit weight for the kaolin clay of 17.44 kN/m^3. This ensured that the total vertical stress with depth provided by the fluid in front of the wall would match that provided by the soil behind it and prevent premature heaving of the formation level. Adopting this specific gravity with K_o=1 would result in the total horizontal stresses, provided by the fluid against the wall, to be less than those that would have been provided by the soil that was removed in front of the excavation during model making. As a consequence, it was accepted that during inflight consolidation and establishment of hydrostatic pore pressures the wall would be expected to move in slightly towards the excavation and up against the prop provided at the retained surface level.

Elshafie (2008) and McNamara (2001) both reported the benefit of using latex rubber bags as a separating membrane which provide little restraint to either wall or fluid because of the low material stiffness. The latex bag, shown in Figures 5.21 and 5.22, was used for all tests in this study. It was dipped from natural latex using a polypropylene former by Precision Dippings Ltd, U.K. The bag was designed to be 1 mm thick to avoid being easily punctured or damaged during model preparation or centrifuge testing. Natural latex

was selected for its semi-transparency which would allow visual inspection of the drainage of fluid from the bag during excavation simulation via the live camera feed. The bag was constructed in two parts with an upper collar adhered to the lower section using liquid latex. The collar section allowed the latex bag to be secured to the prop plate using a collar clamp, see Figure 5.19, to prevent it collapsing and being potentially damaged during the test. The collar clamp also served to allow visual confirmation of the SPT fluid level during the filling process prior to spinning up.

It was considered desirable to limit the volume of SPT within the excavation to reduce the demand and time taken to drain the fluid. A solid polypropylene block measuring 200 x 25 x 90 mm, seen in Figure 5.18, was bolted to the underside of the prop plate against the right strongbox wall. The displaced volume of this block in consideration with the latex bag construction reduced the total volume needing to be drained to approximately 2700 ml.

The right strongbox wall had a 9.55 mm diameter clearance hole drilled at a 9.5 mm centre above formation level and a 19 mm diameter by 2.7 mm deep counter bore on the inside face, at this same position. This recess and hole allowed flush fitting of the SPT drainage fitting attached to the latex bag, illustrated in Figure 5.23, to permit draining of the SPT fluid with minimal influence on the formation heave expected during flight.

Figures 5.24 and 5.25 illustrate the key features and location of the heavy fluid piston pump used in this study. The heavy fluid pump was designed to allow a controlled drainage rate of the SPT in simulating the excavation process. A DC Maxon servo motor and 156:1 planetary reduction gearbox assembly drove two 5 mm pitched lead screws via a single drive and two counter spur gears with gear ratio of 1. Counter rotation of the left and right-handed lead screws permitted the ballnuts attached to a rigid travelling plate to be linearly actuated. The linear actuation of the plate allowed linear motion of the piston inside the cylinder. The piston was attached to the travelling plate via a 12 mm stainless steel rod. An aluminium cylinder and piston with an internal bore of 154.4 mm and maximum stroke of 170 mm provided a volumetric capacity of about 3180 ml. Drainage of the Sodium polytungstate solution was achieved by drawing the piston up using the drive mechanism. The heavy fluid pump was designed such that the fluid level when full, at the minimum piston stroke, was below the formation level of the excavation. This prevented any back flow of SPT into the excavation following simulation of the event, eliminating the need for isolation valves inflight. The heavy fluid pump was mounted

onto a 25 mm thick aluminium plate positioned behind the strongbox with 12 high tensile screws. The heavy fluid pump overhung the front edge of the swing by 135 mm owing to space restrictions on the swing bed. Gusset plates beneath this overhang stiffened and partially supported the weight of the heavy fluid pump against the front face of the swing. A 16 mm thick U shaped plate secured the heavy fluid pump to the top of the strongbox. The heavy fluid pump allowed drainage to simulate a staged excavation. This approach would allow for potential pauses in excavation to initiate grouting with movements observed from the LVDTs in later grout injection tests. Two initial baseline tests, 2HH and 3HH, made use of the heavy fluid pump to provide a reference of movements pertaining to excavation only. As no grouting was modelled in these tests it was thought appropriate to continually drain the fluid. However, owing to the bit count limit of the servo motor optical encoder, it was necessary to reset the control program twice during the excavation simulation. This resulted in a three staged excavation, with each stage equal to about 3.6-3.8 m deep excavations at prototype scale. Owing to the invert level of the outlet of the fitting, used to drain out the SPT being about 6 mm above the formation level, it was not possible to fully drain all the heavy fluid. The duration of each stage was approximately 2.5 minutes with a maximum delay of 30 seconds before commencement of the following stage. This equated to a total period of about 8.5 minutes at model scale or around 60 days at prototype scale.

Following a critical review of the apparatus after these tests, with consideration of the requirements for modelling compensation grouting, it was decided to abandon the heavy fluid pump and seek a simpler solution for simulating the excavation. This was due to the lack of consistency in withdrawing the heavy fluid during the last stage by the pump in both early tests. The large size of the heavy fluid pump assembly significantly limited access to the space behind the strongbox, where access would be required later for the grouting tests. Securing the heavy fluid pump on the swing and lowering the piston to inject the pre-filled Sodium polytungstate solution in the cylinder into the latex bag was also considered to be too time and labour intensive. Adoption of the gravity driven drainage approach utilised by McNamara (2001) and Elshafie (2008) was considered to provide a better consistency in the SPT drainage rate and time. It had been proven to be a simpler system requiring less time to prepare on the swing and operate during the test. Such a system would also reduce potential equipment failure and consequent abandonment of tests.

Figure 5.26 illustrates the revised apparatus used for simulating excavation. The cylinder from the heavy fluid pump was recycled to provide enough volumetric capacity and was modified to be vented to atmosphere. This cylinder is hereinafter referred to as the heavy fluid (HF) cylinder. Stainless steel tubing with a 1/8" diameter by 1/16" bore connected the SPT drainage manifold (discussed in section 5.2.6) to the cylinder via an actuated stainless steel plug valve assembly to initiate and control drainage. Initial calculations showed this size pipe with the length needed for connection would permit the SPT to drain in about 4 minutes or 28 days at prototype scale. A 110^0 rotary solenoid, manufactured by Magnet Shultz, seen in Figure 5.27 and driven by an on-board 70V DC power supply was used for the first grouting test (6HH) to actuate the plug valve. During this test the plug valve was shown to slowly rotate to a half open position. Post-test investigation revealed a misalignment of the coupling connecting the valve and solenoid and insufficient torque capacity to easily overcome the resulting internal friction within the plug valve, leading to its very slow actuation. To prevent a reoccurrence, the plug valve and solenoid assembly were cleaned, aligned and lubricated prior to each test with the actuation checked prior to spin up. Although this proved to be successful in the following two tests, 7HH and 8HH, better assurance was required in the actuation of the drainage plug valve and consequently a new geared motorised valve assembly was developed, illustrated in Figure 5.26. The motorised rotary valve assembly, consisted of the plug valve, manufactured by Hoke, connected via a coupling to the output shaft of a geared 12 V DC synchronous motor assembly. The motorised valve assembly provided up to 2 Nm of torque to rotate the plug valve 90^0 between its closed and open position in a period of 3 seconds. The new motorised valve assembly was used without fault from test 9HH onwards.

5.2.5 Compensation grouting apparatus

5.2.5.1 Grouting injection tubes

The initial concept to permit the modelling of compaction grouting was taken from pressuremeters which involve the controlled expansion of a cylindrical rubber membrane within a soil to determine soil strength and stiffness. Au (2001) successfully used the injection of grout into a latex balloon to simulate the development of idealised compaction grout bulbs. It was decided to adopt a similar method in the centrifuge model with the expansion of a latex sleeve by injection of the water 'grout' medium. Using a sealed latex sleeve would prevent any bleeding or penetration of the grout into the soil. Figures 5.28-5.30 show details of the grout injection tubes used for tests in this study. A typical

150 mm diameter tube á manchette at prototype scale would scale down to 1.5 mm diameter tube in the centrifuge at a 100 *g*. Use of such small diameter pipe work would lead to relatively large pressure losses owing to frictional losses and demand a larger pump capacity to achieve the required pressures to initiate grout injection. The pressure losses in the small bore pipe work would also consequently limit injection flow rates which is important when attempting to carry out an undrained event in the centrifuge. For these reason previous researchers (Au, 2001 and Chin and Bolton, 1999) have used larger bore piping, given the focus on the consequent soil behaviour to grout injection. This provided confidence in using similar larger bore pipework within the tests.

Natural rubber latex sleeves dipped by Chainbond Ltd, U.K. using 4 mm diameter aluminium rods as formers with a specified thickness of 1.5 mm + 0.1 mm/-0.2 mm. This tolerance had to be allowed for owing to the manual dipping process involved. The wall thickness was chosen as it would provide sufficient resistance against tearing or bursting with the expected injection pressures.

To permit expansion of these sleeves by the injected water and prevent collapsing under the soil self-weight during flight it was necessary to provide an internal supporting mandrel. High pressure flexible Nylon pipe (6 mm external diameter and 4 mm internal bore) 400 mm in length was used to support the latex within the clay during consolidation. This length also provided easier connection of the injection tubes to the injection system piping outside the strongbox, described in section 5.2.5.2. To encourage the uniform expansion of a cylinder during injection to simulate plane strain compaction grouting, 2 mm diameter outlet holes were provided at regular intervals. The holes were machined at the quadrants of the circular cross section, as illustrated in Figures 5.28-5.30, at 15 mm centres. The grout tubes were inserted into the model in the orientation indicated in Figures 5.28-5.29. The holes at the front and back edge of the tube were centred 10 mm away from the strongbox and Perspex window faces. The expansion of a uniform cylinder in the plane strain model was considered to be analogous to individual grout bulbs injected at close spacing as so to effectively lift the settling soil above them. A 5 mm long Nylon plug was threaded and glued into the front edge of the support tube. The plug prevented the injected water exiting through the front of the tube and pushing back or bending the injection tube within the soil. In order to contain the injected volume within the latex sleeve, 0.5 mm diameter stainless steel wire wraps were provided at the end of the latex sleeve near the back strongbox wall. To allow these to properly seal the latex against the Nylon, 0.25 mm deep by 0.5 mm wide grooves were machined into the outer

diameter of the inner Nylon tube. These provided better seating for the latex and wire wrappings. Pressure tests on various samples proved this sealing method was capable beyond a water pressure of 2 MPa, much greater than the minimum pressures expected, based on the overburden stress at the deepest injection depth in the model. Figures 5.28-5.29 show the details and photographs of the wire wrap sealing system adopted for the grout injection tubes. The wire wraps were positioned to sit within the injection port of the strongbox back wall to minimise their influence on the expanding shape during injection, see Figures 5.28-5.30.

In the initial injection tests where the injection tubes were located at depths d< 0.5H below the retained surface it was found the tubes did not expand as uniform cylinders. The cavities were found to have a tapered profile with the larger diameter near the Perspex window. To prevent this effect for later tests at shallower depths, a 5 mm long by 0.5 mm thick brass retaining collar was machined and positioned over the front end of the injection tube closest to the Perspex window, as illustrated in Figures 5.28-5.30. Contact between the brass collar and Perspex window may have led to restraint of the injection tube and soil movements. The collar was therefore positioned to provide a 0.5-1 mm clearance from the window face, with only the latex in contact. Details of observations from all the tests are discussed in chapter 6. The effects on the recorded soil movements in tests with and without the provision of the brass collar are discussed further in section 6.2.

5.2.5.2 Grout injection system

A fluid extraction system, developed by Divall (2013) to control fluid in and out of model tunnels, was modified to permit injection of the water 'grout'. Figure 5.31 shows a view of the arrangement of the modified assembly used in this study, herein referred to as the injection system. A Bishop ram served as a piston pump, with the piston actuated via rotation of the lead screw against an internal brass lead screw nut. The internal bore of the Bishop ram was 37.8 mm. The lead screw had an external diameter of 12.7 mm with a BSC (British Standard Cycle) thread providing a thread pitch of 26 TPI (turns per inch). A Maxon DC servo motor driving a 156:1 planetary gearbox was connected to a 30 teeth module 1.0 hardened steel spur gear. This spur gear drove a 30 tooth, module 1.0 aluminium toothed bar serving as an idler gear. The working length of the tooth bar was machined to 120 mm with 6 mm diameter shafts supported at each end. Use of the idler toothed bar accommodated a 120 mm linear stoke of the Bishop ram piston. With this stroke length the maximum available volume for injection during the test was

approximately 135 ml. The idler geared bar drove another hardened steel 30 tooth, module 1.0 spur gear connected to the end of the Bishop ram lead screw. All gears and the toothed bar for this setup were supplied by HPC Gears Ltd, U.K. The entire injection system was found to have a pumping capability in excess of 2 MPa that was again much greater than the theoretical cavity expansion pressures expected. Calibration of this injection system showed one turn of the threaded shaft connected to the Bishop Ram piston provided 1.078 ml of fluid through the outlet.

The injection rate intended to be used for all grout injection tests was 0.359 ml/s, the maximum available rate from the injection system. However as detailed in section 6.1 several problems initiating the injection system were encountered during the grout injection tests. This resulted in the utilised injection rates being lower than the intended maximum available in order to obtain some data from the tests.

Two G1/4 BSPP outlet ports were provided at the base of the Bishop ram. A one quarter turn ball valve fitting was secured to the left outlet port, seen in Figures 5.31-5.32. This was used to aid in the de-airing and priming process prior to each test and was left closed afterwards. The right outlet port was connected to an aluminium manifold block which housed the Druck PDCR810 PT described in section 4.8. Another one quarter turn isolation ball valve was attached to the outlet of this manifold to again aid in the priming of the system before the test. Two G1/4 BSPP ports on the top and bottom of the manifold were also used in the priming and de-airing process and plugged afterwards. A single G1/4 BSPP filling port was provided at the base of the Bishop ram.

To prime the injection system all taps and ports, including the eventual pressure transducer port, were plugged and shut. The assembly was turned upside down to access the filling port and the Bishop ram piston withdrawn to provide the maximum available capacity within the cylinder. Using a 50 ml syringe and extended needle distilled, de-aired water was tremied into the cylinder to avoid the trapping of air bubbles via a Perspex standpipe, see Figure 5.32. Once filled to capacity with water, the Bishop ram was connected to a vacuum pump via the Perspex standpipe and gently agitated to encourage out any trapped air. After ensuring all trapped air was removed, the Perspex standpipe was detached and the filling port plugged with care taken to not introduce any air pockets into the Bishop ram cylinder.

The same semi-rigid Nylon pipe used in the grout injection tubes was used to pipe the injection system to the injection tubes in the model. Quick release push in fittings were

used to allow easy connection and priming of the piping before spinning up the model. For all grout injection tests, the injection pipework lengths connections and fittings between the grout injection system and the 400 mm long grout injection tube (inserted into the model during model making) were kept the same for consistency. This minimised variation in pipe frictional losses between tests, addressed further in section 6.4.2. The same apparatus as the single injection tube tests was used with the addition of a T-fitting used to split the feed pipe from the injection system into each injection tube for the dual injection tubes in tests 12HH and 13HH before entering the backwall of the strongbox. Consequently, the injection of the water grout into the individual tubes in these tests and their expansion were uncontrolled, although the total volume injected and total injection pressure was still recorded using the revolutions counted by the encoder on the injection system motor by the controlling software.

Often in the field, grouting pressures are measured close to the point of injection to provide a better understanding of its performance. It was not possible to measure the injection fluid pressure at the entry point of the grout tubes in the model. An aluminium manifold, referred to as the injection manifold, was externally placed relatively close to the grout tubes, as discussed in section 5.2.6 and shown in Figure 5.26. The manifold housed a Druck PDCR810 pressure transducer, discussed in section 4.8, and was secured to the top plate of the heavy fluid cylinder. A G1/4 BSPP port was made available to this manifold to allow priming of the manifold and pipe work when on the swing bed. A one quarter turn isolation valve connected to the outlet side of this manifold feeding the grout tube aided in the priming process on the swing.

5.2.6 Location of instrumentation

The various instruments utilised through the series of centrifuge tests in this study have been detailed in section 4.8. An aluminium gantry setup, shown in Figure 5.33, was bolted on top of the prop plate support frame, allowed fixing of the nine LVDTs using collar clamps bolted down onto the LVDT bars. The 25.4 mm square hollow section LVDT bars were machined with fixing points at 5 mm centres to permit flexible positioning of the LVDTs.

Two G1/4 BSPP tapped holes at the far left field of the model were provided in the back wall of the strongbox for insertion of the two Druck PDCR-81 PPTs. These PPTs were monitored to confirm when the hydrostatic pore pressure profile associated with the water table set had reached equilibrium before beginning the test. The heights and positions of

these pore pressure transducers within the reference frame of the model are shown in Figure 5.34. The position of the third pore pressure transducer used to measure local soil pore water pressure response close to the grout injection points for each test is shown in Figure 5.35.

The positioning of the two Druck PDCR810 pressure transducers used to measure injection fluid pressures are described in section 5.2.5 and shown in Figure 5.26. The third Druck PDCR810 pressure transducer was used to measure the pressure head at the base of the water column in the standpipe. This pressure transducer was centred 25.4 mm above the base of the swing (Figure 5.12).

The external SPT drainage manifold (Figure 5.26), attached to the SPT drainage fitting also housed the XP5 pressure transducer. This pressure transducer permitted measurement of the heavy fluid pressure approximately 9 mm above formation level.

The de-stoned PDCR-81 pore pressure transducer (functioning as a pressure transducer) to measure SPT fluid pressures at formation level was inserted into the excavation support latex bag through the latex bag collar clamp prior to spin up, seen in Figure 5.36(a). The slotted aluminium sleeve shown in Figure 5.36(b) was attached behind the head of the pressure transducer. It served as a ballast to ensure the transducer head lay horizontal at the base of the bag during flight. Owing to the rigidity of the pressure transducer wire it was often difficult to position the pressure transducer head along the centre line of the model, where calculations of the theoretical SPT support pressure were carried out and assumed.

5.3 Experimental procedure

5.3.1 Sample preparation

In accordance with normal practice at the Research Centre for Multi-Scale Geotechnical Engineering at City, University of London the clay samples for the tests were prepared from a slurry at a water content of 125%. This was approximately twice the liquid limit of Speswhite kaolin clay. The slurry was prepared in an industrial ribbon blade mixer using distilled water and dry kaolin powder which required about 6 hours to fully mix.

The consolidation of a sample with a final minimum 300 mm depth from a 125% water content slurry required the preparation of at least 66.5 litres of slurry in the mixer. As the strongbox was only 375 mm high, a 300 mm high extension with the same plan dimensions was bolted above to allow consolidation of the volume required.

McNamara (2001) provides details of the typical procedures, adopted at the Research Centre for Multi-Scale Geotechnical Engineering Centre at City, University of London, in the preparation of the strongbox container, extension, pouring of the clay slurry and its placement into a consolidation press. These same procedures were adopted for all tests in this study, however a hydraulic rather than the pneumatic consolidation presented by McNamara (2001) was utilised instead.

Figure 5.37 illustrates the loading schedule adopted in the pre-consolidation of the sample in the hydraulic press for all tests. The maximum pressure, 500 kPa was achieved by the third day. On the eighth day the sample was swelled to 250 kPa and typically left for 24 hours prior to its removal from the press for model making. A dial gauge placed on top of the loading platen was used to measure changes in vertical displacement to assess the degree of consolidation of the sample prior to reducing the applied pressure to 250 kPa and removal from the press.

5.3.2 Model preparation

The calibrated and de-aired pore pressure transducers were installed through the plugged holes in the back strongbox wall using special equipment about four hours after reducing the pressure on the sample to 250 kPa. Monitoring of the top loading platen via the dial gauge placed on top showed negligible swelling of the sample before pore pressure transducer installation. McNamara (2001) provides details of the equipment and procedure adopted in the installation of the miniature pore pressure transducers, typical of the practice adopted at the Research Centre for Multi-Scale Geotechnical Engineering Centre at City, University of London.

The exposed model clay surfaces, after removal from the press, were sealed during model making and every care was taken to carry out model making and prepare the model for flight as quickly as possible. These steps were necessary to prevent excessive drying of the clay surfaces and consequently reduce the dissipation of suction pressures generated upon removal from the consolidation press, such that the effective vertical stress remained as close to 250 kPa as possible. Further details regarding model making and preparation times for each of the tests are presented in section 6.1. Indication of any loss of suction from the model could only be gained from the far field pore pressure transducers, shown in Figure 5.34, after spinning up of the centrifuge but not before this time owing to the limitations of the transducers to measure such large suctions.

On removal of the strongbox from the press, the extension and front aluminium wall were removed. The front exposed clay surface was lightly scraped to remove excess lithium based grease and expose the white kaolin surface required for good image analysis. This surface was then immediately sealed with a 100 cS viscosity silicone oil to prevent drying. The top surface level was reduced using a tube cutter before trimming to the required level with an extruded aluminium box section. The cutter was guided by a 150 mm wide aluminium shelf angle bolted to the strongbox, as shown in Figure 5.38.

Previous researchers (i.e. McNamara, 2001; Divall, 2013) in the sealing and prevention of drying of the top clay surface during model making have used a layer of 100 cS viscosity silicone oil or paraffin liquid. With this fluid, brass bunds or clay berms have been necessary to prevent seepage of the fluid on to critical surfaces where interaction was important. Even with great care taken to remove any potential seepage paths the inherent fluid nature of these wet methods always presented a risk of seepage. These fluids although less dense than water also imposed a very small surcharge on the model. Gorasia (2013) successfully trialled and exploited an alternative dry sealing system with the sprayed liquid application of a quick air drying plastic, commercially available as Plasti Dip. Before sealing the top trimmed surface of the model, the edges of the clay in contact with the box walls were depressed with the tip of a finger. This prevented ingress of the liquid Plasti Dip into the boundary faces of the model. A thin coat applied to the top surface was found to be touch dry in 3 to 4 minutes. A blanking plate was used to cover the excavation footprint to prevent overspray as the Plasti Dip coating was not required in this area.

An elaborate aluminium guide, shown in Figure 5.39, was used to form the remaining cut faces of the final model excavation geometry. The tube and box cutters were used to trim the horizontal and vertical faces true. Cutting of the trench for the retaining wall toe embedment required a special cutting tool, seen in Figures 5.40 and 5.41. A cutter with an adjustable blade was guided along a track to allow the cut depth to be varied with each pass. The mounting plate of the track was pinned and secured in position to ensure consistency in geometry for every test. Cut depths of 5 mm were required for each pass to provide a final clean smooth trench. A 4 mm diameter location pin system shown in Figure 5.42 was machined to reduce the time in adjusting the blade position between each cutting pass. The hardened steel blade was ground oversized by 0.5 mm to provide clearance for inserting the wall. After applying a bead of silicone grease along the front and back seals of the wall it was gently pushed in from the front face of the model; care

was taken to avoid smearing and trapping any clay on the leading edge. The verticality of the inserted wall was checked using an engineer's square against the top machined edge of the strongbox back wall. The prop plate assembly was also temporarily inserted into position to check the wall was in contact with both the leading edge of the prop plate and the cut clay face on the retained clay side of the model wall. The edges of the formation against the strongbox and model wall were slightly depressed and a bead of silicone grease applied. This prevented any potentially spilt SPT used at a later stage seeping into the boundary surfaces. At this stage the model was ready for the excavation support apparatus to be placed. The SPT drainage fitting was attached to the latex bag (Figure 5.23) which was then secured to the prop plate using the collar clamp on the day preceding model making. This allowed the assembly to be quickly placed into position. The drainage fitting was pushed through the hole in the right strongbox wall and the SPT drainage manifold fitted (Figure 5.23) ready for connection of the pipe work on the swing. Once placed, the wall and latex bag effectively sealed the cut clay faces during the remaining model preparation and testing period. The pre-placed black imaging targets into a special template, in a grid at 10 mm centres, were then pushed into the front face of model using a specially profiled brass rod.

In the tests modelling the excavation and grouting process it was necessary to cut and insert the grout injection tubes into the model before inserting targets into the front vertical face, illustrated in Figure 5.43. A similar method adopted for the insertion of the pore pressure transducers was adopted. A long brass cutter guide, screwed into the strongbox injection tube port, was used to guide a thin walled stainless steel cutting tube. The 100 mm long guide, reamed to the 10 mm external diameter of the cutting tube, ensured the tube would be inserted in the correct position below the surface and behind the model wall. The cutting tube was used to remove clay cores in approximate 30 mm passes through the width of the clay model. In the last 20 mm pass a clear Perspex plate was lightly pressed against the front face of the model in alignment with the cutter tube for reaction. This allowed the final clay plug to be removed without disturbing the surrounding soil on the front model face. The 10 mm external diameter by 0.5 mm wall thickness tube provided a cavity 1 mm larger in diameter than the external injection tube diameter. For the tests where the brass retaining collar was used on the tubes the cored hole provided just enough clearance to pass the tube and brass collar through without disturbing the cored hole. A 3.5 mm diameter stainless steel rod inserted inside the inner Nylon tube served as a mandrel to guide the tube to the front model face through the cored

hole. Following insertion of the injection tube a 400 mm long by 3 mm diameter needle attached to a syringe were used to fill and prime the tube with distilled de-aired water. Care was taken to ensure as far as possible that all air was removed from the injection tube which was then temporarily plugged until connection of the Nylon injection pipework on the swing. For tests where the brass front collar was used on the injection tubes, a rigid clear Perspex sheet was pressed against the front face of the model and tube to ensure the collar would not later come into contact with the Perspex window. After securing the injection tube fittings and insertion of black imaging targets, the lubricated Perspex window incorporating the image processing control targets was bolted in place. All edges of the retained soil surface were then slightly depressed with a fingertip and a bead of silicone grease applied at the perimeter.

The LVDT gantry and injection system were finally secured to the strongbox before weighing the assembled model. The heavy fluid pump (in early tests) or the heavy fluid cylinder setup (in later tests) and the standpipe assembly were positioned at the edges of the swing before placement of the strongbox owing to space restrictions.

5.4 Testing

A significant amount of work remained to be carried out once the model was on the swing. The connection of instruments to junction boxes, motors and rotary valves to power supplies and water supply to the standpipe assembly were of a standard nature. To save time the positions of the CCD cameras were adjusted on the day preceding the model preparation.

For the excavation only tests using the heavy fluid pump all that remained at this point was the connection of the outlet of the SPT drainage manifold to the heavy fluid pump using 3/16” external diameter by 1/8” internal bore semi-rigid Nylon pipe. The latex bag in the excavation was then filled by driving the piston in the heavy fluid pump down which was pre-filled and primed with the required volume of SPT prior to model preparation. This method ensured there was no air locks in the pipe work preventing proper drainage during the test.

In later tests, grouting and excavation were modelled using the injection system and heavy fluid cylinder drainage tank. For these tests it was necessary to ensure that no air was present in the piping connecting the injection system to grout tubes in the model. The Nylon pipe work consisted of a number of sections joined together using quick release

push fittings, shown in Figure 5.26. The piston of the Bishop ram was slowly actuated using the servo motor with the outlet tap open to sequentially push water through the pipework sections as they were connected together. This was continued until no air bubbles were seen exiting from the open end of the pipe before final connection to the pre-primed grout injection tubes in the model. Great care was taken in this procedure of bleeding and priming the pipe work with water to ensure the injected volume measured by the encoder on the motor would be true during the test. The motor control program was able to provide an accurate count of the number of revolutions taken by the motor shaft via the optical encoder and consequently the volume injected. The next step involved the connection of the SPT drainage manifold to the rotary valve and heavy fluid cylinder assembly (Figure 5.26) using 1/8" diameter by 1/16" bore stainless steel pipe. This permitted the filling of the SPT into the support latex bag using a funnel before inserting the de-stoned pressure transducer into the base of the bag. The rotary valve was opened for a very short period to allow some SPT to drain through and then closed to ensure no air locks were present in the piping. The level in the bag was then topped up. The final steps involved checking and securing all cables and wires and adjusting the counterweight position. The back drainage tap connecting the standpipe and model was opened immediately before spinning up to prevent the sample prematurely swelling. Figure 5.44 shows a photograph of the model ready for spin up.

Once reaching 100 *g*, the model was left to reconsolidate and the pore pressures to come into equilibrium. The readings from the far field pore pressure transducers (Figure 5.34) were used to monitor when pore pressure in the model had reached their expected hydrostatic values based on the induced ground water level. Owing to the clay depth in the model, this reconsolidation and pore pressure equalisation stage typically took at least 48 hours before the testing could commence.

In the excavation only baseline tests (2HH and 3HH) the heavy fluid pump was used as detailed in section 5.2.4.2. Excavation was only initiated once synchronous instrumentation and image processing data logging had commenced. After completion of the third and final drainage stage the model was left to spin at 100 *g* for a further 10 minutes to observe long term movements.

For all other tests, excavation was simulated with the free drainage of the SPT solution into the heavy fluid cylinder and grouting modelled via the injection system and grout

tubes previously described. The general procedure for these tests was as follows after initiating data and image logging and energising the servo:

- Open rotary valve to commence SPT drainage and excavation simulation.
- Initiate injection system pump after observing predefined surface settlement trigger value from the LVDTs.
- Continue injection until LVDT reading above injection tube returned to initial zero value or no heave response observed. Injection stopped if significant horizontal displacement of the model wall confirmed visually from the live image feed.
- In the tests where the LVDT was returned to its initial zero value from the first injection pass, subsequent injection passes were initiated to attempt maintaining the corrected position.

During the entire process it was necessary to record the commencement and completion of each injection pass against the sample count of the LabVIEW program logging the instrumentation response. The number of motor revolutions counted by the encoder was also recorded to allow later calculation of injected volumes. The consistent duration of the SPT solution drainage in these tests, about four minutes, provided a sufficient window to initiate at least one pass of injection into the model during excavation simulation. Following passes were also made after the excavation had been carried out in some tests in an attempt to correct post excavation and long term surface settlements. With completion of the last injection pass the model was permitted to spin for at least 5 minutes to observe the long term response from the soil following the modelled events.

6. EXPERIMENTAL WORK

This chapter details the tests conducted and the performance of the apparatus described in chapter 5. A total of 13 centrifuge tests were carried out. The basic results recorded and fundamental observations from 10 successfully conducted tests are presented. Two basic forms of tests were conducted; reference tests to establish soil and wall movement patterns and magnitudes with simulation of the excavation only and a series of excavation and grout simulation tests with only the location of grouting varied.

6.1 Details of tests

Time constraints following the lengthy period spent in apparatus development dictated that only the depth and distance behind the retaining wall of the grouting simulation was varied between tests. These were envisaged to be the simplest parameters to investigate and would enable variations in soil and structure behaviour between the different grouting positions to be apparent.

A total of 10 successful tests were conducted, the details of which are described in Table 6.1. Of these tests two, 3HH and 10HH, provided reliable reference data for excavation only induced movement. A third reference test, 2HH was also conducted, however the confidence in the soil and wall response were brought into question as a result of a lower initial excavation support pressure and an issue experienced with the standpipe feed to the model. A total of eight grouting tests, 6-13HH (see Figure 6.1) were conducted using the apparatus described in chapter 5 to simulate grouting at varying distances behind and below the model retaining wall and retained clay surface, respectively, the details of which are described in Table 6.1

Tests 6-11HH were conducted using a single point of injection at various positions. Following a brief overview of the soil behaviour, retaining wall and grouting response from these tests, it was decided to conduct tests 12HH and 13HH with at least two simultaneous points of injection. As illustrated in Figure 6.1, these dual injection tubes were positioned at fixed horizons below the retained surface. The distance of the injection tubes behind the wall were decided based on the observed surface displacements in previous tests, with the intention of minimising the influence of injection on horizontal wall movements. In the single point injection tests, control and measurement of injected volumes and pressures into the tubes was possible with the equipment and instrumentation described in chapter 5. However, without significant modifications and

additions to the injection apparatus, only the combined injection pressures and total volumes for both tubes could be monitored in tests 12HH and 13HH. Tests 1HH, 4HH and 5HH, were considered failures as no data was obtained on the excavation simulation, grout injection event or the test was abandoned on spin up owing to equipment failure. Consequently, the results and observations from these tests have not been presented here, although they provided valuable insight into improvements that were needed in the modelling technique, model making and functionality of the apparatus.

Test 1HH was the first attempt to model the excavation process with the newly developed apparatus to provide a datum of soil and wall movements to which subsequent tests could be compared. Although the individual pieces of apparatus had been bench tested and procedures for model making written down to minimise errors, it was inevitable that unforeseen problems would arise during the model making period for early tests. This resulted in an 11 hour preparation time from removal of the sample from the consolidation press to a completed model, with all instrumentation and apparatus connected, on the swing ready for spin up. In the following tests 2HH and 3HH, the time for preparing the model ready for spin up on the swing was reduced to about 7 hours. This was possible through additional efforts made to prepare all items of apparatus and equipment, including priming of the heavy fluid pump on the day prior to model making and spin up. With the removal of the heavy fluid pump and simplification of the excavation simulation method in subsequent tests the time taken in model making and on the swing was reduced further by nearly 1 hour. However, the additional apparatus and model making procedures introduced with injection grouting added to the model complexity, resulting in a preparation time of 9 hours for the first grouting test 6HH. This was an unavoidable consequence in using the grouting tubes and apparatus that had been implemented together as a whole system for the first time and the care taken to ensure the injection tubes and piping were primed with water and bled of air. In the following tests a duration of about 6 to 6.5 hours between removing the model from the consolidation press and spin up was maintained, with test 9HH requiring the shortest time of 5.5 hours. The significance of minimising this time has been outlined in section 5.3.2. Even with the measures described in section 5.3.2 to minimise dissipation of the suction pressures within the model it was apparent from the far field pore pressure transducers (Figure 5.34) both before and after spinning up of the centrifuge that the loss of suction was significant for all tests. With the longest model making duration, the pore pressures transducers in test 6HH indicated a loss of suction to around one third of the ideal -250 kPa. For the

other tests which in general had shorter model making durations, the two distant transducers recorded a dissipation of suction up to a value approximately equal to half the ideal value, in which no suction loss would occur. McNamara (2001) experienced similar changes on a series of tests which also required minimal time for model making, suggesting that such changes were therefore unavoidable.

In most of the tests two pressure transducers, detailed in section 5.2.6, were provided to monitor the SPT fluid pressures during flight and simulated excavation. In initial tests 2HH and 3HH the internal de-stoned pressure transducer was unavailable, leaving only the measurements from the external XP5 pressure transducer. For all subsequent tests the SPT fluid pressure was measured by both pressure transducers. During all tests the external pressure transducer was shown to be sensitive to the opening of the rotary plug valve upon initiating excavation as an instant pressure drop of 25-35 kPa was recorded. The external pressure transducer was also observed to be sensitive to the change in fluid medium being measured; a noticeable jump to negative pressure values was logged at the end of simulation, where the fluid in contact would change from SPT to air. Figure 6.2 shows this typical response from the external pressure transducer for test 7HH. In contrast, the internal pressure transducer, where available, provided a far more stable output as shown in Figure 6.3. It was for these reasons that where available the internal pressure transducer readings were used to determine excavation progress in the model tests conducted.

It was originally envisaged that all tests would essentially be the same with regards to simulated excavation duration and initiation of grouting when a predetermined maximum settlement trigger value of 0.125 mm or 0.1%H was observed in the LVDT located x= 0.5H behind the wall, in accordance with the behaviour in baseline test 3HH. This settlement was close to the maximum observed by Gaba *et al.* (2017) for excavations in very firm to stiff clays, shown in Figure 2.15. From the excavation only tests this settlement was found to occur after one third of the excavation had been completed. Adopting this settlement trigger for grouting would enable a direct comparison between tests, with the only primary variable being the position of grouting and injected volumes. However, achieving this aim relied on the consistent and satisfactory performance of various components of the apparatus, in particular the grout injection apparatus. The details of the tests and problems encountered (see Table 6.1) with apparatus in the various tests and their influence on the tests are discussed below.

For consistency the specific gravity of the SPT fluid was checked and adjusted to 1.78 prior to model making. The SPT was filled to the top of the latex bag retaining collar for all tests to account for the additional volume required as the bag would stretch and seat into the corner of the pre-cut excavation upon spin up. A visual check was made prior to spin up to ensure no large air pockets existed in the bag beneath the prop plate that could potentially displace at a later stage, thereby reducing the SPT fluid level and pressure. This was not possible in the initial test 2HH where a black opaque latex bag was used and a subsequent lower than expected support pressure was recorded during the consolidation period prior to testing, shown in Table 6.2. At the time a decision was made to not to interrupt the test to check the SPT fluid level and top up if required considering the lengthy period taken to prepare and spin the model up. In all subsequent tests greater care was taken during filling to check for trapped air bubbles in the latex bag beneath the prop plate. These additional precautions ensured the initial SPT support pressure prior to testing were consistent to within approximately 10 kPa between the tests, as presented in Table 6.2. The level of the SPT was also monitored during spin up and flight through the translucent latex bag used in tests 3HH onwards using the live camera feed into the control room.

The heavy fluid pump apparatus was used in the initial excavation only tests 2HH and 3HH. As detailed in section 5.2.4.2, the limitations of the motor control software and optical encoder driving the piston of the heavy fluid pump restricted its range of movement, allowing removal of the SPT from the latex bag in a stepwise or staged manner. In order to remove all the fluid from the excavation it was intended to carry out three linear stages of removal of equal duration and reduction in pressure. This meant an overall time of about 8-8.5 minutes including two 20-30 s break periods to reset the software would have been required to simulate excavation. McNamara (2001) also observed similar excavation durations and recorded relatively large excess pore pressures changes during the unloading stage from PPTs installed close to the excavation. This was indicative of a largely undrained excavation and provided confidence in the use of an approximate 8 minute duration for the excavation with the heavy fluid pump. Figure 6.4 shows the successful removal of the fluid in the first two stages for tests 2HH and 3HH. Each stage resulted in a reduction of approximately 60 kPa over 2.5 minutes from the initial pre-excavation pressure, with the break required to reset the encoder in between. However as discussed in section 5.2.4.2, in both tests approximately half way through the third stage of fluid removal the Maxon motor driving the heavy fluid pump stopped

responding for an unknown reason. This resulted in reduced excavation durations of about 7 minutes for the two tests with a 17 s difference between them. Several attempts were made to reinitiate the motor with no success resulting in recorded values of 22 kPa and 29 kPa of pressure (see Figure 6.4) remaining at the base of the excavation for test 2HH and 3HH, respectively. With a SPT specific gravity of 1.78, these pressures equated to unexcavated soil depths of 1.2 m and 1.6 m at prototype scale, respectively. These depths would have been less along the model centre line owing to the curved free surface of the SPT fluid present as a result of the radial acceleration. Post-test inspection and drainage of the remaining SPT fluid suggested that lesser depths and volumes of fluid remained in the bag than those indicated by the pressure recorded by the external pressure transducer.

Following the issues experienced with the heavy fluid pump all subsequent tests adopted the simplified free drainage method described in section 5.2.4.2. As expected with the adoption of the simpler free drainage method and apparatus, see Table 6.1, excavation durations were maintained at about 4 minutes for most of the tests. A deviation of 7 s was noted between the shortest and longest excavation periods, shown in Table 6.2. Figure 6.3 illustrates good consistency in the SPT drainage rates under free drainage for nearly all of the grouting tests with the exception of 6HH. Test 6HH had the longest excavation period of about 820 s at model scale. Post-test investigation found the solenoid only turned the plug valve to a half open position, for the reasons presented in section 5.2.4.2 The problems with the solenoid-plug valve assembly were temporarily resolved for test 7HH.

In test 8HH the functionality of the solenoid-plug valve assembly was checked prior to spin up however the solenoid failed to actuate when attempting to initiate the excavation. As no SPT fluid had been drained it was considered feasible to spin the model down to resolve this issue. The investigation and repair of the solenoid-plug valve assembly required about 25 minutes in total during which time the model was spun down twice. Following the final spin up of the model to 100 *g*, the far field installed PPTs indicated immediate changes of about 40 kPa and -14 kPa, respectively, in the bottom and top PPTs from the initial equalised pore pressures. Figure 6.5 illustrates the pore pressure response in the far field PPTs during the aforementioned events to address the solenoid issue. With the unloading and reloading of the clay model to the same total stress (with spinning down and back up again) the measured changes in the pore pressures suggested the clay model underwent some softening and swelling whilst stationary, even with the isolation of the standpipe feed to the model base. Consequently the pore pressure changes, relative to the

initial equalised values, following the final spin up of the model would have required more time at 100 *g* to dissipate and return to the original equilibrium state. However, adding duration to the test would have introduced an unacceptable risk of a possible repeat failure of the solenoid-plug valve assembly at a later stage, with the increased stresses at 100 *g*, which would have forced abandonment of the test. It was therefore decided to accept the relatively small change in model stresses and carry out the test.

In subsequent tests 9HH-13HH, the 12 V DC synchronous motor assembly with a higher torque output, detailed in section 5.2.4.2 was used, to avoid a reoccurrence of the problems in test 6HH and 8HH. Figure 6.3 shows the different durations and rates of excavation between the two excavation simulation methods used.

During the typical 48 hour consolidation period and after simulation of excavation and grouting, no signs of water accumulation as a result of seepage through the formation level in the pre-formed excavation were seen through the Perspex window. Following removal of the models from the swing it was noticed that a thin layer of silicone fluid used to lubricate the Perspex window during model making was coating the formation level. This was probably dragged off the window in the region of the pre-formed excavation during flight under its self-weight. With the latex bag secured to the prop plate by the collar clamp the base of the bag was also noted to remain in contact with the formation level both during and after SPT fluid drainage. It is reasonable to assume that both these factors significantly reduced seepage into the formation thereby reducing the magnitude of heave induced through softening of the base consistently across all tests. It is also reasonable to assume the same groundwater level was imposed (with the exception of tests 2HH and 8HH) across the tests programme, thus providing confidence in consistent geostatic stresses being established in the soil model prior to simulation of the excavation and injection events.

It was intended in all grouting tests to initiate injection upon observation of the surface settlement trigger value, discussed previously, at an injection rate of 0.359 ml/s. Injection at this rate was comparable with the rates adopted by Au (2001) under undrained loading conditions in kaolin clay samples. Similar conditions were also required for the tests in this study to minimise consolidation induced movements during injection as a result of the excess pore pressures generated locally around the injection location. Adoption of this systematic method of grout injection relative to generated settlements and thus excavation

progress would have aided comparisons of the effects of injection on soil and wall movements between tests.

However as briefly described in chapter 5 problems were experienced with initiation of the Maxon motor on the injection system even after reducing the injection rate to 0.230 ml/s for tests 6-9HH. For the remaining tests (10-13HH) this injection rate had to be further reduced to 0.115 ml/s owing to several non-responsive attempts made in test 10HH. It was necessary to opt for successful operation of the injection system at lower than intended rates in order to obtain useable data rather than abandon the tests as a result of being unable to inject. The problems with the motor also resulted in varying injection start times relative to excavation progression and observed LVDT surface settlements in all tests, with the exception of tests 12HH and 13HH. In these tests injection was successful at the first attempt when around 0.125 mm of surface settlement was observed. In all other grouting tests different magnitudes of soil and wall movements had developed before injection. Table 6.1 summarises the problems encountered with the injection attempts for each of the grouting tests. The effects of these delays on the soil and wall displacements are presented in section 6.4 and discussed further in chapter 7.

6.2 Comparison of LVDT and image processing vertical measurements at the retained surface

Movements at the retained surface were measured using both image processing of the targets and the fixed position LVDTs, shown in Figure 5.33. Measurements of the surface settlements using image processing were available from the top row of targets placed 5 mm below the soil surface for comparison against the LVDTs at the surface. However, during reconsolidation some small visible swelling of the surface tended to move the top row of targets just beneath the top aluminium section of the Perspex window. With the lighting required to illuminate the front face, positioned near the top edge of the Perspex window, this region was either severely under exposed in tests 2HH and 3HH (with the use of the older halogen lighting system) or over exposed in subsequent tests (using the newly upgraded LED lighting). As a consequence, the image processing software was unable to consistently track these targets across the visible retained surface thus requiring the use of the second row beneath at depth 12-15 mm below the surface, for comparison against LVDT measurements.

Three types of tests were conducted; 1) excavation only, 2) excavation and injection without the provision of brass collars and 3) excavation and injection with the provision

of brass collars on the injection tubes, as summarised in Table 6.1. In the two reference tests 2HH and 3HH no injection tubes were included, however for the excavation only dataset provided by test 10HH (see section 6.4.1.1) an injection tube with a brass collar was present. In tests 6HH and 7HH no brass collars were provided and as a consequence non-linear expansion of the injection tubes across the 200 mm model width were observed from post-test resin castings, as described in section 6.4.1.2. In the following tests, 8HH-13HH the injection tubes were provided with a brass collar on the front of the tube (see section 5.2.5) to successfully enable linear expansion of the cavity, as discussed further in section 6.4.1.2.

The two independent methods adopted for measuring vertical displacements near to or at the retained surface enable an assessment of the plane strain behaviour of the model, particularly in the soil regions surrounding the latex injection tubes. This is examined in the following sections by comparison of the two datasets, for the excavation and excavation and injection events both with and without the provision of the brass collars on the injection tubes. The comparison also enables consistency of the measurement methods to be assessed.

6.2.1 Excavation tests

Figure 6.6 presents the difference in the vertical displacements, ΔS_v measured between the LVDTs (at the surface) and image processing targets (on the wall and the second row of targets embedded in the soil, 12-15 mm below the retained surface, and at distances x= 0.25H, 0.5H, 1.0H and 1.5H behind the wall) for the excavation only events in tests 2HH, 3HH and 10HH, up to 133 s after completion of the excavation. Although different magnitudes of settlement and different excavation durations were observed between the three tests (as detailed in section 6.4.1.1) the development and magnitudes of ΔS_v for all three tests show remarkable consistency. Greater noise was observed in tests 2HH and 3HH in comparison to 10HH which was probably owed due to the angled positions of the two CCD cameras and lower light levels provided by the halogen lamps in comparison to the single camera and LED strip lighting adopted in later tests.

Comparison of ΔS_v values on the wall, obtained from the LVDT on top of the wall and the closest embedded wall target to the retained surface, show effectively zero difference in the response from both measurement methods in all three tests. This behaviour would be expected given that it would be likely that the wall would displace vertically as a rigid body across the 200 mm width of the model, with a bending stiffness 34% greater than

the longitudinal bending stiffness of the wall along its retained length. The behaviour observed also demonstrates the validity of both measurements methods used. At distance x= 0.25H little difference (up to a magnitude of 25 μm) was also observed between the two datasets across the three tests. Table 6.3 shows the similar order of magnitudes of ΔS_v values recorded for each of the tests at the end of excavation and 133 s after.

A gradual increase to similar orders of magnitude in ΔS_v values was noted for increasing distances behind the wall where x≤ 1.5H for all tests. Even with the shorter excavation duration in test 10HH compared to tests 2HH and 3HH, all three tests show a gradual increase in ΔS_v with time (for distances x≥ 0.5H behind the wall) up to the end of excavation. Following this the values of ΔS_v remain constant which is different to the behaviour observed by Grant (1998) and McNamara (2001). Both previous researchers observed a stick-slip mechanism in which the offset between the measurements increased with excavation and then gradually decreased following the excavation event to a constant value of around 100 μm. This was attributed to frictional effects at the front Perspex-clay window interface. Grant (1998) found the viscosity and quantity of the silicone fluid applied to reduce friction effects had significant influences on the magnitudes of offsets, with increasing fluid viscosity leading to progressively smaller offsets. The same viscosity silicone fluid used by Grant (1998) and McNamara (2001) was used in the tests for this study. In general, an even thickness of around 1 mm of lubricant was applied over the window area prior to securing the window to the front of the model.

In all three of the reference tests in this study the LVDTs generally recorded greater magnitudes of settlements than the image processing targets at the front face. This behaviour was expected considering the effect of the propagation of settlements at the surface through to the subsurface horizon at which the second row of targets were located. The magnitude of the offsets between the measurements were also noted to increase with distance behind the wall up to distance x= 1.5H in all the tests within this study (prior to the influence of injection and brass collars), as presented in the following sections, 6.2.2 and 6.2.3.

6.2.2 Grouting and excavation tests (without a brass collar)

Figures 6.7-6.8 present the development of absolute vertical displacements recorded by the LVDTs and imaging targets at corresponding distances behind the wall throughout the excavation and injection events in tests 6HH and 7HH. Injections were simulated at distance x= 0.5H behind the wall at depths d= 0.5H and 0.25H beneath the retained surface, respectively for test 6HH and 7HH. Although the excavation durations (see Table 6.2) and consequently timings of the injections differ by several magnitudes between both tests, a general trend was apparent with the LVDTs recording greater settlements than the imaging targets at the retained surface.

Without the provision of the brass collars at the front of the injection tubes, near to the Perspex-clay interface, the grout injections in both tests resulted in the expansion of non-linear cavities along the longitudinal axis of the injection tube, as pictured in Figure 6.40. This resulted in the soil closest to the front face of the model experiencing greater displacement than that along the longitudinal centre line of the model. This is demonstrated by significant localised heave manifesting in the targets above the injection tubes for both tests in Figures 6.7-6.8. As expected with a shallower injection in test 7HH, where the injection event was closer to the second row of imaging targets, a greater maximum magnitude of heave was recorded above the tube in comparison to the deeper injection in test 6HH (even with the larger injected grout volume in test 6HH). A significant reduction in the development of excavation settlement, followed by heave and a return to gradually increasing settlement following the first injection, was detected by the LVDT above the injection tube in the shallower injection of test 7HH. In comparison, the corresponding LVDT in test 6HH showed a small momentary reduction in settlement rate before increasing towards the end of injection. This behaviour was also reflected in the target above the injection locations although a larger magnitude in the settlement reduction was recorded compared to the LVDT. During the second injection in test 7HH, heave was detected by the targets but not the LVDT located at distances x= 0.25H and 0.5H behind the wall.

Figures 6.9-6.10 show the ΔS_v offsets between LVDT and image processing target readings of the vertical settlements at various distances behind the wall in tests 6HH and 7HH. These distances corresponded to the fixed positions of the LVDTs. Table 6.3 lists the values of ΔS_v at the beginning and end of each injection event and excavation. With the exception of the heave experienced above the injection tube and at distance x= 0.25H, the data in the table and figures indicate similar orders of magnitude for ΔS_v were

established in the two tests at the other measurement locations, by the end of excavation and at the start and end of the first injection pass. As would be expected the offset values for the shallow injection in test 7HH were marginally larger in comparison to test 6HH. Similar to the reference tests, discussed in section 6.2.1, the offset between the LVDT on the wall and topmost visible embedded wall target was observed to be effectively zero throughout the tests duration, reaffirming the behaviour expected of the model wall. At distance x= 1.5H behind the wall, ΔS_v was noted to gradually develop for both tests during the first injections and up to the end of excavation. Following this period, the offset values were shown to stabilise to similar values, even with the second smaller volume injected in test 7HH. Comparisons of the offset values at the end of excavation between the excavation only tests and test 6HH and 7HH, in Tables 6.3 and 6.4, show a good correlation in the magnitudes at the far field distance x= 1.5H behind the wall or 120 mm from the injection tube location in the two tests. Closer to the injection, at distance x= 1.0H behind the wall (60 mm from the injection tube) a greater offset was observed in the shallower injection of test 7HH in comparison to the magnitudes observed in test 6HH.

In line with the observations from the excavation tests, the LVDTs in tests 6HH and 7HH presented larger settlements than the image processing targets particularly above the injection tube location. This localised effect was attributed to the non-linear cavity expansion resulting in greater heave being detected at the front model face in comparison to the model centre line along which the LVDTs were located.

6.2.3 Grouting and excavation tests (with a brass collar)

Figure 6.11 presents the offsets, ΔS_v for test 8HH between the LVDT and imaging target measurements of the vertical displacements above the wall (close to the retained surface) and at distances corresponding the positions of LVDTs behind the retaining wall.

The injection in test 8HH was the deepest of all tests at d= 0.75H (90 mm) below the surface and x= 0.5H behind the wall. The behaviour observed in this test closely resembled that observed in the excavation only reference tests, which was probably due to the distance between the injection tube and the second row of imaging targets. As a consequence, the injection tube (with collar) appeared to have an insignificant effect either locally around the tube or globally on the retained soil mass at a depth of d= 0.75H below the retained surface. Comparison of Table 6.3 with Table 6.5 and Figure 6.6 with Figure 6.11 indicate remarkably similar magnitudes of ΔS_v values and their development

between test 8HH and the reference tests at the end of excavation and injection. As with the reference tests a consistent increase in the ΔS_v values is noted with increasing distance behind the wall. Measurements at the wall and distance x= 0.25H show little discrepancy between the two measurement methods, as with previously discussed tests.

The injections in tests 10HH and 12HH were conducted at the same depth beneath the retained surface at d= 0.25H. For test 10HH the single injection tube was located at distance x= 0.75H behind the wall. In test 12HH grouting was carried out simultaneously into two injection tubes located at x= 0.5H and 0.75H that are referred to as the right and left injection tubes, respectively, in this section for simplicity. Limitations in the grouting apparatus prevented the control of independent volume injection into each tube in tests 12HH and 13HH. As a consequence, the extent of expansion of the two tubes in each test differed, as detailed further in section 6.4.1.4. Figures 6.12-6.13 illustrate the absolute vertical displacements throughout tests 10HH and 12HH logged by each measurement system above the wall and at distances behind that correspond with the LVDT positions. Figures 6.12-6.13 indicate the LVDTs, located above the injection tubes, in tests 10HH and 12HH were more responsive to the heave induced by both injection events. This would be expected with the provision of the brass collars on the injection tubes at the front face of the model essentially restraining the front 5 mm of the tubes, nearest to the imaging targets, from expanding in proportion with the central portion of the tube above which the LVDTs were located.

Figures 6.14-6.15 present the offset values between the LVDT and image processing targets, ΔS_v for tests 10HH and 12HH. Table 6.6 lists the ΔS_v values for both tests. Following the start of the first injection ΔS_v is similar for both tests at distances local to the injection tube and in neighbouring measurement locations. As with previous tests, a small discrepancy up to 20 μm was observed at the top of the wall. At the far field distance x= 1.5H, magnitudes for ΔS_v of 250-275 μm were observed in both tests, which are similar to those in previously discussed tests following the completion of excavation. After completion of the first injection in tests 10HH and 12HH, ΔS_v values were noted to generally stabilise along the retained surface and continued to do so through the second injection pass, with the exception of the locations above the injection tubes. This was expected given the close proximity between the retained surface, second row of imaging targets and injection tube depths. A similar response in magnitude was observed at the LVDT located at distance x= 1.0H behind the wall (+30 mm from the injection tube) in

test 10HH and (+30mm from the left tube) in test 12HH, following the completion of the second injection pass. The discernible difference between the two tests observed at distance x= 0.25H was expected with the presence of the right injection tube in 12HH.

The vertical distance between the retained surface, second row of imaging targets and injection tubes was the same for tests 9HH, 11HH and 13HH. Figures 6.16-6.18, present the absolute displacements logged by each measurement system for all three tests above the wall and at distances coinciding with the location of the LVDTs behind the wall. As with tests 10HH and 12HH, the LVDTs above the injection locations in tests 11HH and 13HH appeared to be more sensitive to the changes in displacement caused by injections of grout in comparison to the targets. This was expected with the restraining effect provided by the brass collars.

Figures 6.19-6.21 show the offset values between the two measurement systems, ΔS_v for tests 9HH, 11HH and 13HH. As with all previous tests no discernible offset was observed for measurements of the vertical displacement of the wall. The development and magnitude of ΔS_v values at distance x= 1.5H behind the wall also showed notable consistency with the values and behaviours observed in all the other tests. This further supported the limiting extent to which the provision or lack thereof of brass collars, different injection locations and events had on the measurements made by the two methods. Inspection of Figures 6.19-6.21 and Table 6.7, which lists the ΔS_v values at each event, highlight the overall consistent behaviour between the tests; a short time after starting injection the ΔS_v values tended to positive values (indicating LVDT settlements < target settlements) for measurements above the injection tube and at neighbouring sites ±30 mm from the injection tube. The offsets at these sites very gradually then reduced down prior to the end of injection and continued to do so following the event. This was in contrast to the constant behaviour observed for the shallower injections in tests 10HH and 12HH. For measurements at a distance 0.25H behind the wall, the different offset magnitudes reflect the relative proximity to the injection tube for each of the tests, with tests 9HH (injection at x= 0.5H) and 13HH (injection at x= 0.5H- right tube and x= 0.75H- left tube) showing larger values in comparison to 11HH (injection at x= 0.75H behind wall).

Comparison of test set 10HH and 12HH with test set 9HH, 11HH and 13HH showed in general larger offset values in the locality of the injection sites behind the wall as would be expected given the closer proximity between surface, targets and injection tubes in the

first set. This pattern also occurred where the measurement sites were a short longitudinal distance from the injection location, with larger offsets noted the closer the point of measurement was to the injection tube.

Comparison of both test sets with the non-brass collared tests 6HH and 7HH, clearly indicated that even with similar or closer vertical proximity to the surface, smaller offsets in general were recorded between the measurement methods as a result of providing the collars. However, it is also clear that with the exception of the far field measurements at distance x= 1.5H and those above the wall the absolute magnitudes and development of the offsets varied in location between each test. These variations were seen overall to be a function of horizontal and vertical proximity between the injection tubes, the retained surface and imaging targets as well as the provision or lack thereof of brass collars. The consistency observed in the measurements of the wall provided reassurance in the ability of the image processing system to track relatively rigid body movements of the wall. The key difference observed between the collared and uncollared injection tests was the decreased sensitivity of the image processing targets locally around and above the injection tube locations with the provision of the brass collars as expected with the restraint provided. In the uncollared test 7HH, the maximum difference in LVDT and targets measurements was located above the point of injection was up to 12.4 mm. In comparison for the collared test 10HH (with injection at the same depth beneath the surface as test 7HH), the maximum difference between measurements, also located above the point of injection, was recorded to be only 1.28 mm. This was an entire magnitude smaller than in test 7HH. Similar orders of magnitude in the maximum differences between the measurements were observed between the other collared and uncollared tests, as detailed in Tables 6.4-6.7.

6.3 Image processing of wall and formation level displacements

In early tests 2HH and 3HH the two CCD cameras, PULNIX and TELI, enabled independent measurements to be made of a relatively substantial region of the soil behind the wall, the wall itself and a limited region in front of the wall at formation level. This was made possible because these regions were within the field of view of both cameras (see Figure 4.6). The use of two cameras permitted the accuracy of the measurements, determined from their images, to be assessed. The differing specifications of the cameras, notably the focal lengths and significantly different positions, meant that comparison of the data was not straightforward.

For each of the cameras the image processing software, VisiMET, required the selection of all visible targets embedded in the soil and wall before assigning identification numbers and calculating their pixel co-ordinates. The visible control targets (machined onto the inside face of the Perspex window) in each camera view, of which their positions and numbers were known and specified, were then selected and subsequently used by the software to calculate the camera positions through an iterative process. The software was then able to correlate the embedded target pixel coordinates against the visible control targets using the calibrated positions of the cameras and calculate the positions of all targets in the front soil plane. However, with different control targets visible in each camera, the assignment of identification numbers of the embedded targets visible in both fields of view were also different. This meant the task of finding and matching the data for the same targets in each camera became a very arduous and lengthy task.

In view of the limited scope of the investigation it was decided instead to focus on the displacement of a relatively small set of targets embedded in the wall and beneath the formation level at significant events in both tests. Comparison of the vertical measurements made by LVDTs and the embedded wall targets, made previously in section 6.2, displayed close to zero discrepancy between the two measurements close to the top of the wall. Figures 6.22 and 6.23 show plots of the horizontal and vertical displacements of the wall and formation in tests 2HH and 3HH using image processing from both cameras. The dotted and dashed lines with triangular and square solid markers represent data at the end of excavation and 133 s after, respectively, as recorded by the TELI camera. The solid line with hollow triangular and square markers, respectively, represent data at the end of excavation and 133 s after obtained with the PULNIX camera. Figure 6.22 shows that in general the PULNIX camera measurements of the embedded wall targets and soil beneath, at both stages in both tests, were marginally larger than the TELI camera measurements with a maximum difference observed of around 70 μm in test 2HH and 50 μm in test 3HH. In contrast the vertical measurements of the formation level in Figure 6.23 made by the PULNIX camera appeared to be smaller than those of the TELI camera. Similar differences of 30 μm and 50 μm were observed between the two camera measurements, respectively, in tests 2HH and 3HH at both stages in the tests. These small differences in the vertical displacements of the formation level fall in line with expectations, given the close proximity to the unloading horizon with the heavy excavation support fluid and relative isolation from the injection event. The number of targets at formation level visible to the PULNIX camera image processing in 2HH were

severely limited owing to shadows created by lighting during the test which meant the software was unable to detect their presence.

The magnitudes of differences between camera measurements were noted to be less than 0.065%H in test 2HH and less than 0.05%H in test 3HH for both the maximum horizontal wall and vertical formation level displacements recorded 133 s after excavation. These relatively small differences together with the resolution capabilities of the image processing method provided greater certainty about the accuracy of the camera measurements. These marginal differences in measurements as well as the adjustable position of the TELI camera, enabling it to capture more of the region of interest around the excavation, wall and formation level, justified the use of the TELI camera data for tests 2HH and 3HH. For consistency, the TELI camera and subsequent data recorded by the camera were used to present the wall and formation level displacements for subsequent single camera tests 6-13HH. In summary, the notable agreement observed between measurements of both cameras and the consistency observed in the vertical measurements made by LVDTs and image processing above the wall, discussed in section 6.2, provided confidence in the performance of the VisiMET software and consistency in the behaviour and response of the wall to excavation and injection.

6.4 Observations and Results

6.4.1 Soil and wall movements

The following sections present the basic results and fundamental observations of soil and wall displacements from the 10 tests conducted. The tests results have been grouped together based on the position of the injection point below the retained clay surface or behind the back face of the retaining wall.

In the following sections the retained surface, wall and formation level movements at the start of injection and end of injection are presented where relevant. With the differences in starting injection times and the durations and volumes of injection, it is necessary to establish a system of notation which allows easier identification of the start and end of the injection events relative to either the progression of excavation (drainage of support fluid) or time post excavation. This enables a clearer understanding of the magnitude of movements between grouting tests against movements established at equivalent stages in the excavation only tests.

For injection events which started or ended during excavation, their position within this period is described using the fraction of fluid support pressure present at the time relative to the total fluid support removed during excavation (i.e. percentage of excavation). A leading decimal value is used to refer to the fraction of the total heavy support fluid, E (see Tables 6.9-6.16), with subscripts referencing the test number. For example, in test 7HH the first injection pass was started at $0.53E_7$ or after the excavation support fluid pressure had been reduced by 53% of the total fluid present at the start of the excavation. This system permits comparisons between movements during grouting and the reference test, where comparable boundary conditions existed in both, in relation to SPT fluid levels and excavation progress.

The elapsed time following excavation completion is used as a referencing system to describe events in this period of the tests with the notation of T used to reference the total test excavation duration, time after excavation in model scale and subscripts indicating the test number (see Tables 6.9-6.16). For example the start of the second injection pass in test 7HH occurred 103 s after completion of the excavation or T_7 + 103 s. Following drainage of the supporting fluid it is reasonable to assume soil and wall movements were largely time and seepage dependent without any external influence (i.e. grout injection). It is therefore sensible to use this system to observe differences in the effects of grouting in test 6-13HH against the reference excavation tests at equivalent stages after excavation, although consideration must be made for the differences in the excavation duration periods between the tests, previously described in section 6.1. Figure 6.24 shows the relative position of the various events in the grouting tests using these two referencing notations with respect to test 3HH; this is used to compare movements at the relevant and equivalent positions either during excavation or post excavation. The justification for using 3HH as the reference test is provided below.

6.4.1.1 Tests 2HH, 3HH and 10HH

A test that successfully simulated excavation without grouting was necessary to establish a datum against which later tests with grouting could be compared. The datum test would also aid in determining the locations where the grouting should be focused based on the positions of maximum vertical soil and horizontal wall movements. Such a test was therefore repeated twice intentionally using the heavy fluid pump apparatus, as previously mentioned, to provide confidence in the consistency of the results before progressing onto the grouting tests. As described in section 6.1, simulation of the excavation in the grouting

tests was conducted without the heavy fluid pump, instead allowing the SPT fluid to drain under its own self-weight. A plan was made to conduct a third excavation only datum test using the new simulation method to allow comparison against the earlier datum test results. However, during the grouting test series, a failed response in the injection system motor resulted in an unintentional delay in the commencement of grouting in test 10HH, such that grouting was delayed until 133 s after excavation completion. This initial period of the test provided data for comparison with tests 2HH and 3HH.

As previously detailed in section 5.2.2 it was intended to set a water table 25 mm below the retained clay surface for all tests which was controlled by the height of the overflow pipe in the standpipe assembly. However, owing to an unidentifiable source of leakage in the standpipe assembly in test 2HH, the water level in the standpipe was below the head of the overflow pipe. This led to the water table within the model being at an unknown lower elevation beneath the retained clay surface, as indicated by lower equalised pore pressure readings, presented in Table 6.8, of -3.5 kPa and 179.7 kPa in the top and bottom far field PPTs, respectively, for test 2HH in comparison to average values of 5.5 kPa and 204.5 kPa for tests 3HH, 6-7HH and 9-13HH in the top and bottom PPTs, respectively. Table 6.8 shows good consistency in the values of hydrostatic pore pressures established in the models, which are within 5 kPa of each other, with the exception of test 8HH for the reasons discussed earlier in section 6.1. The datum test using the heavy fluid pump apparatus was repeated with relative success in test 3HH and it is this test data which is directly comparable with pre-injection data from test 10HH.

Figure 6.25 shows settlements of the retained surface and the top of the model wall (measured by the LVDTs) at the end of excavation in tests 2HH, 3HH and 10HH. The data points between the wall and the adjacent LVDT have been connected as similar behaviour was observed locally with the image analysis from the embedded tracking targets in all of the tests conducted. The maximum settlement was seen to occur at a distance x= 0.5H behind the wall, although the inclusion of an LVDT at x= 0.75H in test 10HH suggests the settlement trough to be less steep locally than that observed in tests 2HH and 3HH. Good correlation was observed between tests 3HH and 10HH, with 15% difference in the maximum settlement value, S_{vmax} as opposed to 50% difference between tests 2HH and 3HH. Small settlements, up to 0.190 mm for test 10HH, were seen to extend a distance 3H behind the wall with the strongbox boundary at x= 3.25H.

Observation of the surface settlements 133 s after the end of excavation in each test (before starting injection in test 10HH) is indicated by the dashed lines in Figure 6.25. The disparity between tests 3HH and 10HH was seen to reduce further at this point with the difference in S_{vmax} reducing to about 7% compared to 47% between tests 2HH and 3HH. However, owing to the difference in effective stresses in the ground in test 2HH compared to tests 3HH and 10HH, similarity was not expected in comparisons of their data.

The horizontal wall displacements at the end of excavation and 133 s post excavation are shown in Figure 6.26. The embedded tracking targets in the wall and the vertical line of targets immediately below were used to track horizontal movements of the wall and soil beneath. At the end of excavation maximum horizontal displacements, S_{hmax} in all tests were shown to coincide at depth d= 0.75H beneath the retained soil surface. This position remained constant for tests 2HH and 3HH 133 s after excavation and increased marginally to d= 0.79H for test 10HH prior to injection. The data showed good correlation between tests 3HH and 10HH with displacements from test 2HH being significantly smaller. S_{hmax} for test 2HH was about 30% smaller than test 3HH at both stages of the tests. At both, the end of excavation and 133 s later, a negligible difference was observed in the S_{hmax} value between tests 3HH and 10HH. With the rigid prop at the retained soil surface level preventing horizontal translation of the wall into the excavation there was significant rotation of the wall near this horizon with visible bending taking place throughout the wall length as initially expected with the low bending stiffness of the wall. The horizontal displacements measured beneath the wall near to the bottom of the strongbox in tests 2HH, 3HH and 10HH indicated little influence on the movements from the boundary.

The vertical movements of the formation level recorded by image analysis at the end of excavation and 133 s after are plotted in Figure 6.27. Maximum heave was seen immediately in front of the wall as one would expect with rotation and bending of the wall about the prop in each of the tests. As with the retained surface and horizontal wall displacements good correlation was observed between the data from tests 3HH and 10HH with reduced magnitudes of heave in test 2HH. In tests 3HH and 10HH the most significant differential heave of the formation level was observed to extend approximately 60 mm in front of the wall face beyond which the gradient of the surface tended to reduce with more uniform heave occurring over the remaining visible formation width. Because only a single image processing camera was available after test 3HH it was not possible to

observe displacements at the formation level beyond a distance of 80 mm in front of the wall in these tests. This was due to the need to focus the available field of view around the retaining wall, the retained surface and soil surrounding the injection tubes.

A greater degree of confinement of the formation level across the 200 mm model width was provided by the heavy fluid support filled bag and strongbox rigid boundaries in comparison to the free retained soil surface. It is therefore reasonable to assume the measured soil displacement offsets, between imaging targets at the front of the model and LVDTs along the model centre line, at the free retained surface would have at least been of a smaller magnitude across the formation level.

Figure 6.28 presents the development of S_{vmax} in tests 2HH, 3HH and 10HH up to 133 s after excavation. Figure 6.29 shows the observed behaviour of the embedded model wall imaging target located at the S_{hmax} depth d= 0.75H (90 mm) below the retained surface. A clear difference is apparent in the rates of increase of S_{vmax} and S_{hmax} with time between tests 2HH and 3HH compared to test 10HH as a result of the different excavation simulation methods adopted, resulting in step wise development of displacements in the two earlier tests. Regardless of this difference a close correlation is observed in the displacement magnitudes at the end of excavation between tests 3HH and 10HH. A difference of 114 μm and 200 μm was observed between S_{vmax} values at the end of excavation and 133 s after, respectively between tests 3HH and 10HH. For S_{hmax}, smaller differences of 30 μm and 40 μm were noted at these two stages of tests 3HH and 10HH.

The smaller displacements observed in test 2HH in comparison to tests 3HH and 10HH in Figures 6.25-6.29 is expected with the lower than expected water table, discussed previously, leading to an increase in the effective stresses and hence the stiffness of the soil. This indicates that there is a greater dependency of soil and wall movements on the soil stress state rather than the duration of the excavation. It is clear from these tests that even with a difference in duration of excavation between tests 3HH and 10HH, by a factor of around 1.8, the similarity in magnitudes of soil and wall displacements at the end of excavation clearly indicate the tests were predominantly undrained during this period. In the subsequent 133 s after excavation, where no events were occurring, the displacements developed were most probably due to consolidation. The similarity in displacements after 133 s in tests 3HH and 10HH were expected given the similar stress states in the ground and displacements up to the end of excavation.

The parallels observed in the development and magnitudes of soil and wall displacements between tests 3HH and 10HH during the different duration undrained excavation events provided confidence in using the dataset obtained from test 3HH as a datum or reference against which the displacements caused by grout injection could be compared. Owing to the eventual injection event in test 10HH, significantly more excavation only data was available to use as a reference data set in test 3HH.

As discussed in section 2.2.1 the aspect of basal heave failure is a dominating source of ground movements for excavations in soft to medium clays. Although the undrained shear strengths of the soil model used in the tests of this study were expected to represent a medium to stiff clay, as discussed in section 5.2.2, it is worthwhile examining the factor of safety against basal heave, FS_{Heave}, of the model geometry and soil properties. This permits assessment of how much, if any, potential basal heave would have impacted the ground and wall measurements made in the baseline test 3HH before using the data from it as a datum for comparison in later grouting tests.

Using Figure 2.6(a) with the prototype scale dimensions of the full width excavation geometry in the model tests (H=12 m; B= 30.25 m; D= 18 m - formation level to strongbox base boundary; L= 20 m), γ=17.44 kN/m^3, $S_{u,1}$= 43 kPa, $S_{u,2}$= 58 kPa (values determined from shear vane data- see section 6.5) and N_c= 7.3 (after Skempton, 1951), FS_{Heave} simulated in the model tests is about 2.4. This value is close to the suggested lower limit of 2.5 for medium to stiff clays, as discussed in section 2.2, beyond which no clear correlation between the support system stiffness and soil and wall displacements was observed and where the aspect of basal heave failure does not contribute as a significant source of soil surface ground movements around the excavation. It is therefore reasonable to assume that basal heave would not have had a major influence in the development of soil and wall displacements in the model tests.

6.4.1.2 Tests 6-9HH

Grouting tests 6-9HH consisted of a single latex injection tube positioned at four different depths below ground surface at distance x= 0.5H behind the wall. This position coincided with the maximum settlement position observed in reference test 3HH. Placing the injection tubes at this horizontal distance would create, if effective, localised reductions in the settlement profile. Such reductions in the settlement trough have obvious potential for avoiding the notoriously damaging angular distortions associated with differential settlement of shallow buried services and structures. It was decided to vary the depth of

the injection tube with each test to observe its impact on the effectiveness of injection to control retained soil surface settlements and the effects on wall displacements. A depth spacing interval of 0.25H was used for tests 6-8HH, with a limiting depth of d= 0.75H for test 8HH, based on the observed depth of S_{hmax} in the reference tests. It was assumed that injections below this depth would be detrimental to the stability of the excavation given the proximity to the wall toe and would have limited influence on the retained surface. The decision to inject at a depth d= 0.375H (45 mm) below the surface in test 9HH was made following the observed behaviour in tests 6HH and 7HH. The injection rate available from the injection system for these four tests was 0.230 ml/s.

As a result of problems with the injection system as described in section 6.1, in tests 6-9HH, varying degrees of movement had developed prior to the initiation of injection. Figures 6.30-6.31 show the development of the vertical settlements at the retained surface and horizontal wall displacements with reference to the different timings of the injection and excavation events. The development of S_{vmax} and S_v above the injection tube location is presented in Figure 6.30. The figure clearly displays the effects of the softer soil model in test 8HH with larger movements and the significant difference in excavation duration between test 6HH and the other tests. Figure 6.31 shows the development of S_h at d= 0.75H beneath the retained surface where maximum horizontal displacements were noted in the reference test data. This permits an easier datum for comparison of the effects of injection on the wall and soil surface between tests as the position of S_{hmax} was observed to change between each of the tests, as shown in Figures 6.33 and 6.36.

The first injection pass for tests 7-9HH was started within the period of excavation. The solenoid issue (described in section 6.1) in test 6HH resulted in the excavation period being just over 3.5 times longer than the other tests. Injection in this test started after 74% of the excavation had been completed. The first pass for test 7HH began 53% of the way through simulation. A second smaller volume injection pass was made in test 7HH 103 s after excavation completion, as shown in Figure 6.35. The injection for test 8HH was started 31% of the way through excavation. Injection in test 9HH was only possible shortly before excavation completion, at 94%. Comparison of the general magnitudes and profiles of soil and wall displacements generated in tests 6-9HH at the start of injection, with the movements in test 3HH at the end of excavation (see Figures 6.32-6.34) show a logical and expected development in magnitude and shape at increasing stages throughout excavation. With injection commencing close to the end of excavation in test 9HH the

vertical settlements show a good correlation with the end of excavation settlements in test 3HH up to distance x= 0.5H behind the wall. Beyond this distance the vertical settlements for test 9HH were recorded to be marginally larger than those observed in test 3HH.

Figure 6.32 shows the position of S_{vmax} at the start of the first injection in tests 6-9HH to be in good agreement with the position in test 3HH, at a distance x= 0.5H behind the wall. Larger settlements were observed at distances greater than x= 1.5H behind the wall in test 8HH when compared to the later starting first injection in test 7HH. The far field settlement profile of test 8HH indicated more uniform settlement of the surface compared to the other tests. It is reasonable to assume this response was a result of the soil model undergoing consolidation as pore pressures returned to their equilibrium state following the model being spun down twice, as detailed in section 6.1. The depth of S_{hmax} in tests 6HH, 7HH and 9HH correlated closely with test 3HH at depth d= 0.75H, shown in Figure 6.33. As injection in test 8HH was carried out comparatively early, the magnitude of horizontal displacements generated were quite small, thus the position of S_{hmax} was not as well defined as in the other tests. However, it was clear maximum displacements were developing between $0.25 \leq d/H \leq 0.75$ below the retained surface. Maximum heave at formation level in tests 6HH, 7HH and 9HH, shown in Figure 6.34, was localised immediately in front of the wall as in test 3HH. The zone of greatest localised heave of the surface was shown to extend roughly 45 mm in front of the wall. However, after only 31% of the excavation period in test 8HH a more uniform heave of the formation level was observed from the image analysis.

Figures 6.35-6.37 compare the surface settlements, wall displacements and formation heave at the end of the first injection passes in tests 6-9HH to the movements in 3HH at the equivalent stages in excavation progression or time after completion. Tables 6.9-6.12 detail the total volumes injected at model scale at the end of each injection pass and the duration of injection in each test. The volumes differed for each test because an attempt was made to see a positive response in the retained soil surface to grout injection. The injected volumes at the end of the first injection pass were 64.51, 29.49, 41.93 and 34.33 ml, respectively for tests 6HH, 7HH, 8HH and 9HH. Injection duration and therefore volumes in tests 6HH, 8HH and 9HH were greater than in test 7HH as no immediate response was observed in the retained surface shortly after beginning injection. It was therefore decided to continue injecting until a significant response was observed. Injection was stopped once significant bending of the wall or signs of excavation failure were visible through the live camera feed. This prevented any potential permanent

damage to the model wall and latex bag within the excavation space. In test 7HH a second shorter and smaller volume pass of an additional 7.83 ml was made after a positive response in reducing surface settlements was observed after the first pass to investigate the effectiveness of controlling the surface with injection at a later stage.

The settlement profiles in Figure 6.35 clearly indicate that injection, at distance x= 0.5H behind the wall, had the effect of moving the position of S_{vmax} closer to the wall to distance x= 0.25H in all tests compared to the position observed in test 3HH. This change of position of S_{vmax} was likely due to the larger magnitudes of wall deflections generated with the injections, as shown in Figure 6.36. The injections significantly increased the magnitude of S_{vmax} observed in test 3HH by factors of 3.7, 1.25, 4.3 and 3.3, respectively for tests 6-9HH. In tests 6HH and 7HH the settlements at x≥ 1H behind the wall showed good agreement with those of test 3HH. In this region the range of differences in settlements between the grouting tests and reference test was observed to be within 0.05-0.125 mm. For test 9HH the range was slightly smaller but magnitudes larger, between 0.1-0.2 mm. In contrast the range and magnitudes for test 8HH were significantly larger, between 0.6-1.4 mm.

The first injection in test 7HH in Figure 6.35 showed a marked reduction in the settlement locally above the injection tube to under half the magnitude observed in test 3HH. The influence of the injection was observed to extend back to x= 1.5H behind the wall with notable reductions in the gradients of the soil surface relative to 3HH. Injection was stopped at this point as there was concern that continuing could cause a blowout at the soil surface.

The second injection pass in test 7HH, of smaller volume and duration, was made 103s after the end of excavation. Some small additional surface settlements up to a maximum value of 0.1 mm at x= 0.5H behind the wall developed between the end of the first and start of the second injection pass. The second pass was unable to correct these settlements. It was clear that at such a late stage after excavation in both grouting tests and reference tests there was very little increase in settlements. As such the second injection in test 7HH did not appear to cause any further noticeable increase in settlements at this point. This response was also reflected in the horizontal wall and formation level displacements, shown in Figures 6.36 and 6.37.

Based on the surface response of the shallow injection in test 7HH it would be reasonable to assume injections at greater depths would have a reduced positive effect on the surface leading to greater settlements. This assumption can be seen to apply to tests 7HH and 8HH. In contrast the magnitudes of vertical settlements in test 9HH (at a normalised injection depth d/H= 0.375) were generally larger than in the deeper injection of test 6HH (normalised injection depth d/H= 0.5) across the retained surface length. However, this behaviour can be explained by the larger magnitude of surface settlement developed prior to starting injection in test 9HH when compared to 6HH, as observed in Figure 6.32. The direct effects of grout injection on the retained surface at the location above the injection tube are discussed in detail in chapter 7.

The plot of wall displacements in Figure 6.36 show the injections in tests 6-9HH induced significantly larger horizontal displacements, S_h, relative to the data from test 3HH. A general trend is presented showing an increase in the magnitude of S_h with increasing depth of injection and distance from the stiff prop horizon (which prevented horizontal translation of the wall at the crest of the excavation). At the end of the first injection pass the magnitudes of S_{hmax} for tests 6HH, 7HH, 8HH and 9HH were about 3.5, 1.6, 4.2 and 2.4 times greater than in test 3HH, respectively. Little change was observed in the difference of S_{hmax} values between test 7HH and the equivalent stage in test 3HH, following the second injection event in test 7HH. Contrary to the behaviour observed at the retained surface in Figure 6.35, the horizontal displacements in test 6HH were greater than of test 9HH, as shown in Figure 6.36. This can probably be attributed to the larger volume injected in test 6HH and the increased horizontal confinement provided by the stiff prop in the shallower injection in test 9HH compared to test 6HH. The large horizontal displacements observed in test 8HH provide an explanation for the larger far reaching global surface settlements observed in Figure 6.35.

The position of S_{hmax} in Figure 6.36 was shown to increase in depth for all four grouting tests in comparison to d= 0.75H observed in test 3HH. A marginal increase in the depth of S_{hmax} to around d= 0.79H was seen in test 7HH. Contrary to the expectation of the depth of S_{hmax} increasing with injection depth, the position of S_{hmax} was seen to be lower in test 9HH, at d= 0.9H below the retained clay surface level, than the deeper larger injected volume in test 6HH, where S_{hmax} occurred at a shallower depth of around d= 0.82H. The wall displacement in 8HH showed S_{hmax} to occur around 26 mm below the formation level (d~ 1.22H). Significant bending of the low stiffness model wall was

apparent in tests 6HH, 7HH and 9HH. However, in test 8HH less bending was visible with the large displacement observed at the wall toe which was around 8 times larger than the displacement observed in test 3HH. Displacements of similar orders of magnitude were recorded at the wall toe in tests 6HH and 9HH, around 4.5 and 3.5 times the values in 3HH, respectively. The smallest displacements at toe level were seen in test 7HH with values around 1.8 and 1.7 times the equivalent stage displacement in test 3HH, for the first and second injection passes, respectively. The relatively large movements near the top of the wall just below the level of the retained surface and prop suggest significant rotation of the wall in the grouting tests relative to test 3HH. As the prop plate only prevented horizontal translation of the wall at the excavation crest these rotations resulted in the vertical settlements of the wall shown in Figure 6.35. Larger movements of the soil beneath the wall in Figure 6.36 were noted in the grouting tests in comparison to test 3HH. The largest displacements of the soil in this region were observed in test 8HH which correlate well with the behaviour seen at the retained soil surface (Figure 6.35) and formation level (Figure 6.37).

The heave of the formation level shown in Figure 6.37 shows significant increases in magnitude in all four grouting tests compared to test 3HH. Test 8HH produced the greatest heave. As expected from the behaviour of the wall toe in Figure 6.36 maximum vertical displacements, S_{vmax} occurred immediately in front of the wall for tests 7-9HH. In test 6HH, S_{vmax} was shown to occur at a distance approximately 20 mm away from the wall front face, even with the development of similar wall toe displacements to test 9HH (see Figure 6.36). Although S_{hmax} for the wall in test 6HH was greater than test 9HH, similar formation level heave patterns and magnitudes were presented beyond distances of 20 mm in front of the wall. For test 7HH the zone of largest surface distortion was limited to 50 mm in front of the wall. Beyond this distance the pattern of heave was more uniform, in line with the behaviour observed in test 3HH.

Inspection of the front face of the model in test 8HH immediately after removal of the Perspex window showed a clear rupture line, indicating the development of a failure plane, extending back about 60 mm diagonally from the wall toe to the invert of the latex tube position, shown in Figure 6.38. A rupture line was also seen extending diagonally in front the wall from the toe in addition to apparent shear bands radiating vertically upwards from the injection tube location. A similar response was observed after test 9HH. However with the smaller horizontal translation of the toe compared to test 8HH, no rupture line or failure plane had developed in front of the wall, as depicted in Figure 6.39.

As previously mentioned in section 5.2.5.1 brass collars were provided on the front of the latex injection tubes for test 8HH onwards following the non-uniform cylindrical cavities created during tests 6-7HH. The effect of these non-uniform cavity expansions is shown in Figure 6.40 with the resin castings of the tapered cavities created in tests 6HH and 7HH. Figure 6.40(a) shows the cavity created in test 6HH to have a more linear and gradual increase in its diameter from the back model face to the front face. In contrast, the casting of the cavity created in test 7HH in Figure 6.40(b) shows a more localised grout distribution, concentrated around the front third of the injection tube from the front model face. This difference in the shape of the uncollared tests was probably owed to the lower overburden stress in test 7HH compared to test 6HH. Figure 6.41 shows the more uniform cylindrical expansion created during injections in tests 9HH and 11HH with the use of the front brass collar. This was typical of the cavities created in tests following test 7HH where brass collars were provided. It is therefore clear that had brass collars been provided for tests 6HH and 7HH, the response observed by the LVDTs along the model longitudinal centre line would have provided a different representation in Figure 6.35 in response to injection. A detailed analysis of the effects of the provision or lack thereof of brass collars on the injection tubes in the grouting tests on the recorded vertical retained surface movements has been presented in section 6.2.

The resin castings were taken following removal of the front Perspex window from the model after removing it from the centrifuge swing where a two part urethane resin (filled with aluminium oxide powder) was mixed and poured into the cavity created, following removal of the injection tube. During the period of decelerating the centrifuge after the tests the pressure within the injection tubes was reduced by removing water from the tube using the injection system to match the reducing overburden stress above the tube with reducing *g* level. This was necessary to avoid possible blowout of the clay above the tubes and prevent the tubes from bursting. However, this had the effect of the causing the cavities to reduce in size from their original expanded volume following grout injection. As a consequence, the resin castings were only able to provide a general idea of the shape of the cavities created as the soil compressed around the reducing volume with fluid removal under the relatively high acceleration fields.

6.4.1.3 Tests 10-11HH

Following the retained soil surface and wall response observed in tests 6-9HH it was decided to increase the distance of injection behind the wall to x= 0.75H for tests 10-11HH. The depths of injection for tests 10HH and 11HH were selected to be the same as tests 7HH and 9HH, respectively, as the injection in these tests were shown to have the least impact on wall displacements but showed potential to provide compensation of surface settlements. Two injections passes were made in test 10HH and a single one in test 11HH. An injection rate of 0.115 ml/s was available from the injection system for these tests, for the reasons discussed in section 6.1

Figure 6.42 shows the development of vertical surface displacements above the injection tube location and at the position of maximum vertical settlement. Figure 6.43 presents the development of the horizontal wall displacement at d= 90 mm, coinciding with the position of S_{hmax} in tests 3HH. The development of the soil surface and wall displacements is presented with reference to the timings of the excavation and injections events relative to the start of excavation. Both figures clearly illustrate the differences in the behaviour of the soil and wall with injections at increasing depth as well as the effects of delayed injections in controlling the settlement of the retained surface vertically above the injection point. The influence of injection depth, volume and timing is addressed in detail in chapter 7. Figures 6.44-6.46 compare the displacements at the retained surface, wall and formation level established at the start of the first injection passes in tests 10HH and 11HH.

A volume of 29.61 ml was injected during the first injection pass in test 10HH with an additional 4.72 ml injected during the second. A larger total volume of 47.46 ml was injected in the single pass of test 11HH. Tables 6.13 and 6.14 show the injected volumes and timings relative to the start of excavation.

Consistent with test 3HH, the position of S_{vmax} was observed to occur at distance x= 0.5H behind the wall for both tests prior to injection, as shown in Figure 6.44. S_{vmax} in test 10HH, at the start of the first injection, was around 2.2 times greater than in test 11HH owing to the later injection in test 10HH. Settlements measured on top of the wall in test 10HH were about three times larger than in test 11HH which can be explained by the greater apparent bending of the wall and rotation about the prop observed in Figure 6.45 as a result of the delay in starting injection.

Figure 6.45 shows S_{hmax} at the start of injection in test 11HH developed at depth d= 0.63H (76 mm). As previously stated in section 6.4.1.1, S_{hmax} at the start of the first injection pass in test 10HH occurred at depth d= 0.79H; close to the depth observed in test 3HH. This position was shown to remain constant following the second injection pass in test 10HH (see Figure 6.48). As with S_{vmax}, S_{hmax} in test 10HH was observed to be approximately twice as large as in test 11HH. Near the wall toe, a significant difference by a factor of around 6 was observed between the two tests. An increase of 30% in S_{hmax} and a 45% increase in wall toe displacements was noted between the start of the two injection passes in test 10HH as a result of the first injection pass.

A uniform heave profile was noted in Figure 6.46 at the formation level at the start of injection in test 11HH which fits with the small horizontal displacements seen at the toe of the wall. In contrast, for test 10HH significant differential heave displacements of the formation level had developed before injection, extending approximately 60 mm in front of the wall. This was indicated by the increased gradients between imaging targets in this zone relative to those at greater distances from the front face.

Following both injections in test 10HH, the location of S_{vmax} remained at distance x= 0.5H behind the wall. Injection in test 11HH caused S_{vmax} to move forward to distance x= 0.25H, although the settlements at this distance were only marginally greater than at x= 0.5H. Despite the presence of the injection event, good agreement to within 0.1 mm was observed in surface settlements between tests 10HH, 11HH and 3HH, at distances $1.5 \leq x/H \leq 3.0$ behind the wall, as shown in Figure 6.47. The injections in both grouting tests caused a noticeable reduction in the surface gradients between measurement locations at distances $1.0 \leq x/H \leq 2.0$ behind the wall and a reduction of S_v at distance x= 1.0H by 34%, relative to test 3HH. The most significant difference in behaviour between the two grouting tests and reference test was observed for distances $x \leq 0.75H$ behind the wall. The first injection of test 10HH was able to compensate the surface locally above the injection tube by 100% (i.e. back to its original pre-excavation position). Figure 6.47 shows a negligible increase in the settlements occurred at distances x= 0.25H and x= 0.5H behind the wall, between the first and second injection passes for test 10HH. The second injection pass of test 10HH caused the surface above the tube to heave by 0.150 mm above the original pre-excavation surface whilst causing small increases up to values of 0.085 mm in the settlements between the centre line of the wall and distance x= 0.5H behind the wall. The increased settlements at these distances corresponded to

differences of up to a maximum of 30% above the wall and a minimum of 7% at distance x= 0.5H, compared to the equivalent stage in test 3HH representing the end of the second injection pass in test 10HH. In contrast, the earlier initiated and larger injected volume of test 11HH caused the settlement above the injection tube to increase by 17% from the interpolated settlement value in test 3HH at distance x= 0.75H. The greatest detrimental impact of injection for test 11HH was observed between the measurement on top of the wall and at distance x= 0.5H behind the wall where settlements were noted to increase by 364% and 170%, respectively, relative to test 3HH.

Figure 6.48 compares the wall displacements in tests 10HH and 11HH at the end of injection against the equivalent times in test 3HH. The position of S_{hmax} in test 10HH was shown to remain relatively constant at a depth of around d= 0.8H through the two injection passes. The first injection in test 10HH produced a 22% increase in the magnitude of S_{hmax} relative to the value prior to initiating injection. A 4% increase was observed in S_{hmax} between start and end of the second injection. In the time between the two passes an increase of 3% in S_{hmax} was recorded. In test 11HH the position of S_{hmax} developed to d= 0.82H following injection. The larger volume and lower position of injection in test 11HH resulted in S_{hmax} increasing by about 5 times the value prior to injection. The relatively small increase in the depths of S_{hmax} in both tests, between the start and end of the injection events, clearly show injecting at distance x= 0.75H had relatively little impact on the occurrence of S_{hmax} along the wall depth below the retained surface. Comparison of the magnitudes of S_{hmax} at the end of injection for the grouting tests and the equivalent data in test 3HH showed an increase by a factor of 1.13 and 1.16 after the first and second injection passes in test 10HH. A factor close to 2.4 was observed following injection in test 11HH. Similar differences relative to test 3HH were also apparent close to the wall toe with the measurements increasing by factors of 1.3 and 1.4 for the first and second passes of test 10HH and 3.2 for test 11HH. Movements of the soil beneath the wall were similar for both grouting tests although these were greater in comparison to test 3HH. The larger horizontal displacements and wall toe movement observed in test 11HH, relative to test 10HH, were probably due to the greater rotation of the wall about the prop with the deeper injection depth.

At the formation level both grouting tests showed the largest vertical heave zone extending 20 mm in front of the wall, as shown in Figure 6.49. The magnitudes of heave were significantly greater in test 11HH compared to tests 10HH and 3HH, as expected

with the larger magnitude of movements observed in Figures 6.47 and 6.48. S_{vmax} values for test 11HH were 2.7 times larger than in test 3HH. Following the first and second injections of test 10HH the heave was 1.25 and 1.2 times greater than in test 3HH. The first injection of test 10HH produced an increase in the heave in front of the wall by 30% which increased by a further 6% between injections. The second injection pass induced an additional increase by 4%. In comparison the injection in test 11HH induced an increase in S_{vmax} equal to a factor of almost 15 times the pre-injection value.

6.4.1.4 Tests 12-13HH

It was decided to simulate injection into two grouting tubes simultaneously located at distances x= 0.5H and x= 0.75H behind the wall at two shallower depths d= 0.25H and d= 0.375H in tests 12HH and 13HH, respectively. The behaviour observed in tests 7HH, 9HH, 10HH and 11HH suggested that injecting into an array of tubes would enable better control of the retained surface profile in comparison to single point injections.

Figures 6.50-6.51 present the development of soil surface and wall displacements against the elapsed time after the start of excavation. Reference is made to the end of excavation and the start and end of each injection event in tests 12HH and 13HH. Figure 6.50 illustrates the vertical surface displacements above the left and right (as viewed from the front of the model) injection tube locations as well as the maximum settlement. Figure 6.51 presents the horizontal wall displacement recorded by the embedded wall targets at depth d= 0.75H below the retained surface where S_{hmax} was observed in the reference test 3HH. Both figures illustrate the varying degrees of influence the dual injection tubes (at different depths beneath the retained surface) had on both wall and soil surface displacements with each of the two injection passes.

Figures 6.52-6.54 show the vertical retained surface, horizontal wall and vertical formation level movements at the start of the first injection pass. Movements recorded at the start of the second pass are presented in Figures 6.55-6.57 to allow direct comparison of the development of movements between the end of the first and start of the second injection pass.

In both tests an injection rate of 0.115 ml/s was adopted from the beginning following the problems with injection system motor in tests 10HH and 11HH. As a result, it was possible to initiate injection upon observation of a settlement value close to the intended surface settlement trigger value of 0.125 mm. Injection was initiated when approximately

a third of the excavation had been completed in both tests. Consequently, the developed soil and wall movements presented in Figures 6.52-6.54 show similar behaviours and magnitudes at this early stage in the excavation. Consistent with test 3HH the occurrence of S_{vmax} for tests 12HH and 13HH was observed at distance x= 0.5H behind the wall with a value of around 0.140 mm in both tests. The surface settlements in both tests were noted to be in good agreement with each other, with discernible settlements extending back to a distance x= 2H behind the wall. Similar profiles in the wall displacements and soil beneath the toe for both tests was also recorded, although the distinction of the depth of S_{hmax} between the two tests was less clear due to the small magnitudes of movement developed and the limiting 50 μm resolution available from the image processing system. Similar behaviour was also noted at the formation level with the magnitude of movements recorded laying within the limits of the image processing system.

It was assumed that because both tubes in each test were experiencing the same overburden their expansion would be relatively equal. However, for both tests the retained surface movements at the end of the first injection pass, shown in Figure 6.55, clearly indicate greater vertical movements above the left injection tube (at distance x= 0.75H behind the wall). This may be a result of the greater degree of lateral confinement provided to the right tube (at distance x= 0.5H behind the wall) by the wall itself or by the stiff prop in comparison to the left tube. At the end of the first injection pass, 42.16 ml of water was injected into both tubes in test 13HH, approximately 40% more than the 30.18 ml injected in 12HH (see Tables 6.15 and 6.16). In the second injection passes a significantly smaller volume of about 1.8 ml was introduced in test 12HH compared to 6.22 ml for test 13HH. Figure 6.55 shows the first injection in both tests significantly reduced settlements relative to the equivalent stages in test 3HH at distances between $1.0 \leq x/H \leq 1.5$ behind the wall. The influence of injection in both tests was shown to extend back to x= 1.5H behind the wall, indicated by a clear reduction in surface gradients between distances $1.0 \leq x/H \leq 1.5$ relative to test 3HH. At distances up to x= 1H behind the wall a clear increase in the gradient of the surface between LVDT locations, relative to test 3HH, was evident as a result of the expansion of the two injection tubes particularly between $0.25 \leq x/H \leq 0.5$ behind the wall. The position of S_{vmax} was moved forward to distance x= 0.25H behind the wall for both grouting tests compared to x= 0.5H in test 3HH. Comparison of the magnitudes of S_{vmax} in tests 12HH and 13HH to test 3HH show an increase by factors of 1.08 and 1.11 in test 12HH and 1.27 and 1.86 in test 13HH, for the first and second injection passes, respectively. The increase in

settlements observed between the end of the first and start of the second injection pass in test 12HH were significantly smaller than those observed in test 13HH. The second injection pass in test 13HH also caused a significant increase in settlements at distances up to x= 1H behind the wall in comparison to test 12HH. This behaviour was also reflected on top of the wall.

In both tests similar changes in horizontal displacements between the first and second injection passes to those at the retained surface are shown in Figure 6.56. Significant increases in horizontal displacements of the wall relative to 3HH were observed for both tests. Following the first injection in test 12HH, S_{hmax} was shown to occur at a depth between d= 0.7-0.8H increasing to d= 0.8H after the second injection. Similarly, for test 13HH the position of S_{hmax} was observed to occur at d= 0.8H following the first pass, increasing marginally to d= 0.81H after the second injection. A consistent increase by a factor of 1.35 was noted in S_{hmax} values at the end of both injections in test 12HH, relative to the equivalent stages in test 3HH. Significantly larger differences were recorded at the end of the injections in test 13HH relative to the values in test 3HH by factors of 1.7 and 2.1 for the end of the first and second injection, respectively. Similar movements were also noted at the wall toe. Although larger than in test 3HH, the soil movements beneath the wall in both grouting tests were shown to be relatively similar. Figure 6.58 illustrates the diagonal rupture lines traced on the front face of the model following test 13HH which were not observed in test 12HH. A rupture line was seen extending from the back corner of the wall toe to the position of the left injection tube. Open fractures were also noted locally around the front of the injection tubes shown by the shaded region as well as separation of the soil from the front wall face just beneath the formation level.

Figure 6.57 presents the vertical displacements of the formation level at the end of both injection passes and the start of the second for visual comparison of movements developed between injections. As with all the other tests conducted maximum heave was observed immediately in front of the wall with significant increases in heave along the surface compared to those observed in test 3HH. The behaviour observed between the start and end of the first and second injection passes at the retained surface and wall were also reflected at formation level. The injections of test 13HH generated greater differential displacements of the formation level when compared to test 12HH, extending up to 70 mm in front of the wall before notable decreases in the surface gradients between tracked imaging targets was recorded.

6.4.2 Injection and local pore pressure response

The two Druck PDCR810 pressure transducers (PTs) located near the outlet of the grouting injection system and in the injection manifold (closer to the entry point of the injection tube into the soil model) were intended to provide a means to check for consistency of pressure losses in the pipework between the injection tests. Using two PTs also provided a redundancy in the event of one of them failing. Table 6.17 shows the relatively consistent pressure losses, ΔP_{loss} measured in the pipework between the two PTs, in tests where they were available, with a small error range of about 6 kPa between the tests. In tests 6HH and 10HH the PT in the injection manifold stopped responding during the consolidation period. However, with the consistency observed in the pressure losses in the other grouting tests the median pressure loss value shown in Table 6.17 was used to forecast the pressure at the manifold; this allowed a better representation of the injection pressure P_i in these tests.

Post-test inspection of the injection tubes, following removal of any water showed the outer latex membrane to have collapsed back onto the outside diameter of inner Nylon spandrel tube. With the fixed outer diameter of the inner Nylon tube of 6 mm, measurements of the total external diameter (Nylon + latex membrane) were taken along the length of each injection tube to check for consistency in the latex thickness between tests. These external diameters allowed calculation of the volume of the initial cavity, V_o established in the soil model after achieving effective stress equilibrium and before commencement of the test. Table 6.18 summarises the average measured total external diameters and V_o of the injection tubes in each test. The external diameters suggested differing latex wall thicknesses ranging between 1.25-1.7 mm. Following the grouting test series, a selection of the thinnest, thickest and average wall thickness injection tubes were manually inflated with water using a Bishop ram connected to a digital pressure indicator to observe any differences in the pressure response when separating the latex from the inner Nylon tube. This manual expansion showed little difference in the behaviour and latex separation pressures; a variation of about 6 kPa was recorded between the thinnest and thickest latex walled tubes. This pressure difference was considered negligible in comparison to the magnitudes of injection pressures recorded, thus providing confidence in the behaviour of the injection tubes when installed within the soil model.

As illustrated in Figure 5.35 PPTs were installed locally around the injection tube in each grouting test. Table 6.19 summarises the radial distances between the injection tube and local injection zone PPT during the grout tests.

Figures 6.59-6.66 show plots of the injection pressure, P_i measured by the manifold PT and the pore pressure response of the local PPT (u_{inj}) for each test. For the first grouting test 6HH the PPT was installed further from the tube owing to a lack of confidence in the expected magnitude of pore pressures at closer distances, given the working limit of the PPT (350 kPa). Following the measured changes in pore pressures in this test (see Figure 6.59), the PPT was installed in the closest available pre-drilled port to the injection tube in the back wall of the strongbox for subsequent tests.

It is clear from the period prior to the start of injection in Figures 6.59-6.66 the local PPT recorded the development of negative excess pore pressures as a result of excavation. However, with excavation and injection events overlapping for most of the grouting tests, except for test 10HH, it was difficult to separate their effects from the changes induced in local pore pressures solely due to injection. The different locations of the local PPTs relative to the injection tube, distance behind the wall and depth below the surface also contribute to the difficulty of direct comparisons between the pore pressure responses to injection in the tests.

However, it is possible to outline some of the common aspects of the behaviour observed. With the exception of tests 6HH, 7HH and 9HH, shown in Figures 6.59, 6.60 and 6.62, the injections were shown to cause an increase in the rate of pore pressure reduction from the pre-injection values. In these tests a delayed increase in pore pressure following an increased rate of reduction was recorded. For most of the tests local pore pressures were shown to generally stabilise after injection, very gradually decreasing with time. In test 12HH, shown in Figure 6.65 pore pressures continued to reduce between injection events before injection in the second pass induced a small increase in pore pressures. In contrast, a recovery of some pore pressure reductions from injection and excavation were noted in the period between the first and second injection events for tests 7HH, 10HH, and 13HH. The behaviours observed in test 10HH where injection started 133 s after the end of excavation (see Figure 6.63) confirm the general observations and effects of injection on the local pore pressures.

In all grouting tests a small delay was observed before a response in the local pore pressure transducer was recorded following the first injection pass. With the short

duration of these delays, between starting injection and local pore pressure transducer response, it would be sensible to assume the injection events were largely undrained. At the end of the first pass and during the second pass, where applicable, an immediate response was observed between injection and local pore pressures. This behaviour was observed for both of the different injection rates used in the grouting tests, as outlined in Table 6.1. An explanation for these different behaviours observed during the injection events can be provided by considering the stress strain response and the development of the elastic and plastic zones in the soil around the injection tube within the framework for cavity expansion; assuming the soil to be an infinite elastic-perfectly plastic medium. Prior to injection of grout and expansion of the injection tubes, the soil surrounding the tube and local pore pressure transducer were in an elastic state; here changes in pore pressures are equal to zero, i.e. $\Delta u=0$, as illustrated in Figure 6.67(a). However, upon initiating injection the soil locally around the injection tube is plastically strained, creating an encircling plastic soil zone with radius r_p, shown in Figure 6.67(b) that increases with continued injection. During this short time after initiating injection it is possible, given the relatively large radii between the local pore pressure transducers and injection tube centres (see Table 6.19), that the plastic zone had not extended as far as the pore pressure transducer location. However, with continued injection and for subsequent injections the plastic soil zone would have expanded sufficiently to encompass the local pore pressure transducer, as illustrated in Figure 6.67(c). This would explain the initial short delay observed between injection and local pore pressure response and the immediate responses on succeeding injections.

Using this explanation based around the cavity expansion theory framework and the observations made by Au (2001), regarding pore pressure responses around expanding cavities in clays (discussed in section 3.2), the grout injection in each test should have produced locally positive excess pore pressures (in the plastic zone- see Figure 6.67). This should have been detected by the local PPT even in the tests with the 'overlapping period' of negative changes in pore pressures (generated during excavation) given their relatively close proximity to the injection point. This response should have been particularly noticeable in test 10HH where injection was started after excavation; at this point there was relatively little change in the pore pressures measured by the local PPT, shown in Figure 6.63. However, from Figures 6.59-6.66, it is shown that during the first injection pass the changes in pore pressures between the start and end of injection, relative to those established prior to starting injection, were largely negative in most of the tests. An

exception to this was observed in tests 6HH, 9HH and 11HH where a delayed but positive change in pore pressures was noted at some point in time during the injection pass resulting in a near net positive change in pore pressures due to injection. The contrasting behaviour in pore pressure changes around the cavities to that expected from cavity expansion theory can be explained by the dominant and probably larger negative pore pressures generated (in the retained soil mass) by the additional horizontal wall displacements from grout injection compared to the relatively smaller magnitude, more localised positive pressures generated in the plastic zones around the cavities in the overconsolidated clay of the model. This dominance of negative change in pore pressures (from the additional horizontal wall displacement) in addition to the negative change created by the excavation event over the smaller localised positive excess pore pressures around the cavity resulted in the net negative excess pore pressures largely observed in Figures 6.59-6.66. However, it is worth noting that cavity expansion theory and associated pore pressure behaviour, assuming an infinite elastic-perfectly plastic soil, inherently fails to account for the influence of local boundaries, especially deformable boundaries such as a retaining wall within relatively close proximity of the expanding cavity. For cavity expansions or contractions in a finite elastic-perfectly plastic soil, Yu (2000) showed that a small excess pore pressure (opposite in sign to the internal cavity pressure) was present in the elastic zone around a cavity. A similar behaviour was observed by Au (2001) during the idealised compaction grouting cavity expansions in overconsolidated clays. This behaviour also provides a possible explanation as to the general negative change in pore pressures observed in the PPTs immediately upon initiating injection (whilst being in the elastic zone- see Figure 6.67) before showing a small but positive change as the radius of the plastic zone (r_p) around the cavity tended towards the radius of the PPT location, relative to the centre of injection (r_{PPT}) (see Table 6.13).

Table 6.20 summarises the peak injection pressures and the associated total injected volumes recorded for each of the tests. The values of normalised peak injection pressure against the theoretical overburden stress ($P_{i,PEAK}/\sigma_v$) above the injection tube and normalised injected volumes at peak injection pressure against the initial cavity volume ($\delta V_{i,PEAK}/V_o$) are also presented. A general trend was visible showing an increase in $P_{i,PEAK}$ with depth in tests 6-11HH as expected with the increasing overburden stress to be overcome to enable expansion of the cavity. Good agreement was also noted in the peak pressures corresponding to injections at the same depth below the retained surface. Tests

6-11HH also exhibited similar magnitudes of normalised injected volumes at peak injection pressures ($\delta V_{i,PEAK}/V_o$). In tests 12HH and 13HH where the two injection tubes were expanded simultaneously the peak pressures were significantly lower than the pressures recorded at equivalent depths in the single injection tubes. However, with the limitations of the apparatus and instrumentation, described in section 5.2.5.2, it was difficult to assess the true injection pressures and volumes injected into each of the injection tubes in these tests.

6.4.3 Far field pore pressures

The main purpose of the PPTs, shown in Figure 5.34 was to provide real time pore pressures measurements at these horizons during consolidation to establish when the model had reached an equilibrium state where the effective stresses had become stable. Figure 6.68 illustrates the typical response recorded from the two PPTs with the associated standpipe pressure, during effective stress equalisation. With the PPTs installed 290 mm behind the model wall it was known prior to testing that the recorded response during excavation and injection would provide limited information in response to the events, particularly for the relatively short durations of the events when compared to the typical 48 hour equalisation period.

6.5 Soil strengths

Undrained shear strength, S_u readings for the soil model were recorded from hand shear vane tests carried out at 1 *g* in various locations for tests 3-13HH to monitor the consistency of the soil state between tests. Readings were taken immediately after the test once the centrifuge was stationary and the water feed to the model via the base drain isolated, to prevent excessive softening and swelling of the sample and consequential reduction in the soil strength. For test 3HH the distances of the shear vane sites behind the wall were the same as subsequent tests however readings were taken along the soil model longitudinal centre line, indicated by the starred position numbers in Figure 6.69(a), after removal of the LVDT gantry. In subsequent tests the shear vane sites were offset from the model longitudinal centre line to reduce time spent removing the gantry. This reduced the elapsed time between the model becoming stationary after the test and the taking of the readings, to again avoid any unwanted softening of the soil.

Figures 6.69(b)-(d) show the readings taken at each of the three locations defined in Figure 6.69(a). Owing to the physical dimensions of the shear vane it was only possibly to take readings at 50 mm depth intervals. With the exception of test 8HH, the S_u readings

observed at each sample site for the tests correlated well with each other throughout the model depth. The error bars shown in Figure 6.69(b)-(d) show the soil strengths for these tests lay within ±5% of the average S_u profile of all readings, signified by the solid black line. The lower soil strengths observed in test 8HH, for the reasons previously outlined in section 6.1, explain the larger magnitudes of soil and wall displacements observed and discussed in section 6.4.1.2. This inconsistency as well as the consistencies observed in S_u between the other tests must be taken into consideration in chapter 7 when making comparisons against the reference test data in test 3HH. The similarities in undrained shear strengths also provide reassurance of the consistency maintained in the model making and testing procedures across most of the tests.

The measured undrained shear strengths of the soil model in the testing programme were in good correlation with the values presented by previous researchers who adopted similar stress histories and model depths for their centrifuge model tests, as discussed in section 5.2.2.

6.6 Summary

6.6.1 Test details

A detailed description of the tests conducted has been provided. Different excavation times occurred in the two initial reference tests compared to all subsequent tests as a consequence of changing the method of removal of the heavy fluid supporting the excavation. Significant events and problems encountered in both reference and grouting tests which might affect the results have been described in detail.

6.6.2 Measurement of vertical soil and horizontal wall displacements

Comparisons have been made between the vertical settlement measurements made at the retained surface by LVDTs and image processing targets embedded around 15 mm below the surface. This exercise permitted the assessment of the plane strain behaviour of the models and frictional effects that were present at the Perspex-clay interface in each test.

Remarkable consistency across all tests was noted with near zero difference between LVDT and image processing measurements of the vertical displacement above the wall; this confirmed the plane strain response of the model wall across the tests as would be expected from a wall, relatively rigid in the direction perpendicular to the measurement plane. In addition to this response, the horizontal wall and vertical formation level displacements measured using dual cameras with the image processing system, in tests

2HH and 3HH showed the precision of the method to be within 1.5 times its resolution capacity. As such the data recorded for the wall and formation level displacements for all tests could be presented with a high level of confidence and used for discussion later in chapter 7.

At a distance x= 1.5H behind the wall the offset between LVDT and target measurements (ΔS_v) for all test was shown to develop similar values of 250-300 μm by the end of excavation where it remained relatively constant, irrespective of the excavation or injection timing during the test. In general, for all tests, a common pattern demonstrating the presence of varying frictional effects within each test was observed from increasing ΔS_v values with distance behind the wall, prior to the localised influence of any injection events on the vertical retained surface displacements.

6.6.2.1 Excavation tests

In the excavation only tests 2HH, 3HH and 10HH a remarkable similarity was observed in the magnitudes and development of the offsets, ΔS_v between LVDTs and imaging target measurements at corresponding distances behind the wall for all three tests. As with previous studies of a similar nature these offsets remained constant following excavation although the magnitudes were noted to be in general larger than the 100 μm noted by McNamara (2001) and Grant (1998). The LVDTs were largely shown to be more sensitive to settlements than the imaging targets. This behaviour indicated the clear presence of a relatively consistent frictional effect at the Perspex-clay interface that was dependent on the excavation event, irrespective of its duration and the soil stiffness, as in the case of test 2HH where a lower than expected water table most probably resulted in a stiffer soil model. In general, little variability in ΔS_v values were noted between the excavation only reference tests, even with the difference in excavation durations between tests 2HH and 3HH with 10HH and the stiffer soil in test 2HH.

6.6.2.2 Grouting tests

With regard to the provision or lack of brass collars a clear contrasting behaviour was observed between LVDT and image processing measurements of the vertical displacements close to the retained surface. In tests 6HH and 7HH excessive localised heave above the injection tube and at the neighbouring measurement locations was indicated by the image processing targets in comparison to the corresponding LVDTs which detected little to no heave along the model longitudinal centre line. This behaviour

was expected given the non-linear expansions of the injections cavities as a consequence of not providing brass collars to the front of the injection tubes. In these tests the LVDTs in general recorded greater settlements than the targets across the measured retained surface.

Injection in test 8HH which was provided with a brass collar on the tube at depth d= 0.75H (90 mm) below the surface was shown to have little effect on the measured ΔS_v offsets compared to subsequent tests 9-13HH, which were also provided with a brass collar. Similar behaviours and magnitudes to those observed in the reference tests were noted. This highlighted the possible limiting influence of injection and brass collars on the measurements from the two methods. In following tests 9-13HH, a consistent trend was observed showing the LVDTs to be more sensitive to both heave and settlements than the imaging targets. In general, the LVDTs located (along the longitudinal model centre line) above the injection tubes were shown to detect either significant reduction in the excavation induced settlements or significant heave during injection in comparison to the front embedded targets. This was expected given the restraint provided by the injection collars at the front model face, thus dulling the localised response of the soil at this front plane in response to injection. Consequently, the magnitudes and variability of ΔS_v values in these collared tests were significantly smaller than those without collars provided. As with tests 6HH and 7HH, the injection in later tests 9-13HH were shown to have an influence on measurement locations neighbouring the injection tubes but to a lesser extent. A consistent observation made across all grouting tests was the correlation between ΔS_v magnitudes and the vertical and horizontal proximity of the LVDTs and second row of targets to the injection tube location; ΔS_v was noted to reduce with increasing distance (both vertical and horizontal) between injection location and the corresponding target and LVDT.

With the larger variability, relative to the reference test, observed in the imaging target data surrounding the injection tube in two of the test sets conducted; 1) excavation and grouting (without brass collars) and 2) excavation and grouting (with brass collars) it was decided to use only the LVDT data in the presentation of the vertical displacements at the retained surface for chapters 6 and 7. Although the LVDT data was skewed in tests 6HH and 7HH as a result of the non-linear expansions, the LVDTs in general provided a more robust and consistent means of measuring vertical retained surface displacement data for all tests; being along the model longitudinal centre line guaranteed their independence

from any frictional effects at the Perspex-clay interface and were beyond the influence of the brass collars. As such the LVDTs may have provided a better average settlement response in the two tests where the collar was not used. The LVDTs were also capable of higher resolution measurements of 10 μm in comparison to the 50 μm capacity of the image processing system.

6.6.3 Observations

Good agreement was observed between the excavation only data in tests 3HH and 10HH thus verifying the consistent development of soil and wall displacements during the largely undrained event, even with the difference in excavation durations between the two tests. This provided confidence in using the dataset from test 3HH as a reference against which the movements recorded in the grouting tests could be compared.

Owing to the different timings, durations and consequently volumes of injections in the grouting tests relative to the start of excavation, comparisons with test 3HH was possible by finding the data in test 3HH at an equivalent stage to the injection event either in terms of the fraction of excavation complete or time elapsed after completion of excavation. The established soil and wall displacements prior to commencement of injection for each test have been presented to describe the variation in magnitudes as result of the different injection starting times.

In tests 6-9HH which were conducted at increasing depths and at equal distance behind the wall (x= 0.5H), a clear trend was noted indicating a reduction in capacity of the injections to compensate and control retained surface settlements locally above the injection position with increased depth. This behaviour was also reflected in subsequent tests in which the distance from the wall to the point of injection was increased for tests 10-11HH (x= 0.75H) and with the execution of simultaneous expansions of two cavities in tests 12HH and 13HH (x= 0.5H and x= 0.75H, right and left injection tubes, respectively). Significant reduction in the gradients of the retained surface were noted to extend back to distance x= 0.5H back from the injection point in tests 6-9HH, increasing to x= 0.75H for tests 10-13HH, compared to the surface profile presented in test 3HH. In front of the injection tube location the magnitudes of vertical settlements were in general (with the exception of the shallowest injections) much larger in comparison to the magnitudes observed in test 3HH. The position of maximum vertical settlement was also closer to the wall, relative to the position observed with excavation only.

With regards to the wall, horizontal displacements were recorded to be much larger for all grouting tests compared to the displacements during excavation only simulation in test 3HH. However as with the vertical settlements at the retained surface, the detrimental effect on wall displacements relative to test 3HH data increased with depth; the shallowest injections of tests 7HH, 10HH and 12HH had the least impact on wall displacements in comparison to the other tests. As might be expected, increasing the depth of injection had the effect of moving the position of maximum horizontal wall displacement further down below the retained surface horizon. Deeper injections caused greater rotation of the wall about the prop and as such displaced the soil immediately in front of the wall to a greater extent. Maximum vertical heave of the formation level was noted immediately in front of the wall for all test as might be expected with the single prop arrangement of the model.

Pore pressure transducers installed close to the injection tubes indicated a generally undrained soil response although a short delay was noted after initiation of the first injection. For tests with a second injection the local pore pressures responded immediately. An explanation has been provided for this observed behaviour based around the cavity expansion theory framework. Peak injection pressure was noted to increase with injection depth due to the increase in overburden stress with depth. An explanation has also been provided why in general negative pore pressure changes were observed locally around the injection cavities when cavity expansion theory dictates these should have been positive in the clay models. Owing to available ports in the back wall of the strongbox, the positioning of the local pore pressure transducers relative to the injection point varied between each test. As such it was difficult to provide an absolute comparison of the injection pressure behaviours observed with each injection.

6.6.4 Soil strengths

Undrained shear strength readings taken in the clay sample immediately after completion of each test indicated a good consistency between the soil models for all tests with the exception of test 8HH, where a weaker soil sample was noted. Parallels in S_u values observed by previous researchers from soil models adopting similar stress histories and model depths support the reliability of the shear vane measurements.

7. DISCUSSION

7.1 Introduction

The purpose of this chapter is to present a summary of the significant findings from the series of centrifuge tests undertaken and to provide an explanation of the behaviour observed.

The reason for applying compensation grouting beneath the retained surface behind an excavation is to provide some control and mitigation of vertical settlements of the retained soil surface and subsurface; which are consequences of the stress changes during the excavation process. In order to understand the effectiveness of the application, it is necessary to compare the development of soil and wall displacements resulting from injection and excavation against those solely from excavation. Doing so enables any relationships to be determined and similarities in characteristic behaviours to be drawn from the model tests.

The chapter is structured to allow examination of the effects of injection timing, volume and position, respectively on soil and wall displacements relative to the observed displacements in reference test 3HH (excavation only), both during and after the simulated excavation.

The focus in the following sections is on the localised difference in displacements between the grouting tests and reference tests. The vertical surface movements locally above injection and the horizontal wall displacements at depth d= 0.75H, rather than positions of maximum vertical and horizontal displacement, were selected as the points of interest. This depth along the wall coincided with the position of S_{hmax} in the reference test. Observing the difference in displacements at these locations was preferred over the location of the individual maximum displacements in each test as the latter were shown to be highly dependent on the injection position. The positions of maximum displacements would also in practice be different given the unrealistic single point injections modelled in many of the tests in this study.

The effects of grouting on the formation level movements have not been addressed in this chapter owing to the limited range of imaging targets available for the analysis of movements at the formation level. It has been shown in chapter 6 that the extent of heave displacements at the formation level were largely dependent on the lateral displacements and rotations of the wall about the prop. Therefore, with the single prop arrangement used

in the model tests one would expect that examining the effects of injection on wall displacements relative to the reference tests would provide some indication of the corresponding response at the formation level.

7.2 Consideration of the test results within existing frameworks

Peck (1969) necessarily ignored the effects of individual excavation geometries, wall types, system stiffnesses and boundary conditions for a large number of excavations in order develop an overall framework for a wide range of ground conditions, using good quality monitoring information. The chart, illustrated in Figure 2.7 and reproduced in Figure 7.1, was the outcome of the data. At the time of being published, the chart represented the first real attempt to collate and summarise case study data to enable the estimation of an upper bound for movements expected in different soil types.

Data used to develop the chart was primarily sourced from different excavations using soldier and sheet piles, which in general are less stiff than current available methods. Excavation movements where the first shallow support was installed very early on in the excavation process were also considered. As such, the chart provides a reasonable first reference point for comparison of the movements observed in the excavation only tests 3HH and 10HH in this study, with the low stiffness of the model wall used.

Figure 7.1 shows the vertical settlement, S_v and distance behind the wall, x both normalised against the excavation depth, H in tests 3HH and 10HH for the end of excavation displacements at the retained surface. This allows presentation of the data non-dimensionally against those presented by Peck (1969). Comparison with data from Peck (1969) shows that the settlements in tests 3HH and 10HH lie within the upper and lower bounds of zone 2 for movements in soft clays to limited depth. This is quite reasonable given the observed strengths of the soil from the measured undrained shear strengths taken after the two tests at 1 *g* and the general consistency of the soil during deconstruction of the model which indicated the soil to be akin to a soft to firm clay. However with a soft to firm clay in the model tests it would be expected that movements following excavation should instead lie closer to the boundary between zones 1 and 2 (profile between soft to hard clays and soft to very soft clays).

A better comparison of the normalised soil movements in test 3HH and 10HH against a more recent existing framework is made in Figure 7.1, with the bounding profiles for soft to firm and stiff soils (with high and low support stiffnesses as defined by Carder, 1995)

presented by Gaba *et al.* (2017). The bounding curves for stiff soils was presented using collated data from case studies published by several previous authors (i.e. Clough and O'Rourke, 1990; Carder, 1995; Fernie and Suckling, 1996; Carder *et al.,* 1997; Long, 2001 and Moorman, 2004) for movements resulting from excavation in front of bored pile, diaphragm and sheet pile walls and horizontal wall deflection. The profile for soft to firm clays was provided by Gaba *et al.* (2017) as an upper bound to data collated from Clough and O'Rourke (1990), Carder (1995), Finno *et al.* (2002) and Moorman (2004). In the description of the profile for soft to firm soils, Gaba *et al.* (2017) highlighted the inability to distinguish between the data representing walls embedded in stiff clay retaining some soft and firm clays from those embedded wholly in soft to firm clays.

Comparison against the profiles presented by Gaba *et al.* (2017) show the data for test 3HH and 10HH, at the end of excavation, clearly lie between the bounding curves for stiff and soft to firm clays. This is reasonable given the measured range in undrained shear strength of the clay in the model tests. The provision of the prop at the crest of the excavation, prior to simulating excavation (analogous to wishing the stiff prop in place) clearly had the effect of keeping the end of excavation movements in the model tests well within the upper bound profile for soft to firm soils at distances $x \leq 2.5H$. This was the case even with the comparatively lower wall and support system stiffness than those used in the collated case study data presented by Gaba *et al.* (2017). The movements in this region represent local movements. Beyond this distance, the normalised vertical movements (representing global excavation induced movements) for the two tests fall outside the profile for soft to firm soils but follow the general shape of the profiles presented for stiff soils. This is expected given the relative large degree of isolation from the localised excavation event. It is also worth noting the bounding curves presented by the authors represent data from non-greenfield sites in contrast to the greenfield movements in the model tests. As such, movements observed by Gaba *et al.* (2017) at these distances would have been influenced by overlying and surrounding structures and services, which in turn would affect the magnitude of the relatively small movements generally expected at such distances compared to greenfield conditions.

Peck (1969) suggested the presence of measurable movements up to distance $x= 4H$ behind the wall, whilst Gaba *et al.* (2017) found the movements for firm to stiff clays extended as far back as $x= 3.5H$. The distance, at which vertical displacements became negligible in the model tests, could not be confirmed because of the limiting boundary of the strongbox end wall at distance 3.25H behind the wall. However, the close correlation

with the profile presented by Gaba *et al.* (2017) for firm to stiff soils in non-greenfield conditions suggests the settlements in tests 3HH and 10HH would probably have been limited to distance x= 3.5-4H behind the wall.

Examining the position of maximum settlement in tests 3HH and 10HH in Figure 7.1 against the maximum settlement positions shown by Gaba *et al.* (2017) for both soft to firm and stiff clays, more clearly presented in Figures 2.14 and 2.15, respectively, shows a clear similarity. Figure 7.2 shows the normalised settlements in the two tests decreased more gradually with distance from the wall, than the profile proposed by Hseih and Ou (1998), applicable to both soft and stiff clays. A close resemblance to this profile shape is observed with a notable change in surface gradient beyond a distance of x= 2H behind the wall. Hseih and Ou (1998) identified this distance as the boundary between the primary and secondary influence zones and stated that movements in the former were those which have the greatest potential to cause damage to overlying structures.

A comparison of the normalised maximum horizontal wall displacements in tests 3HH and 10HH against the field measurements for excavations in firm to stiff clays (Moorman, 2004) are shown in Table 7.1. Moorman (2004) reviewed 530 case studies including those presented by previous researchers. The horizontal wall displacements in tests 3HH and 10HH are larger than expected, by factors of 1.67-1.7. A possible explanation for this difference is that the model wall and overall system stiffness were significantly more flexible than the typical walls from which the data was collected. This explanation also correlates with the conclusions of Long (2001) who also reported significantly greater wall displacements than the normal expectations, when examining case histories in which a more flexible retaining system was adopted.

7.3 Influence of the grouted volume

Owing to the non-linear expansions in tests 6-7HH, the unknown volumes injected into each tube in test 12-13HH and consequential impacts on displacements recorded by the LVDTs, it is difficult to establish the direct influence of the injected volumes on the displacements at the retained surface above each tube and the wall. This therefore leaves the data recorded in single injection tube tests 8HH, 9HH, 10HH and 11HH (provided with a brass collar) to be examined to enable an understanding of the effects of the injected volumes in the following sections. Tables 6.11-6.14 detail the total injected volume in each of the four tests.

The following sections examine the changes due to the effects of injection alone on vertical displacements above the injection tube, $\Delta\delta S_v$ and horizontal wall displacements at depth d= 0.75H, $\Delta\delta S_{h,\ d=0.75H}$ between the grouting and reference excavation only test. The changes are plotted from the start of injection against the normalised injected volumes, V_i/V_o. The displacement changes are normalised by the depth of injection. This is in an attempt to isolate the effects of injection depth which, as discussed further in section 7.5, are shown to have a relatively linear effect with depth on the surface (vertical) and wall (horizontal) displacements relative to the excavation only scenario in the model tests. The depth of injection is also shown, in section 7.5, to have a greater influence on the compensation of vertical settlements at the retained surface than the distance behind the wall.

The changes in displacements solely due to injection were calculated by subtracting the movements recorded in the excavation only test from the corresponding data in the grouting tests, thereby isolating displacements caused by the excavation process.

7.3.1 Vertical displacements at the retained surface

Figure 7.3 shows the development of changes in normalised vertical displacements between the grouting tests and excavation only reference data relative to the start of injection against the normalised injected volumes for each test. The cumulative injected volumes are normalised against the initial cavity volume created by the injection tube in the test. The injection pressures normalised by the total overburden stress above each injection location are also shown.

In normalising the changes in displacements by the injection depth, one would expect to see very similar changes in displacements with the same normalised injected volume if there existed a common relationship between volume injected and relative displacements induced at the surface. However, as can be seen in the figure and considering the total volumes injected from Tables 6.11-6.14, this was not the case.

A clear net positive effect was noted in the shallow injection of test 10HH in contrast to the overall negative effect in the deeper injection in test 8HH from the start of injection. In tests 9HH and 11HH, where injections were conducted at depth d= 0.375H for both tests but at distances x= 0.5H and x= 0.75H behind the wall, respectively, a similar positive response in the relative normalised displacement changes were noted up to normalised volumes of about 1.55 and 2.34, respectively. The introduction of additional

volumes beyond this point resulted in the deterioration of the positive changes in displacements established, leading to overall net negative effects at the end of injection. This clearly shows that different optimum volumes existed for each of the two tests for which positive compensation of the surface locally above the injection would have been noted.

It is worth noting that a different but critical volume existed in all of the tests shown but 10HH, at which point the rate in the change in displacements relative to the excavation only data were shown to significantly increase, noted by the change to a steeper gradient following the initial injection period in Figure 7.3. This is possibly due to the higher position of grouting in test 10HH and consequently closer proximity to the lateral confinement provided by the stiff prop in comparison to the other tests. The normalised injected volumes at which this rate of displacement increases was also shown to coincide with the same point where a significant change in the normalised injection pressures were noted; after which they begin to reduce at an increased rate.

It therefore follows given the different behaviours observed between the different injected volumes that no clear or direct relationship existed solely between the injected volume and displacement changes at the retained surface above the injection location in the model tests.

The difference in behaviour between the tests, even when normalising by their respective injection depths, suggests that the influence of the position of grouting, in particular the proximity to the surface, dominates over the injected volume for displacements at the retained surface, at least locally, above the injection location. This follows from the general pattern of decreasing positive compensation effect to increasing negative effect with increasing injection depth.

One would expect however from a practical point of view, that less volume should be required to generate positive compensation effects as distance to the surface reduces, at least for injections that are carried out above the limiting depth of d= 0.5H, discussed further in section 7.5.

7.3.2 Horizontal wall displacements

The normalised change in horizontal wall displacements between the grouting and reference tests at a depth of d= 0.75H are plotted against the normalised injected volume from the start of injection in Figure 7.4. The figure clearly shows, as described in chapter 6, that all of the grouting tests had a negative effect on the wall displacements relative to the behaviour observed from excavation only.

As with the changes in vertical displacements discussed in the previous section, no clear or distinct relationship is apparent between the total volume injected and the changes in displacements due to injection alone.

In line with the behaviour observed in Figure 7.3 the phenomena of a sudden increase in the rate of negative displacements for all test, except the shallowest injection in test 10HH, was observed at the same critical volumes for each test. This clearly indicates that the addition of extra volume into the cavity beyond this volume results in significant worsening of the negative wall displacements relative to the excavation only scenario. Halting the injection process at these critical volumes, particularly in tests 9HH and 11HH, would have resulted in both a positive compensation effect at the retained surface and minimal negative effect on the wall displacements in comparison to the responses at the end of the total injected volume in the tests.

Contrary to the behaviour observed at the retained surface in Figure 7.3, a larger negative effects was observed in Figure 7.4 for the shallower smaller volume injection of test 9HH compared to the deeper injection in test 8HH. This was observed irrespective of the fact that changes in displacements relative to the reference test, from the start of injection, were normalised by the injection depth. If a linear relationship existed between the injected volume, horizontal wall displacements induced and injection depth, one would expect similar responses from each of the four tests at the same normalised injected volumes.

In comparing tests 9HH (x= 0.5H, d= 0.375H) and 11HH (x= 0.75H, d= 0.375H) it can be seen that the normalised changes in displacements were relatively similar up to a normalised injected volume of about 1.0. However, beyond this volume, further injection in test 9HH induced larger negative changes in displacements on the wall than that observed in test 11HH. This was similar to the behaviours observed at the retained surface for the two tests in Figure 7.3. In line with the normalised changes in displacements at the retained surface injections beyond normalised volumes of around 1.55 and 2.34 for tests

9HH and 11HH, respectively resulted in the increased rate and deterioration of wall displacements by the end of injection. This again suggests that they were optimum volumes in the particular conditions of these tests at which the negative effects on the model wall could have been minimised. In contrast to tests 8HH, 9HH and 11HH the shallower injection in 10HH, being closer to the prop horizon showed a relatively linear increase in normalised wall displacements with normalised injected volume.

It therefore follows from these observations that factors, other than the injected volume, appear to dictate the behaviour of the wall displacements examined at depth d= 0.75H.

7.4 Influence of the timing of grout injection

This section focuses on the effect of the timing of grout injection relative to the excavation event for two sets of tests; 1) 7HH and 10HH and 2) 9HH and 11HH where similarities existed in injected volumes and positions below the retained surface but significant differences in the time periods before the initiation of injection and the duration of injection existed between each test. As such the behaviours observed within each set provide a tool to compare the effect of grout injection timing on the development of vertical retained surface movements above the injection location and horizontal wall displacements at depth d= 0.75H. The datasets are compared to the excavation only dataset.

7.4.1 Vertical displacements at the retained surface

Injection in test 7HH was conducted at the same depth as test 10HH but closer to the wall. For test 7HH injection was carried out at distance x= 0.5H and for test 10HH x= 0.75H. Crucially in test 7HH injection of the first pass was initiated and completed during the excavation period in comparison to the post excavation, initiation and completion of both injection passes in test 10HH.

The development of settlements in these tests at the retained surface, above the injection tube location, are illustrated in Figures 7.5 and 7.6, during excavation and the time after, respectively. In line with the behaviour observed across the grouting tests, regardless of the timing of starting injection, the deviation in settlements from those attributed to excavation only, prior to commencing injection, was relatively small for all four tests 7HH, 9HH, 10HH and 11HH, up to an equivalent value of 0.08%H (or 0.0008H). This indicates that prior to injection the soil was behaving as expected solely due to excavation.

The relatively early start of injection in test 7HH following 53% completion of the excavation showed a small delay in response at the surface, before gradually increasing to provide a positive compensation effect equivalent to 0.65%H by the end of injection, after 97% completion of the excavation, as summarised in Table 7.2. Following this period, relatively little change in this positive effect was observed even with the introduction of a second smaller volume 103 s after excavation. Dissimilarly the first post excavation injection in test 10HH resulted in a greater positive compensation effect, by a factor of around two, as illustrated in Table 7.2.

Upon initial examination this trend suggests that even with a smaller injected volume in test 10HH compared to 7HH (a volumetric difference of around 10%), late (post excavation) injection yielded better compensation effects than the early injection during excavation. However, the effect of the non-linear cavity expansion in test 7HH must also be taken into consideration, as discussed in section 6.2, which resulted in an underrepresentation of the actual influence of injection in the data recorded by the LVDTs, at the surface along the model centre line, used in Figure 7.5-7.6.

It was shown in Figure 6.8 and Table 6.4 that a significantly greater heave was noted at the front face of the model in test 7HH in the imaging target than the LVDT, above the injection tube location at the end of the first and second pass. Comparison of the vertical displacements recorded by the imaging target close to the surface above the injection tube in test 7HH to the vertical displacements observed in the reference test 3HH would have provided δS_v values of -7.57 mm at the end of the first injection pass and -13.12 mm at the end of the second pass; both these values are significantly larger than those presented in Figures 7.5-7.6. Considering the average vertical displacements (S_v) values obtained by the LVDT and target measurements (above the injection tube location at the end of each injection event), shown in Figure 6.8, allows for some redistribution of the injected volume along the length of the cavity, had a brass collar been provided, to be taken into account. Subtracting these average values from the vertical displacement recorded in the reference test and then normalising by the excavation depth, H would have instead provided positive compensation effects to the order of -3.48% and -5.77% at the end of the first and second pass, respectively. Comparison of these average $\delta S_v/H$ values against those presented in Table 7.2 (obtained solely using LVDT data) suggests that, if a brass collar been provided for the injection tube, to enable a more uniform cavity expansion along its length, the early injection in test 7HH would have possibly been at least 2.5 times more efficient than the positive effects of the late injection in test 10HH.

Consequently this analysis of the vertical displacements logged by the LVDTs and imaging targets for the non-linear cavity expansion in test 7HH make it possible to suggest with good confidence that an equal or greater positive compensation effect would have been observed from the early (during the simulated excavation) injection event in test 7HH compared with test 10HH. This observation would be consistent with the trend observed in comparing tests 9HH and 11HH, as discussed below.

Comparison is made of the difference in localised surface settlements above the injection tubes in test 9HH and 11HH, relative to the reference excavation only settlement developments in Figure 7.5 and 7.6. The figures show the earlier initiated (starting after 68% excavation completion) but larger injected volume (with a volumetric difference of 30%) in test 11HH, yielded a significantly smaller negative compensation effect on the local vertical settlement than the late starting injection (after 94% completion of the excavation) in test 9HH.

Figures 7.5 and 7.6 show that the earlier injection in test 11HH and later injection in test 9HH were both able to correct the small deviation in local surface settlements up to a value equal to 0.06%H, that had developed prior to injection commencing above the injection tube by the end of the simulated excavations. Consequently the settlements above the tube were in line with those observed from the excavation only test. This was achieved even with the larger volume injected by the end of the simulated excavation in test 11HH compared to test 9HH, as summarised in Table 7.3.

Although both tests 9HH and 11HH had a net negative compensation effect at the end of injection (in contrast to tests 7HH and 10HH) the indication of the momentary positive effect during injection before causing unfavourable settlements in both tests hint at the potential for injections at similar depths to provide a positive compensation effect.

It is also worth noting the effect of different waiting times between the first and second injection passes in tests 7HH and 10HH. In test 7HH the elapsed time between the end of the first pass and start of the second pass of 119 s was almost twice the 61 s time period between two injection passes in test 10HH, summarised in Table 7.4. As these periods were after simulation of the excavation the development of settlements in the model at this time would primarily have been due to consolidation, as the localised -Δu generated from excavation and dominant -Δu caused by the additional wall displacement after the first injection (discussed in 6.4.2) dissipated before the influence of the upcoming injection event.

The reduced period between injections in test 10HH resulted in an increase in the positive compensation effect from the second injection pass by 0.05%H in comparison to an apparent decrease in the effect by 0.14%H for test 7HH (as shown in Table 7.4) possibly due to the non-linear effects present in the expansion of the cavity in test 7HH. This behaviour fits with the conclusions presented by Soga *et al.* (2004), Au (2001) and Lee *et al.* (2000), who described improved grouting efficiencies with shorter waiting periods between injections by taking advantage of the compensation effect of the previous injection prior to its reduction as a result of dissipation in localised pore pressures, which ultimately lead to an increase in settlements due to consolidation.

7.4.2 Horizontal wall displacements

It is likely that despite the non-linear cavity expansion in test 7HH, the measured horizontal displacements using the targets embedded on the front seal of the retaining wall were representative of movements across the model width. This is due to the observations presented in chapter 6, which provided evidence that the wall displaced largely as a rigid body. In addition, given that the bending stiffness of the wall in the out of plane direction was significantly greater than its stiffness along depth of the wall, differential wall displacements between the front face and longitudinal centre line of the model would have been very small, if not negligible.

In general, it was found in chapter 6 that all grouting tests had a detrimental effect on wall displacements in the context of displacements observed from excavation only. However, the extent of these effects on wall displacements, with respect to timing of the injection events, can be better understood by examining the two sets of tests individually; tests 7HH with 10HH and 9HH with 11HH.

In contrast to the behaviour observed at the retained surface (in section 7.4.1), an immediate response to the start of injection in terms of wall displacements was noted for both tests. Figure 7.7 shows that the early initiation and completion of the injection in test 7HH (in comparison to 10HH) resulted in a gradual increase in wall displacements by 0.91%H at the end of injection relative to test 3HH, as summarised in Table 7.5. This negative effect on wall displacements was shown to remain relatively constant in the period following injection and excavation, seen in Figure 7.8, and appeared to be unaffected by the introduction of the second smaller volume 103 s after the simulated excavation.

As expected, with the comparisons made between tests 3HH and 10HH in chapter 6, a very good correlation was observed in the wall displacements at d= 0.75H prior to the commencement of injection in test 10HH, shown in Figure 7.7. Initiation of the late injection 133 s after excavation (shown in Figure 7.8) with a similar injected volume to that in test 7HH, resulted in a significantly smaller detrimental effect on the wall at d= 0.75H in test 10HH. This produced an increase in horizontal displacements by 0.26%H (Table 7.5) relative to test 3HH, which again by and large appeared to remain constant during the following period and through the much later second injection pass. However, it is worth noting that the point of injection in test 7HH is closer to the wall than in 10HH, discussed further in section 7.5. This provides a reasonable explanation of the larger effect on the wall in test 7HH compared to test 10HH, as would be expected.

In contrast to the effect of timing observed in tests 7HH and 10HH, the different starting times for injection in tests 9HH and 11HH in Figure 7.7 (see Tables 6.12 and 6.14) resulted in a relatively small difference in the final impact of injection on the wall displacements at d= 0.75H compared with the reference test. This was the case even with the larger injected volume in test 11HH and closer proximity to the wall in test 9HH as shown in Figure 7.8. Table 7.5 summarises the normalised effect of injection on wall displacements relative to the excavation only data. A small difference of only 0.09%H was observed between the negative effects on the wall in tests 9HH and 11HH. Following completion of injection, the gradual rate of increase in wall displacements relative to test 3HH was similar for tests 9HH, 10HH and 11HH.

Contrary to the similar rates of increase in δS_h following injection, in tests 9HH, 10HH and 11HH (shown in Figure 7.8), the early initiated and completed injection in test 7HH resulted in a visibly lower rate of increase in the period after excavation and injection, where movements are governed by consolidation.

7.5 Influence of the position of grouting

This section focuses on the effects of the different grouting positions adopted in all of the grouting tests on the vertical displacements locally above the injection tube and on the horizontal wall displacements at depth d= 0.75H, relative to the displacements observed in the reference test at the same positions.

7.5.1 Vertical displacements at the retained surface

Figures 7.9-7.10 show, δS_v, the difference in vertical settlements between the excavation only data in test 3HH and the injection test data for tests 6-9HH locally above the injection tube during excavation and the period after, respectively. As with all the grouting tests, regardless of the timing of starting injection, the deviation in settlements from those attributed to excavation only, prior to commencing injection, was relatively small. In tests 6-9HH this deviation was up to an equivalent value of 0.08%H (or 0.0008H), showing that prior to injection the soil was behaving in accordance with the excavation only data.

In agreement with the general pattern found in chapter 6, the beneficial effect at the end of injection (with respect to compensating settlements induced solely by excavation) at the retained surface above the injection tube appears to decrease with depth as indicated by tests 6-8HH (see Figure 7.9) by the end of excavation. Although injection in test 9HH was started very late during the excavation period this general behaviour was reflected after completion of injection in the test, as illustrated in Figure 7.10.

Table 7.2 summarises the positive and negative compensation effects of the injections in tests 6-9HH at the end of the first injection pass relative to test 3HH when normalised against the excavation depth, H. The shallowest injection in test 7HH had the greatest positive compensation effect and the deepest injection in test 8HH had the greatest negative compensation effect. The values in the table suggest injections, regardless of volume or timing, from a depth d= 0.5H and below produce unfavourable vertical retained surface displacements with respect to the excavation only scenario.

However, as previously discussed in section 7.4.1, the vertical displacements at least locally above the injection tube recorded by the LVDTs (reflected in Figures 7.9-7.10) were underrepresented in tests 6HH and 7HH due to the non-linear cavity expansions resulting from not having a brass collar at the front of the tube during injection.

Consideration of the average δS_v values, using the average of the LVDT data and target data close to the surface and above the injection location in test 7HH, was shown in

section 7.4.1 to represent significantly greater positive compensation effects (relative to the excavation only event) at the end of the first and second pass than those presented solely using LVDT data in Table 7.2.

Conducting a similar analysis for test 6HH shows that the injection (if a brass collar had been provided) had the potential to produce a positive compensation effect such that $\delta S_v/H$= -0.196% in comparison to the value in Table 7.2. This suggests that injections up to and including a depth of d= 0.5H have the potential to reduce settlements generated solely due to excavation, at least locally above the point of injection. Consideration of this potential compensation effect for test 6HH would suggest the brass collared, shallower and smaller total volume injection in test 9HH had a marginally greater negative effect than the deeper and larger volume injection in test 6HH, even during the short period where a positive effect was observed during injection equal to $\delta S_v/H$= 0.17% in test 9HH. However, it is worth noting again that injection in test 9HH was initiated quite late during the simulated excavation and completed after excavation. This was contrary to test 6HH which was started and completed before the end of excavation as shown in Figure 7.9.

It is therefore possible to suggest, based on the discussion and findings in section 7.4, that if injection in test 9HH been carried out earlier (i.e. during the excavation period) the magnitude of the momentary positive effect observed during injection would have possibly been larger than the potential positive effect observed for test 6HH, had the injected volume been distributed linearly along the injection tube length.

It also worth noting the significantly longer excavation period experienced in test 6HH, which was about three times the durations in tests 7-9HH. The displacements prior to injection in test 6HH are shown in Figure 7.9 to be in line with the excavation only displacements observed in the reference test 3HH and test 10HH (prior to initiating injection- see section 6.4.1.1).

Also, worth noting from Figure 7.9 is the sudden and sharp increase in the rate of settlements due to injection relative to the excavation only scenario shortly after injection in the two deep grouting tests 6HH and 8HH. This behaviour was not reflected in the shallower injections test 7HH and 9HH, where a more gradual change in displacements was recorded. The sudden sharp behaviour observed would cause significant problems in the field as not only would the increase in settlements relative to excavation cause further damage (in addition to that solely from excavation) to any overlying structures but would

also come about unexpectedly, allowing little time to react and arrest the settlements or to stop the grouting operation. A similar effect was also noted in tests 6HH and 8HH on the horizontal wall displacements at depth d= 0.75H, as discussed in section 7.5.2.

It therefore follows, that the behaviour observed and discussed with respect to the timing of injection for tests 7HH, 9HH, 10HH and 11HH in section 7.4.1 also applies for injection up to a depth d= 0.5H, such that early injection (i.e. initiation and completion during the excavation period) up to a depth d= 0.5H has the potential to positively compensate settlements generated due to the excavation process.

Consequently, it is possible that, for injection depths up to d= 0.5H, timing is as significant a factor as the position of grouting. Below this depth, as shown in the behaviour during test 8HH (injection at d= 0.75H), the earlier start and completion of injection during excavation had little positive effect on the settlements relative to the excavation only scenario. At such large depths the indication is that timing and volume become irrelevant and that negative compensation effects are always generated at the retained surface.

Comparison of test 7HH with 10HH and test 9HH with 11HH, shown in Figures 7.5-7.6, enable a preliminary examination of the effects of distance of injection behind the wall. The figures clearly show that for injection at depth d= 0.25H in tests 7HH and 10HH, a greater positive compensation effect was generated with injection at an increased distance from the wall. However this behaviour was somewhat skewed between the effects of the non-linear cavity expansion in test 7HH and the significantly late injection in test 10HH, as discussed in section 7.4.1. A similar response is also noted for injections at d= 0.375H in tests 9HH and 11HH, even during the short period where a maximum positive compensation effect of $\delta S_v/H$ equal to -0.17%H and -0.20%H for test 9HH and 11HH was observed, respectively, before deteriorating to the values shown in Table 7.2 at the end of injection.

Test 7HH with 10HH and test 9HH with 11HH serve as comparative tools to assess the behaviour exhibited in tests 12HH and 13HH, respectively as the injection positions in the former test sets represented the left and right hand injection tube positions in the latter tests at depths d= 0.25H and d= 0.375H, respectively (see Figure 6.1- positions of grout injections).

Figures 7.11-7.14 compare the development of vertical displacements relative to test 3HH above the location of the injection tubes at the retained surface for the single and dual injection tube tests, both during excavation and the period after. Table 7.6 summarises the compensation effects achieved in the single and dual injection tube tests. As with tests 6-9HH it is clear greater positive effects were observed in the shallower injections at depth d= 0.25H for tests 7HH, 10HH and 12HH in comparison to the deeper injections at d= 0.375H in tests 9HH, 11HH and 13HH. It is apparent from the figures that the injections at the same depths generated very similar general responses to the injected volumes regardless of the different volumes and timings of injection events. In line with all other grouting tests, all six tests show negligible differences in settlements prior to the start of injection as expected with excavation only simulation.

The second injection in test 12HH (at d= 0.25H) further improved on the positive compensation effects observed at the end of the first. This was in contrast to the second injection of similar volume in test 7HH (closer to the wall at x= 0.5H) but in line with the second volume injected in test 10HH (further from the wall at x= 0.75H). In contrast the secondary injections in test 13HH (at d= 0.375H) resulted in deterioration of the positive compensation effect achieved above both injection locations. It is difficult to compare the secondary injection behaviour of test 13HH with tests 9HH and 11HH, conducted at the same injection depth, as no secondary injections were made in the two single point injection tests.

Tests 7HH and both injections (left and right) of test 12HH showed a very similar response in magnitude to injection, with grout injection commencing during the excavation, as shown in Figure 7.11. Figure 7.12 shows that even with delayed injection in test 10HH the magnitudes of the positive compensation achieved were very similar to the values achieved in both injection locations of test 12HH.

Greater positive compensation effects were noted in test 12HH above the injection tube located at distance x= 0.75H than at distance x= 0.5H, suggesting that a larger volume was injected into the left hand tube than the right. This was plausible as there was no control over the individual volumes injected into the tubes. It is also possible the larger compensation effect in the left tube was observed owing to lower horizontal confinement that was provided compared to the right tube by the stiff prop and closer wall proximity. However, this contradicts the findings of Au (2001) who reported increased compensation efficacies with reduced spacing between simultaneous grout bulb expansions and the

surrounding rigid boundary in Speswhite kaolin clay samples. It is worthwhile highlighting that the model wall used in this study was far from being representative of a rigid boundary; this possibly helps in explaining the contrast in observations between Au (2001) and those made from tests 12HH, 10HH and 7HH. A similar pattern is also apparent between tests 7HH and the more distant (from the wall) injection in test 10HH. It is however worth noting at this point that the positive effects achieved in test 12HH were done so with a very similar total volume injected between both injection tubes to that of the individual total volumes injected in test 7HH and 10HH respectively.

In line with tests 7HH, 10HH and 12HH (injections at d= 0.25H), very similar general responses between all three injections in tests 9HH, 11HH and 13HH (injections at d= 0.375H) were noted irrespective of the different volumes and injection timings, as shown in Figures 7.13-7.14.

In contrast to tests 9HH and 11HH, the simultaneous injections in test 13HH generated a net positive effect above both injection tubes, although this effect was shown to reduce at a faster rate after completing injection than the observed post injection response in tests 9HH and 11HH.

A possible explanation for this behaviour can be provided with reference to the larger change in excess pore pressures observed in test 13HH than in tests 9HH and 11HH (as shown in Figures 6.62, 6.64 and 6.66). Also, a greater and quicker recovery of the pore pressures after injection was seen in 13HH than observed in the single injection tests. Consequently, greater consolidation induced settlements were probably generated with the larger pore pressure change in test 13HH than the other two tests, resulting in a comparatively greater rate of reduction of the immediate post injection compensation effects shown in Figure 7.14.

As in test 12HH, the left hand injection tube at distance x= 0.75H in test 13HH was noted to have a greater positive compensation effect than the right hand tube at distance x= 0.5H; this suggests again that a larger proportion of the total volume may have been injected in the left tube than the right. However, it also worth noting from chapter 6 that the single tube injections in tests 6-11HH had the effect of causing a significant increase in the maximum settlements which moved closer to the wall from the point of injection. Therefore, it is possible the larger injected volumes in the left hand tubes in tests 12HH and 13HH caused a significant increase in settlements, which moved forward towards the

wall and thereby increased the settlements to be compensated by the right hand tube at distance x= 0.5H.

It clearly follows that better efficiencies in injected volume can achieve very similar positive compensation effects above the injection location if an array of injection tubes up to depth d= 0.375H are utilised instead of single point injections at the same depths.

7.5.2 Horizontal wall displacements

Figures 7.15-7.16 show the development of the horizontal displacement of the wall at depth d= 0.75H in tests 6-9HH relative to those observed from the excavation only reference test.

The figures clearly show an increasing negative and unfavourable effect on the wall displacements with injection depth. Table 7.5 summarises the increase in magnitudes of the differences, as a result of injection, observed against the excavation only data normalised by the excavation depth, $\delta S_{h(d=0.75H)}/H$. As would be expected from the effects of excavation only, already discussed for tests 7HH, 10HH, 9HH and 11HH in section 7.4.2, the movements prior to injection were in line with the reference test wall displacements.

Figure 7.15 shows that the injection in tests 6HH and 8HH at depth d≥ 0.5H resulted in similar but significant negative effects on the wall. Also, in line with the sharp and sudden displacements at the retained surface, the same behaviour is reflected in the wall at d= 0.75H for both tests. This sudden and sharp increase in wall displacements in both tests probably contributed to the sudden behaviour observed at the retained surface and clearly shows injections below depth d= 0.5H produce unexpected and unwanted soil and wall responses.

Following the injection events in the period after excavation (Figure 7.16), the negative effects on the wall remained relatively constant for injections at d≤ 0.5H. However, for test 8HH, with injection at d= 0.75H and being completed at the end of the simulated excavation, there was a noticeable increase in wall displacements, suggesting that injection at this position severely destabilised the excavation. This ties in with the fracture or slip planes that developed and were observed at the end of the test (as shown in Figure 6.38), suggesting the excavation was close to failure and that this state was clearly influenced by the grout injection.

Comparison of test 7HH with 10HH and test 9HH with 11HH against the wall displacements generated solely due to excavation, shown in Figures 7.7-7.8, generally indicate a trend where the negative effects due to injection reduce with distance from the wall, which would be expected. The least negative effect on the wall was noted in test 10HH, being the shallowest and furthest from the wall and largest unfavourable effect from test 9HH, being the deepest and closest to the wall of the four tests, as shown in Table 7.5. A smaller negative effect was observed in test 7HH in comparison to test 9HH which was most probably due to the closer proximity to the stiff prop that would have provided significantly more lateral confinement to the added grout volume behind the wall in test 7HH than in test 9HH.

Examining Figures 7.17-7.18 shows a smaller detrimental effect on wall displacements with increasing distance from the wall in tests 7HH, 10HH and 12HH, confirming the previously discussed observations. The earlier injection in test 12HH (with expansion, as previously suggested to be biased towards the tube at distance x= 0.75H) resulted in a smaller negative effect on wall displacements in comparison to the closer and later injection in test 7HH. The significantly later injection in test 10HH, at the same depth but at greater distance than test 7HH, had the least detrimental effect on wall displacements.

Comparison of the behaviours for tests 7HH, 10HH and 12HH in Figures 7.17-7.18 with tests 9HH, 11HH and 13HH in Figure 7.19-7.20, where injections were conducted at d= 0.375H, indicates again that the shallower injections had a significantly smaller unfavourable effect on horizontal wall displacements. Figure 7.20 clearly indicates very similar general behaviours between tests 9HH, 11HH and 13HH, even with the introduction of a secondary smaller additional volume in test 13HH.

In contrast to the behaviours observed for tests 7HH, 10HH and 12HH in Figures 7.17-7.18, the dual simultaneous injections in test 13HH had a significantly smaller negative effect on wall displacements than tests 9HH and 11HH. This was possibly partly due to the biased expansion of the left hand cavity at distance x= 0.75H over the right hand injection tube at distance x= 0.5H, resulting in lesser influence from the smaller volume injected in the right side tube. It is also worth noting that grout injection for tests 9HH, 11HH and 13HH were all initiated at some point during the excavation period in contrast to the timing variation between tests 7HH and 12HH with test 10HH in starting grout injection.

Table 7.5 shows a very similar order of negative effects due to injection in both tests 9HH and the greater distanced injection in test 11HH, with the latter producing a marginally larger negative effect. This was contrary to the behaviour observed between tests 7HH and 10HH, suggesting the differences in the negative impacts on horizontal displacements, with increased distance of injection behind the wall, become less noticeable with increased distance below the surface and the horizon of lateral confinement provided by a prop.

7.6 Summary

7.6.1 Volume of injected grout

Comparison of the normalised changes in displacements between the grouting tests and reference test at the retained surface locally above the injection with the normalised injected volume, showed no clear or distinct relationship between the total volume injected and the compensation achieved relative to the start of injection. A clear difference in behaviours between the four single injection, brass collared tests examined indicated instead that at least in the model tests, the proximity to the retained surface has a greater influence on the surface displacements than the volume injected. Similar changes in the soil and wall displacements and the general behaviour from the start of injection were noted between tests 9HH and 11HH where injection was conducted at the same depth below the surface, irrespective of the larger horizontal distance from the wall in the latter test.

In examining the changes in the horizontal displacements of the wall at depth d= 0.75H, again no clear relationship between the total injected volumes and effects on the wall displacements relative to the excavation only data was observed. This suggests that factors other than volume control the changes in relative displacements observed at the wall.

A clear and common feature between the behaviours at the retained surface and retaining wall displacements was noted amongst the four tests examined. Different but critical volumes were noted in the four tests where a significant increase in the rates of displacements, both vertically (at the retained surface) and horizontally (at wall depth d= 0.75H), were noted. The addition of grout beyond these critical volumes resulted in significantly greater negative effects in tests 8HH, 9HH and 11HH by the end of the injection event.

7.6.2 Timing of injection grouting

The observed behaviour in the two sets of tests 7HH with 10HH and 9HH with 11HH show that injection timing has some impact on the overall magnitude of compensation achieved, summarised as follows:

- Initiating injection earlier, at least before 70% completion of the excavation, has greater potential to positively compensate for excavation induced settlements rather than at a stage closer to the end of excavation.
- It is clear from these tests that this impact of injection timing may be secondary to the position of the grout injection, discussed further in section 7.5, and that the magnitude of positive or negative compensation generated by injection is at least partially dependent on the position.
- Shallower injections (i.e. $d \leq 0.25H$) near the surface have significantly greater capacity to mitigate excavation induced settlements local to the injection position if carried out and completed during the excavation rather than in the period after.
- Deeper injections, up to a depth of $d = 0.375H$, initiated at least before 70% of excavation completion can yield a positive compensation effect on local surface settlements.
- Conducting secondary injections, even if of significantly smaller volume than the first pass, were shown to be far more effective in the compensation of local vertical settlements if conducted closer to the end of the first injection. Doing so possibly allows advantage to be taken of the strengthening effect on the soil created by its localised compression after the first injection.
- Reducing the time between the first and second injection was observed to potentially provide a reduction in the change of negative localised pore pressures, as shown in Table 7.4, generated by the initial injection. This could possibly have led to smaller additional consolidation induced settlements developed after injection as a result of the smaller change in effective stresses in the high hydraulic gradient region created around the injection.

The contradictory behaviour between the two test sets examined with respect to injection timing provides difficulty in clearly determining the true impact of grout injection timing on wall displacements but suggests that for displacements at the retained surface timing is less influential than grouting position, discussed further in section 7.5.

7.6.3 Position of grouting

Negligible differences were noted between the grouting tests and reference test displacements (both above the injection location and at a wall depth of d= 0.75H) prior to initiating injection as expected from the simulation of excavation only. This was the case even though there existed a difference in excavation durations by a factor of around 1.75 between the reference test and the majority of the grouting tests. Even when the difference in duration was a factor of around 3.4 for test 6HH there was negligible difference in displacements prior to injection. This confirms the consistent and largely undrained soil response to excavation in all the tests considered.

The observed behaviour in all of the grout injection tests show that the position of grouting has the most influential impact on the overall compensation capabilities and magnitudes of the injection event. A clear relationship was also noted between the effects of injections on the retained surface and retaining wall and the distance behind the wall. The following two sets of points summarise the key trends identified in relation to the grouting position with respect the retained surface locally above injection and on the wall at a depth of 0.75H, below the surface.

Vertical displacements at the retained surface:

- A decrease from the greatest positive vertical settlement compensation effect at injection depths of d= 0.25H to the greatest negative compensation effect at injection depth d= 0.75H were found in examining tests 6-9HH. This behaviour with depth was reflected also in the other tests.
- In considering the non-linear cavity expansions in tests 6HH and 7HH it was found that the injections in these tests had the potential to increase the positive compensation effects at the retained surface. This indicated that injection, down to and including a depth of d= 0.5H, had the potential to compensate and reduce settlements of those expected from an excavation only event.
- With this consideration it was also found that shallow injections at d= 0.25H can provide a greater positive compensation effect if conducted during the excavation period, as in test 7HH in comparison to injections after the excavation, as with test 10HH.
- Injection beneath d= 0.5H resulted in significant negative effects on both the surface and wall compared to the excavation only scenario.

- A phenomenon observed both at the surface and at the wall for injections below d= 0.5H indicated that the addition of a grout volume at these depths can result in a sudden and sharp increase in the rate of unfavourable displacements which would pose significant concern in the prototype.
- A greater positive compensation effect with increased distance from the wall was noted by comparing the two tests sets 7HH with 10HH and 9HH with 11HH, despite the non-linear cavity expansion problems in test 7HH.
- The general response in the tests at the same depth but different distance behind the wall clearly indicate the depth below the surface as the predominant factor determining the compensation of settlements at the surface rather than the distance behind the wall.
- Comparison of the single injections in tests 7HH and 10HH (at d= 0.25H) and 9HH and 11HH (at d= 0.375H) with the dual simultaneous injections in tests 12HH and 13HH at the corresponding depths showed a greater positive compensation effect at the surface could be achieved using an array of tubes rather than a single point of injection. A greater volumetric efficiency was also noted in the dual injection tests over their single injection counterparts as similar total injected volumes between the two injection tubes resulted in greater positive compensation of the settlements than in the total volumes injected into the single tubes.
- The general response between the single and dual injections tests at their respective injection depths and locations behind the wall were shown to be very similar.

Horizontal wall displacements:

- All grouting tests showed that the introduction of an additional volume into the soil mass behind the retaining wall resulted in greater horizontal wall displacements than would be observed from excavation only.
- As with the trends observed at the retained surface, the negative effects of injection on the wall displacement increased with injection depth.
- The greatest negative effects were noted for injections where d≥ 0.5H. Both tests conducted at or below d= 0.5H showed similar orders of negative effects on the wall displacements at the end of the injection at a wall depth of d= 0.75H (relative to the excavation only simulation).

- Injection at the deepest depth, d= 0.75H, in test 8HH resulted in a comparatively larger rate of increase in horizontal displacement following injection than in the other shallower grouting tests. This behaviour clearly suggests that not only does injection at this depth cause significant increases in wall displacements relative to the excavation only scenario but that it also appears to significantly destabilise the excavation.
- Examining test 7HH with 10HH and 9HH with 11HH showed a reduced negative effect with increased distance behind the wall for injections at the same depth.
- Equally comparing these test sets with the dual simultaneous injections in tests 12HH and 13HH, respectively, showed in general a reduced negative effect when using an array of injection points rather than single points. However this data was probably affected by the biased expansion of the left injection tube at distance x= 0.75H over the right injection tube at distance x= 0.5H.
- The least negative effect on wall displacements was noted in test 10HH where injection was conducted at the shallowest depth and therefore closer to the horizon of the stiff prop and also the furthest horizontal distance from the wall.

8. CONCLUSION

8.1 Introduction

The work described thus far was conducted to investigate the influence of applying compensation grouting, in particular through the use of compaction grouting, behind a deep retained excavation to control ground movements. In this chapter the experimental approach is summarised and conclusions drawn. The limitations of the conclusions are considered and recommendations for further research are proposed.

8.2 Experimental procedure

Apparatus was designed and manufactured to enable a total of ten successful tests to be conducted using the geotechnical centrifuge facility at City, University of London. Two reference tests modelled a prototype scale 12 m deep retained excavation supported by a stiff prop at the top of the wall. The remaining eight tests modelled idealised compaction grouting injections into the soil mass behind the retained excavation simultaneously with the excavation processes. Six single injection point grouting tests and two dual simultaneous grouting tests were carried out, all using water as the grout medium. The injections were simulated by pushing the water into latex rubber injection tubes inserted into the soil mass behind the excavation. The injection tubes were constructed of an outer latex tubing to contain the grout, which was then supported internally by a perforated Nylon tube acting as a mandrel to prevent the tubes from collapsing under the weight of the soil during the initial effective stress equilibrium phase of the soil model on the centrifuge at 100 *g*. In the first two grouting tests the injection events resulted in the expansion of non-linear cavities along the length of the tubes. To prevent a reoccurrence of this phenomenon in subsequent tests a thin brass collar was provided externally to the injection tubes close to the front of the model and Perspex window interface.

The models were made from overconsolidated samples of Speswhite kaolin prepared from slurry at 1 *g* in a hydraulic consolidation press. Prior to simulation of the excavation, support to both the vertical and horizontal surfaces was provided by the use of a dense fluid contained within a thin walled latex bag. The models were left to reach effective stress equilibrium after acceleration to 100 *g* in the centrifuge, at which point the excavation was simulated together with grout injection in the majority of tests.

Miniature pore pressure transducers were used to monitor changes in the far field pore pressures during the effective stress equalisation stage and to determine when the model

was ready for testing. A local miniature pore pressure transducer was also provided in close proximity to the injection locations in the grouting tests to provide some indication of the changes in pore pressure induced in the soil by the grouting event. Measurement of the support fluid pressure was provided by a miniature pressure transducer positioned at the base of the latex bag. Injection pressures were measured at two locations; at the outlet of the injection pump and close to the point of insertion of the injection tubes into the strongbox. Nine LVDT's were used to measure vertical displacements at the retained surface and model retaining wall. CCD cameras mounted on the swing were used to take images of tracking targets embedded in the front face of the soil and model wall. The images were processed using specialist software to determine the magnitude and spread of vertical and horizontal displacements at the retained and formation level and horizontally for the wall. The use of the target data in representing subsurface movements elsewhere was limited owing to different frictional and localised effects observed at the window for each test, particularly around the injection tube locations in the grout injection tests.

Owing to problems encountered with the initiation of the motor, used to drive the injection system in the majority of the grouting tests, the timing at which injection was initiated varied for each test from the intended trigger settlements. Injection in each grouting test was continued until either a positive compensation of the maximum vertical retained surface settlements was observed or significant horizontal displacements of the wall were noted visually from the CCD camera feed.

8.3 Conclusions

This study has explored the performance of the novel method of applying compensation grouting, with the principal focus on compaction grouting, behind deep retained excavations in order to control surface ground movements. The influence of three parameters: 1) grout injection volume, 2) grout injection timing and 3) grout injection position on the retained surface and horizontal wall displacements were the key focus of the tests conducted in this study. Examination of these parameters enabled a preliminary understanding of the conditions under which the novel application of compensation grouting behind excavations would be effective. The following sections summarise the main findings relevant to the injected grout volumes, timing and position.

8.3.1 Grouted volume

- Comparison of the different total injected volumes in four tests (with linear cavity expansions along their length) showed no clear relationship between the development of displacements at the retained surface (locally above the injection position), along the wall at a depth d= 0.75H and the total injected volumes.
- The differing behaviour and magnitudes of the displacements induced by the injected volumes between the tests suggests that factors other than the injected volume dictate the compensation response at the retained surface and any unfavourable horizontal displacements of the wall induced by the injected volume.
- A significant phenomenon was observed in tests where injection was conducted below a depth of d= 0.25H. In these tests a critical injected volume could be identified, beyond which a positive compensation of the retained surface significantly deteriorated or a negative compensation increased at a greater rate. The increased rate of displacement was also reflected in the horizontal wall displacements at depth d= 0.75H at the same critical volumes.

8.3.2 Grout injection timing

- The initiation of injection before at least 70% excavation completion was shown to have greater potential to positively compensate the excavation induced surface settlements compared with injections initiated closer to the end of the excavation period.
- Grout injections down to a depth of d= 0.5H in the model tests were shown to have greater potential to reduce excavation induced settlements when the injection event was initiated and completed within the excavation period compared with injection events after excavation.
- For deeper injections below depth d= 0.5H in the model, the timing of injection was shown to be irrelevant to the development of increased settlements at the retained surface (above the injection) and increased horizontal wall displacements at depth d= 0.75H, relative to the excavation only scenario.
- The addition of secondary volumes following the first injection pass were shown to be far more effective in compensating vertical settlements above the injection if conducted closer to the end of the first pass.

- The observed behaviour for the two sets of tests examined clearly indicated that the timing of injection has an impact on the overall magnitudes of compensation achieved at the retained surface but that it is less influential than injection position.
- The contradictory behaviour observed between the examined tests made it difficult to confidently identify the influence of grout injection timing on horizontal wall displacements.

8.3.3 Position of grouting

Comparisons of differences in displacements vertically (at the retained surface above injection) and horizontally (at wall depth d= 0.75H) between all the grout injection test data and the excavation only test data showed that the position of grout injection has the greatest impact on the magnitudes of compensation achieved at the surface and unfavourable displacement of the wall. The depth of the injection below the retained surface was observed to have a greater influence on settlement compensation than distance behind the wall.

Figure 8.1 provides a summary of δS_v, the difference in vertical displacements at the retained surface above the injection point between the excavation only reference test and grouting tests, at the end of the first injection event. δS_v is normalised against S_{vref}, the displacements in the reference test, in order to provide a quantification of the proportion of the settlement that was compensated for in the different grouting positions. Positive $\delta S_v/S_{vref}$ values indicate where the vertical settlements induced by excavation were reduced or compensated for by the grout injection event. Values greater than unity illustrate where heave of the retained surface above the injection location was achieved.

The figure provides an indication of a relatively linear relationship between the depth of injection and proportion of settlement either positively or negatively compensated. This is illustrated by the linear grey dashed best fit line through the data points with a coefficient of determination (R^2) equal to 0.902.

The data shows that injections, both at single and dual points, up to depth d= 0.375H in the model tests clearly had the potential to achieve positive compensation of the settlements induced by excavation alone, with the shallowest injection depths at depth d= 0.25H (30 mm) in the model having the greatest compensation efficiency.

Consideration of the behaviour observed in tests 9HH and 11HH, prior to the addition of injected volumes beyond the critical volumes identified in section 7.3, shows that

injections at depths of down to d= 0.375H in the model had the potential to provide positive compensation at the retained surface if the volumes and response at the retained surface were closely monitored and halted upon achieving compensation of the surface. This is noted by the dotted positive error bars in Figure 8.1. It is also worth noting that injection in test 9HH was initiated very close to the end of excavation and therefore has the potential to achieve a greater compensation based on the findings summarised in section 8.3.2, relating to grout injection timing.

The provision of dual injection tubes at depths down to d= 0.375H were observed to provide greater and more volumetrically efficient positive compensation of the surface above the injection location when compared to single point injections at corresponding depths. Notably, the general response between the single and dual injection tubes at the same depths were remarkably similarly, thus confirming that the injection depth below the surface is the principle factor influencing the compensation achieved with injection.

Greater positive compensation efficiencies were noted with increased distance behind the wall for injections down to depths of d= 0.375H when compared with equivalent injection depths closer to the wall. This was in contrast to the observation presented by Au (2001) where increased confinement resulted in increased grouting efficiency as a result of the interaction of the boundary and the excess pore pressure zone generated around each cavity. However, owing to the use of only two distances behind the wall in the model tests it is difficult to provide a detailed assessment on the variation in grouting efficiencies and magnitudes on the soil surface with increasing distances from the model wall.

It is also worth noting the potential ranges of positive compensation at the retained surface that could have been achieved by the injection positions in test 6HH and 7HH had the injection cavities expanded linearly along the length of the injection tubes. These ranges are indicated by the solid blue error bars in Figure 8.1. The approach in deriving these ranges of potential compensation is detailed in section 7.4.1 It is possible therefore to suggest that injections as deep as d= 0.5H (60 mm) in the model can provide reductions in the settlements induced by excavation alone. This depth is similar to the findings presented by El-Kelesh *et al.* (2001) and Nishimura *et al.* (2011) in the experimental studies of compaction grouted piles where heave at the ground surface was realised for injections above a depth of about 5 m.

The largest negative compensation was observed with injection at depth d= 0.75H (90 mm) which resulted in very significant increases in settlements by a factor of about

3.2, relative to those solely from excavation alone. Observations of the soil post-test provided indications that injection at this depth significantly destabilised the model excavation, resulting in the development of fracture or slip planes propagating from the retaining wall toe, both on the active and passive stress sides of the excavation.

Figure 8.2 provides a summary of δS_h, the changes in horizontal wall displacements between the reference tests and grouting test observed at the end of injection normalised by the displacements observed in the reference tests, S_{href}. Positive values along the vertical axis indicate the magnitude of negative or unfavourable wall displacements induced in addition to the excavation only scenario, by the introduction of the grout volumes behind the excavation. It is immediately clear that injection at all the various positions in the model grouting tests had an overall net negative effect on the wall.

In line with the findings at the retained surface, a relatively linear relationship was noted between injection depth and the magnitudes of negative effects on the wall. This is noted by the grey dashed best fit line through the data points in each test with a R^2 value of about 0.815 in Figure 8.2. The shallowest injections at depth d= 0.25H (30 mm) had the least effect. The response at injection depth d= 0.75H (90 mm) in the model resulted in the largest increase in wall displacements relative to excavation only. This was also reflected in the behaviour at the retained surface.

It is clear that the negative effects on the wall displacements decrease with increased distance behind the wall as one would expect. The employment of dual injection tubes at depths up to d= 0.375H were again noted in general to perform better than the single injection points at the corresponding injection depths.

Based on the conclusions presented, Figure 8.3 provides a schematic illustration of the regions or zones behind the excavation simulated in the model where the application of compensation grouting has different effects on the retained surface locally above the injection point and at the wall. The region of overlap between zones 1 and 3 indicate where the potential to compensate settlements at the retained surface exist but not without causing significant increases in the wall displacements relative to those observed from excavation alone. The ideal region of injection with the single propped excavation arrangement used in the physical modelling tests is identified in the overlapping region between zones 1 and 2a. The region identified by the zone 2b is where the influence of grout injections on the retained surface and wall displacements are unknown but would likely have little positive or negative effects on the displacements

In summary it appears from the model tests conducted only shallow injections are beneficial to the retained soil surface with deep injections causing significant wall distortions with no compensation of vertical settlements.

8.4 Implications and limitations of the research

The work within this study has identified quantifiable and physical limits to a zone where positive compensation of the retained surface can be achieved by grout injection and also the physical locations that would very likely result in significant negative effects and destabilisation of the retaining wall and excavation. These along with the conditions, recognised with respect to grout injection timing, enable the designer in the field or future researchers to optimise the application of compensation grouting for excavations with similar arrangements to that utilised in this study. The presence of the different but critical volumes have been identified. Beyond these critical points it was recognised that further injection can either cause significant settlement of the compensated surface and wall displacements, in the case of injections below certain depths, or can provide increasing positive compensation with minimal negative impact on wall displacements for shallower injection.

However, the findings presented from the study are limited to a retained excavation with a single prop at the top and a relatively low stiffness model wall. It is likely that the suggested limiting positions and regions at which positive compensation of the retained surface can be achieved whilst minimising the negative effect on wall displacements, would not necessary be linearly applicable for deeper excavations or for different support system arrangements and stiffnesses.

Investigation of the distortions, horizontal strains, relative deflections and shear strains induced in the soil near and at the surface by the grout injections in the model test and their effects on overlying structures was not the key focus of this research. As such, these variables have not been quantified, nor the implications assessed of the grout injections on potential overlying structures using the damage assessment criteria assessment available in literature (i.e. Boscardin and Cording, 1989; Boone, 1996; Finno *et al.,* 2005 and Son and Cording, 2005); typically these are used in the field to provide performance limits of the excavation induced movements upon which to initiate and stop grouting operations.

The response of the soil surface to grout injections in the model tests would also be different with the presence of an overlying structure due to influence from the stiffness and restraint provided by the foundations of the structure on the soil beneath and adjacent to it and the grout 'bulbs'. This would in turn affect the magnitudes of distortions, relative deflections and the horizontal and shear strains recorded at the soil surface or close to the overlying structure or service.

One of the main features of the experimental work is that the simulation of compaction grouting was necessarily idealised in order to achieve close to plane strain conditions within the model. In the model the expansion of the single and dual cavities along the length of the injection tubes, being inserted parallel to the excavation, could be considered analogous to the injection of grout bulbs at close centre to centre spacing along the length or width of an excavation in the field.

The simulated grouting events via single and dual injection tubes in the model tests were unrepresentative of the typical multiple points of compensation grouting in the field. The localised compensation effects observed in the model tests would be different from field measurements of multiple grout injections, owing to the interaction effects between the grout masses and the surrounding soil.

In the model tests water was used as a grout medium in order to keep the demand for injection pressures required from the injection system low. As such any of the interaction effects (e.g. bleeding, partial fracturing around cavity) that would be expected between the suspension grouts typically employed in the field and surrounding soil were not simulated in the model tests.

Owing to the water 'grout' lacking shear strength or ability to set the shape of the injected grout mass could change as the deformations developed within the soil and wall. This is unlike the behaviour of typical quick setting cementitious suspension grouts employed in the field. As such the localised behaviours observed at the locations of the soil surface and model wall examined in this study would be different with the use of realistic grout materials.

The simulated excavation was simplified and idealised to enable reliable and repeatable conditions to be maintained when modelling grout injections in the model tests. It is also worth noting the influence of overlying structures or buried services that would exist in the field were not modelled or considered in the model. The presence of these structures

and services would be expected to have a significant effect on the observed soil and wall displacements from both the excavation and injection events and would probably result in different responses to the compensation effects observed in the model tests.

8.5 Recommendations for further research

It is clear, from the behaviour observed in the two sets of tests examined with respect to the influence of injection timing in section 7.4, that a further series of tests would be required in which both the injected volume and positions of grouting were kept constant and only the timing of grout initiation relative to the start excavation was varied.

A series of tests should be undertaken where the optimum timing of injection initiation, taken from the previously suggested series, and position should be kept constant, but the total volumes injected varied. This would provide a larger dataset in which comparisons could be made to determine the true effects of grouted volume on the retained surface and wall.

Following this, tests should be conducted to continue to explore the efficiencies of grouting at alternative positions to those investigated in this study. A subseries of these tests should include:

- A large test series in which an array (of more than two injection tubes) of injections at depths up to the recommended limiting depth from this study. It would be necessary to control the individual injected volume in each tube. This series of test would provide a more realistic real world response of the soil and wall deformations than the single point injections conducted within this study.

In addition, the following recommendations would provide an understanding of the different interactions between the soil, structure and grout injections. This would enable the appropriate selection and design of the elements in the field:

- Instrumentation of the prop and wall to enable the changes in prop loads, strains and therefore bending moments to be found.
- Investigating the effect of prop positioning relative to grouting positions on the compensation grouting efficacies achieved at the retained soil surface and the impact on wall displacements and induced bending moments. This could be achieved by grouting in line with different propped horizons below the retained clay surface.

- Series of grouting tests with different single prop and multi propped excavation arrangements to provide an understanding of the interaction between the different lateral supports and grout injections.
- A series of grouting tests where wall stiffness is varied to investigate its influence on compensation grouting efficiencies and wall displacements
- Varying the model soil stiffness to investigate different behaviours of the soil and retaining structure to compensation grouting.
- Investigating the variation in compensation grouting efficiency on the retained soil surface with increasing distances from the wall.
- Use experimental data to validate numerical analysis and then use numerical analysis to explore effects of changing parameters such as grout depth, distance from wall and variations with propping.
- Investigation of the effects of the grout bulb expansions, in similar excavation simulated model tests, on overlying structures by examining the induced relative deflections, horizontal strains, angular distortions and shear strains in the soil below.

REFERENCES

Al-Tabbaa, A. (1987). *Permeability and stress-strain response of Speswhite kaolin*. Ph.D. Thesis, University of Cambridge, U.K.

Anderson, W.F., Yong, K.Y. and Sulaiman, N. (1985). Shaft adhesion on bored piles and cast *in situ* piles. In: *Proc. 11th Int. Conf. on Soil Mechanics and Foundation Engineering*, San Francisco, CA, 12-16th August 1985, Balkema: Rotterdam, pp. 1333-1336.

ASCE. (2010). *Compaction grouting Consensus Guide*. Reston, VA. ASCE/GI 53-10.

Au, S.K.A. (2001). *Fundamental study of Compensation grouting*. Ph.D. Thesis, University of Cambridge, U.K.

Azevedo, R.F. and Ko, H.-Y. (1988). In-flight centrifuge excavation tests in sand. In: Corte, J.F. (ed.), *Proc. Conf. Centrifuge '88,* Paris, France, 25th-27th April 1988, Balkema: Rotterdam, pp. 119-124.

Baker, W.H., Cording, E. J. and MacPherson, H.H. (1983). Compaction grouting to control ground movements during tunnelling. *Underground Space*, Vol. 7, pp. 205-212.

Bjerrum, L. and Eide, O. (1956). Stability of Strutted Excavation in clay. *Géotechnique*, 6(1), pp. 32-47.

Bolton, M.D. and Powrie, W. (1987). Behaviour of diaphragm walls: retaining walls prior to collapse. *Géotechnique*, 37(3), pp. 335-353.

Bolton, M.D., Chin, C.Y. and Lu, Y.C. (1994). Compensation grouting. In: Lee, F.H., Leung, C.F. and Tan, T.S. (eds.), *Proc. Conf. Centrifuge '94*, Singapore, 31st Aug.- 2nd Sept. 1994, Balkema: Rotterdam, pp. 719-724.

Bolton, M.D. and Whittle, R.W. (1999). A non-linear elastic-perfectly plastic analysis for plane strain undrained expansion tests. *Géotechnique*, 49(1), pp. 133-141.

Boone, S.J. (1996). Ground Movement Related Building Damage. *Journal of Geotechnical Engineering*, 122(11), pp. 886-896.

Boscardin, M.D. and Cording, J.C. (1989). Response to excavation-induced Settlement. *Journal of Geotechnical Engineering*, 115(1), pp. 1-21.

Boscardin, M.D. and Walker, M.P. (1998). Ground Movement, Building Response, and Protective Measures. In: *Effects of Construction on Structures: Proceedings of sessions of Geo Congress '98*, Boston, Massachusetts, 18th-21st October 1998, ASCE: Reston, VA, pp. 45-55.

Bowles, J. (1988). *Foundation Analysis and Design*. 4th Ed., McGraw-Hill: New York.

Brown, D.R. and Warner, J. (1973). Compaction grouting. *Journal of the Soil Mechanics and Foundations Division*, 99(8), pp. 589-601.

Bruce, D.A. (1994). An Overview of Grouting Developments. *Geotechnical News*, 12 (4), pp. 36-40.

Burland, J.B., Simpson, B. and St John, H.D. (1979). Movements around excavations in London Clay. In: *Proc. 7th European Conf. on Soil Mechanics and Foundation Engineering*, Brighton, U.K., Vol. 1, pp. 13-30.

Carder, D.R. (1995). *Ground movements caused by different embedded wall construction techniques*. TRL report No. 172, Transport Research Laboratory: Berkshire, U.K.

Carder, D.R., Morley, C.H. and Alderman, G.H. (1997). *Behaviour during construction of a propped diaphragm wall founded in London Clay at Aldershot road underpass*. TRL239, Transport Research Laboratory: Crowthorne, U.K.

Carter, J.P., Booker, J.R. and Yeung, S.K. (1986). Cavity expansion in cohesive frictional soils. *Géotechnique*, 36(3), pp. 345–358.

Chin, C.Y. and Bolton, M.D. (1999). Factors influencing hydro-fracture in clay. In: *Proc. 13th ASCE Engineering Mechanics Conference,* The John Hopkins University, Baltimore, MD, 9th-15th June 1999, ASCE: Baltimore, MD.

Cirone, A. (2016). *Geotechnical modelling of CPR Grouting*. M.Sc. Thesis, Politecnico di Milano, Italy.

Clough, G.W., Smith, E.M. and Sweeney, B.P. (1989). Movement Control of Excavation Support Systems by Iterative Design. In: Kulhawy, F.H. (ed.), *Foundation Engineering: Current Principles and Practices: Proceedings*, Evanston, Illinois, 25th-29th June 1989, ASCE: New York, Vol. 2, pp. 869-884.

Clough, G.W. and O'Rourke, T.D. (1990). Construction induced movements of *in situ* walls. In: Lambe, P. and Hansen, L. (eds.), *Proc. ASCE Conf. on Design and Performance of Earth Retaining Structures,* Geotechnical Special Publication (GSP) 25, Ithaca, NY, 18th-21st June 1990, ASCE: New York, pp. 439-470.

Cooper, M.A.R. and Robson, S. (1996). Chapter 2: Theory of close range photogrammetry. In: Atkinson, K.B. (ed.), *Close Range Photogrammetry and Machine Vision*, Whittles: Caithness, U.K , pp. 9-51.

Culligan-Hensley, P.J. and Savvidou, C. (1995). Chapter 8- Environmental Geomechanics and transport processes. In: Taylor, R.N. (ed.), *Geotechnical Centrifuge Technology*, Blackie Academic and Professional: Glasgow, pp. 196-263.

Divall, S. (2013). *Ground movements associated with twin-tunnel construction in clay*. Ph.D. Thesis, City, University of London, U.K.

El-Kelesh, M., Mossaad, M.E. and Basha, I.M. (2001). Model of compaction grouting. *Journal of Geotechnical and Geoenvironmental Engineering*, 127(11), pp. 955-964.

El-Kelesh, M. and Matsui, T. (2002). Compaction grouting and soil compressibility. In: Chung, J.S, Sayed, M., Kashiwagi, M., Setoguchi, T. and Hong, S.W. (eds.), *Proc. of the 12th Int. Offshore and Polar Engineering Conference*, Kitakyushu, Japan, 26th-31st May 2002, ISOPE: Cupertino, California, Vol. 2, pp. 563-568.

Elshafie, M. (2008). *Effect of building stiffness on excavation-induced displacements*. Ph.D. Thesis, University of Cambridge, U.K.

Essler, R. D., Drooff, E. R. and Falk, E. (2000). Compensation grouting, concept, theory and practice. In: Krizek, R.J. and Sharp, K. (eds.), *Advances in grouting and ground modification*: *Proceedings of Sessions of Geo-Denver 2000*, Geotechnical Special Publication (GSP) 104, Denver, Colorado, 5th-8th August 2000, ASCE, pp. 1-15.

Fernie, R. and Suckling, T. (1996). Simplified approach for estimating lateral wall movement of embedded walls in U.K. ground. In: Mair, R.J. and Taylor, R.N. (eds.), *Proc. Int. Symp. On Geotechnical Aspects of Underground Construction in Soft Ground*, City University, London, 15th-17th April 1996, Balkema: Rotterdam, pp. 131-136.

Finno, R. J., Bryson, S. and Calvello, M. (2002). Performance of a stiff support system in soft clay. *Journal of Geotechnical and Geoenvironmental Engineering,* 128(8), pp. 660–671.

Finno, R. J., Voss, F. T., Rossow, E. and Tanner Blackburn, J. (2005). Evaluating damage potential in buildings affected by excavations. *Journal of Geotechnical and Geoenvironmental Engineering*, 131(10), pp. 1199-1210.

Gaba, A., Hardy, S., Doughty, L., Powrie, W. and Selemetas, D. (2017). *Guidance on embedded retaining wall design*. CIRIA: London (CIRIA C760).

Gibson, R.E. and Anderson, W.F. (1961). *In situ* measurement of soil properties with the pressuremeter. *Civil Engineering and Public Works Review*, 56(658), pp. 615-618.

Goldberg, D.T., Jaworski, W.E. and Gordon, M.D. (1976). *Lateral support systems and underpinning*. FHWA: Washington, D.C (Report No. FHWA-RD-75-128), Vol. 1.

Gorasia, R. J. (2013). *Behaviour of ribbed piles in clay*. Ph.D. Thesis, City, University of London, U.K.

Graf, E.D. (1969). Compaction grouting technique and observations. *Journal of the Soil Mechanics and Foundations Division*, 95(5), pp. 1151-1158.

Grant, R.J. (1998). *Movement around a tunnel in two-layer ground*. Ph.D. Thesis, City, University of London, U.K.

Hsieh, P.G. and Ou, C.Y. (1998). Shape of ground surface settlement profiles caused by excavation. *Canadian Geotechnical Journal*, 35(6), pp. 1004-1017.

Kantartzi, C. (1993). *Ground movements during diaphragm wall installation in clays*. Ph.D. Thesis, University of London, U.K.

Kimura, T. and Takemura, J. (1994). Excavation in soft clay using an in-flight excavator. In: Lee, F.H., Leung, C.F. and Tan, T.S. (eds.), *Proc. Conf. Centrifuge '94*, Singapore, 31st Aug.- 2nd Sept. 1994, Balkema: Rotterdam, pp. 649-654

Kopsalidou, K. (2000). *A numerical investigation of ground movements around multi-propped deep excavations*. M.Sc. Thesis, City, University of London, U.K.

Lam, S.Y., Haigh, S.K., Elshafie, M.Z.E.B. and Bolton, M.D. (2012). A new apparatus for modelling excavations. *International Journal of Physical Modelling in Geotechnics*, 11(1), pp. 24-38.

Lee, S.W., Bolton, M.D., Mair, R.J., Soga, K., Dasari, G.R. and Hagiwara, T. (2000). The influence of injection sequence in compensation grouting. In: Couture, R. and Evans, S.G. (eds.), *53rd Canadian Geotechnical Conference*, Montreal, CA, 15th-18th October 2000, pp. 1013-1020.

Lings, M.L., Nash, D.F.T., Ng, C.W.W. and Boyce, M.D. (1991). Observed behaviour of a deep excavation in Gault Clay: A preliminary appraisal. In: *Proc. 10th Int. Conf. on Soil Mechanics and Foundation Engineering*, Florence, Italy, 27th-30th May 1991, Vol. 2, pp. 467-470.

Littlejohn, S. (2003). The Development of Practice in Permeation and Compensation Grouting- A Historical Review (1802-2002): Part 2: Compensation Grouting. In: Johnsen, L., Bruce, D.A. and Byle, M.J. (eds.), *Proc. 3rd International Conference on Grouting and Ground Treatmen*t, Grouting and Ground Treatment (GSP) 120, New Orleans, Louisiana, 10th-12th February 2003, ASCE, pp. 100-144.

Liu, J. (2003). Compensation Grouting to Reduce Settlement of Buildings during an Adjacent Deep Excavation. In: Johnsen, L., Bruce, D.A. and Byle, M.J. (eds.), *Proc. 3rd International Conference on Grouting and Ground Treatmen*t, Grouting and Ground Treatment (GSP) 120, New Orleans, Louisiana, 10th-12th February 2003, ASCE, pp. 837-844.

Loh, C.K., Tan, T.S. and Lee, F.H. (1998). Three-dimensional excavation tests in the centrifuge. In: Kimura, T., Kusakabe, O. and Takemura, J. (eds.), *Proc. Conf. Centrifuge '98*, Tokyo, Japan, 23rd-25th September 1998, Balkema: Rotterdam, pp. 649-652.

Long, M. (2001). Database for Retaining Wall and Ground Movements due to Deep Excavations. *Journal of Geotechnical and Geoenvironmental Engineering*, 127(3), pp. 203-224.

Lu, Y. C. (1996). *Compensation grouting in clay*. Ph.D. Thesis, Department of Engineering, University of Cambridge, U.K.

Lyndon, A. and Schofield, A.N. (1970). Centrifuge model test of short term failure in London Clay. *Géotechnique*, 20(4), pp. 440-442.

Mair, R.J. (1994). Report on Session 4: Displacement. In: Bell, A.L. (ed.), *Grouting in the ground: Proceedings of the conference organized by the Institution of Civil Engineers*, London, 25th-26th November 1992, Thomas Telford: London, pp. 375-384.

Mair, R.J. and Hight, D.W. (1994). Compensation Grouting. *World Tunnelling and Subsurface Excavation*, 7(8), pp. 361-367.

Mair, R.J., Harris, D.I., Love, J.P., Blakely, D. and Kettle, C. (1994). Compensation grouting to limit settlement during tunnelling at Waterloo Station. In: *Tunnelling '94: papers presented at the 7th International Symposium*, London, 5th-7th July 1994, Chapman and Hall: London and New York, pp. 279-300.

Mair, R.J., Rankin, W.J., Essler, R.D. and Chipp, P.N. (1995). Compensation grouting-Informal Discussion. *Proceedings of the Institution of Civil Engineers- Geotechnical Engineering*, 113(1), pp. 55-57.

Mana, A.I. and Clough, G.W. (1981). Prediction of Movements for Braced Cuts in clay. *Journal of the Geotechnical Engineering Division*, 107(6), pp. 759-777.

Mayne, P.W. and Kulhawy, F.H. (1982). K_o - OCR relationships in soil. *Journal of the Geotechnical Engineering Division*, 108(6), pp. 851-872.

McNamara, A.M. (2001). *Influence of heave reducing piles on ground movements around excavations*. Ph.D. Thesis, City, University of London, U.K.

McNamara, A.M., Divall, S., Goodey, R.J., Gorasia, R.J., Halai, H., Rose, A.V., Stallebrass, S.E., Taylor, R.N. and Xu, M. (2012). The London Geotechnical Centrifuge Centre at City, University of London. In: *2nd European Conference on Physical Modelling in Geotechnics (Eurofuge 2012)*, Delft, Netherlands, 23rd-24th April 2012. Available at: uuid: a27c15cb-8a72-49de-a628-e1106a1cc48a.

Ménard, T.L. (1975). The Menard pressuremeter: interpretation and application of the pressuremeter test results to foundation design. *Sols Soils*, No. 26, pp. 5-44.

Moormann, C. and Moormann, H.R. (2002). A Study of wall and ground movements due to deep excavations in soft soil based on worldwide experiences. In: Kastner, R., Emeriault, F., Dias, D. and Guilloux, A. (eds.), *Proc. 3rd Int. Symp. On Geotechnical Aspects of Underground Construction in Soft Ground*, Toulouse, France, 23rd-25th October 2002, Spécifique: Lyon, pp. 477-482.

Moormann, C. (2004). Analysis of wall and ground movements due to deep excavations in soft soil based on a new worldwide database. *Soils and Foundations*, 44(1), pp. 87-89.

Nishimura, S., Takehana, K., Morikawa, Y. and Takahashi, H. (2011). Experimental study of stress changes due to compaction grouting. *Soil and Foundations*, 51(6), pp. 1037-1049.

O'Rourke, T.D. (1981). Ground movements caused by braced excavations. *Journal of the Geotechnical Engineering Division*, 107(9), pp. 1159-1178.

Ou, C.Y., Hsieh, P.G. and Chiou, D.C. (1993). Characteristics of ground surface settlement during excavation. *Canadian Geotechnical Journal*, 30(5), pp. 758-767.

Padfield, C.J. and Mair, R.J. (1984). *Design of retaining walls embedded in stiff clay*. CIRIA: London (CIRIA R104).

Palmer, A. C. (1972). Undrained plane-strain expansion of a cylindrical cavity in clay: a simple interpretation of the pressuremeter test. *Géotechnique*, 22(3), pp. 451-457.

Pantelidou, H. (1994). *Changes in soil stiffness associated with diaphragm walling*. Ph.D. Thesis, University of London, U.K.

Peck, R.B. (1969). Deep excavations and tunnelling in soft ground. In: *Proc. 7th Int. Conf. on Soil Mechanics and Foundation Engineering*, Mexico City, Mexico, pp. 225-290.

Phillips, R. (1995). Chapter 3- Centrifuge modelling: practical considerations Geotechnical centrifuge technology. In: Taylor, R.N. (ed.), *Geotechnical Centrifuge Technology*, Blackie Academic and Professional: Glasgow, pp. 34-60.

Potts, D.M. and Fourie, A.B. (1984). The behaviour of a propped retaining wall: results of a numerical experiment. *Géotechnique*, 34(3), pp. 383-404

Potts, D.M. and Fourie, A.B. (1986). Discussion: The behaviour of a propped retaining wall: results of a numerical experiment. *Géotechnique*, 36(1), pp. 119-121.

Powrie, W. (1986). *The behaviour of diaphragm walls in clay*. Ph.D. Thesis, University of Cambridge, U.K.

Powrie, W. and Li, E.S.F. (1991). Finite element analyses of an *in situ* wall propped at formation level. *Géotechnique*, 41(4), pp. 499-514.

Powrie, W. and Kantartzi, C. (1993). Installation effects of diaphragm walls in clay. In: Clayton, C.R.I., (ed.), *Retaining Structures: Proceedings of the Conference organized by the Institution of Civil Engineers*, Cambridge, U.K., 20th-23rd July 1992, Thomas Telford: London, pp. 37-45.

Powrie, W. and Kantartzi, C. (1996). Ground response due to diaphragm wall installation in clay: centrifuge model tests. *Géotechnique*, 46(4), pp. 725-739.

Powrie, W., Pantelidou, H. and Stallebrass, S. E. (1998). Soil stiffness in stress paths relevant to diaphragm walls in clay. *Géotechnique*, 48(4), pp. 483-494.

Rampello, S., Stallebrass, S.E. and Viggiani, G.M.B. (1998). Panel Report: Ground movements associated with excavations in stiff clays- Current prediction capability. In: Evangelista, A. and Picarelli, L. (eds.), *The Geotechnics of Hard Soil- Soft Rocks: Proc. 2nd Int. Symp. On Hard Soils-Soft Rocks*, Naples, Italy, 12th-14th October 1998, Vol. 3, pp. 1527-1540.

Rawling, C.G., Hellawell, E.E. and Kilkenny, W.M. (2000). *Grouting for ground engineering*. CIRIA: London (CIRIA C514).

Richards, D.J. (1995). *Centrifuge and numerical modelling of twin propped retaining walls*. Ph.D. Thesis, University of London, U.K.

Richards, D.J. and Powrie, W. (1998). Centrifuge model tests on doubly propped embedded retaining walls in overconsolidated kaolin clay. *Géotechnique*, 48(6), pp. 833-846.

Rose, A.V. (2012). *Behaviour and efficiency of perimeter pile groups*. Ph.D. Thesis, City, University of London, U.K.

Schofield, A.N. and Taylor, R.N. (1988). Development of standard geotechnical centrifuge operations. In: Corte, J.F. (ed.), *Proc. Conf. Centrifuge '88,* Paris, France, 25th-27th April 1988, Balkema: Rotterdam, pp. 29-32.

Skempton, A.W. (1951). The bearing capacity of clays. In: *Proc. Building Research Congress*, London, U.K., Vol. 1, pp. 180-189.

Soga, K., Bolton, M.D., Au, S.K.A., Komiya, K., Hamelin, J.P., Van Cotthem, A., Buchet, G. and Michel, J.P. (1999). Development of compensation grouting modelling and control system. In: Kusakabe, O. (ed.), *Proc. Int. Symp. On Geotechnical Aspects of Underground Construction in Soft Ground*, Tokyo, Japan, 19th-21st July 1999, Balkema: Rotterdam, pp. 425-430.

Soga, K., Au, S.K.A., Jafari, M. R. and Bolton, M.D. (2004). Laboratory investigation of multiple grout injections into clay. *Géotechnique*, 54(2), pp. 81-90.

Son, M. and Cording, E.J. (2005). Estimation of building damage due to excavation-induced ground movements. *Journal of Geotechnical and Geoenvironmental Engineering*, 131(2), pp. 162-177.

Stewart, D.I. (1989). *Ground water effects on in-situ walls in stiff clay*. Ph.D. Thesis, University of Cambridge, U.K.

Takemura, J., Kondoh, M., Esaki, T., Kouda, M. and Kusakabe, O. (1999). Centrifuge model tests on double propped wall excavation in soft clay. *Soils and Foundations*, 39(3), pp. 75-87.

Taylor, R.N. (1995). Chapter 2- Centrifuges in modelling: Principles and scale effects. In: Taylor, R.N. (ed.), *Geotechnical Centrifuge Technology*, Blackie Academic and Professional: Glasgow, pp. 19-44.

Taylor, R.N., Grant, R.J., Robson, S. and Kuwano, J. (1998). An image analysis system for determining plane and 3-D displacements in soil models. In: Kimura, T., Kusakabe, O. and Takemura, J. (eds.), *Proc. Conf. Centrifuge '98*, Tokyo, Japan, 23rd-25th September 1998, Balkema: Rotterdam, pp. 73-78.

Tedd, P., Chard, B. M., Charles, J. A. and Symons I. F, (1984). Behaviour of a propped embedded retaining wall in stiff clay at Bell Common Tunnel. *Géotechnique*, 34(4), pp. 513-532.

Terzaghi, K. (1943). *Theoretical Soil Mechanics*. John Wiley and Sons, Inc.: New York, U.S.A.

Timoshenko, S.P. and Goodier, J.N. (1970). *Theory of Elasticity*. McGraw-Hill: New York, U.S.A.

Vesic, A.S. (1972). Expansion of cavities in infinite soil mass. *Journal of the Soil Mechanics and Foundation Division*, 98(3), pp. 265-290.

Wong, H.Y. (1971). *Compaction of soil during pressure grouting*. Private Rep., Cementation Research Ltd., Rickmansworth, U.K.

Wong, H.Y. (1974). Discussion of compaction grouting by Brown, D.R. and Warner. *Journal of the Geotechnical Engineering Division*, 100(5), pp. 556-559.

Wong, L.W., Shau, M.C. and Chen, H.T. (1996). Compaction Grouting for Correcting Building Settlement. In: Yonekura, R., Terashi, M. and Shibazaki, M. (eds.), *Grouting and Deep mixing: Proc. IS-Tokyo '96, the 2nd Int. Conf. on Ground Improvement Geosystems*, Tokyo, Japan, 14th-17th May 1996, Balkema: Rotterdam, Vol. 1, pp. 231-236.

Wood, D.M. (2004). *Geotechnical Modelling (Applied Geotechnics)*. Spon Press: New York, U.S.A.

Yu, H.-S. (2000). *Cavity Expansion Methods in Geomechanics*. Kluwer Academic Publishers: Netherlands.

TABLES

Support stiffness	Description/examples
High	Top-down construction, temporary props installed before permanent props at high level
Moderate	Temporary props of high stiffness installed before permanent props at low level
Low	Cantilever wall, temporary props of low stiffness or temporary props installed at low level

Table 2. 1 Support stiffness categories for excavations (after Carder, 1995).

No	Description	Bottom depth	Unit weight, γ	Water content, w	Void ratio, e	Modulus, E	Shear Strength	
		m	kN/m^3	%	--	MPa	c kPa	ϕ ^{0}
(1)	(2)	(3)	(4)	(5)	(6)	(7)	(8)	(9)
2	Yellow clay	2.4~4	18.15	30.2	1.03	7.81	9.6	19
3	Grey silty clay	8.5~10	17.36	42.1	1.30	3.34	18.8	12
4	Grey clay	17~19	17.07	48.8	1.32	1.96	19.5	12
5	Grey silty clay	19~21	17.85	37.6	0.99	3.93	21.0	14
6	Green silty clay	26~29	19.82	22.3	0.68	3.57	26.2	16

Table 3. 1 Physical and geotechnical properties of Shanghai Clay (after Liu, 2003).

Monitoring point (1)	G2 (2)	G3 (3)	G4 (4)	G5 (5)	G6 (6)	G7 (7)	G8 (8)	G9 (9)	G10 (10)
Distance from grouting (m)	0.2	3	6	9	12	15	18	21	24
Before grouting (mm/day)	1.89	2.04	2.11	1.73	1.87	1.57	0.87	0.68	0.59
During grouting (mm/day)	0.46	1.02	0.92	0.96	0.93	0.51	0.65	0.8	0.54
After grouting (mm/day)	1.37	1.29	1.25	1.01	0.54	1.04	0.94	0.86	0.72

Table 3. 2 Ground settlement changes due to compaction grouting in Shanghai, China (after Liu, 2003).

Quantity	Metric unit	Prototype	Centrifuge at N gravities
Length	m	1	1/N
Mass density	Kg/m^3	1	1
Acceleration	m/s^2	1	N
Bending Stiffness, EI	Nm	1	$1/N^4$
Axial Stiffness, EA	N	1	$1/N^2$
Stress	$Pa= N/m^2$	1	1
Force	$N= kg\ m/s^2$	1	$1/N^2$
Force/unit length	N/m	1	1/N
Strain	-	1	1
Displacement	m	1	1/N
Permeability (Darcy's Law)	m/s	1	N
Time (diffusion)	s	1	$1/N^2$
Hydraulic gradient, i	-	1	1
Dynamic Viscosity, μ	Ns/m^2	1	1
Young's Modulus	N/m^2	1	1
Curvature	m^{-1}	1	N
Moment of inertia, I	m^4	1	$1/N^4$
Bending moment	Nm	1	$1/N^3$

Table 4. 1 Scaling factors relating parameters at prototype scale to centrifuge model scale.

Excavation modelling method	Advantages	Disadvantages
Increasing acceleration of pre-cut excavated model to failure (Lyndon and Schofield, 1980).	Correctly reproduce prototype σ_v.	Continually changing scale factor, N Unable to simulate progressive ground movements due to excavation.
Using an inflight excavator (Kimura and Takemura, 1994; Loh *et al*., 1998; Takemura *et al.*, 1999 and Lam *et al.*, 2012).	Permits realistic modelling and sequence of excavation and propping. Provides appropriate initial ground conditions and stresses prior to excavation.	Highly complicated and complex system to develop.
Drainage of heavy support fluids retained in rubber bags, with fluid at the same density of model soil (Bolton and Powrie, 1987; Powrie, 1986; McNamara, 2001 and Elshafie, 2008).	Simple and quick method. Correctly simulates σ_v with depth inside excavation. Provides good approximation of earth pressures associated with cast in place walls (Richards *et al.*, 2006).	With the fluid having K_o=1, the method is unable to correctly model prototype stresses and deformations with respect to excavation progress.
Removal of a bag of material from the excavation area (Azevedo and Ko, 1988).	Realistic stress history simulated by using the same soil in the bag as the model. K_o within excavation is consistent with the rest of the model.	Difficult to quantify interaction between interfaces of soil bags and wall.

Table 5. 1 Previous methods for modelling excavations in a geotechnical centrifuge.

Symbol	Parameter	Value
A	coefficient in relationship for $G'_{max(NC)}$	1964
N	exponent in relationship for $G'_{max(NC)}$	0.65
M	exponent in relationship for $G'_{max(OC)}$	0.2
κ	average gradient of swelling line in ν: lnp' space	0.035
λ	gradient of compression line in ν: lnp' space	0.18
M	stress ratio at critical state (q': p')	0.89
Γ	specific volume at critical state when p'= 1kPa	2.994
N	specific volume on NCL when p'= 1kPa	3.05
ϕ'_c	critical state angle of shearing resistance	23°
γ	unit weight of soil (saturated for clay) (kN/m^3)	17.44

Table 5. 2 Speswhite kaolin clay properties (after Grant, 1998).

Test ID	Excavation modelling method	Position of injection tubes behind retaining wall	Injection tube depth below retained surface	Injection rate (ml/s)	Injection tube with brass collar	Comments
2HH	HFP	NA	NA	NA	NA	HFP initiated and reset for each stage of SPT removal. 1st and 2nd stages removed without issues. Motor failure during 3rd stage of removal. 18 kPa of SPT recorded in base of excavation at end of motor failure. De-stoned PPT not available to record SPT pressure at base of latex bag. Water leak in standpipe assembly observed resulting in lower unknown level of water table.
3HH	HFP	NA	NA	NA	NA	HFP initiated and reset for each stage of SPT removal. 1st and 2nd stages removed without issues. Motor failure during 3rd stage of removal. 28 kPa of SPT recorded in base of excavation at end of motor failure. Standpipe assembly leak fixed and water table set -25 mm below top of retained clay and in subsequent tests.

Table 6. 1 Details of tests conducted showing development of experimental technique with comments on performance of apparatus (cont'd).

Test ID	Excavation modelling method	Position of injection tubes behind retaining wall	Injection tube depth below retained surface	Injection rate (ml/s)	Injection tube with brass collar	Comments
6HH	Free drainage	60 mm (0.5H)	60 mm (0.5H)	0.230	No	Solenoid unable to fully open plug valve resulting in slow drainage of SPT and longer than expected excavation process. Injection system motor failed to run at injection rate of 0.359 ml/s, at settlement trigger of 0.125 mm in LVDT positioned 0.5H behind wall. Motor speed lowered to provide injection rate of 0.230 ml/s. Time of injection significantly delayed from intended point in excavation owing to motor failure. Injection carried out during excavation event.
7HH	Free drainage	60 mm (0.5H)	30 mm (0.25H)	0.230	No	Rotary solenoid used to permit drainage of SPT into reservoir tank. Solenoid actuation successful; plug valve fully opened. Injection system motor set at injection rate of 0.230 ml/s; to be initiated when trigger value of 0.125 mm observed from surface LVDTs. 1st injection attempt at trigger value failed owing to motor control program crashing; no injection occurred. Control program reset and delayed 1st successful injection pass conducted. 2nd injection pass successfully made after excavation event following positive response from 2nd pass to correct surface movement from LVDT measurements.

Table 6. 1 (cont'd) Details of tests conducted showing development of experimental technique with comments on performance of apparatus.

Test ID	Excavation modelling method	Position of injection tubes behind retaining wall	Injection tube depth below retained surface	Injection rate (ml/s)	Injection tube with brass collar	Comments
8HH	Free drainage	60 mm (0.5H)	90 mm (0.75H)	0.230	Yes	Centrifuge stopped 16 hours after spinning up owing to faulty out of balance load cell. Restarted after stationary for 3 hours. Model allowed to continue consolidating for additional 30 hours. Expected equilibrium pore pressures established after this period. Solenoid unresponsive on initiation of excavation. Model spun down, solenoid fixed and spun up again in short period. Hydrostatic pore pressures slightly different from expected equilibrium values. Insufficient time to allow re-establishment of pore pressures. Test carried out with functioning solenoid-plug valve assembly. Successful injection pass initiated at 0.25 mm settlement value observed from LVDT 0.5H behind wall after software reset following crash on 1st attempt. Injection stopped after visual observation of significant horizontal wall deflection and development of failure plane ruptures behind wall and in front of embedded toe.
9HH	Free drainage	60 mm (0.5H)	45 mm (0.375H)	0.230	Yes	New geared motorised valve assembly used to drain SPT. Motor failure for 1st injection attempt at lower trigger value of 0.125 mm. Failed 2nd attempt owing to control program crashing. Successful 3rd attempt= 1st injection pass carried out close to end of excavation event. Single injection pass made for test.

Table 6. 1 (cont'd) Details of tests conducted showing development of experimental technique with comments on performance of apparatus.

Test ID	Excavation modelling method	Position of injection tubes behind retaining wall	Injection tube depth below retained surface	Injection rate (ml/s)	Injection tube with brass collar	Comments
10HH	Free drainage	90 mm (0.75H)	30 mm (0.25H)	0.115	Yes	Motor failure at injection rate of 0.230 ml/s at trigger value of 0.125 mm. Control program and motor reset with injection rate reduced to 0.115 ml/s to provide successful response from injection system for the 1st injection pass; started 133 s after excavation event. A 2nd smaller volume injection pass was made 425 s after excavation completion to maintain the compensated surface after the 1st pass.
11HH	Free drainage	90 mm (0.75H)	45 mm (0.375H)	0.115	Yes	Motor failure at attempted injection rate of 0.230 ml/s at trigger value of 0.125 mm. Control program and motor reset with injection rate 0.115 ml/s to provide response from injection system for 1st single injection pass; injection started during excavation and completed after the event.

Table 6. 1 (cont'd) Details of tests conducted showing development of experimental technique with comments on performance of apparatus.

Test ID	Excavation modelling method	Position of injection tubes behind retaining wall	Injection tube depth below retained surface	Injection rate (ml/s)	Injection tube with brass collar	Comments
12HH	Free drainage	Left tube: 90 mm (0.75H) Right tube: 60 mm (0.5H)	Left tube: 30 mm (0. 25H) Right tube: 30 mm (0.25H)	0.115	Yes	Simultaneous injection of water into two latex tubes with different positions behind wall. Investigation into soil response with 'horizon' of grouting tubes. Both tubes expanded with no control over volume between them. Lower injection rate used owing to issues observed in previous tests. 1st injection pass started close to settlement trigger value of 0.125 mm. 2nd smaller volume injection pass made to reduce settlements after 1st pass.
13HH	Free drainage	Left tube: 90 mm (0.75H) Right tube: 60 mm (0.5H)	Left tube: 45 mm (0. 375H) Right tube: 45 mm (0.375H)	0.115	Yes	Simultaneous injection of water into two latex tubes with different positions behind wall. Both tubes expanded with no control over volume between them. 1st injection pass started close to settlement trigger value of 0.125 mm during excavation and continued beyond end of event. 2nd smaller volume injection pass made to observe its affect following the 1st pass.

Notes:

HFP: Simulation of excavation using the heavy fluid pump to remove SPT from the excavation supporting latex bag.

Free drainage: Simulation of excavation by allowing supporting SPT fluid to drain into a reservoir under induced increased gravitational acceleration field.

H: Model excavation depth (120 mm).

Table 6. 1 Details of tests conducted showing development of experimental technique with comments on performance of apparatus.

Test ID	Excavation duration (s)	Initial SPT support pressure (pre-excavation) (kPa)	Change in support pressure (kPa)
2HH	405	160.3	138.3
3HH	422	175.8	156.1
6HH	820	182.7	182.2
7HH	249	184.0	180.1
8HH	242	181.9	179.1
9HH	247	189.3	185.0
10HH	245	190.6	186.7
11HH	248	187.3	185.5
12HH	244	191.0	185.7
13HH	247	186.5	185.3

Table 6. 2 Summary of simulated excavation durations and SPT support pressures for all tests.

Test	Event (relative to Exc./time post Exc.)	Time (s) (relative to Exc. Start)	ΔS_v (LVDT-Target movement) (mm)				
			Relative distances/positions behind the wall				
			Wall	0.25H	0.5H	1.0H	1.5H
2HH (No Inj. tube)	Exc. End (E_2, T_2)	405	0.007	0.010	-0.072	-0.179	-0.251
	Post exc. +133 s (T_2+133 s)	538	-0.024	0.002	-0.093	-0.186	-0.289
3HH (No Inj. tube)	Exc. End (E_{11}, T_{11})	422	-0.024	-0.023	-0.071	-0.172	-0.238
	Post exc. +133 s (T_2+133 s)	555	0.004	0.002	-0.100	-0.170	-0.269
10HH (With Inj. Tube and brass collar)	Exc. End (E_{13}, T_{13})	245	-0.015	-0.017	-0.082	-0.180	-0.267
	Post exc. +133 s (T_2+133 s)	378	-0.022	-0.022	-0.097	-0.182	-0.271
Note: Negative ΔS_v values: LVDT settlements larger than target settlements.							

Table 6. 3 Difference in settlements between LVDTs and image processing targets (15 mm below the surface) above the wall and at distances x= 0.25H, 0.5H, 1.0H and 1.5H behind the wall during excavation and up to 133 s post excavation completion in tests 2HH, 3HH and 10HH.

Test (without a Brass collar)	Depth of injection	Event (relative to Exc. /time post Exc.)	Time (s) (from Exc. Start)	ΔS_v (LVDT-Target movement) (mm)				
				Relative distances/positions behind the wall				
				Wall	0.25H	0.5H	1.0H	1.5H
6HH	0.5H (60 mm)	*Relative distances from Inj. tube:*		-	*-30 mm*	*Inj. Tube*	*+60 mm*	*+120 mm*
		Injection 1 Start ($0.74E_6$)	509	0.003	-0.024	-0.051	-0.043	-0.231
		Injection 1 Stop ($0.98E_6$)	789	0.009	-0.404	-3.368	-0.210	-0.288
		Exc. End (E_6, T_6)	820	-0.006	-0.429	-3.453	-0.222	-0.294
7HH	0.25H (30 mm)	Injection 1 Start ($0.53E_7$)	105	0.025	-0.077	-0.016	-0.057	-0.096
		Injection 1 Stop ($0.97E_7$)	233	0.003	-0.331	-6.792	-0.213	-0.249
		Exc. End (E_7, T_7)	249	0.015	-0.326	-6.910	-0.220	-0.289
		Injection 2 Start (T_7+103 s)	352	0.019	-0.332	-7.049	-0.239	-0.316
		Injection 2 Stop (T_7+137 s)	386	-0.007	-0.611	-12.394	-0.243	-0.309
Note: Negative ΔS_v values: LVDT settlements larger than target settlements.								

Table 6. 4 Difference in settlements between LVDTs and image processing targets (15 mm below the surface) above the wall and at distances x= 0.25H, 0.5H, 1.0H and 1.5H behind the wall in tests 6-7HH, where no brass collar was provided at the front of the injection tube.

Test (with Brass collar)	Depth of injection	Event (relative to Exc./time post Exc.)	Time (s) (from Exc. Start)	ΔS_v (LVDT-Target movement) (mm)				
				Relative distances/positions behind the wall				
				Wall	0.25H	0.5H	1.0H	1.5H
8HH	0.75H (90 mm)	*Relative distances from Inj. tube:*		-	*-30 mm*	*Inj. Tube*	*+60 mm*	*+120 mm*
		Injection 1 Start ($0.31E_8$)	60	-0.010	0.000	0.010	0.001	-0.009
		Exc. End/ Injection 1 Stop (E_8)	242	-0.014	-0.009	-0.102	-0.177	-0.267
Note: Negative ΔS_v values: LVDT settlements larger than target settlements.								

Table 6. 5 Difference in settlements between LVDTs and image processing targets (15 mm below the surface) above the wall and at distances x= 0.25H, 0.5H, 1.0H and 1.5H behind the wall in test 8HH, where a brass collar was provided at the front of the injection tube.

Test (with Brass collar)	Depth of injection	Event (relative to Exc./time post Exc.)	Time (s) (from Exc. Start)	ΔS_v (LVDT-Target movement) (mm)					
				Relative distances/positions behind the wall					
				Wall	0.25H	0.5H	0.75H	1.0H	1.5H
10HH	0.25H (30 mm)	*Relative distances from Inj. tube:*			*-60 mm*	*-30 mm*	*Inj. Tube*	*+30 mm*	*+90 mm*
		Exc. End (E_{10}, T_{10})	245	-0.015	-0.017	-0.082	-0.215	-0.180	-0.267
		Injection 1 Start (T_{10}+133 s)	378	-0.022	-0.022	-0.097	-0.225	-0.182	-0.271
		Injection 1 Stop (T_{10}+364 s)	609	-0.015	0.064	0.231	1.086	0.000	-0.269
		Injection 2 Start (T_{10}+425 s)	670	-0.011	0.044	0.262	1.072	0.011	-0.239
		Injection 2 Stop (T_{10}+465 s)	710	-0.021	0.057	0.232	1.277	0.023	-0.264
12HH	0.25H (30 mm)	*Relative distances from Inj. tube:*			*-30 mm*	*Right Inj. tube*	*Left Inj. tube*	*+30 mm*	*+90 mm*
		Injection 1 Start (0.32E_{12})	62	0.009	-0.009	-0.034	-0.022	-0.032	-0.032
		Exc. End (E_{12}, T_{12})	244	0.005	0.117	0.306	0.256	-0.106	-0.244
		Injection 1 Stop (T_{12}+80 s)	324	0.008	0.245	0.901	0.897	-0.025	-0.243
		Injection 2 Start (T_{12}+390 s)	634	0.009	0.244	0.895	0.862	-0.047	-0.253
		Injection 2 Stop (T_{12}+421 s)	665	0.007	0.257	1.184	1.134	-0.048	-0.254
Note: Negative ΔS_v values: LVDT settlements larger than target settlements.									

Table 6. 6 Difference in settlements between LVDTs and image processing targets (15 mm below the surface) above the wall and at distances x= 0.25H, 0.5H, 0.75H, 1.0H and 1.5H behind the wall in tests 10HH and 12HH, where a brass collar was provided at the front of the injection tube.

Test (with Brass collar)	Depth of injection	Event (relative to Exc./time post Exc.)	Time (s) (from Exc. Start)	ΔS_v (LVDT-Target movement) (mm)					
				Relative distances/positions behind the wall					
				Wall	0.25H	0.5H	0.75H	1.0H	1.5H
9HH	0.375H (45 mm)	*Relative distances from Inj. tube:*		-	*-30 mm*	*Inj. Tube*	-	*+60 mm*	*+120 mm*
		Injection 1 start ($0.94E_9$)	221	-0.019	0.036	-0.099	-	-0.186	-0.253
		Exc. End (E_9, T_9)	247	-0.011	0.053	-0.023	-	-0.121	-0.280
		Injection 1 Stop (T_9+123 s)	370	0.010	0.168	0.008	-	-0.173	-0.282
11HH	0.375H (45 mm)	*Relative distances from Inj. tube:*		-	*-60 mm*	*-30 mm*	*Inj. Tube*	*+30 mm*	*+90 mm*
		Injection 1 Start ($0.68E_{11}$)	142	-0.023	-0.010	-0.119	-0.143	-0.238	-0.213
		Exc. End (E_{11}, T_{11})	248	-0.015	0.040	-0.088	-0.231	-0.277	-0.228
		Injection 1 Stop (T_{11}+306 s)	554	0.009	0.077	0.336	0.250	-0.115	-0.254
13HH	0.375H (45 mm)	*Relative distances from Inj. tube:*		-	*-30 mm*	*Right Inj. tube*	*Left Inj. tube*	*+30 mm*	*+90 mm*
		Injection 1 Start ($0.34E_{13}$)	64	0.019	-0.020	-0.021	-0.035	-0.011	-0.009
		Exc. End (E_{13}, T_{13})	247	0.012	0.067	-0.115	-0.222	-0.097	-0.247
		Injection 1 Stop (T_{13}+183 s)	430	0.012	0.186	0.037	-0.011	0.000	-0.275
		Injection 2 Start (T_{13}+376 s)	623	0.012	0.140	-0.053	-0.136	-0.066	-0.276
		Injection 2 Stop (T_{13}+430 s)	677	0.018	0.167	-0.221	-0.276	-0.082	-0.281
Note: Negative ΔS_v values: LVDT settlements larger than target settlements.									

Table 6. 7 Difference in settlements between LVDTs and image processing targets (15 mm below the surface) above the wall and at distances x= 0.25H, 0.5H, 0.75H, 1.0H and 1.5H behind the wall in tests 9HH, 11HH and 13HH, where a brass collar was provided at the front of the injection tube.

Test ID	Initial pre-test hydrostatic pore pressures (kPa)	
	Top PPT	Bottom PPT
2HH	-3.5	179.7
3HH	7.7	209.8
6HH	3.6	203.4
7HH	3.2	202.2
8HH	-5.2	247.4
9HH	7.4	206.1
10HH	7.4	205.3
11HH	6.6	203.7
12HH	6.6	204.7
13HH	1.2	200.7

Table 6. 8 Pre-test hydrostatic pore pressures established in model, measured by the top and bottom far field PPTs.

Event description, 6HH	Time (s)	Total injected volume, V_i (ml)
Start Excavation	0	-
Injection 1 Start ($0.74E_6$)	509	0
Injection 1 Stop ($0.98E_6$)	789	64.51
Exc. End (E_6, T_6)	820	64.51

Table 6. 9 Summary of event times relative to the start of excavation and injected volumes in test 6HH.

Event description, 7HH	Time (s)	Total injected volume, V_i (ml)
Start Excavation	0	-
Injection 1 Start ($0.53E_7$)	105	0
Injection 1 Stop ($0.97E_7$)	233	29.49
Exc. End (E_7, T_7)	249	29.49
Injection 2 Start (T_7+103 s)	352	29.49
Injection 2 Stop (T_7+137 s)	386	37.32

Table 6. 10 Summary of event times relative to the start of excavation and injected volumes in test 7HH.

Event description, 8HH	Time (s)	Total injected volume, V_i (ml)
Start Excavation	0	-
Injection 1 Start ($0.31E_8$)	60	0
Injection 1 Stop (E_8)	242	41.93
Exc. End (E_8, T_8)	242	41.93

Table 6. 11 Summary of event times relative to excavation initiation and injected volumes in test 8HH.

Event description, 9HH	Time (s)	Total injected volume, V_i (ml)
Start Excavation	0	-
Injection 1 start ($0.94E_9$)	221	0
Exc. End (E_9, T_9)	247	5.99
Injection 1 Stop (T_9+123 s)	370	34.33

Table 6. 12 Summary of event times relative to the start of excavation and injected volumes in test 9HH.

Event description, 10HH	Time (s)	Total injected volume, V_i (ml)
Start Excavation	0	-
Exc. End (E_{10}, T_{10})	245	-
Injection 1 Start (T_{10}+133 s)	378	0
Injection 1 Stop (T_{10}+364 s)	609	26.61
Injection 2 Start (T_{10}+425 s)	670	26.61
Injection 2 Stop (T_{10}+465 s)	710	31.33

Table 6. 13 Summary of event times relative to the start of excavation and injected volumes in test 10HH.

Event description, 11HH	Time (s)	Total injected volume, V_i (ml)
Start Excavation	0	-
Injection 1 Start ($0.68E_{11}$)	142	0
Exc. End (E_{11}, T_{11})	248	12.21
Injection 1 Stop (T_{11}+306 s)	554	47.46

Table 6. 14 Summary of event times relative to the start of excavation and injected volumes in test 11HH.

Event description, 12HH	Time (s)	Total injected volume, V_i (ml)
Start Excavation	0	-
Injection 1 Start ($0.32E_{12}$)	62	0
Exc. End (E_{12}, T_{12})	244	20.97
Injection 1 Stop (T_{12}+80 s)	324	30.18
Injection 2 Start (T_{12}+390 s)	634	30.18
Injection 2 Stop (T_{12}+421 s)	665	31.97

Table 6. 15 Summary of event times relative to the start of excavation and injected volumes in test 12HH.

Event description, 13HH	Time (s)	Total injected volume, V_i (ml)
Start Excavation	0	-
Injection 1 Start ($0.34E_{13}$)	64	0
Exc. End (E_{13}, T_{13})	247	21.08
Injection 1 Stop (T_{13}+183 s)	430	42.16
Injection 2 Start (T_{13}+376 s)	623	42.16
Injection 2 Stop (T_{13}+430 s)	677	48.38

Table 6. 16 Summary of event times relative to the start of excavation and injected volumes in test 13HH.

Test	Available Injection PTs (S= System PT, M= Manifold PT, B= Both PTs)	Average pressure loss between the Injection system and manifold PTs, ΔP_{loss} (kPa) (= Injection system PT reading – Injection manifold PT reading)
6HH	S	n/a
7HH	B	169.7
8HH	B	167.1
9HH	B	159.9
10HH	S	n/a
11HH	B	172.2
12HH	B	164.3
13HH	B	167.6
	median	166.1
	error range	6.1

Table 6. 17 Average pressure losses measured between the Injection system PT and Manifold PT (close to the point of injection tube into the back wall of the strongbox).

Test ID	Average external diameter of injection tube (mm) (inc. inner Nylon tube: external diameter= 6 mm)	Initial injection tube volume, V_o (ml) (tube length= 200 mm)
6HH	8.50	11.35
7HH	8.70	11.89
8HH	9.17	13.20
9HH	9.07	12.91
10HH	9.10	13.01
11HH	9.23	13.39
12HH (L, x= 90 mm)	9.13	13.10
12HH (R, x= 60 mm)	9.17	13.20
13HH (L, x= 90 mm)	8.73	11.98
13HH (R, x= 60 mm)	8.77	12.07

Table 6. 18 Initial cavity volumes of the injection tubes in tests 6-13HH.

Test	Radial distance between injection tube and local PPT, r_{PPT} (mm)
6HH	60
7HH	42.4
8HH	42.4
9HH	33.5
10HH	30
11HH	33.5
12HH (L)	42.4
12HH (R)	30
13HH (L)	33.5
13HH (R)	61.8

Table 6. 19 Radial distance between the injection grouting tube and locally installed injection zone pore pressure transducer.

Test ID	Injection depth below retained surface (mm)	Peak injection pressure, $P_{i,PEAK}$ (kPa)	Injected volume at peak injection pressure $\delta V_{i,PEAK}$ (ml)	Vertical total stress above each injection tube, σ_v (kPa) (theoretical)	Peak injection pressure normalised against vertical total stress $P_{i,PEAK}/\sigma_v$	Injected volume at peak injection pressure normalised against initial cavity volume $\delta V_{i,PEAK}/V_o$
6HH	60	409.2	19.35	101.96	4.01	1.71
7HH	30	354.9	18.43	49.98	7.10	1.55
8HH	90	436.8	14.75	155.96	2.80	1.12
9HH	45	374.4	17.28	75.72	4.94	1.34
10HH	30	320.0	14.75	49.98	6.40	1.13
11HH	45	369.9	19.47	75.72	4.89	1.45
12HH	30	270.6	28.11	49.98	5.42	2.14
13HH	45	324.3	27.19	75.72	7.16	2.26

Table 6. 20 Peak injection pressures, associated injected volumes, overburden stresses above each tube and normalised injection pressures against overburden stresses for all grouting tests.

Test	Normalised depth of S_{hmax} (d/H) (below retained surface level)	S_{hmax}/H (%)	Typical value of S_{hmax}/H (%) in Firm clays (S_u< 75 kPa) by Moormann (2004)
3HH	0.75	1.70	1 (>1 for low stiffness walls i.e. sheet piles)
10HH	0.75	1.67	

Table 7. 1 Normalised magnitude of maximum horizontal wall displacement at the end of simulated excavation in tests 3HH and 10HH shown in the context of expected limits in firm clays from monitoring data by Moorman (2004).

Test	Normalised distance, x/H	Normalised depth, d/H	Normalised impact of injection at the surface above the injection tube, δS_v/H (%) at end of 1st injection pass *(at end of 2nd injection pass)*
7HH	0.5	0.25	-0.65* *(-0.61)*
10HH	0.75	0.25	-1.27** *(-1.42)*
9HH	0.5	0.375	0.85**
11HH	0.75	0.375	0.21**
6HH	0.5	0.5	1.21*
8HH	0.5	0.75	3.66*

Note:
Negative δS_v/H (%) value: positive compensation effect (i.e. reduction in settlements relative to excavation only data).
*: First injection pass completed during excavation simulation.
**: First injection pass completed after excavation simulation.

Table 7. 2 Normalised impact of the injection passes in tests 7HH, 9HH, 10HH and 11HH on the vertical surface settlements above the injection tube relative to test 3HH.

Test	Total injected volume, ml (at end of excavation simulation)
6HH	64.51*
7HH	29.49*
8HH	41.93*
9HH	4.15**
10HH	N/A
11HH	12.21**
12HH	21.20**
13HH	21.08**
Note: *: First injection pass completed during excavation simulation **: First injection pass ongoing after excavation simulation N/A: Injection not yet started at end of excavation	

Table 7. 3 Total injected volumes in test 6-13HH at the end of simulated excavation.

Test	Total elapsed time between 1st and 2nd single injection pass (s)	Change in normalised effect on vertical settlement at surface above injection, $\Delta\delta S_v/H$ (%)	Change in pore pressures between injection passes measured in local injection zone PPT, Δu_{inj} (kPa)
7HH	119	-0.14	5.4
10HH	61	0.05	1.1
Note: Negative $\Delta\delta S_v/H$ (%) value = decrease in positive compensation effect.			

Table 7. 4 Effect of timing between injection passes on the compensation effect in single point injection tests 7HH and 10HH.

Test	Normalised distance, x/H	Normalised depth, d/H	Normalised impact of injection on wall at depth d= 0.75H (90 mm), $\delta S_{h(d=0.75H)}/H$ (%) at end of 1st injection pass *(at end of 2nd injection pass)*
7HH	0.5	0.25	0.91* *(0.99)*
10HH	0.75	0.25	0.26** *(0.37)*
9HH	0.5	0.375	2.79**
11HH	0.75	0.375	2.88**
6HH	0.5	0.5	4.03*
8HH	0.5	0.75	4.46*
12HH	0.5(R), 0.75(L)	0.25	0.68** *(0.77)*
13HH	0.5(R), 0.75(L)	0.375	1.51** *(2.36)*

Note:
Positive $\delta S_{h(d=0.75H)}/H$ (%) value: unfavourable impact (i.e. increased horizontal displacements relative to excavation only data).
*: First injection pass completed during excavation simulation.
**: First injection pass completed after excavation simulation.

Table 7. 5 Normalised impact of the injection passes in all grouting tests on the horizontal wall displacements at a depth d= 0.75H below the retained surface relative to test 3HH.

Test	Normalised depth, d/H	Normalised effect of injection at the surface above the injection tube, $\delta S_v/H$ (%) at end of 1st injection pass *(at end of 2nd injection pass)*	
		Normalised distance behind wall, x/H	
		0.5	0.75
7HH	0.25	-0.65 *(-0.61)*	-
10HH	0.25	-	-1.27 *(-1.42)*
12HH	0.25	-1.17 *(-1.44)*	-1.40 *(-1.63)*
9HH	0.375	0.85	-
11HH	0.375	-	0.21
13HH	0.375	-0.72 *(-0.24)*	-1.04 *(-0.79)*

Note:
Negative $\delta S_v/H$ (%) value: positive compensation effect (i.e. reduction in settlements relative to excavation only data).

Table 7. 6 Normalised impact of injection between single point injections in tests 7HH, 9HH, 10HH and 11HH and dual point simultaneous injections in test 12HH and 13HH on the vertical displacements at the retained surface above the injection location.

FIGURES

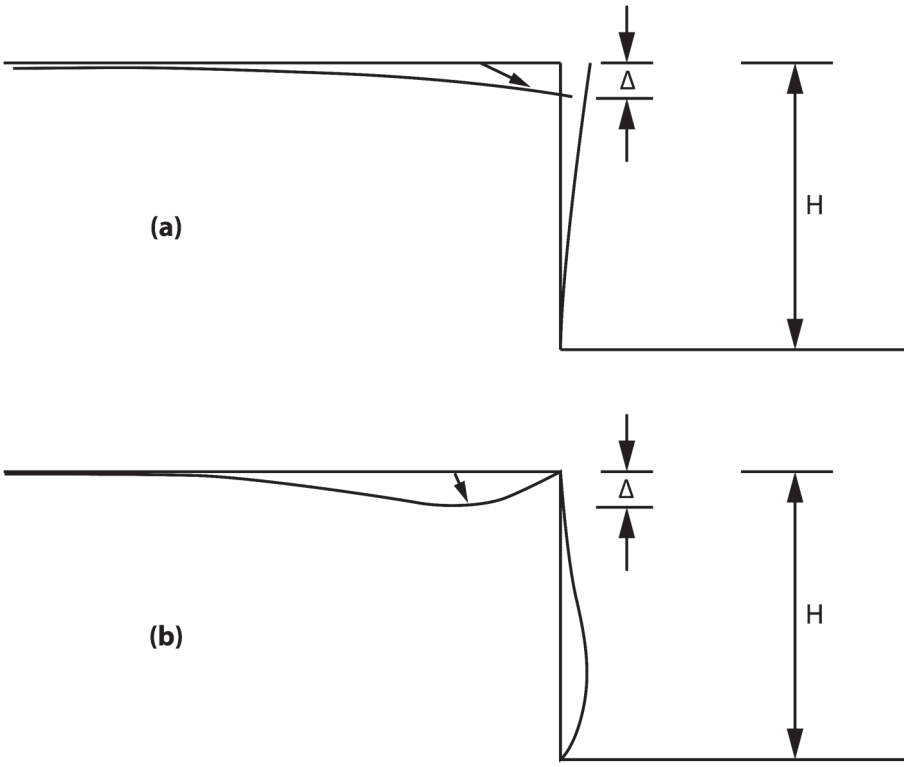


Figure 2. 1 Typical pattern of displacements behind retaining walls (after Burland *et al.*, 1979).

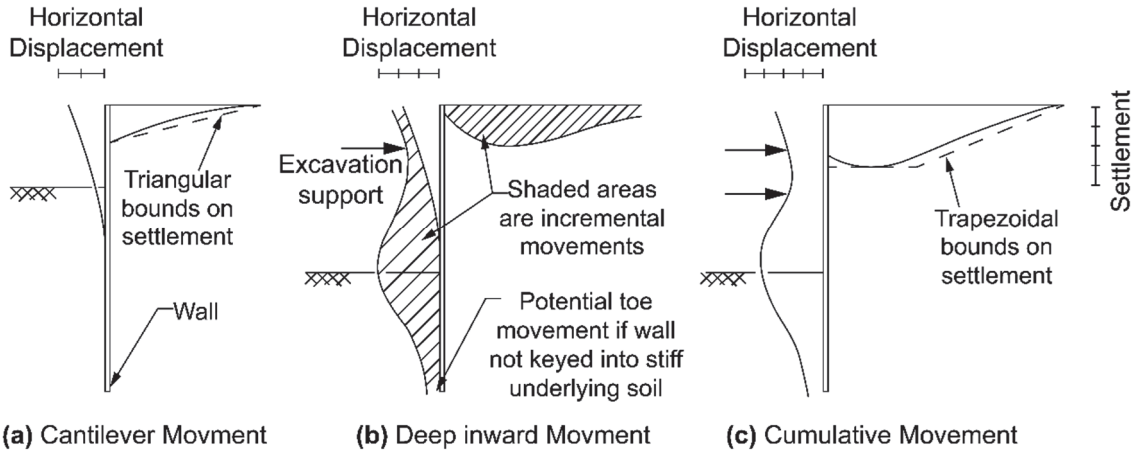


Figure 2. 2 Typical profiles of movement for braced and tieback walls (after Clough and O'Rourke, 1990).

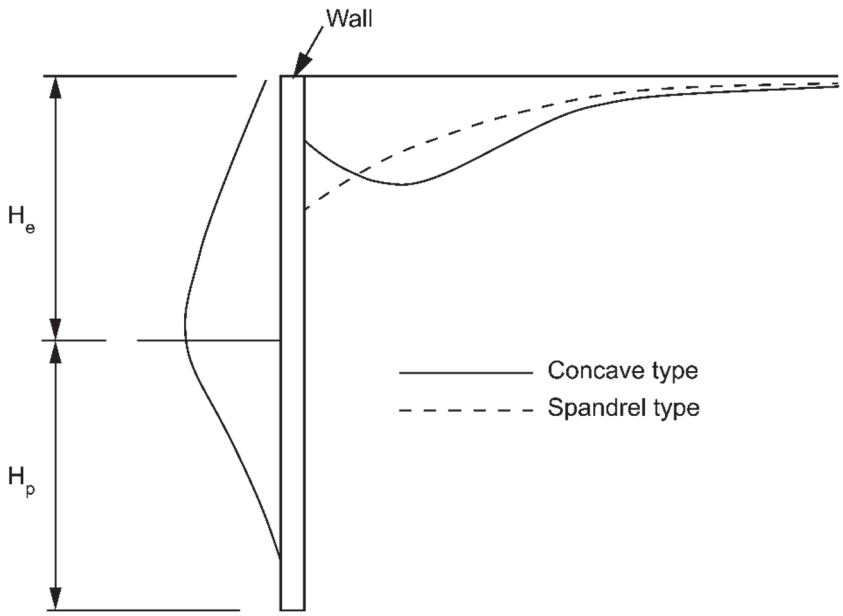


Figure 2. 3 Types of settlement profiles (after Hsieh and Ou, 1998).

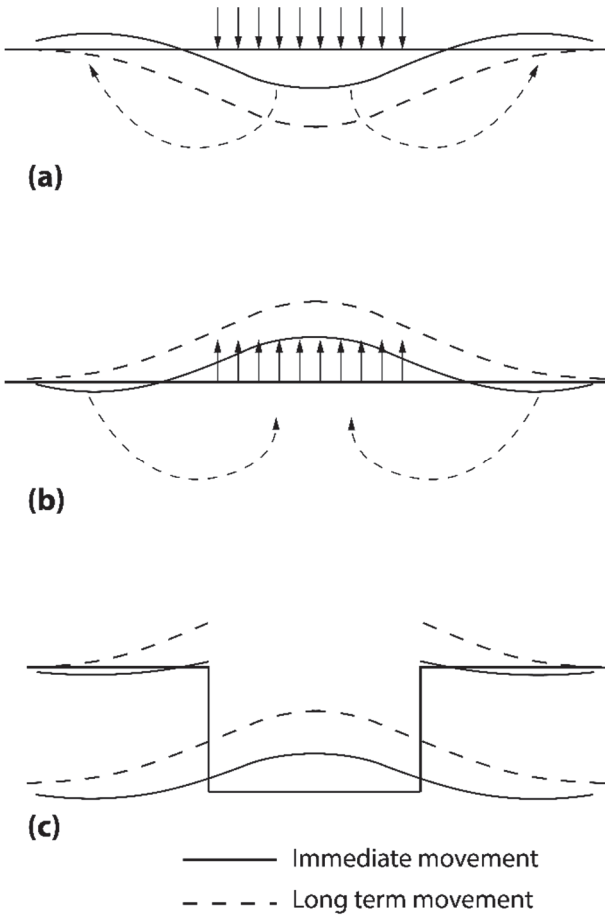


Figure 2. 4 Vertical soil response to vertical unloading caused by excavation (after Burland *et al.*, 1979).

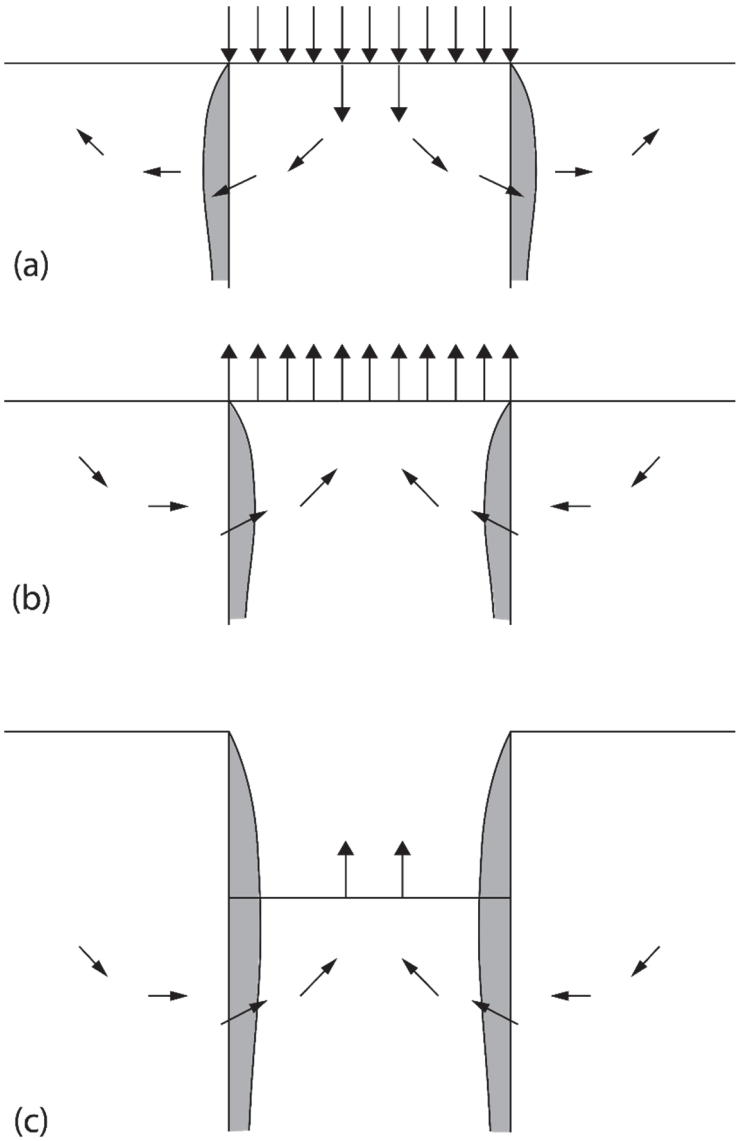
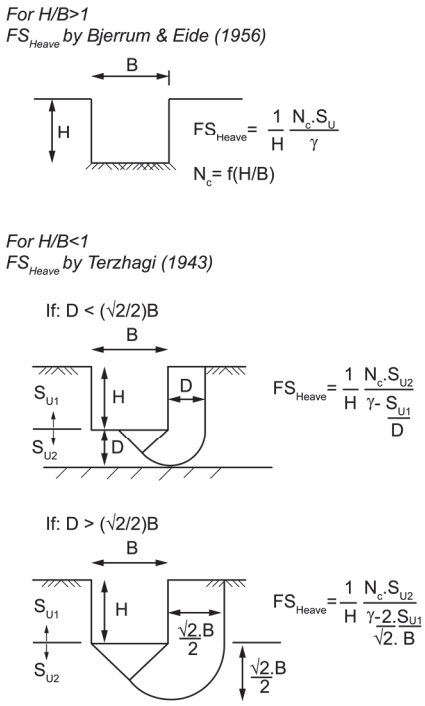
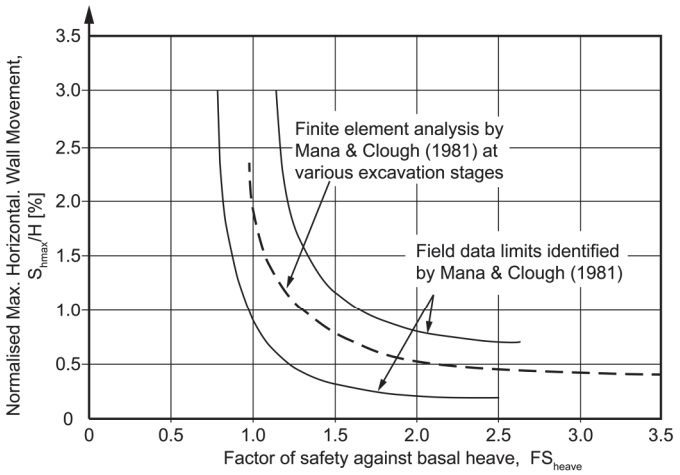


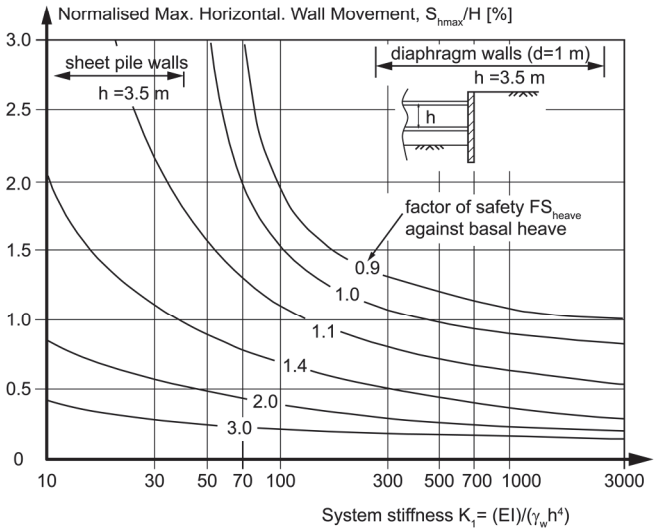
Figure 2. 5 Horizontal soil response to vertical unloading caused by excavation (after Burland *et al.*, 1979).



(a) Calculation of factor of safety against basal heave (after Terzhagi, 1943; Bjerrum & Eide, 1956)



(b) Relationship between factor of safety against basal heave and normalised maximum horizontal wall movement (after Mana & Clough, 1981)



(c) Design curves for estimating normalised maximum horizontal wall movement in soft-medium clays considering system stiffness and factor of safety against basal heave (after Clough *et al*, 1989)

Figure 2. 6 Effect of factor of safety against basal heave (FS_{Heave}) and support system stiffness (K_1) on normalised maximum horizontal wall movements in soft to medium clays (after (a) Terzaghi, 1943; Bjerrum and Eide, 1956, (b) Mana and Clough, 1981 and (c) Clough *et al.*, 1989).

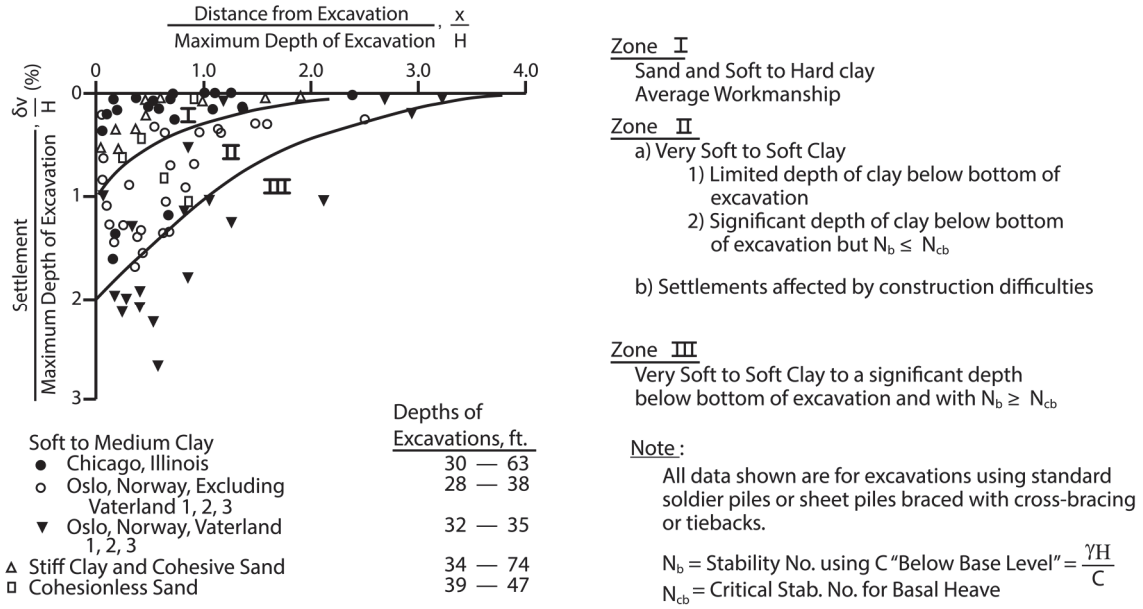


Figure 2. 7 Summary of settlements adjacent to open cuts in various soils, as a function of distance from edge of excavation (after Peck, 1969).

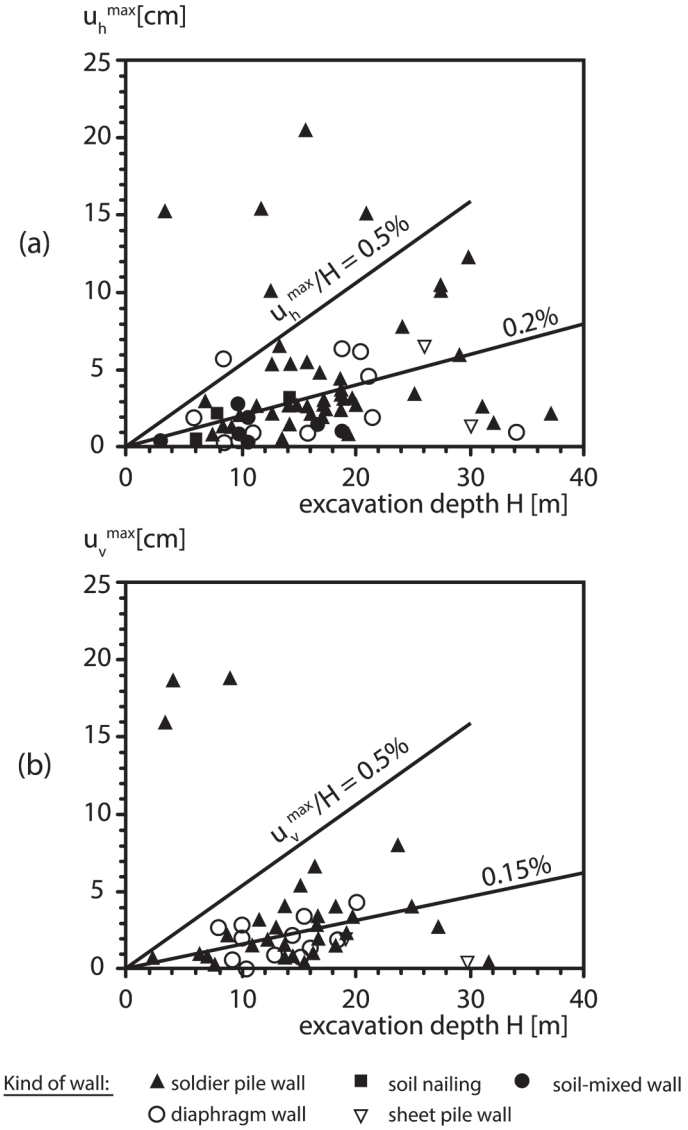


Figure 2. 8 Observed maximum: (a) wall deflections and (b) vertical settlements for stiff clays, residual soils and sands (after Clough and O'Rourke, 1990; reproduced from Moorman, 2004).

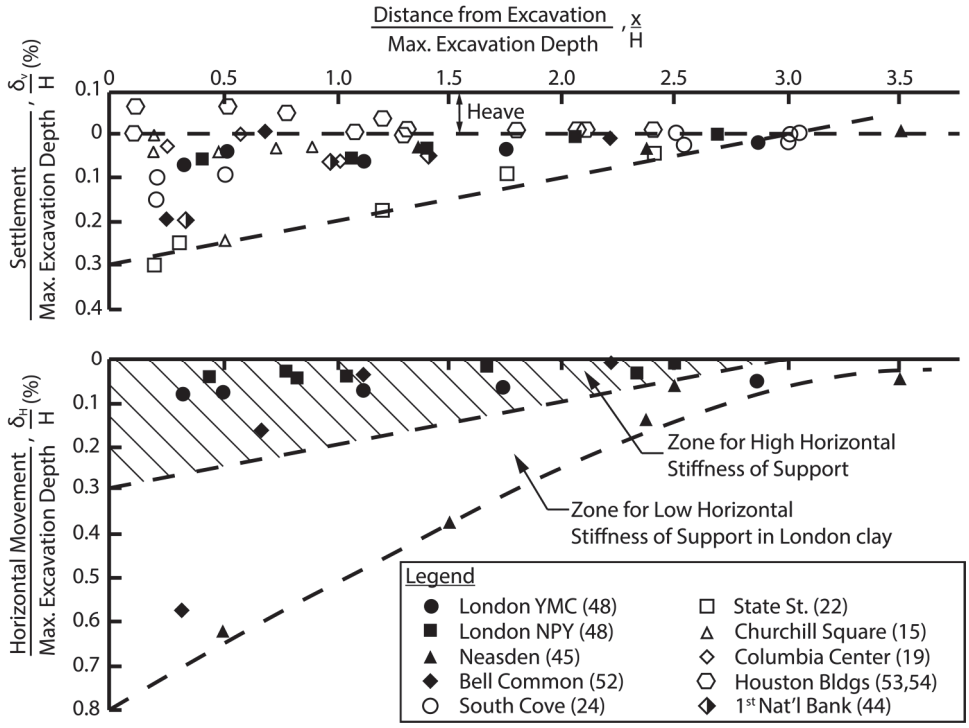


Figure 2. 9 Summary of vertical soil and horizontal wall displacements adjacent to excavations in stiff to very hard clays (after Clough and O'Rourke, 1990).

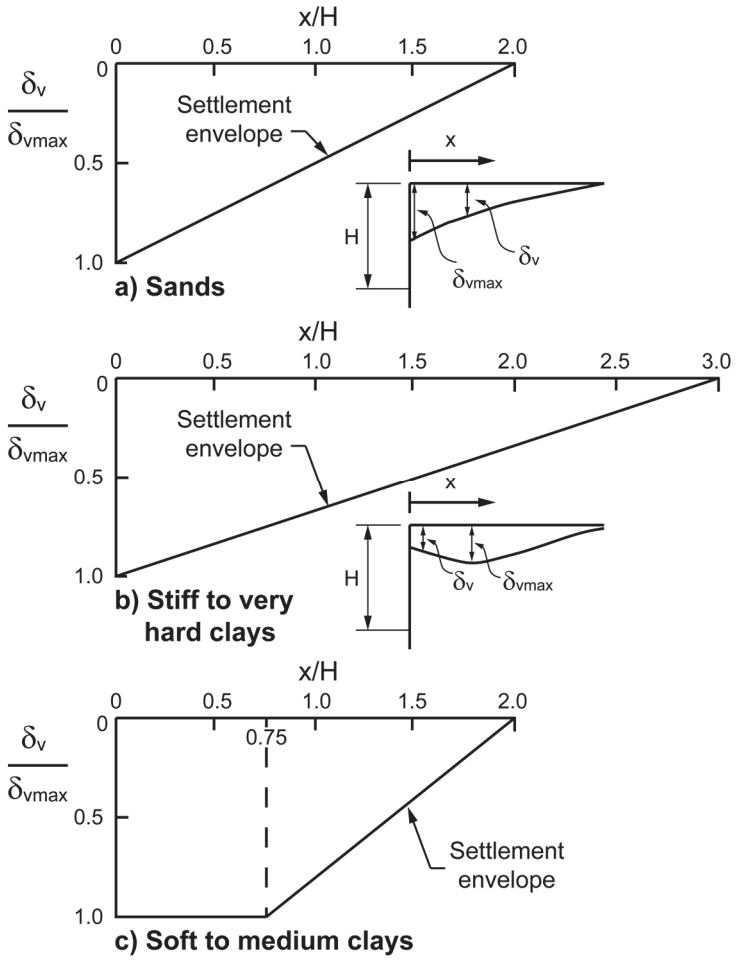


Figure 2. 10 Dimensionless settlement envelopes for estimating settlements adjacent to excavations in different soil types (after Clough and O'Rourke, 1990).

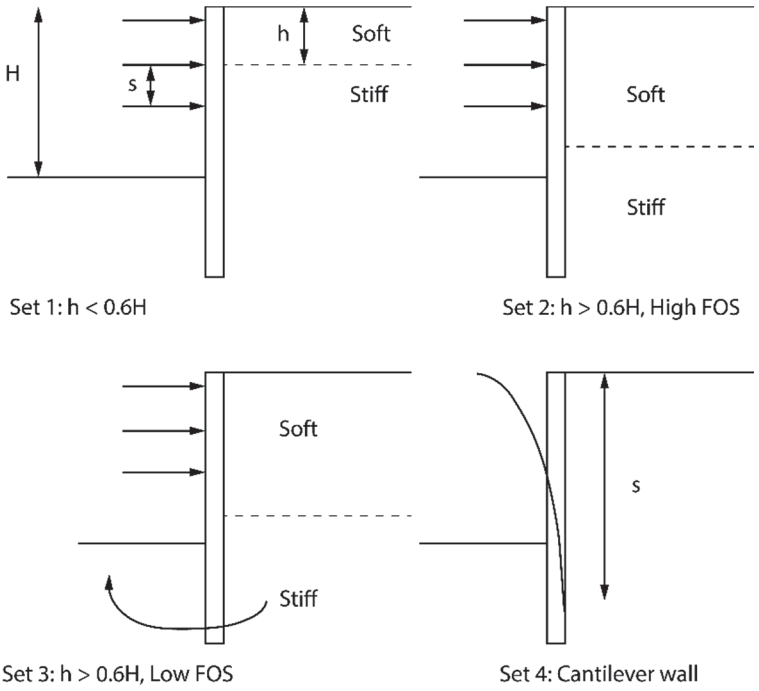


Figure 2. 11 Subdivision of case history data by Long (2001).

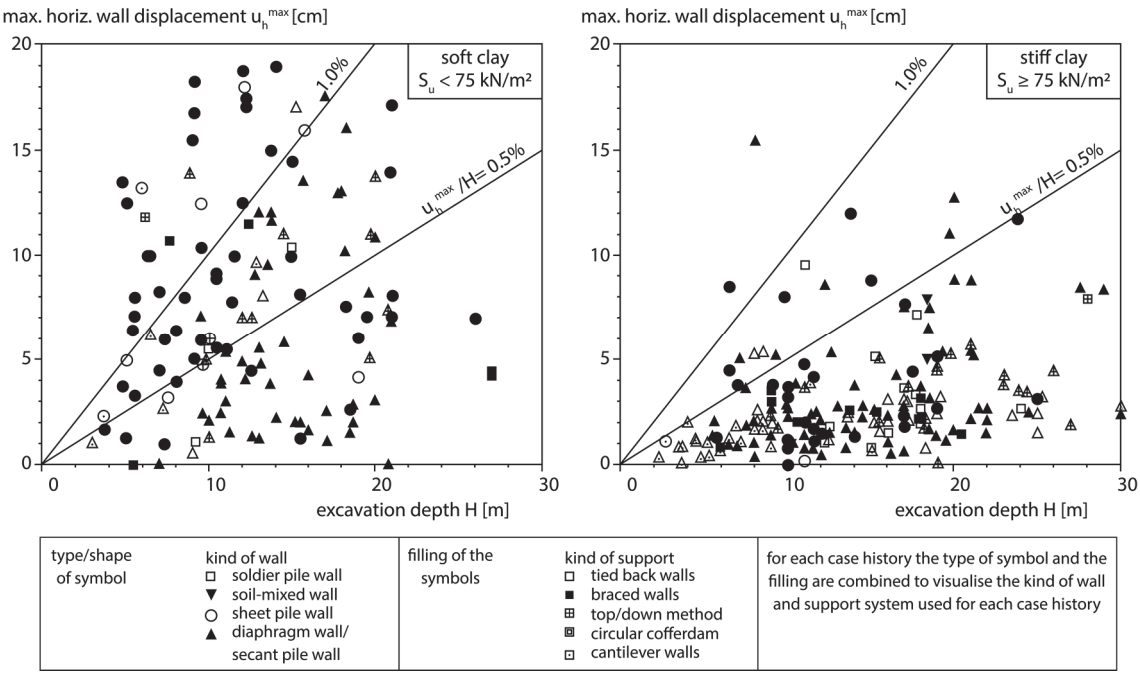


Figure 2. 12 Normalised maximum horizontal wall displacements against excavation depths observed in soft and stiff clays (after Moormann, 2004).

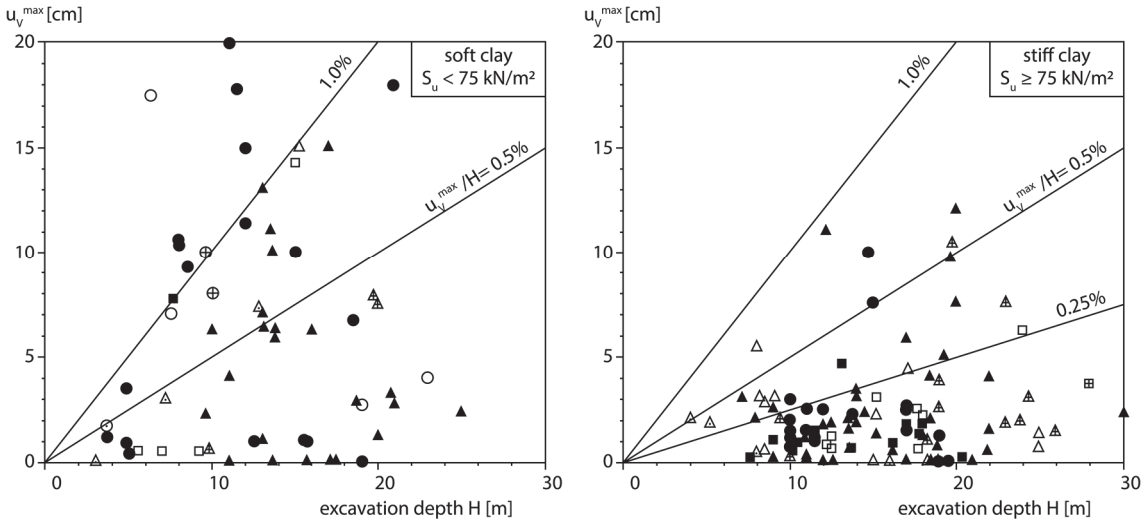


Figure 2. 13 Normalised maximum vertical settlements against excavation depths observed in soft and stiff clays (after Moormann, 2004).

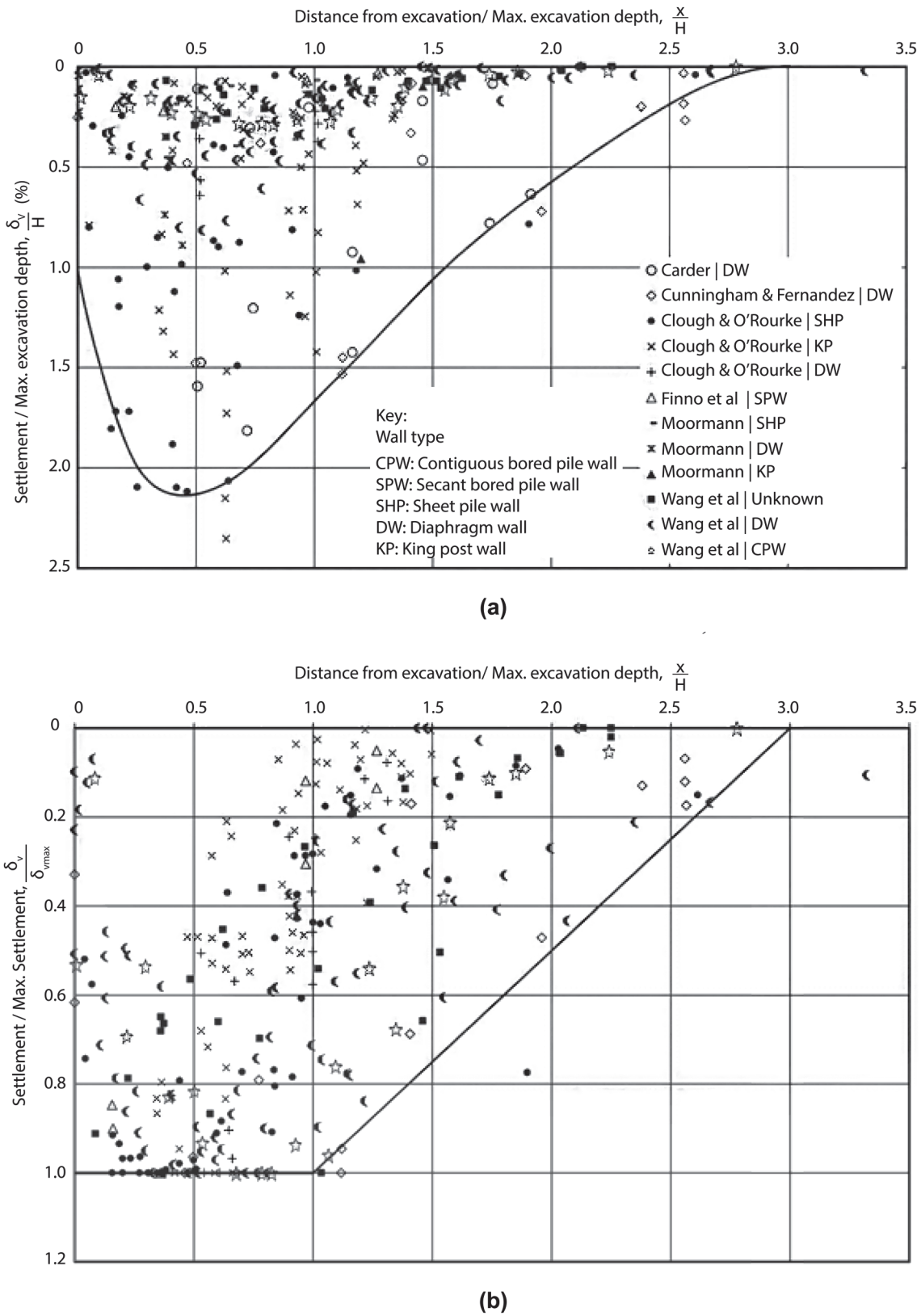


Figure 2. 14 (a) Normalised ground surface displacements due to excavation and (b) settlements normalised against maximum settlement behind the wall in soft to firm clays (after Gaba *et al.*, 2017).

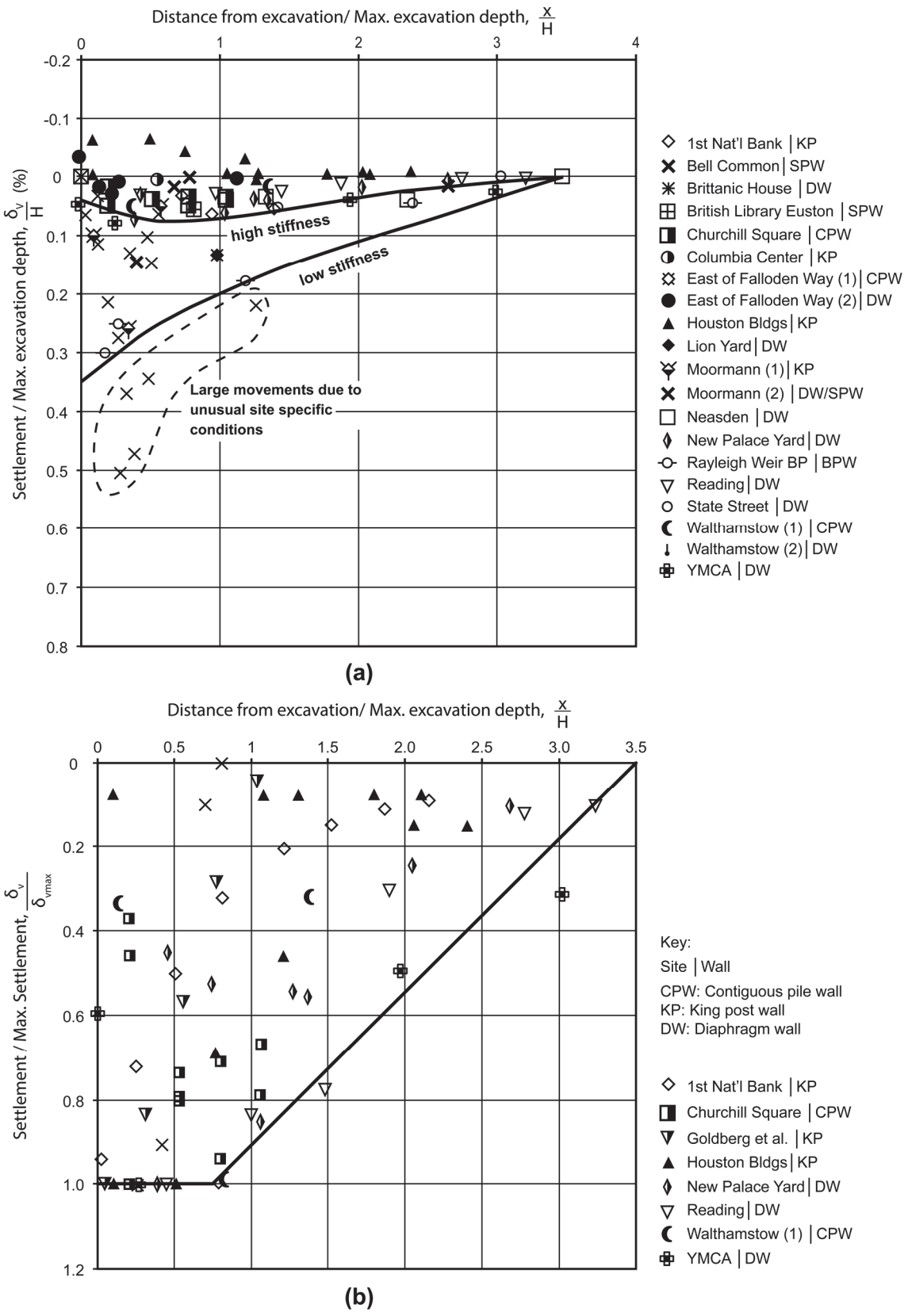


Figure 2. 15 (a) Normalised ground surface displacements due to excavation and (b) settlements normalised against maximum settlement behind the wall in stiff clays (after Gaba *et al.*, 2017).

.

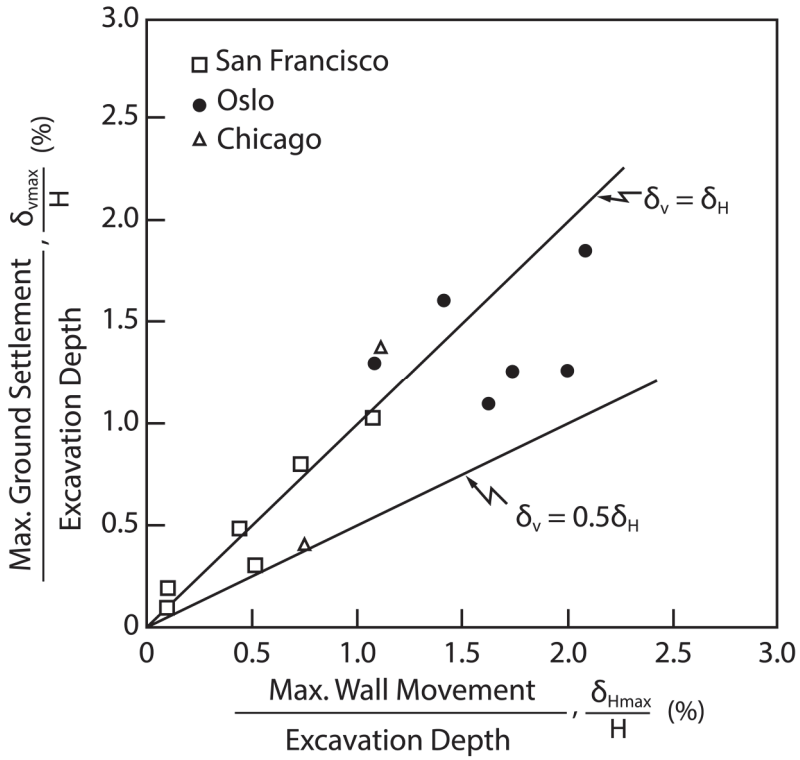


Figure 2. 16 Relationship between normalised maximum ground settlements and lateral wall movements (after Mana and Clough, 1981).

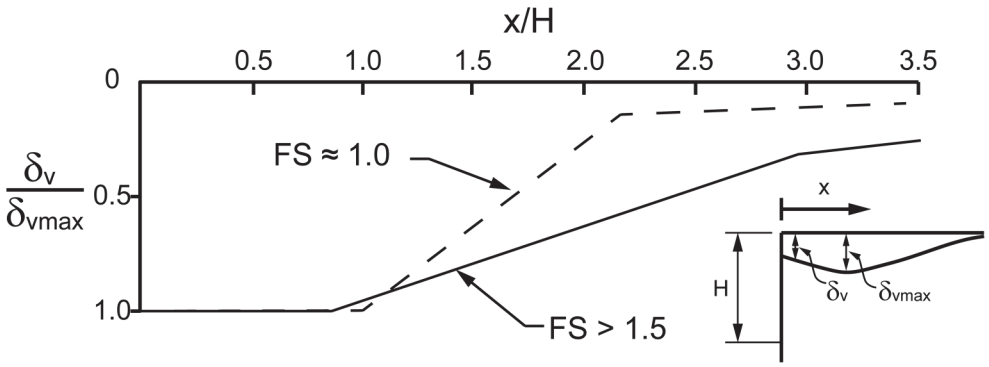


Figure 2. 17 Normalised ground settlement profile envelopes (after Mana and Clough, 1981).

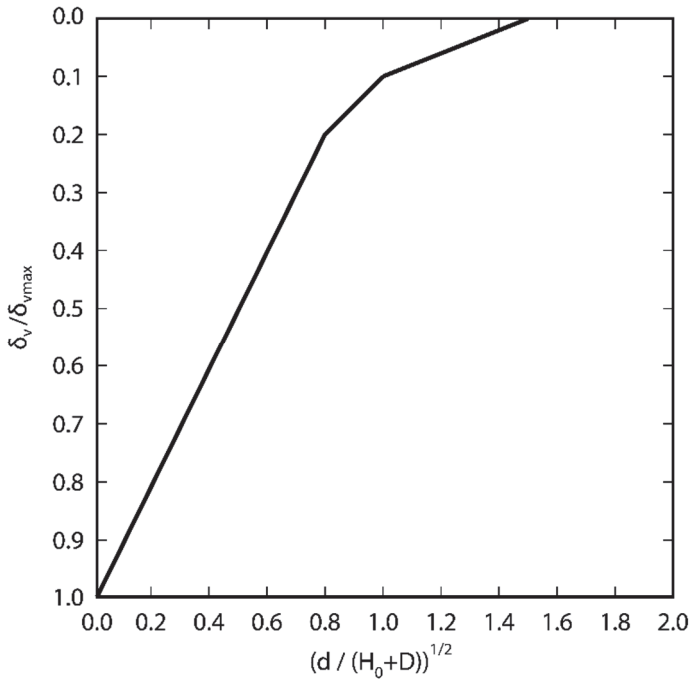


Figure 2. 18 Proposed method for predicting a spandrel type settlement profile (after Ou *et al.*, 1993).

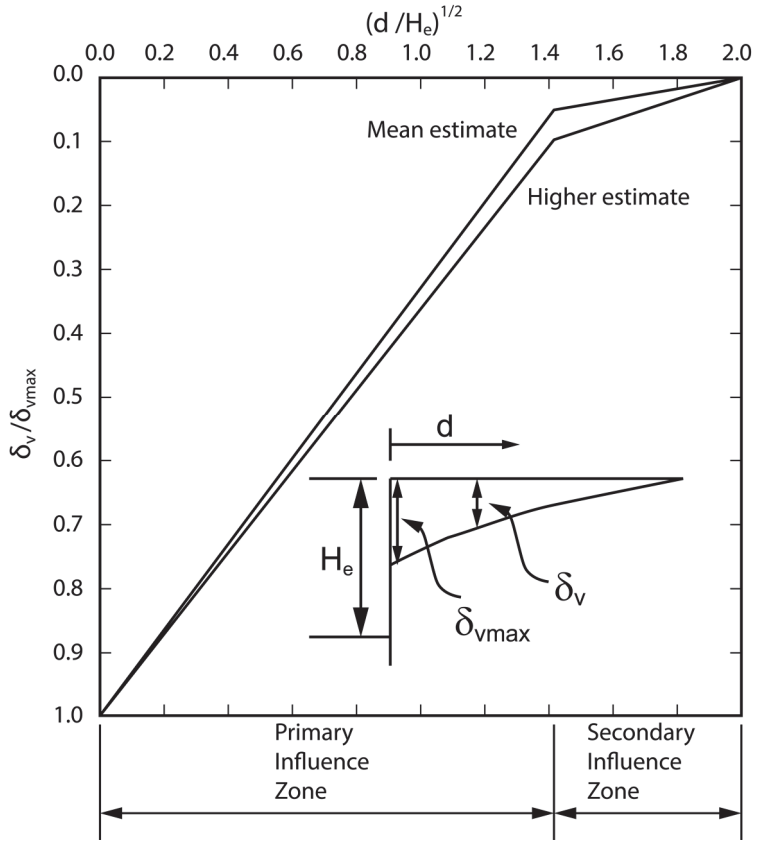


Figure 2. 19 Modified method for predicting a spandrel type settlement profile following Ou *et al.* (1993) (after Hseih and Ou, 1998).

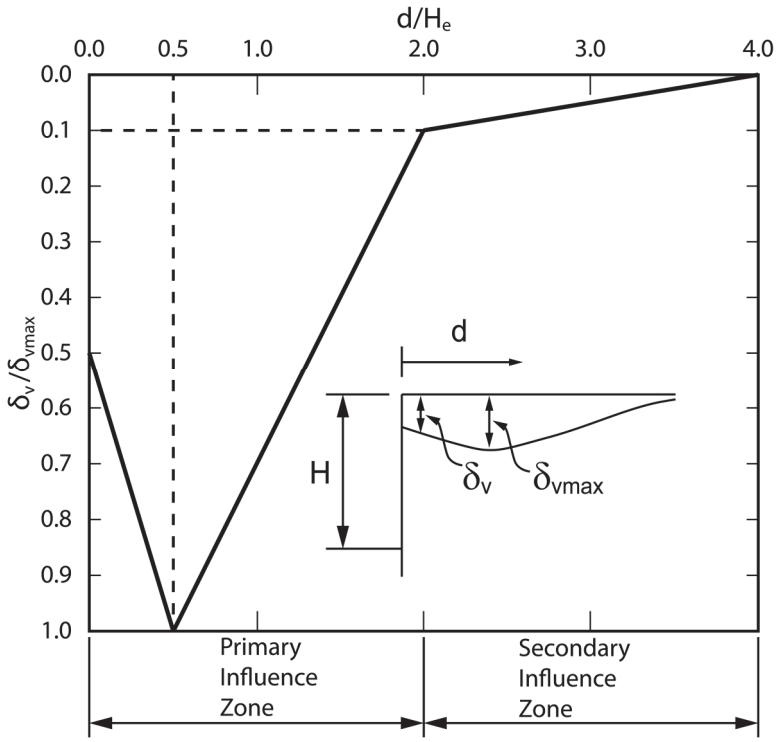


Figure 2. 20 Proposed method for predicting a concave settlement profile (after Hseih and Ou, 1998).

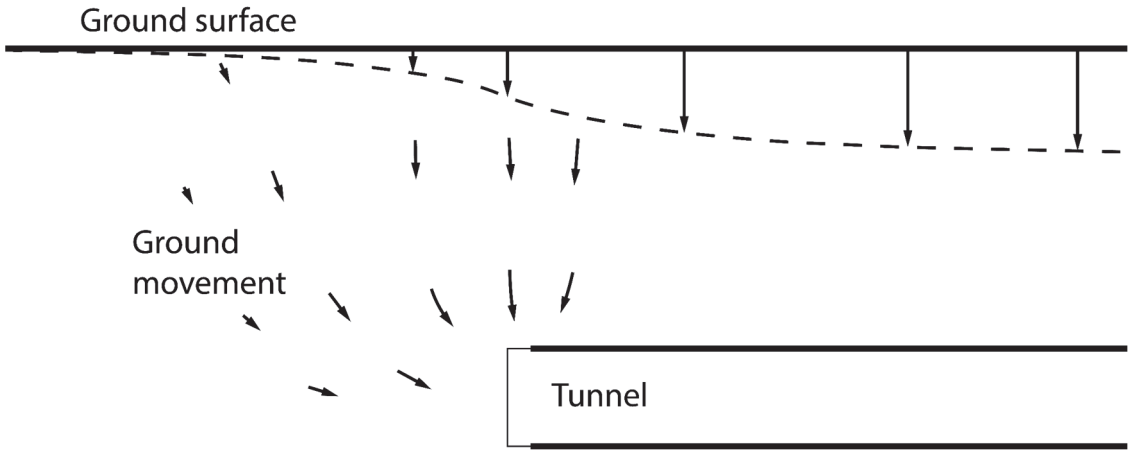


Figure 3. 1 Development of ground movement ahead of a tunnel heading in clay (after Mair *et al.*, 1995).

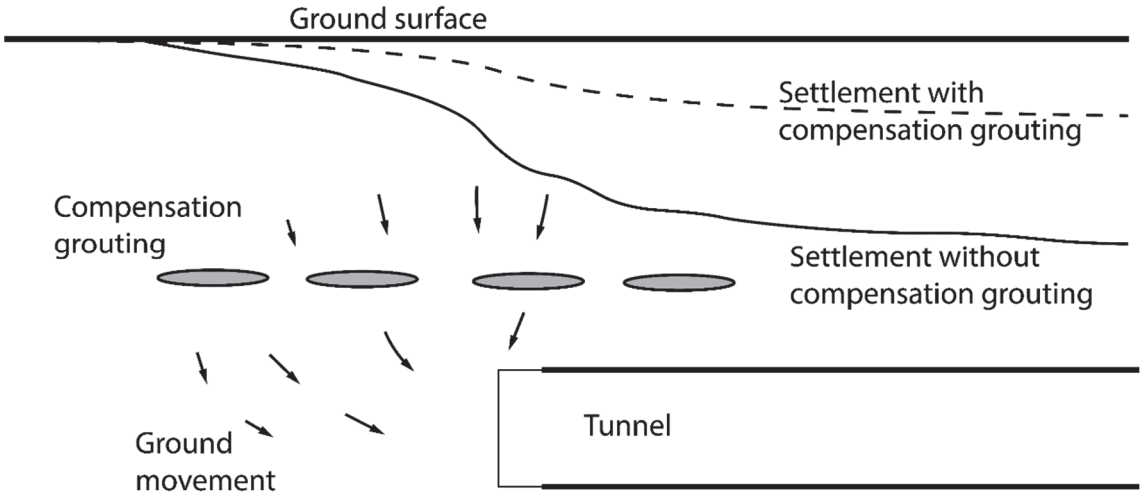


Figure 3. 2 Basic principle of compensation grouting (after Mair and Hight, 1994).

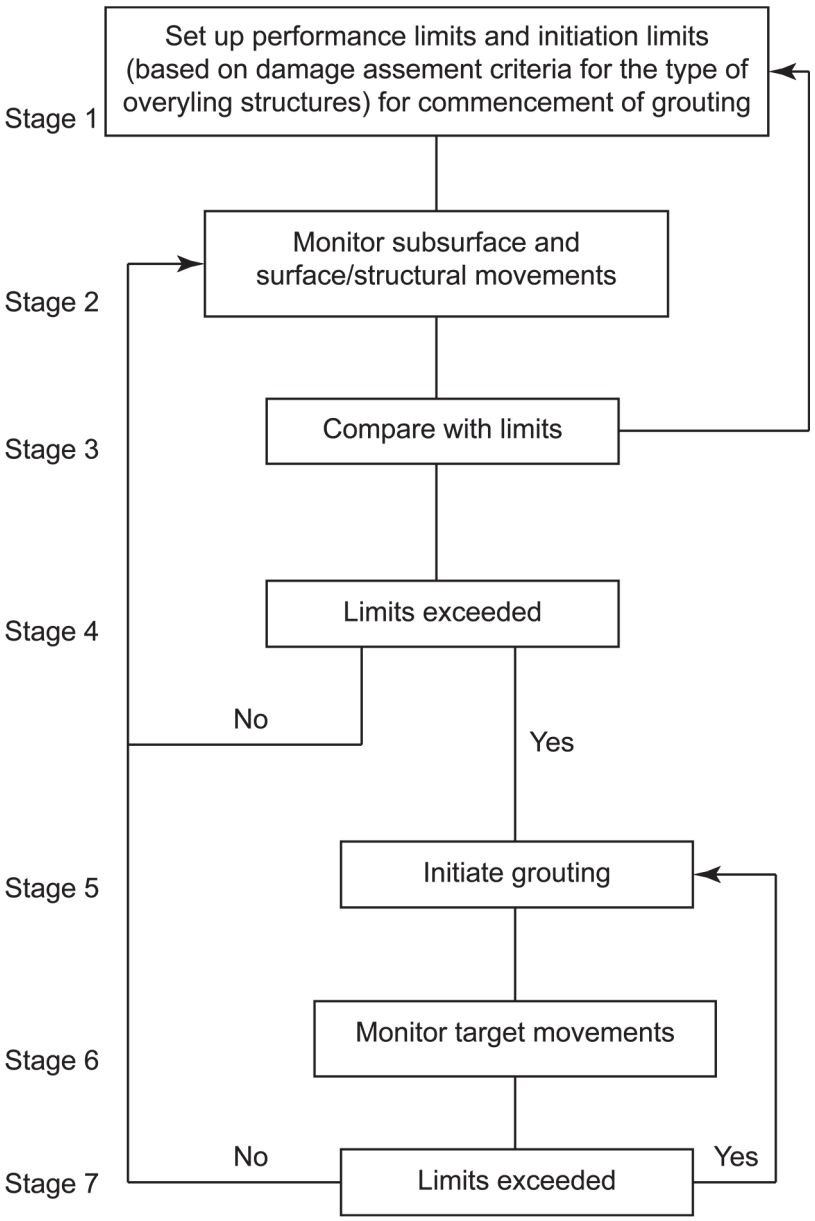


Figure 3. 3 Compensation grouting process (modified after Mair *et al.*, 1995).

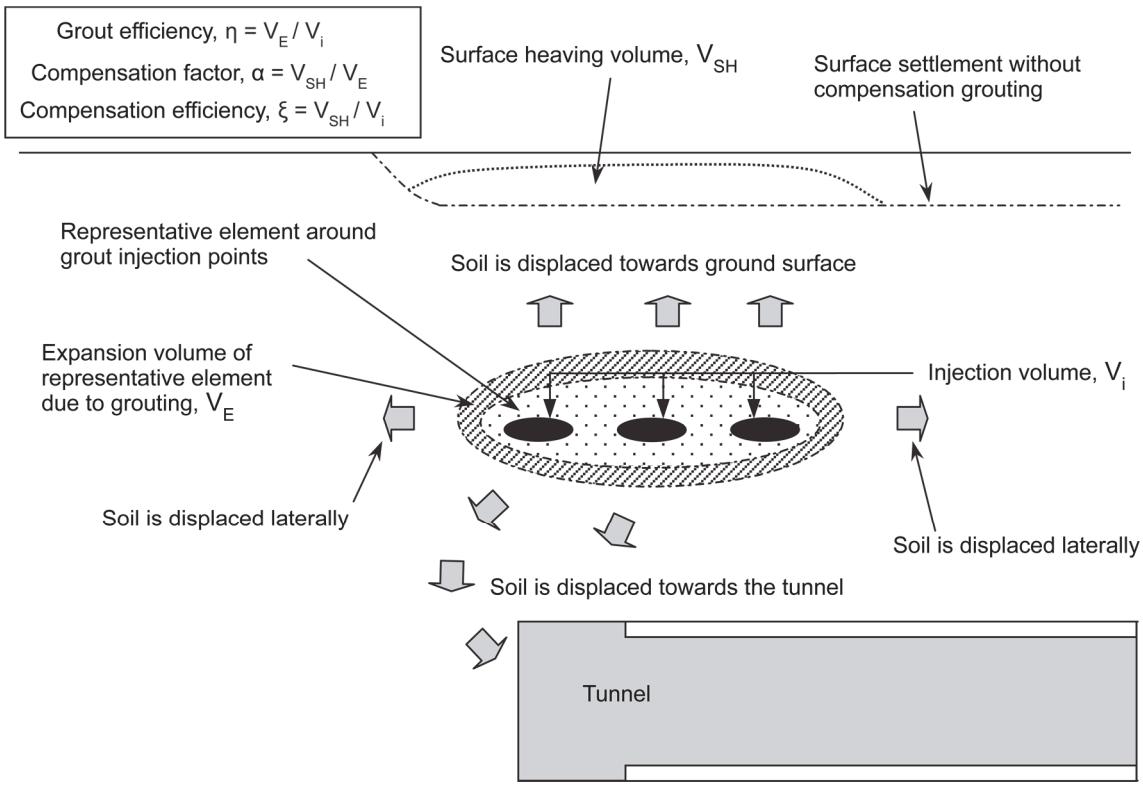


Figure 3. 4 Soil displacements induced by compensation grouting (after Soga *et al.*, 2004).

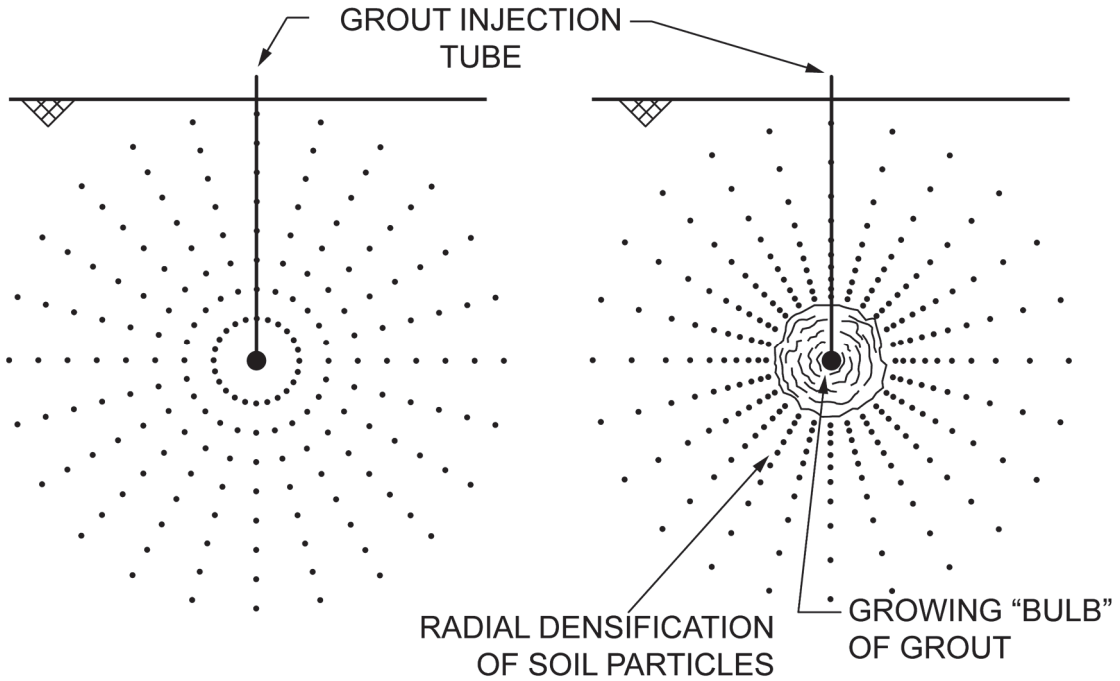
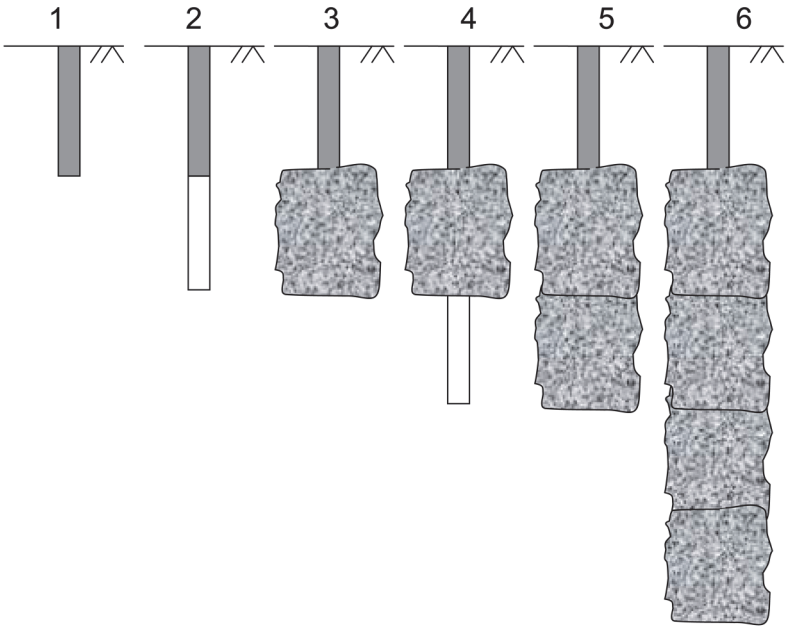
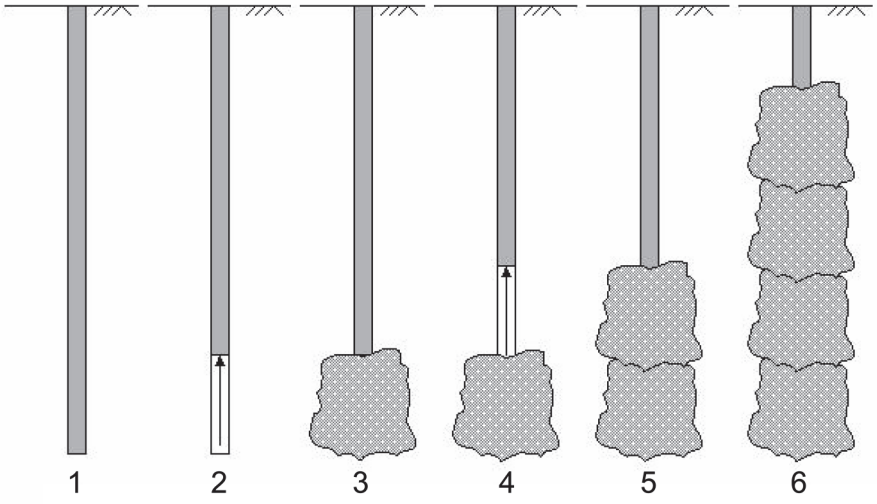


Figure 3. 5 Compaction grouting concept (after Graf, 1969).



Top-down process: **1)** cement casing into oversized hole that extends to top of 1st stage, **2)** drill through casing to extend hole to bottom of intended stage, **3)** grout 1st stage and allow to set, **4)** drill through 1st stage and extend hole to bottom of 2nd stage, **5)** grout stage and allow grout to set, **6)** repeat steps 4) & 5) until bottom hole is reached (indicated by low grout volume take or high pressure)

(a)



Bottom-up process: **1)** install casing, **2)** retract casing to top of deepest stage, **3)** grout 1st stage, **4)** raise casing to top of next stage, **5)** grout next stage, **6)** repeat steps 4) & 5) to top of improvement zone

(b)

Figure 3. 6 Typical compaction grouting processes with: (a) top down and (b) bottom up methods (after ASCE, 2010).

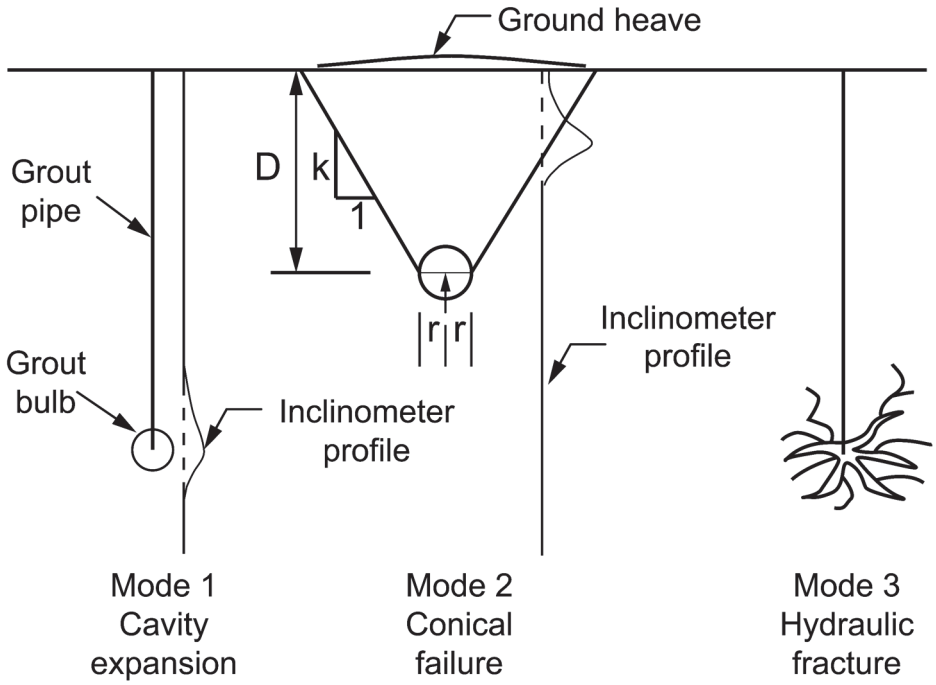


Figure 3. 7 Modes of soil mass deformation by compaction grouting (after Wong *et al.*, 1996).

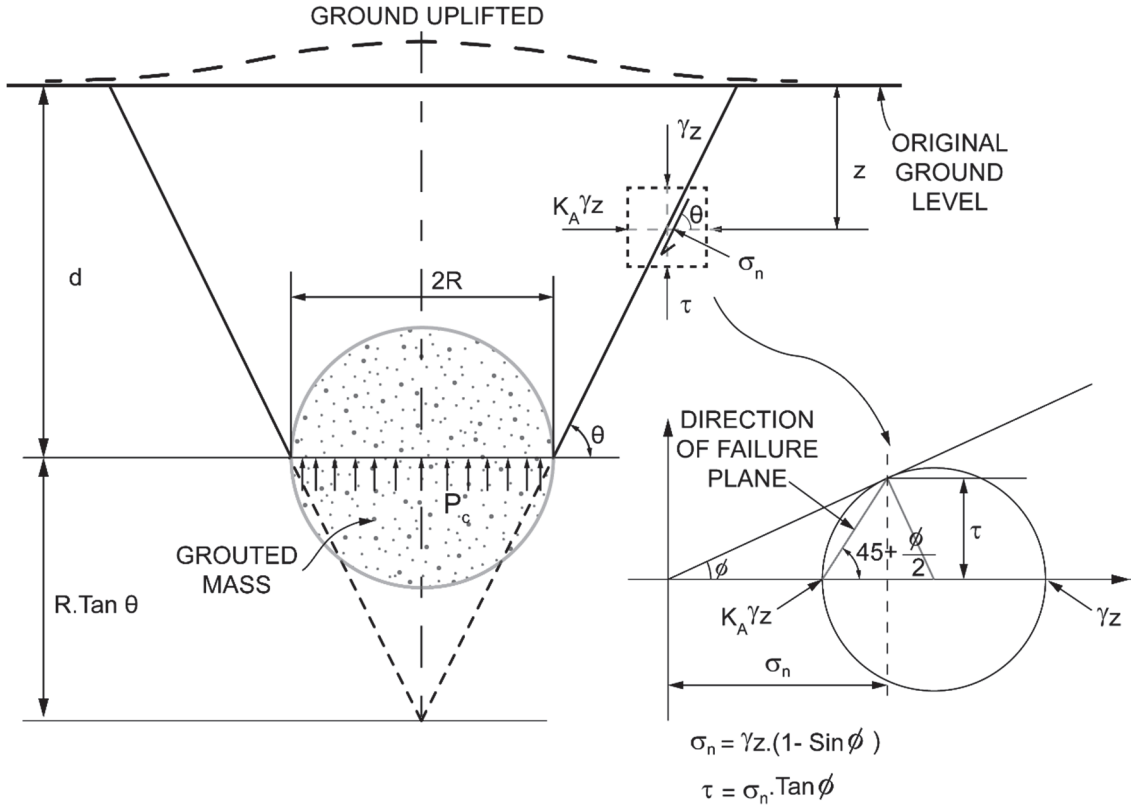


Figure 3. 8 Conical shearing failure above spherical grout bulb (after Wong, 1974).

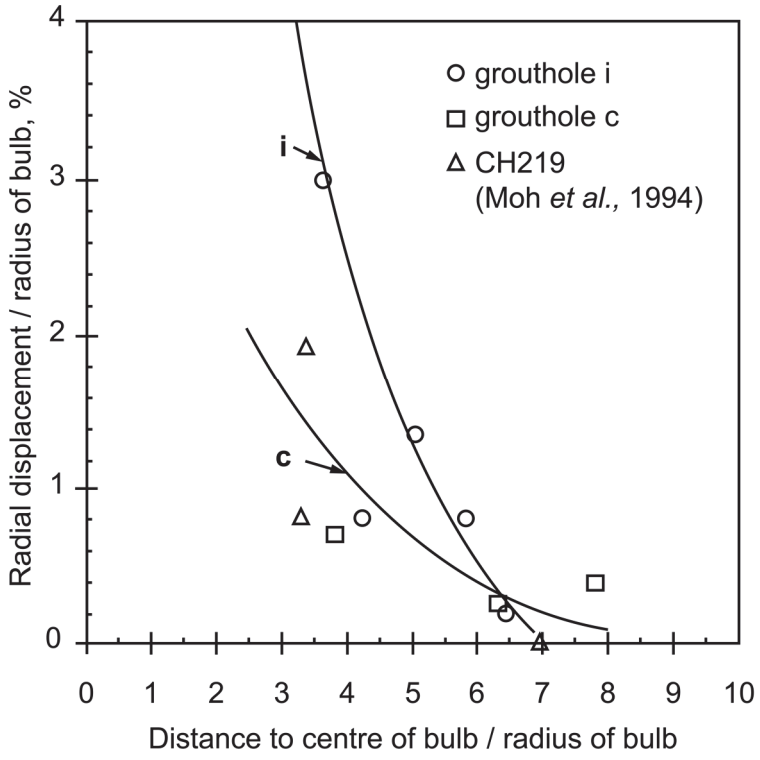


Figure 3. 9 Distributions of normalised radial displacements with normalised radial distance to grout bulbs from compaction grouting (after Wong *et al.*, 1996).

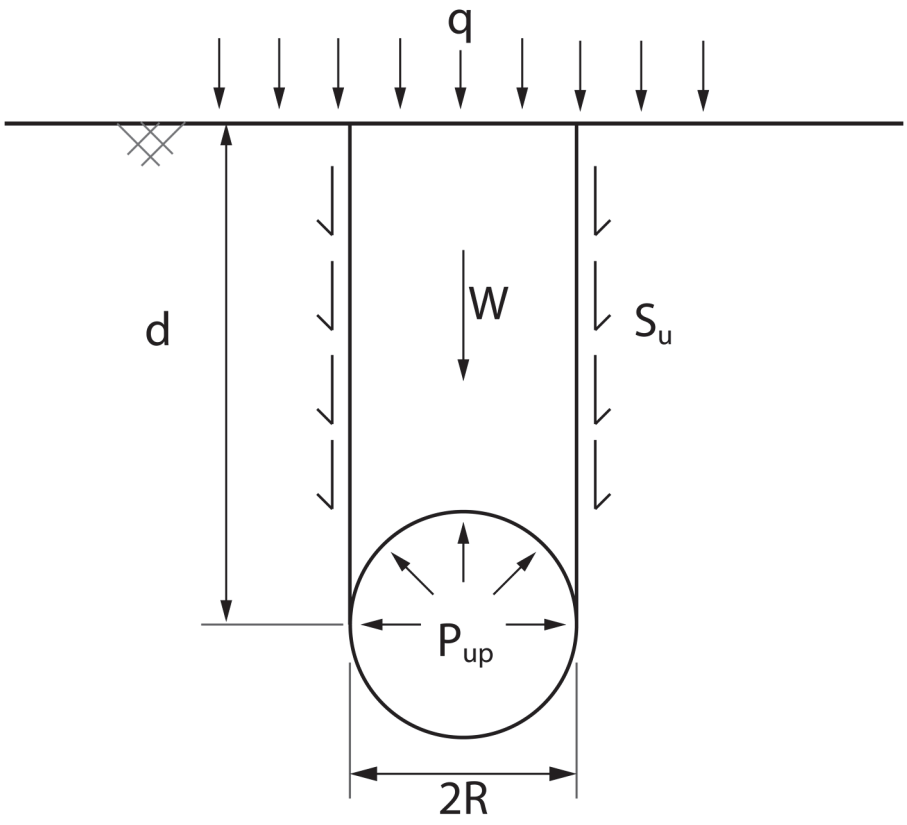


Figure 3. 10 Cylindrical shear failure mechanism above a spherical expanding cavity in clay (after Cirone, 2016).

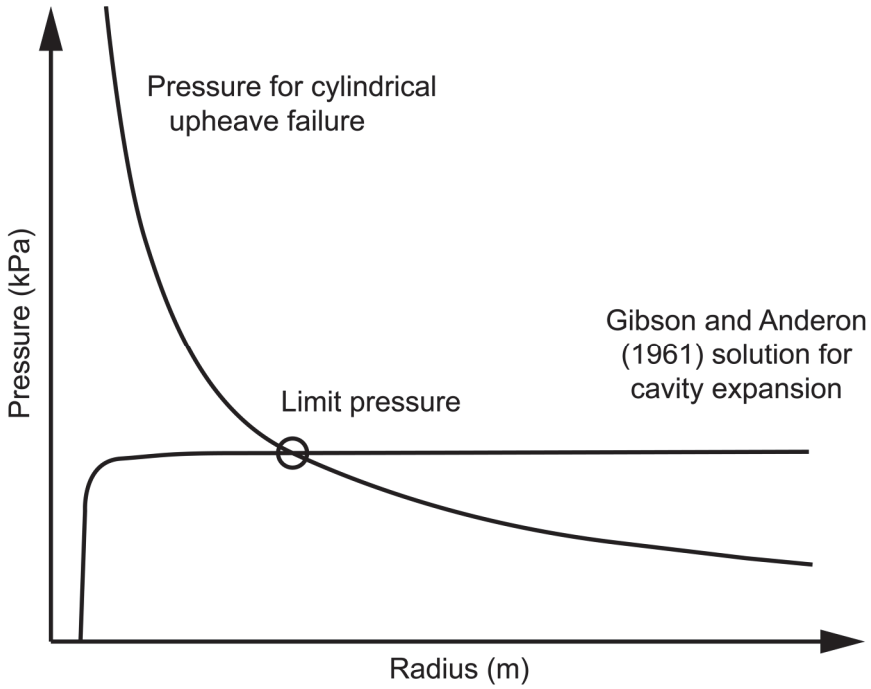


Figure 3. 11 Injection pressure-cavity radius relationship representing the two mechanisms that occur during the compaction grouting process as proposed by Cirone (2016).

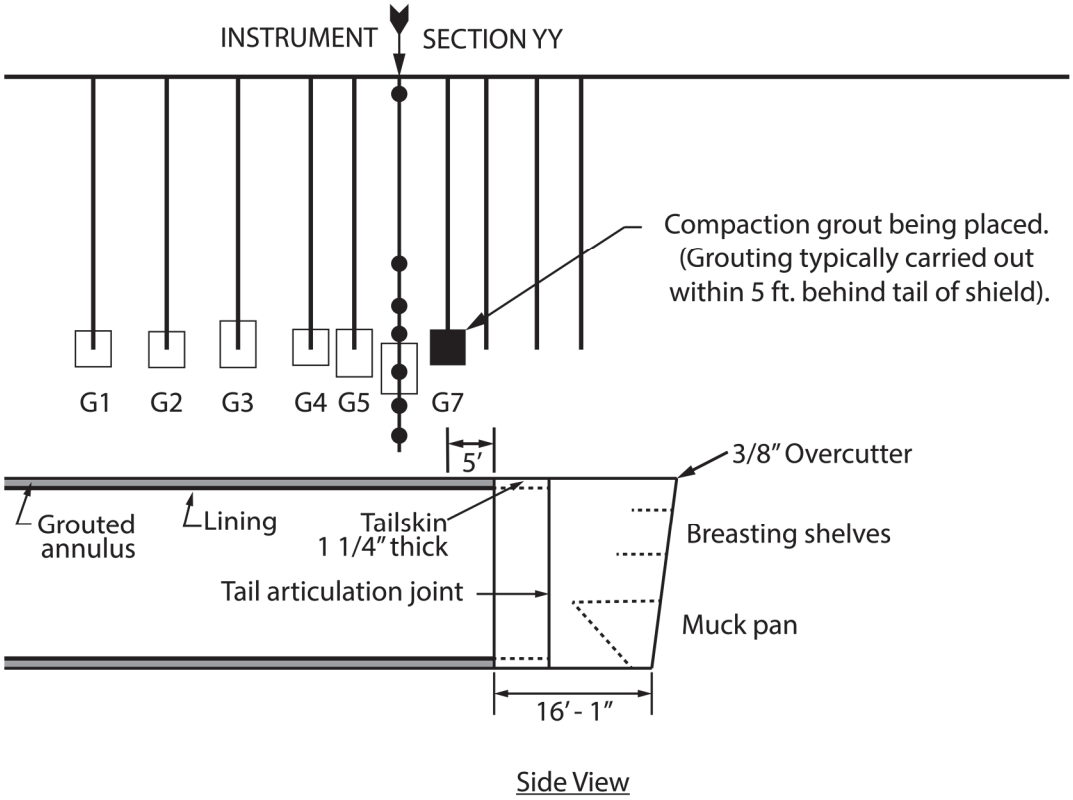


Figure 3. 12 Layout of the compaction grout bulbs over the first tunnel shield in Baltimore, U.S.A. (after Baker *et al.*, 1983).

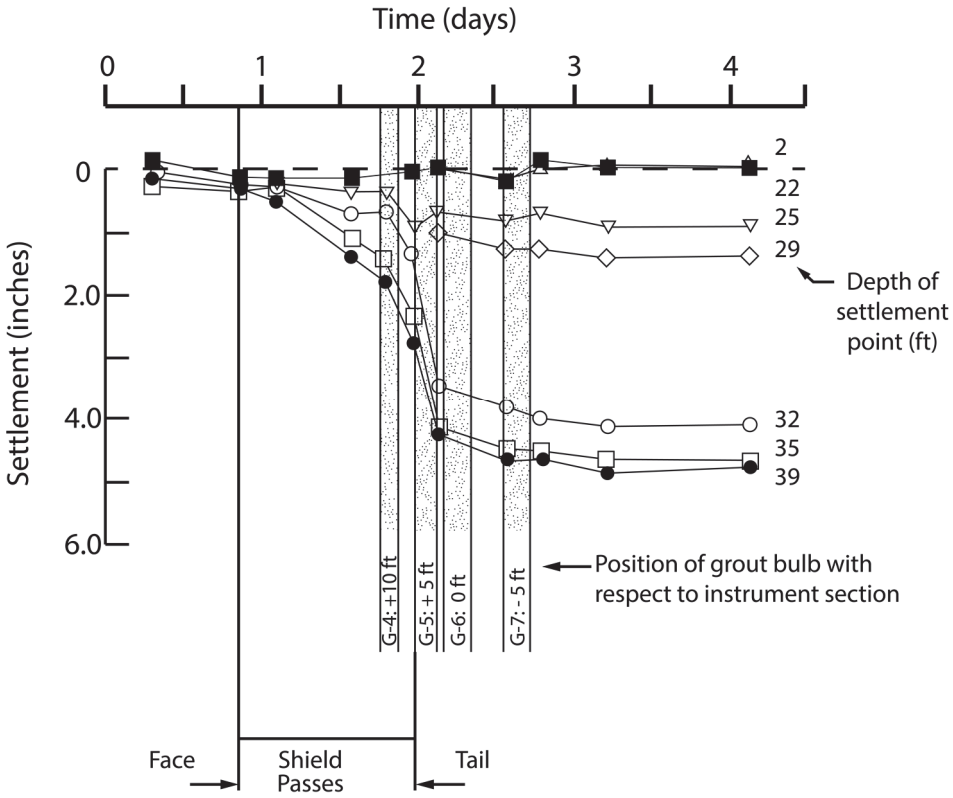


Figure 3. 13 Influence of the compaction grouting on soil settlements above the tunnel at various times in Baltimore, U.S.A. (after Baker *et al.* 1983).

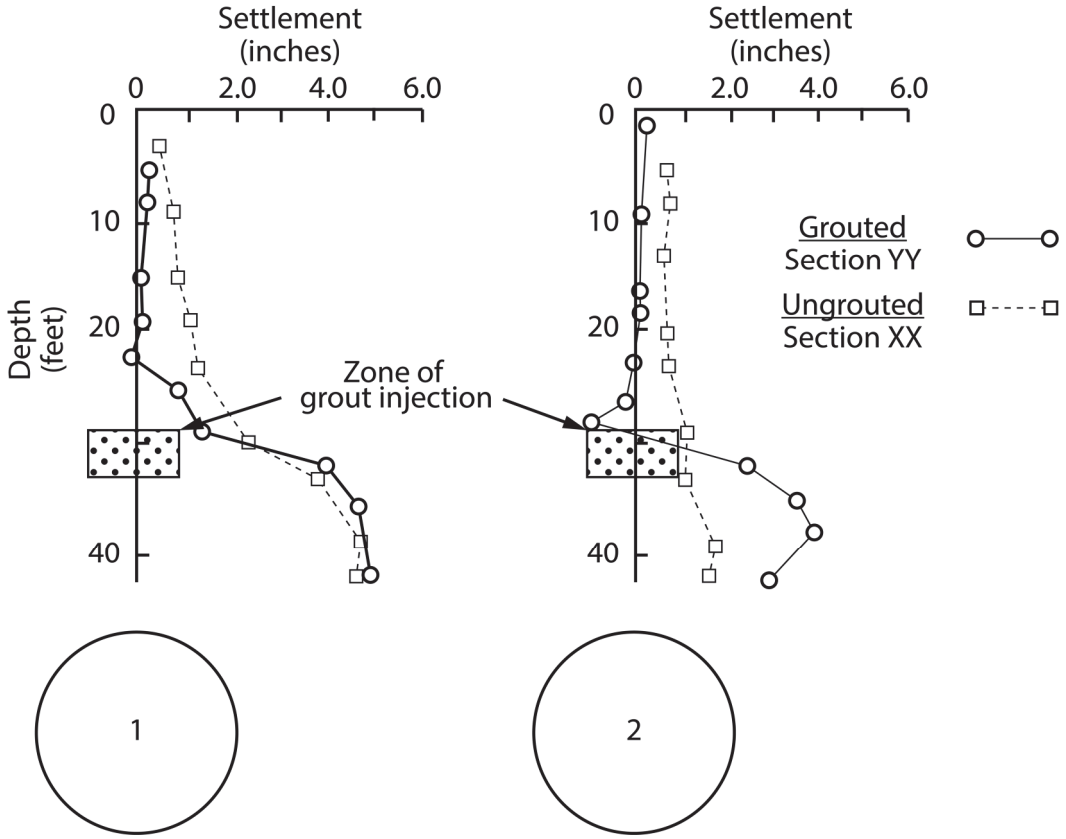


Figure 3. 14 Displacement-depth profiles for grouted and ungrouted sections of the tunnels in Baltimore, U.S.A. (after Baker *et al.*, 1983).

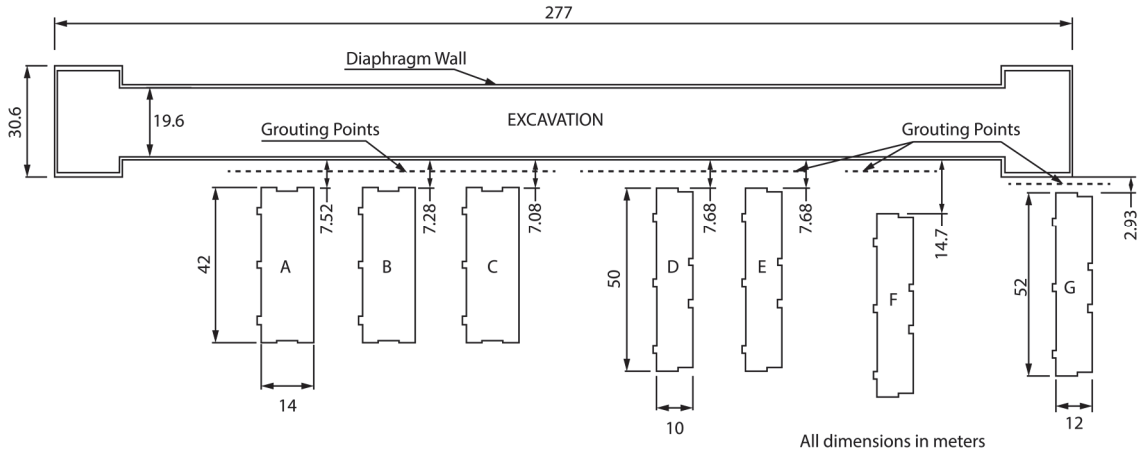


Figure 3. 15 Layout of the excavation and buildings in Shanghai, China (after Liu, 2003).

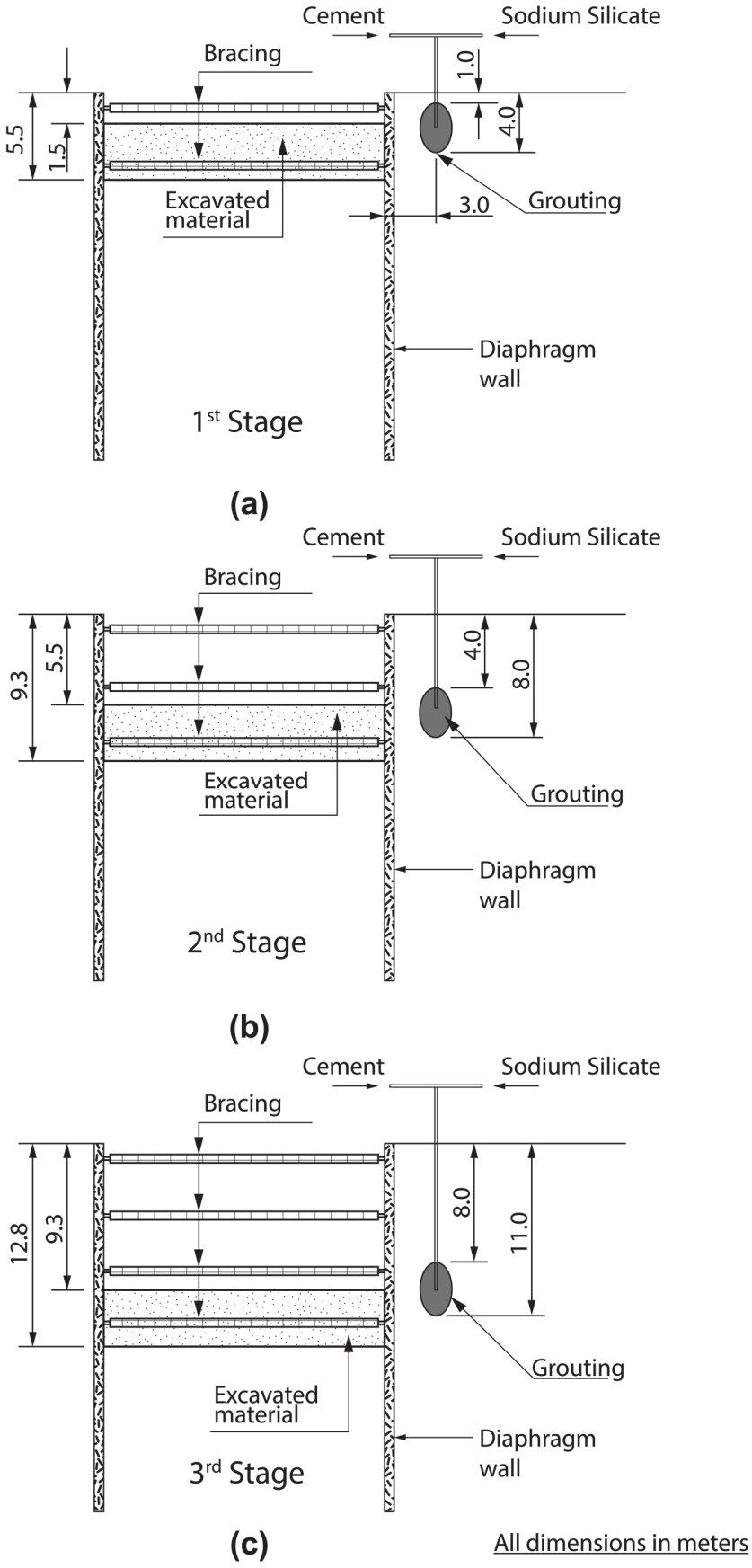


Figure 3. 16 Procedure of compaction grouting during the deep excavation in Shanghai, China (after Liu, 2003).

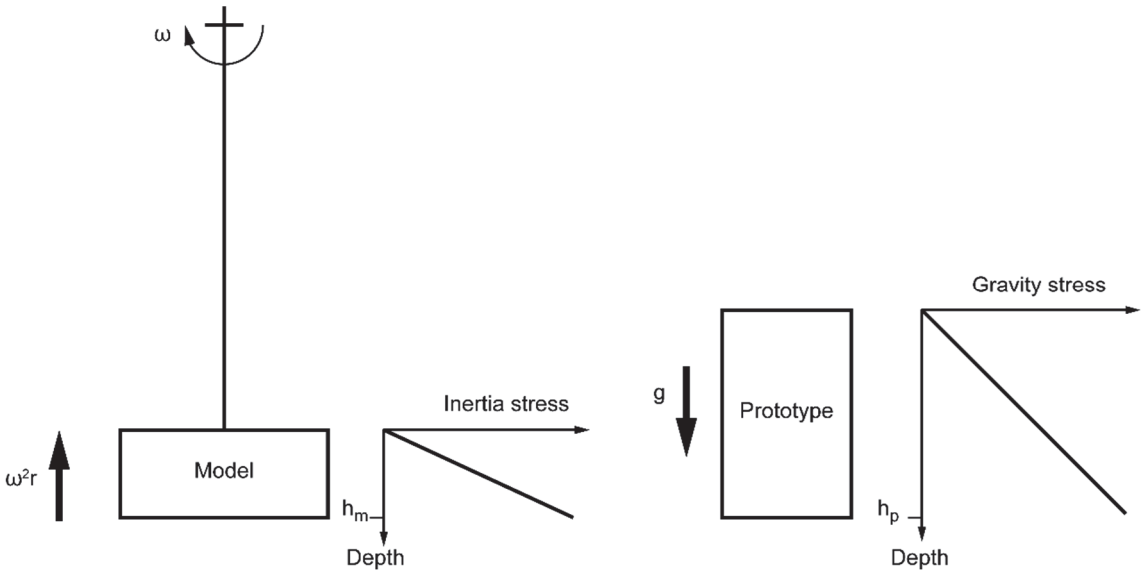


Figure 4. 1 Inertial stresses in a centrifuge model induced by rotation about a fixed axis compared to a corresponding prototype (after Taylor, 1995).

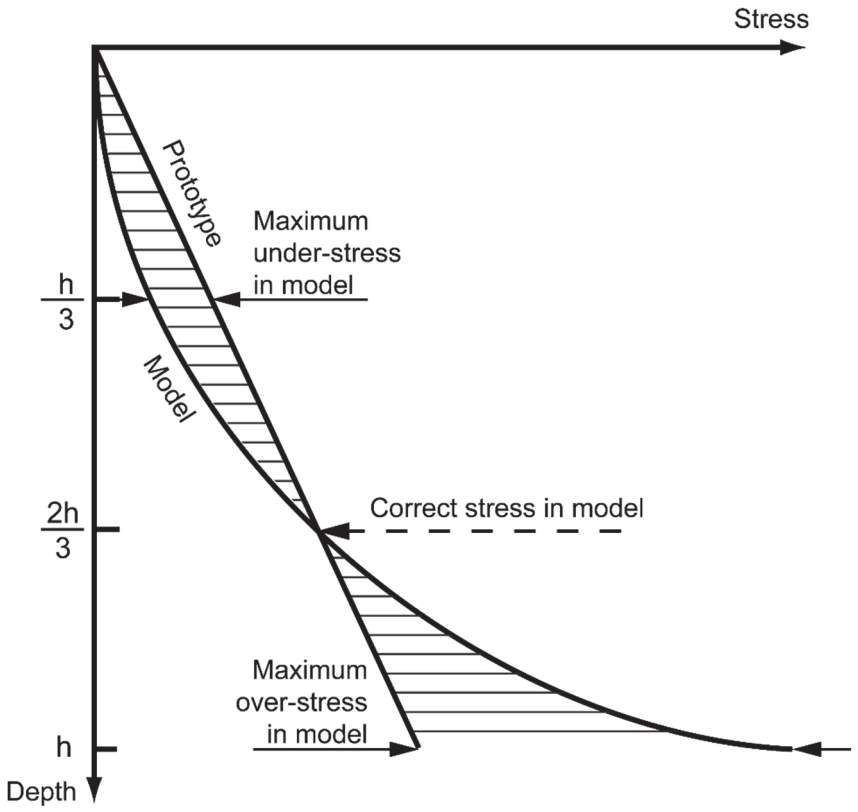


Figure 4. 2 Stress variation with depth in a centrifuge model compared to a corresponding prototype (after Taylor, 1995).

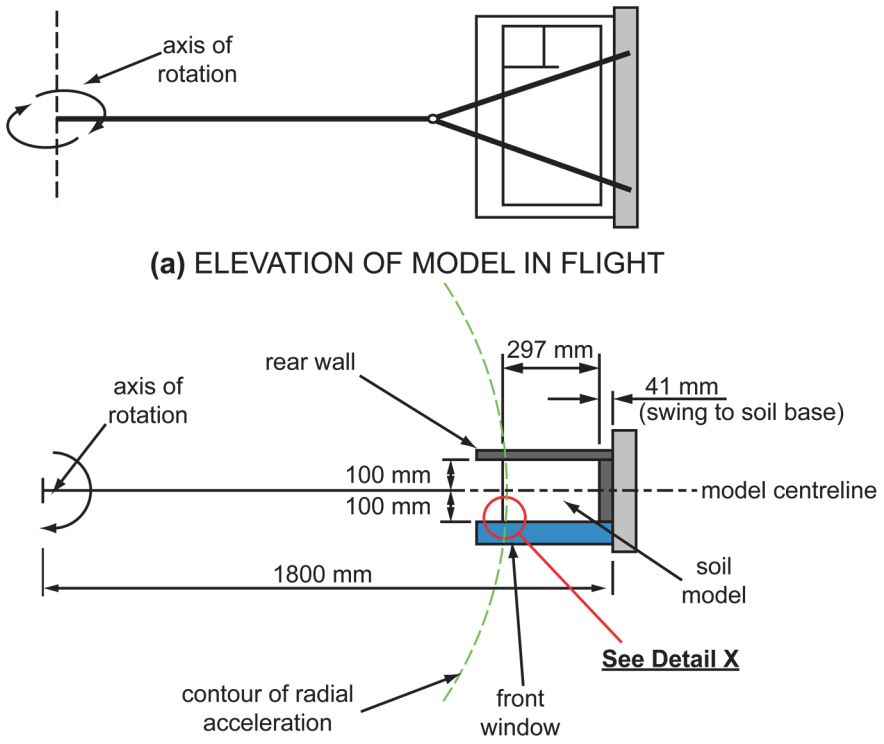


Figure 4. 3 Geometry of a typical model on the Acutronic 661 geotechnical centrifuge at City, University of London showing a) elevation of the model inflight; b) plan view of model inflight with components of induced acceleration (after Grant, 1998).

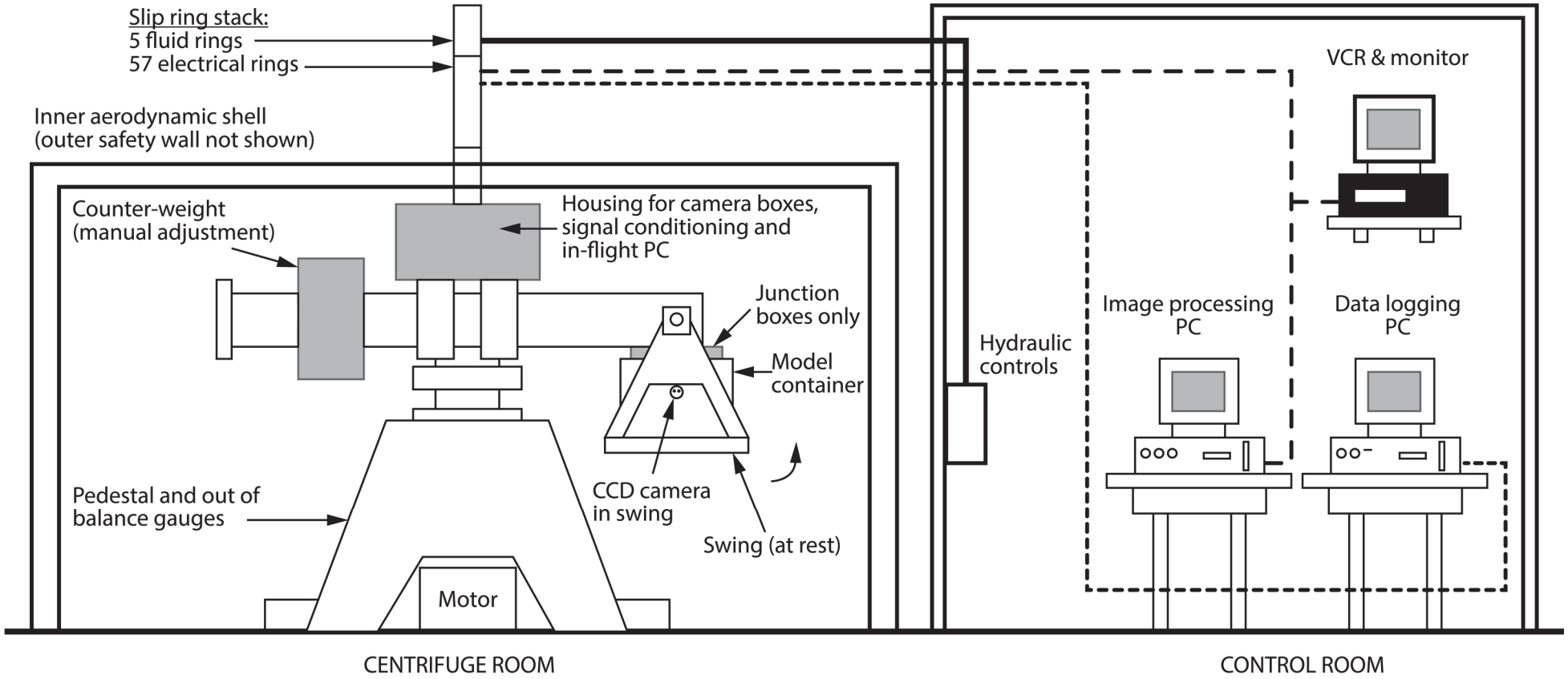


Figure 4. 4 Schematic diagram of the previous Acutronic 661 geotechnical centrifuge testing facility at City, University of London, prior to upgrading and refurbishment of the facility (after Grant 1998).

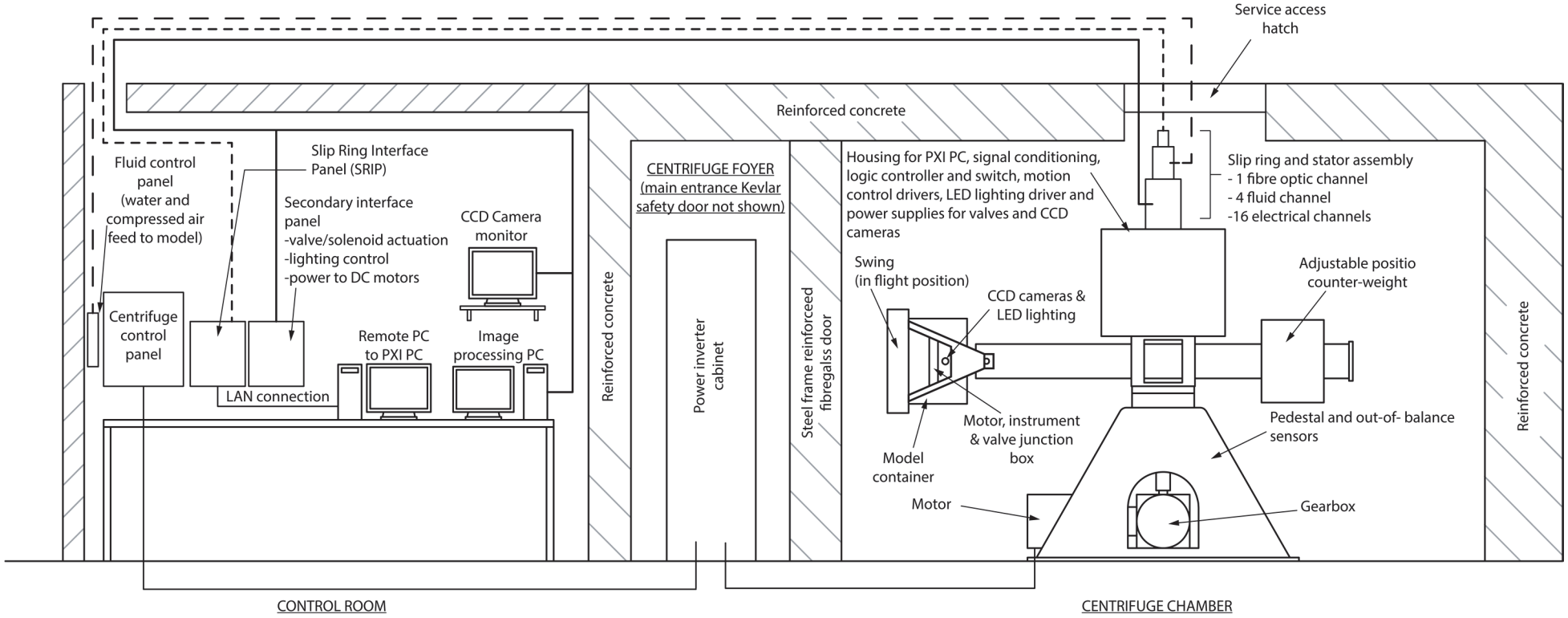
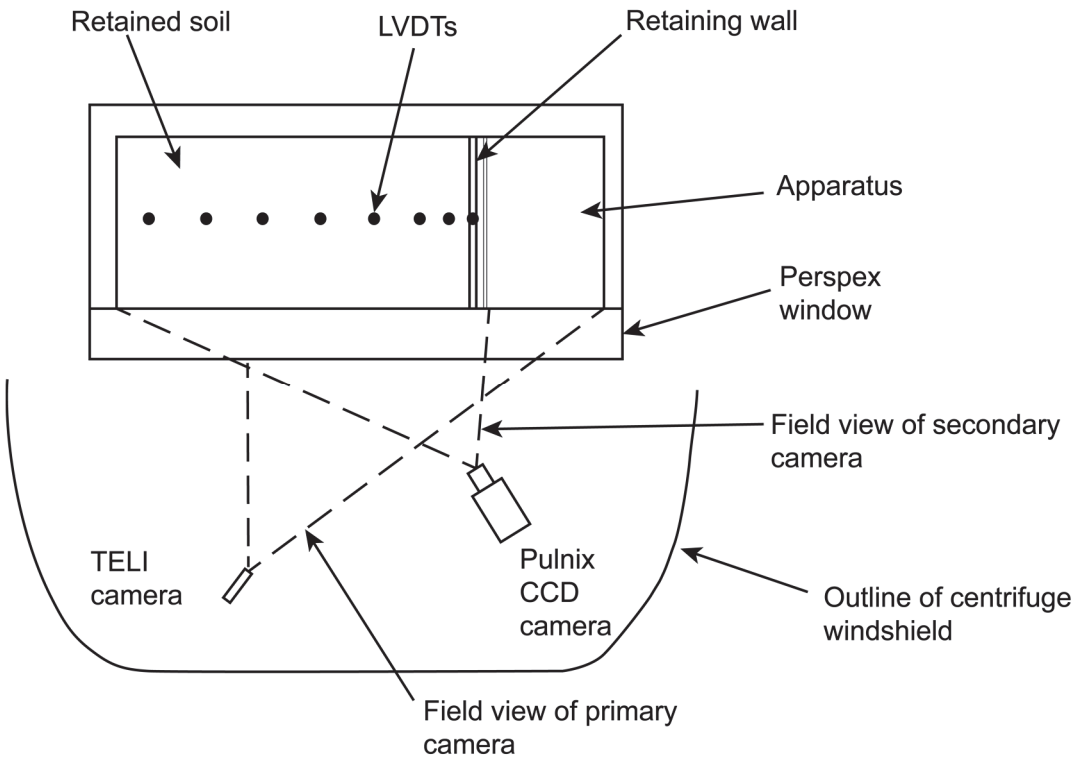
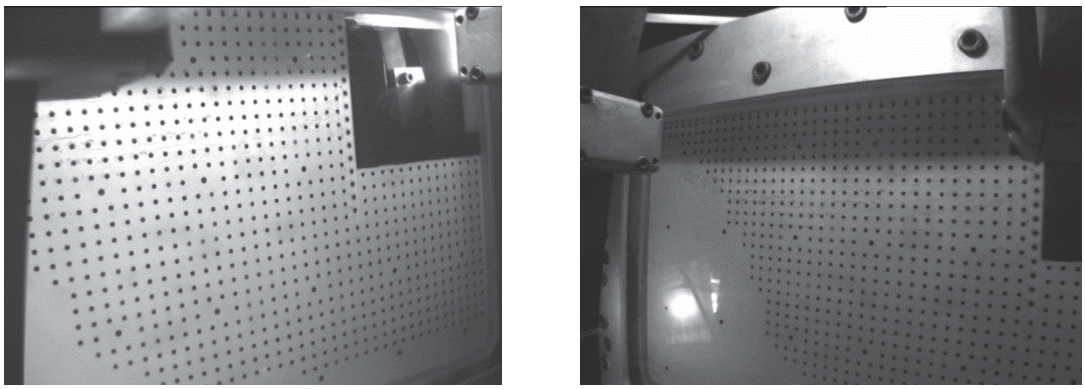


Figure 4. 5 Schematic diagram of the current Acutronic 661 geotechnical centrifuge testing facility at City, University of London (used from test 6HH onwards).



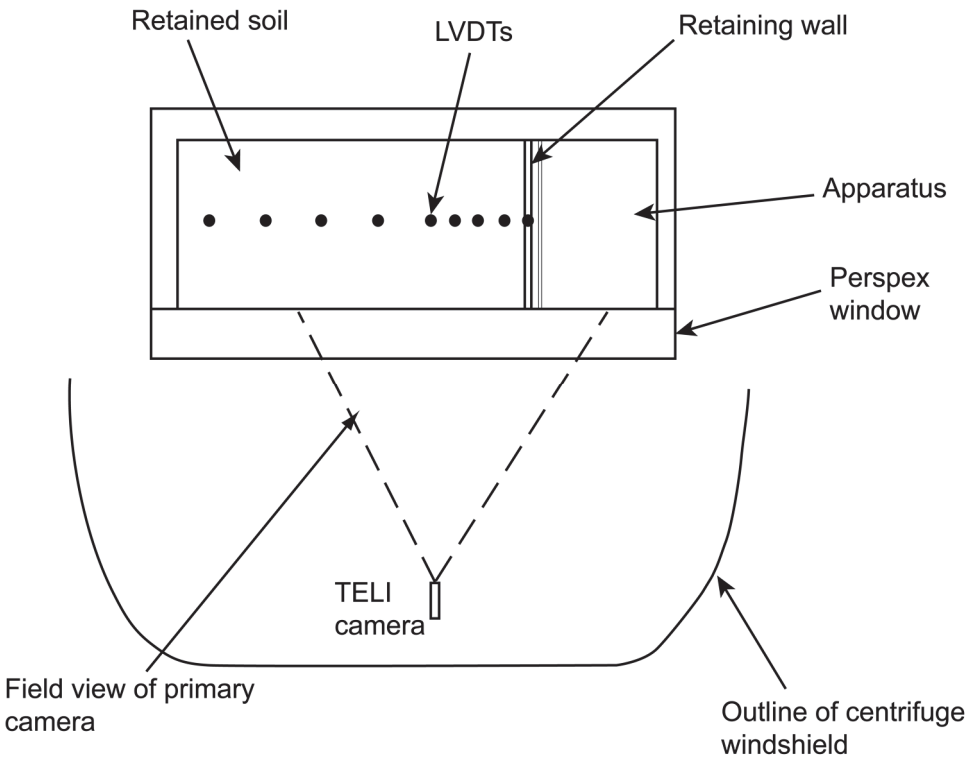
(a)



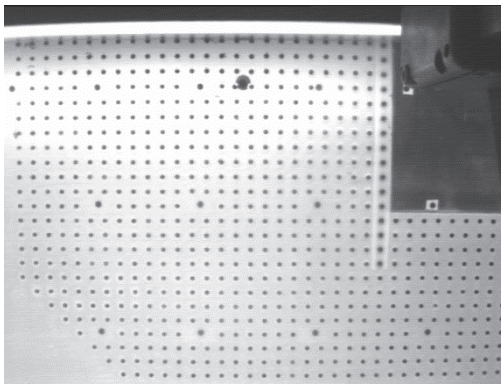
TELI CAMERA VIEW **PULNIX CAMERA VIEW**

(b)

Figure 4. 6 General arrangement of the dual TELI and PULNIX CCD camera setup for tests 2HH and 3HH showing: a) schematic plan view of positions and b) typical fields of view captured by each camera (before January 2014).



(a)



TELI CAMERA VIEW

(b)

Figure 4. 7 General arrangement of the single TELI CCD camera setup for test 6HH onwards showing: a) schematic plan view of position and b) typical field of view captured by the TELI camera (after January 2014).

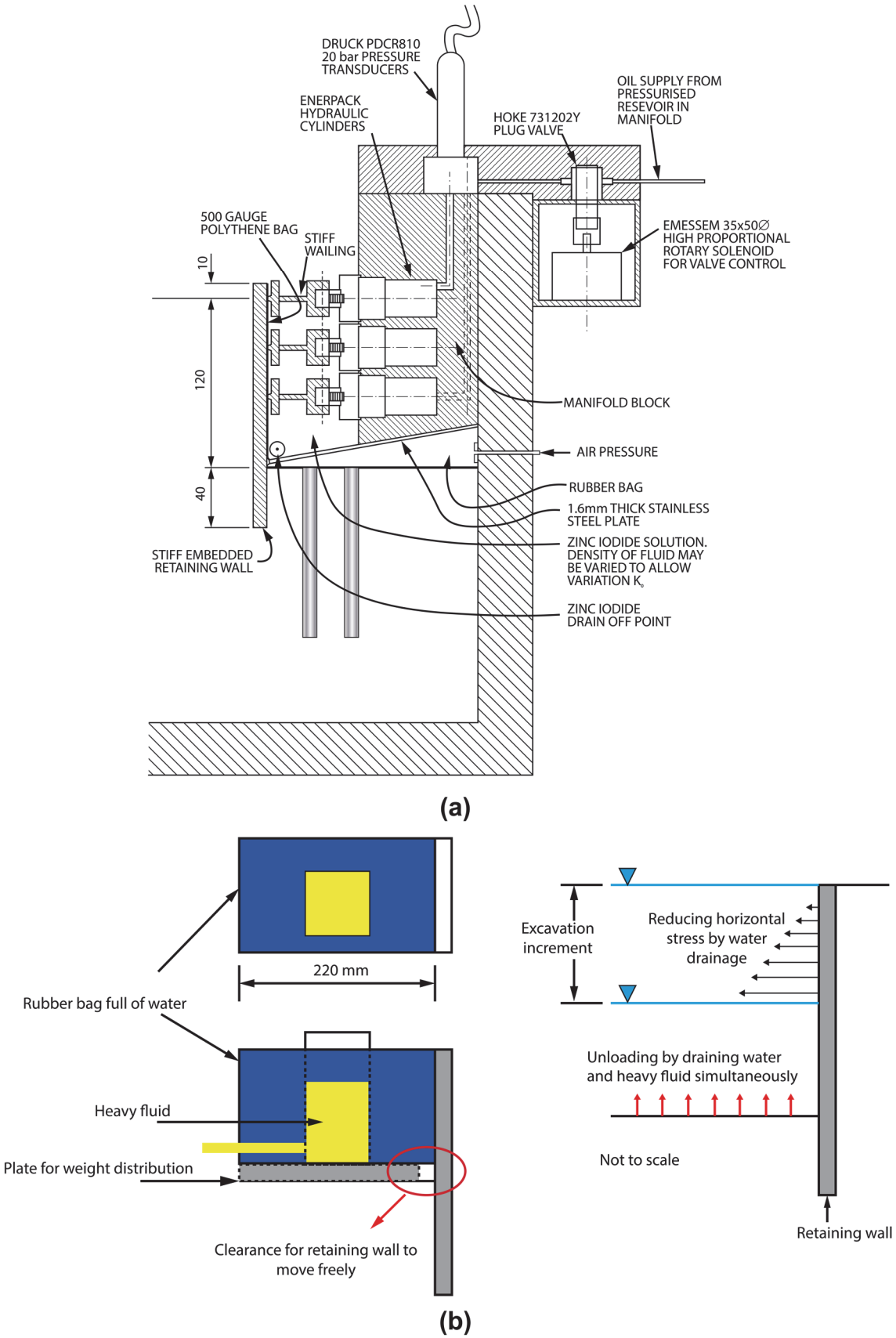
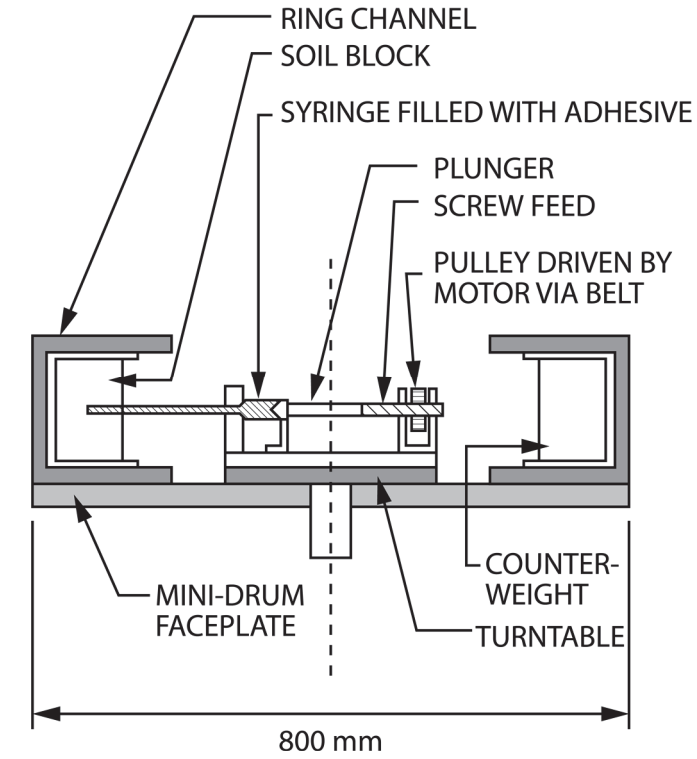
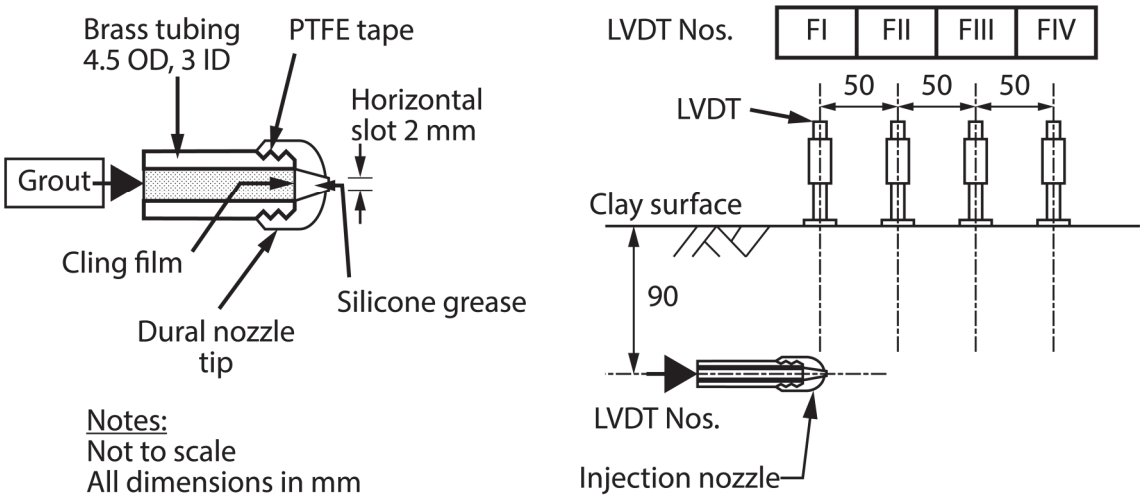


Figure 5. 1 Simulation of excavation methods using two fluids adopted by: (a) McNamara (2001) and (b) Elshafie (2008).



Cross -section of ANS&A mini-drum centrifuge with fluid injection equipment



Details of injection nozzle and model set up

Figure 5. 2 Schematic diagram of model and tests apparatus developed by Chin (1996) for modelling fracture grouting in a geotechnical centrifuge.

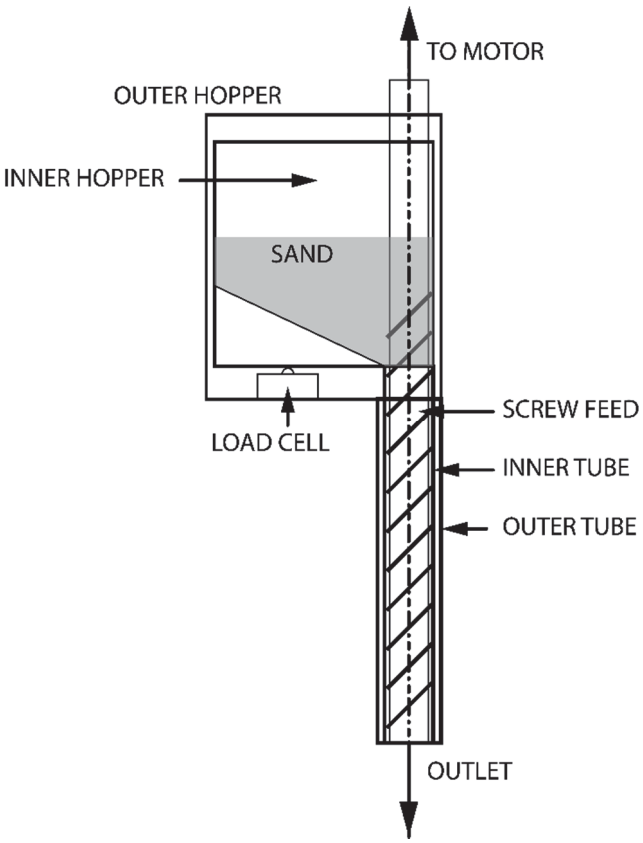


Figure 5. 3 Schematic diagram showing the granular grout injection apparatus developed by Lu (1996) for centrifuge modelling compaction grouting.

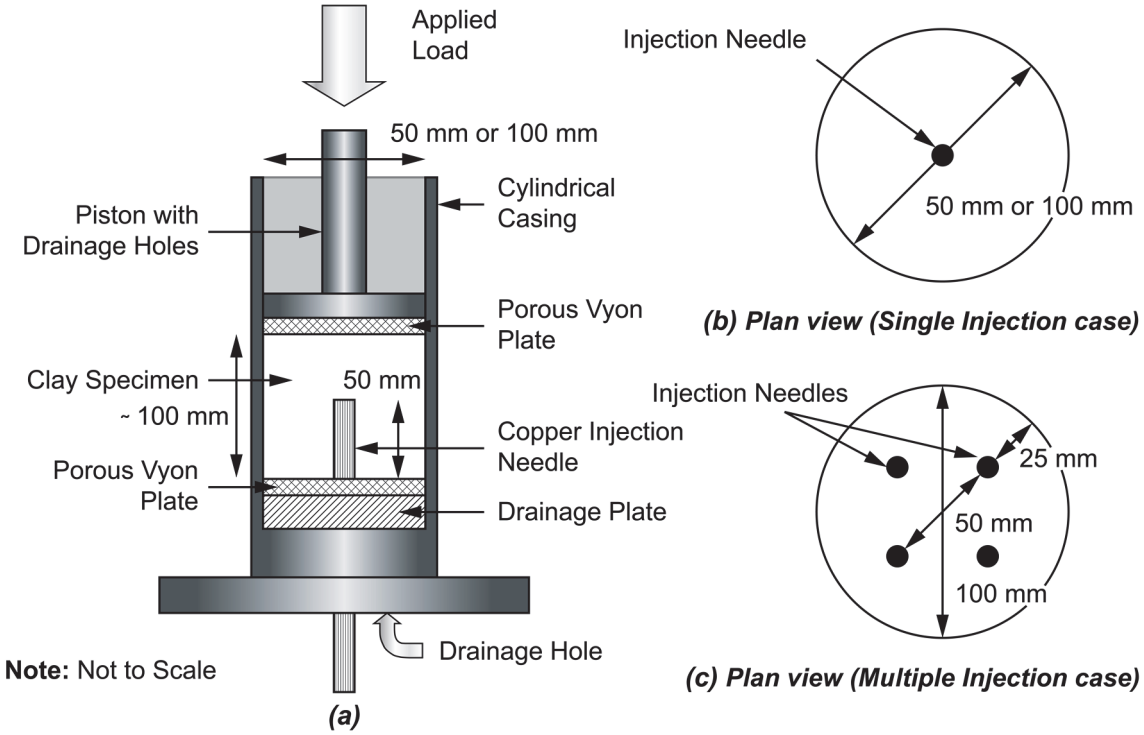


Figure 5. 4 Compensation grouting apparatus developed by Au (2001).

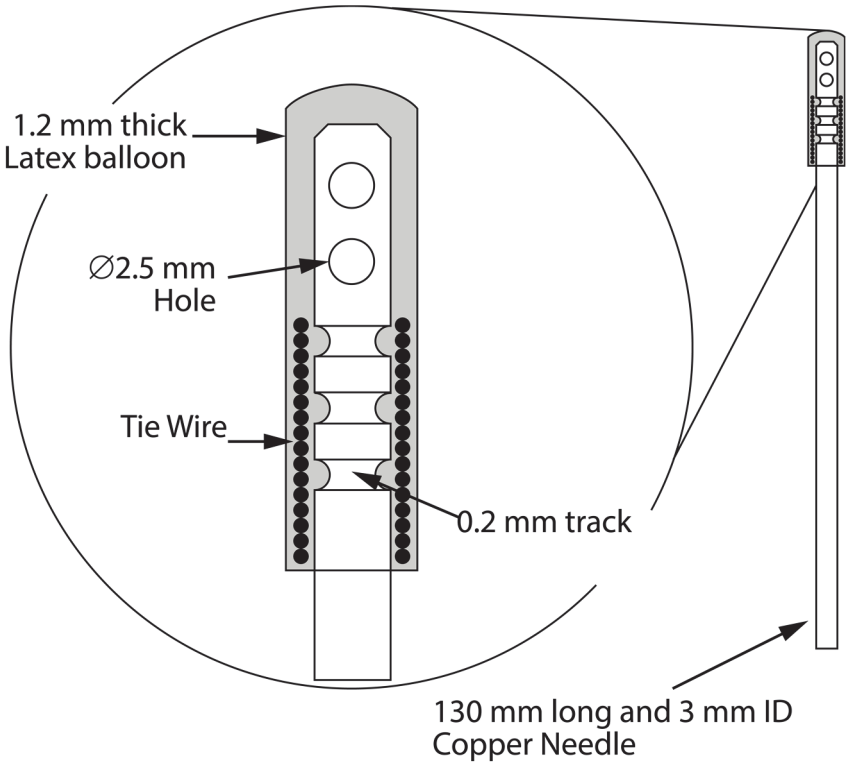


Figure 5. 5 Expandable latex balloon system developed by Au (2001) for the modelling of idealised compaction grouting.

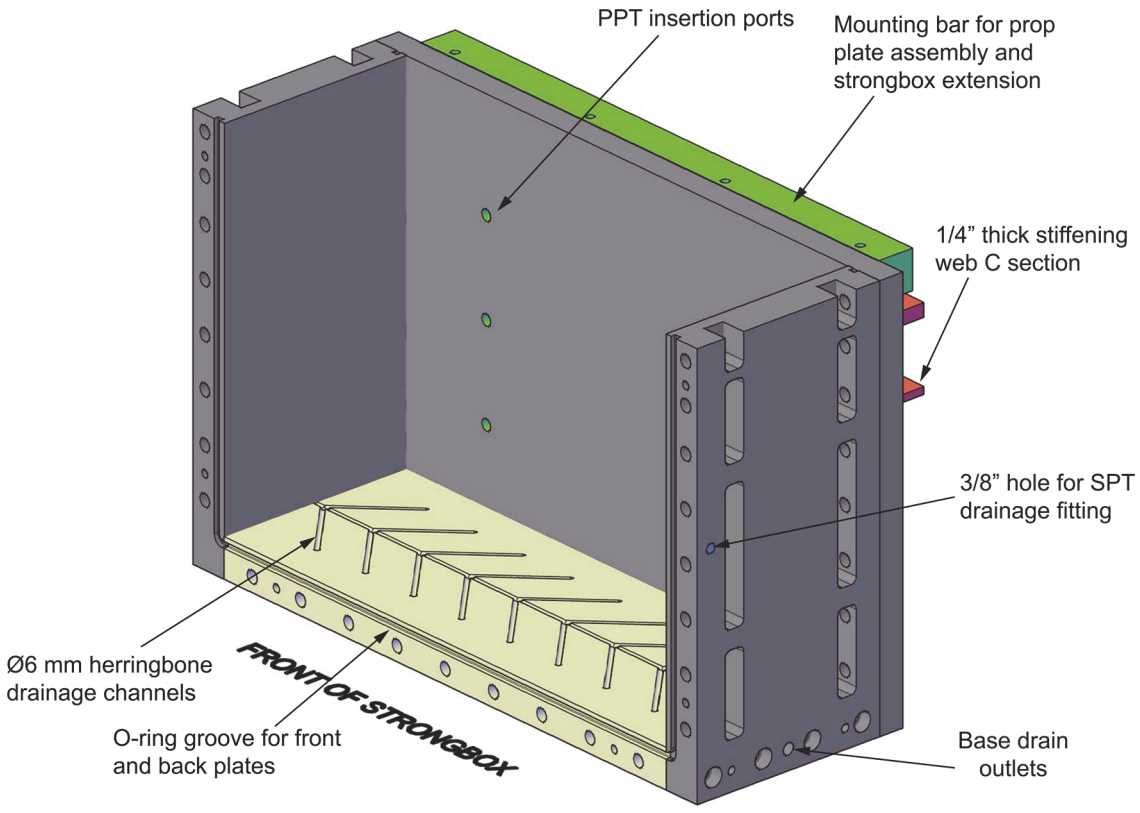


Figure 5. 6 Conceptual image of the aluminium strongbox used in the centrifuge model tests.

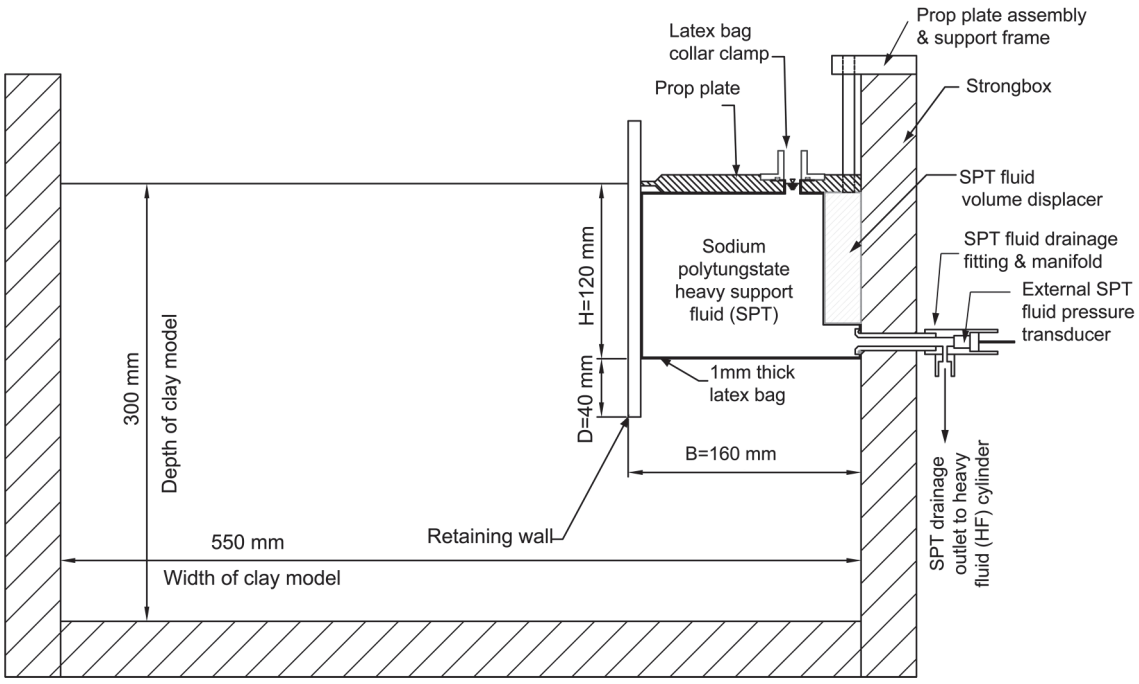


Figure 5. 7 Schematic diagram showing the layout of the excavation in the centrifuge model tests conducted.

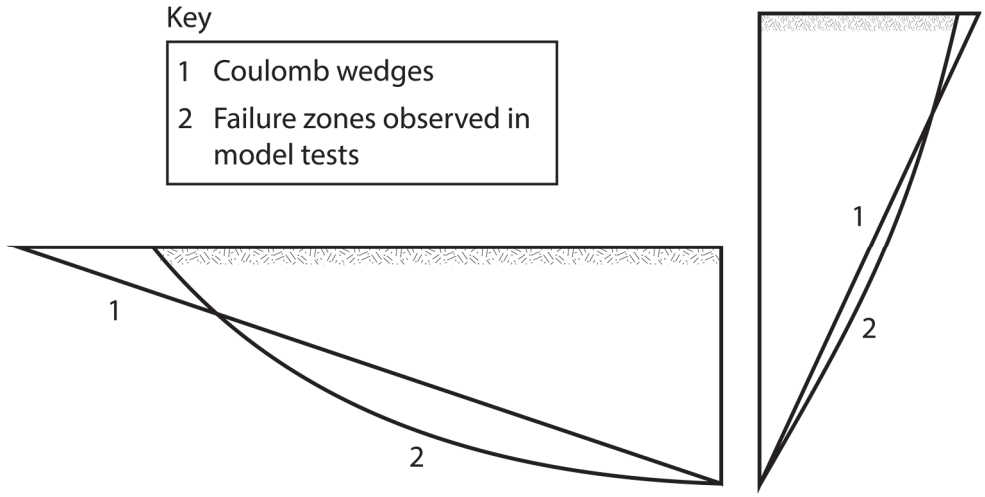


Figure 5. 8 Comparison of failure modes behind and in front of a retaining wall (after Padfield and Mair, 1984).

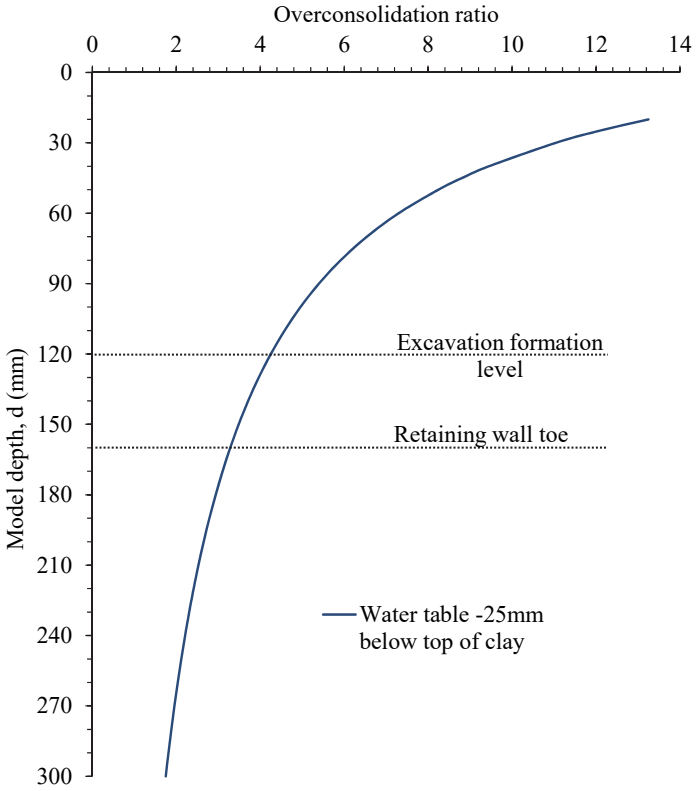


Figure 5. 9 Variation of overconsolidation ratio with soil depth in the centrifuge model.

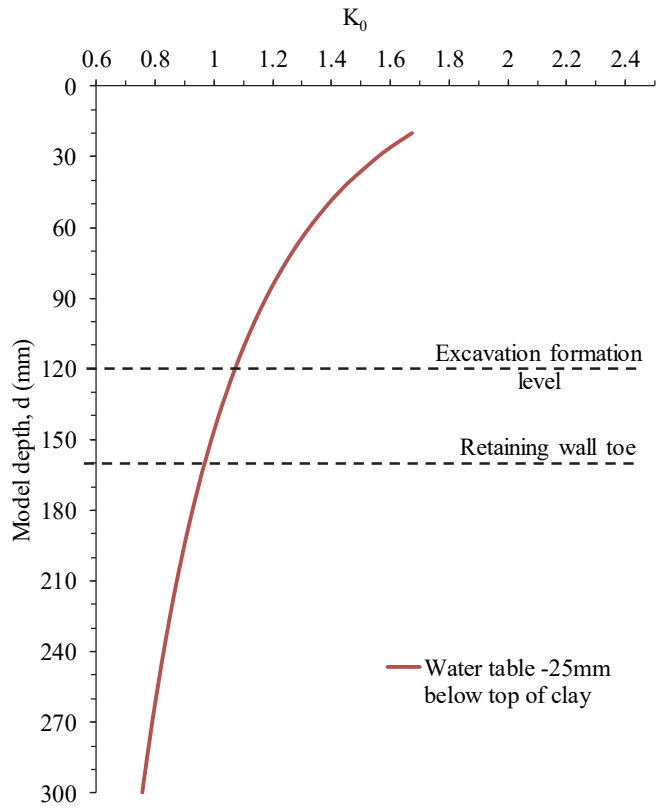


Figure 5. 10 Variation in K_o with soil depth in the centrifuge model.

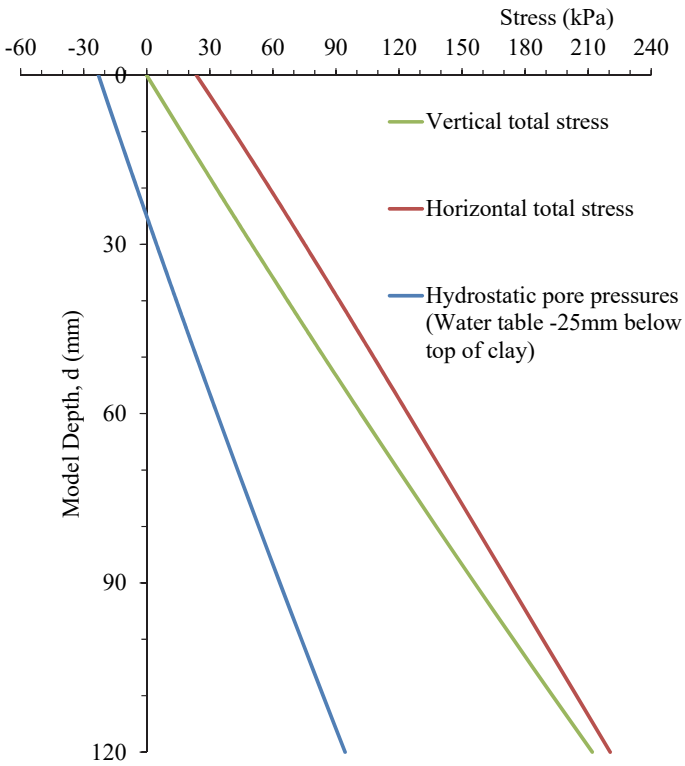


Figure 5. 11 Theoretical total vertical and horizontal stresses and hydrostatic pore pressures with the water table used in the model.

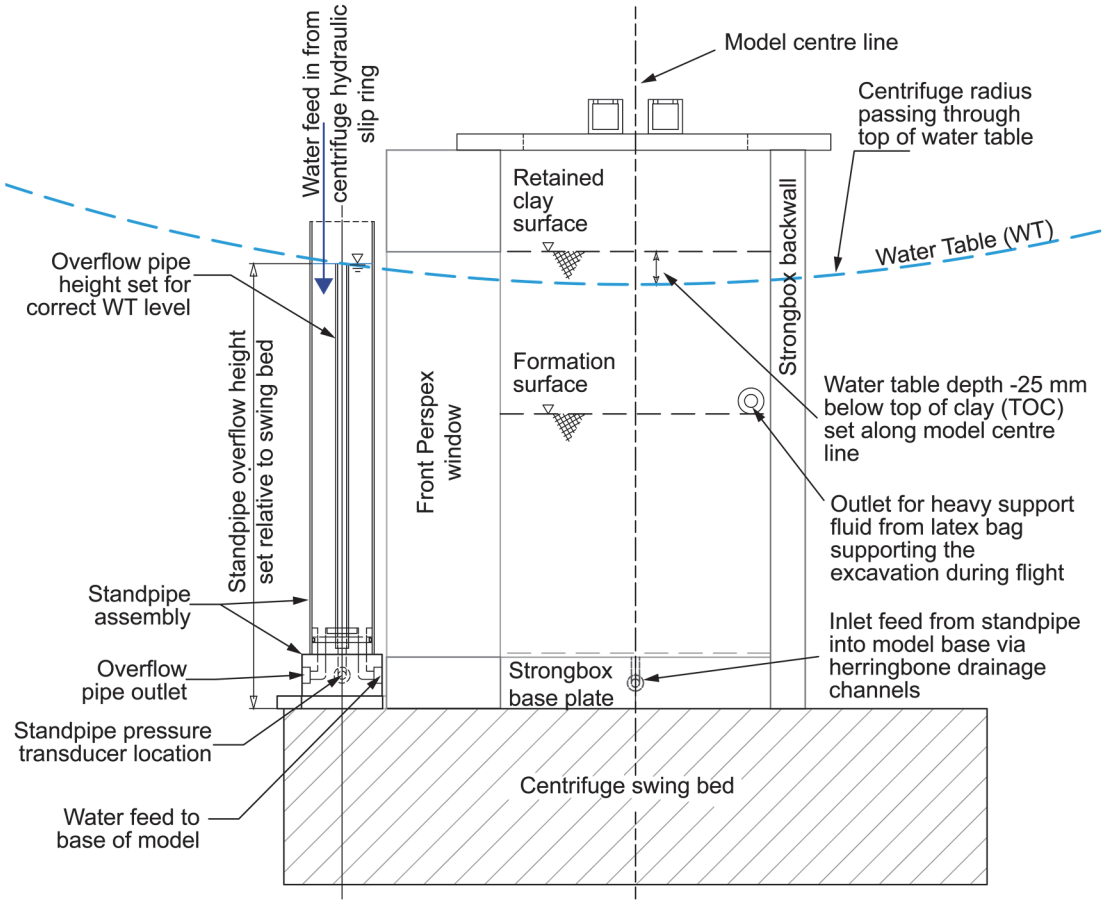


Figure 5. 12 Diagram showing the standpipe configuration for setting up the correct water table level within the model.

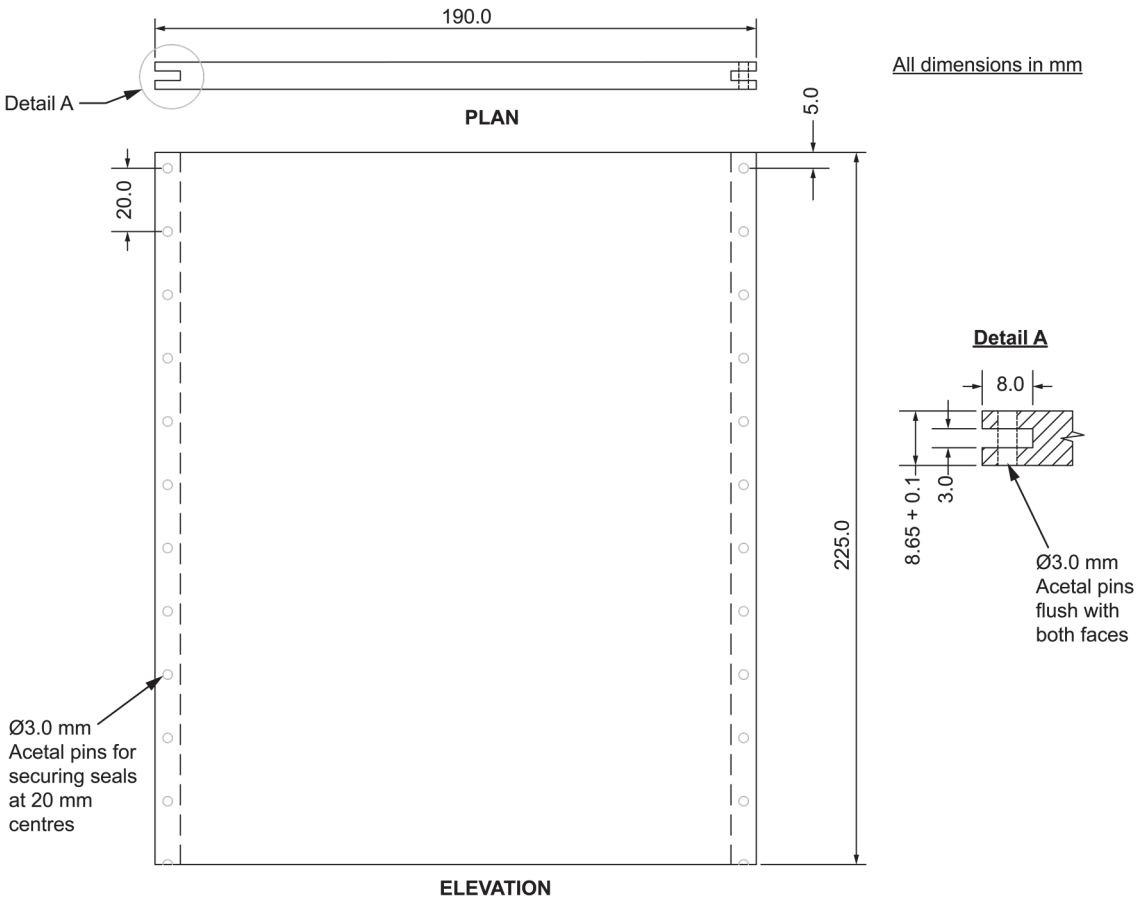


Figure 5. 13 Detailed drawing of the model retaining wall.

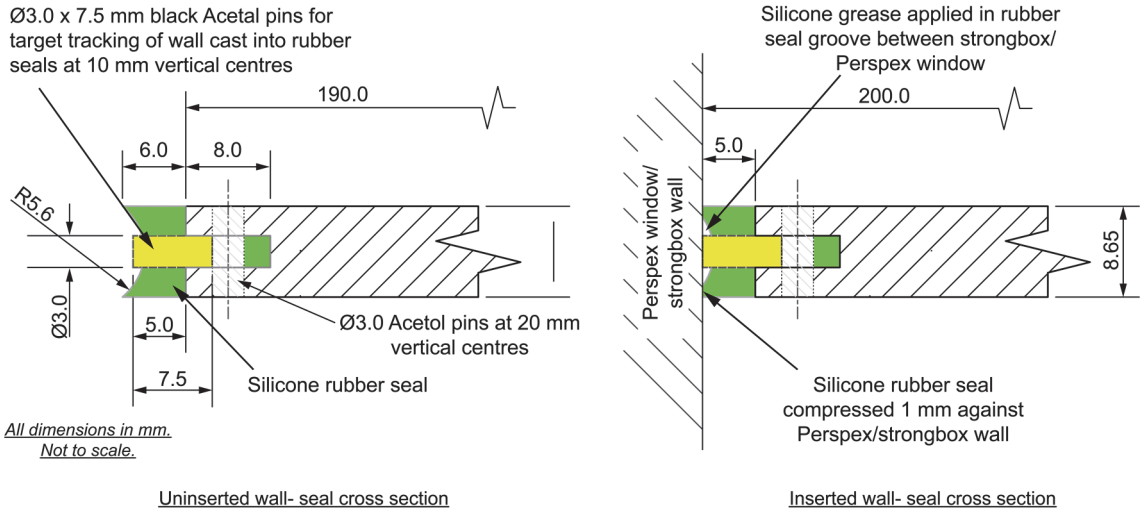


Figure 5. 14 Details of the cast silicone RTV rubber seals used on the front and back faces of the model retaining wall.

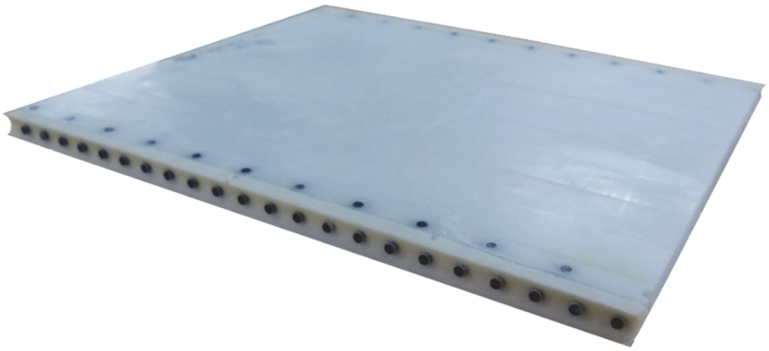


Figure 5. 15 Photograph showing the 3 mm external diameter black tracking targets inserted into the front rubber seal of the model retaining wall for tracking of horizontal wall displacements.

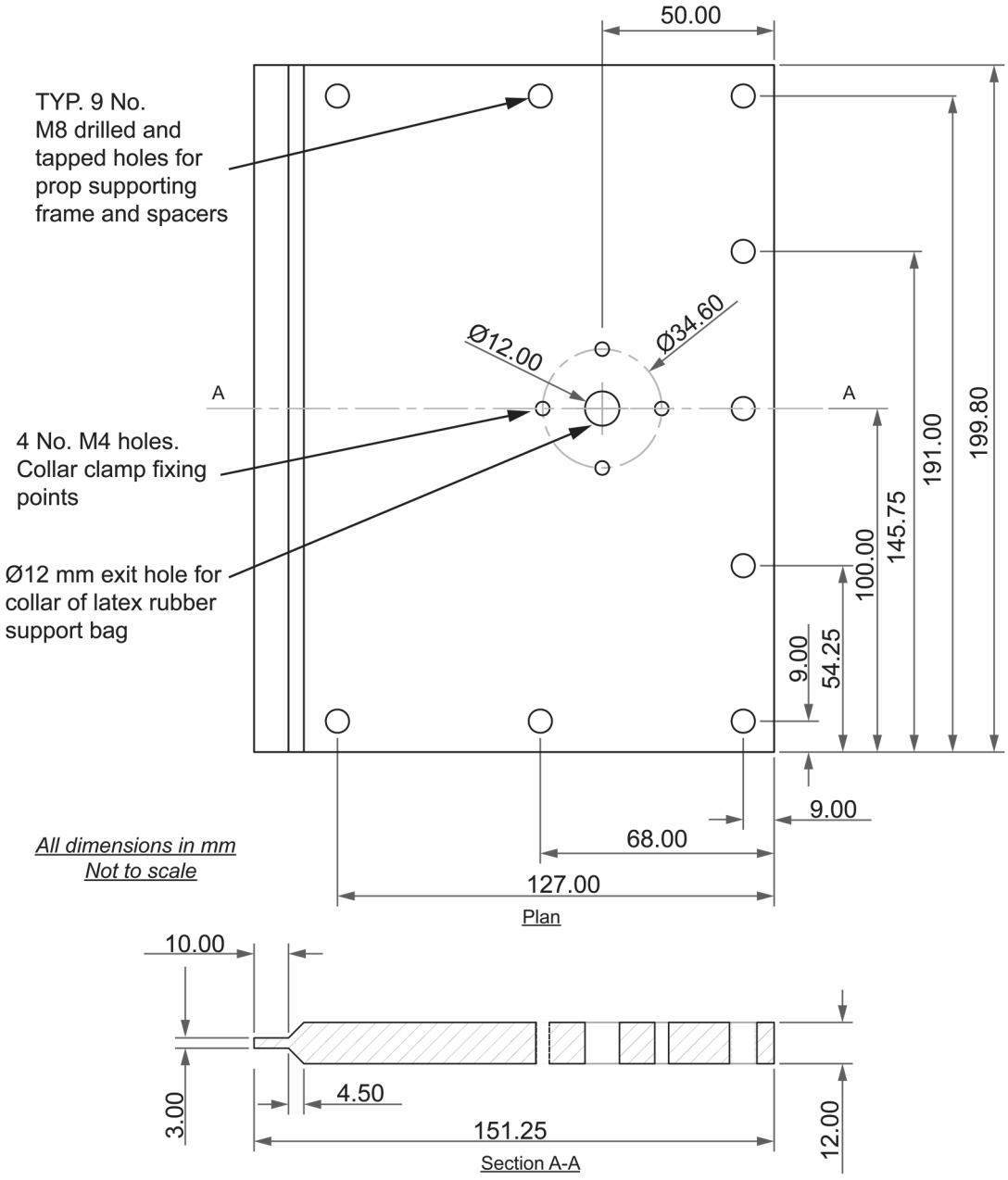


Figure 5. 16 Detailed drawing of the aluminium prop plate.

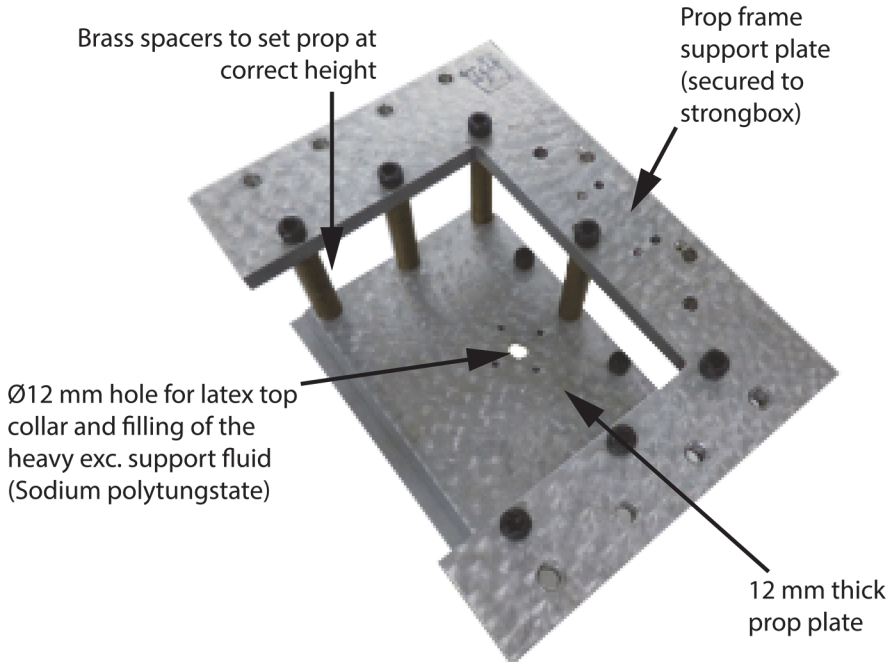


Figure 5. 17 Prop plate support frame and spacers.

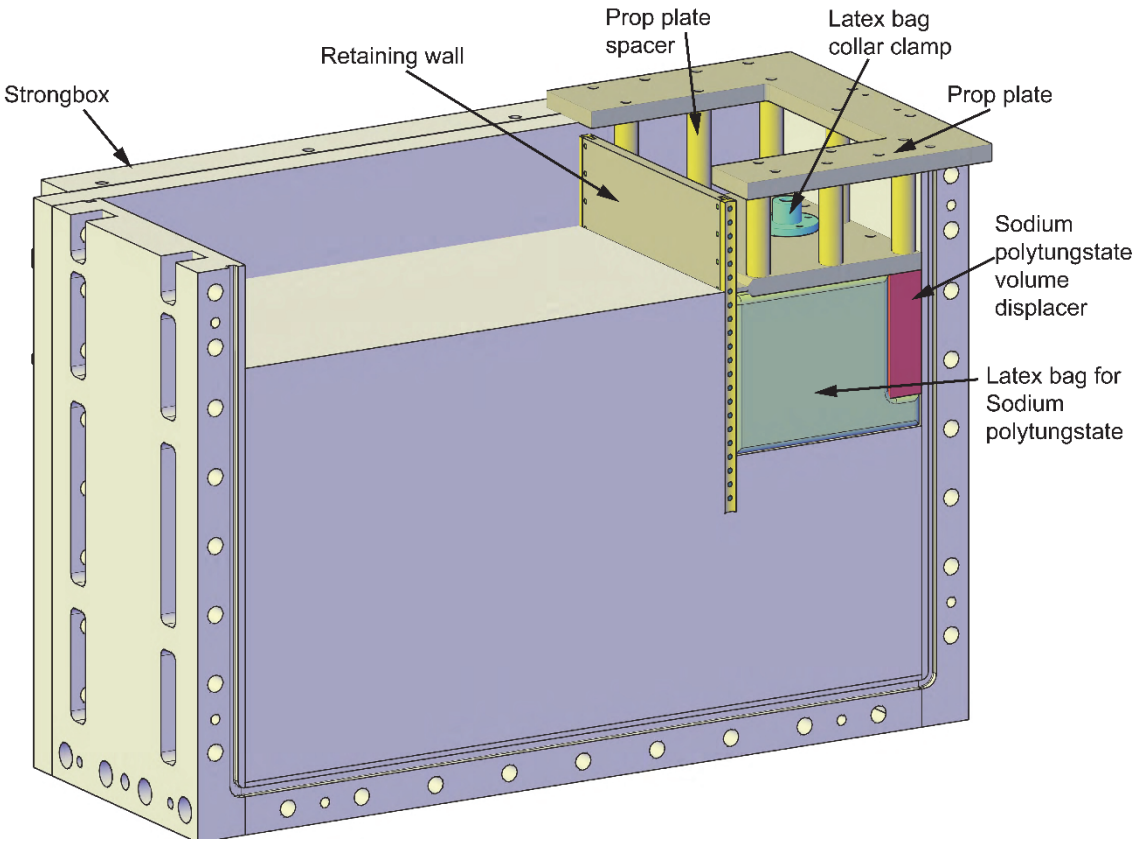
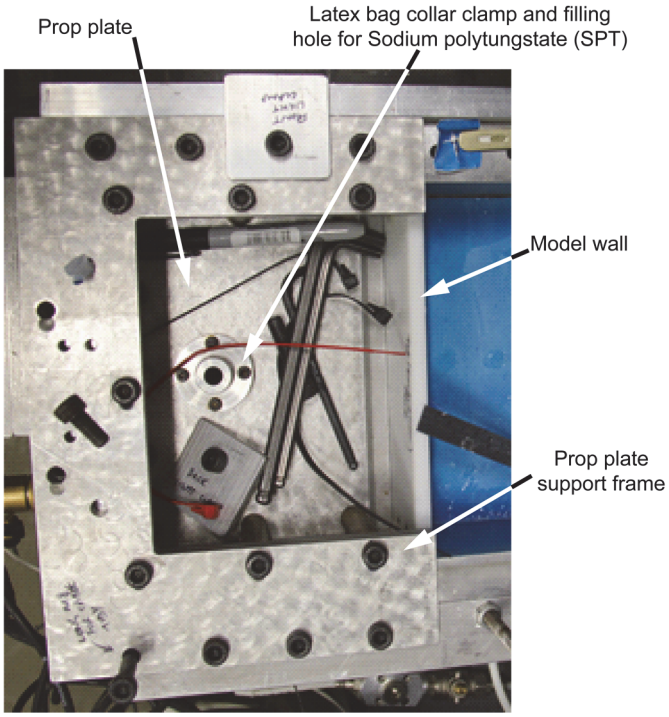
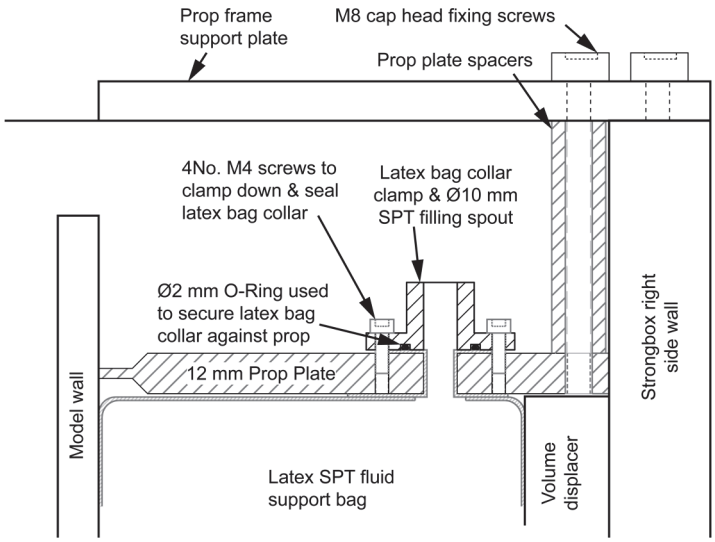


Figure 5. 18 Conceptual diagram of the apparatus arrangement for modelling of the excavation.



(a)



(b)

Figure 5. 19 (a) Photograph of the collar clamp used to secure the SPT filled excavation support latex bag to the prop plate during flight and (b) schematic diagram showing configuration of latex support bag and collar clamp.

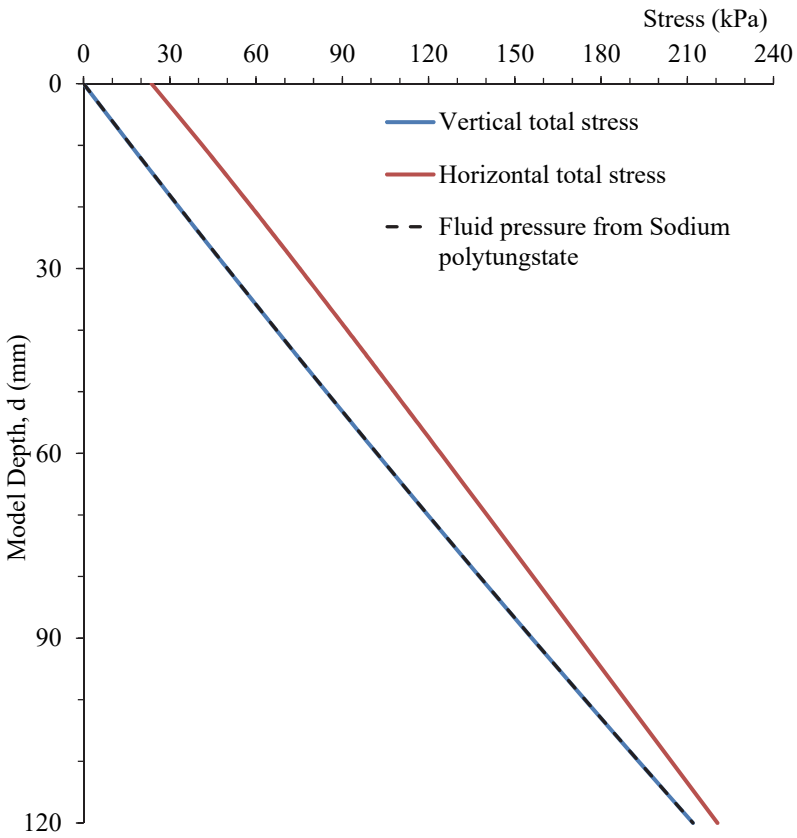


Figure 5. 20 Non-linear distribution of the total vertical and horizontal stresses with the model excavation depth and comparison with the stresses imposed by the Sodium polytungstate solution.

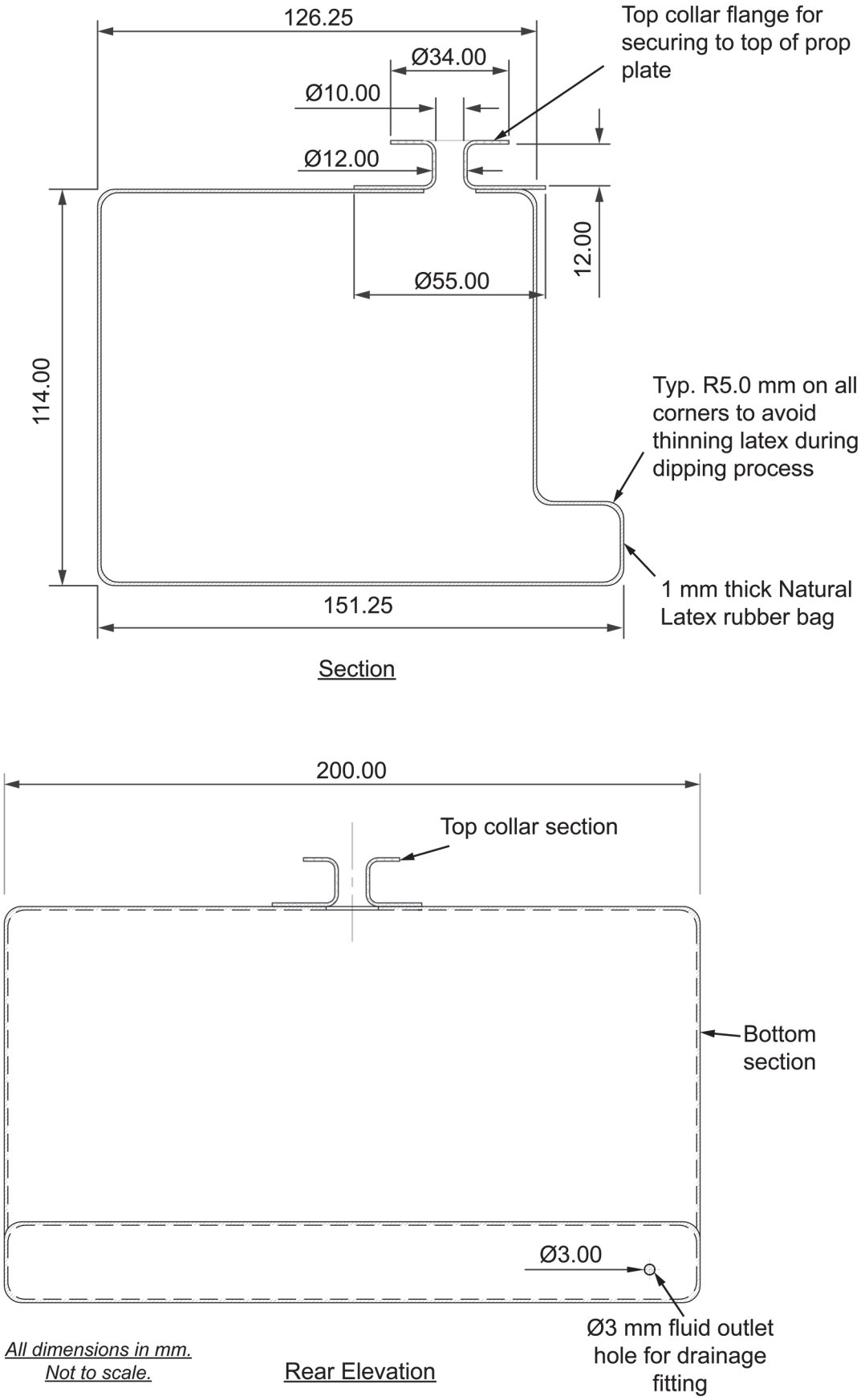


Figure 5. 21 Details of the latex bag used for containing the excavation heavy Sodium polytungstate (SPT) support fluid.

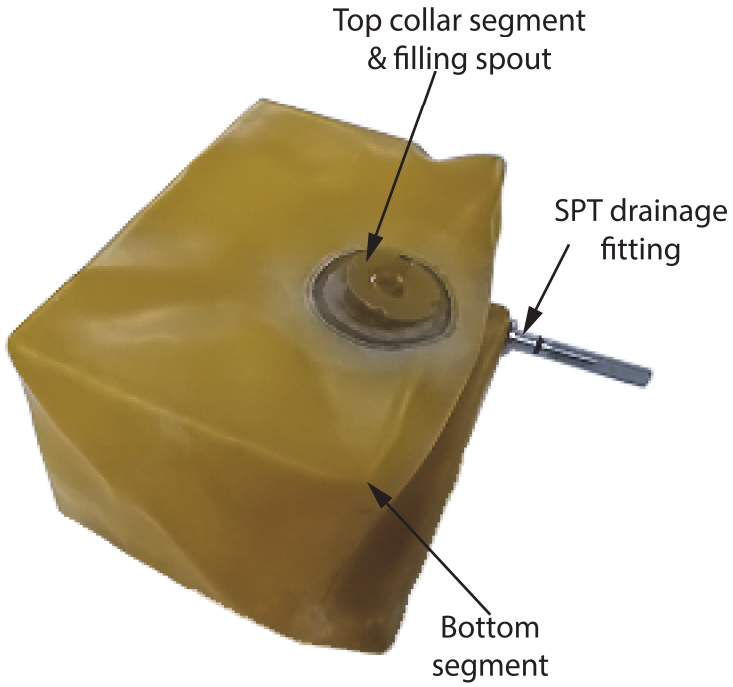


Figure 5. 22 Photograph of the natural latex bag used to contain the SPT fluid and support the pre-cut excavation during flight.

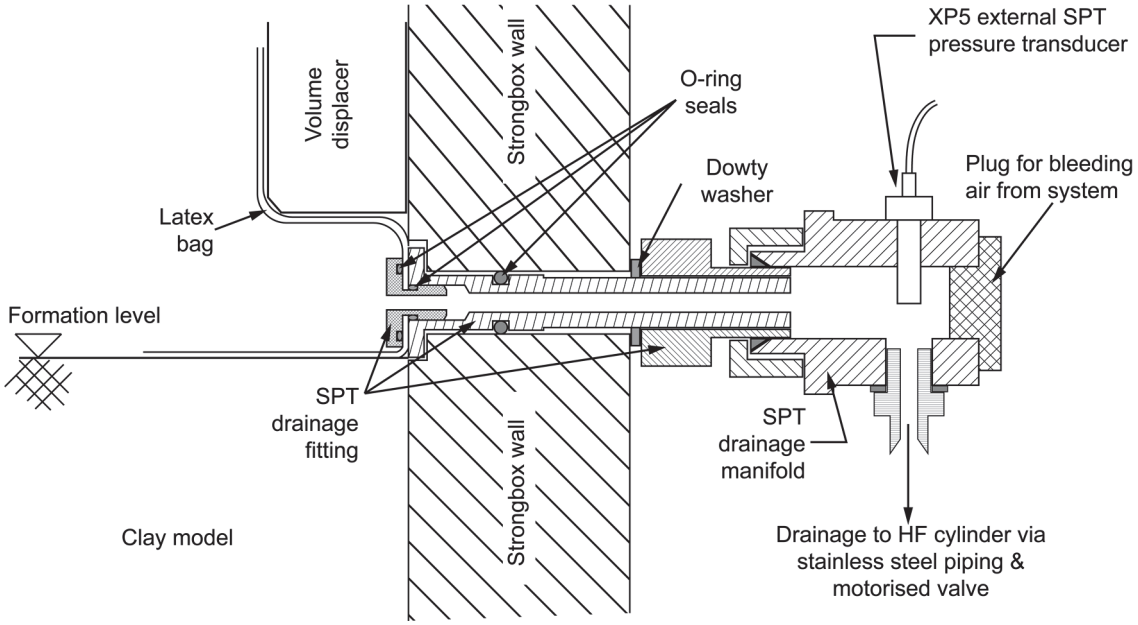


Figure 5. 23 Detail of the SPT drainage fitting connection to the excavation support latex bag, manifold and external SPT pressure transducer.

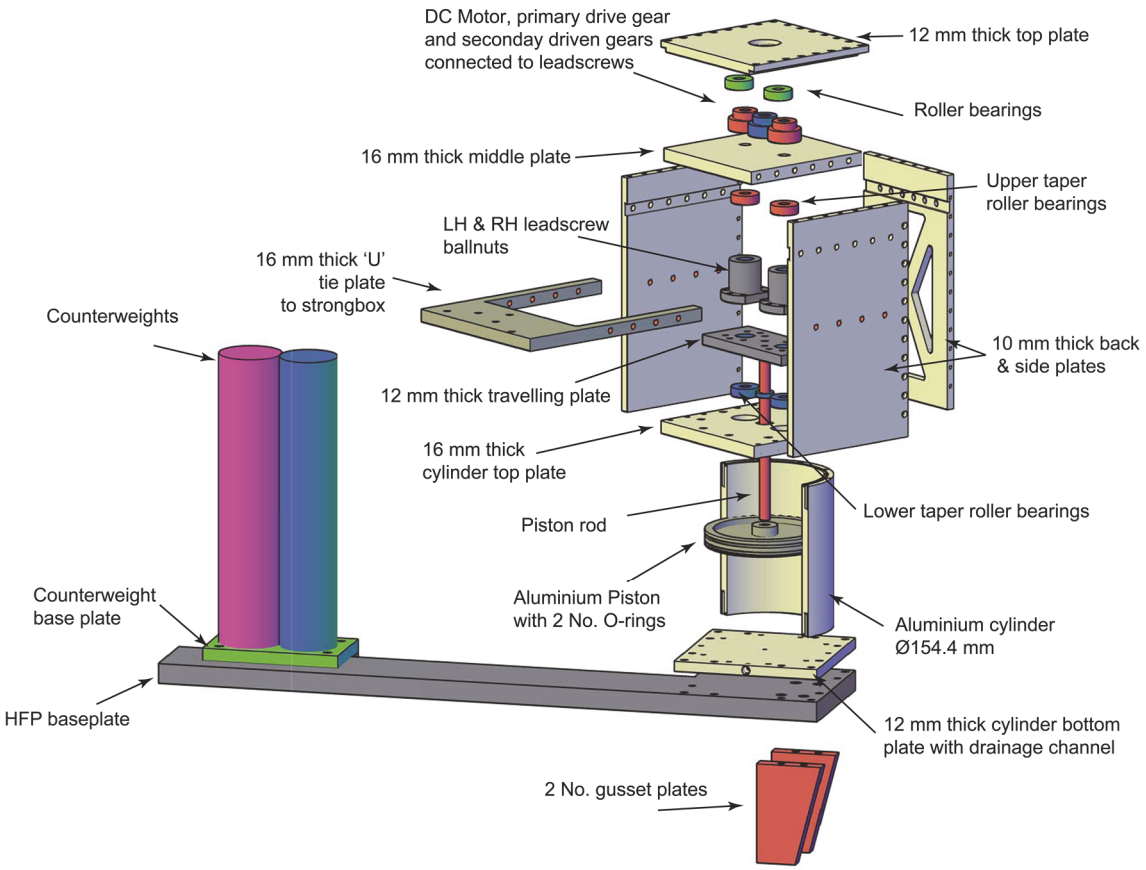


Figure 5. 24 Conceptual diagram (exploded) of the heavy fluid pump (HFP) used to drain the SPT fluid in excavation only tests 2HH and 3HH.

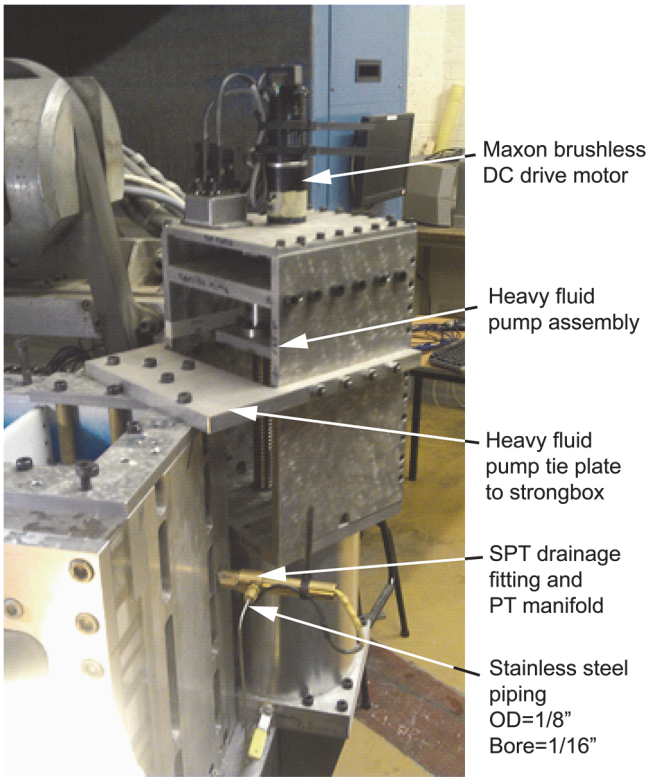


Figure 5. 25 Photograph showing the position and arrangement of the heavy fluid pump on the swing.

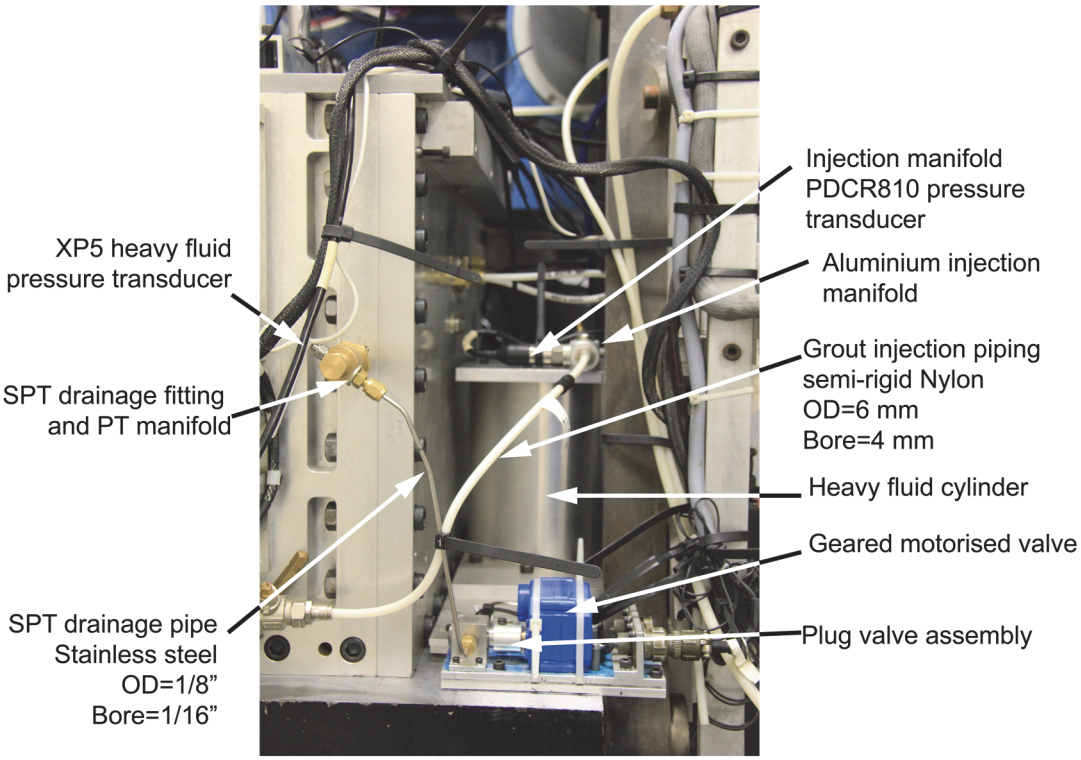


Figure 5. 26 Photograph showing the configuration used for the draining and pressure measurement of the SPT excavation support fluid and injection pressures from tests 7HH onwards.

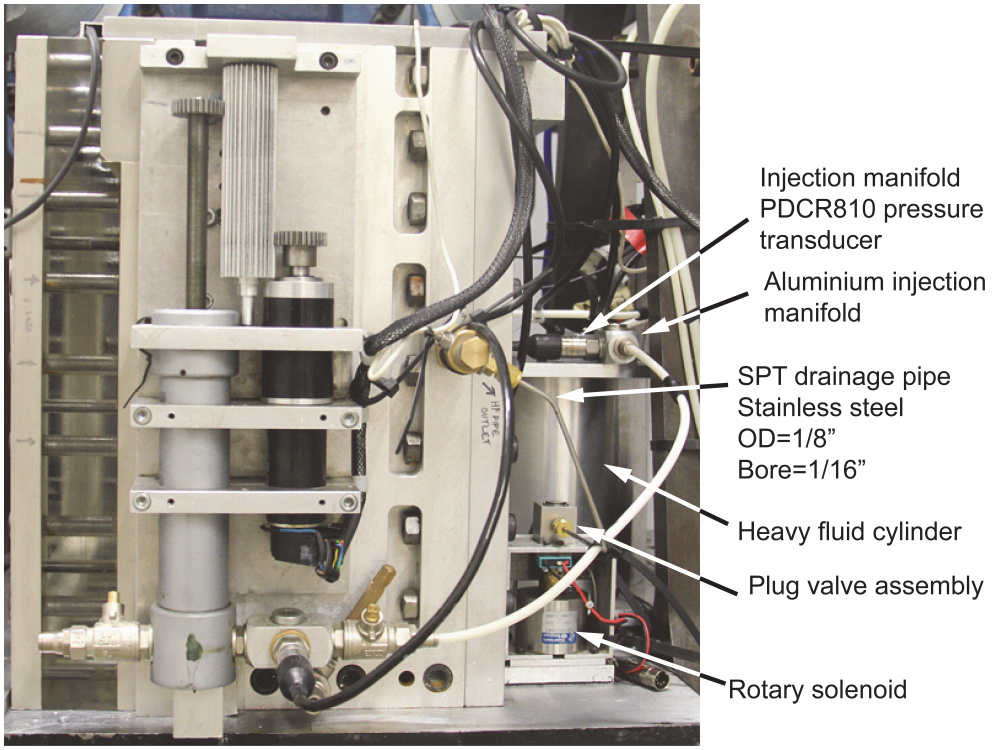


Figure 5. 27 Photograph showing the rotary solenoid assembly used to drain the SPT fluid in test 6HH.

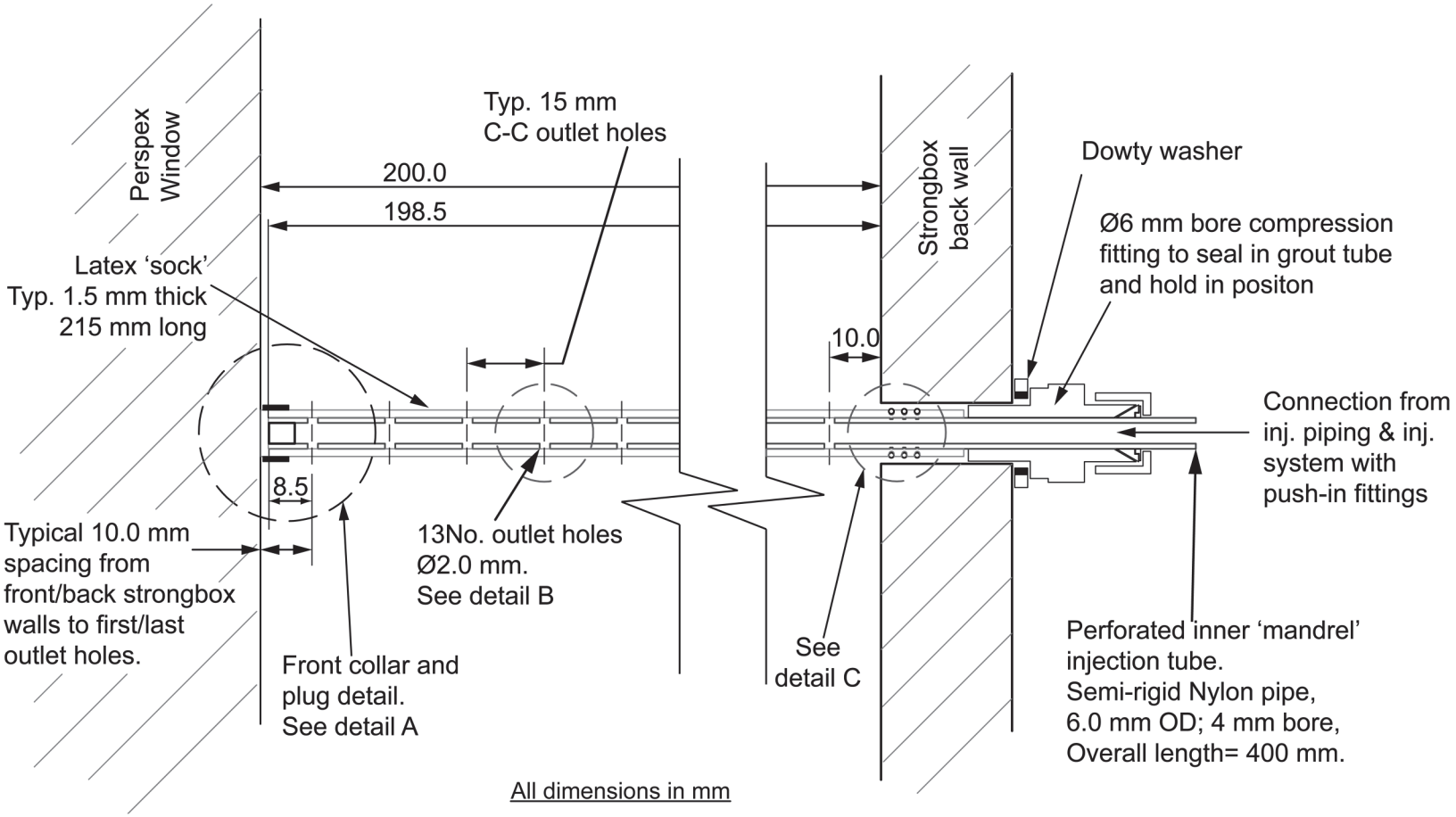


Figure 5. 28 Typical detail of the grout injection tube within the model (see Figure 5.29 for details A to C).

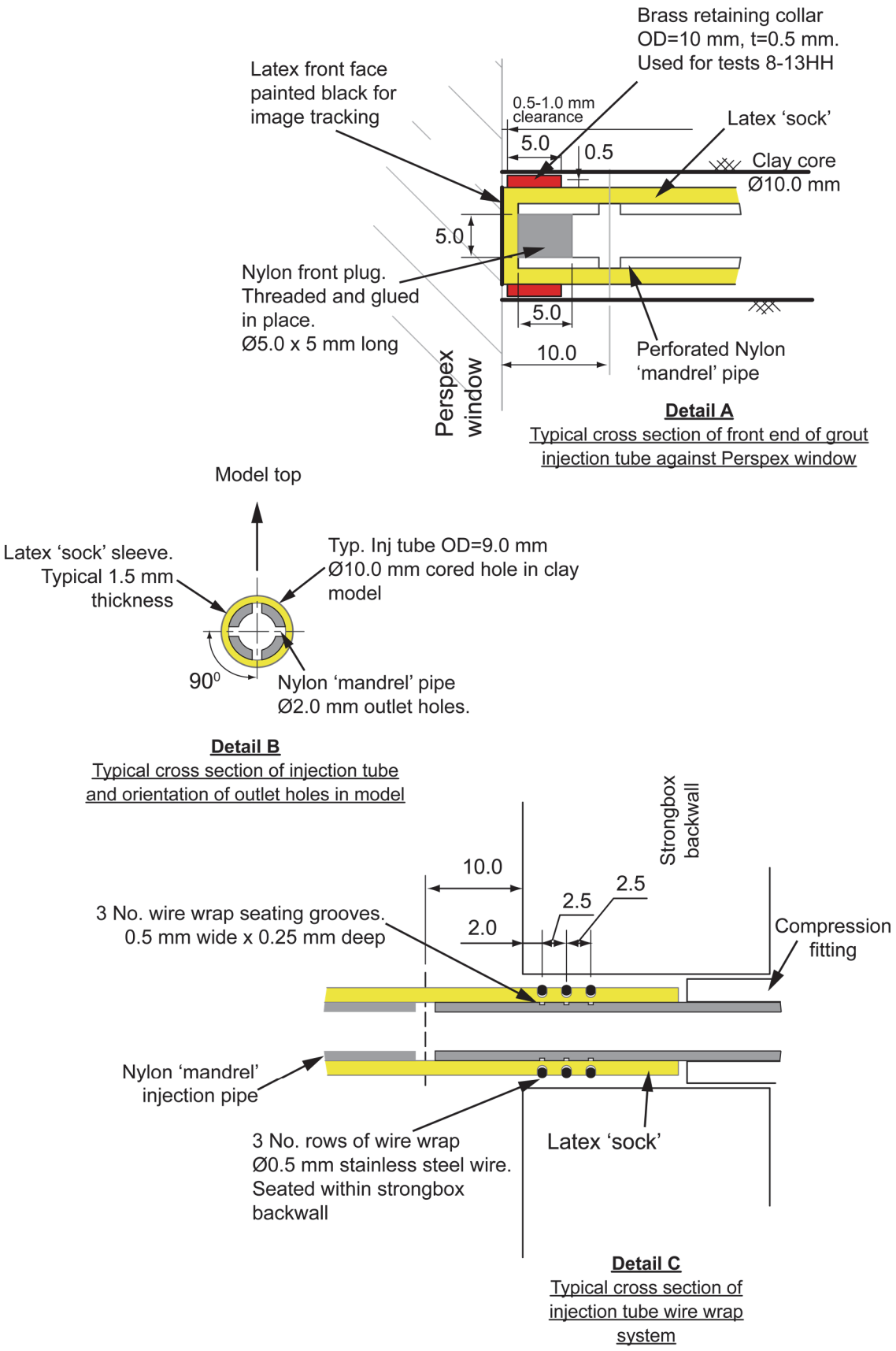


Figure 5. 29 Details A to C from Figure 5.28 of the grout injection tube construction within the model.



(a)



(b)



(c)



(d)

Figure 5. 30 Photographs of: (a) the grout injection tube without the front brass retaining collar used in tests 6-7HH, (b) the front brass retaining collar used in tests 8-13HH, (c) the wire wrap seating grooves in the inner Nylon mandrel injection pipe and (d) application of the outer wire wrap around the latex membrane.

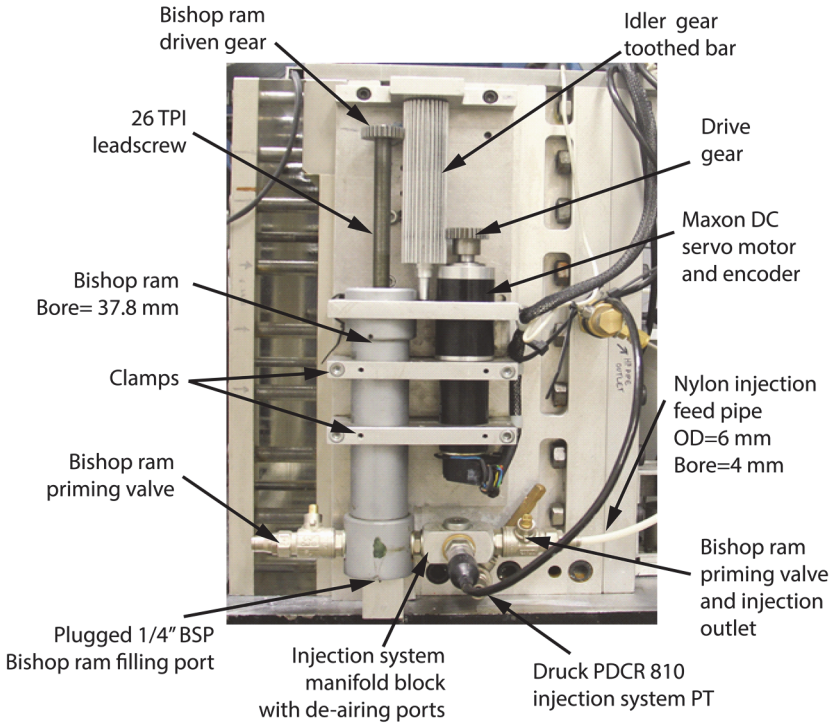


Figure 5. 31 Photograph showing details of the grout injection system.

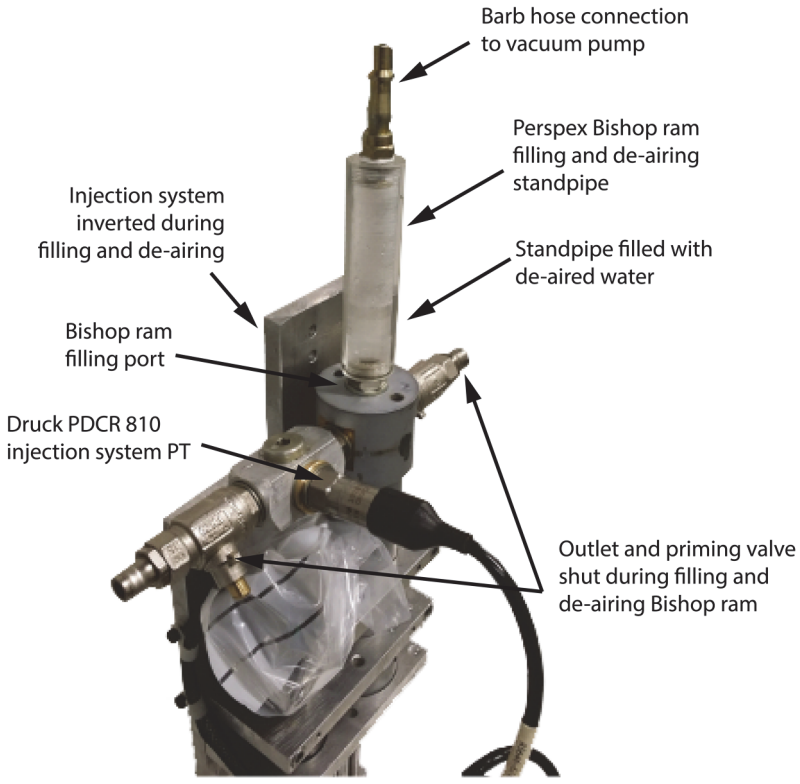


Figure 5. 32 Photograph showing details of the de-airing standpipe used to prime and fill the injection system.

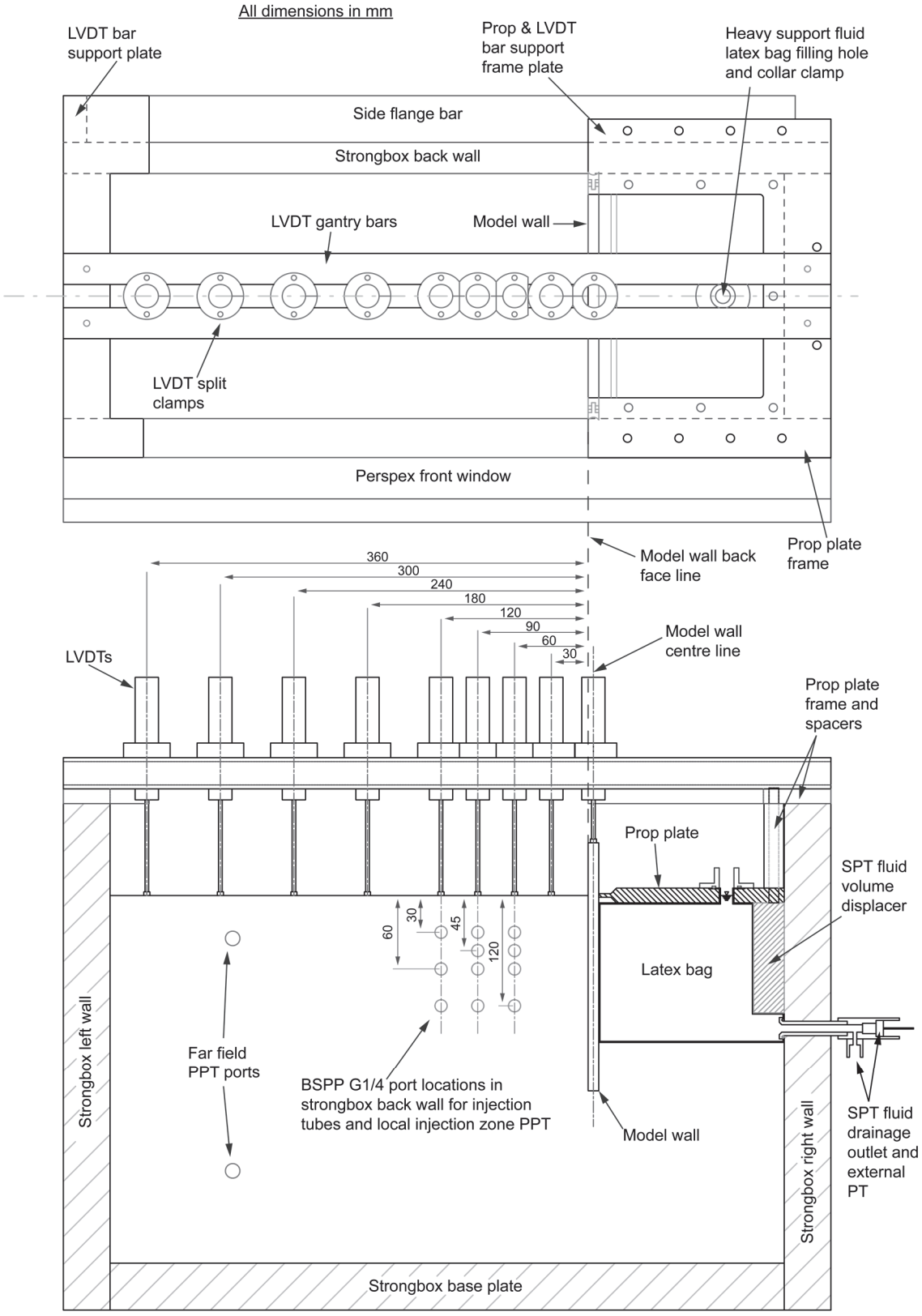


Figure 5. 33 Plan and section view of the LVDT gantry set up in the model tests.

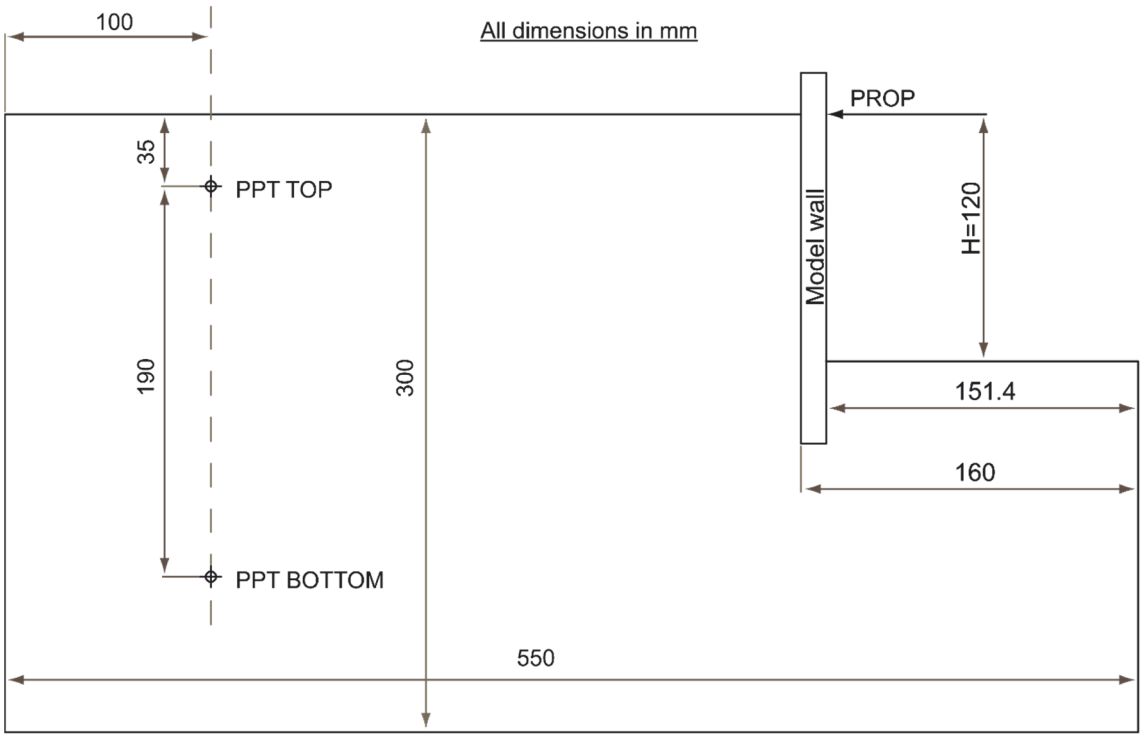
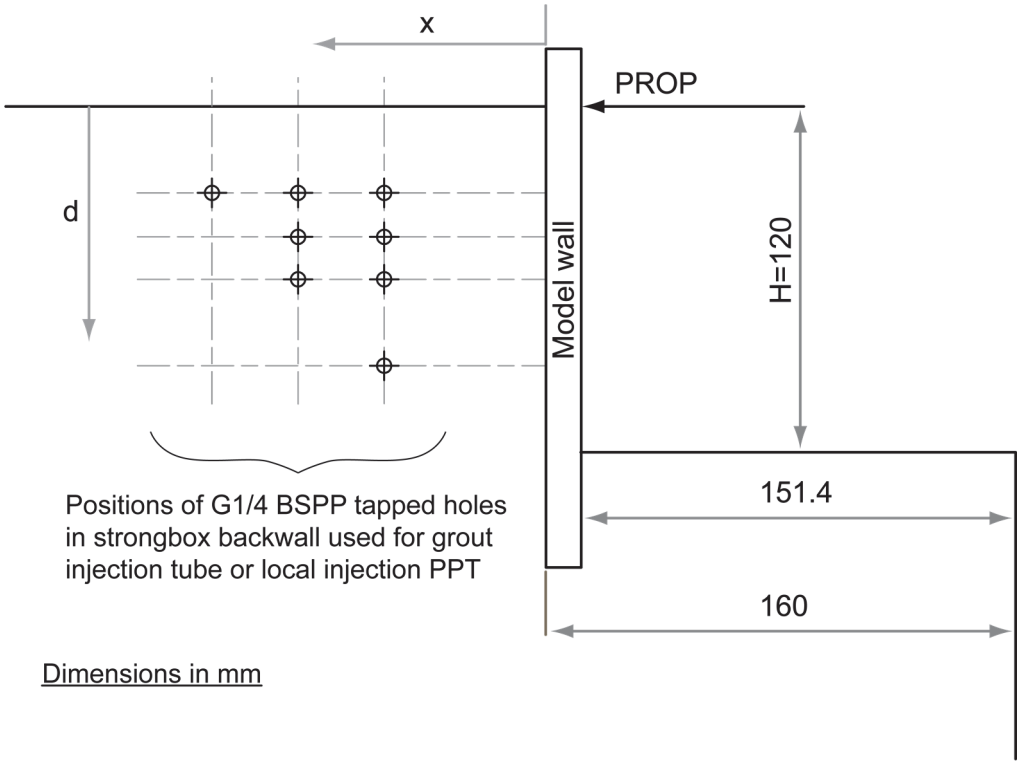


Figure 5. 34 Positions of the far field PPTs used to assess hydrostatic pore pressure equilibrium within the model prior to testing.



Test No.	Injection Zone PPT		Grouting location	
	x (mm)	d (mm)	x (mm)	d (mm)
6HH	120	60	60	60
7HH	90	60	60	30
8HH	90	60	60	90
9HH	90	60	60	45
10HH	120	30	90	30
11HH	120	60	90	45
12HH	60	60	L=90; R=60	30
13HH	120	30	L=90; R=60	45

Figure 5. 35 Positions of the installed PPTs locally around the grout injection tube locations in the grouting tests 6-13HH.

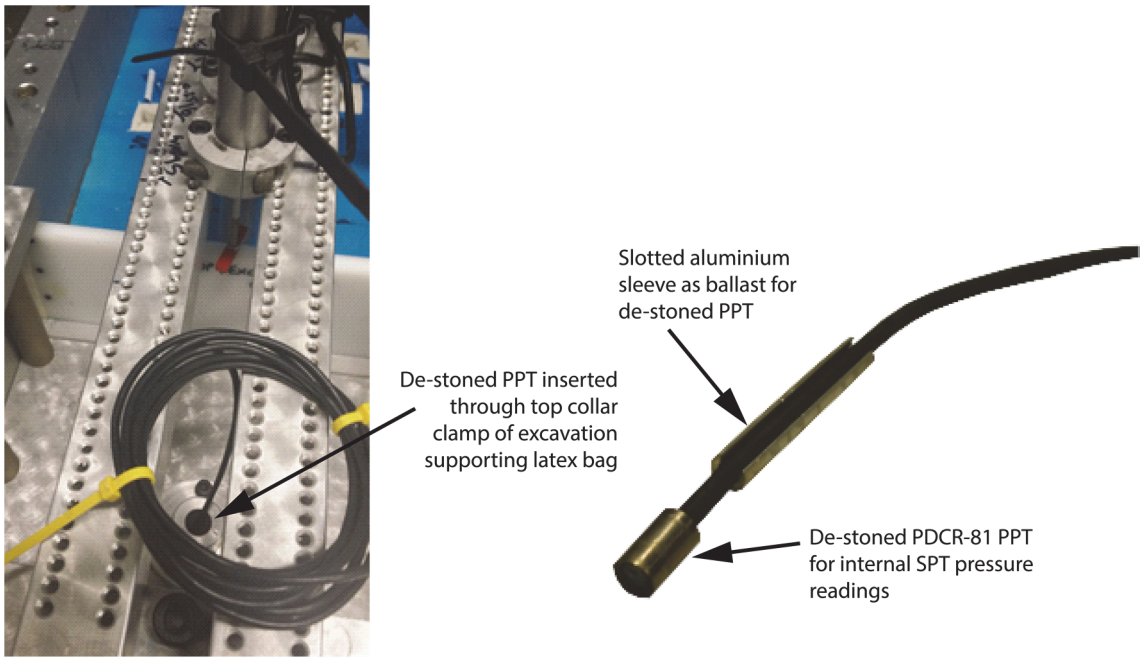


Figure 5. 36 Photographs showing: (a) insertion of the de-stoned Druck PDCR-81 PPT and (b) the slotted ballast sleeve attached behind the de-stoned PPT to ensure its positioning at the bottom of the SPT filled excavation support latex bag.

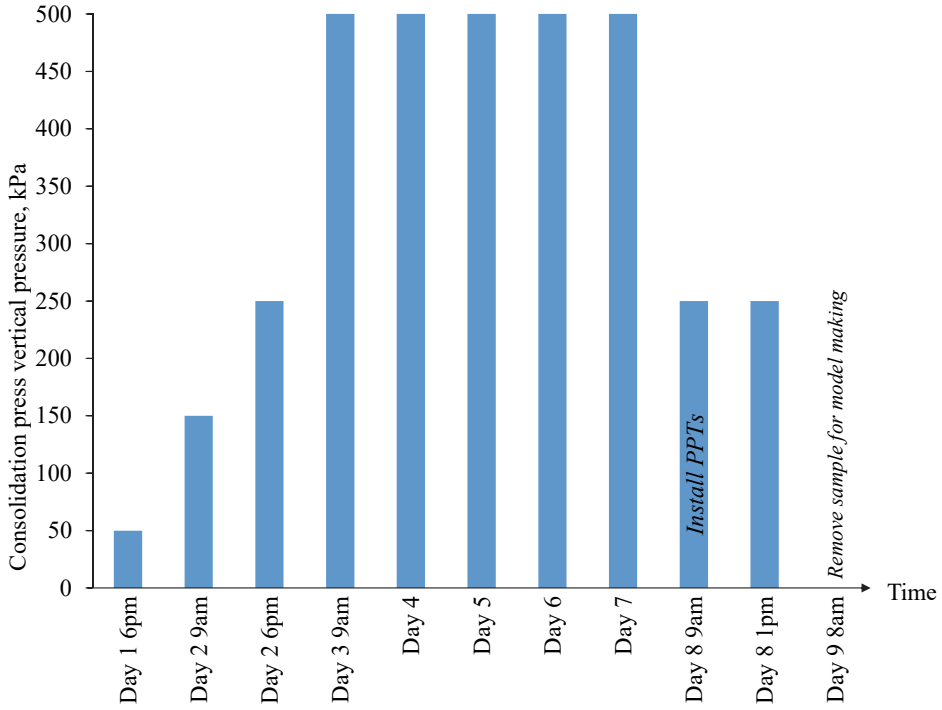


Figure 5. 37 Clay sample stress history during one dimensional consolidation in the hydraulic press prior to model making.

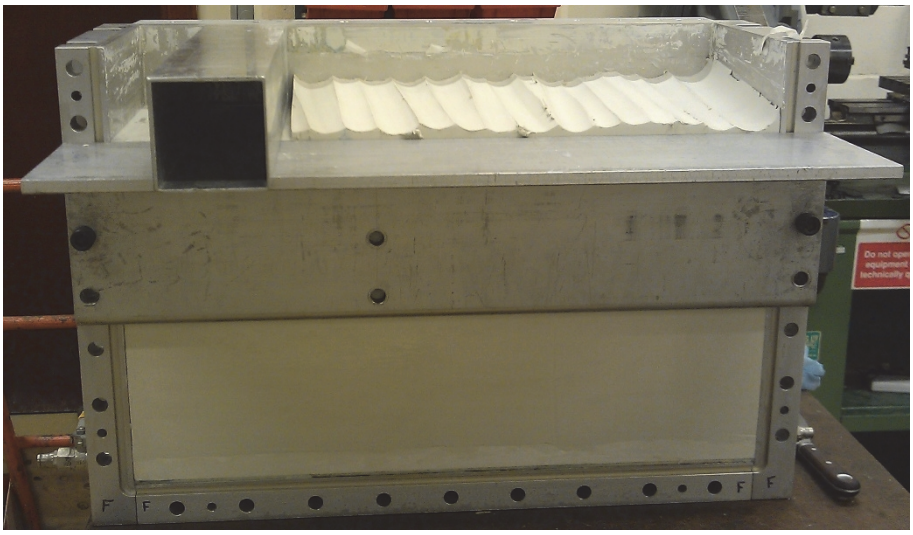


Figure 5. 38 Photograph showing the final trimming of the top model surface using an aluminium box cutter.

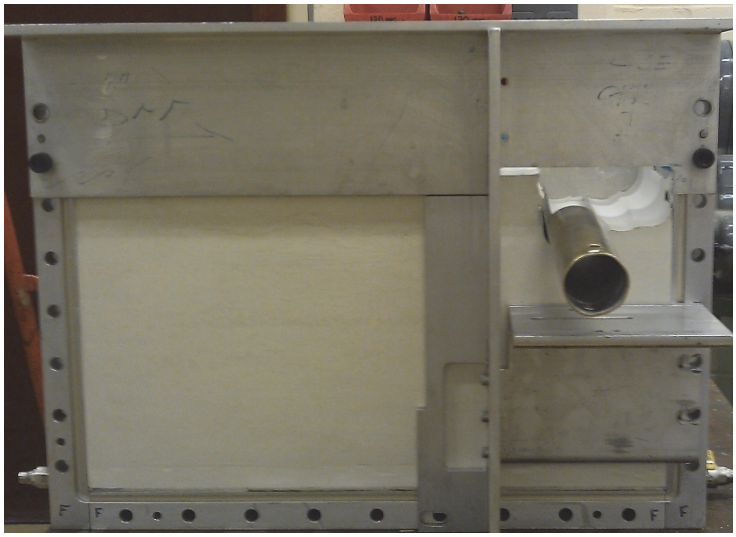


Figure 5. 39 Photograph showing the excavation trimming guide being used to rough cut the excavation cavity using the brass tube cutter.



Figure 5. 40 Guide and cutter for forming the 40 mm deep slot for the model wall toe embedment.

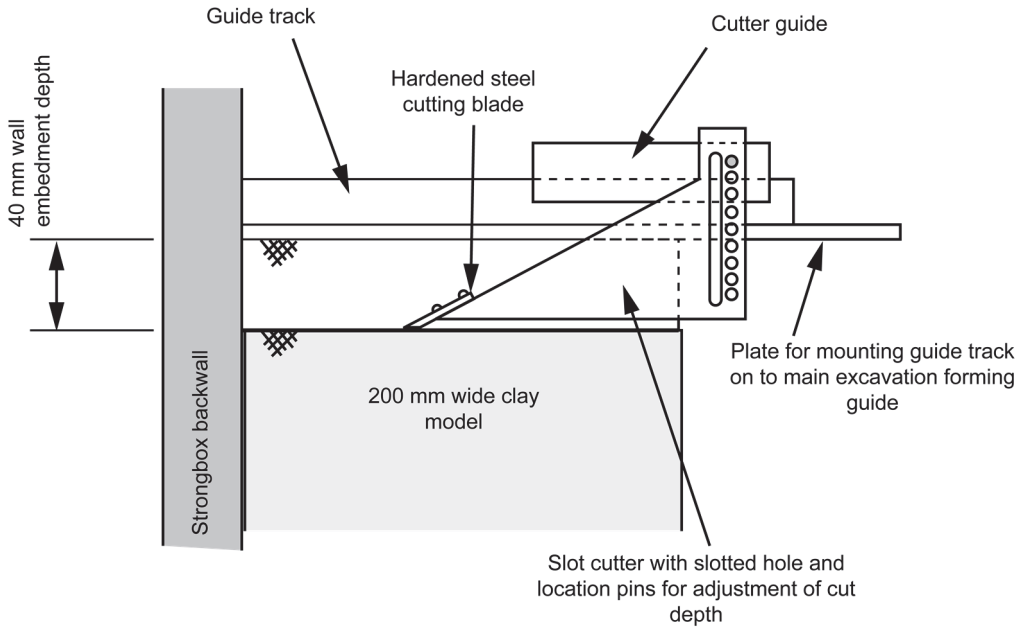


Figure 5. 41 Schematic drawing of the model wall embedment slot cutter and guide (after McNamara, 2001).

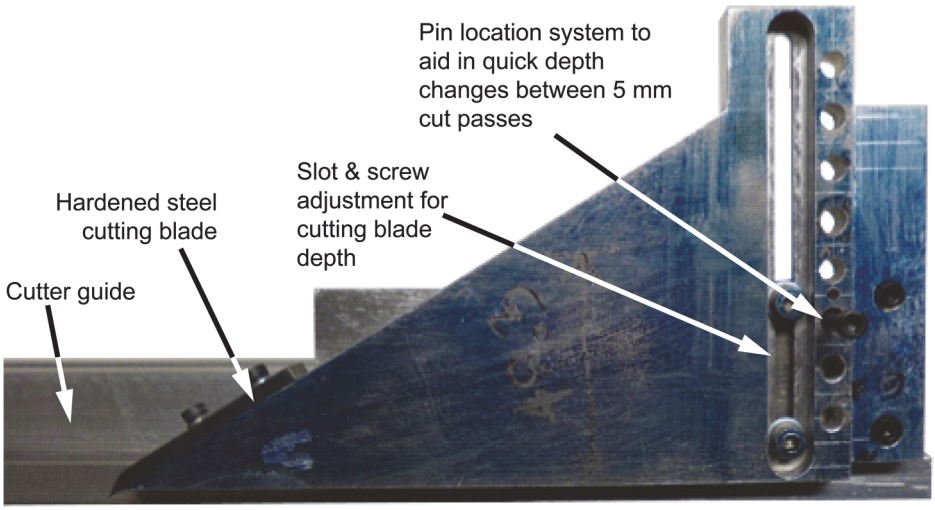


Figure 5. 42 Photograph showing the pin location system on the wall embedment slot cutter for quick adjustment of the cutting depth.

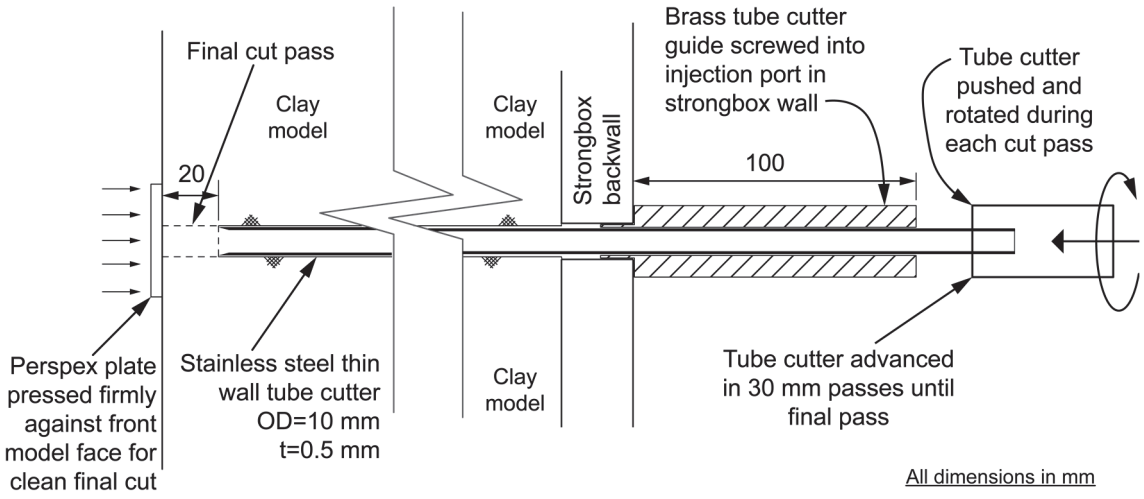


Figure 5. 43 Diagram showing the clay coring apparatus for insertion of the grout injection tube.

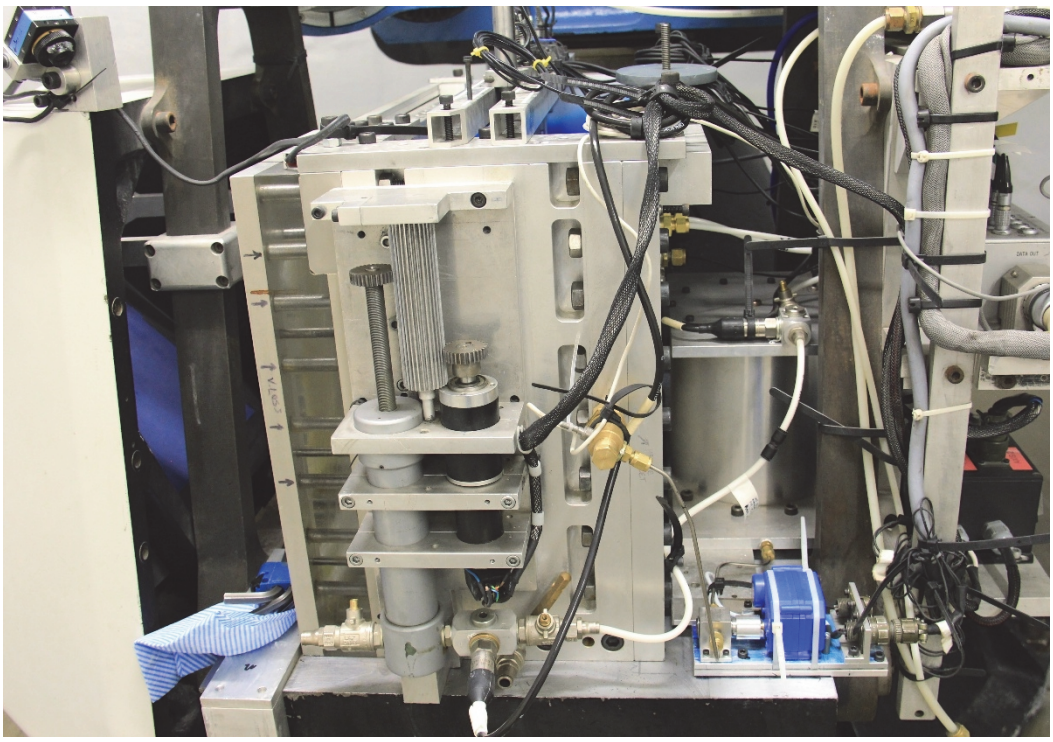


Figure 5. 44 Photograph showing the prepared model, apparatus and instrumentation setup following the model making procedure, ready for flight.

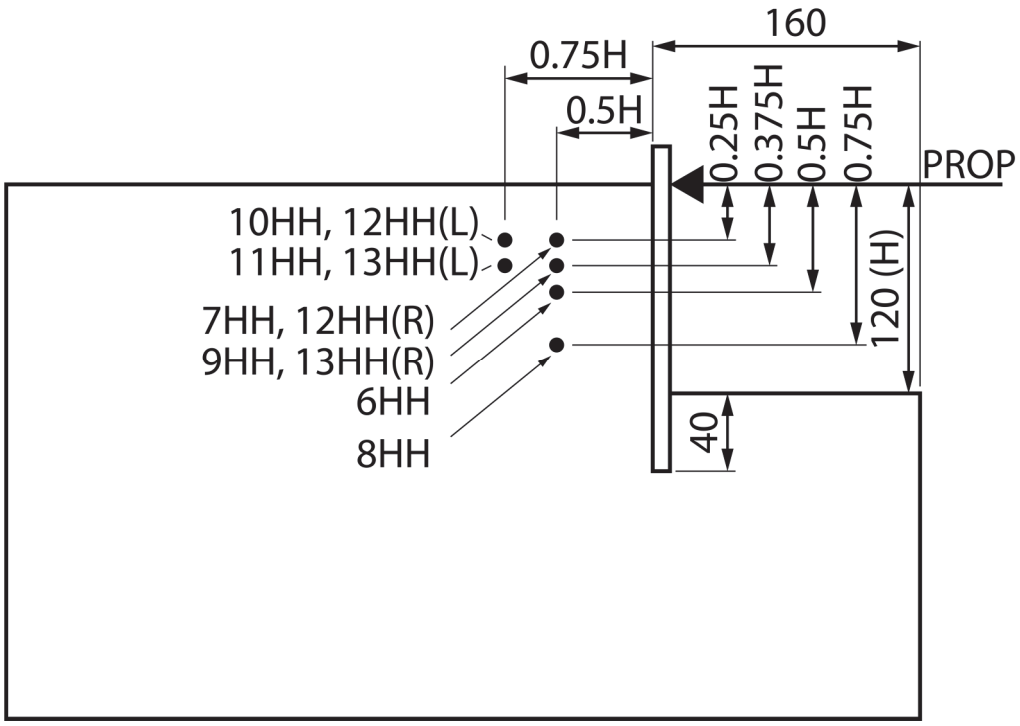


Figure 6. 1 Schematic illustration of the grouting positions for each test relative to the retained surface and back face of the model wall.

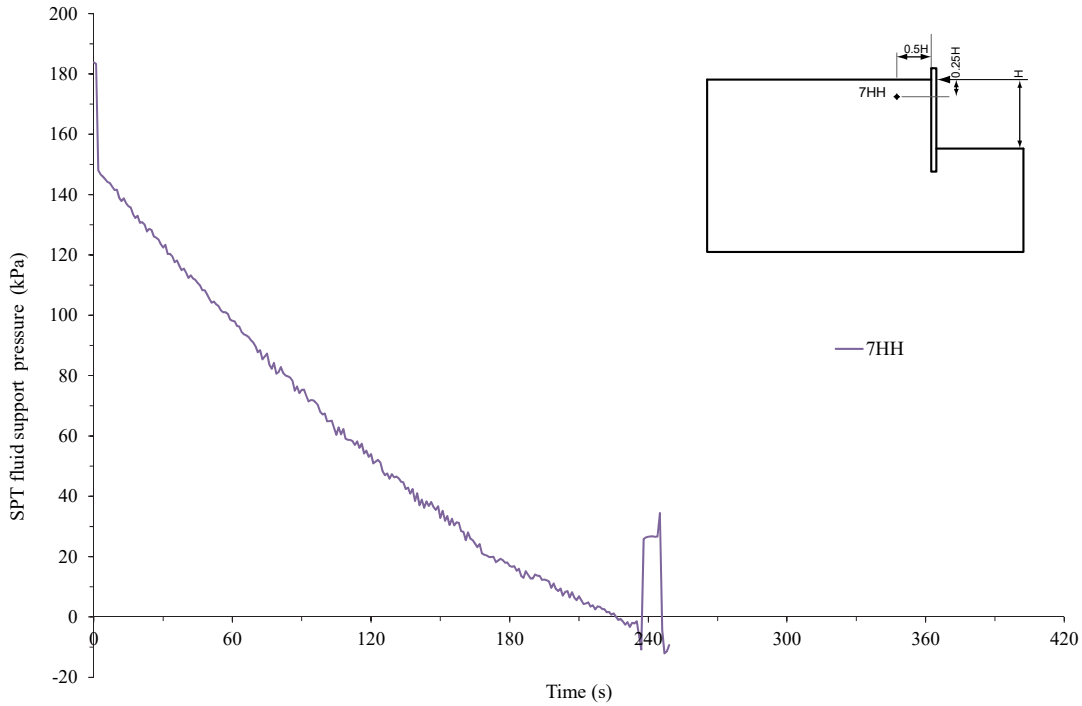


Figure 6. 2 Typical SPT excavation support pressure response recorded by the externally located PT during excavation simulation in test 7HH.

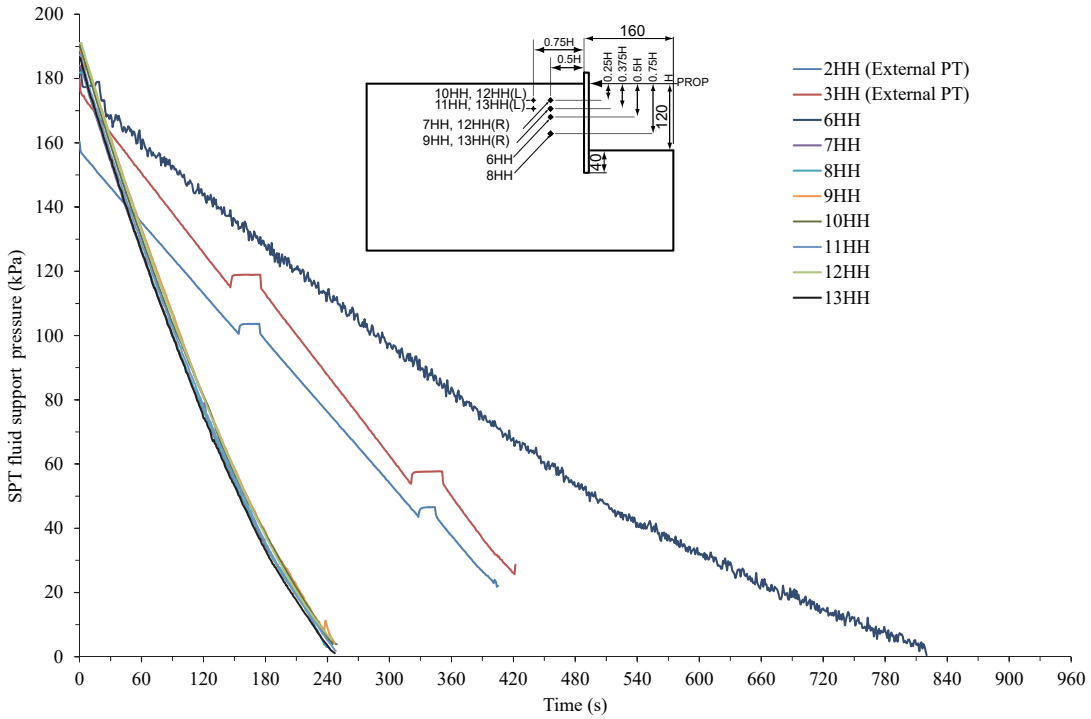


Figure 6. 3 Pressure transducer readings (from the external PT for tests 2-3HH and internal PT for tests 6-13HH) of the SPT support fluid pressure during the simulated excavation period.

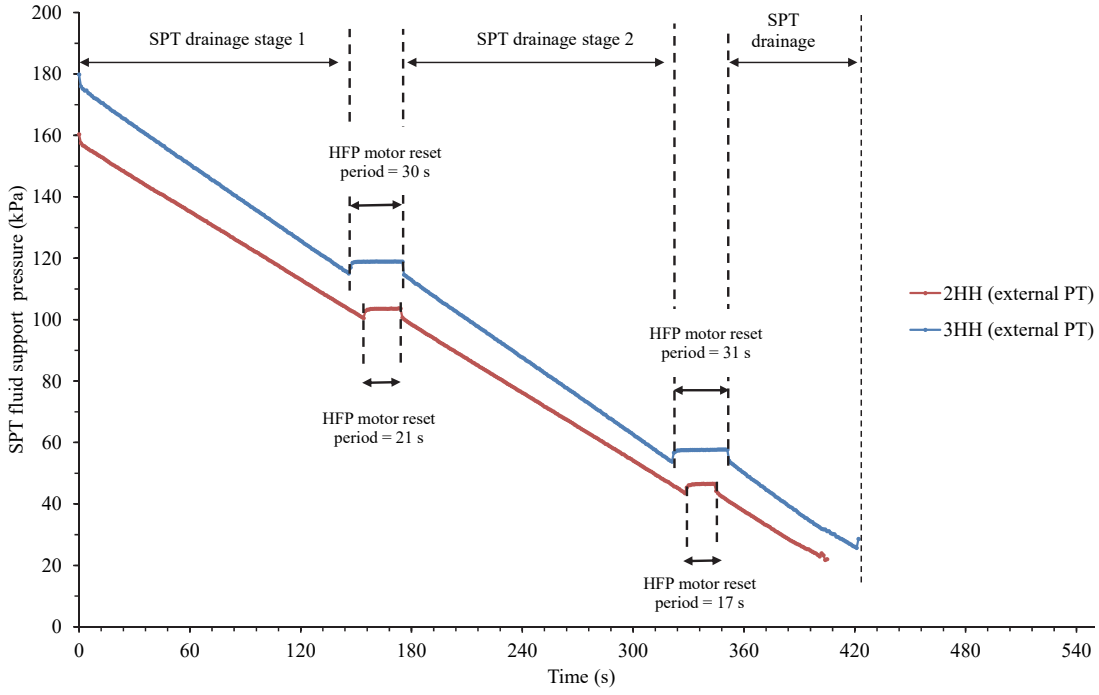


Figure 6. 4 Staged SPT excavation support pressure response in tests 2-3HH (using the HFP to remove the SPT fluid) during excavation simulation.

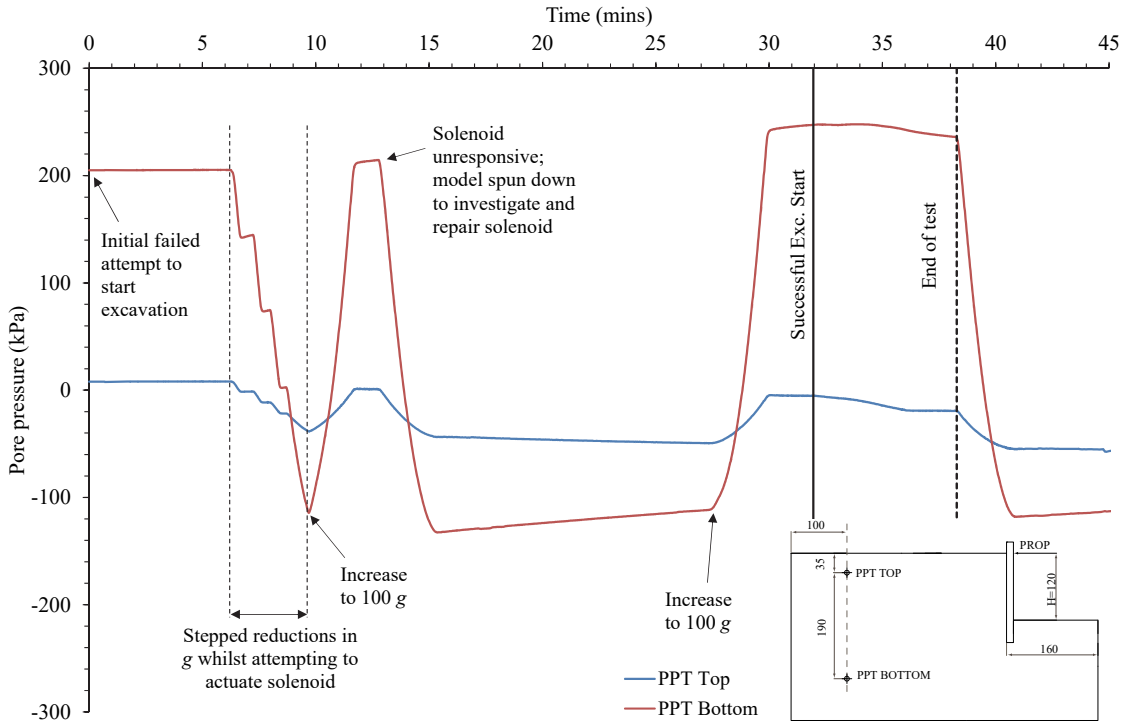


Figure 6. 5 Effect of spinning down the model in test 8HH on the far field pore pressures (following an unresponsive solenoid-plug valve assembly on the first actuation attempt).

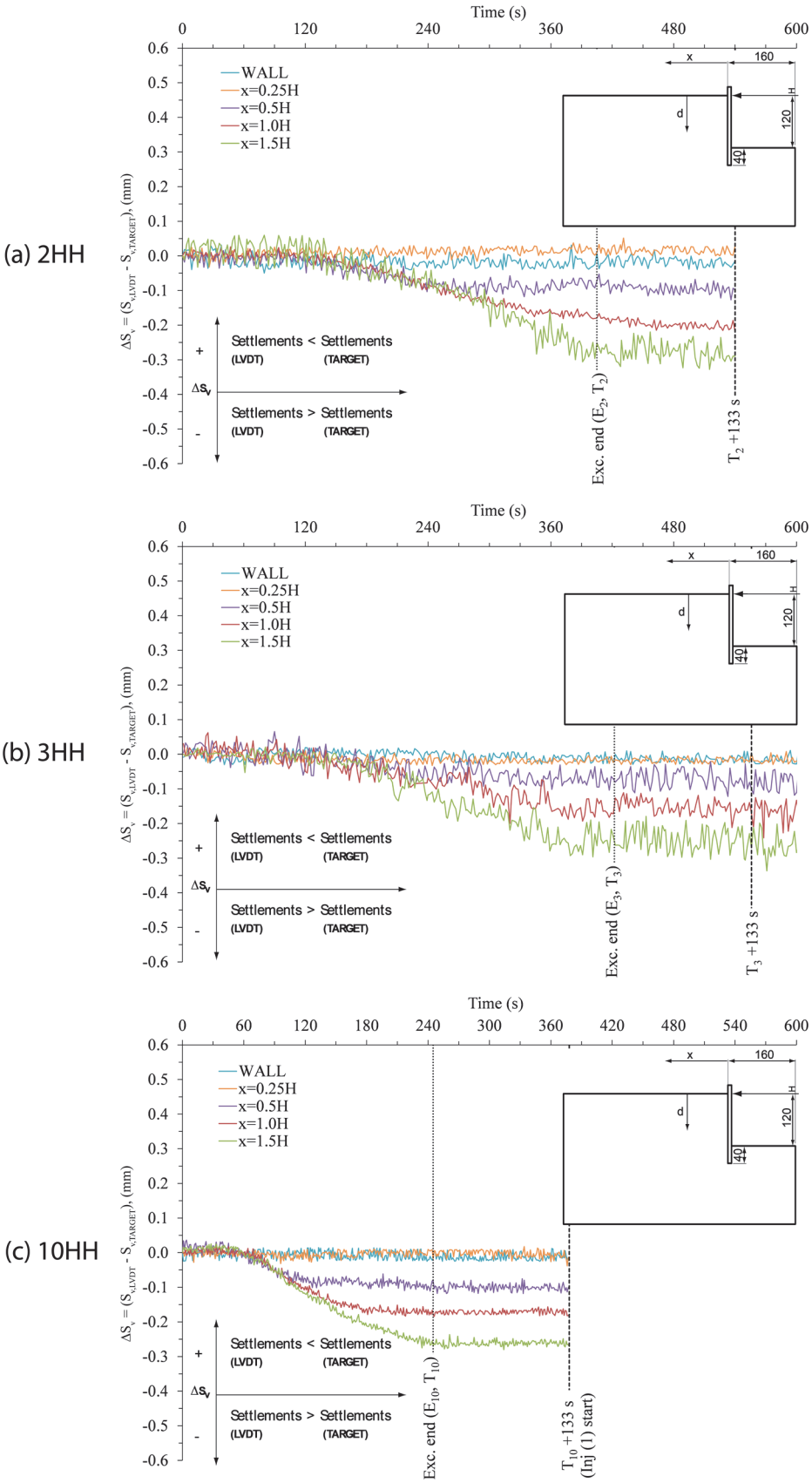


Figure 6. 6 Differences in vertical displacements between LVDTs and image processing targets above the wall and at distances x= 0.25H, 0.5H, 1.0H and 1.5H behind the wall in tests: (a) 2HH (b) 3HH and (c) 10HH, up to 133 s after excavation completion (prior to injection in test 10HH).

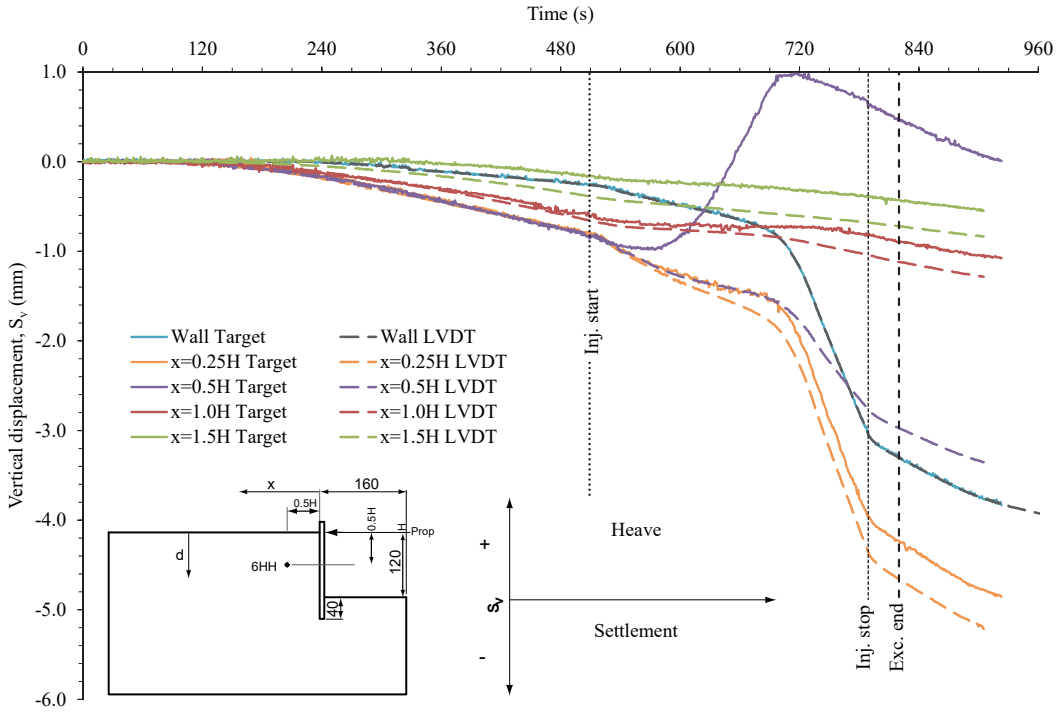


Figure 6. 7 Retained surface vertical displacements measured by LVDTs and image processing targets (15 mm below the surface) in test 6HH above the wall and at distances x= 0.25H, 0.5H, 1.0H and 1.5H behind the wall.

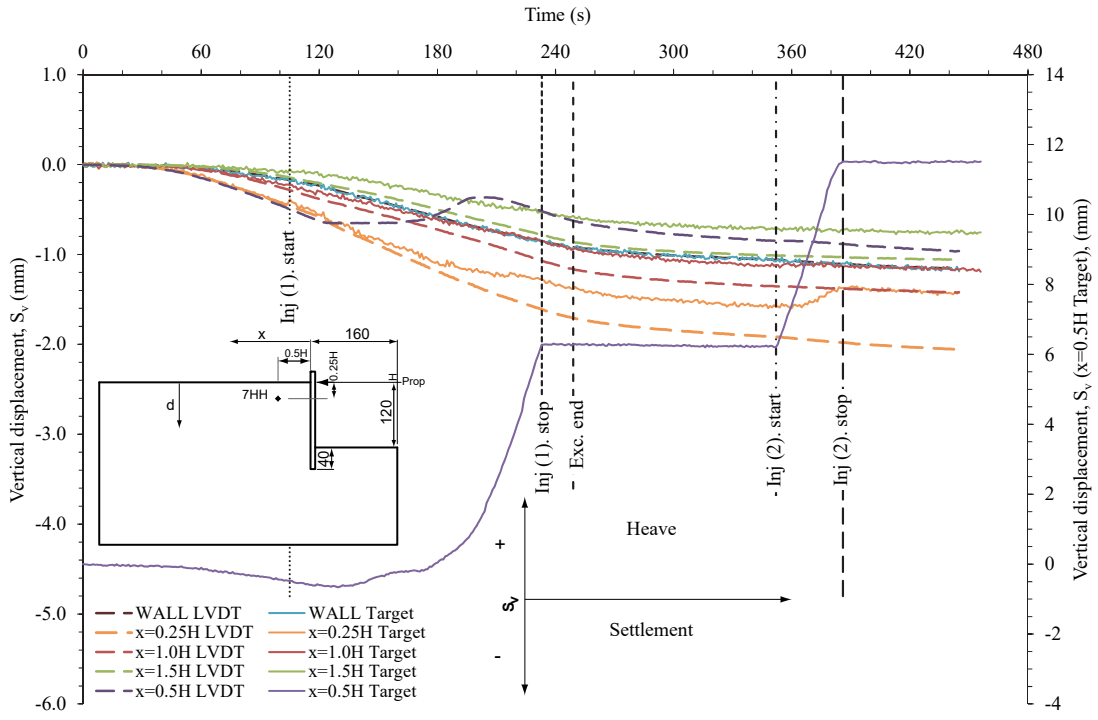


Figure 6. 8 Retained surface vertical displacements measured by LVDTs and image processing targets (15 mm below the surface) in test 7HH above the wall and at distances x= 0.25H, 0.5H, 1.0H and 1.5H behind the wall.

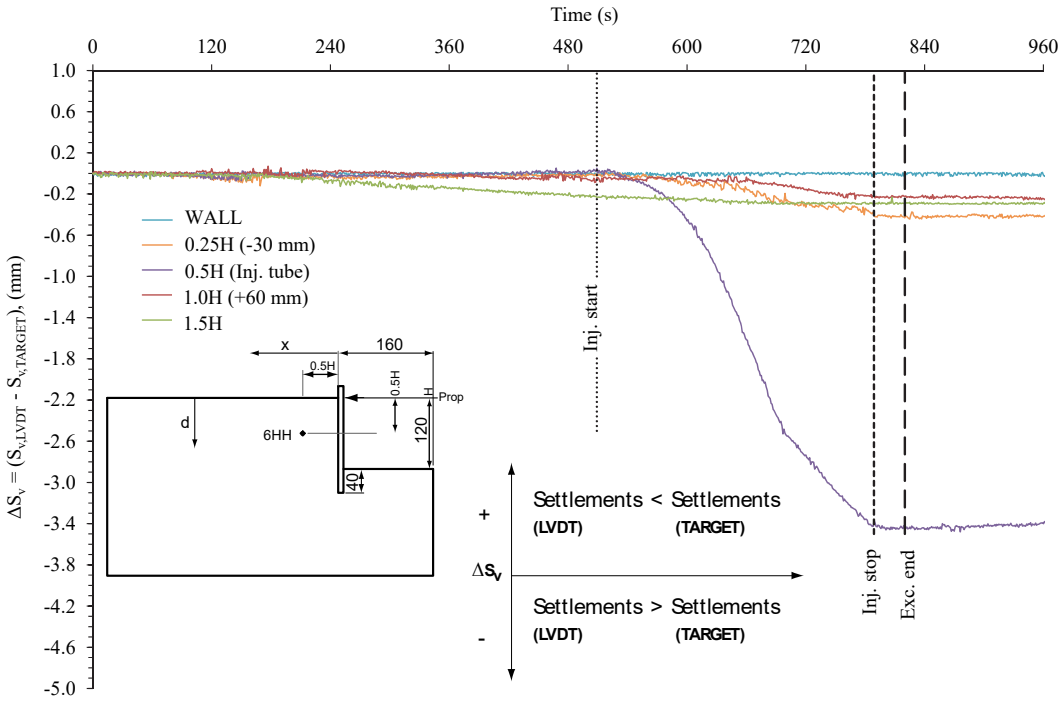


Figure 6. 9 Differences in vertical displacements between LVDTs and image processing targets during test 6HH above the wall and at distances x= 0.25H, 0.5H, 1.0H and 1.5H behind the wall.

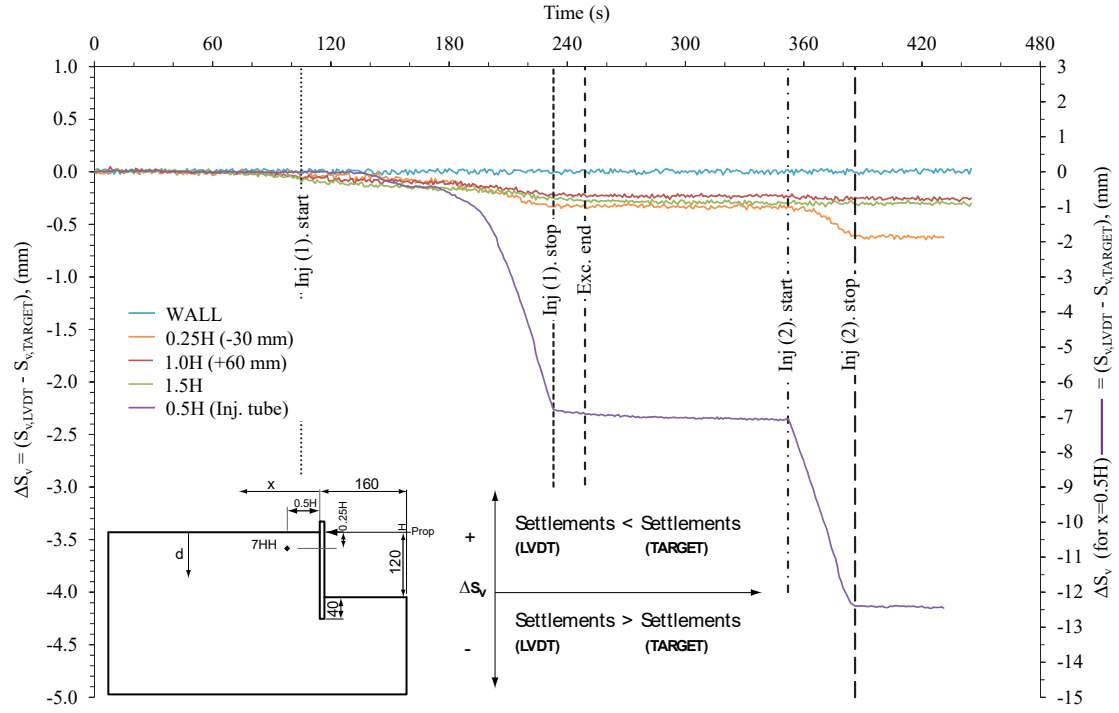


Figure 6. 10 Differences in vertical displacements between LVDTs and image processing targets during test 7HH above the wall and at distances x= 0.25H, 0.5H, 1.0H and 1.5H behind the wall.

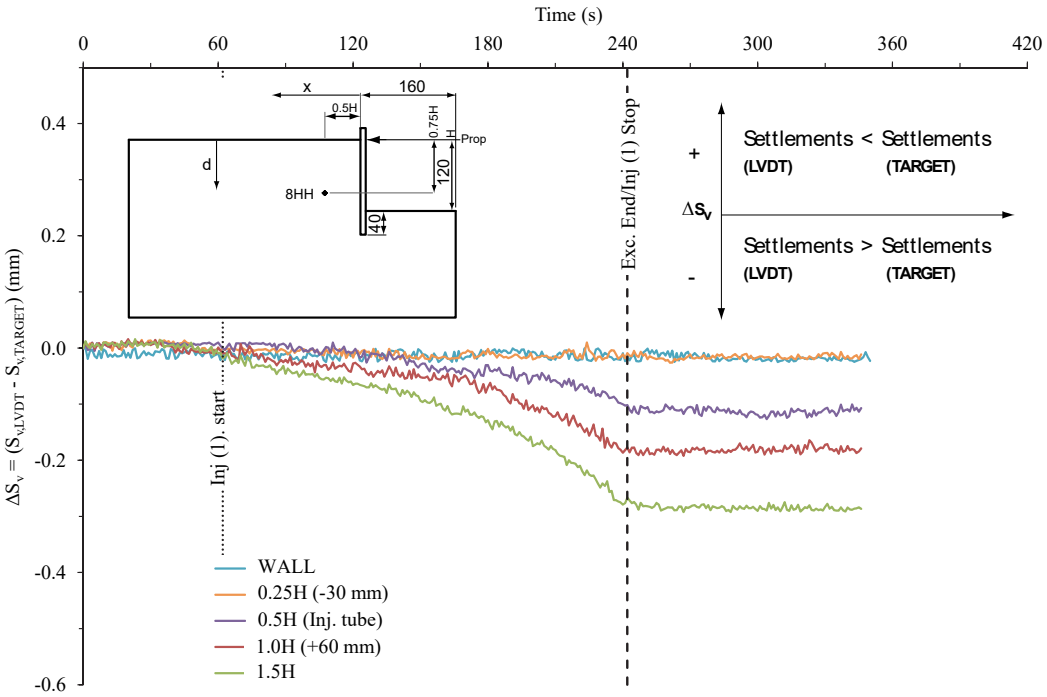


Figure 6. 11 Differences in vertical displacements between LVDTs and image processing targets during test 8HH above the wall and at distances x= 0.25H, 0.5H, 1.0H and 1.5H behind the wall.

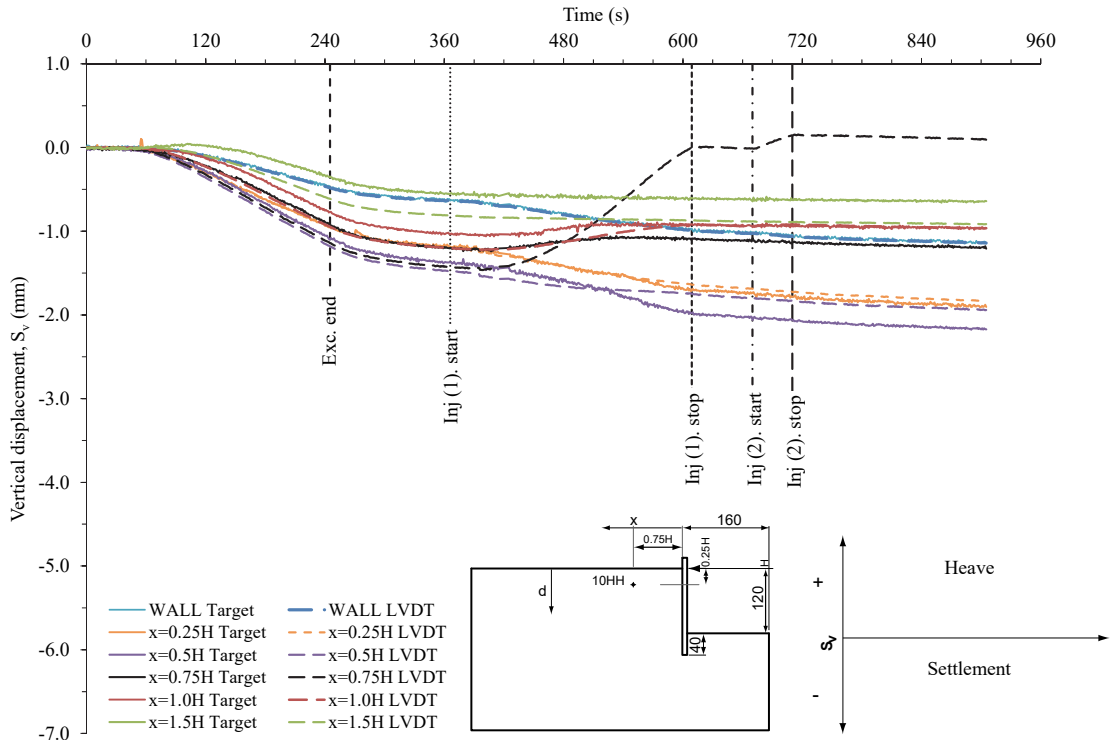


Figure 6. 12 Retained surface vertical displacements measured by LVDTs and image processing targets (15 mm below the surface) in test 10HH above the wall and at distances x= 0.25H, 0.5H, 0.75H, 1.0H and 1.5H behind the wall.

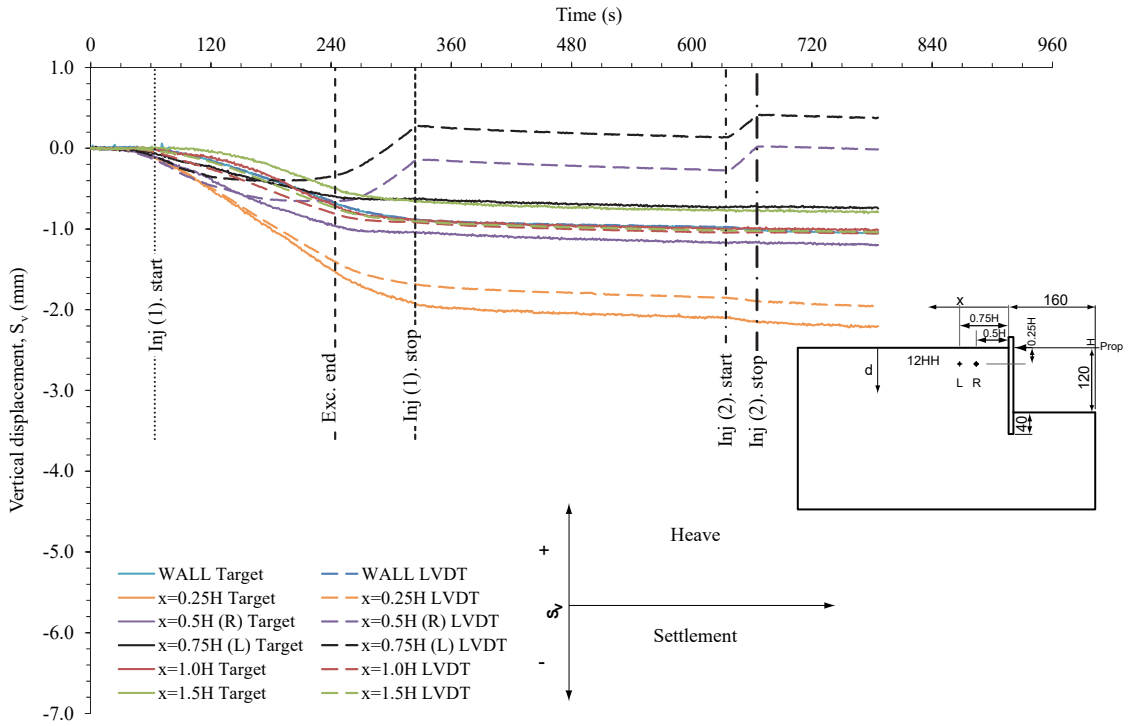


Figure 6. 13 Retained surface vertical displacements measured by LVDTs and image processing targets (15 mm below the surface) in test 12HH above the wall and at distances x= 0.25H, 0.5H, 0.75H, 1.0H and 1.5H behind the wall.

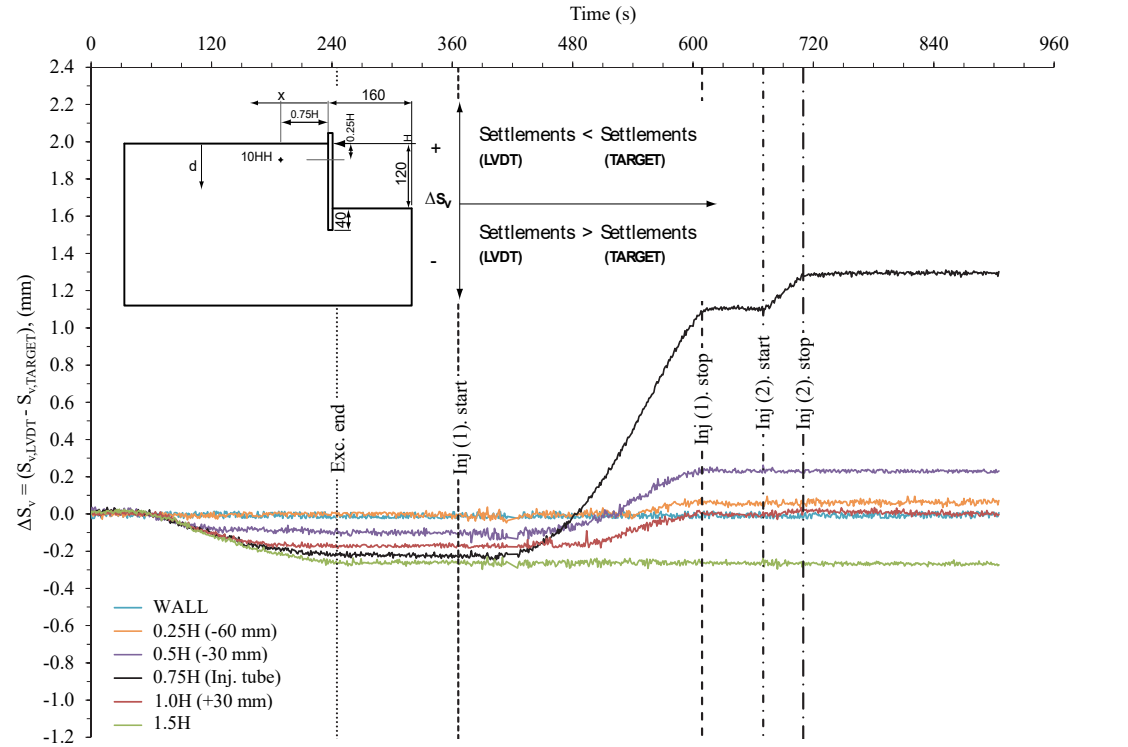


Figure 6. 14 Differences in vertical displacements between LVDTs and image processing targets during test 10HH above the wall and at distances x= 0.25H, 0.5H, 0.75H, 1.0H and 1.5H behind the wall.

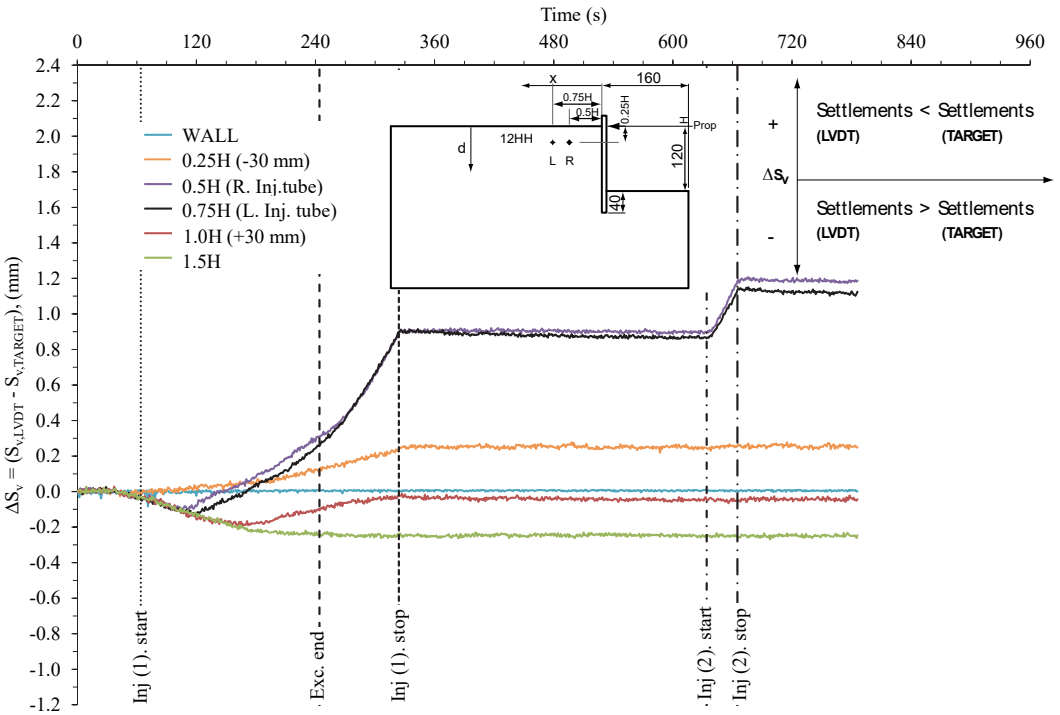


Figure 6. 15 Differences in vertical displacements between LVDTs and image processing targets during test 12HH above the wall and at distances x= 0.25H, 0.5H, 0.75H, 1.0H and 1.5H behind the wall.

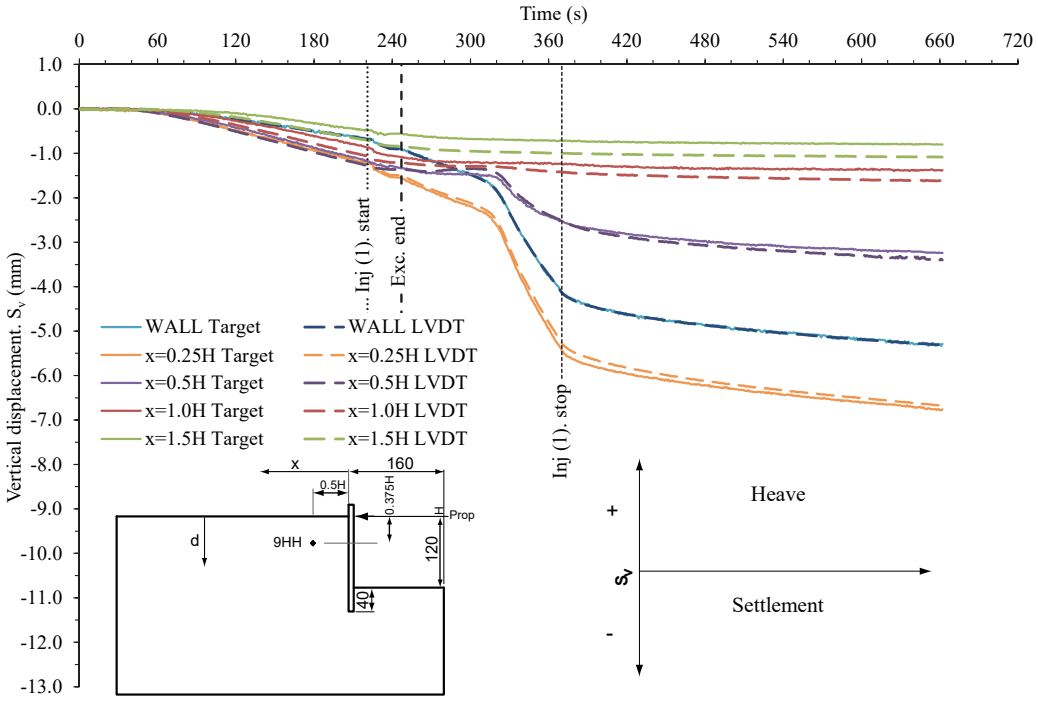


Figure 6. 16 Retained surface vertical displacements measured by LVDTs and image processing targets (15 mm below the surface) in test 9HH above the wall and at distances x= 0.25H, 0.5H, 1.0H and 1.5H behind the wall.

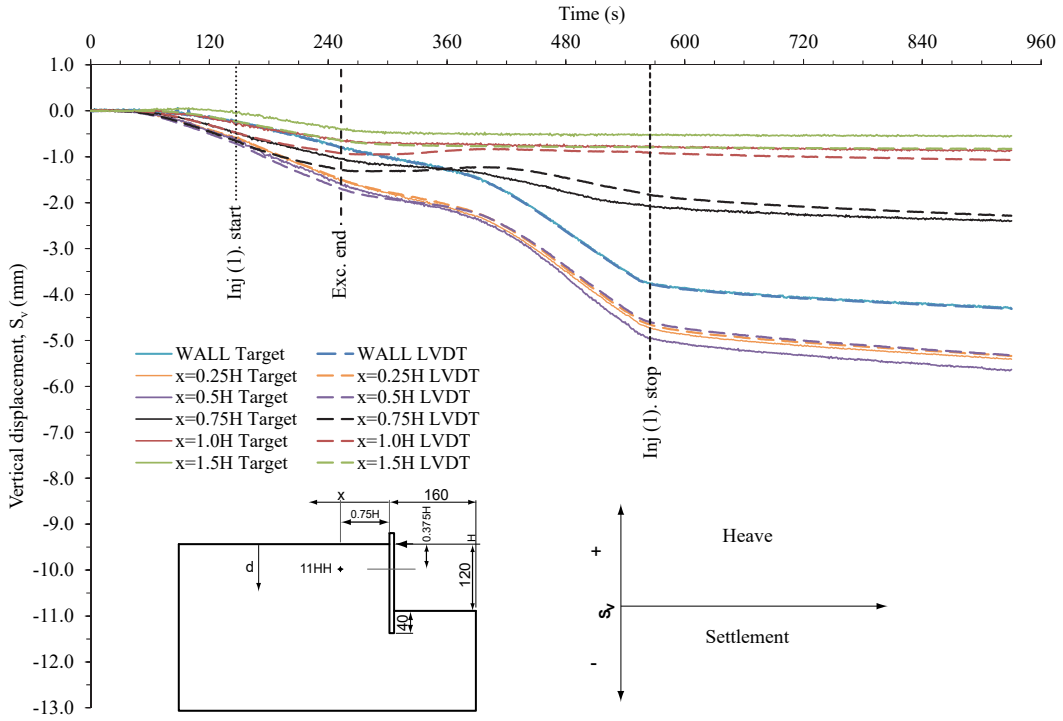


Figure 6. 17 Retained surface vertical displacements measured by LVDTs and image processing targets (15 mm below the surface) in test 11HH above the wall and at distances x= 0.25H, 0.5H, 0.75H, 1.0H and 1.5H behind the wall.

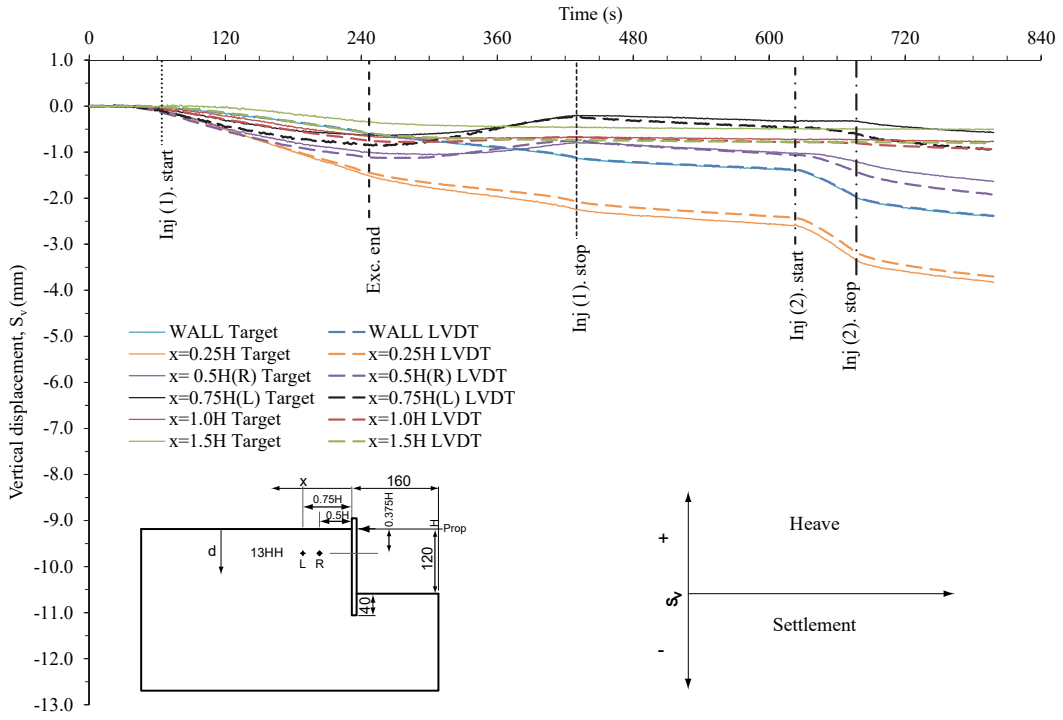


Figure 6. 18 Retained surface vertical displacements measured by LVDTs and image processing targets (15 mm below the surface) in test 13HH above the wall and at distances x= 0.25H, 0.5H, 0.75H, 1.0H and 1.5H behind the wall.

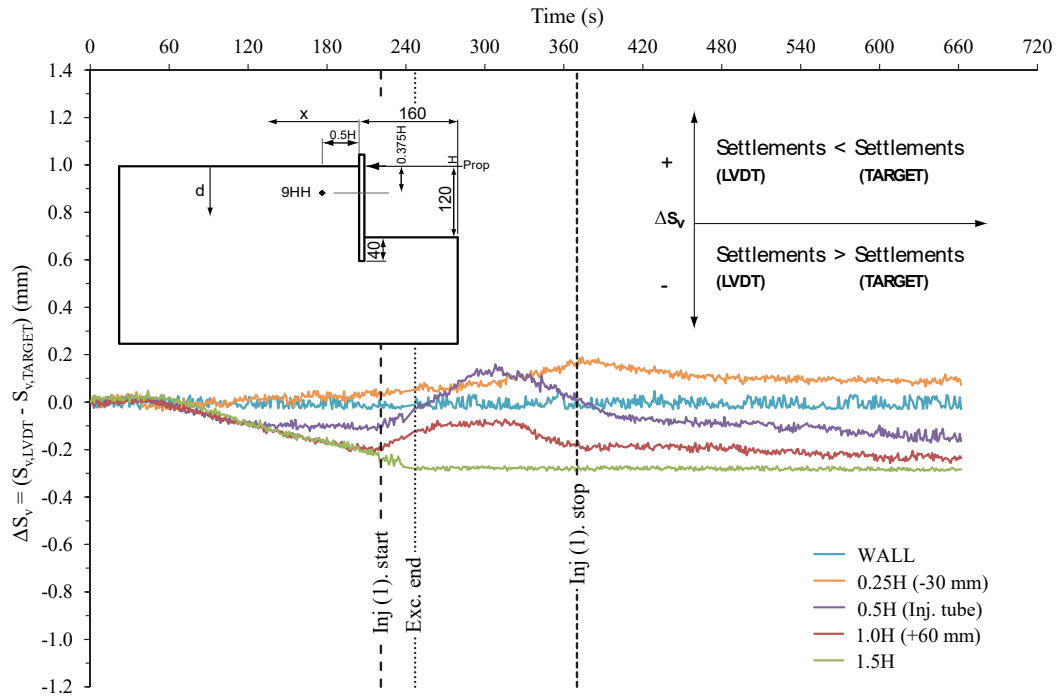


Figure 6. 19 Differences in vertical displacements between LVDTs and image processing targets during test 9HH above the wall and at distances x= 0.25H, 0.5H, 1.0H and 1.5H behind the wall.

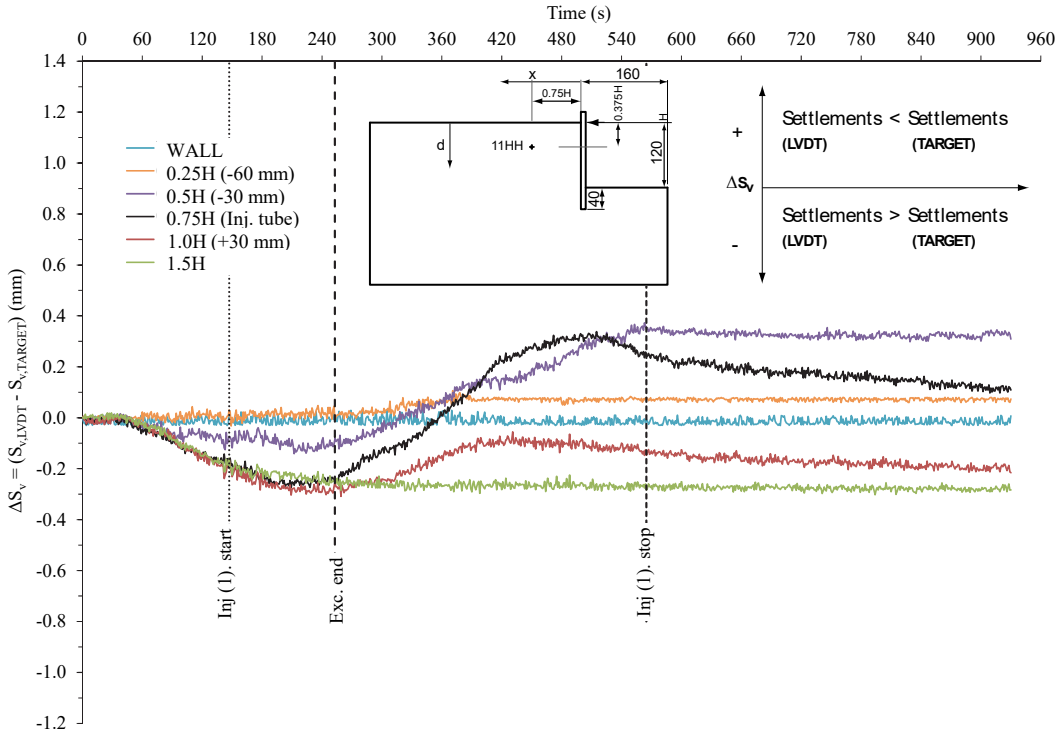


Figure 6. 20 Differences in vertical displacements between LVDTs and image processing targets during test 11HH above the wall and at distances x= 0.25H, 0.5H, 0.75H, 1.0H and 1.5H behind the wall.

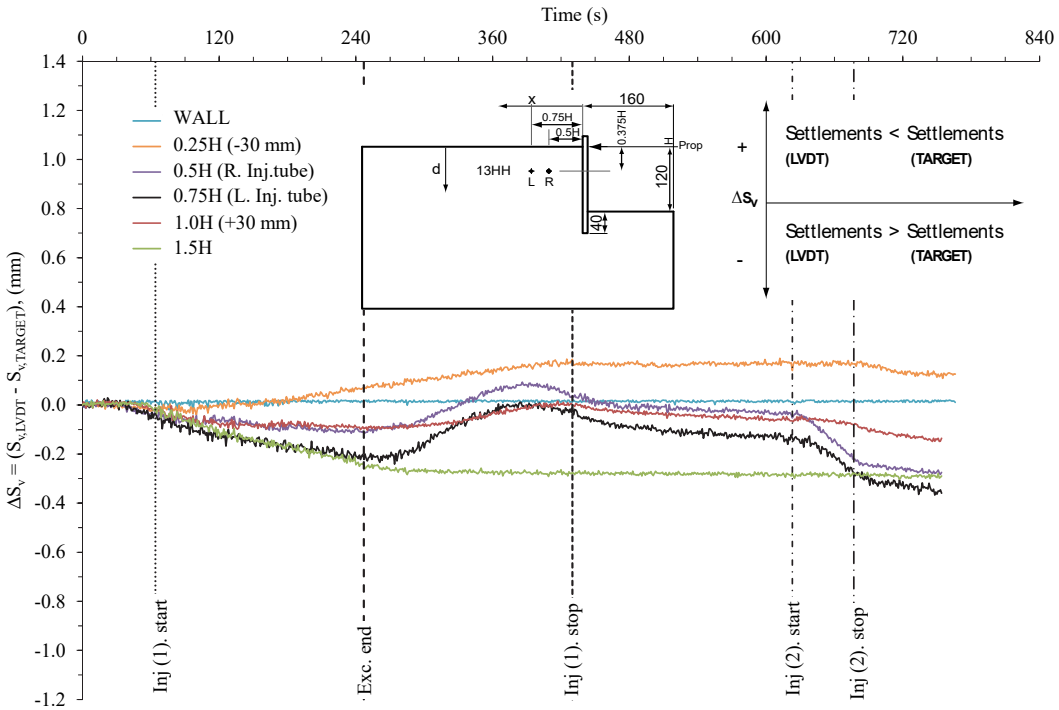


Figure 6. 21 Differences in vertical displacements between LVDTs and image processing targets during test 13HH above the wall and at distances x= 0.25H, 0.5H, 0.75H, 1.0H and 1.5H behind the wall.

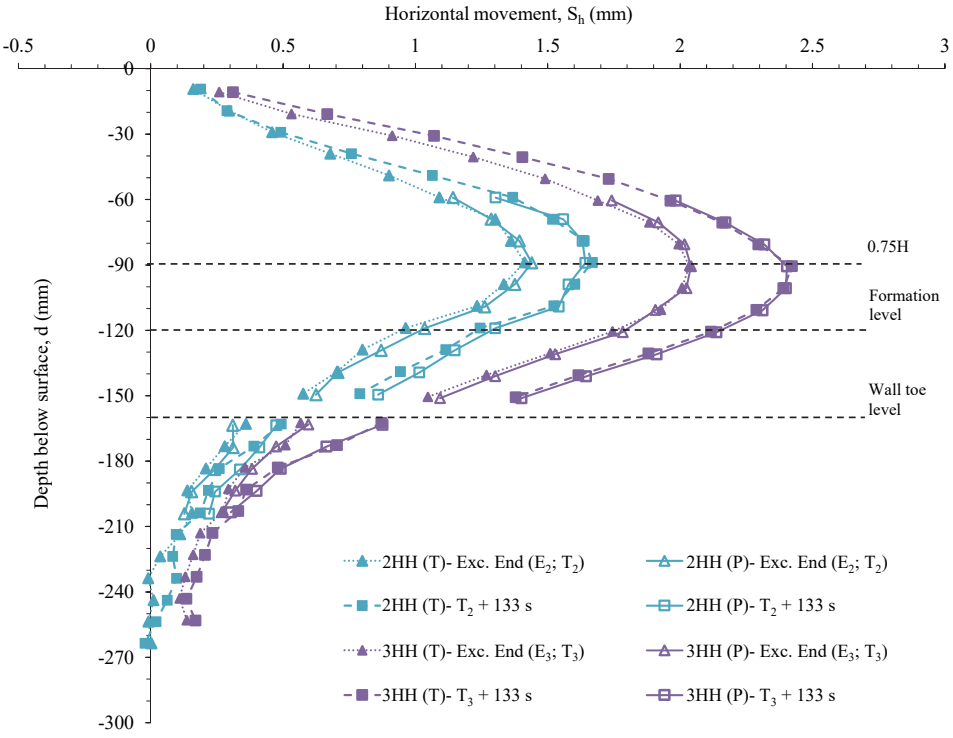


Figure 6. 22 Horizontal wall target displacements measured using the embedded image processing targets from the TELI and PULNIX cameras in tests 2-3HH.

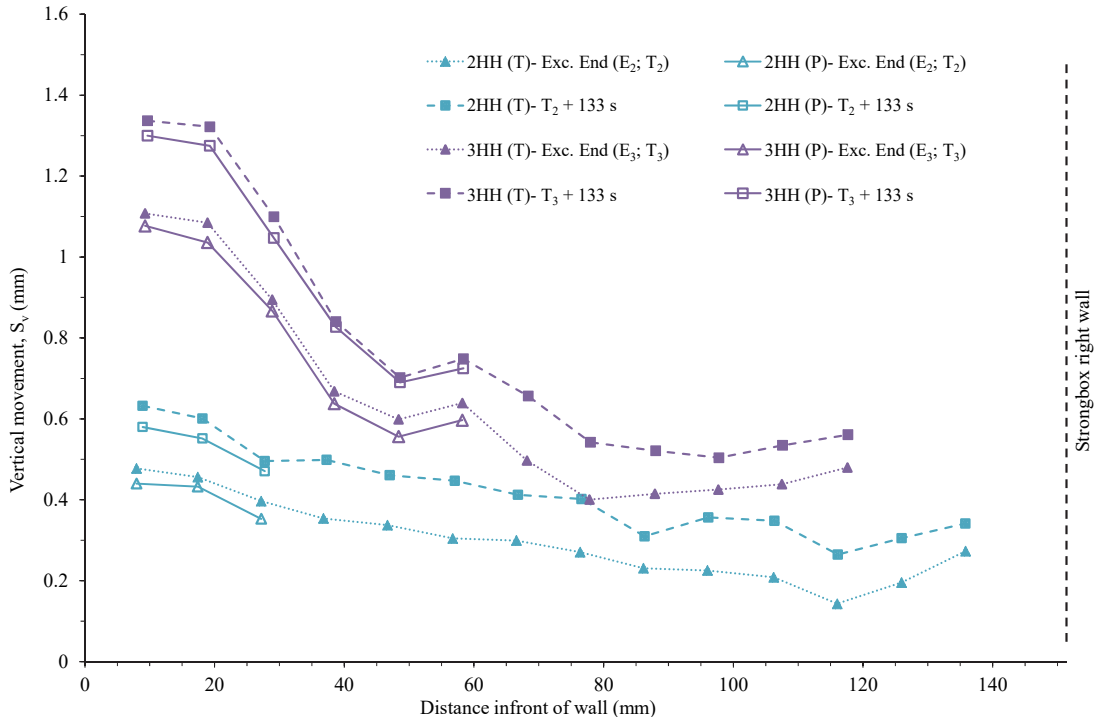


Figure 6. 23 Vertical formation level target displacements measured using the embedded image processing targets from the TELI and PULNIX cameras in tests 2-3HH.

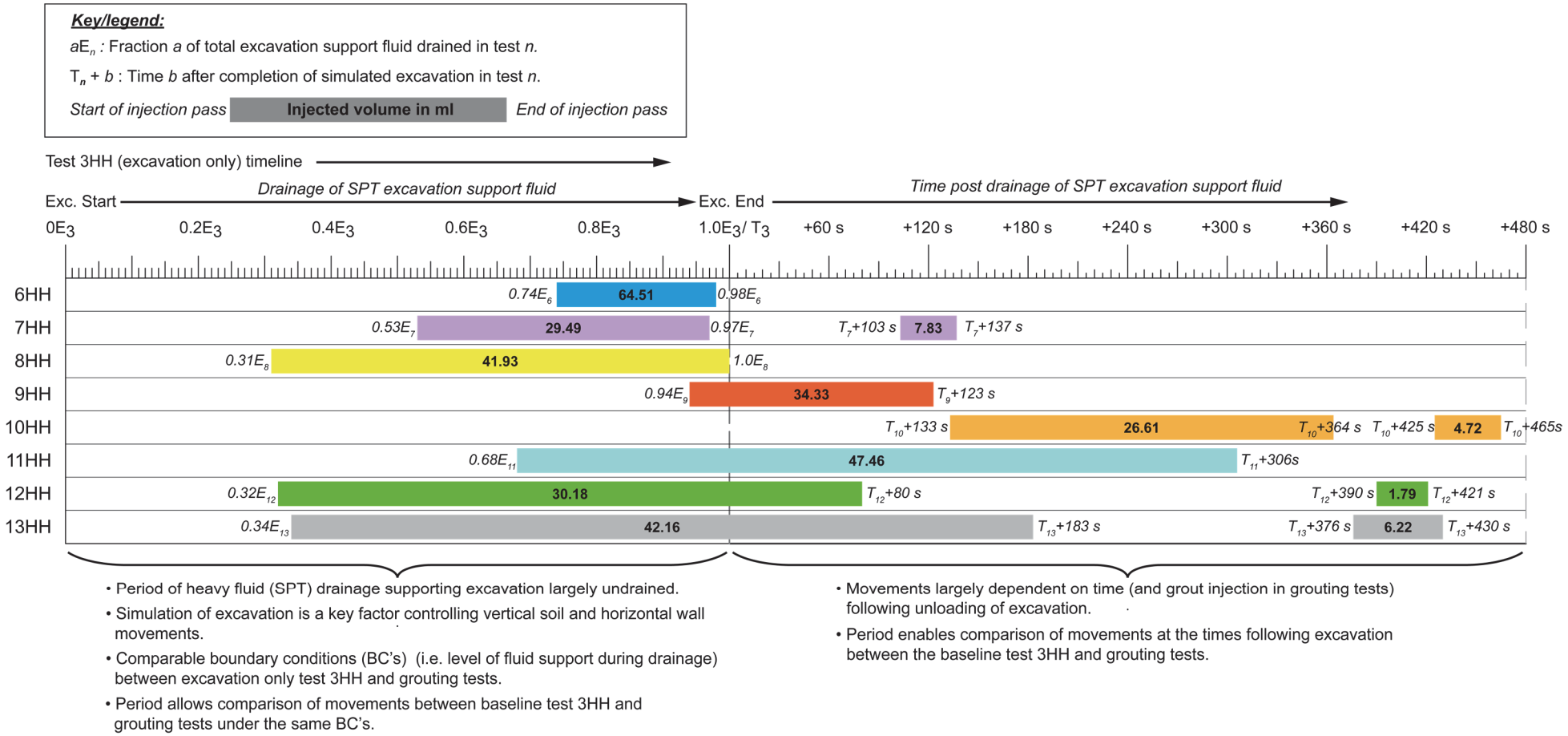


Figure 6. 24 Gantt chart showing the injection events (with grout volumes injected) in tests 6-13HH with reference to the fraction of excavation progression (relative support fluid level) and time elapsed after excavation in baseline test 3HH to enable comparison of movements.

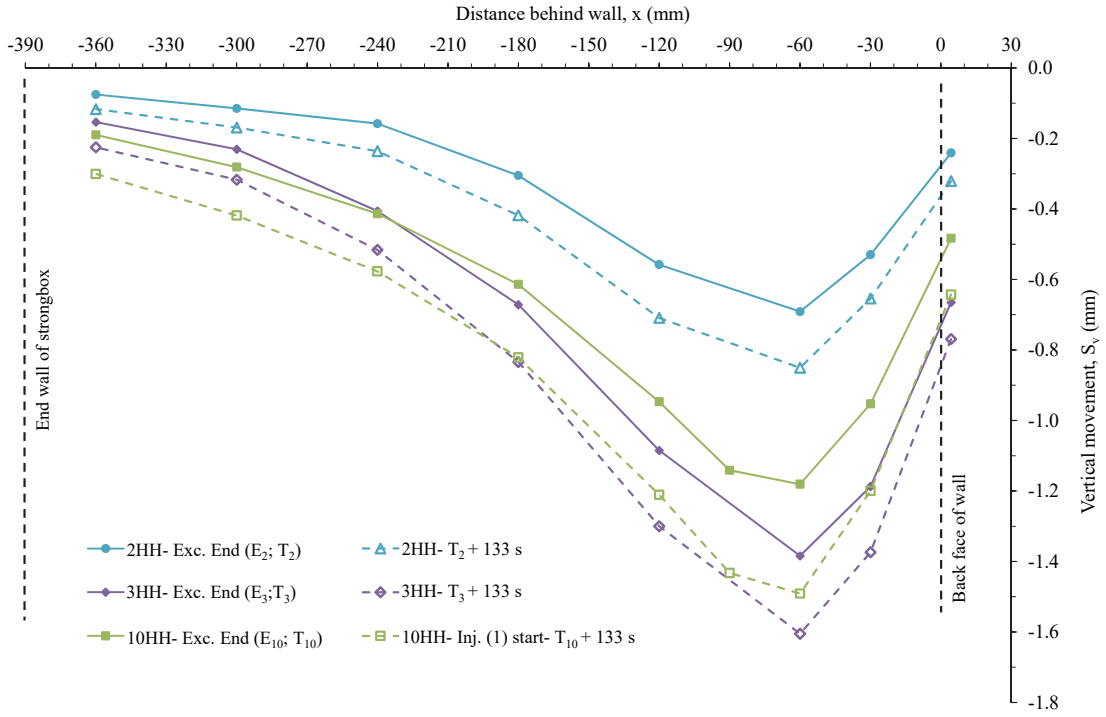


Figure 6. 25 Vertical LVDT retained surface displacements at the end of excavation and 133 s after for tests 2HH, 3HH and 10HH (prior to the start of injection in 10HH).

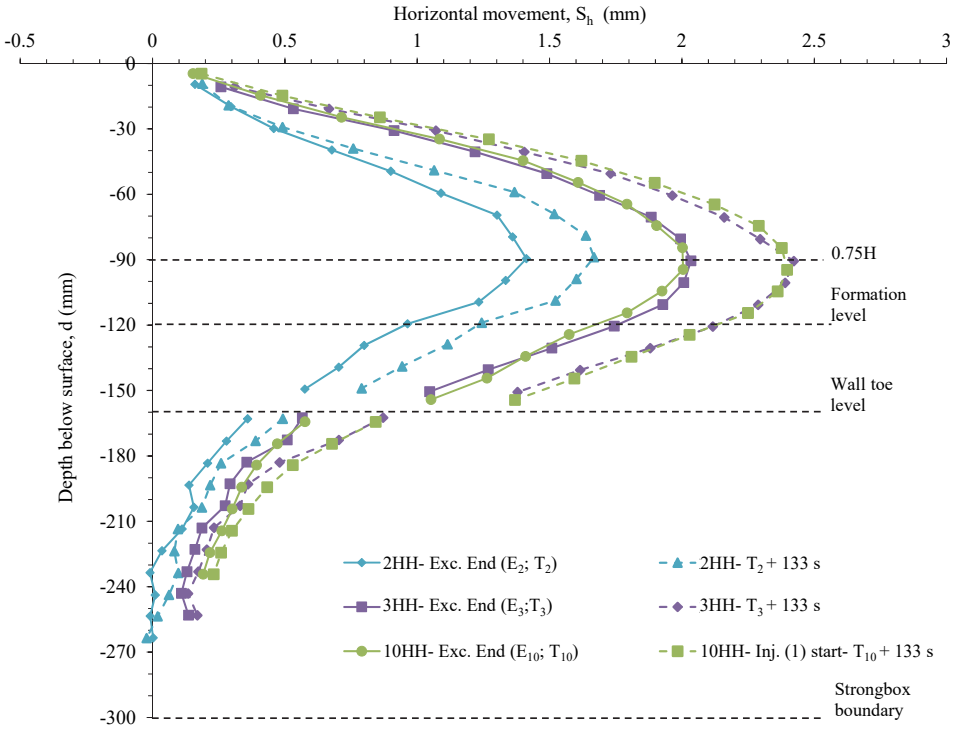


Figure 6. 26 Horizontal displacements of the retaining wall and soil beneath using image processing for tests 2HH, 3HH and 10HH at the end of excavation and 133 s after (prior to the start of injection in test 10HH).

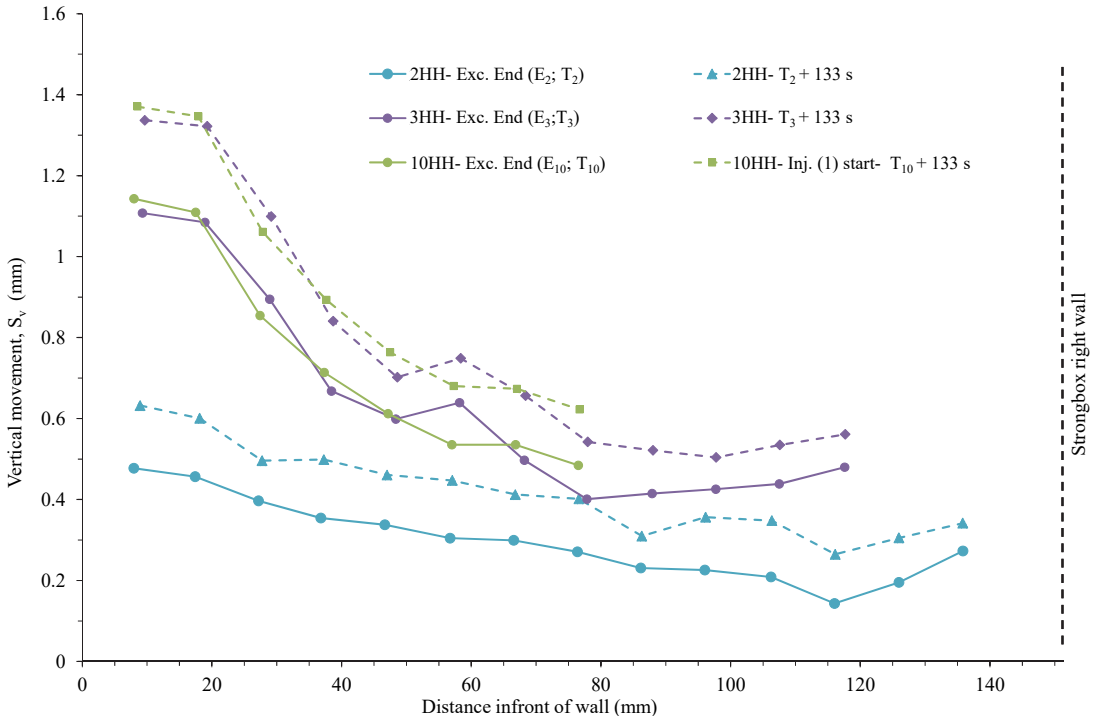


Figure 6. 27 Vertical displacements at the formation level using image processing for tests 2HH, 3HH and 10HH at the end of excavation and 133 s after (prior to the start of injection in test 10HH).

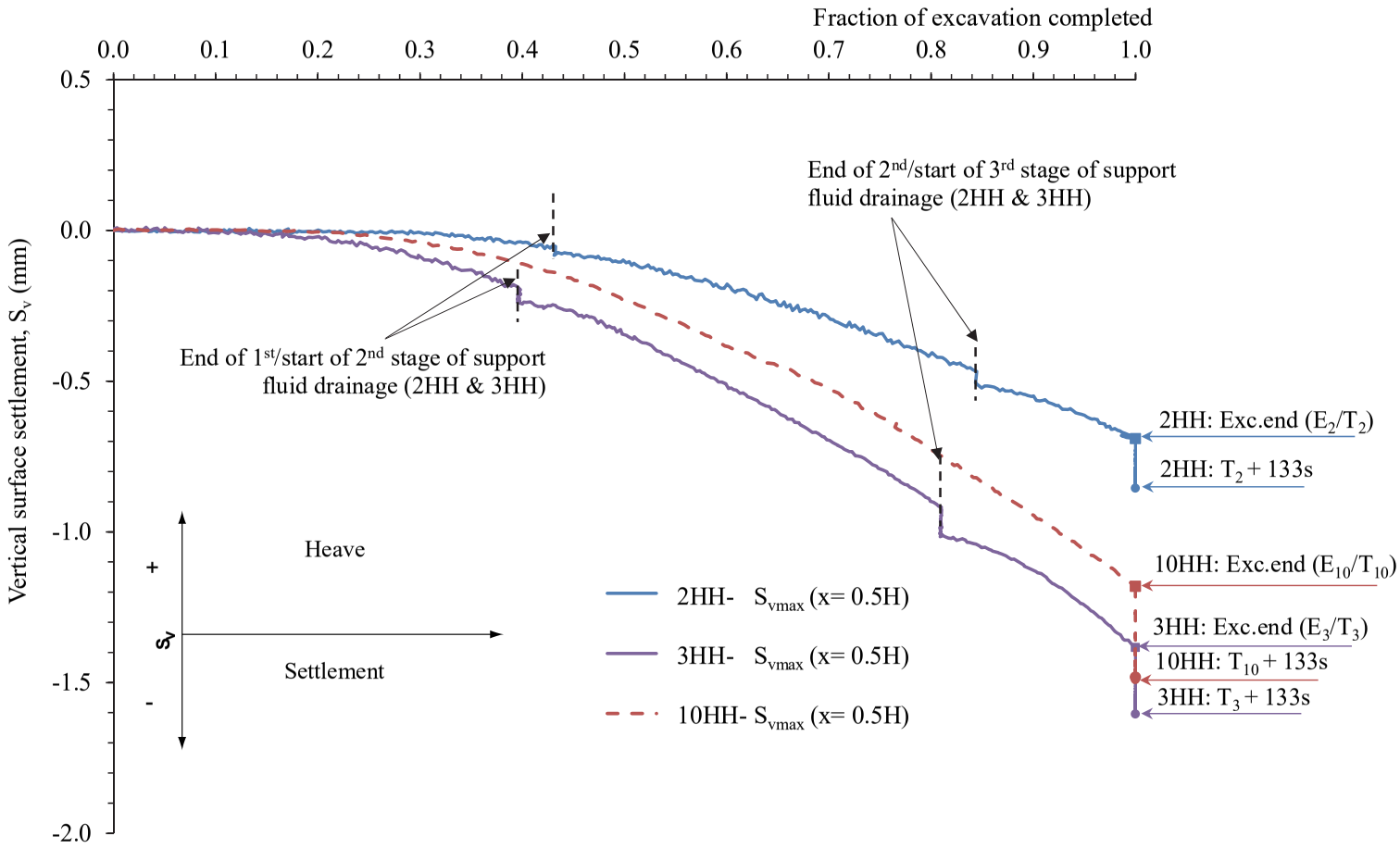


Figure 6. 28 Development of the excavation induced maximum vertical surface settlements measured by the LVDTs at distance x= 0.5H (position of S_{vmax}) behind the wall in tests 2HH, 3HH and 10HH, up to 133 s after excavation.

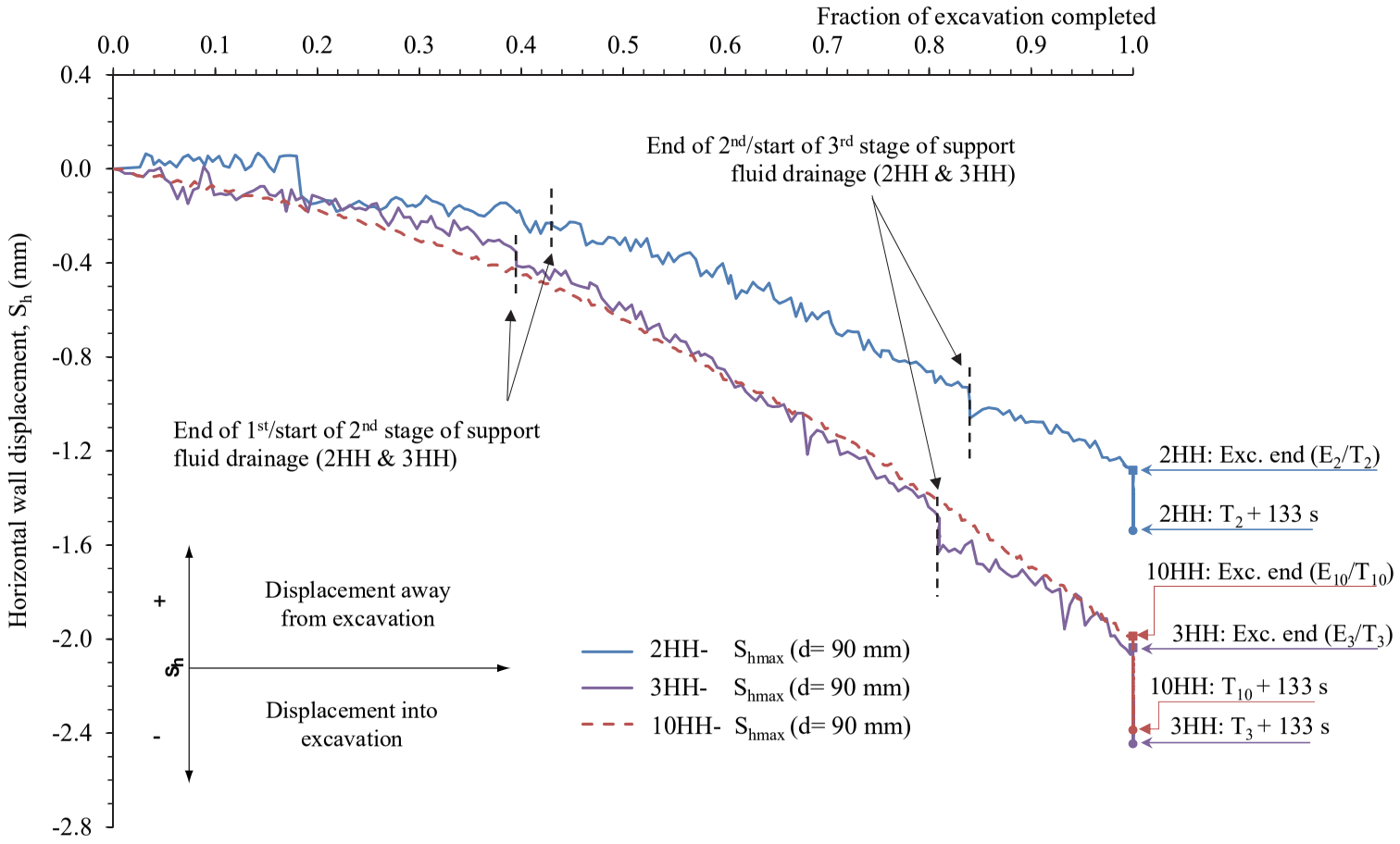


Figure 6. 29 Development of the excavation induced maximum horizontal wall displacements (S_{hmax}) at depth d= 0.75H (90 mm) below the retained surface in tests 2HH, 3HH and 10HH, up to 133 s after excavation.

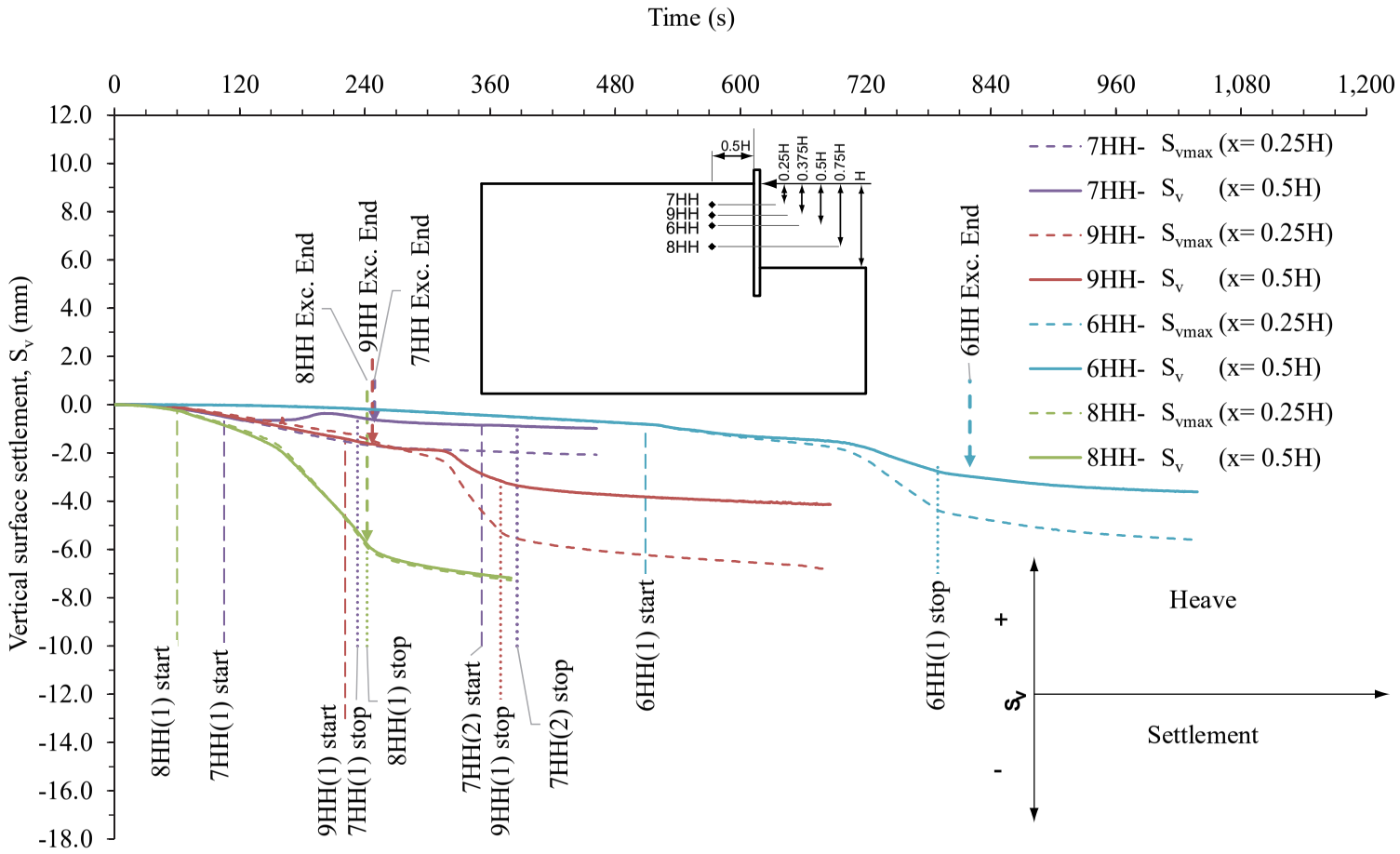


Figure 6. 30 Development of vertical surface settlements (S_v) measured by LVDTs at distances x= 0.25H and 0.5H (above the injection tube) behind the wall in tests 6-9HH.

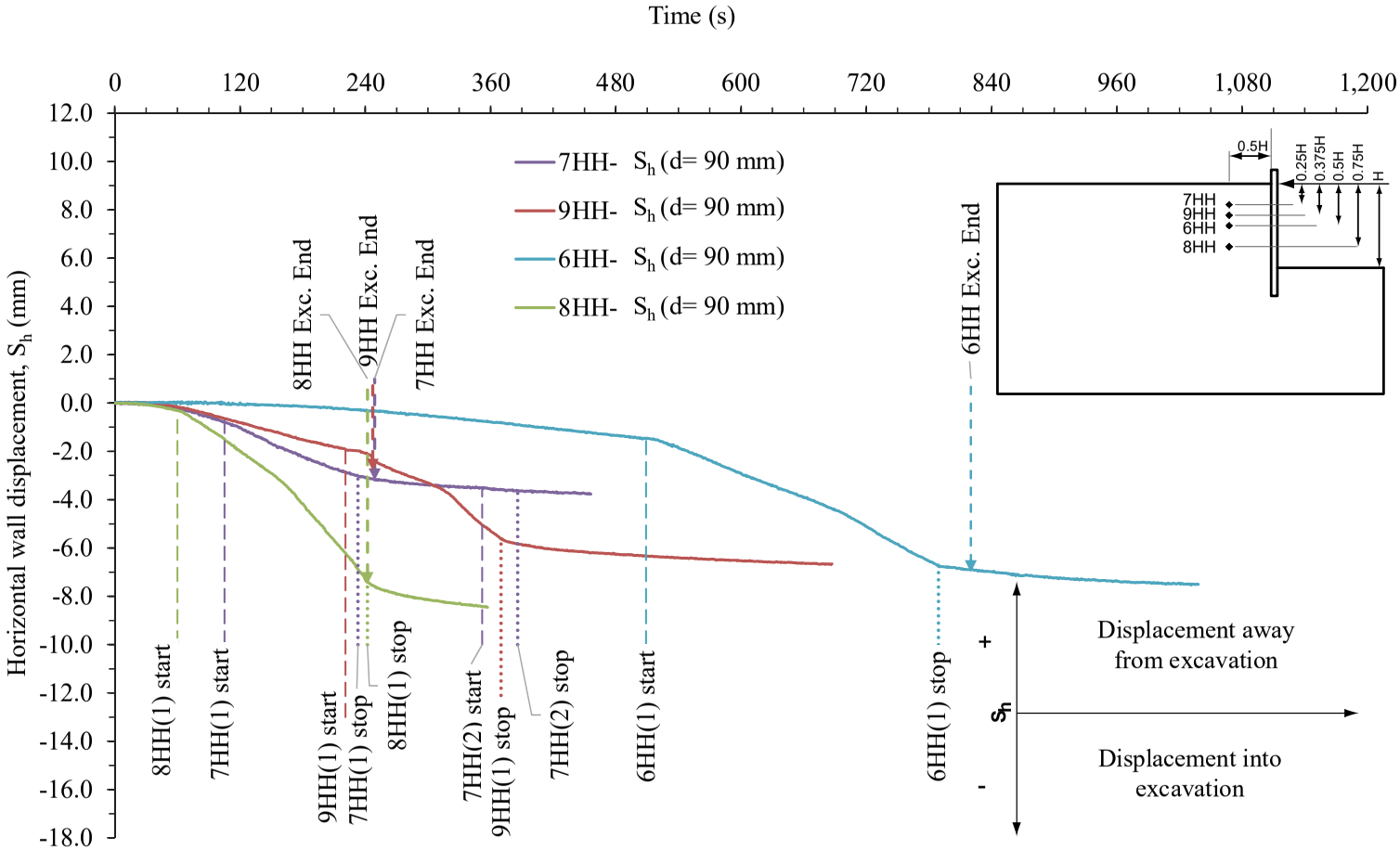


Figure 6. 31 Development of horizontal wall displacements (S_h) at depth d= 0.75H (90 mm) below the retained surface in tests 6-9HH.

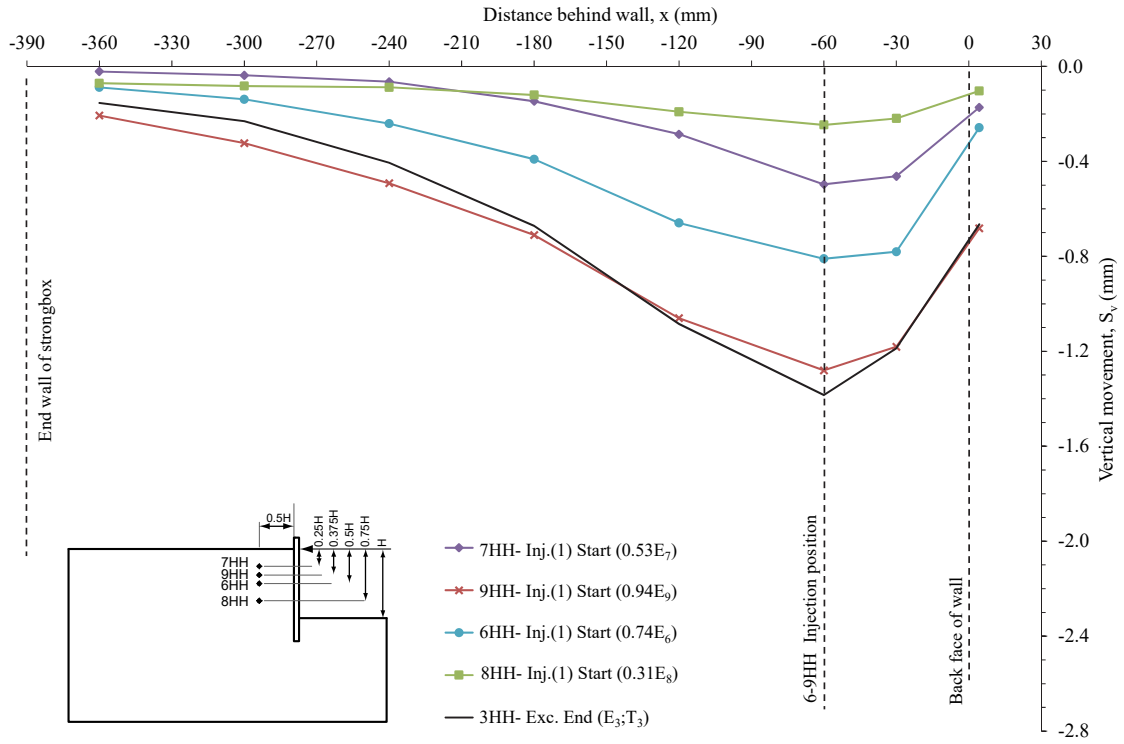


Figure 6. 32 Vertical LVDT retained surface displacements at the start of the 1st injection events in tests 6-9HH against the end of excavation surface settlement envelope in baseline test 3HH.

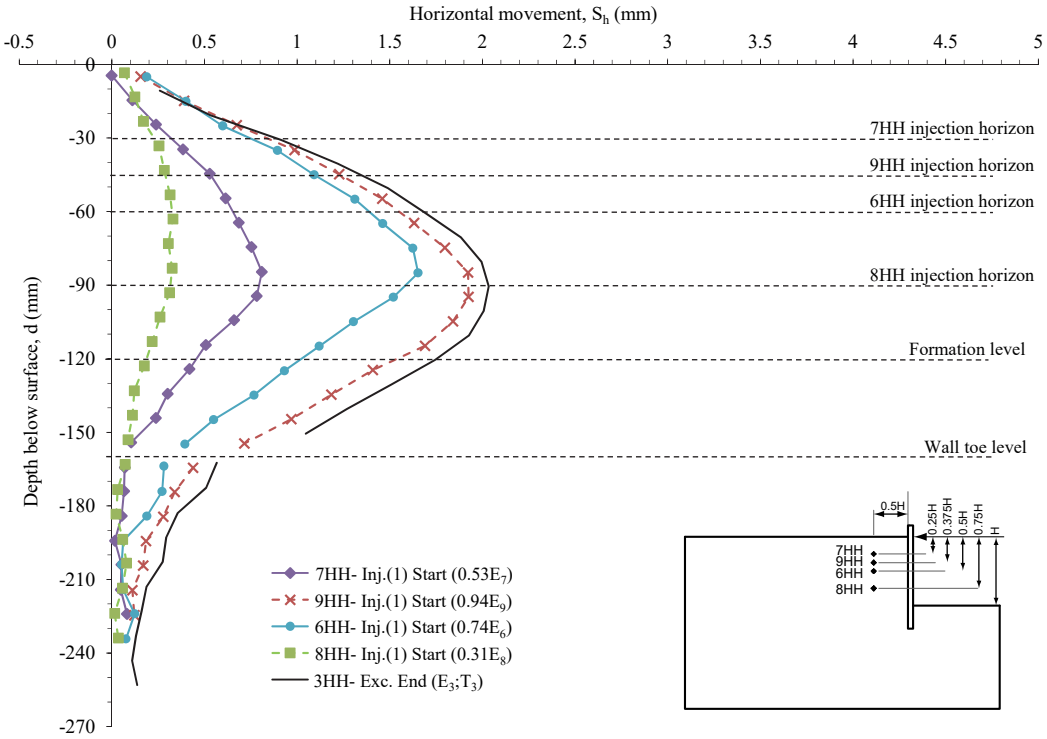


Figure 6. 33 Horizontal wall movements at the start of the 1st injection events in tests 6-9HH against the end of excavation wall displacements profile in baseline test 3HH.

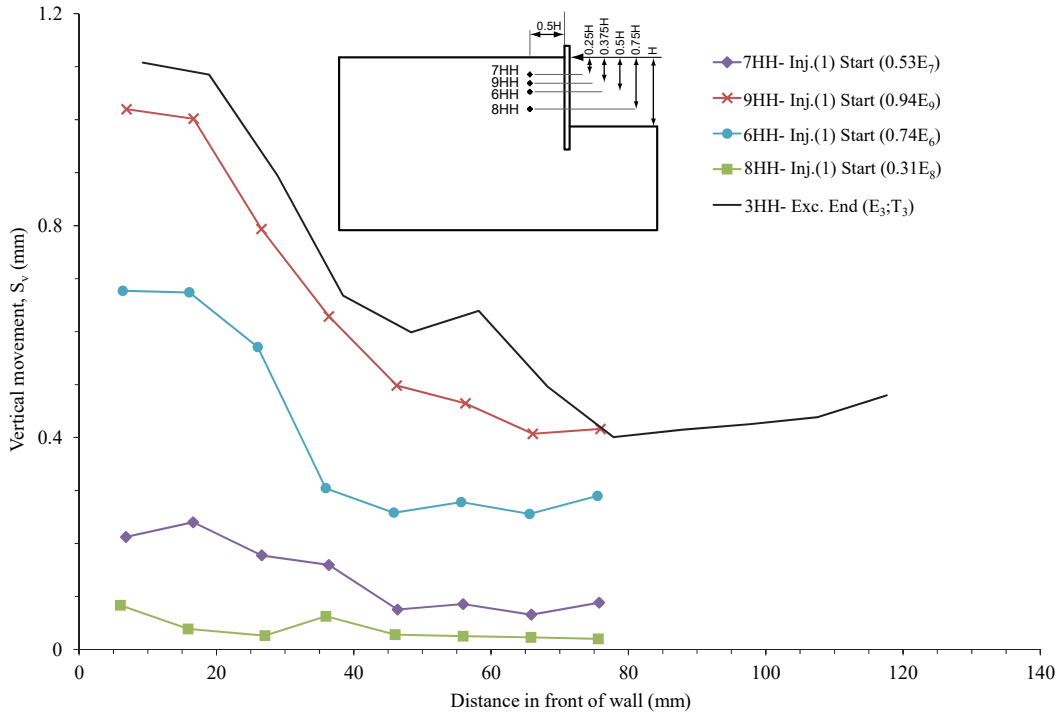


Figure 6. 34 Vertical formation level movements at the start of the 1st injection events in tests 6-9HH against the end of excavation formation level movement envelope in baseline test 3HH.

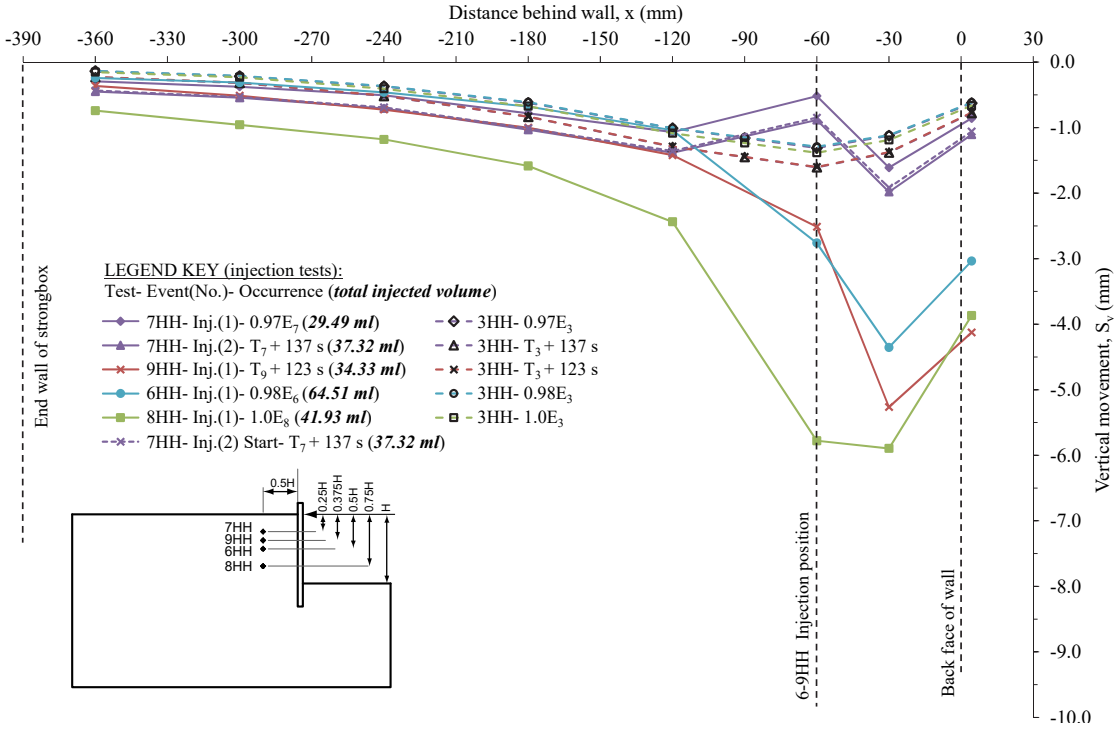


Figure 6. 35 Vertical LVDT retained surface displacements at the end of the injection events in tests 6-9HH (and start of the 2nd injection event in test 7HH) compared to equivalent stages in baseline test 3HH.

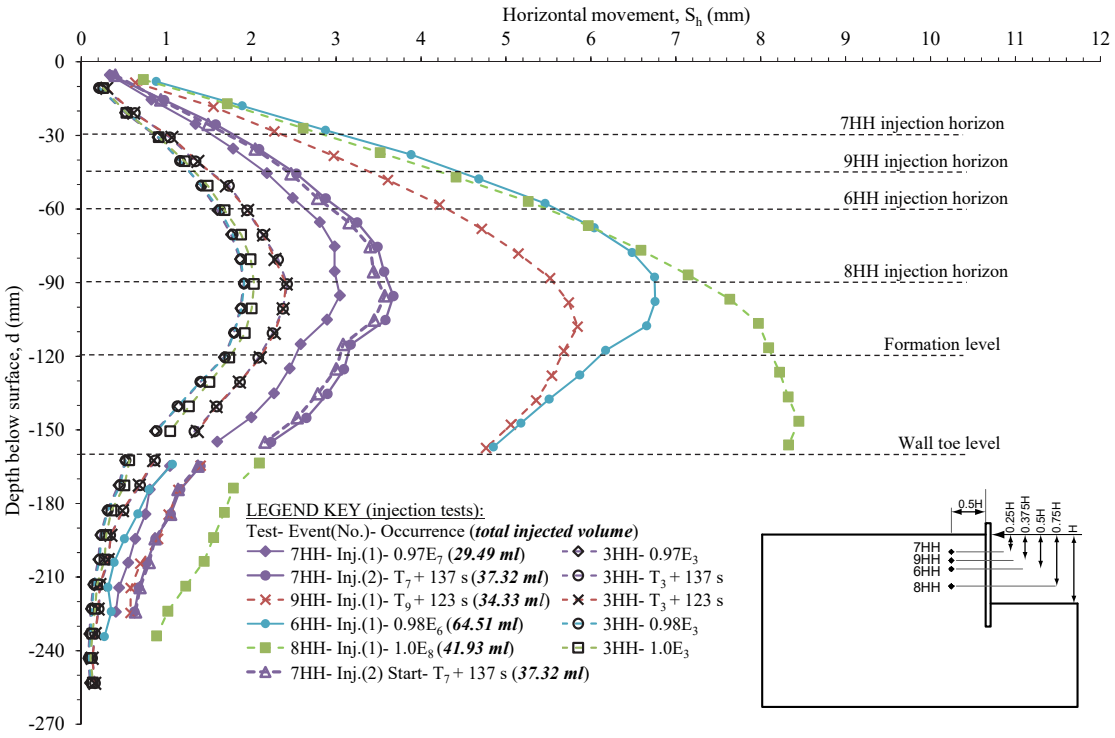


Figure 6. 36 Horizontal wall movements at the end of the injection events in tests 6-9HH (and start of the 2nd injection event in test 7HH) compared to equivalent stages in baseline test 3HH.

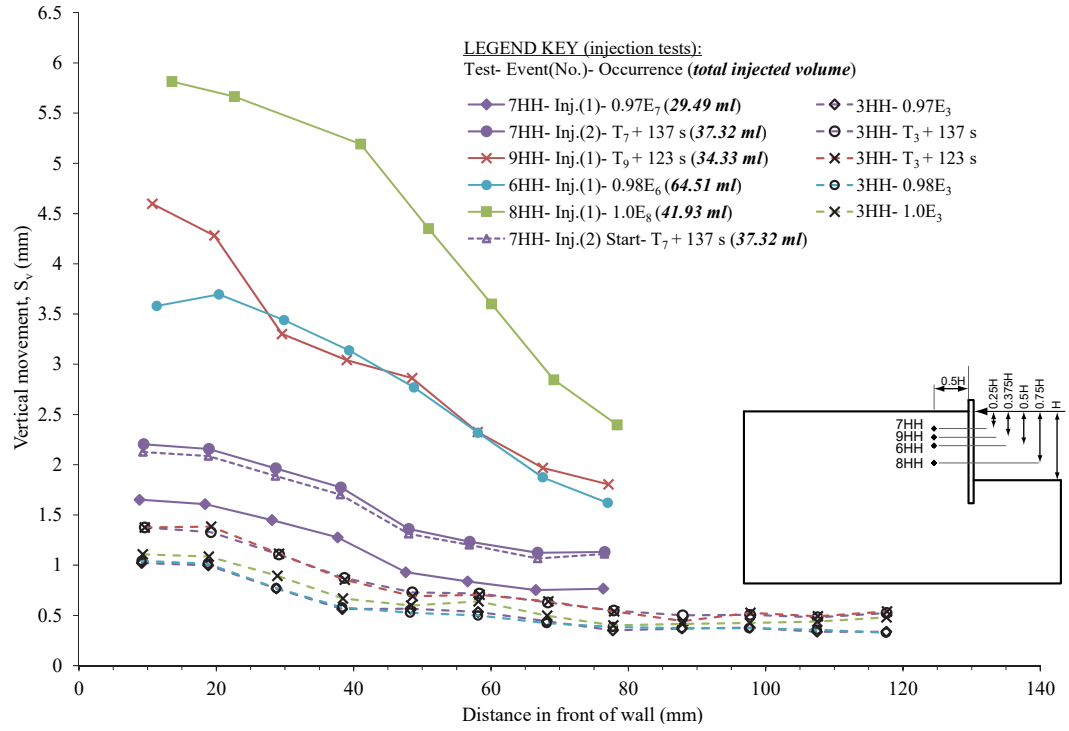


Figure 6. 37 Vertical formation level movements at the end of the injection events in tests 6-9HH (and start of the 2nd injection event in test 7HH) compared to equivalent stages in baseline test 3HH.

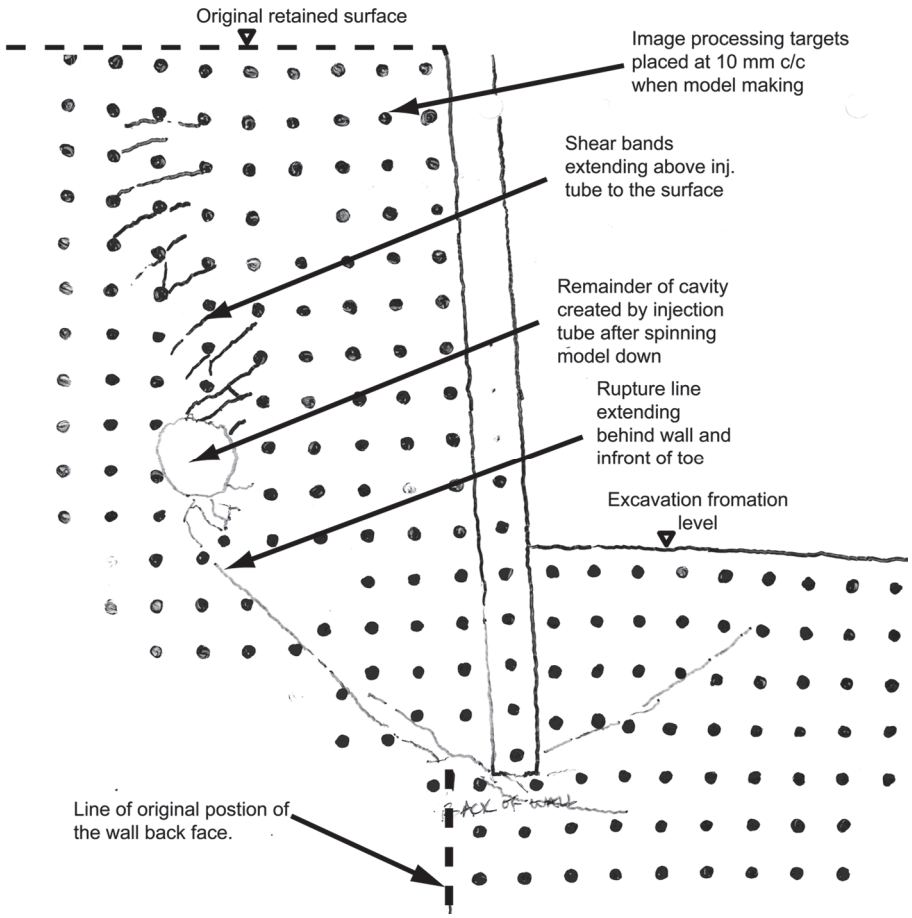


Figure 6. 38 Rupture lines behind and in front of the wall and shear bands above the injection location at the end of test 8HH (traced following removal of the model from the centrifuge swing and removal of the latex injection tube).

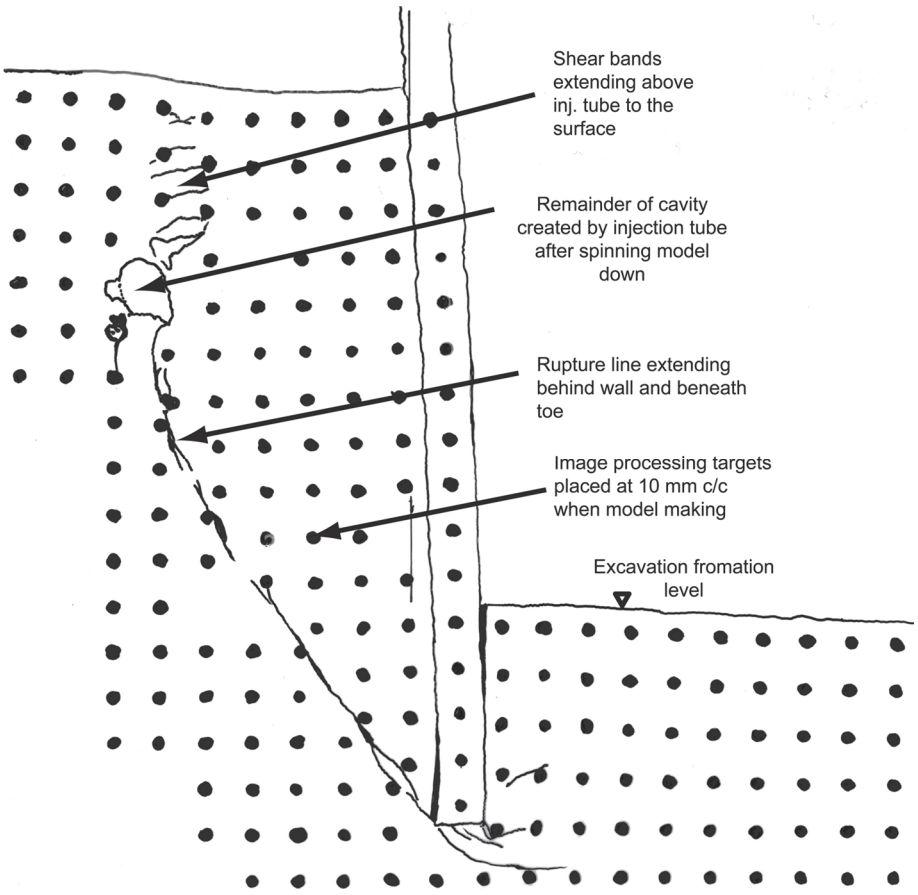
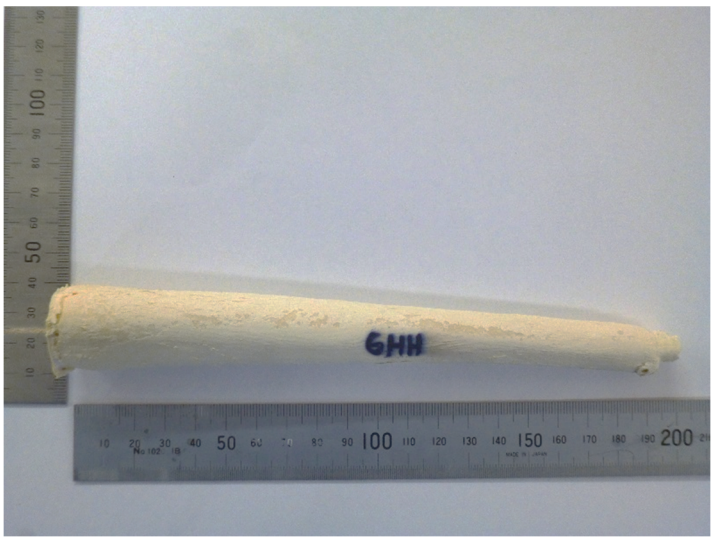
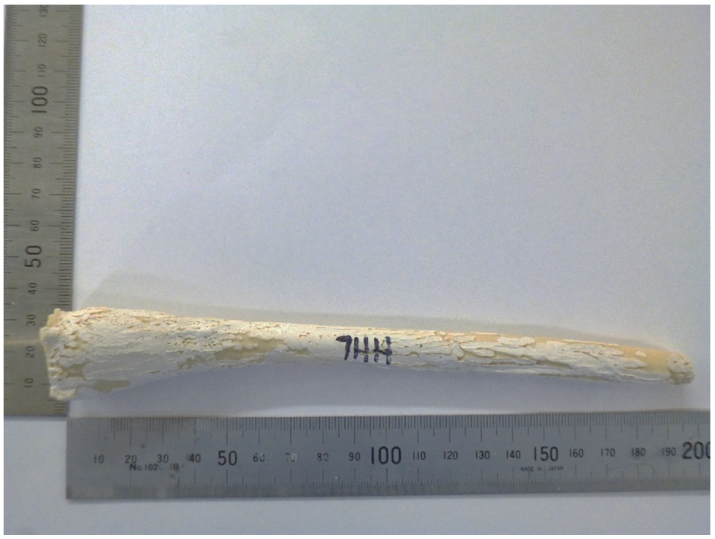


Figure 6. 39 Rupture lines behind and beneath the wall and shear bands above the injection location at the end of test 9HH (traced following removal of the model from the centrifuge swing and removal of the latex injection tube).

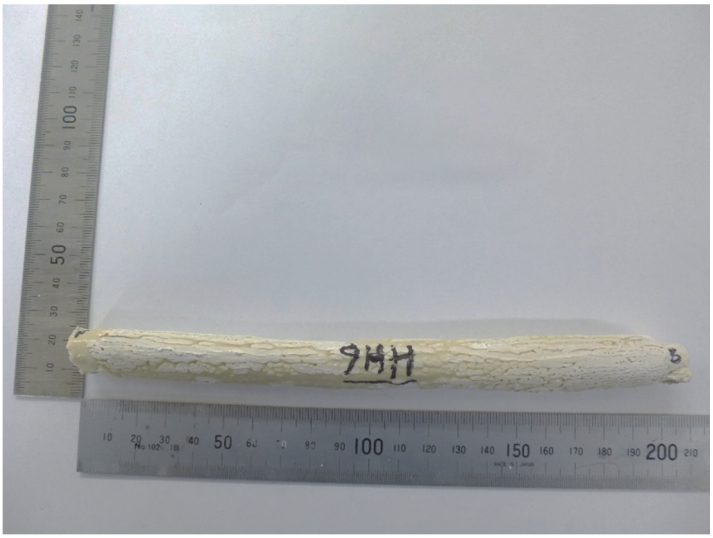


(a)

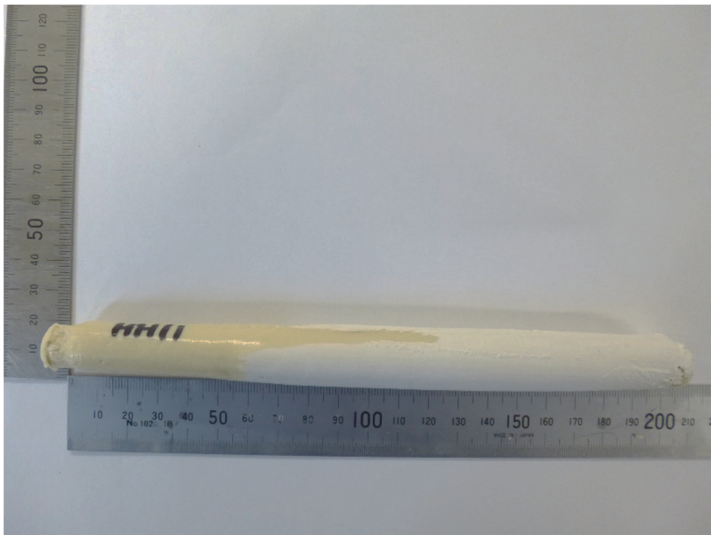


(b)

Figure 6. 40 Photographs of the post-test resin castings of the cavities created by the injection tubes for tests: (a) 6HH and (b) 7HH, showing the tapered shape created without the provision of the front brass retaining collar on the injection tubes.



(a)



(b)

Figure 6. 41 Photographs of the typical uniform cylindrical post-test resin castings of the cavities created by the injections tubes provided with the front brass retaining collar for tests: (a) 9HH and (b) 11HH.

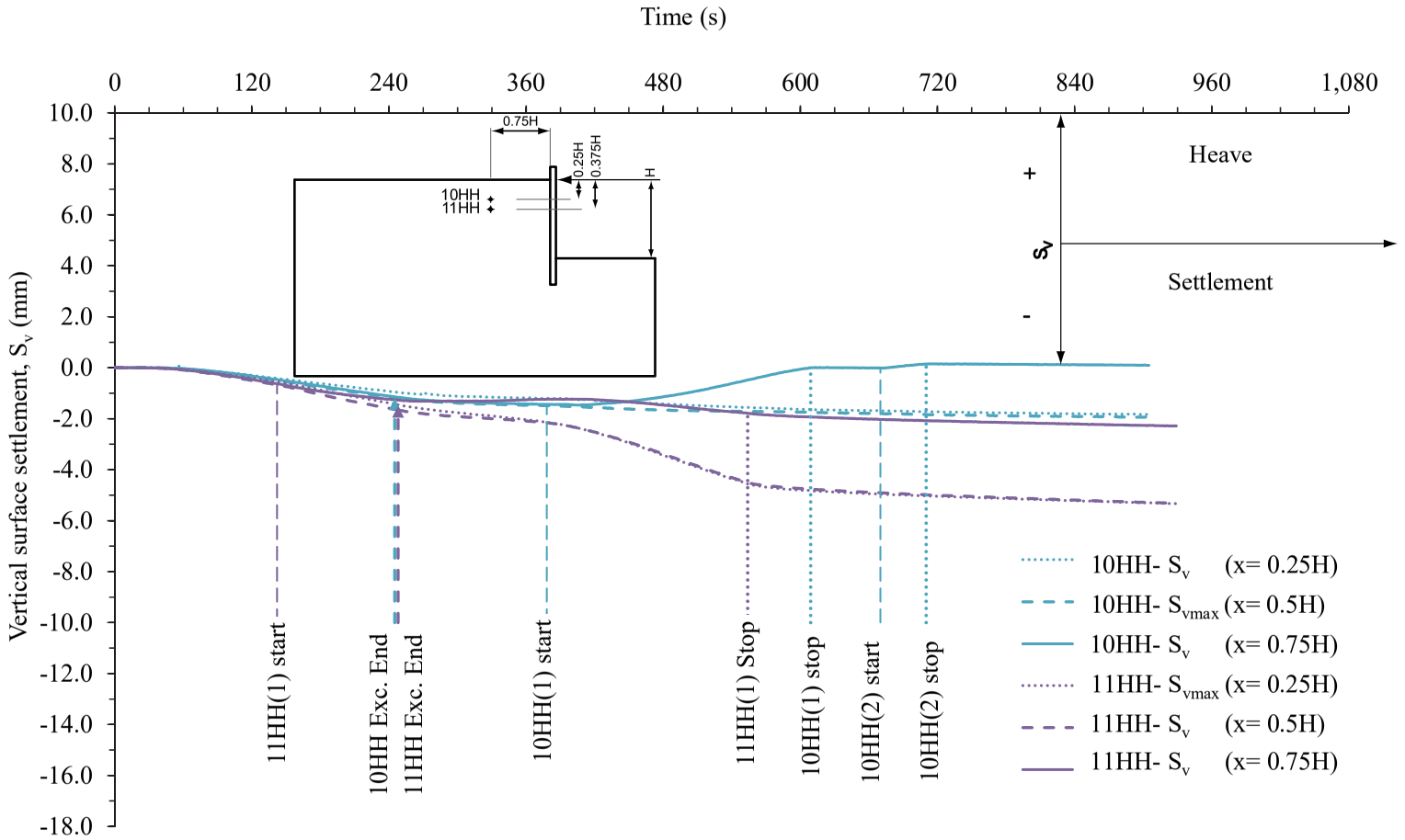


Figure 6. 42 Development of vertical surface settlements (S_v) measured by LVDTs at distances x= 0.25H, 0.5H and 0.75H (above the injection tube) behind the wall in tests 10-11HH.

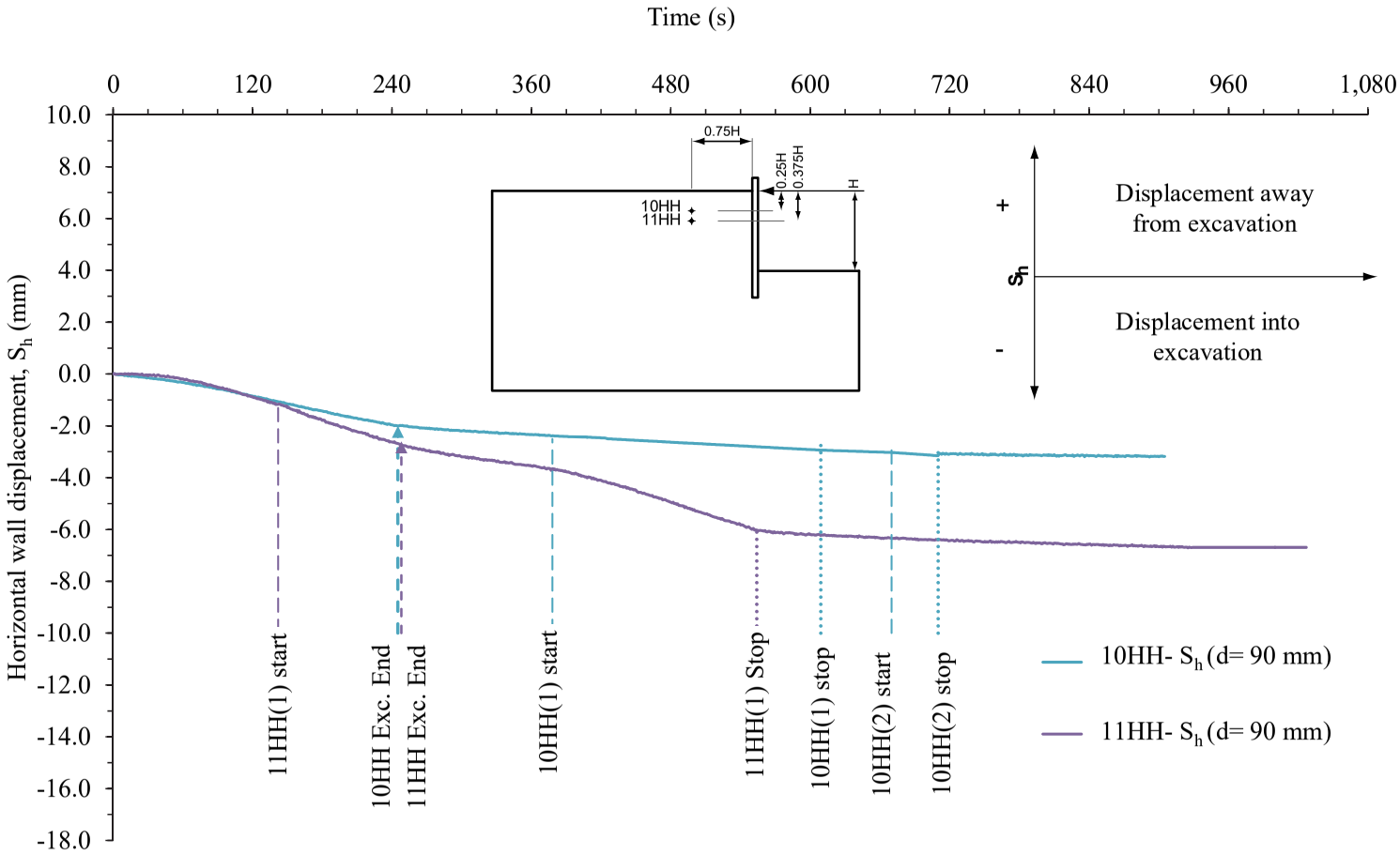


Figure 6. 43 Development of horizontal wall displacements (S_h) at depth d= 0.75H (90 mm) below the retained surface in tests 10-11HH.

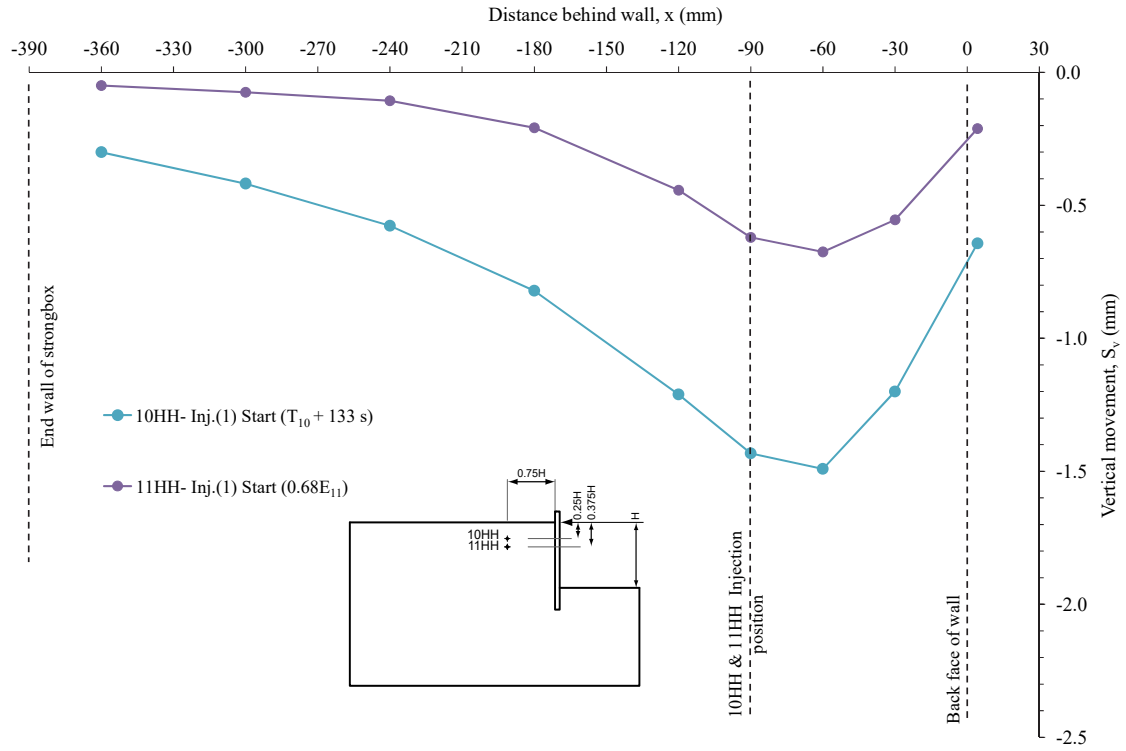


Figure 6. 44 Vertical LVDT retained surface displacements at the start of the 1st injection events in tests 10-11HH.

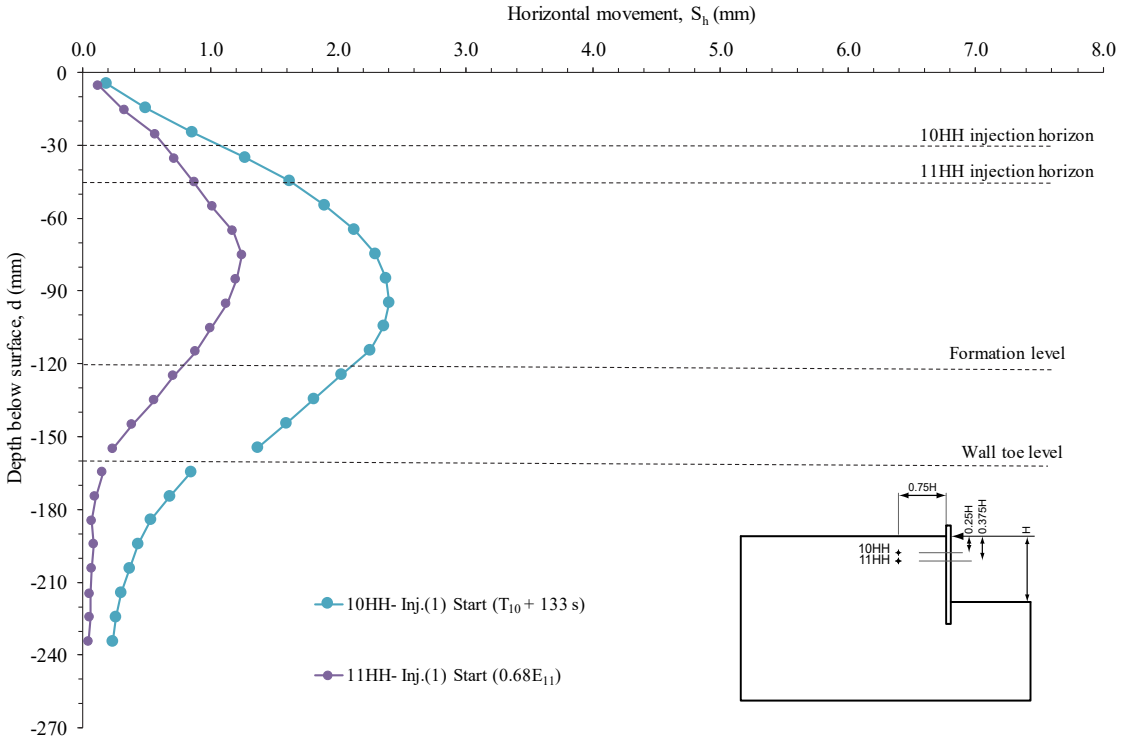


Figure 6. 45 Horizontal wall movements at the start of the 1st injection events in tests 10-11HH.

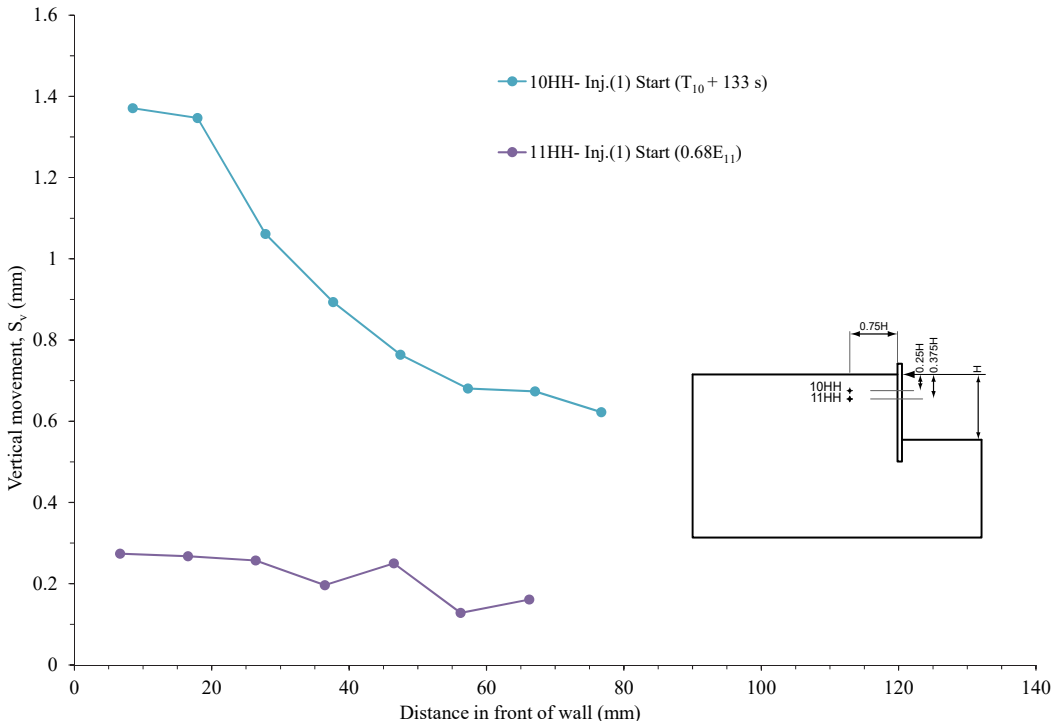


Figure 6. 46 Vertical formation level movements at the start of the 1st injection events in tests 10-11HH.

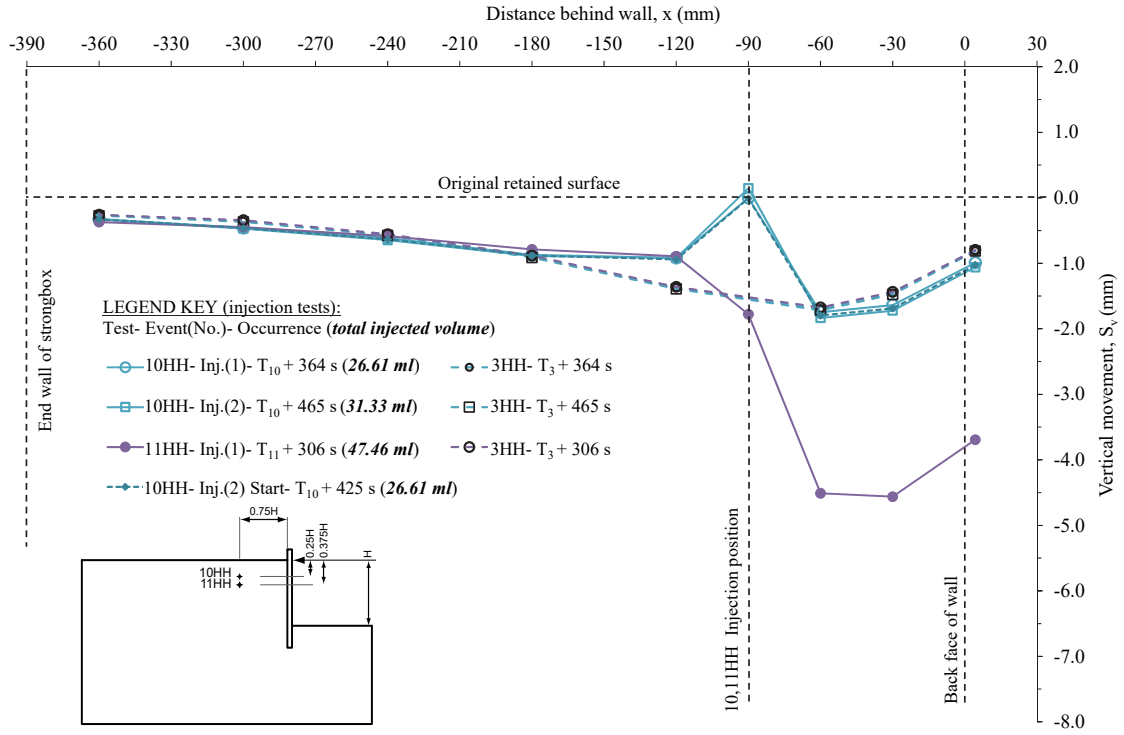


Figure 6. 47 Vertical LVDT retained surface displacements at the end of the injection events in tests 10-11HH (and start of the 2nd injection event in test 10HH) compared to equivalent stages in baseline test 3HH.

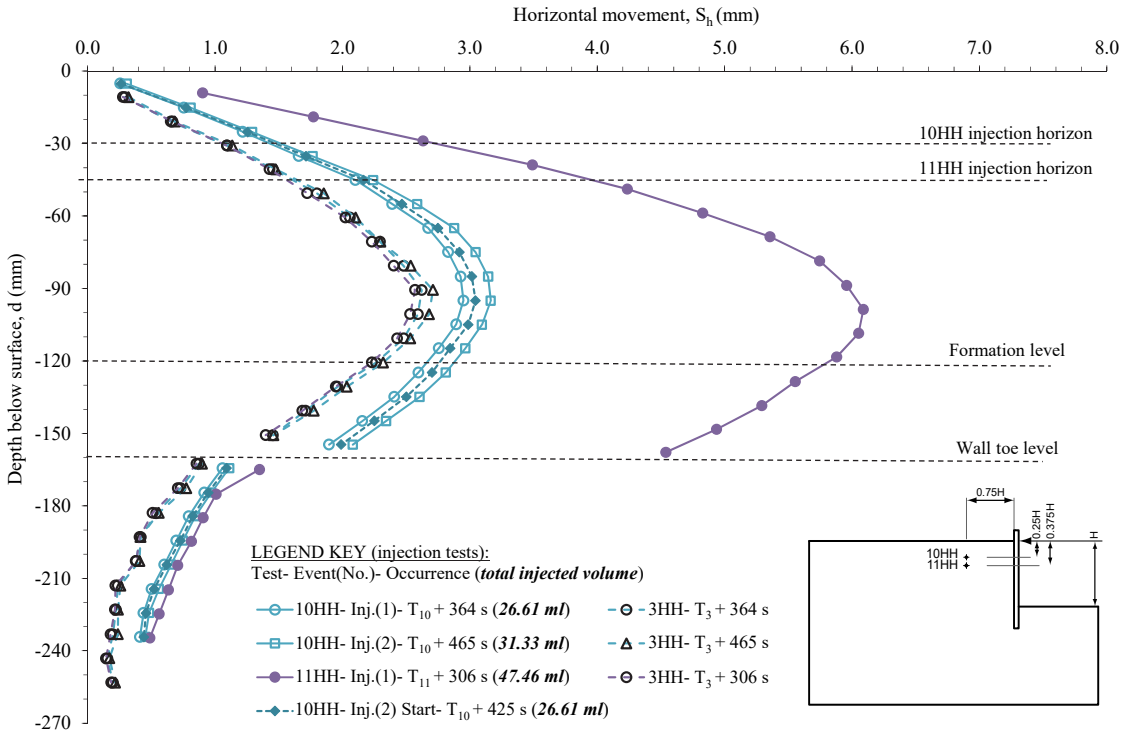


Figure 6. 48 Horizontal wall movements at the end of the injection events in tests 10-11HH (and start of the 2nd injection in 10HH) compared to equivalent stages in baseline test 3HH.

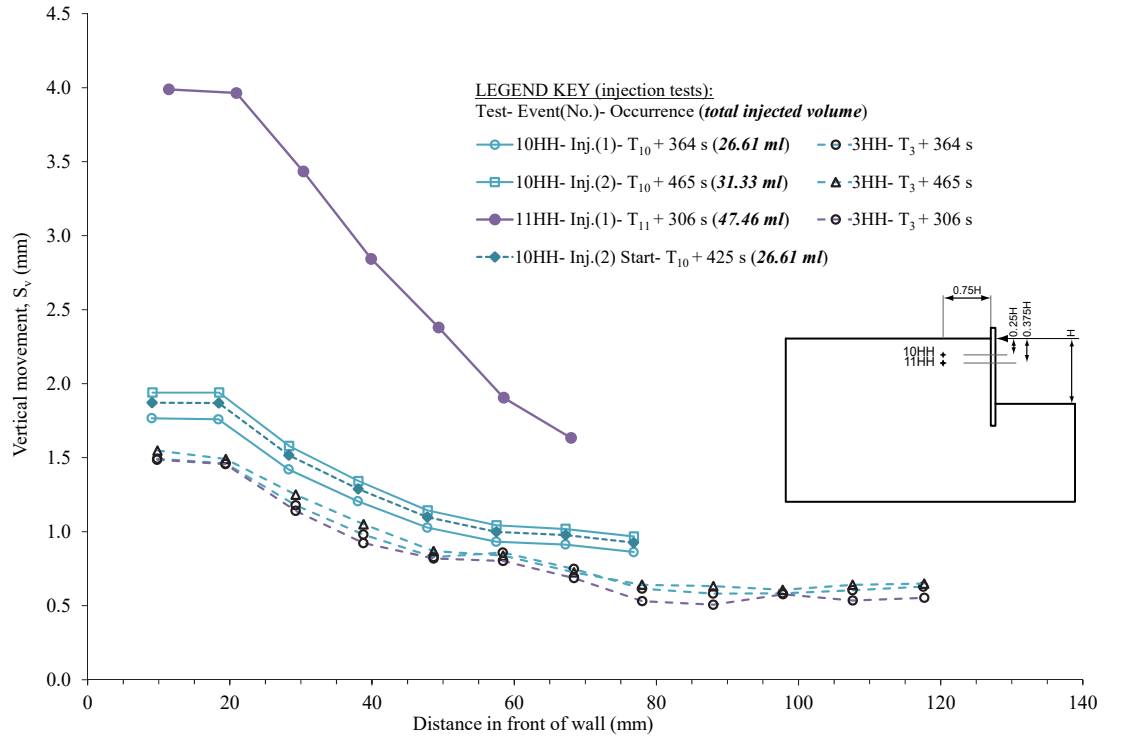


Figure 6. 49 Vertical formation level movements at the end of the injection events in tests 10-11HH (and start of the 2nd injection in 10HH) compared to equivalent stages in baseline test 3HH.

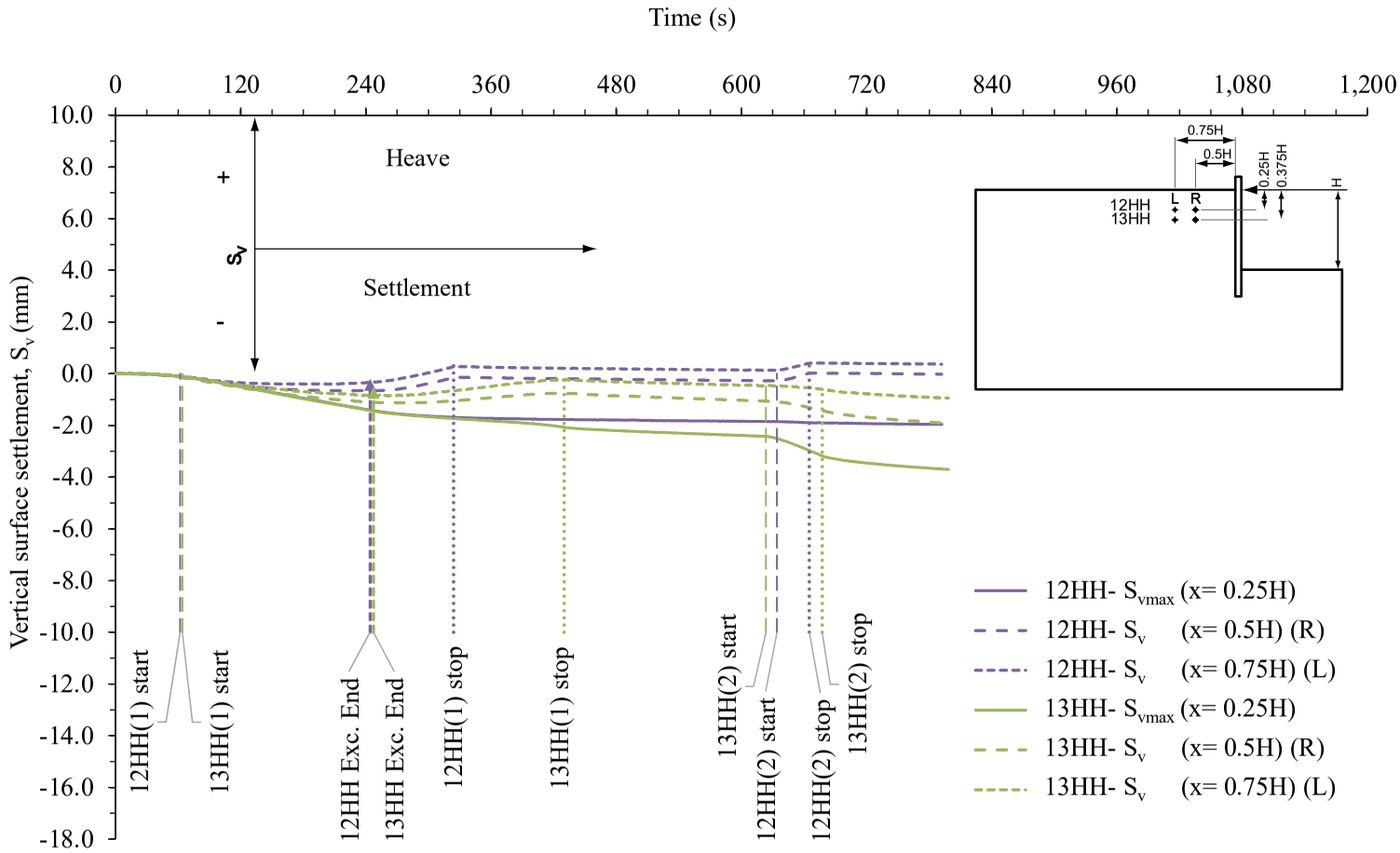


Figure 6. 50 Development of vertical surface settlements (S_v) measured by LVDTs at distances x= 0.25H, 0.5H and 0.75H behind the wall in tests 12-13HH.

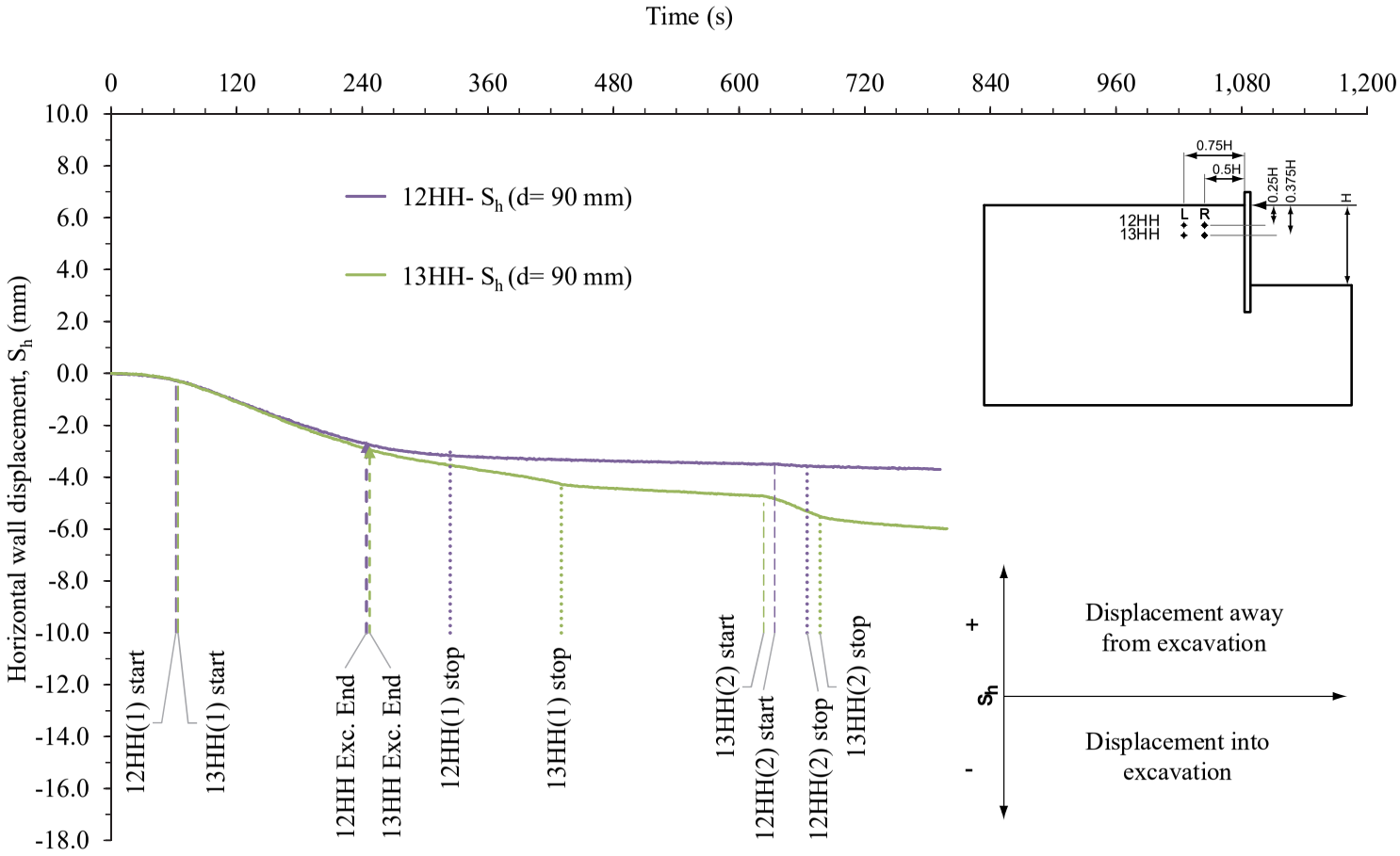


Figure 6. 51 Development of horizontal wall displacements (S_h) at depth d= 0.75H (90 mm) below the retained surface in tests 12-13HH.

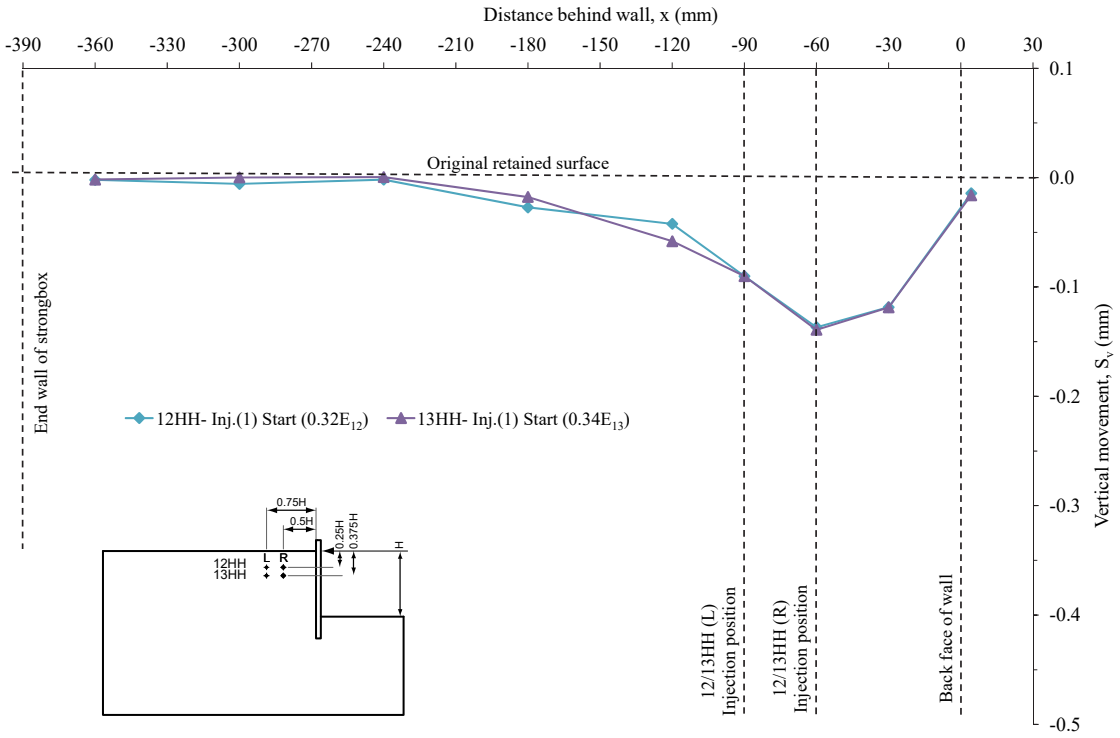


Figure 6. 52 Vertical LVDT retained surface displacements at the start of the 1st injection event in tests 12-13HH.

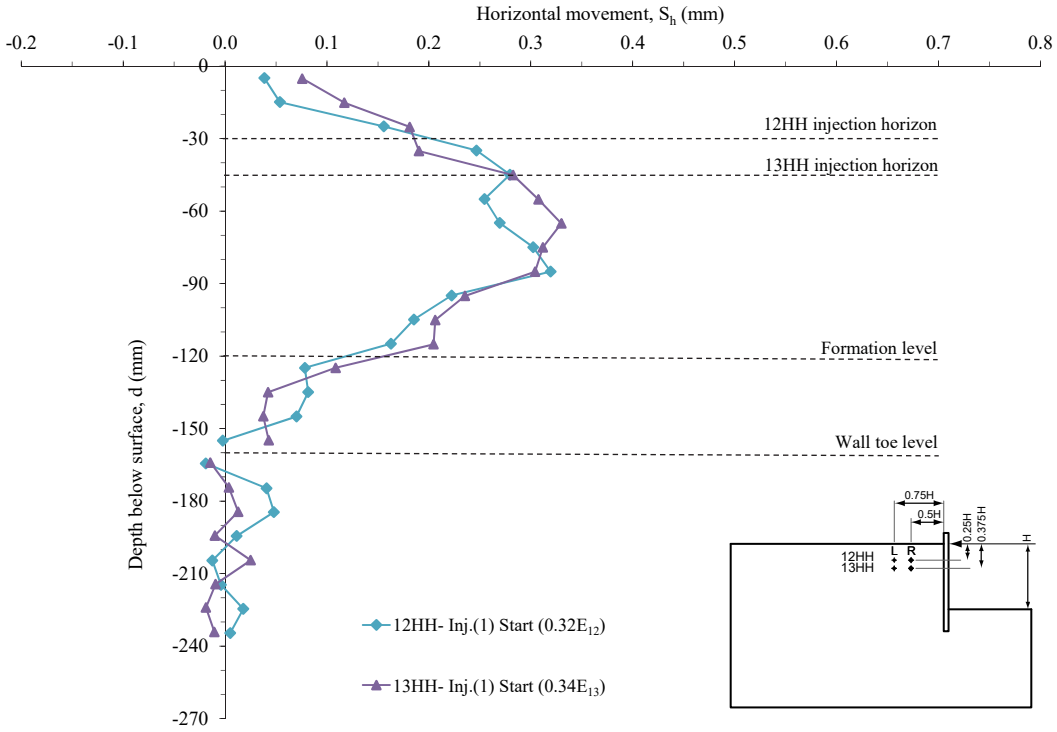


Figure 6. 53 Horizontal wall movements at the start of the 1st injection event in tests 12-13HH.

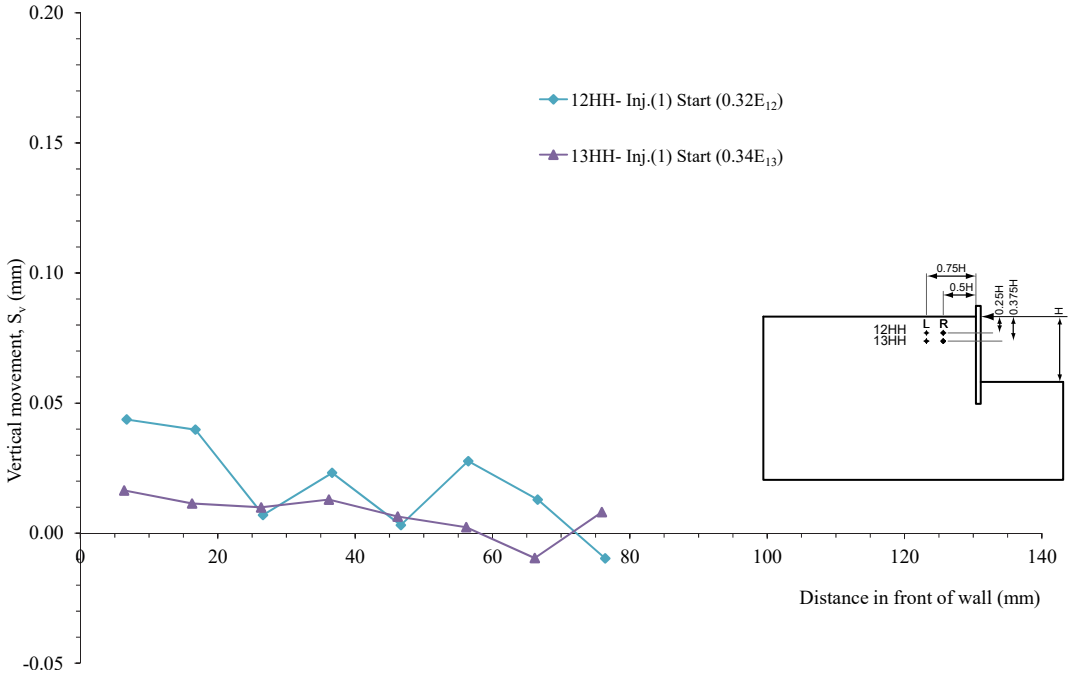


Figure 6. 54 Vertical formation level movements at the start of the 1st injection event in tests 12-13HH.

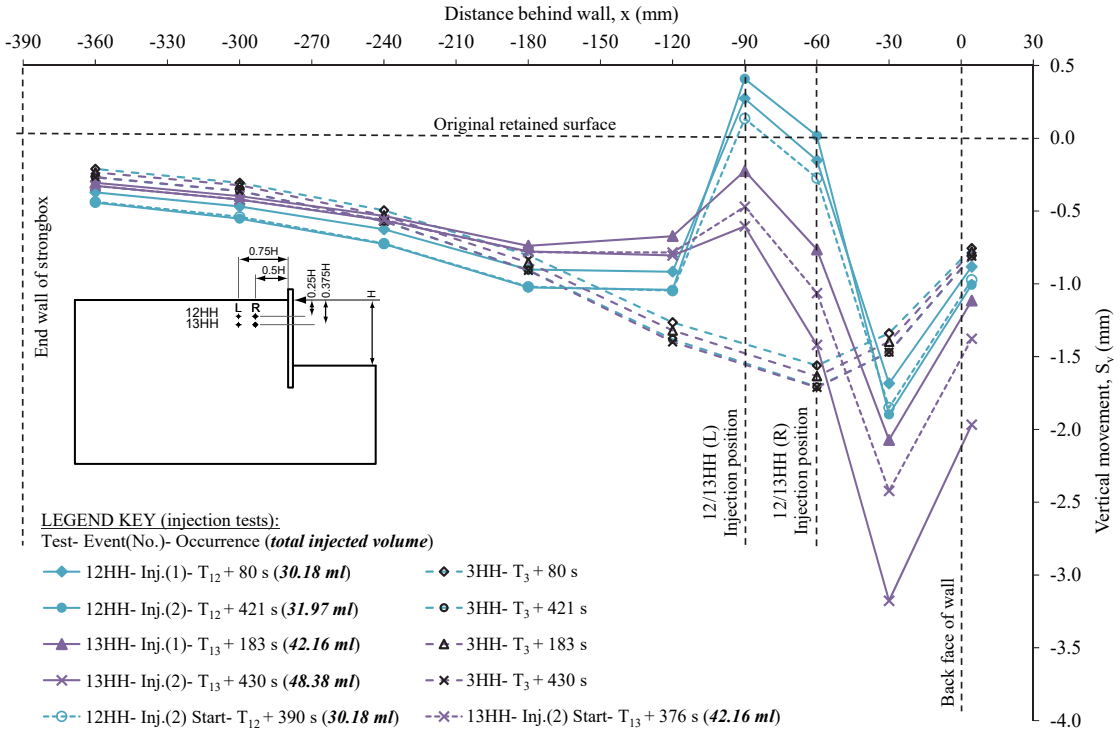


Figure 6. 55 Vertical LVDT retained surface displacements at the end of the injection events in tests 12-13HH (and start of the 2nd injection events) compared to equivalent stages in baseline test 3HH.

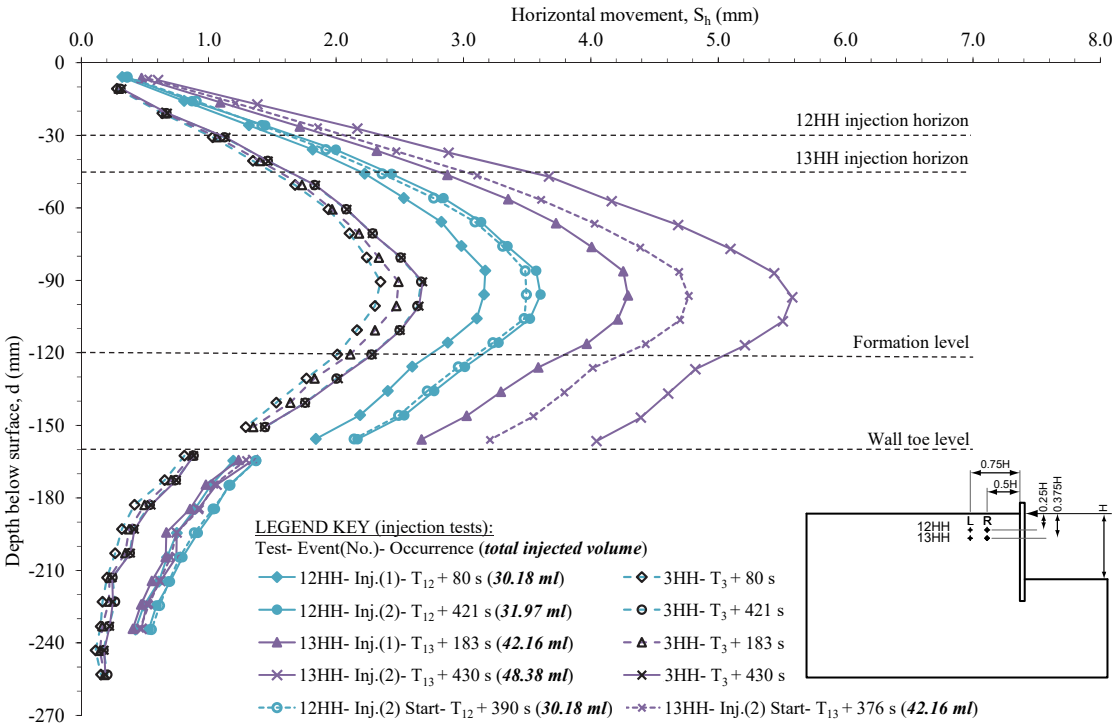


Figure 6. 56 Horizontal wall movements at the end of the injection events in tests 12-13HH (and start of the 2nd injection events) compared to equivalent stages in baseline test 3HH.

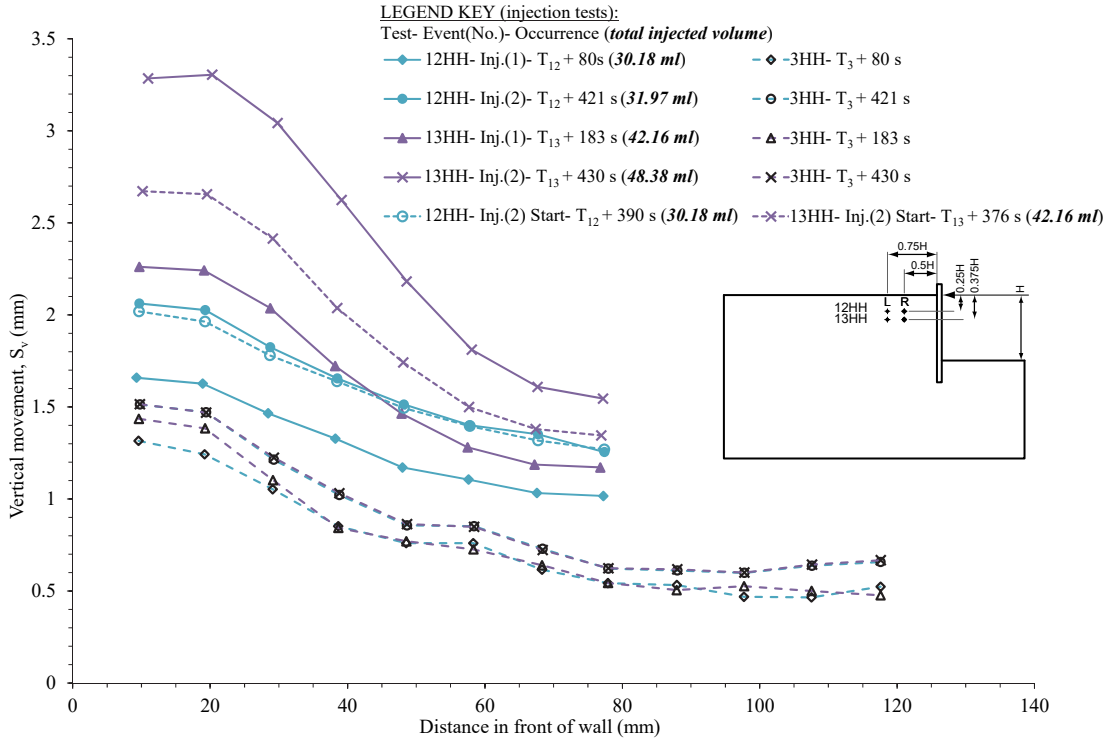


Figure 6. 57 Vertical formation level movements at the end of the injection events in tests 12-13HH (and start of the 2nd injection events) compared to equivalent stages in baseline test 3HH.

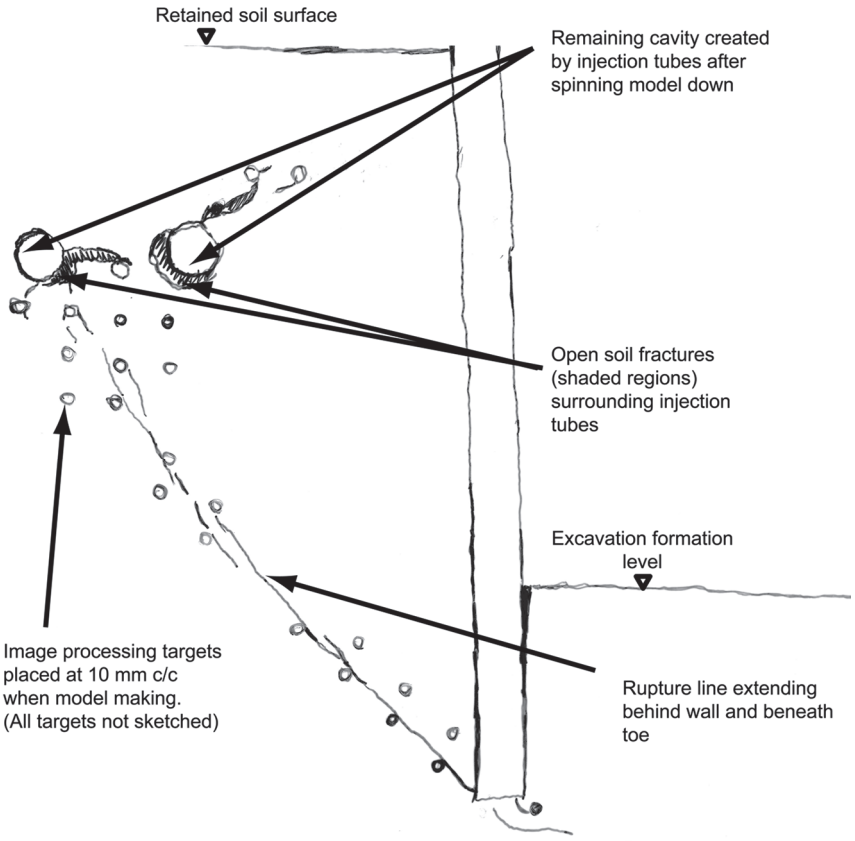


Figure 6. 58 Rupture lines behind and beneath the wall toe and open soil fractures surrounding the injection tube location at the end of test 13HH (traced following removal of the model from the centrifuge swing and removal of the latex injection tube).

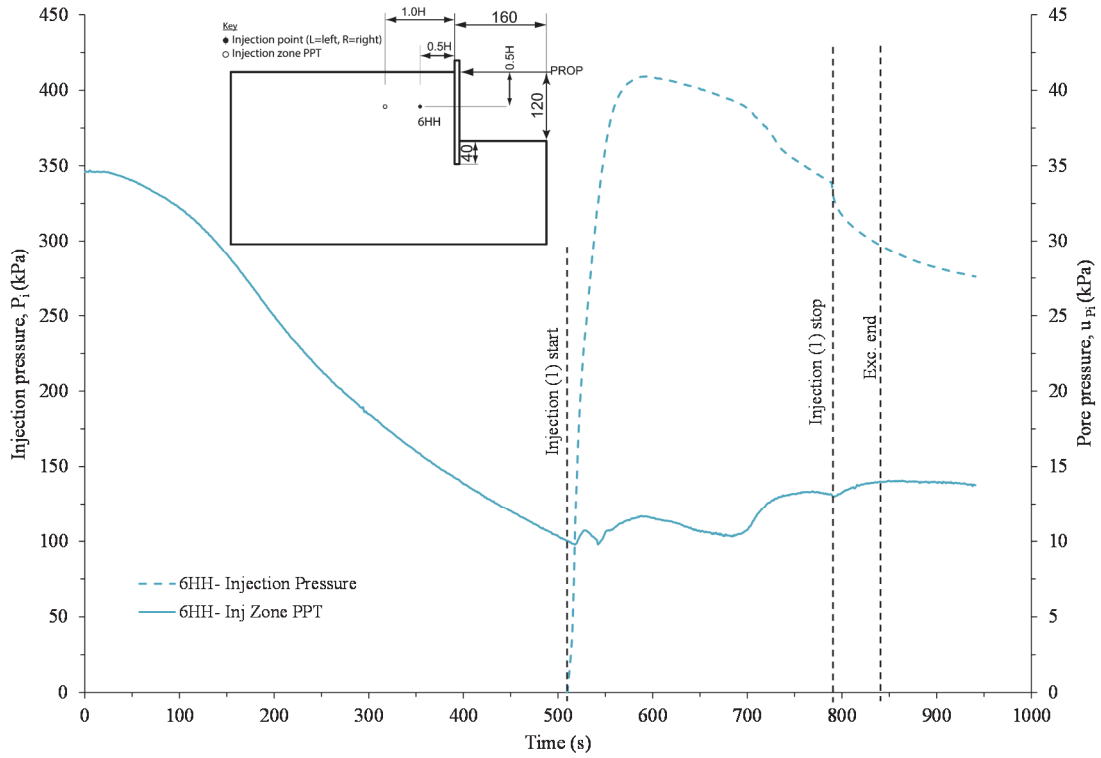


Figure 6. 59 Injection pressure and locally installed injection zone PPT response during test 6HH.

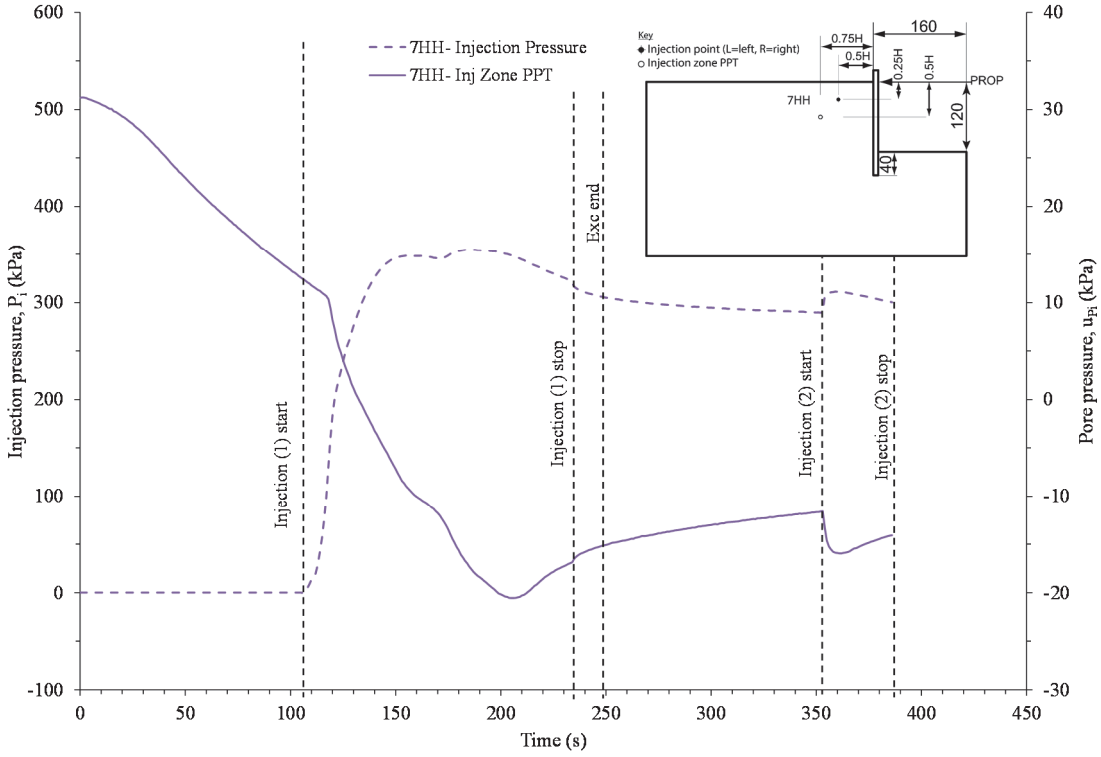


Figure 6. 60 Injection pressure and locally installed injection zone PPT response during test 7HH.

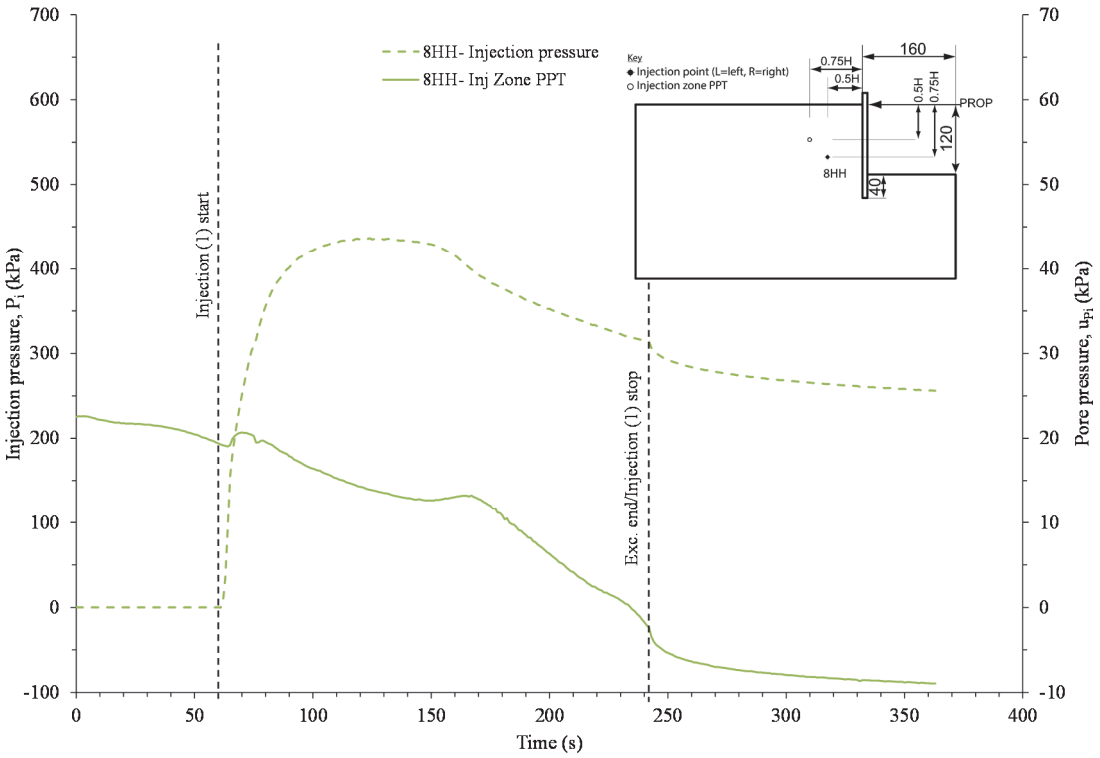


Figure 6. 61 Injection pressure and locally installed injection zone PPT response during test 8HH.

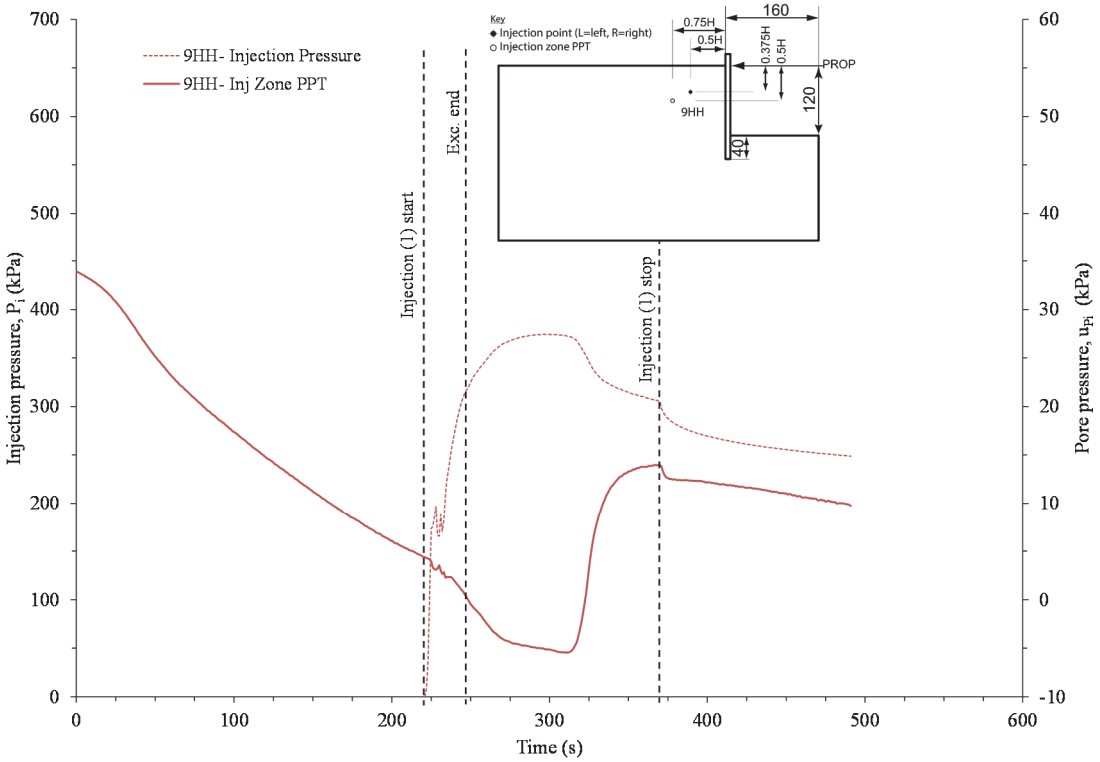


Figure 6. 62 Injection pressure and locally installed injection zone PPT response during test 9HH.

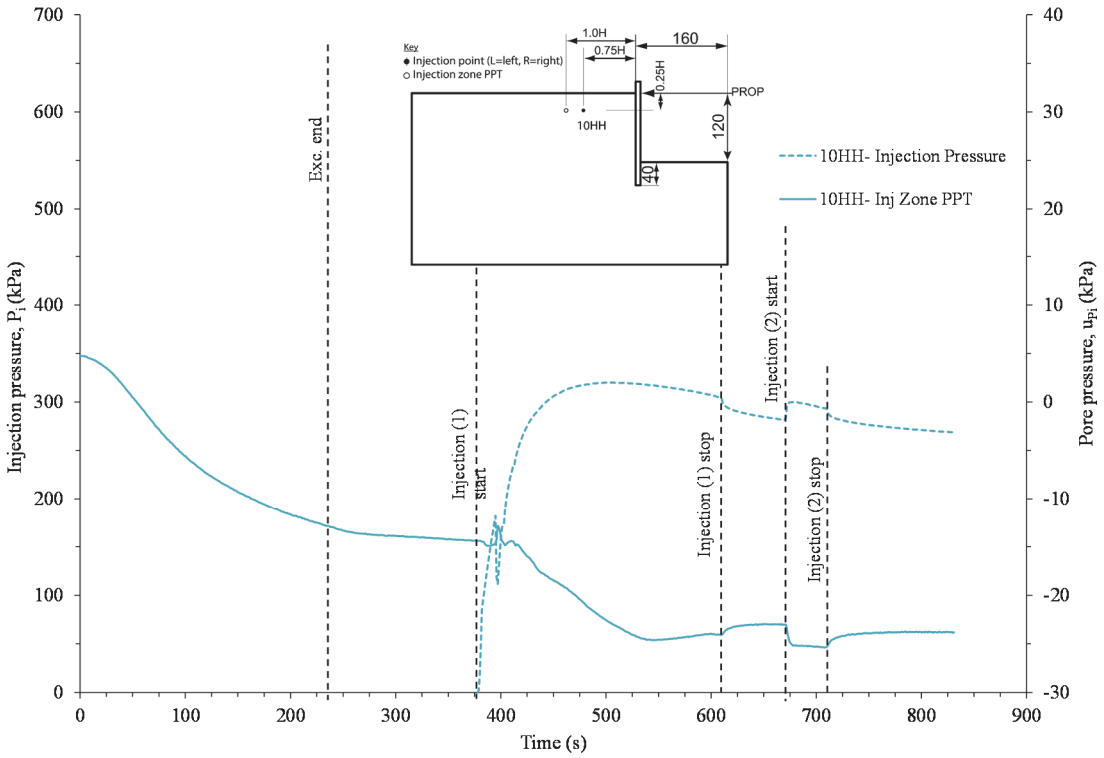


Figure 6. 63 Injection pressure and locally installed injection zone PPT response during test 10HH.

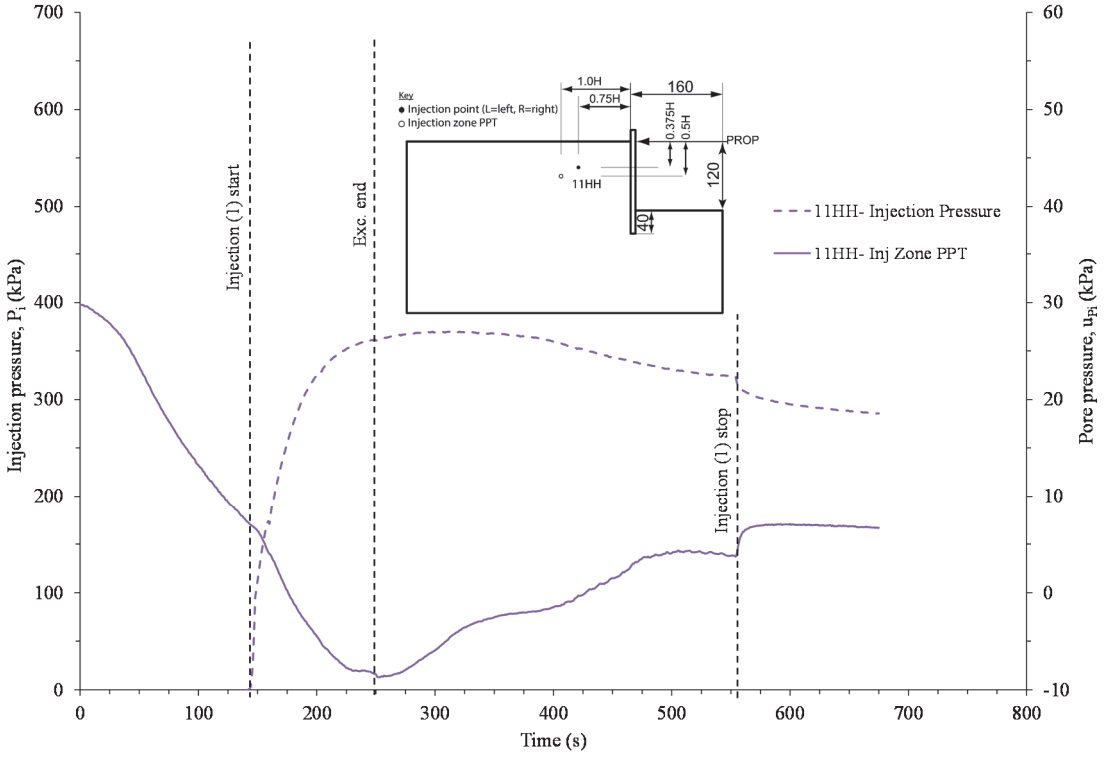


Figure 6. 64 Injection pressure and locally installed injection zone PPT response during test 11HH.

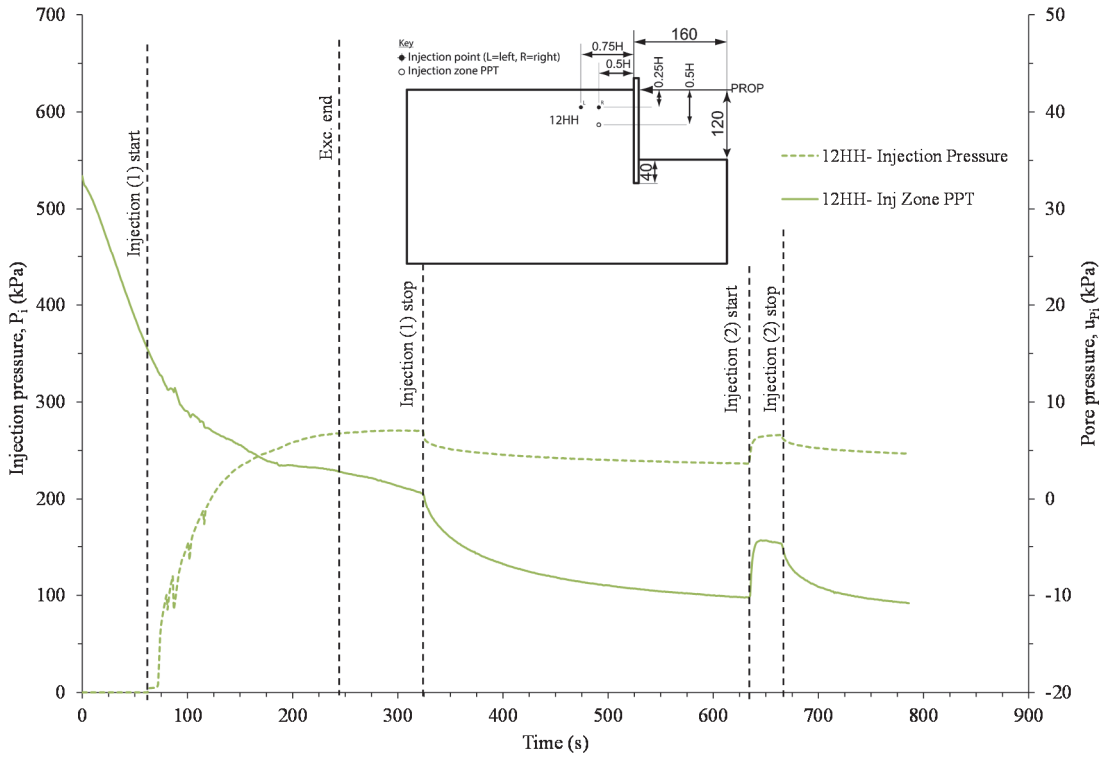


Figure 6. 65 Total injection pressure response from both injection tubes and locally installed injection zone PPT response during test 12HH.

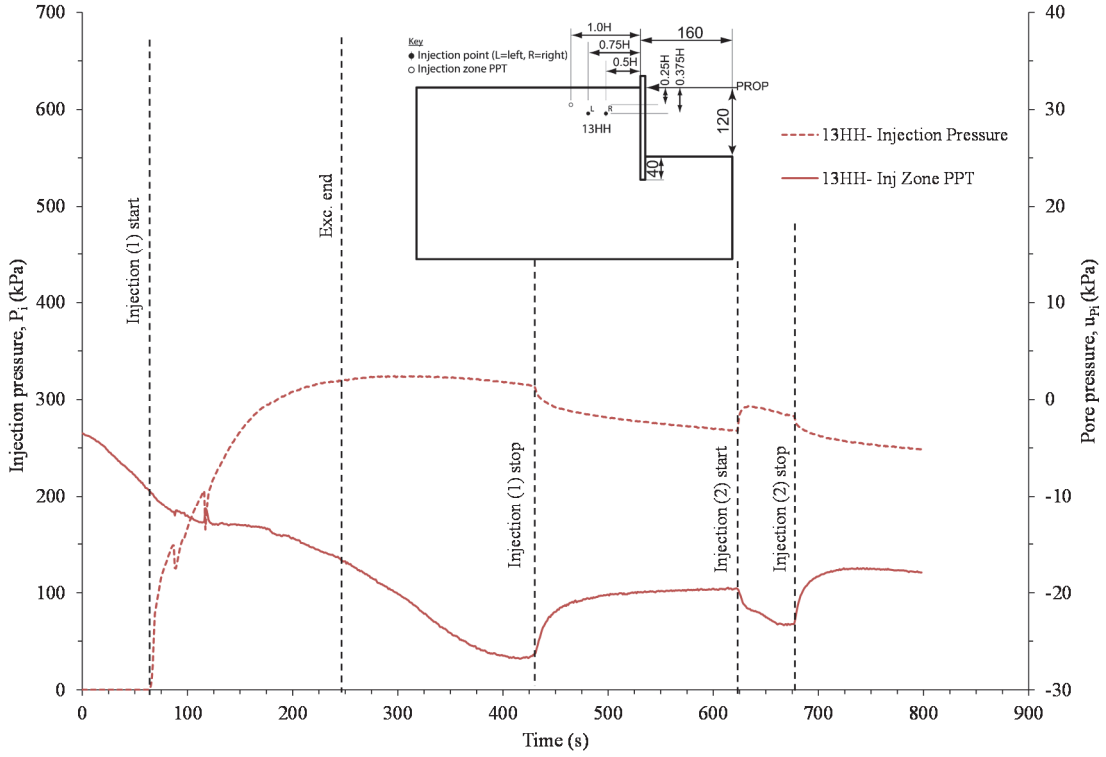


Figure 6. 66 Total injection pressure response from both injection tubes and locally installed injection zone PPT response during test 13HH.

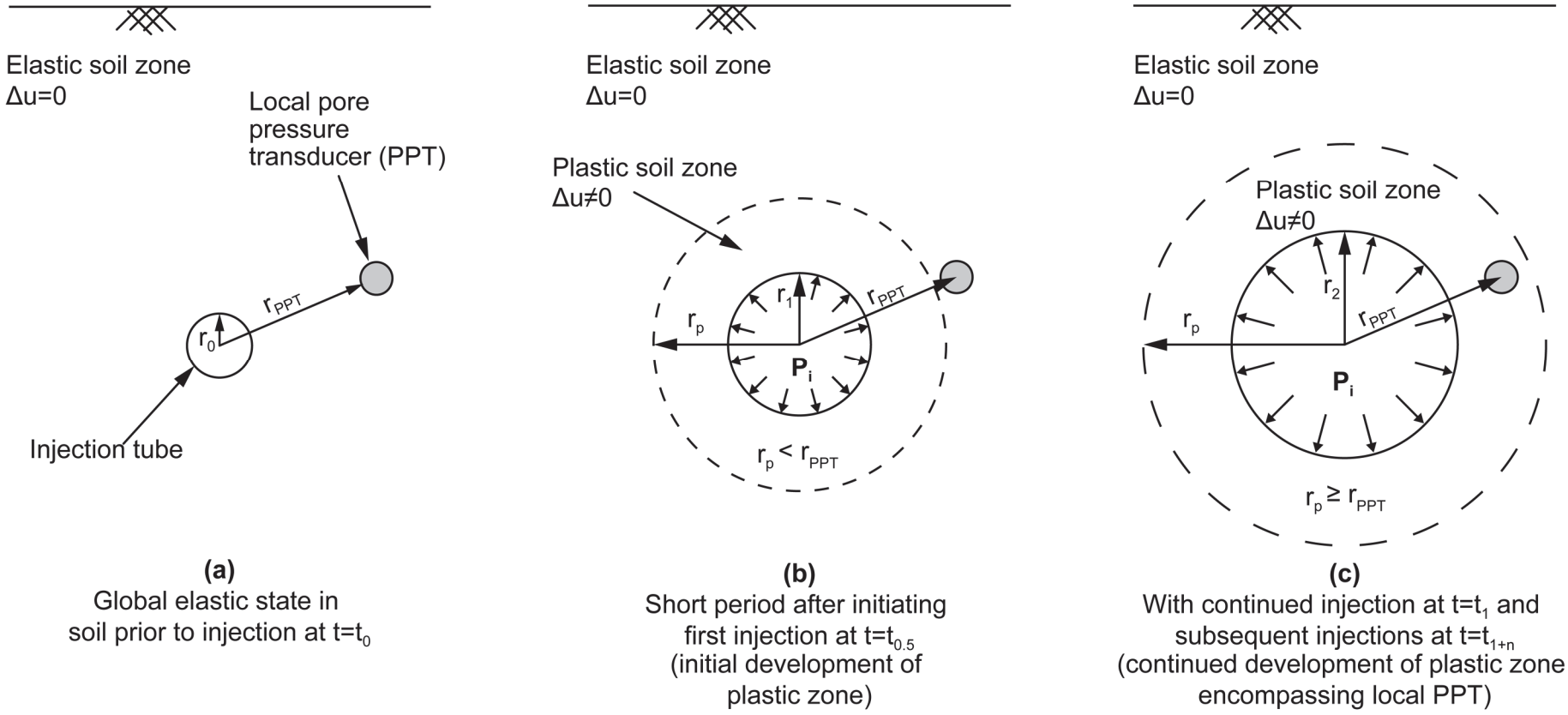


Figure 6. 67 Schematic illustrating the development of the plastic soil zone around the injection tube during injection and its coincidence with the local pore pressure transducer based on cavity expansion theory in an infinite elastic-perfectly plastic soil.

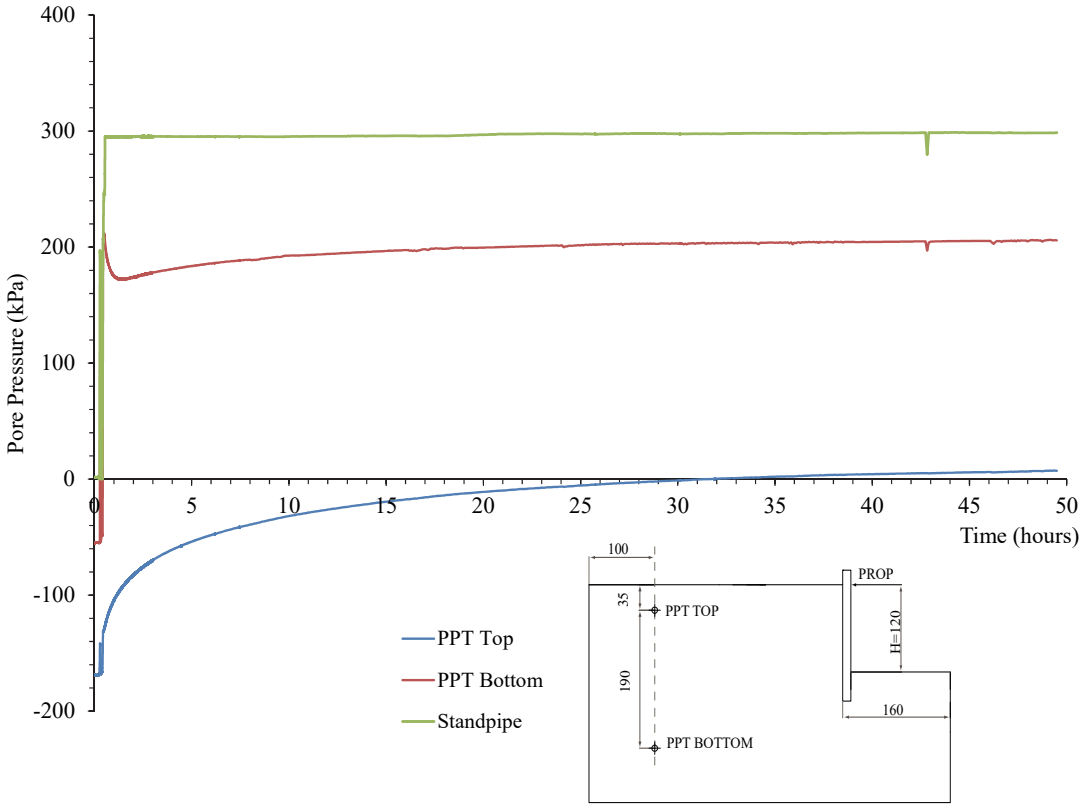


Figure 6. 68 Typical response of the far field PPTs and standpipe PT during consolidation prior to testing.

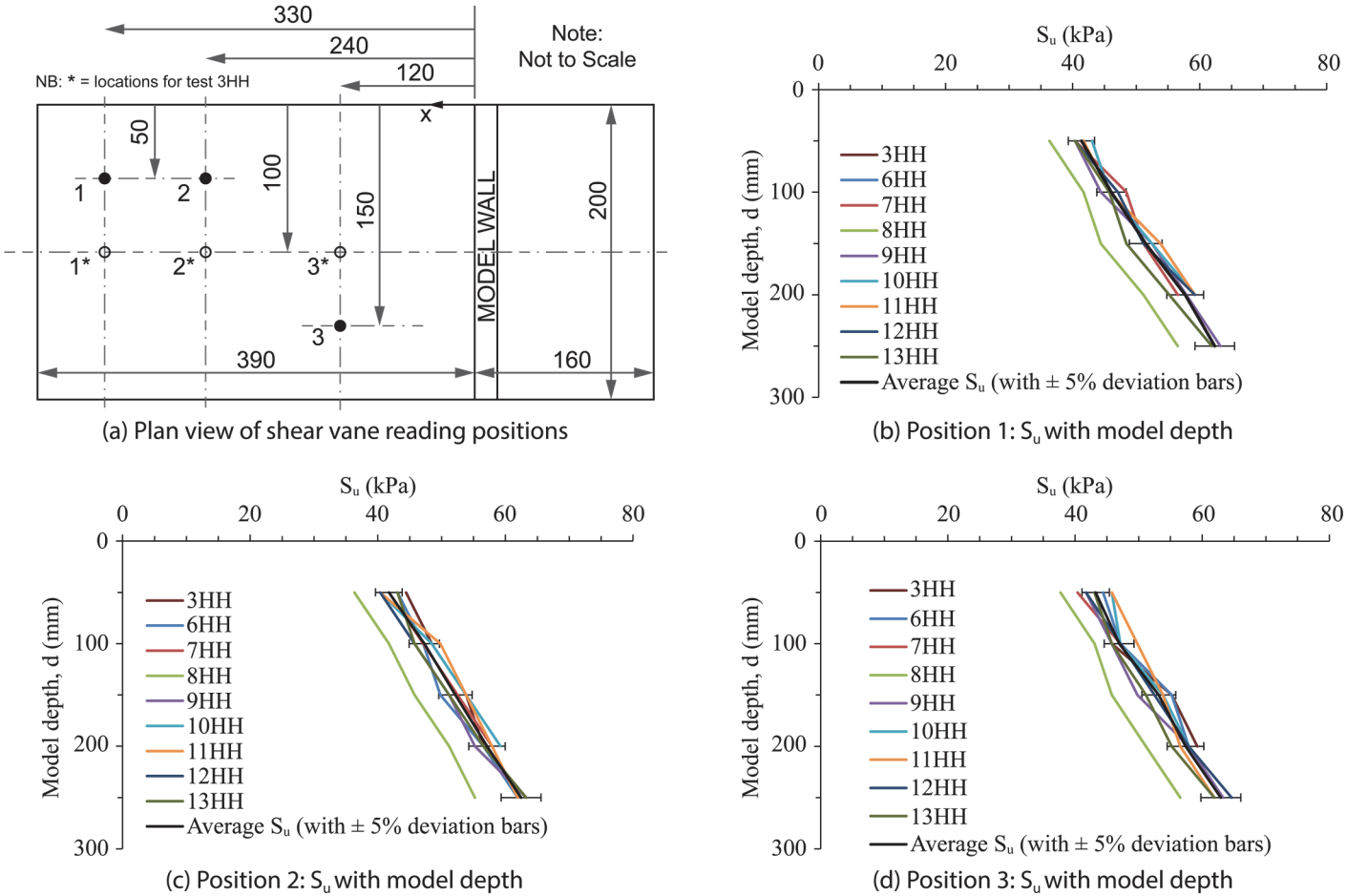


Figure 6. 69 Readings and locations of undrained shear strengths (S_u), using a 19 mm hand shear vane, taken of the soil model immediately after the tests (3-13HH).

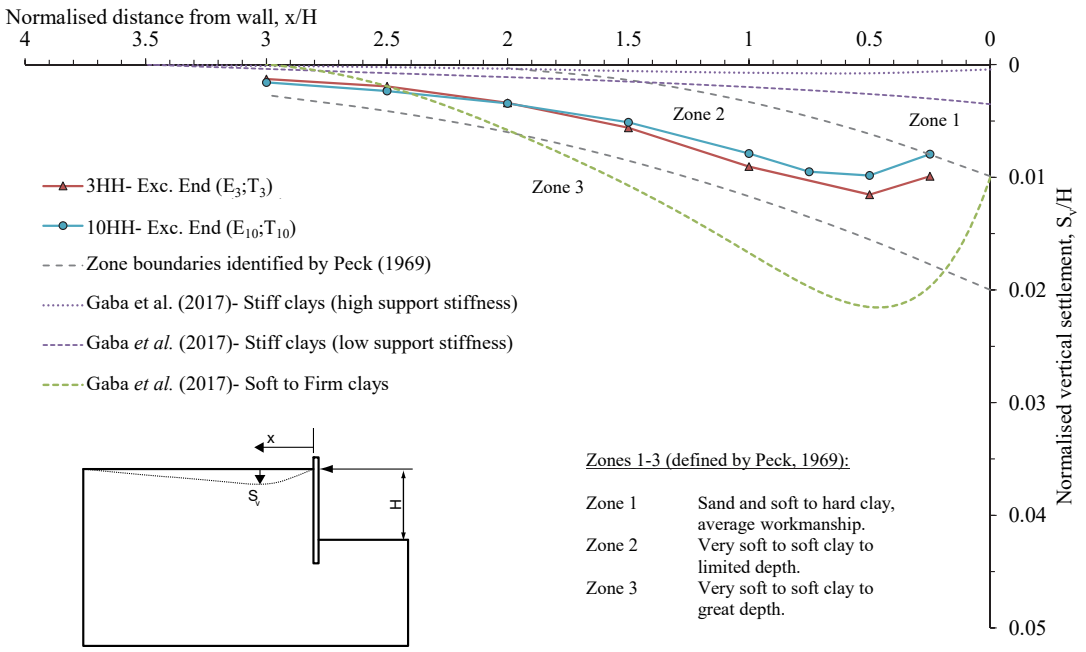


Figure 7. 1 Normalised settlements behind the retaining wall at the end of simulated excavation in tests 3HH and 10HH shown in the context of expected settlements for excavation in various soils from field monitoring data after Peck (1969) and Gaba *et al.* (2017).

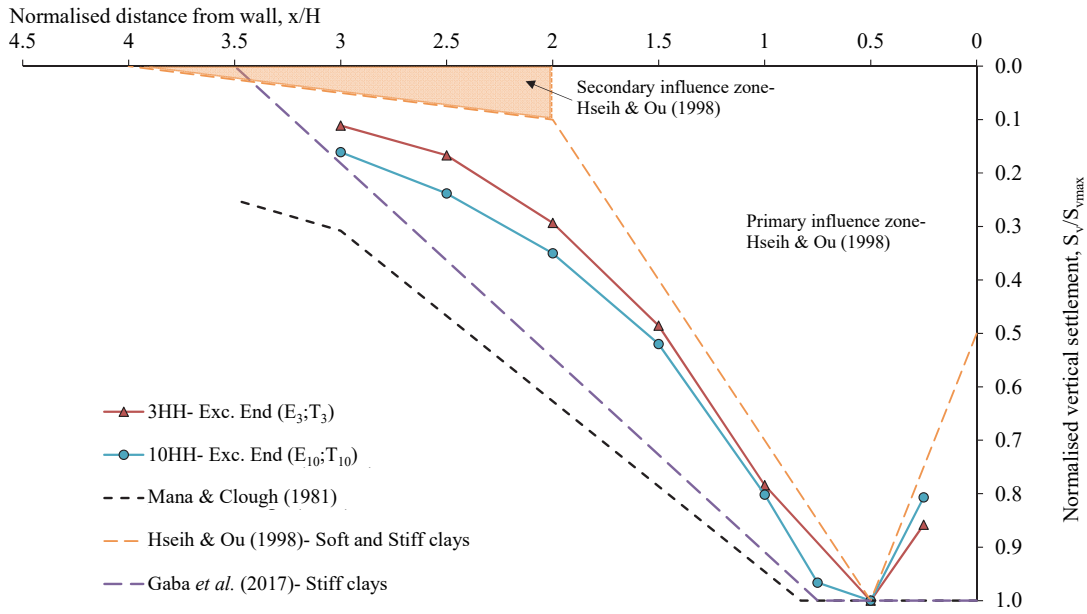


Figure 7. 2 Normalised settlement profile behind the retaining wall at the end of simulated excavation in tests 3HH and 10HH shown in the context of typical bounding profiles in soft-firm soils from field monitoring after Hseih and Ou (1998) and Gaba *et al.* (2017).

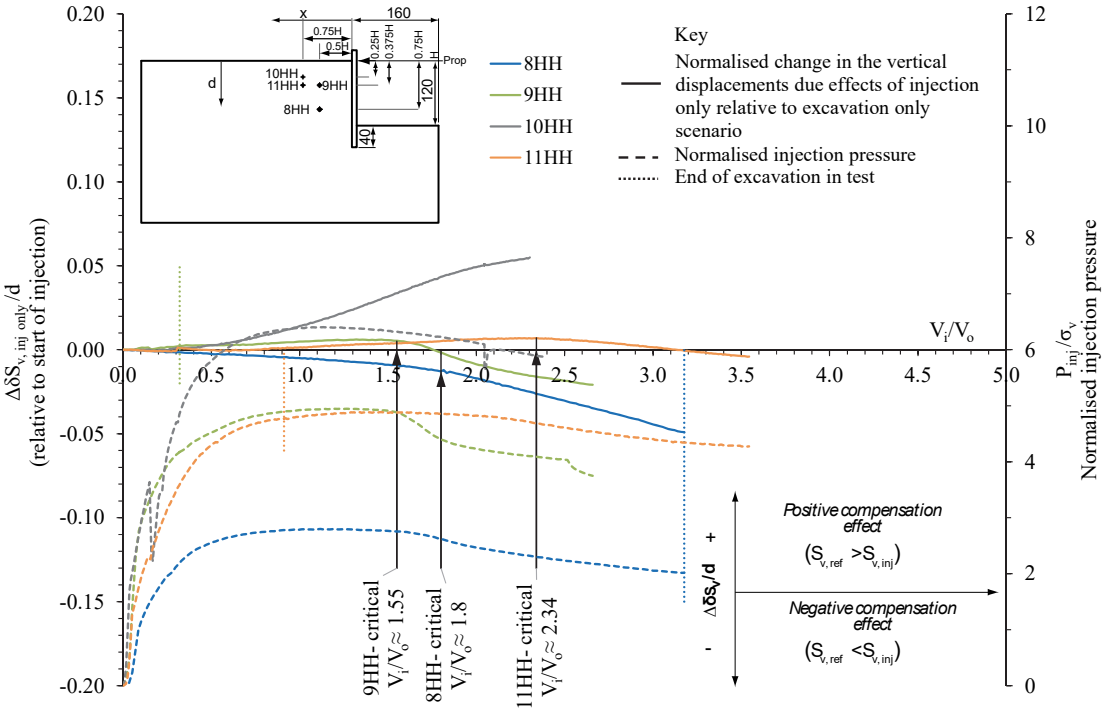


Figure 7. 3 Normalised changes in vertical displacements and injection pressures with injected volume above the injection location relative to the reference test from the start of injection in tests 8HH, 9HH, 10HH and 11HH.

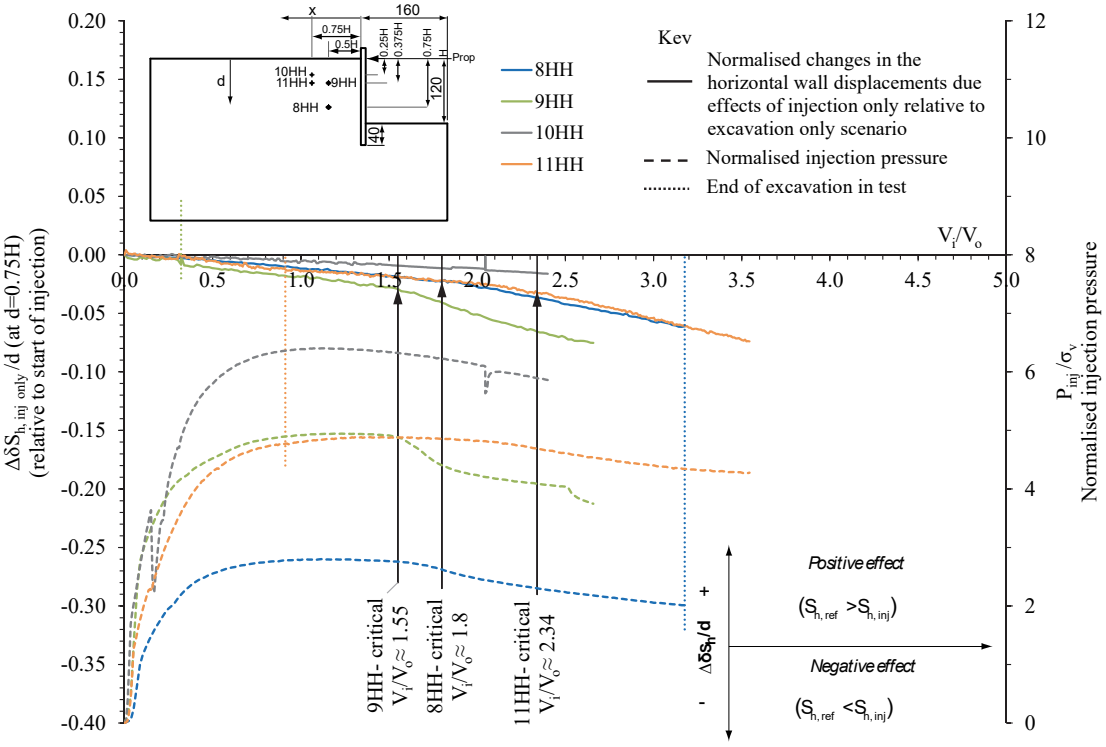


Figure 7. 4 Normalised changes in horizontal wall displacements at depth d= 0.75H, below the retained surface and injection pressures with injected volume, relative to the reference test from the start of injection in tests 8HH, 9HH, 10HH and 11HH.

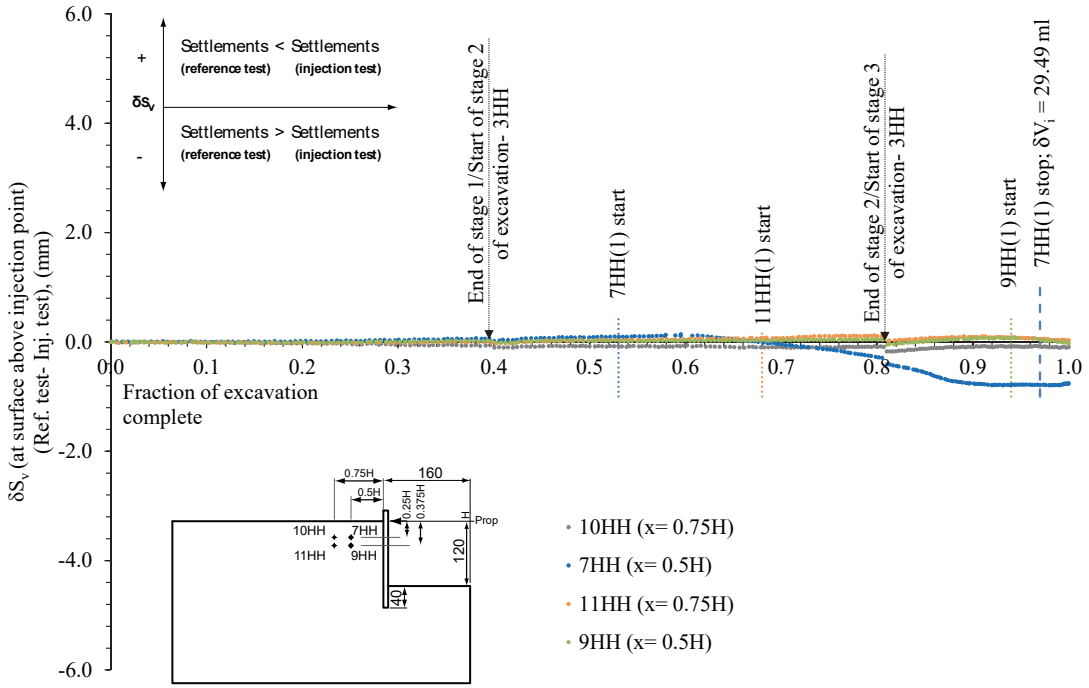


Figure 7. 5 Development of vertical displacements above the injection location at the retained surface in grouting tests 7HH, 9HH, 10HH and 11HH relative to test 3HH during the simulated excavation.

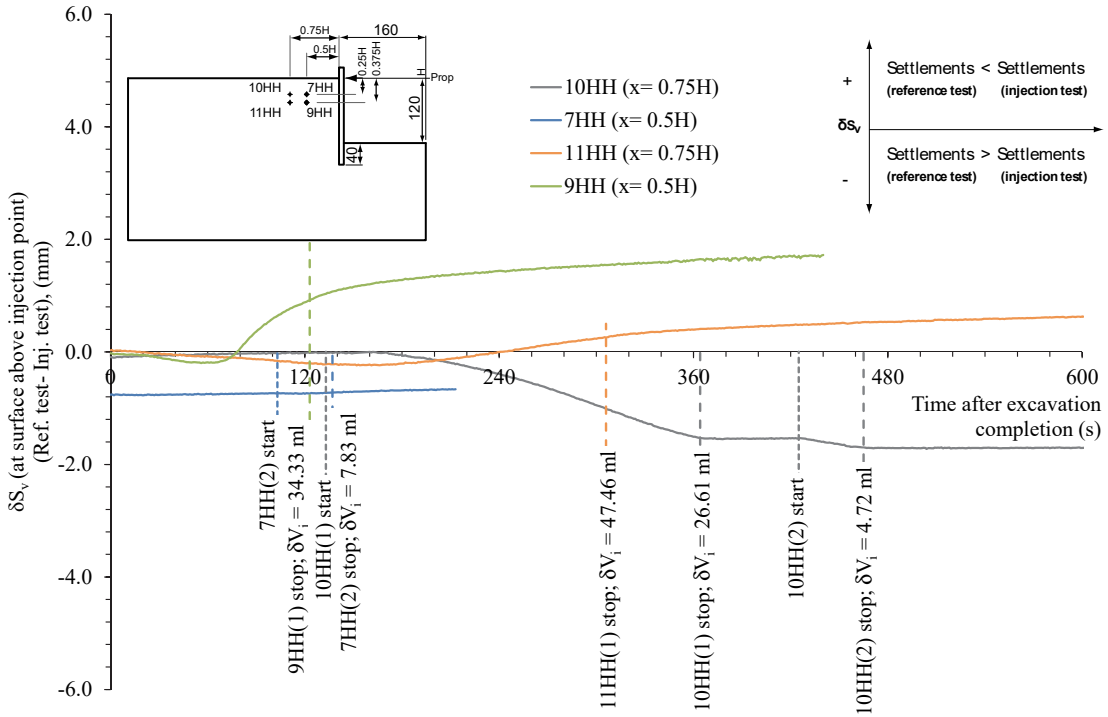


Figure 7. 6 Development of vertical displacements above the injection location at the retained surface in grouting tests 7HH, 9HH, 10HH and 11HH relative to test 3HH after the simulated excavation.

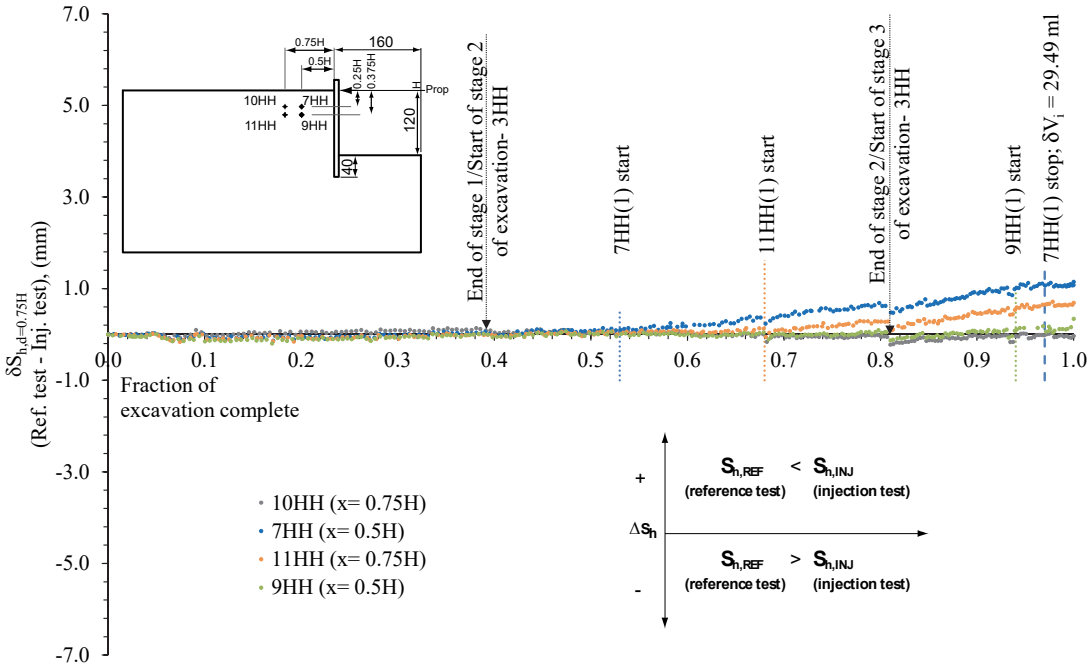


Figure 7. 7 Development of horizontal wall displacements at depth d= 0.75H, below the retained surface, in grouting tests 7HH, 9HH, 10HH and 11HH relative to test 3HH during the simulated excavation.

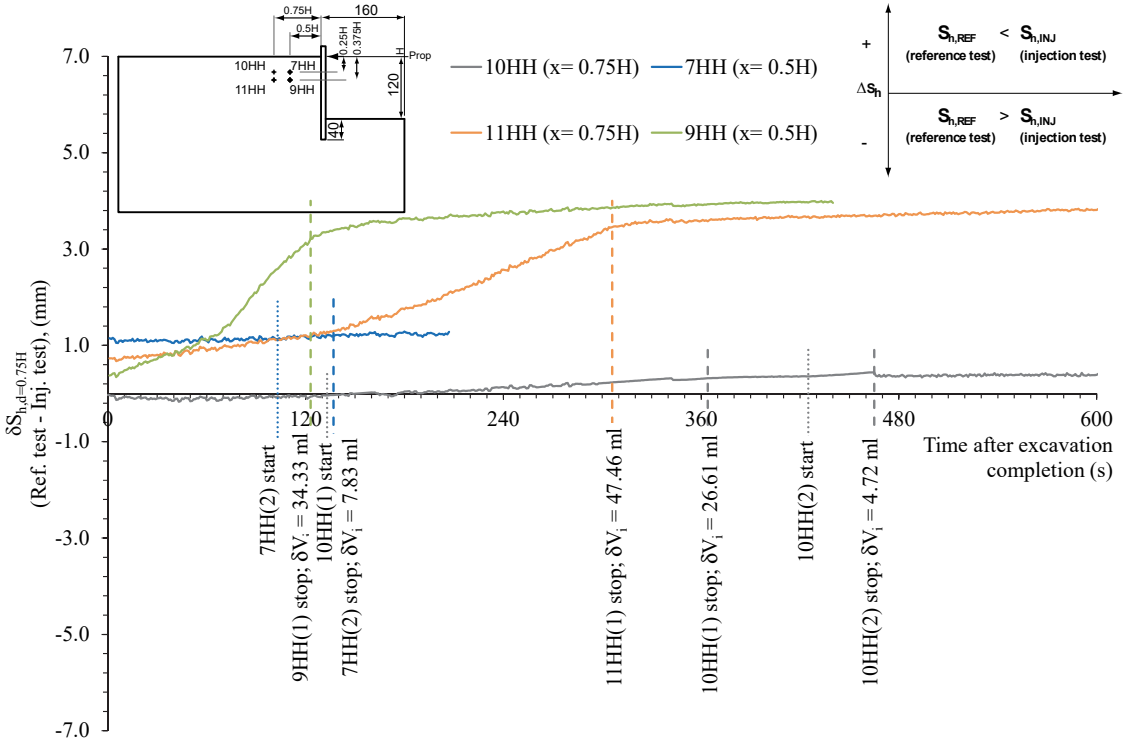


Figure 7. 8 Development of horizontal wall displacements at depth d= 0.75H, below the retained surface, in grouting tests 7HH, 9HH, 10HH and 11HH relative to test 3HH after the simulated excavation.

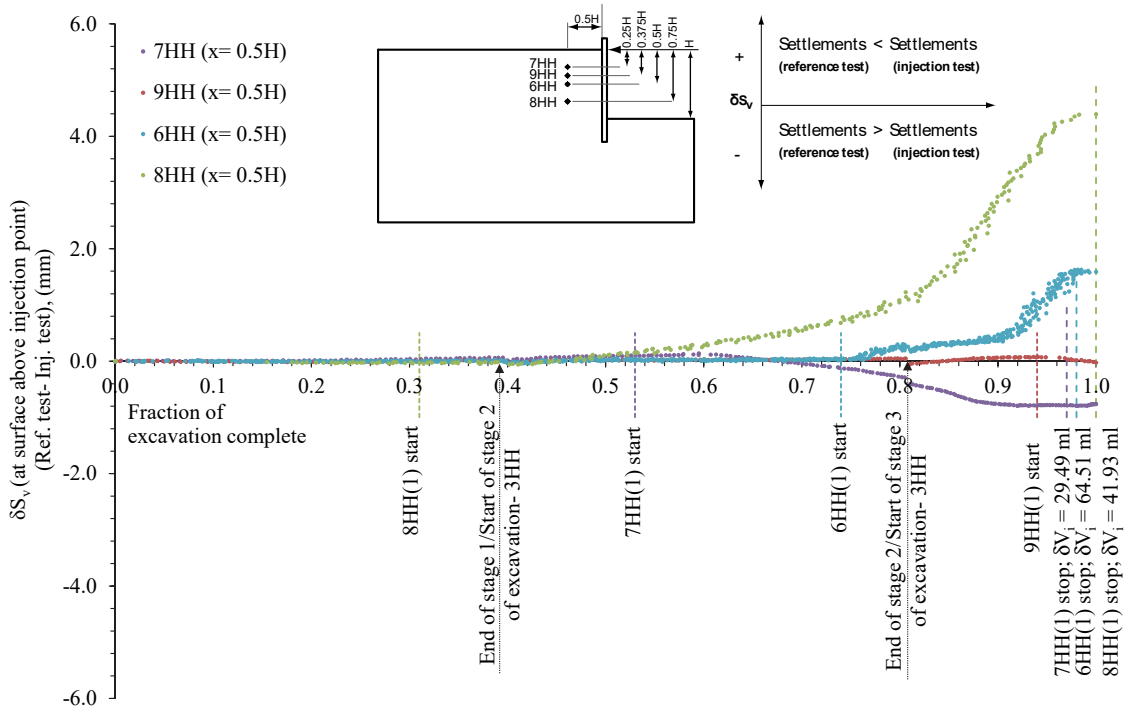


Figure 7. 9 Development of vertical displacements above the injection location at the retained surface in grouting tests 6-9HH relative to test 3HH during the simulated excavation.

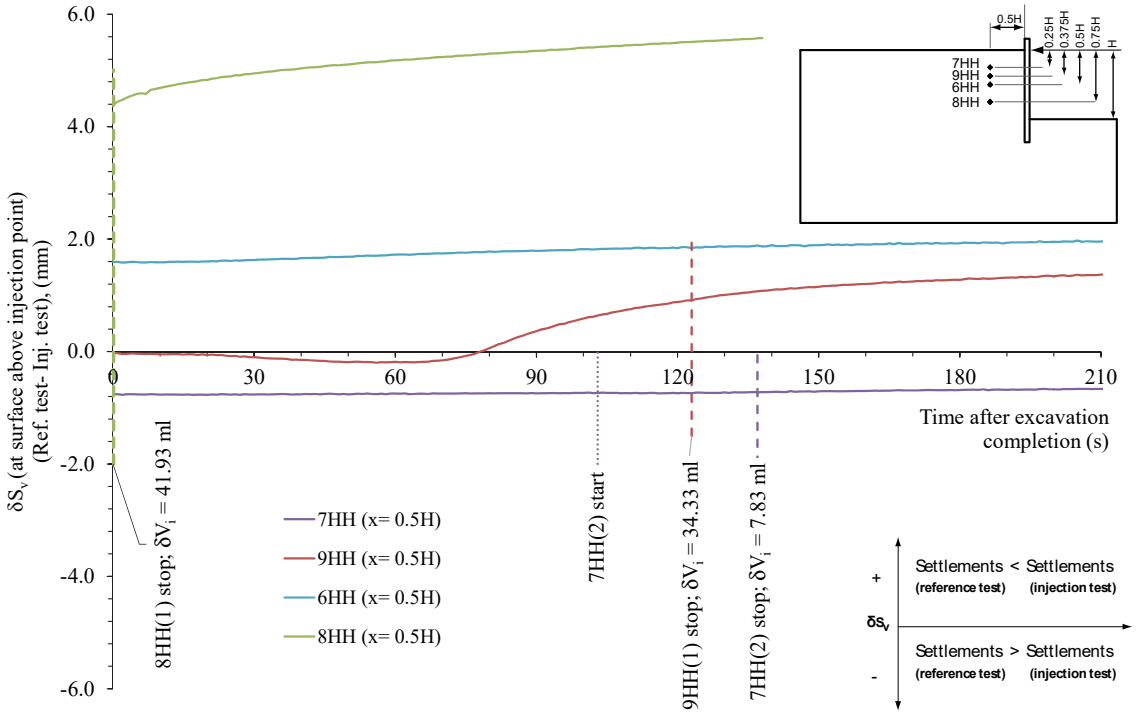


Figure 7. 10 Development of vertical displacements above the injection location at the retained surface in grouting tests 6-9HH relative to test 3HH after the simulated excavation.

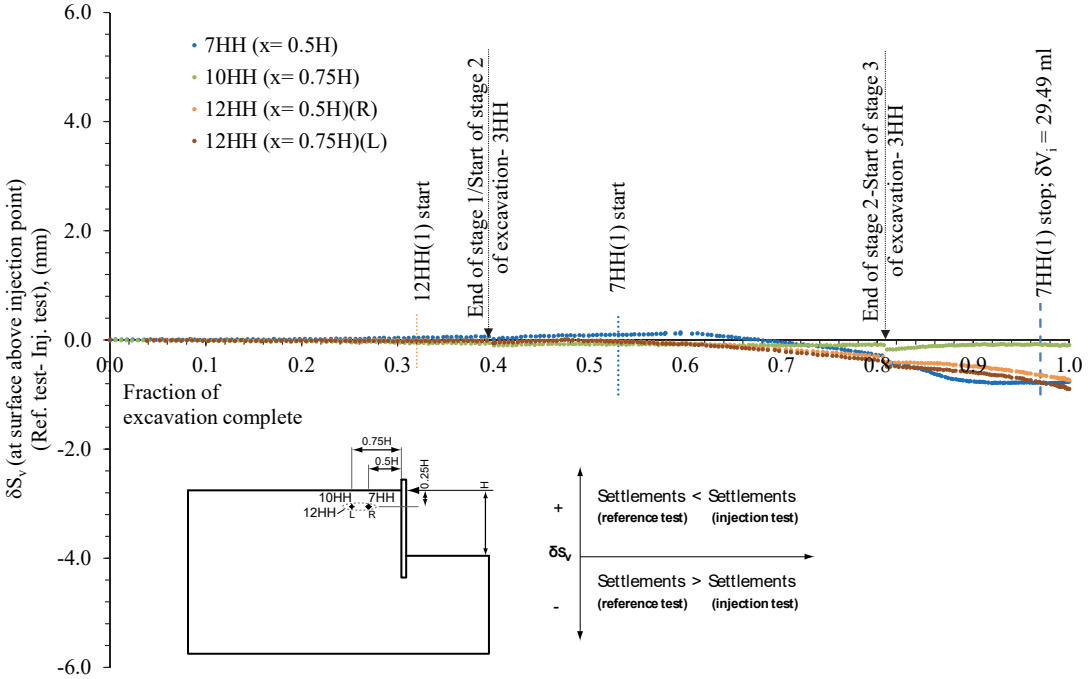


Figure 7. 11 Development of vertical displacements above the injection location at the retained surface in grouting tests 7HH, 10HH and 12HH relative to test 3HH during the simulated excavation.

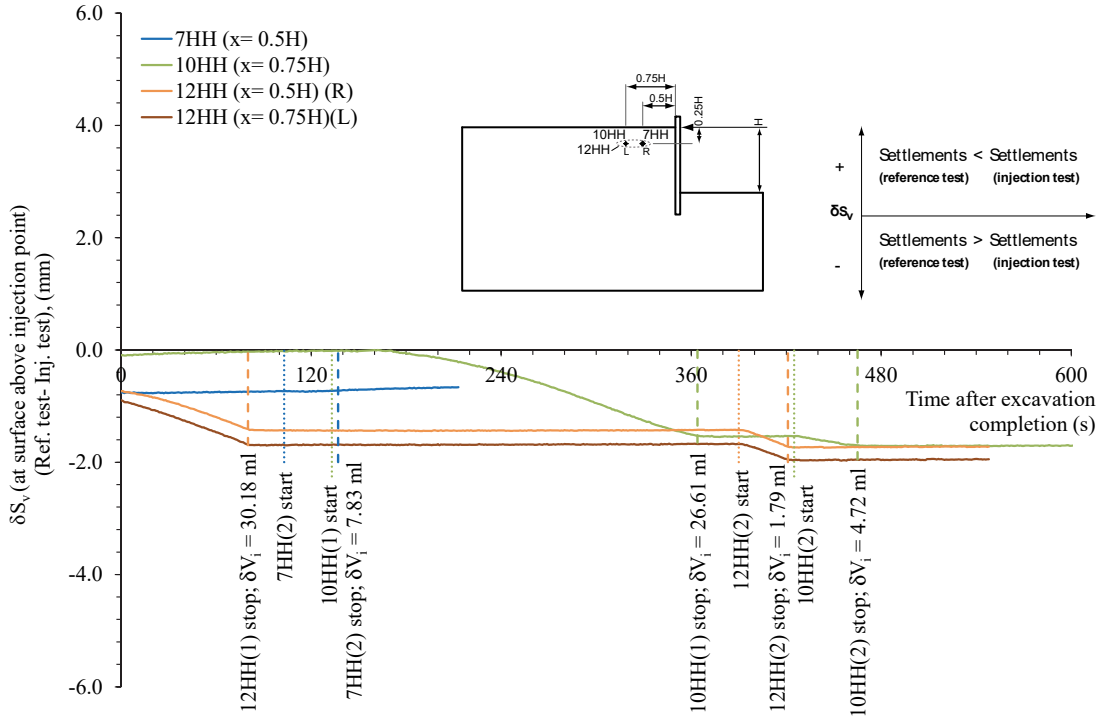


Figure 7. 12 Development of vertical displacements above the injection location at the retained surface in grouting tests 7HH, 10HH and 12HH relative to test 3HH after the simulated excavation.

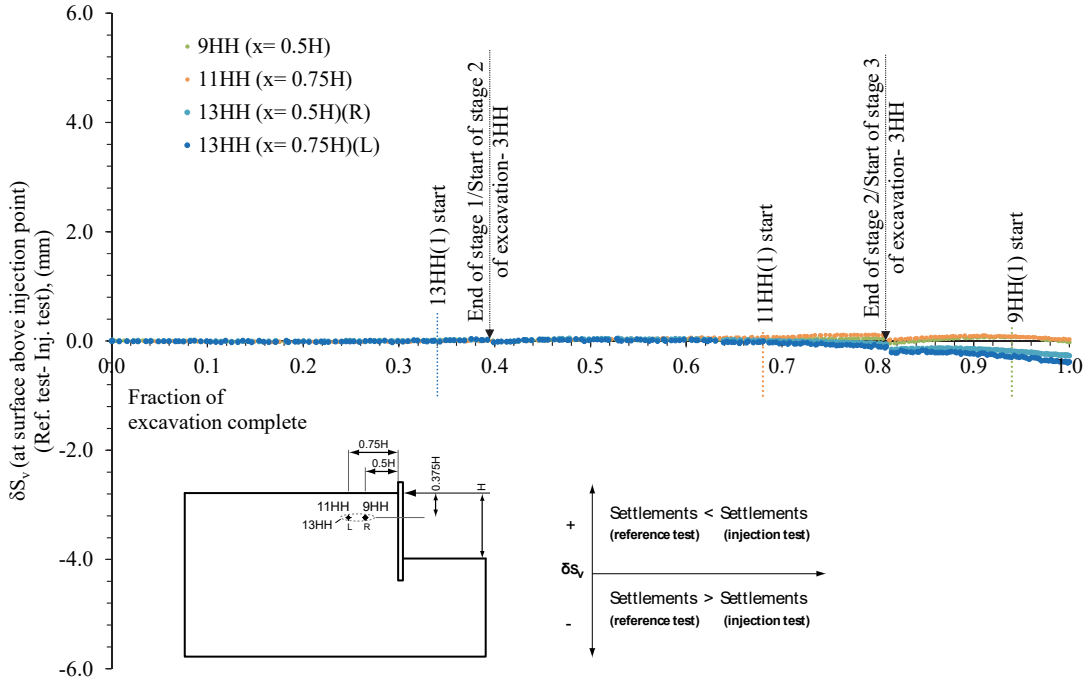


Figure 7. 13 Development of vertical displacements above the injection location at the retained surface in grouting tests 9HH, 11HH and 13HH relative to test 3HH during the simulated excavation.

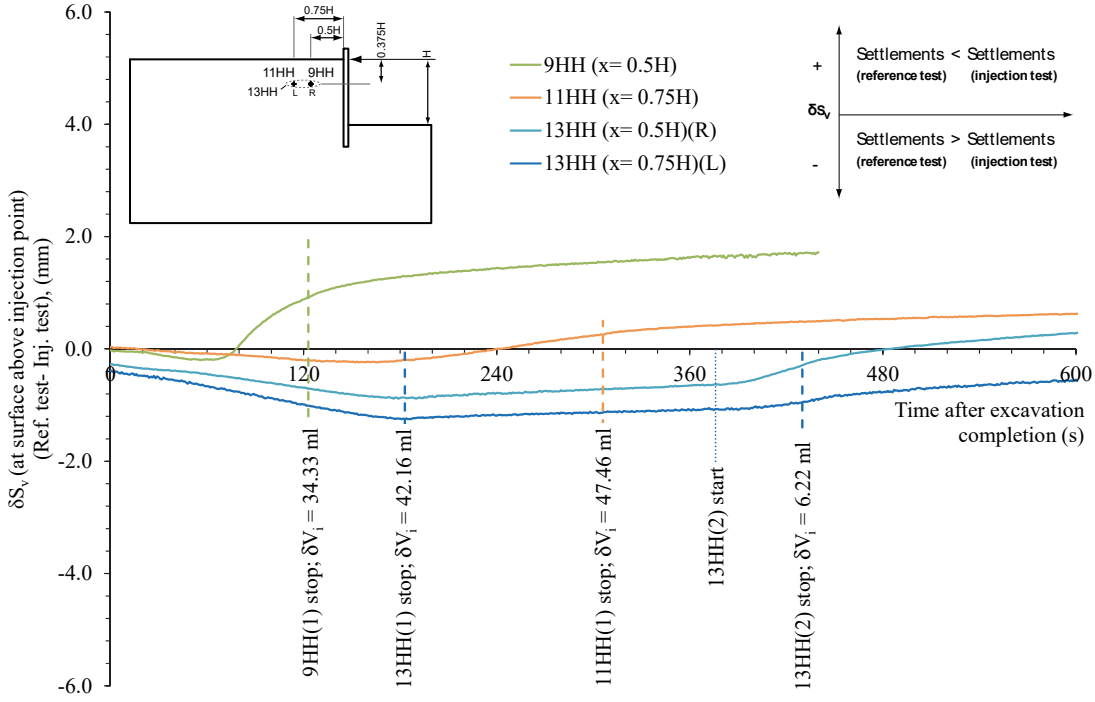


Figure 7. 14 Development of vertical displacements above the injection location at the retained surface in grouting tests 9HH, 11HH and 13HH relative to test 3HH after the simulated excavation.

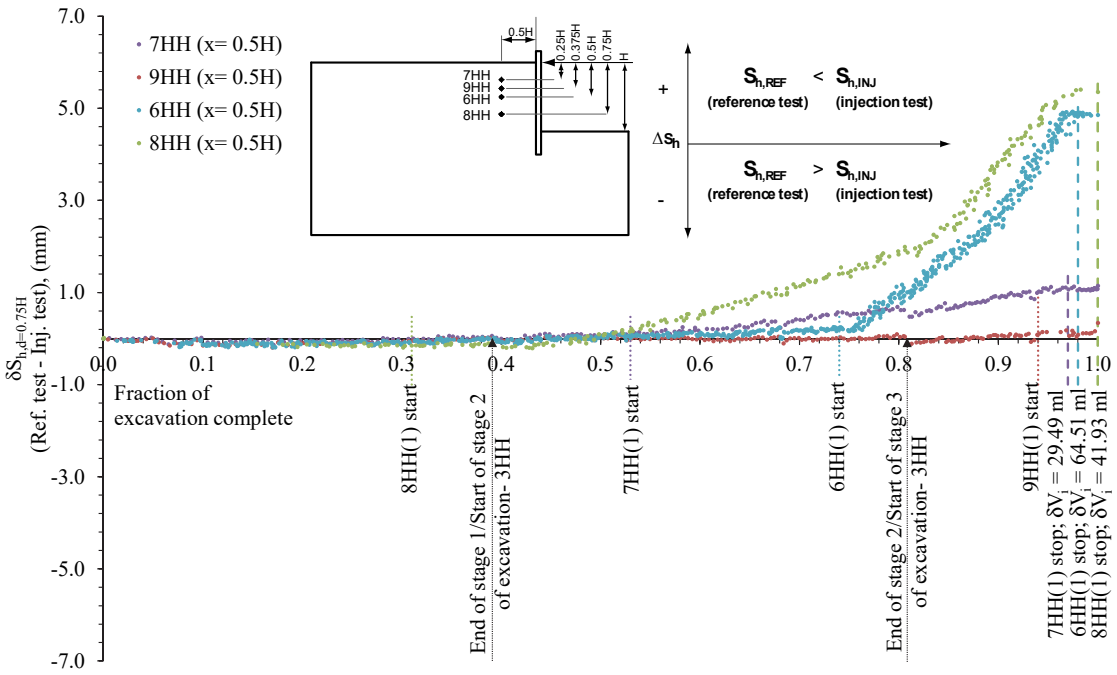


Figure 7. 15 Development of horizontal wall displacements at depth d= 0.75H, below the retained surface, in grouting tests 6-9HH relative to test 3HH during the simulated excavation.

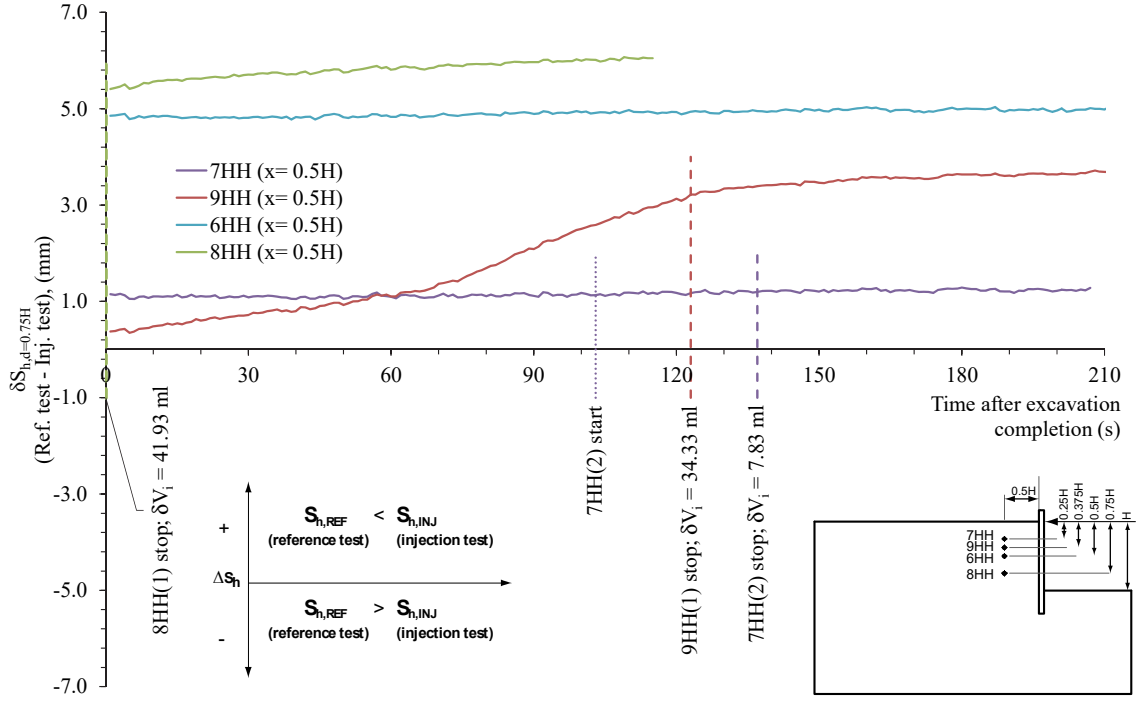


Figure 7. 16 Development of horizontal wall displacements at depth d= 0.75H, below the retained surface, in grouting tests 6-9HH relative to test 3HH after the simulated excavation.

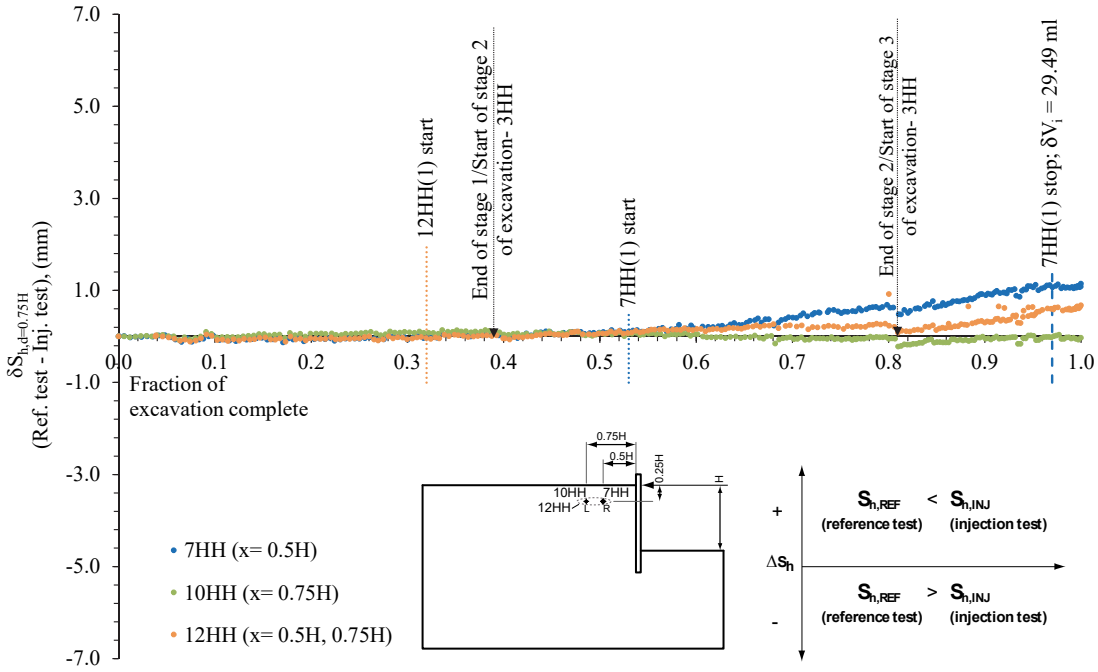


Figure 7. 17 Development of horizontal wall displacements at depth d= 0.75H, below the retained surface, in grouting tests 7HH, 10HH and 12HH relative to test 3HH during the simulated excavation.

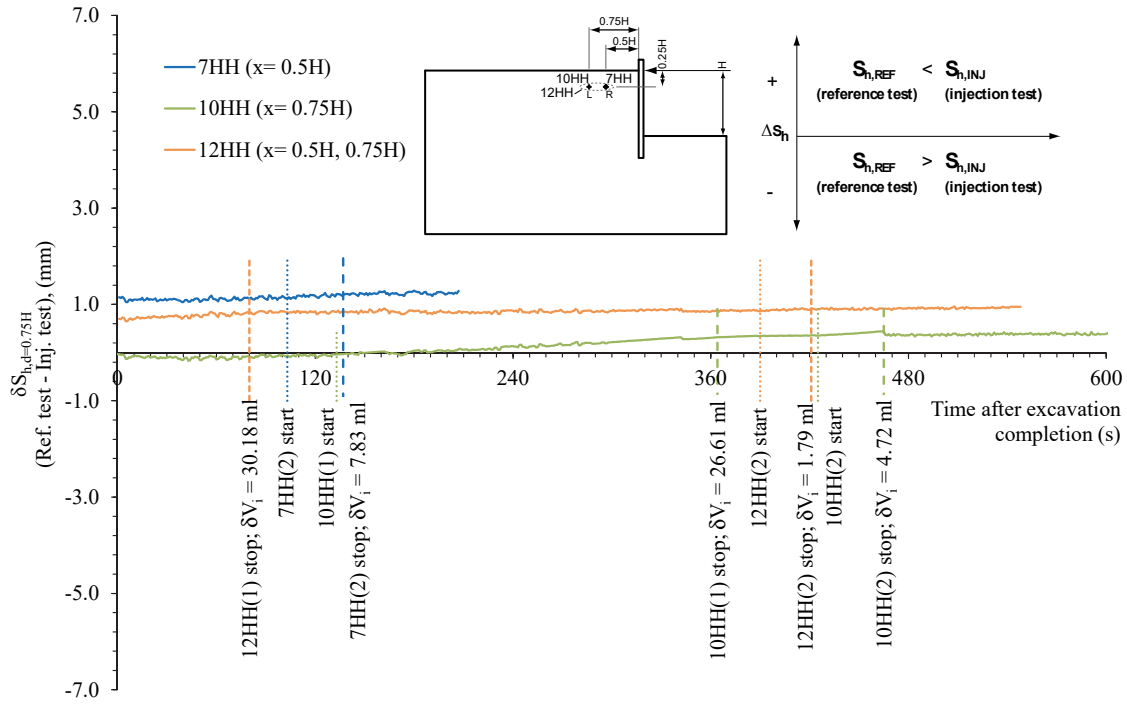


Figure 7. 18 Development of horizontal wall displacements at depth d= 0.75H, below the retained surface, in grouting tests 7HH, 10HH and 12HH relative to test 3HH after the simulated excavation.

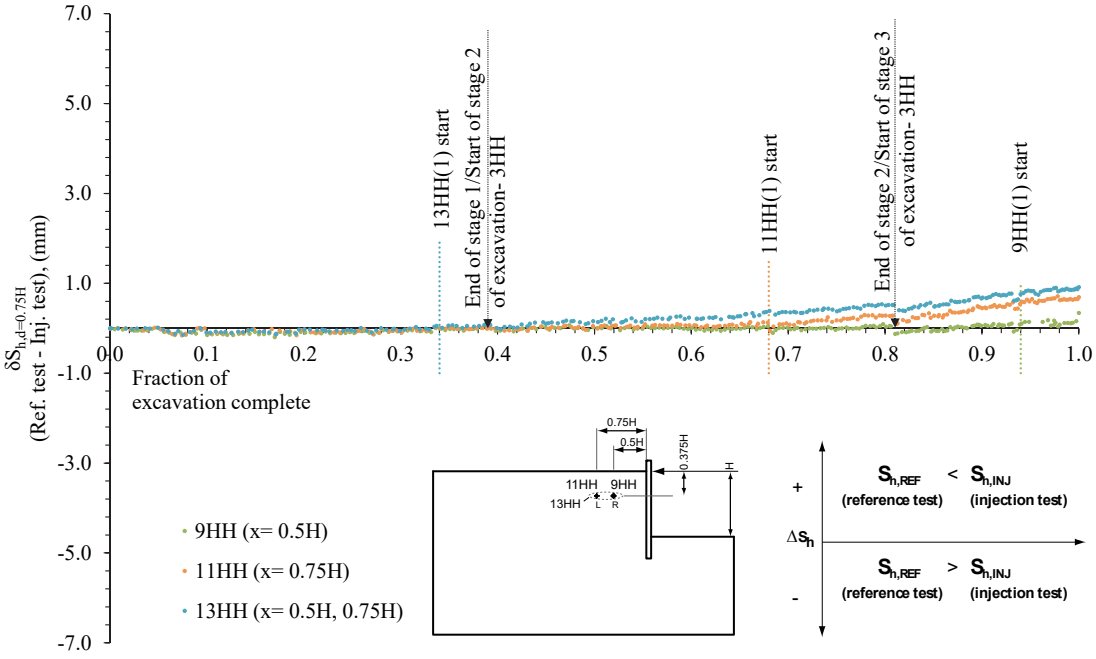


Figure 7. 19 Development of horizontal wall displacements at depth d= 0.75H, below the retained surface, in grouting tests 9HH, 11HH and 13HH relative to test 3HH during the simulated excavation.

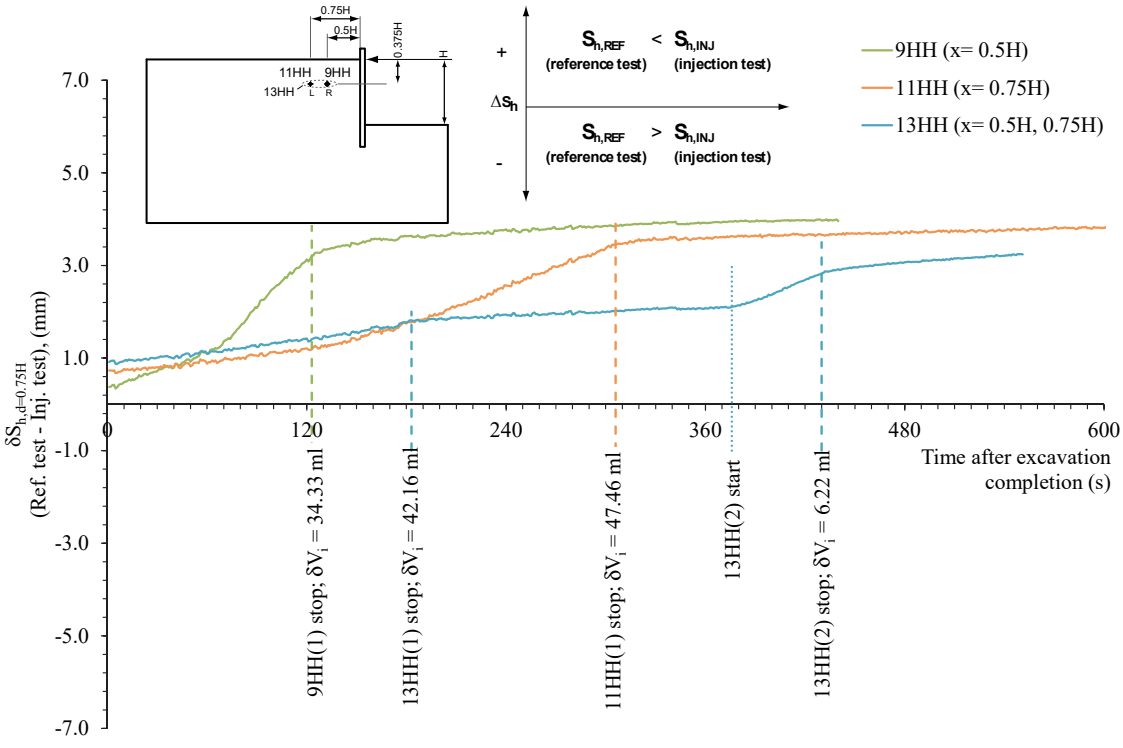


Figure 7. 20 Development of horizontal wall displacements at depth d= 0.75H, below the retained surface, in grouting tests 9HH, 11HH and 13HH relative to test 3HH after the simulated excavation.

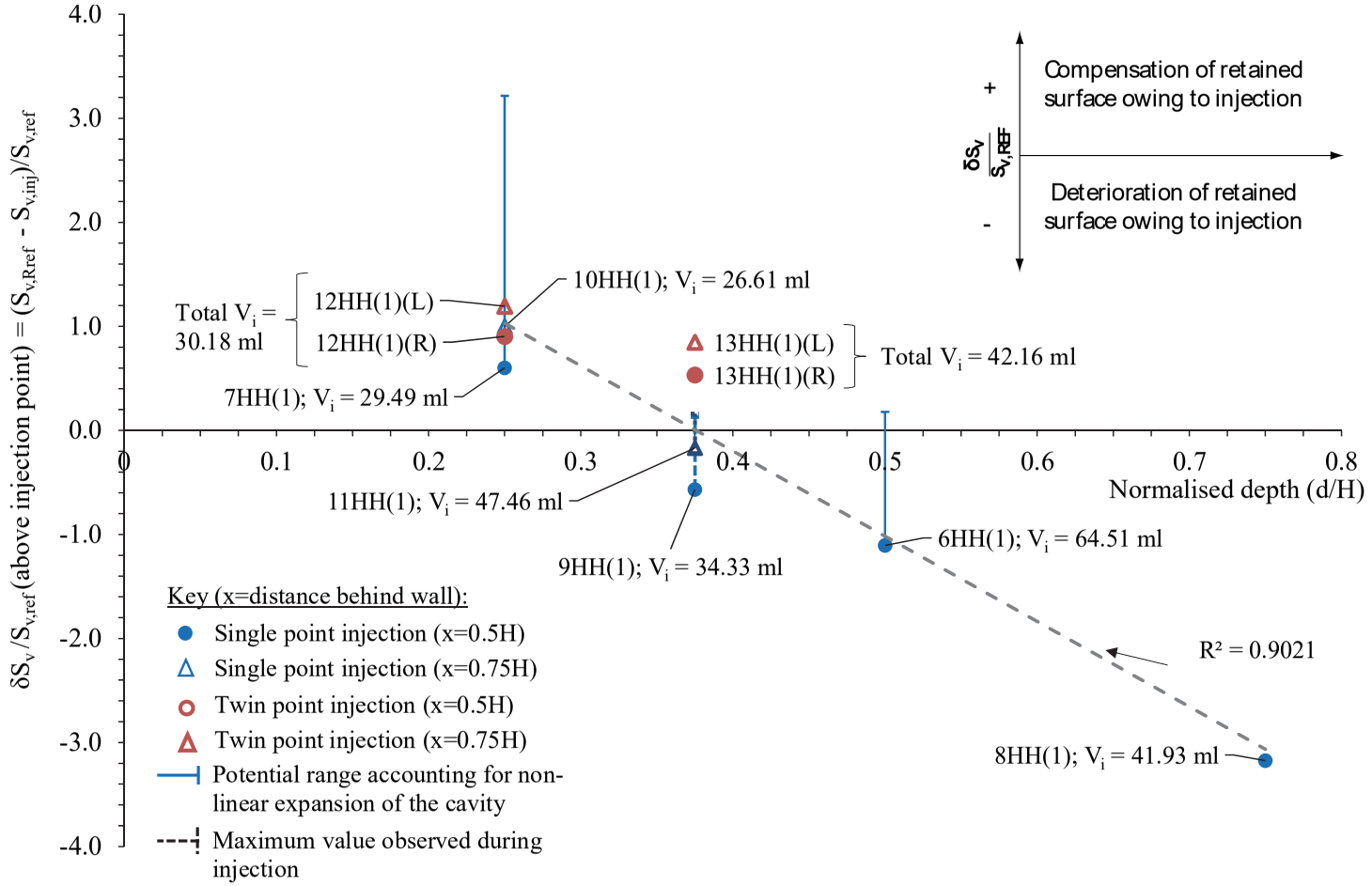


Figure 8. 1 Summary of the compensation effect on vertical displacements above the injection tube location at the retained surface between grouting tests (after the first injection pass) and reference test 3HH.

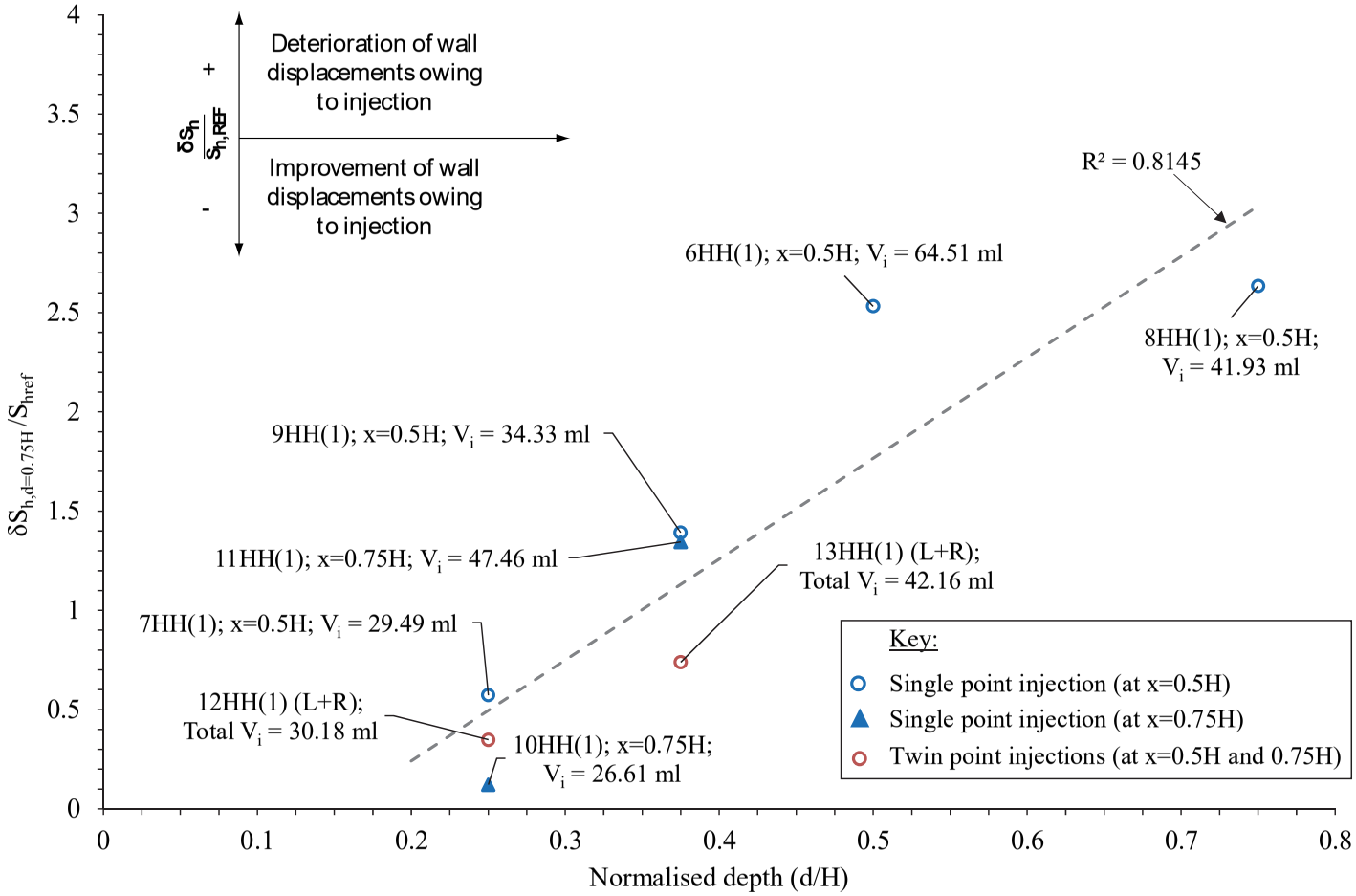
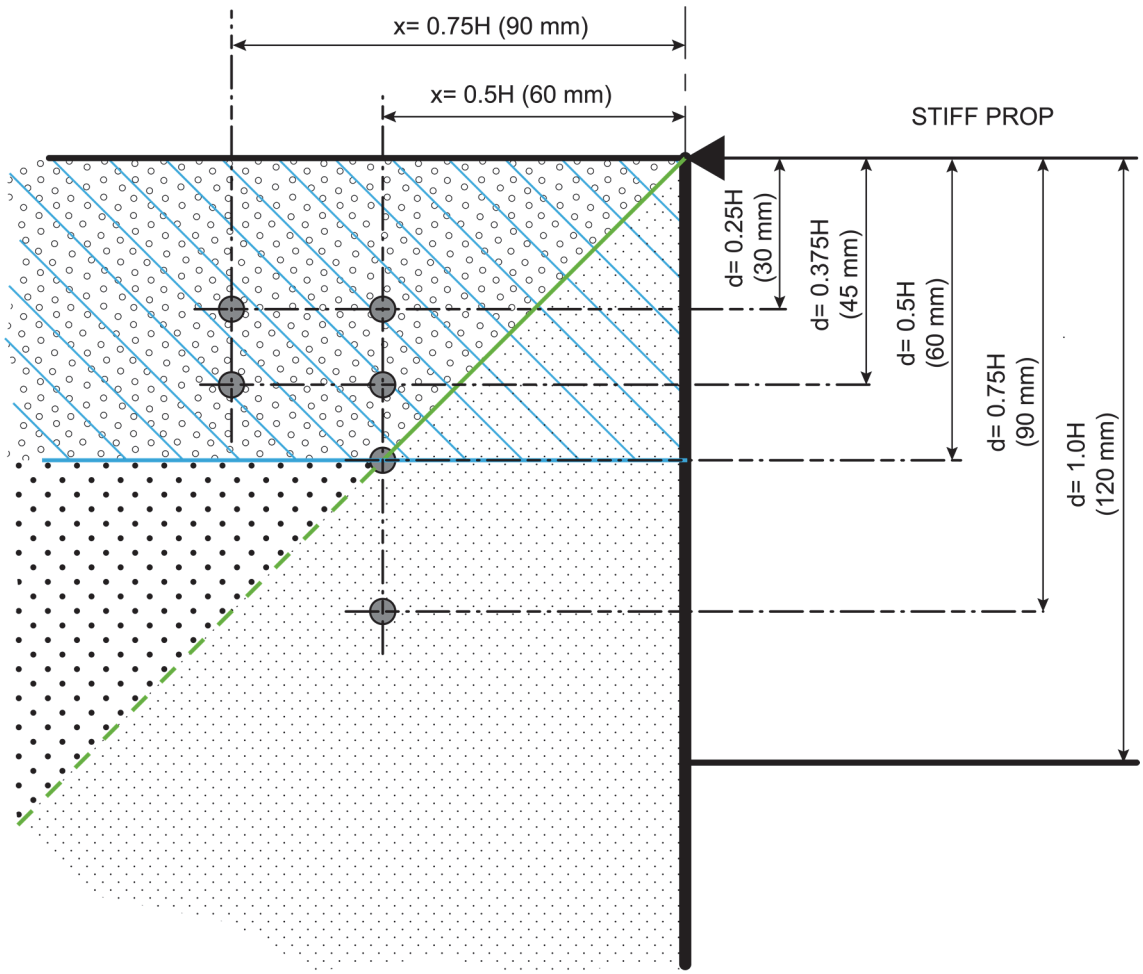


Figure 8. 2 Summary of the effects on wall displacements at depth d= 0.75H, below the retained surface, between grouting tests (after the first injection pass) and reference test 3HH.



KEY

Positions of grout injection investigated in model tests

Zone 1
-Positive compensation of retained surface achievable

Zone 2a
-Positive compensation of retained surface achievable
-Minimal increase of wall displacements relative to excavation only

Zone 2b
-Unknown impact on retained surface and wall displacements

Zone 3
-Significant increases of wall displacements relative to excavation only scenario

Figure 8. 3 Schematic illustration of regions identified from model tests where injection grouting can provide positive compensation of the retained surface and the effects on wall displacements.